201
Advances in Polymer Science

Editorial Board:

A. Abe · A.-C. Albertsson · R. Duncan · K. Dušek · W. H. de Jeu
J.-F. Joanny · H.-H. Kausch · S. Kobayashi · K.-S. Lee · L. Leibler
T. E. Long · I. Manners · M. Möller · O. Nuyken · E. M. Terentjev
B. Voit · G. Wegner · U. Wiesner

Advances in Polymer Science

Recently Published and Forthcoming Volumes

Neodymium Based Ziegler Catalysts – Fundamental Chemistry
Volume Editor: Nuyken, O.
Vol. 204, 2006

Polymers for Regenerative Medicine
Volume Editor: Werner, C.
Vol. 203, 2006

Peptide Hybrid Polymers
Volume Editors: Klok, H.-A., Schlaad, H.
Vol. 202, 2006

Supramolecular Polymers · Polymeric Betains · Oligomers
Vol. 201, 2006

Ordered Polymeric Nanostructures at Surfaces
Volume Editor: Vancso, G. J., Reiter, G.
Vol. 200, 2006

Emissive Materials · Nanomaterials
Vol. 199, 2006

Surface-Initiated Polymerization II
Volume Editor: Jordan, R.
Vol. 198, 2006

Surface-Initiated Polymerization I
Volume Editor: Jordan, R.
Vol. 197, 2006

Conformation-Dependent Design of Sequences in Copolymers II
Volume Editor: Khokhlov, A. R.
Vol. 196, 2006

Conformation-Dependent Design of Sequences in Copolymers I
Volume Editor: Khokhlov, A. R.
Vol. 195, 2006

Enzyme-Catalyzed Synthesis of Polymers
Volume Editors: Kobayashi, S., Ritter, H., Kaplan, D.
Vol. 194, 2006

Polymer Therapeutics II
Polymers as Drugs, Conjugates and Gene Delivery Systems
Volume Editors: Satchi-Fainaro, R., Duncan, R.
Vol. 193, 2006

Polymer Therapeutics I
Polymers as Drugs, Conjugates and Gene Delivery Systems
Volume Editors: Satchi-Fainaro, R., Duncan, R.
Vol. 192, 2006

Interphases and Mesophases in Polymer Crystallization III
Volume Editor: Allegra, G.
Vol. 191, 2005

Block Copolymers II
Volume Editor: Abetz, V.
Vol. 190, 2005

Block Copolymers I
Volume Editor: Abetz, V.
Vol. 189, 2005

Intrinsic Molecular Mobility and Toughness of Polymers II
Volume Editor: Kausch, H.-H.
Vol. 188, 2005

Intrinsic Molecular Mobility and Toughness of Polymers I
Volume Editor: Kausch, H.-H.
Vol. 187, 2005

Supramolecular Polymers
Polymeric Betains
Oligomers

With contributions by
B. Donnio · D. Guillon · A. Harada · A. Hashidzume · W. Jaeger
B. Janowski · S. Kudaibergenov · A. Laschewsky · J. Njuguna
J. Pielichowski · K. Pielichowski · Y. Takashima

Springer

The series *Advances in Polymer Science* presents critical reviews of the present and future trends in polymer and biopolymer science including chemistry, physical chemistry, physics and material science. It is adressed to all scientists at universities and in industry who wish to keep abreast of advances in the topics covered.
As a rule, contributions are specially commissioned. The editors and publishers will, however, always be pleased to receive suggestions and supplementary information. Papers are accepted for *Advances in Polymer Science* in English.
In references *Advances in Polymer Science* is abbreviated *Adv Polym Sci* and is cited as a journal.

Springer WWW home page: springer.com
Visit the APS content at springerlink.com

Library of Congress Control Number: 2006921403

ISSN 0065-3195
ISBN-10 3-540-31923-9 Springer Berlin Heidelberg New York
ISBN-13 978-3-540-31923-8 Springer Berlin Heidelberg New York
DOI 10.1007/11614784

This work is subject to copyright. All rights are reserved, whether the whole or part of the material is concerned, specifically the rights of translation, reprinting, reuse of illustrations, recitation, broadcasting, reproduction on microfilm or in any other way, and storage in data banks. Duplication of this publication or parts thereof is permitted only under the provisions of the German Copyright Law of September 9, 1965, in its current version, and permission for use must always be obtained from Springer. Violations are liable for prosecution under the German Copyright Law.

Springer is a part of Springer Science+Business Media

springer.com

© Springer-Verlag Berlin Heidelberg 2006
Printed in Germany

The use of registered names, trademarks, etc. in this publication does not imply, even in the absence of a specific statement, that such names are exempt from the relevant protective laws and regulations and therefore free for general use.

Cover design: *Design & Production* GmbH, Heidelberg
Typesetting and Production: LE-TEX Jelonek, Schmidt & Vöckler GbR, Leipzig

Printed on acid-free paper 02/3100 YL – 5 4 3 2 1 0

Editorial Board

Prof. Akihiro Abe
Department of Industrial Chemistry
Tokyo Institute of Polytechnics
1583 Iiyama, Atsugi-shi 243-02, Japan
aabe@chem.t-kougei.ac.jp

Prof. A.-C. Albertsson
Department of Polymer Technology
The Royal Institute of Technology
10044 Stockholm, Sweden
aila@polymer.kth.se

Prof. Ruth Duncan
Welsh School of Pharmacy
Cardiff University
Redwood Building
King Edward VII Avenue
Cardiff CF 10 3XF, UK
DuncanR@cf.ac.uk

Prof. Karel Dušek
Institute of Macromolecular Chemistry, Czech
Academy of Sciences of the Czech Republic
Heyrovský Sq. 2
16206 Prague 6, Czech Republic
dusek@imc.cas.cz

Prof. W. H. de Jeu
FOM-Institute AMOLF
Kruislaan 407
1098 SJ Amsterdam, The Netherlands
dejeu@amolf.nl
and Dutch Polymer Institute
Eindhoven University of Technology
PO Box 513
5600 MB Eindhoven, The Netherlands

Prof. Jean-François Joanny
Physicochimie Curie
Institut Curie section recherche
26 rue d'Ulm
75248 Paris cedex 05, France
jean-francois.joanny@curie.fr

Prof. Hans-Henning Kausch
Ecole Polytechnique Fédérale de Lausanne
Science de Base
Station 6
1015 Lausanne, Switzerland
kausch.cully@bluewin.ch

Prof. Shiro Kobayashi
R & D Center for Bio-based Materials
Kyoto Institute of Technology
Matsugasaki, Sakyo-ku
Kyoto 606-8585, Japan
kobayash@kit.ac.jp

Prof. Kwang-Sup Lee
Department of Polymer Science & Engineering
Hannam University
133 Ojung-Dong
Daejeon 306-791, Korea
kslee@hannam.ac.kr

Prof. L. Leibler
Matière Molle et Chimie
Ecole Supérieure de Physique
et Chimie Industrielles (ESPCI)
10 rue Vauquelin
75231 Paris Cedex 05, France
ludwik.leibler@espci.fr

Prof. Timothy E. Long
Department of Chemistry
and Research Institute
Virginia Tech
2110 Hahn Hall (0344)
Blacksburg, VA 24061, USA
telong@vt.edu

Prof. Ian Manners
School of Chemistry
University of Bristol
Cantock's Close
BS8 1TS Bristol, UK
ian.manners@bristol.ac.uk

Prof. Martin Möller
Deutsches Wollforschungsinstitut
an der RWTH Aachen e.V.
Pauwelsstraße 8
52056 Aachen, Germany
moeller@dwi.rwth-aachen.de

Prof. Oskar Nuyken
Lehrstuhl für Makromolekulare Stoffe
TU München
Lichtenbergstr. 4
85747 Garching, Germany
oskar.nuyken@ch.tum.de

Prof. E. M. Terentjev
Cavendish Laboratory
Madingley Road
Cambridge CB 3 OHE, UK
emt1000@cam.ac.uk

Prof. Brigitte Voit
Institut für Polymerforschung Dresden
Hohe Straße 6
01069 Dresden, Germany
voit@ipfdd.de

Prof. Gerhard Wegner
Max-Planck-Institut
für Polymerforschung
Ackermannweg 10
Postfach 3148
55128 Mainz, Germany
wegner@mpip-mainz.mpg.de

Prof. Ulrich Wiesner
Materials Science & Engineering
Cornell University
329 Bard Hall
Ithaca, NY 14853, USA
ubw1@cornell.edu

Advances in Polymer Science
Also Available Electronically

For all customers who have a standing order to Advances in Polymer Science, we offer the electronic version via SpringerLink free of charge. Please contact your librarian who can receive a password or free access to the full articles by registering at:

springerlink.com

If you do not have a subscription, you can still view the tables of contents of the volumes and the abstract of each article by going to the SpringerLink Homepage, clicking on "Browse by Online Libraries", then "Chemical Sciences", and finally choose Advances in Polymer Science.

You will find information about the

- Editorial Board
- Aims and Scope
- Instructions for Authors
- Sample Contribution

at springer.com using the search function.

Contents

Cyclodextrin-Based Supramolecular Polymers
A. Harada · A. Hashidzume · Y. Takashima 1

Liquid Crystalline Dendrimers and Polypedes
B. Donnio · D. Guillon 45

Polymeric Betaines: Synthesis, Characterization, and Application
S. Kudaibergenov · W. Jaeger · A. Laschewsky 157

Polyhedral Oligomeric Silsesquioxanes (POSS)-Containing Nanohybrid Polymers
K. Pielichowski · J. Njuguna · B. Janowski · J. Pielichowski 225

Author Index Volume 201 297

Subject Index 299

Adv Polym Sci (2006) 201: 1–43
DOI 10.1007/12_056
© Springer-Verlag Berlin Heidelberg 2005
Published online: 6 December 2005

Cyclodextrin-Based Supramolecular Polymers

Akira Harada (✉) · Akihito Hashidzume · Yoshinori Takashima

Graduate School of Science, Osaka University, Toyonaka, Osaka, 560-0043, Japan
harada@chem.sci.osaka-u.ac.jp

1 Introduction 2

2 Supramolecular Polymers in the Solid State 3
2.1 Crystal Structure of 6-*O*-(*tert*-Butylthio)-β-Cyclodextrin 5
2.2 Crystal Structure of 6-*O*-(Phenylthio)-β-Cyclodextrin and 6-*O*-(Phenylsulphinyl)-β-Cyclodextrin 5
2.3 Crystal Structure of 2-*O*-[(*S*)-2-Hydroxypropyl]-β-Cyclodextrin, 6-*O*-[(*R*)-2-Hydroxypropyl]-β-Cyclodextrin, and 6-*O*-[(*S*)-2-Hydroxypropyl]-β-Cyclodextrin 6
2.4 Crystal Structure of 6-*O*-(6-Cyclo(L-histidyl-L-leucyl))-β-Cyclodextrin . . . 7
2.5 Crystal Structure of 6-*O*-Azido-α-Cyclodextrin, 6-*O*-Allyl-α-Cyclodextrin and 6-*O*-[(6-Aminohexyl)Amino]-β-Cyclodextrin 8
2.6 Crystal Structure of 6-*O*-6-(1-Propyl)amino-β-Cyclodextrin, 6-*O*-6-[(*R*)-1-Cyclohexylethyl]amino-β-Cyclodextrin, 6-*O*-6-[(*R*)-1-Phenylethyl]amino-β-Cyclodextrin, and 6-*O*-6-[(1*R*,2*S*)-2-Hydroxyindan-1-yl]amino-β-Cyclodextrin 9
2.7 Crystal Structure of β-Cyclodextrin Aromatic Tethers 10
2.8 Crystal Structure of 6-*O*-4-Aminocinnamoyl-β-Cyclodextrins 11

3 Supramolecular Polymers in Solution 12
3.1 Formation of Intramolecular Complexes by Hydrocinnamoyl-β-Cyclodextrin 13
3.2 Formation of Intermolecular Complexes by Hydrocinnamoyl-α-Cyclodextrin 14
3.3 Formation of Supramolecular 6-Cinnamoyl-β-Cyclodextrin Complexes . . 15
3.4 Formation of Intramolecular Complexes by 6-Cinnamamide-β-Cyclodextrin 16
3.5 Formation of a Supramolecular Dimer by 6-Cinnamamide-α-Cyclodextrin 16
3.6 Formation of Supramolecular Polymers by 3-Cinnamamide-α-Cyclodextrin 17
3.7 Formation of Supramolecular Oligomers by 6-Cinnamoyl α-Cyclodextrin . 17
3.8 Cyclic Daisy Chain 18
3.9 Daisy Chains 18
3.10 Formation of Helical Supramolecular Polymers by *p*-*tert*-Boc-Amino-Cinnam-α-Cyclodextrin 19
3.11 Supramolecular Polymers with Alternating α- and β-Cyclodextrin Units . . 19

4 Polyrotaxanes 20
4.1 *pseudo*-Poly(rotaxane)s between Cyclodextrins and Polymers 21
4.2 α-Cyclodextrin Polyrotaxanes and Cyclodextrin Molecular Tube 27
4.3 Molecular Shuttle 28
4.4 β-Cyclodextrin Polyrotaxanes 31

4.5 Cyclodextrin Poly(polyrotaxane) 32
4.6 One-Pot Synthesis of γ-Cyclodextrin Polyrotaxane 33
4.7 Polyrotaxanes Prepared by Inclusion Polymerization (Polythiophene Polyrotaxanes) 34

5 Supramolecular Polymers Formed by CDs and Polymer Side Chains . . . 35
5.1 Side Chain Polyrotaxanes 36
5.2 Alkyl Side Chains 36
5.3 Aryl Side Chains 36
5.4 Utilization of Supramolecular Polymers Formed by CDs and Polymer Side Chains 37

References 38

Abstract Supramolecular polymers were prepared by inclusion of a guest in cyclodextrin via a covalent bond. The structures of the supramolecular oligomers and polymers were determined by X-ray studies, NMR measurements, absorption and circular dichroism spectra. The sizes of the supramolecular polymers were determined by vapor pressure osmometry and pulsed-field gradient NMR. Although hydrocinnamoyl β-cyclodextrin formed an intramolecular complex, hydrocinnamoyl α-cyclodextrin formed intermolecular complexes. Cinnamoyl β-cyclodextrin gave a cyclic dimer and cinnamoyl α-cyclodextrin formed a cyclic trimer. α-Cyclodextrin with cinnamic amide at the secondary hydroxyl side gave supramolecular polymers. Formation of the complexes of cyclodextrins with various polymers has also been described.

Keywords Cyclodextrin · Host-guest interactions · Inclusion complex · Molecular tube · Polyrotaxane · Supramolecular polymer

1 Introduction

In recent years, supramolecular chemistry has been expanding to include supramolecular polymer science [1, 2]. Conventional polymers, such as vinyl polymers and condensation polymers, are made up of covalent bonds. However, supramolecular polymers are made up of non-covalent bonds. The first supramolecular polymers were reported by Lehn et al. [1, 3–5], in which each building block is linked by three hydrogen bonds (Fig. 1). In this case, on average, several building blocks are linked together to form supramolecular oligomers. Later, Meijer et al. [6–8] reported supramolecular polymers formed by four hydrogen bonds in each unit (Fig. 2). In this case, high molecular weight (higher than 10×10^4) supramolecular polymers were obtained. The concentrated solutions are viscous-like solutions of conventional polymers. In addition, the viscosity can be controlled by their concentrations, temperature, and even the addition of a monofunctional unit.

These supramolecular polymers remind us of the discussion concerning the existence of macromolecules over 70 years ago by Staudinger et al. Although macromolecules made up of covalent bonds are of course ubiqui-

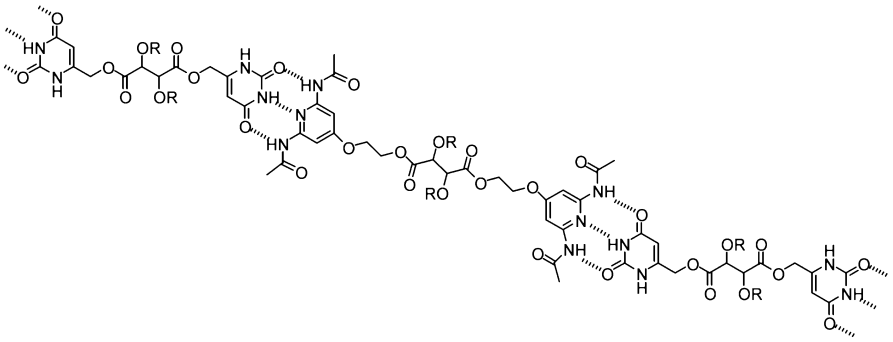

Fig. 1 Supramolecular polymer of bifunctional ureido pyrimidinone derivative reported by Lehn

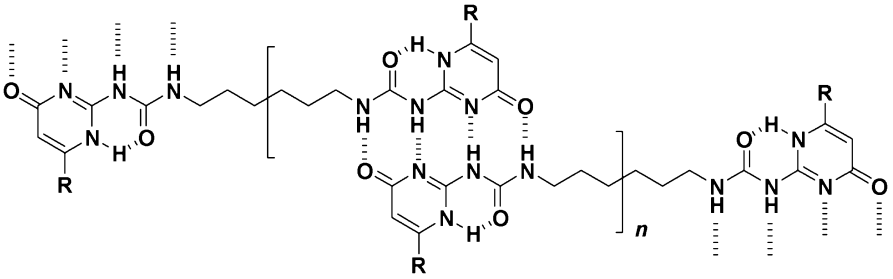

Fig. 2 Supramolecular polymer reported by Meijer

tous in nature and the synthetic world, "macromolecules" made up of noncovalent bonds are also ubiquitous in nature, especially in living creatures and are important in the synthetic world as well.

Many kinds of molecular interactions, such as hydrogen bonding, ionic interactions, van der Waals interactions, and hydrophobic interactions can be used for the design and construction of supramolecular polymers [1–12]. The most important interaction in biological systems are Host-Guest interactions, such as enzyme-substrate, antigen-antibody, microtubules, microfilaments, and flagella. Recently, many kinds of supramolecular polymers have been designed and constructed by synthetic methods. In this Chapter, the authors would like to introduce some supramolecular polymers constructed through Host-Guest systems, especially using cyclodextrins as hosts and some benzene derivatives as guests.

2
Supramolecular Polymers in the Solid State

X-ray crystallography has been a major source of information for the three-dimensional structure of the host-guest complexes. First attempts in the use

of single-crystal X-ray diffraction were applied to α-cyclodextrin (α-CD) and β-cyclodextrin (β-CD) by French and Rundl [13]. James et al. [14] reported the crystallographic data for several α-CD complexes, but their resolution for structural analysis of the iodine complex was very low. After several years, Hybl et al. [15] reported the structure of the complex of α-CD with potassium acetate for a full X-ray structure. Since then, there have been numerous reports on crystal structures of cyclodextrins and their inclusion complexes, as summarized in several reviews [16–20]. Crystal structures of CDs and their inclusion complexes were classified into cage-, channel-, and layer-type structures. These classes are dependent on the relationship between CDs and the included guest molecules. Recently, some monosubstituted CDs were synthesized to give the catalytic activity and the formation of the supramolecular complex. For example: in the crystal structure, 6-*O*-(*tert*-butylthio)-β-CD molecules was arranged along a screw axis and the *tert*-butylmercaptan group was inserted into the next β-CD cavity to form a helically extended polymeric structure [21]. This modified CD behaves not only as a donor of the guest group but also as an acceptor. These types of structure may be termed "supramolecular polymer" in the solid state. This section focuses on the crystal structures of monosubstituted CDs.

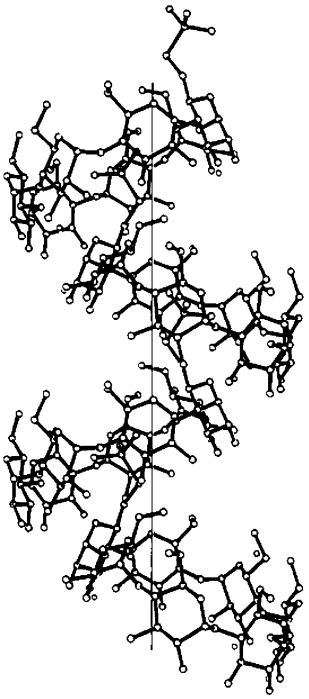

Fig. 3 The crystal structure of 6-*O*-(*tert*-butylthio)-β-CD drawing a helical polymer related by the 2_1 screw axis

2.1
Crystal Structure of 6-*O*-(*tert*-Butylthio)-β-Cyclodextrin

The structure of 6-(*tert*-butylthio)-β-CD was characterized by Tabushi et al. [21]. The compound of 6-*O*-(*tert*-butylthio)-β-CD was prepared from the reaction of 6-*O*-(*p*-toluenesulfonyl)-β-CD with *tert*-butylmercaptan and recrystallized in water. This is the first example of the determination of crystal structure of monosubstituted CD derivatives and the first evidence concerning the supramolecular polymer of an inclusion complex of a monosubstituted CD. The crystal structure of 6-*O*-(*tert*-butylthio)-β-CD was arranged around the two-fold axis to yield a polymeric structure, in which the *tert*-butyl group is intermolecularly included in the cavity of CD (Fig. 3).

2.2
Crystal Structure of 6-*O*-(Phenylthio)-β-Cyclodextrin and 6-*O*-(Phenylsulphinyl)-β-Cyclodextrin

Tabushi and Kamitori et al. [22] also reported that a substituted group was intermolecularly included in the cavity of another CD (Fig. 4). They carried out the X-ray crystallographic study of two compounds, 6-*O*-phenylthio-β-

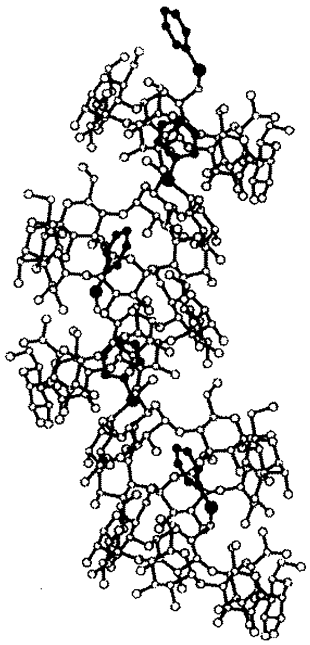

Fig. 4 The crystal structure of 6-deoxy-6-(phenylthio)-β-CD. The phenyl group is shown with *filled circles*. The molecules are arranged along a 4-fold screw axis, and the phenyl group is inserted into the cavity of an adjacent β-CD from its secondary hydroxyl side

CD and 6-*O*-phenylsulphinyl-β-CD. From the molecular structure of 6-*O*-phenylthio-β-CD, it was found that the phenyl group enters the center of the CD cavity from the side of secondary hydroxyl groups. In the case of 6-*O*-phenylsulphinyl-β-CD, the guest phenylsulphinyl group was more deeply included in the host CD cavity than that of 6-*O*-phenylthio-β-CD. In the packing structures, the molecules are arranged around the screw axis to give a unique polymeric inclusion column structure formed from a single species acting both as a guest and as a host. The macrocycles in helical columns are related by a four-fold screw axis for 6-*O*-phenylthio-β-CD and by a two-fold screw axis for 6-*O*-phenylsulphinyl-β-CD.

2.3
Crystal Structure of 2-*O*-[(*S*)-2-Hydroxypropyl]-β-Cyclodextrin, 6-*O*-[(*R*)-2-Hydroxypropyl]-β-Cyclodextrin, and 6-*O*-[(*S*)-2-Hydroxypropyl]-β-Cyclodextrin

Harata et al. [23] reported that the crystal structure of 2-*O*-[(*S*)-2-hydroxypropyl]-β-CD was solved by X-ray diffraction (Fig. 5). The molecules are arranged in a herring-bone fashion to form a cage-type packing structure. The hydroxypropyl group is inserted into the cavity of an adjacent molecule related by a two-fold screw axis.

In the crystal structures of 6-*O*-[(*R*)-2-hydroxypropyl]- and 6-*O*-[(*S*)-2-hydroxypropyl]-β-CD, the 2-hydroxypropyl group is inserted into the β-CD cavity of the next β-CD related by the two-fold screw axis, and a helically extended polymeric structure is formed by repetition of the intermolecular inclusion (Fig. 6). The hydroxyl group of the substituent group penetrates through the β-CD ring from the secondary hydroxyl side and is linked to an

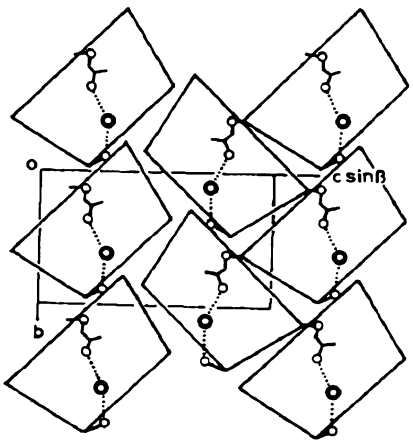

Fig. 5 Packing structure of 2-*O*-[(*S*)-2-hydroxypropyl]-β-CD. Hydrogen bonds involving the hydropropyl group are shown by *dotted lines*

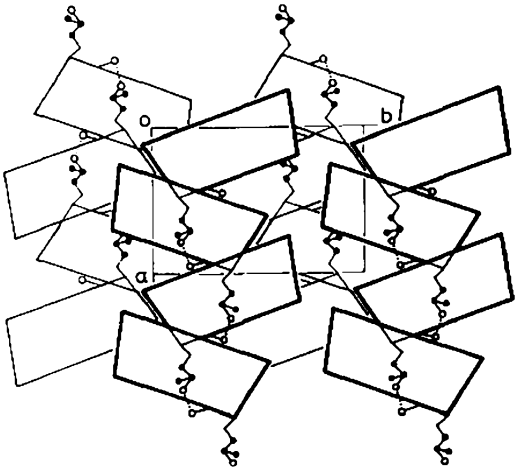

Fig. 6 A schematic drawing of the packing in the crystal viewed along the *c*-axis in 6-*O*-[(*R*)-2-hydroxypropyl]- and 6-*O*-[(*S*)-2-hydroxypropyl]-β-CD

HO-6 group by a hydrogen bond. Comparison of intermolecular contacts of the substituent group indicates that the (*S*)-2-hydroxypropyl group is better fitted to the cavity than the (*R*)-2-hydroxy-propyl group.

2.4 Crystal Structure of 6-*O*-(6-Cyclo(L-histidyl-L-leucyl))-β-Cyclodextrin

In the molecular structure of 6-*O*-(6-cyclo(L-histidyl-L-leucyl)-β-CD, the cyclo(L-histidyl-L-leucyl) group is included in the center of the CD cavity

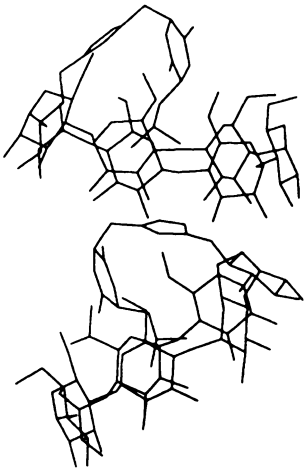

Fig. 7 The crystal structure of 6-*O*-(6-cyclo(L-histidyl-L-leucyl)-β-CD along the *b*-axis

from the side of the primary hydroxyl groups (Fig. 7) [24]. In the packing structure, the molecules are arranged around the two-fold screw axis to give the unique polymeric inclusion column structure formed from a single species acting both as a guest and as a host. The structure of 6-*O*-(6-cyclo(L-histidyl-L-leucyl)-β-CD was arranged along the two-fold screw axis and the cyclo(L-histidyl-L-leucyl) group is inserted into the β-CD cavity.

2.5 Crystal Structure of 6-*O*-Azido-α-Cyclodextrin, 6-*O*-Allyl-α-Cyclodextrin and 6-*O*-[(6-Aminohexyl)Amino]-β-Cyclodextrin

The X-ray crystal structures of 6-*O*-azido-α-CD and 6-*O*-allyl-α-CD were determined by Hanesian et al. [25]. Azido and allyl groups of each CD unit are included in the cavity of adjacent units from the secondary hydroxyl group side to form along the two-fold screw axis (Fig. 8). 6-*O*-[(6-Aminohexyl)amino]-β-CD is arranged along the two-fold screw axis parallel to the *c* crystal axis forming a polymeric column structure (Fig. 9) [26]. 6-Aminohexyl chain groups are inserted into the cavity of the adjacent β-CD moiety from the secondary side. All the atoms of the chain exhibit large thermal motion. The nitrogen atom is found near the secondary hydroxyl group rim of host β-CD and forms a hydrogen-bond with a water molecule. The end of the nitrogen atom in the substituted group was also hydrogen-bonded to

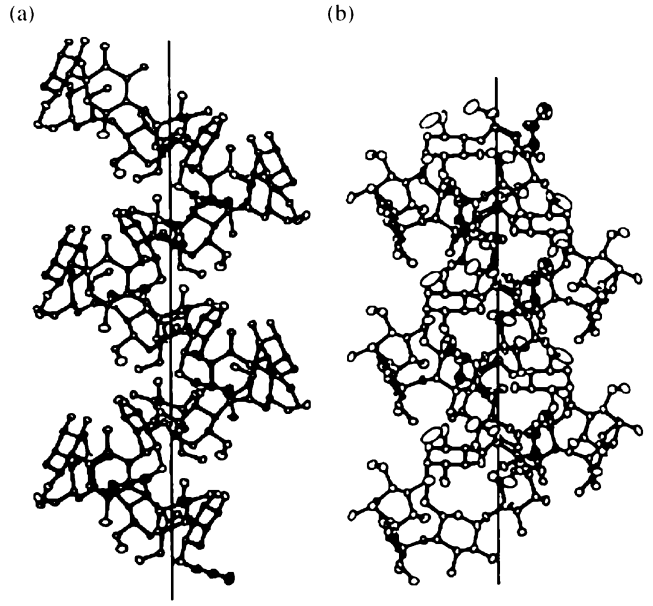

Fig. 8 The crystal structures of 6-*O*-azido-α-CD and 6-*O*-allyl-α-CD drawing a helical polymer penetrated by the 2_1 screw axis

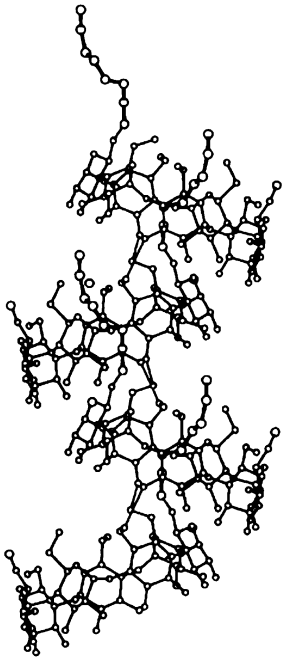

Fig. 9 The crystal structure of 6-*O*-[(6-aminohexyl)amino]-β-CD drawing polymeric-like columns penetrated by the 2_1 screw axis

a water molecule to form a polymeric column. 6-*O*-[(6-Aminohexyl)amino]-β-CD molecules are stacked parallel along the *b* crystal axis and anti-parallel along the *a* axis. Parallel polymeric columns are bound to each other by two hydrogen bonds.

2.6 Crystal Structure of 6-*O*-6-(1-Propyl)amino-β-Cyclodextrin, 6-*O*-6-[(*R*)-1-Cyclohexylethyl]amino-β-Cyclodextrin, 6-*O*-6-[(*R*)-1-Phenylethyl]amino-β-Cyclodextrin, and 6-*O*-6-[(1*R*,2*S*)-2-Hydroxyindan-1-yl]amino-β-Cyclodextrin

Harata et al. [27] reported the crystal structures of four 6-monosubstituted β-CDs, 6-*O*-(1-propyl)amino-β-CD, 6-*O*-[(*R*)-1-cyclohexylethyl]amino-β-CD, 6-*O*-[(*R*)-1-phenylethyl]amino-β-CD, and 6-*O*-[(1*R*,2*S*)-2-hydroxyindan-1-yl]amino-β-CD. They discussed the relationship between crystal packing and the inclusion of the substituent group (Fig. 10). In each crystal, the substituent groups were inserted into the adjacent β-CD cavity from the secondary hydroxyl side. This host-guest type self-association through intermolecular inclusion generates a one-dimensional polymeric chain. 6-*O*-(1-Propyl)amino-β-CD and 6-*O*-[(*R*)-1-cyclohexylethyl]amino-β-CD form

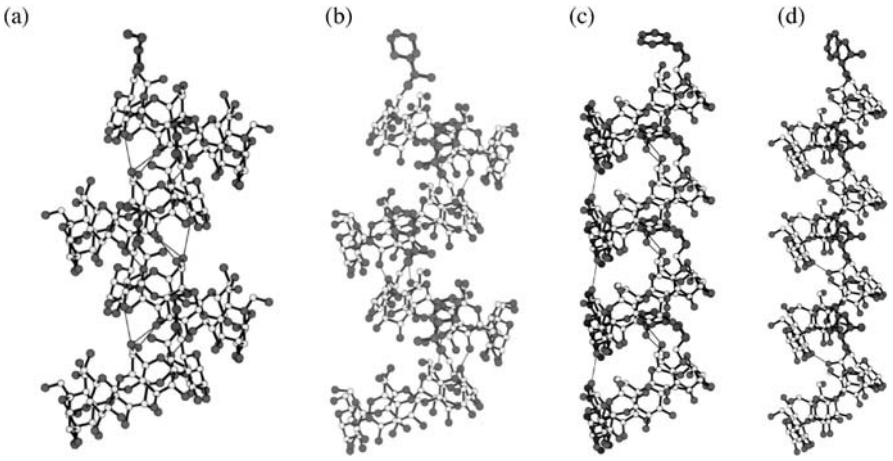

Fig. 10 The crystal structures of 6-*O*-(1-propyl)amino-β-CD (**a**), 6-*O*-[(*R*)-1-cyclohexylethyl] amino-β-CD (**b**), 6-*O*-[(*R*)-1-phenylethyl]amino-β-CD (**c**), and 6-*O*-[(1*R*,2*S*)-2-hydroxyindan-1-yl]amino-β-CD (**d**) drawing a helical polymer penetrated by the 2_1 screw axis

a helically extended chain along the crystallographic two-fold screw axis. 6-*O*-[(*R*)-1-Phenylethyl]amino-β-CD and 6-*O*-[(1*R*,2*S*)-2-hydroxyindan-1-yl]amino-β-CD form a linear extended chain. The crystal packing of 6-*O*-[(*R*)-1-phenylethyl]amino-β-CD was similar to that of a channel-type structure, while the arrangement of the β-CD ring of 6-*O*-[(1*R*,2*S*)-2-hydroxyindan-1-yl]amino-β-CD belongs to the cage-type.

2.7 Crystal Structure of β-Cyclodextrin Aromatic Tethers

Crystal structures of aromatic group-modified β-CD derivatives, such as 6-*O*-anilino-β-CD [28], 6-*O*-(4-formyl-phenyl)-β-CD [29], 6-*O*-(4-bromophenyl)-β-CD [30], 6-*O*-(4-nitrophenyl)-β-CD [30], 6-*O*-(4-formylphenyl)-β-CD [30], 6-*O*-phenylselenyl-β-CD [30], 6-*O*-(4-hydroxybenzoyl)-β-CD [30], and 6-*O*-(*p*-carboxyphenylamino)-β-CD [31], were determined by X-ray crystallography (Fig. 11). 6-*O*-Anilino-β-CD, 6-*O*-(4-formyl-phenyl)-β-CD, 6-*O*-(4-bromophenyl)-β-CD, 6-*O*-(4-nitrophenyl)-β-CD, 6-*O*-(4-formylphenyl)-β-CD, and 6-*O*-(*p*-carboxyphenylamino)-β-CD, form a helically extended chain along the crystallographic two-fold screw axis. 6-*O*-Phenylselenyl-β-CD forms a helically extended chain along the crystallographic four-fold screw axis. 6-*O*-(4-Hydroxybenzoyl)-β-CD forms a tail-to-tail dimer structure, in which the substituents penetrate into the CD cavity. Liu et al. [30] stated this tail-to-tail dimer structure was made possible by the longer and flexible ester linkage in 6-*O*-(4-hydroxybenzoyl)-β-CD rather than other aromatic group-modified β-CDs.

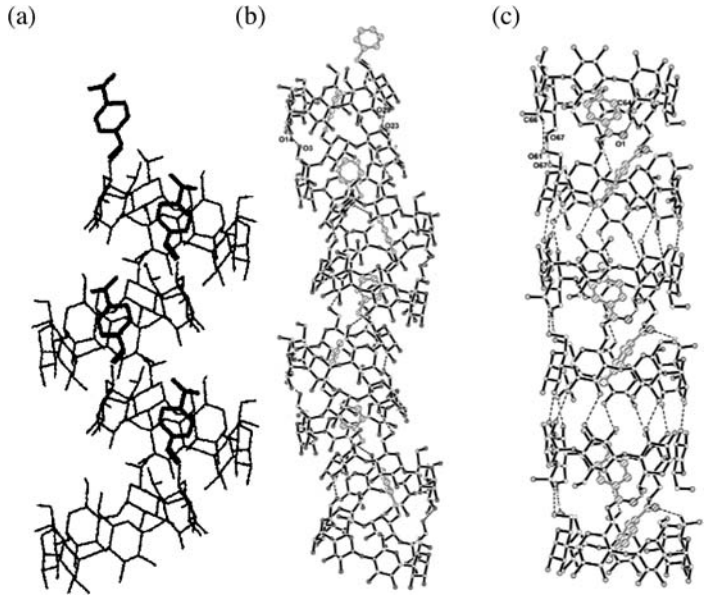

Fig. 11 The crystal structures of 6-*O*-(*p*-carboxyphenylamino)-β-CD penetrated by the 2_1 screw axis (**a**), 6-phenylselenyl-6-deoxy-β-CD penetrated by the 4_1 screw axis (**b**) and 6-*O*-(4-hydroxybenzoyl)-β-CD (**c**) showing the dimeric columnar structure

2.8 Crystal Structure of 6-*O*-4-Aminocinnamoyl-β-Cyclodextrins

The authors studied the X-ray crystallography of 6-aminocinnamoyl-β-CD (6-aminoCiO-β-CD) (Fig. 12) [32]. Some 6-monosubstituted CDs formed a helically extended polymeric structure, in which molecules are related by

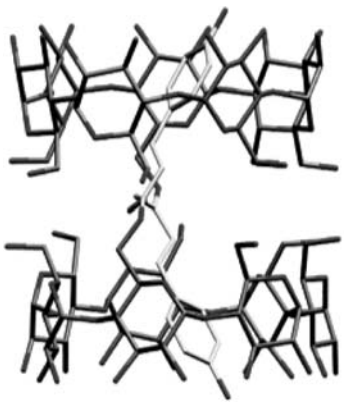

Fig. 12 Crystal structure of 6-aminoCiO-β-CD drawing a dimeric columnar structure

two-fold or four-fold screw axis. The molecular structure of 6-aminoCiO-β-CD is arranged along a dimeric structure and the 6-aminocinnamoyl group is inserted into the adjacent β-CD cavity from the primary hydroxyl group side to form a columnar channel structure.

These crystal structures indicated that the self-assembly of the 6-mono-substituted β-CD was regulated by physical and chemical properties of the substituent group included in the adjacent β-CD ring. This causes variation in the one-dimensional arrangement depending on the shape, size, and orientation of the substituent group.

3 Supramolecular Polymers in Solution

Although the native CDs themselves are of interest as host molecules, the modification of native CDs changes the size, shape and physical properties of the CD ring. Therefore, great efforts have been made for the preparation of CDs covalently attached to guest molecules. When a guest group is covalently attached to the cyclic host molecule, it could form intramolecular [33–42] or intermolecular complexes [30, 32, 43–62] in aqueous solutions by host-guest interactions, depending on the flexibility and length of the substitution part. Many modified CDs have been prepared and its supramolecular structure characterized in aqueous solutions. Most of these formed intramolecular complexes. Ueno et al. [33–35] reported that chromophore-modified CDs act as chemosensors because of the location change of the substitution part from inside to outside of the CD cavities with the inclusion of another guest molecule (Fig. 13). Benzoyl-modified β-CD did not form supramolecu-

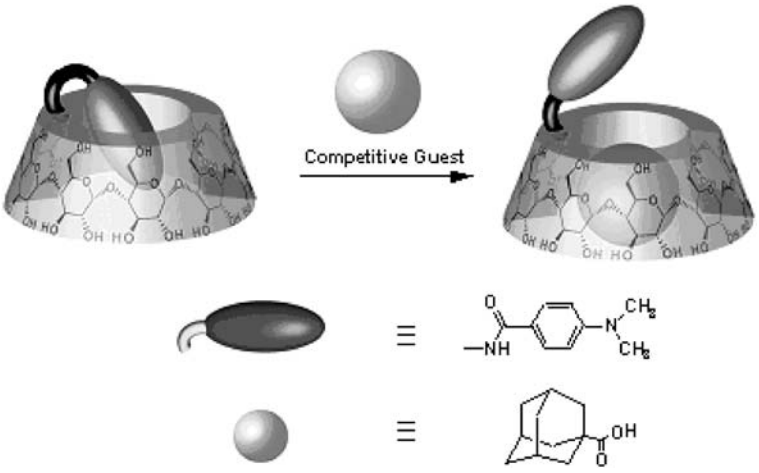

Fig. 13 Schematic illustration of the formation of an intermolecular complex from an intramolecular complex

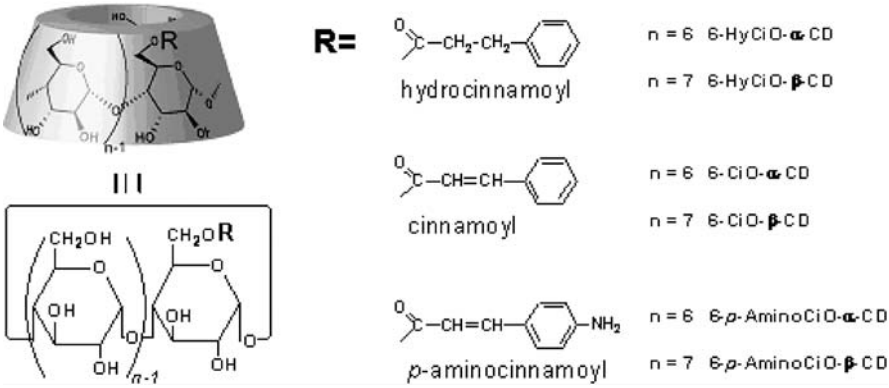

Fig. 14 Chemical structures of hydrocinnamoyl- and cinnamoyl-modified CDs

lar polymers [46]. This result suggests that some spacer groups are required for efficient formation of intermolecular complexes. There are few reports of the formation of supramolecular polymers by host-guest interactions in aqueous solutions, although the formation of supramolecular polymers by these interactions is important in biological systems. The authors [32, 50, 58–62] have been studying the supramolecular structures of modified CDs with a hydrocinnamoyl group or a cinnamoyl group in aqueous solutions (Fig. 14). This section focuses on the formation of the supramolecular polymer constructed by monosubstituted CDs.

3.1
Formation of Intramolecular Complexes by Hydrocinnamoyl-β-Cyclodextrin

The ^{1}H NMR spectra of 6-hydroxycinnamoyl-β-CD (6-HyCiO-β-CD) in D_2O showed that the peaks of the phenyl protons of the hydrocinnamoyl group are shifted to upfield as those of ethylhydrocinnamate with β-CD, indicating that the phenyl ring was included in a CD cavity. The shifts are independent of the concentrations, indicating that 6-HyCiO-β-CD forms intramolecular complexes in D_2O. The ROESY spectrum of that 6-HyCiO-β-CD showed the ROE correlation between the peaks of phenyl protons of hydrocinnamoyl group and inner protons (C(3)-H and C(5)-H) of CDs, indicating that the phenyl ring was included in its own CD cavity. All the signals due to β-CD in the ^{1}H NMR spectrum of 6-HyCiO-β-CD are assigned by measuring various 2D NMR (COSY, TOCSY, ROESY, HMQC) (Fig. 15). The C(3) and C(5) protons in the cavity are shifted. The glucopyranose unit having a hydrocinnamoyl group was abbreviated as A ring and other glucopyranose unit were abbreviated as the B-E rings. The protons of the glucopyranose units of D and E rings are largely shifted to upfield indicating that the phenyl ring is included in the cavity sandwiched by ring A and rings D and E. A proposed structure of 6-HyCiO-β-CD in water is depicted in Fig. 16a.

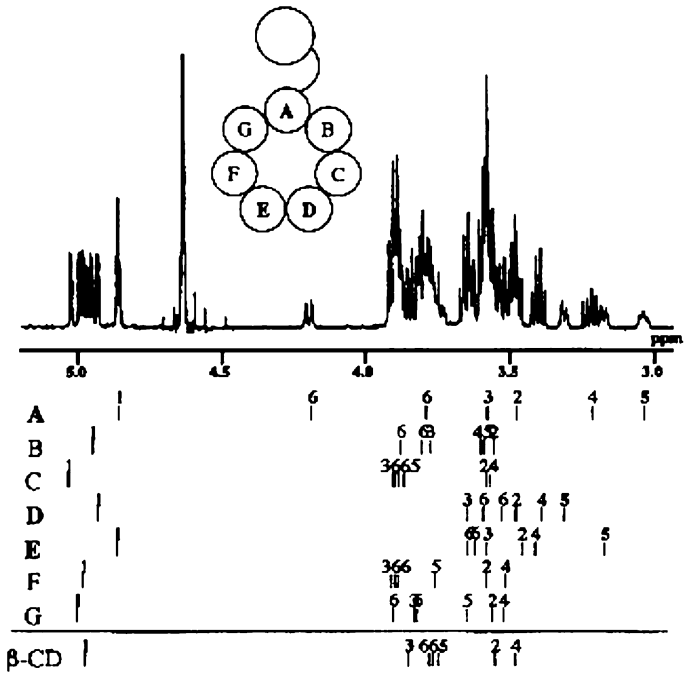

Fig. 15 600 MHz NMR spectrum of 6-HyCiO-β-CD

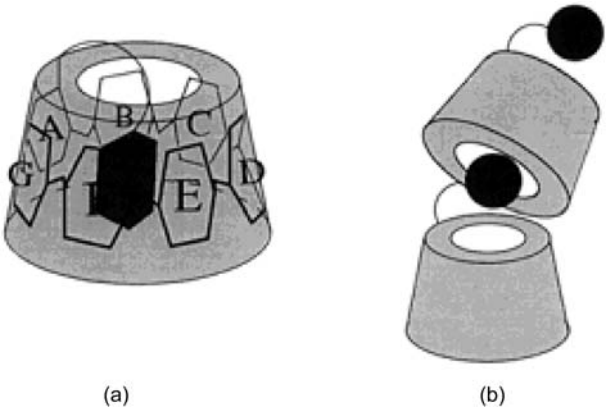

Fig. 16 Proposed structures of 6-HyCiO-β-CD (**a**) and 6-HyCiO-α-CD (**b**)

3.2
Formation of Intermolecular Complexes by Hydrocinnamoyl-α-Cyclodextrin

The ^{1}H NMR spectra of 6-hydrocinnamoyl-α-CD (6-HyCiO-α-CD) in D_2O showed that the peaks of the phenyl protons of the hydrocinnamoyl group are shifted to upfield. However, the shifts are slightly dependent on the con-

centrations in D_2O, indicating that 6-HyCiO-α-CD forms weak intermolecular complexes in D_2O. The ROESY spectrum of 6-HyCiO-α-CD in D_2O showed correlation peaks between the phenyl protons and CD inner protons, indicating that the hydrocinnamoyl group was included in the CD cavity. 6-HyCiO-α-CD has been found to form a intermolecular complex. A proposed structure is shown in Fig. 16b. 6-HyCiO-β-CD formed intramolecular complexes and 6-HyCiO-α-CD formed intermolecular complexes. These results indicate that a hydrocinnamoyl group was too flexible to form intermolecular complexes. Therefore, the authors have decided to use a more rigid spacer like a cinnamoyl group that has a double bond.

3.3 Formation of Supramolecular 6-Cinnamoyl-β-Cyclodextrin Complexes

6-Cinnamoyl-β-CD (6-CiO-β-CD) was sparingly soluble in water, although most 6-substituted β-CDs are soluble. However, 6-CiO-β-CD was solubilized in water on the addition of adamantane carboxylic acid or *p*-iodoaniline which could be included in a β-CD cavity. These results suggest that 6-CiO-β-CD formed supramolecular polymers in the solid state, as shown in the proposed structure in Fig. 17. The X-ray powder pattern of 6-CiO-β-CD was similar to that of the complex between β-CD and ethyl cinnamate, in which β-CDs formed a layer structure. The crystal structure of 6-aminocinnamoyl-β-CD (6-aminoCiO-β-CD) is shown in Fig. 12 and we discussed the relationship between crystal packing and the substituent group in Sect. 2.8.

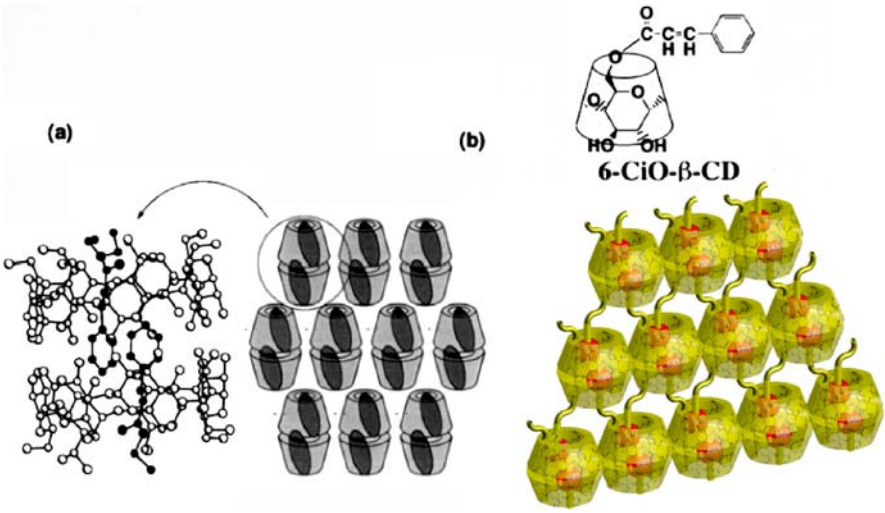

Fig. 17 Crystal structure of the β-CD-ethyl cinnamate complex (**a**) and a proposed structure of 6-CiO-β-CD in the solid state (**b**)

3.4
Formation of Intramolecular Complexes by 6-Cinnamamide-β-Cyclodextrin

6-Cinnamamide-β-CD (6-CiNH-β-CD) is sparingly soluble in water. The solid state NMR studies (^{13}C CP/MAS NMR) show that the phenyl group is included in the β-CD cavity. The X-ray powder pattern showed that 6-CiNH-β-CD forms a layer structure of the CD dimer.

3.5
Formation of a Supramolecular Dimer by 6-Cinnamamide-α-Cyclodextrin

6-Cinnamamide-α-CD (6-CiNH-α-CD) is soluble in water (Fig. 18). The ^{1}H NMR spectra change with its concentrations in D_2O solutions, although the spectra did not change in DMSO-d_6. These results indicate that 6-CiNH-α-CD formed intermolecular complexes in D_2O. The ROESY NMR spectra of 6-CiNH-α-CD showed that the phenyl ring is deeply included into the CD cavity. The molecular weight measured by VPO (vapor pressure osmometry) saturated around 2×10^3, twice as large as that of the monomer unit.

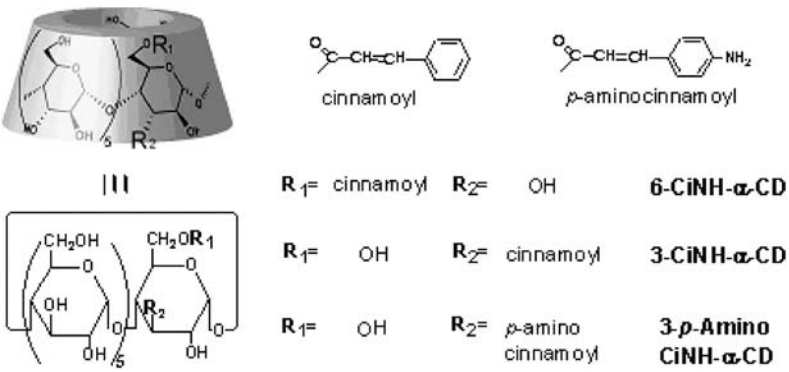

Fig. 18 Structures of cinnamamide-modified CDs

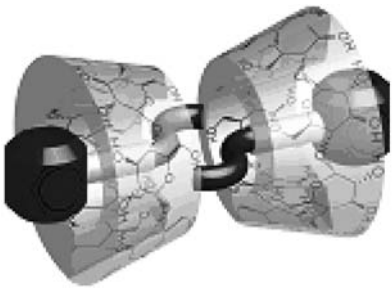

Fig. 19 Structure of supramolecular dimers constructed by 6-CiNH-α-CD in aqueous solution

These observations indicate that 6-CiNH-α-CD formed a rigid supramolecular dimer as shown in Fig. 19.

3.6 Formation of Supramolecular Polymers by 3-Cinnamamide-α-Cyclodextrin

The fact that 6-CiNH-α-CD formed a supramolecular dimer in which cinnamoyl groups are included from the primary hydroxyl groups led us to use 3-cinnamamide-α-CD (3-CiNH-α-CD) as a building unit, because the phenyl group can be included in α-CD from the primary hydroxyl side successively to form supramolecular polymers. Actually, 3-CiNH-α-CD was found to form long supramolecular polymers with a molecular weight higher than 1.6×10^4 (Fig. 20).

3.7 Formation of Supramolecular Oligomers by 6-Cinnamoyl α-Cyclodextrin

The ^{1}H NMR spectra of 6-cinnamoyl-α-CD (6-CiO-α-CD) showed that the phenyl protons shifted to upfield as those of methylcinnamate on addition of α-CD, indicating that the phenyl ring is included in a CD cavity. The shifts are dependent on the concentrations in D_2O although they are independent of their concentrations in DMSO-d_6, indicating that 6-CiO-α-CD forms intermolecular complexes in D_2O. The ROESY spectrum of 6-CiO-α-CD shows a correlation peak between the phenyl signals and CD signals, indicating that the phenyl ring is included in the other CD cavity. The molecular weight of 6-CiO-α-CD measured by VPO at various concentrations in water increased with an increase in the concentrations and the molecular weight reached

Fig. 20 Schematic representation of supramolecular polymers constructed by 3-CiNH-α-CD in aqueous solution

saturation around 3×10^3. This result suggests that 6-CiO-α-CD forms an oligomer. At higher temperature (at 70 °C), the molecular weight observed is lower than that observed at lower temperature (at 40 °C).

3.8
Cyclic Daisy Chain

When supramolecular polymers are treated with bulky stopper groups, they may form poly[2]rotaxane "daisy chains" [32, 60–68]. Cyclic tri[2]rotaxanes (daisy chain necklace) containing cyclodextrins have been prepared from the mixture of 6-(4-aminocinnamoyl)-α-CD and 2,4,6-trinitrobenzene sulfonic acid sodium salt [50, 59] in an agueous solution (Fig. 21). If the molecule changes its conformation (or co-conformation), the ring may expand or shrink by external conditions (temperature, solvents, photochemically, electrochemically). These compounds are important because the cycle can be used as a chemical valve as seen in ion channels in biological membranes.

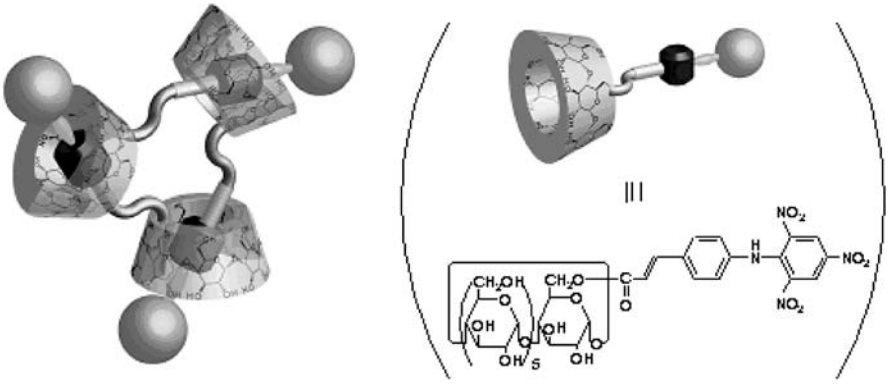

Fig. 21 Harada's daisy chain necklace: cyclic tri[2]rotaxane containing α-CD [41]

3.9
Daisy Chains

The supramolecular polymers formed by 3-CiNH-α-CD were stabilized by attaching bulky stoppers at each end of the guest groups. Poly[2]rotaxanes (Daisy Chain) were obtained. The authors used trinitorobenzene sulfonic acid as a stopping agent. The degree of polymerization of the poly[2]rotaxanes was found to be around 13, characterized by MALDI-TOF Mass spectroscopy. Figure 22 shows a schematic representation of a poly[2]rotaxane based on a supramolecular polymer formed by 3-*p*-aminoCiNH-α-CD.

Fig. 22 Schematic representation of supramolecular polymers constructed by 3-CiNH-α-CD in aqueous solution

3.10 Formation of Helical Supramolecular Polymers by *p-tert*-Boc-Amino-Cinnam-α-Cyclodextrin

α-CD with a *p-tert*-Boc-cinnammoylamino group at the 3-position forms a supramolecular polymer [61]. The existence of substitution/substitution interactions among the adjacent monomers of the supramolecular polymer has been proved by the observation of positive and negative Cotton bands in the circular dichroism spectra. The supramolecular polymers were found to form a left-handed helical conformation. A proposed structure of a supramolecular polymer formed by 3-*p-tert*-BocCiNH-α-CD is shown in Fig. 23. The formation of the helical supramolecular polymer with some cooperativity was shown by the CD spectra. These results remind us that microtubules, microfilaments and flagella are helical supramolecular polymers formed by host-guest cooperative interactions in the biological systems.

Fig. 23 A proposed structure of a helical supramolecular polymer formed by 3-*p*-^{t}BocCiNH-α-CD in aqueous solution

3.11 Supramolecular Polymers with Alternating α- and β-Cyclodextrin Units

6-*p-tert*-BocCiNH-β-CD formed intramolecular complexes. When adamantane carboxylic acid was added in the solution of 6-*p-tert*-BocCiNH-β-CD, the adamantane group was included in the β-CD cavity and the cinnamoyl group was kicked out of the cavity to expose in water [62]. As the extension of the formation of supramolecular polymer, adamantane carboxylic

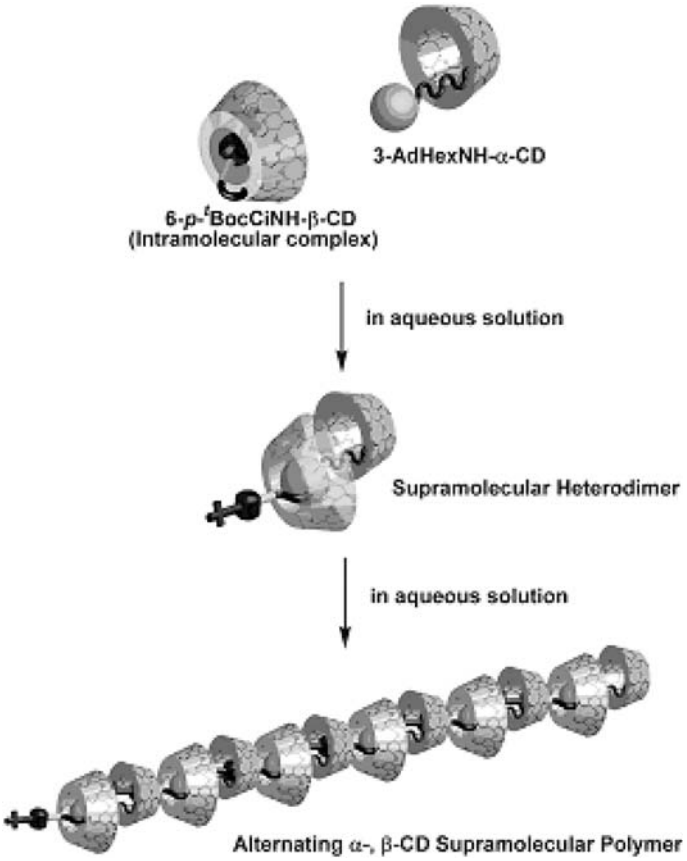

Fig. 24 Proposed structures of supramolecular polymer containing 3-AdHexNH-α-CD and 6-p-^{t}BocCiNH-β-CD

acid was attached to α-CD at the 3-position (3-AdHexNH-α-CD). When the 3-AdHexNH-α-CD was mixed with 6-p-t-BocCiNH-β-CD in D_2O in a one-to-one ratio, they formed a heterodimer, which lines up end-to-end in longitudinal rows to form supramolecular polymers in an alternating manner (Fig. 24).

4 Polyrotaxanes

The chemistry of rotaxanes has progressed well in accordance with the interest in their unique structures and the expectation of development as parts of molecular machines and molecular devices. It was in 1976 that Ogata et al. [69] reported the synthesis of the inclusion complex with polyamide. When β-CD was stirred with aliphatic diamines in water, precipitates were

formed and they were characterized as inclusion compounds. β-CD was used as a rotor of rotaxane by Ogino and Ohata in 1984 [70]. They used metal complexes as stoppers. Since then, some rotaxanes containing γ-CDs have been reported [71–75]. Most of those rotaxanes used metal complexes as stopper groups. However, metal coordination bonds are so labile that CD rings may escape from the bond. All the rotaxanes reported are ionic and thus soluble in water. One example in which all the components are non-ionic and soluble in organic solvents [76] was reported. In such a case there are some interactions between the α-CD ring and the stopper groups. In all cases, there is no clear evidence for the rotary motion of CDs around an axle. The dynamic behavior of the rotaxanes is a subject that remains to be explored. This section focuses on our work concerning polyrotaxanes having CDs. There are some reviews including two comprehensive articles on polyrotaxanes [2, 59, 63–65, 77–91]. Readers can refer to pertinent reviews for a discussion of the other polyrotaxane compounds.

4.1
pseudo-Poly(rotaxane)s between Cyclodextrins and Polymers

pseudo-Polyrotaxanes with CDs have been prepared by polymerization of a *pseudo*-rotaxane monomer in situ. These methods had already been reported by several groups including Ogata et al. [69] and Maciejewski et al. [92–96]. The authors reported the first investigation of *pseudo*-rotaxane formation between polymers and CDs. The authors tested whether CD would form complexes with some water-soluble polymer or not. Table 1 shows the results of the formation of complexes of CDs with some water soluble and insoluble non-ionic polymers, such as poly(vinyl alcohol) (PVA), poly(acrylamide) (PAAm), poly(*N*-vinylpyrrolidone) (PVPo), poly(ethylene glycol) (PEG) [97–103], poly(propylene glycol) (PPG) [98, 99, 103], poly(trimethylene oxide) (PTMO) [104], poly(methyl vinyl ether) (PMVE) [103, 105], poly(ethyl vinyl ether) (PEVE) [103], poly(*n*-propyl vinyl ether) (PnPVE) [103], oligo ethylene (OE) [100, 106], poly(isobutylene) (PIB) [100, 105, 106], squalane [100, 106], poly((trimethylene adipate) (PTA), poly(1,4-butylene adipate) (PBA), poly(ethylene adipate) (PEA) [107], poly(ε-caprolactone) (P(ε-CL)) [108, 109], poly(butadiene) (PB) [110], poly(isoprene) (PIP) [111], poly(dimethyl siloxane) (PDMS) [112, 113], and poly(dimethyl silane) (PSi) [114]. α-CD forms stoichiometric complexes with PEG of various molecular weights in high yields, but did not form complexes with PPG of any molecular weights. β-CD formed crystalline inclusion complexes with PPG. γ-CD formed inclusion complexes with PMVE, PEVE, and PnPVE, although α- or β-CD did not form complexes with these polymers. The yields of the complexes of α-CD with OE were higher than those of β- and γ-CDs under the same condition. β-CD formed complexes with squalane, while α-CD did not. Structures of the complexes of hexa(ethylene glycol) with α-CD

Table 1 Complex formation between CDs and Polymers

Polymer	Structure	$\overline{M_w}/10^3$	yield (%)			ref
			α–CD	β–CD	γ–CD	
PVA	$-(-CH_2\text{-}CH(OH)-)_n-$	22	0	0	0	97-103
PAAm	$-(-CH_2\text{-}CH(CONH_2)-)_n-$	10	0	0	0	97-103
PEG	$-(-CH_2\text{-}CH_2O-)_n-$	1.0	92	0	trace	97-103
PPG	$-(-CH_2\text{-}CH(CH_3)\text{-}O-)_n-$	1.0	0	96	80	98,99,103
PMeVE	$-(-CH_2\text{-}CH(OCH_3)-)_n-$	1.0	0	0	80	103,105
PEtVE	$-(-CH_2\text{-}CH(OEt)-)_n-$	1.2	0	0	71	103
PnPrVE	$-(-CH_2\text{-}CH(OnPr)-)_n-$	1.2	0	0	4	103
OE(20)	$-(-CH_2\text{-}CH_2-)_n-$	0.56	63	0	0	100,106
PP	$-(-CH_2\text{-}CH(CH_3)-)_n-$	ca. 0.8	0	40	7	100,106
Squalane	$-(CH_2\text{-}CH(CH_3)\text{-}CH_2\text{-}CH_2-)_n-$	0.423	0	62	24	100,106
PIB	$-(-C(CH_3)_2\text{-}CH_2-)_n-$	ca. 0.8	0	8	90	100,105, 106

and that of tetra(ethylene glycol) dibromide with α-CD have been determined by X-ray crystallographic analysis (Fig. 25) [115]. α-CDs form columns in a head-to-head (the side of the secondary hydroxyl groups) and tail-to-tail (the side of the primary hydroxyl groups) fashion. Ethylene glycol chains are included in channels formed by α-CDs. The crystal structures of the inclusion complexes of β-CD with polymers, poly(trimethylene oxide) (P3MO, $(\text{-}CH_2CH_2CH_2O\text{-})_n$, average $M_w = 1.4 \times 10^3$), and PPG (average $M_w = 425$) were determined by X-ray crystallographic analysis [116]. P3MO (Fig. 26) and PPG with an all-trans conformation are approximately 97 and 22 Å long and may penetrate 14 and three β-CDs, respectively.

Ripmeester et al. [117] have investigated the single crystal structural analysis of PEG and β-CD (Fig. 27). The crystals of β-CD–PEG inclusion com-

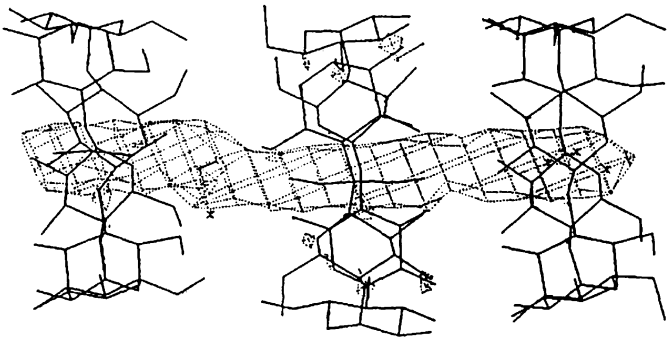

Fig. 25 The electron density of hexa(ethylene glycol) in the complex with α-CD

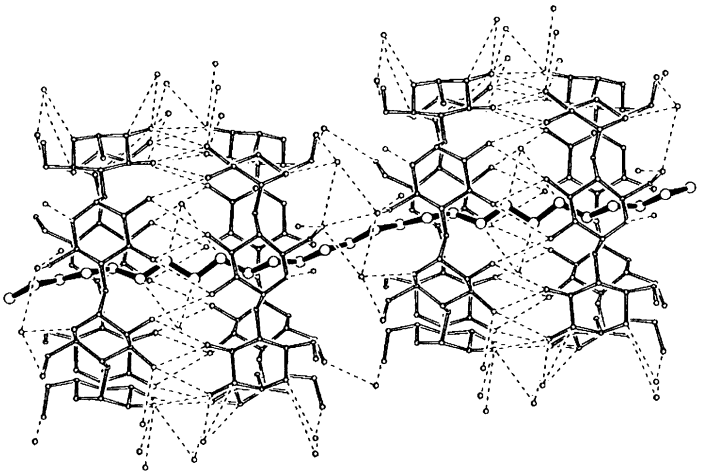

Fig. 26 Column structure composed of four symmetry-related β-CDs (Mol-1, -2, -3, and -4) and P3MO, viewed from the *b*-axis (for clarity, molecules are rotated by 10° along the vertical axis)

plex was monoclinic, space group C_2, $Z = 4$, with the unit cell parameters $a = 18.726$ Å, $b = 24.475$ Å, $c = 15.398$ Å, $\beta = 110.5°$. The structure consists of a PEG chain threaded through hydrogen-bonded head-to-head dimers with one CD for every three monomeric C_2H_4O units. The polymer chain is highly disordered about the axis of the channel that passes through a stack of CD dimers.

The authors also studied *pseudo*-rotaxane formation of CDs with aliphatic polyesters, polydiene, polysiloxane, and polysilane, as summarized in Table 2. CDs were found to form inclusion complexes with aliphatic polyesters, such as PTA, PBA, PEA [107], and P(ε-CL) [108, 109]. α- and γ-CDs formed complexes with these polyesters in high yields, although β-CD gave complexes in moderate yields. Although the yields of the complexes of α-CD with PTA and

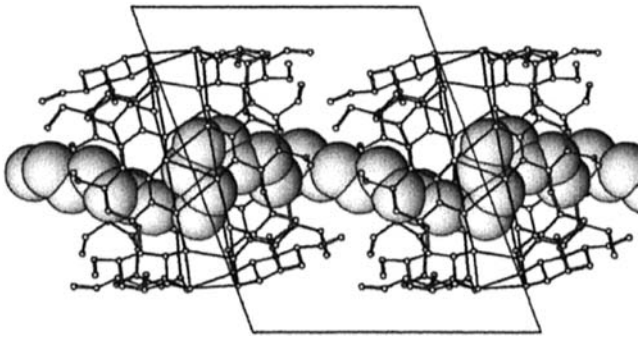

Fig. 27 The crystal structure of β-CD–PEG inclusion complex. The crystal packing structure is head-to-head

Table 2 Complex formation between CDs and Polymers

Polymer	Structure	$\overline{M_w}/10^3$	yield (%)			ref
			α–CD	β–CD	γ–CD	
PEA	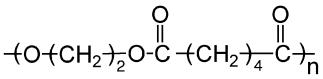	1.0	71	34	68	107
PTA	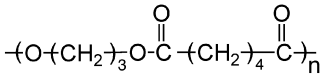	1.0	72	57	80	107
PBA	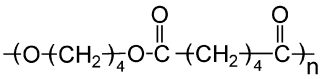	0.84	76	46	77	107
P(ε-CL)	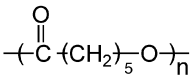	0.53	79	52	71	107, 108
PB	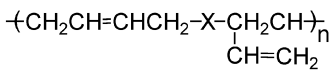	2.0	1.3	31	24	110
PIP	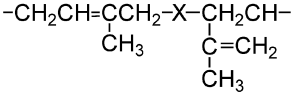	0.62	0	3.0	6.3	111
PDMS	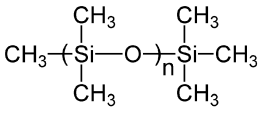	3.2	0	0	72	112, 113
PSi	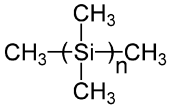	0.8	0	0	57	114

PBA decreased with increasing molecular weight, α-CD formed complexes with PEA in high yields even at higher molecular weights. α-CD-P(ε-CL) complexes were stoichiometric one-to-one (CD: monomer unit) compounds, and γ-CD-P(ε-CL) complexes were one-to-two compounds when the molecular weights of P(ε-CL) are low.

Polybutadienes (PB) [110] and polyisoprenes (PIP) [111] were found to form inclusion complexes with CDs with high selectivity to form crystalline compounds. β-CD formed complexes only with PIP of low molecular weights, whereas γ-CD formed complexes with PIP of high molecular weights. α-CD did not form complexes with PIP of any molecular weights. The yields of γ-CD complexes increased with increasing molecular weights of PIP and reached a maximum at ca. 7×10^3, and then decreased. α- and β-CDs formed complexes only with PB of low molecular weights and high 1,4-addition content, while γ-CD formed complexes with PB of high 1,2-contents in low yields. The yields of the γ-CD complexes decreased with an increase in the molecular weight of PB of similar composition.

β- and γ-CDs formed inclusion complexes with poly(dimethylsiloxane)s (PDMS) [112, 113] and poly(dimethylsilane)s (PSi) [114] of various molecular weights to give crystalline compounds. However, α-CD did not form complexes with PDMS and PSi of any molecular weights. The yields of β-CD-PDMS and β-CD-PSi inclusion complexes decreased with an increase in the molecular weight of the polymer. In contrast, the yields of γ-CD-PDMS and γ-CD-PSi inclusion complexes increased with increasing molecular weight, reaching a maximum around a molecular weight of 760, and gradually decreased at higher molecular weights. The chain-length selectivity is reversed between β-CD and γ-CD. The β-CD-PDMS inclusion complexes were stoichiometric 1 : 1 compounds when the molecular weights of PDMS were low. The γ-CD-PDMS inclusion complexes were 2 : 3 (CD:monomer unit of PDMS) compounds. The γ-CD-PSi inclusion complexes were 1 : 3 (γ-CD : monomer unit of PSi) compounds. The PSi main chain in the cavities of γ-CD takes an all-*trans* conformation. Later, Kira et al. [118] reported that the PSi chain assumes a helical form from the measurements of their circular dichroism spectra.

γ-CD formed a trace amount of complexes with PEG in a series of the preparation of inclusion complexes of CDs. The amount of complexes formed is so small that the authors have not characterized them. Some PEG derivatives, such as bis(3,5-dinitrobenzoyl)-PEG and bis(2,4-dinitrobenzoyl)-PEG, formed crystalline complexes with γ-CD in high yields. However, α-CD did not form inclusion complexes with these PEG derivatives, because the end groups are too large to thread the cavities of α-CD. The authors found the self-assembly of double-strand inclusion complexes consisting of PEG and γ-CD, in which two polymer chains are threaded through the macrocycles [119]. PEG-bearing fluorescent probes at both ends, such as bis(1-naphthylacetyl)-PEG (PEG-1-N_2) and bis(2-naphthylacetyl)-PEG (PEG-2-N_2), were prepared

to investigate the characteristic of the complex formation between γ-CD and PEG derivatives (Scheme 1). Inclusion complexes between PEG-1-N_2 or PEG-2-N_2 and γ-CD formed a PEG:γ-CD ratio of 4 : 1 determined with ^{1}H NMR. Emission spectra of the γ-CD-PEG-1-N_2 and γ-CD-PEG-2-N_2 complexes showed a large contribution from excimers, collective excitations arising from the interactions between two nearby naphthyl groups. It showed only monomer emission in the absence of γ-CD. These complexes are composed of double chains of PEG penetrated to the cavity of γ-CDs.

Most of the supramolecular assemblies have been constructed from the solutions of each component. More recently, the authors found that CD formed inclusion complexes with PEG with high selectivity only by mixing powdered crystals of CDs and polymer samples without any solvents under ambient conditions (Scheme 2) [120]. When crystals of α-CD and PEG (M_w = 400) were mixed without solvent (α-CD : ethylene glycol unit = 1 : 2), the X-ray powder patterns changed; a peak at $2\theta = 22°$ characteristic for the cage type decreased, and a peak at $2\theta = 20°$ characteristic for the channel type appeared

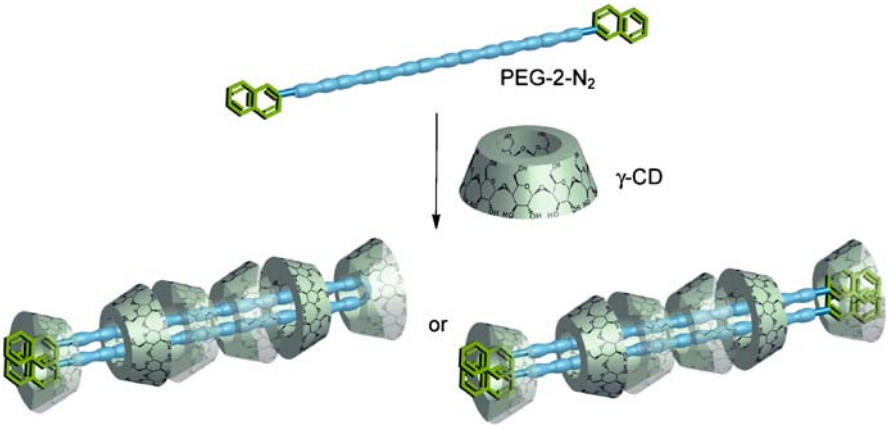

Scheme 1

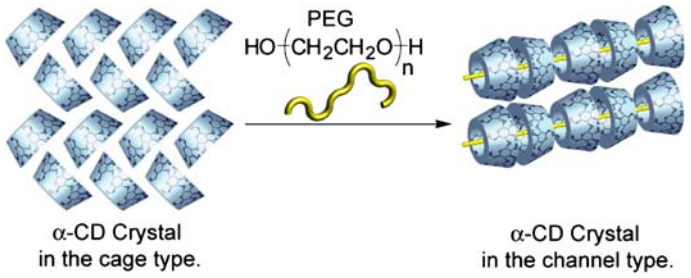

Scheme 2

and increased. Similar changes in X-ray powder pattern were observed in the cases of α-CD and poly(oxytrimethylene) or poly(tetrahydrofuran). PEG carrying large groups, such as 2,4-dinitrophenyl and 3,5-dinitrobenzoyl groups, did not give any changes in the X-ray powder pattern of α-CD even after 2 months, indicating that PEG comes into α-CD cavity from its small end groups.

Tonelli et al. [121] also reported complex formation of α-CD with PEG without solvent. Takata et al. [122] reported the preparation of polyrotaxanes from complexes of α-CD with THF in a similar way.

4.2
α-Cyclodextrin Polyrotaxanes and Cyclodextrin Molecular Tube

Polyrotaxanes in which many α-CD are threaded on a PEG chain were prepared by the reaction of the complexes between α-CDs and PEG bisamines with 2,4-dinitrofluorobenzene which is bulky enough to prevent dethreading [123–125] (Scheme 3). Many kinds of polyrotaxanes were prepared starting from PEG with various molecular weights. Fifteen to 100 α-CD molecules (on average) are captured in each polyrotaxane. A polyrotaxane with ca. 100 α-CD molecules was obtained by the fractionation of the product prepared from PEG of average molecular weight 1.0×10^4 using GPC. This is the first example of a polyrotaxane (not *pseudo*-rotaxane) and was named a "molecular necklace".

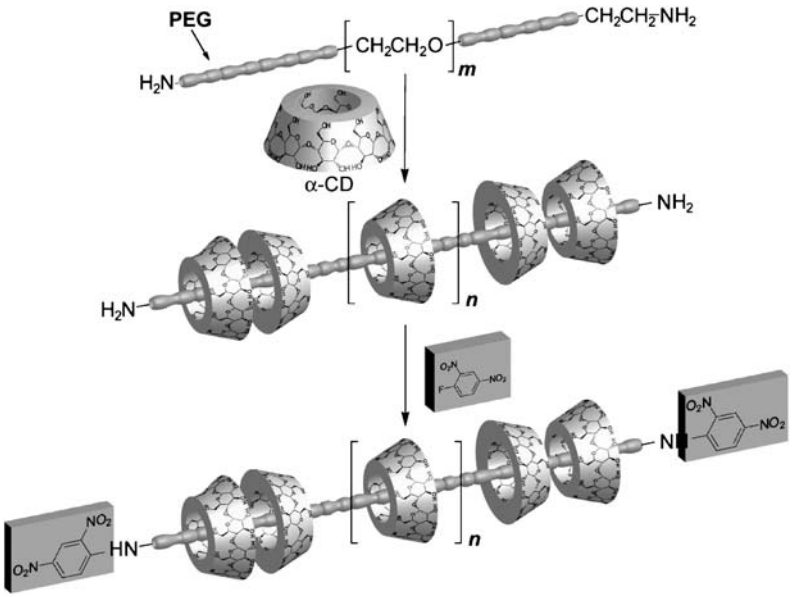

Scheme 3

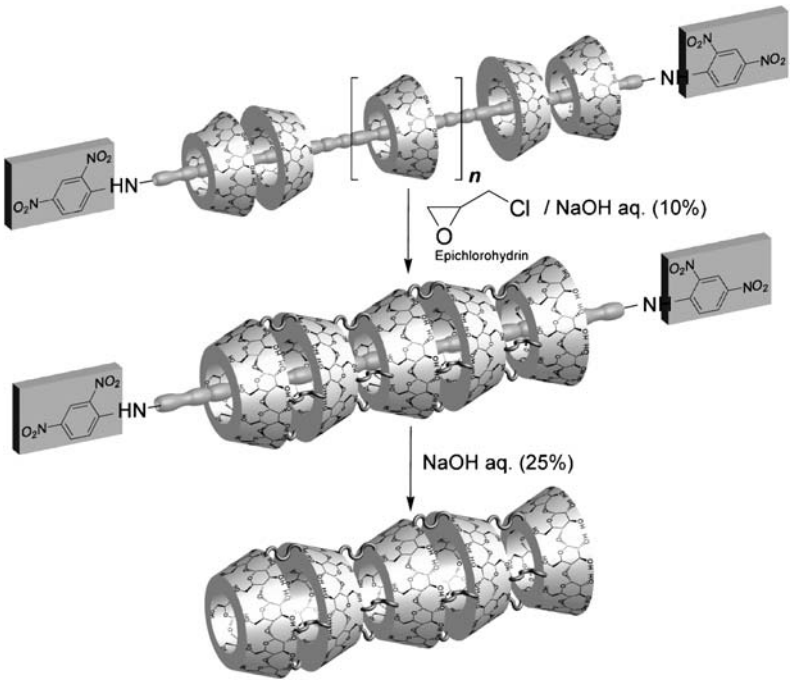

Scheme 4

The authors prepared a "molecular tube" by crosslinking adjacent α-CD units in a polyrotaxane (molecular necklace) [126, 127] (Scheme 4). The molecular necklace was dissolved in 10% NaOH, to which epichlorohydrin was then added. Epichlorohydrin was allowed to react with the hydroxyl groups of the threaded α-CD to link up each α-CD. 2,4-Dinitrofluorobenzene moieties, bulky stoppers, at both ends were removed by the treatment with a strong base (25% NaOH). The yield of molecular tube was 92% and the average molecular weight was estimated to be ca. 2×10^4 by GPC. The molecular tube could accommodate I_3^- ions in an aqueous solution of KI-I_2 efficiently, whereas α-CD could not.

4.3 Molecular Shuttle

CDs form complexes not only with non-ionic polymers but also with ionic polymers, such as linear polymers consisting of bipyridinium (viologen) bridged by polymethylene chains (Scheme 5) [128]. The methylene peaks split in two upon addition of α-CD, although these peaks did not change upon addition of γ-CD. These peaks are broadened upon addition of β-CD. These results indicate that α-CD stays at one of the methylene chains on the ^{1}H

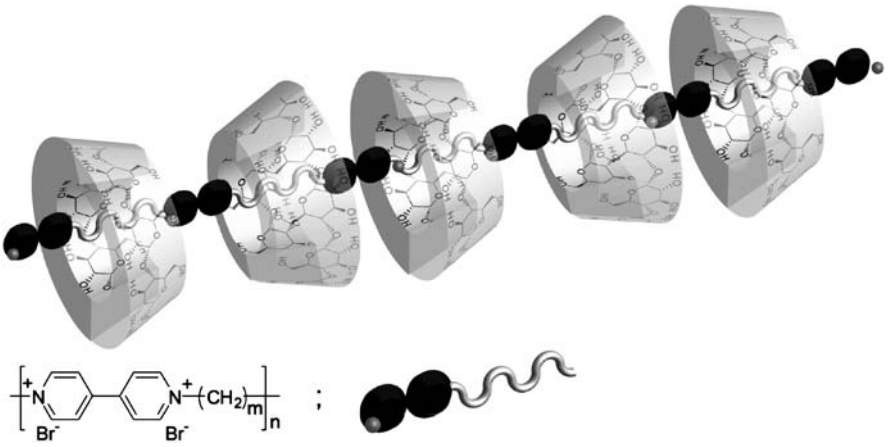

Scheme 5

NMR time scale, and β-CD moves along the polymer chain faster than the ^{1}H NMR time scale. On the basis of these observations, the authors decided to make a molecular shuttle in which α-CD molecule move back and forth along a chain.

A molecular shuttle was designed as follows: α-CD as a ring, two polymethylene chains as stations, 4,4′-bipyridinium units as linkers, and dinitrophenyl groups as stoppers. The molecular shuttles were prepared as shown in Scheme 6. The authors prepared an axle first, and then the axle was treated with an aqueous solution of α-CD. A molecular shuttle consisting of dodecamethylene units, 4,4′-bipyridinium units, and α-CD was obtained by closing the chain end groups with 3,5-dinitrofluorobenzene [129]. The shuttling behavior of the molecular shuttle is sensitive to solvent and temperature,

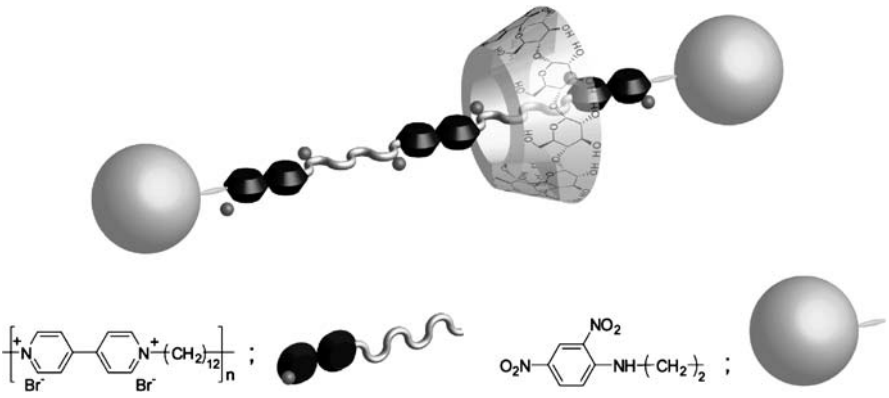

Scheme 6

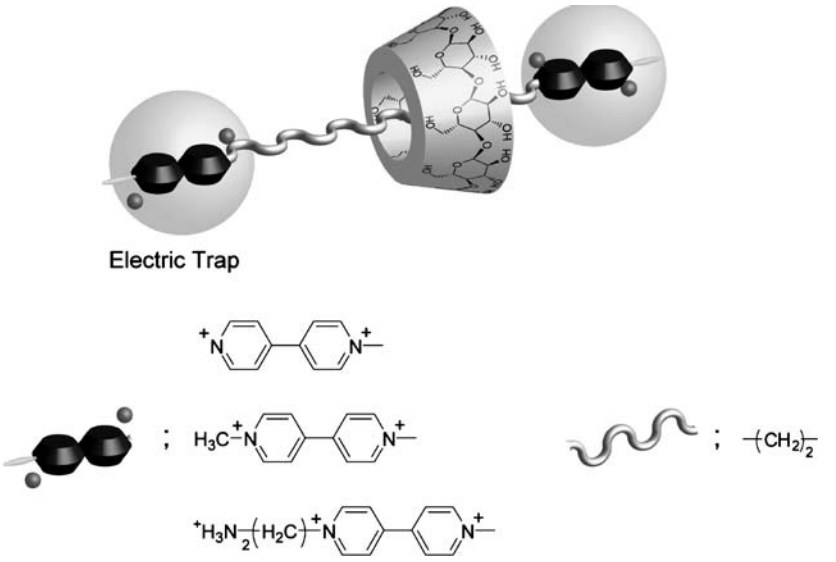

Scheme 7

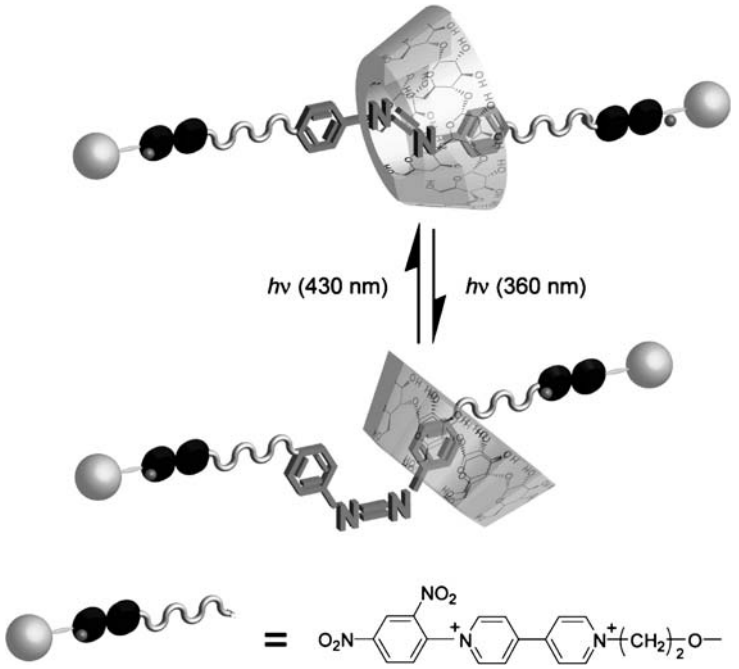

Scheme 8

and could be controlled by double interactions: a hydrophobic interaction between the interior of the CD cavity and the station and a repulsive interaction between α-CD ring and a linker. While the molecular shuttle was prepared, the authors found that cationic groups serve as a potential surface for the translocation of the α-CD ring on a polymer chain. Therefore, the authors studied the interactions between CDs and some dodecamethylene derivatives with different numbers of cationic groups (Scheme 7). The authors found that CD did not escape from a dodecamethylene derivative with three cationic groups at the chain ends. Multiple cationic groups stabilize a rotaxane structure by inhibiting a CD ring from coming off [130]. A rotaxane containing an azobenzene group in its axle and α-CD has been prepared (Scheme 8) [131]. The CD ring stayed around the *trans*-azobenzene site. When the rotaxane was irradiated with UV light, the azobenzene unit was isomerized from *trans* to *cis*, and the α-CD ring moved to encircle one of the ethylene glycol chains. Upon irradiation with visible light, the azobenzene unit was isomerized from *cis* back to *trans*, resulting in shuttling of the CD ring along the chain.

4.4
β-Cyclodextrin Polyrotaxanes

An alternative approach for the preparation of CD-based polyrotaxane using photoreactions is described (Scheme 9). The authors prepared α-CD-based polyrotaxanes by capping ends of α-CD–PPG complexes, in a *pseudo*-polyrotaxane structure, with covalently bound stoppers. A polyrotaxane containing a number of β-CD molecules was prepared by photoreactions of a precursor complex between β-CD with PPG having a triphenylmethyl group at

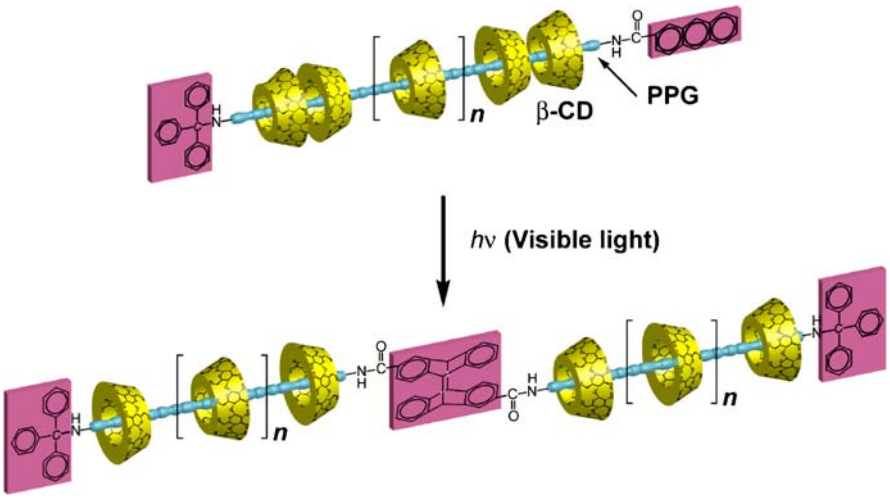

Scheme 9

one end and a 2-anthryl group at the other end [132]. First, the authors prepared a precursor complex of β-CD with a derivative of PPG having a triphenylmethyl group at one end and a 2-anthryl group as the other end. When the precursor complex was irradiated with visible light ($\lambda \geq 340$ nm) using a 500 W Xe lamp and an appropriate cut off filter, the photodimerization of 2-anthryl groups took place to form a polyrotaxane. GPC data indicated that the elution volume of β-CDs polyrotaxane was smaller than that of the starting material, indicating that the hydrodynamic size of β-CDs polyrotaxane was larger than that of the starting material. The fluorescence spectrum of PPG axis molecules attached to a triphenylmethyl group and a 2-anthryl group showed emission around 450 nm, but β-CDs polyrotaxane did not show anthracene emission, showing that the 2-anthryl group in β-CDs polyrotaxane was dimerized by visible light. The authors have successfully prepared a polyrotaxane containing β-CDs by photoreactions of a precursor complex between β-CD with PPG having a triphenylmethyl group at one end and a 2-anthryl group at the other end.

4.5 Cyclodextrin Poly(polyrotaxane)

Bulky substituents, such as dinitorophenyl groups and triphenylmethyl groups, have been used as stoppers to prevent dethreading of the above-mentioned ring compounds. Anthracene groups are large enough to prevent dethreading of α-CD and β-CD from an axle and are able to form dimers by photoirradiation [133]. In this case, poly(polyrotaxane)s and poly(catenane)s could be obtained by photoirradiation of polyrotaxanes with anthracene groups as stoppers. The authors have prepared poly(α-CD-polyrotaxanes) by photoirradiation of polyrotaxanes having 9-anthracene groups as stoppers [133].

First, the authors prepared PEG with an anthracene group at one end of the polymer chain. Then, the modified polymer was treated with α-CD to form *pseudo*-polyrotaxane. Finally, the *pseudo*-polyrotaxane was capped with 9-anthracene carboxylic acid to obtain polyrotaxane (Scheme 10). The ratio of CD and monomer units was found to be 4 : 1 (ethylene glycol unit:CD) by ^{1}H NMR. When a DMSO solution of α-CD-polyrotaxane was irradiated with visible light ($\lambda > 340$ nm) (500 W Xe lamp with UV cut filter) under argon, poly(α-CD-polyrotaxane) was precipitated out. The ^{1}H NMR spectrum of the product showed broad resonance bands due to α-CD and PEG and the absence of the absorption bands due to monomeric 9-anthracene. Characteristic absorption and emission bands due to monomeric 9-anthracene have completely disappeared.

When the DMSO solution was kept at 120 °C after irradiation, UV-visible and fluorescence spectra showed that the anthracene monomer came back again in more than 90% conversion. These spectral changes showed that the reversible photodimerization and dissociation of 9-anthracene end-groups took place.

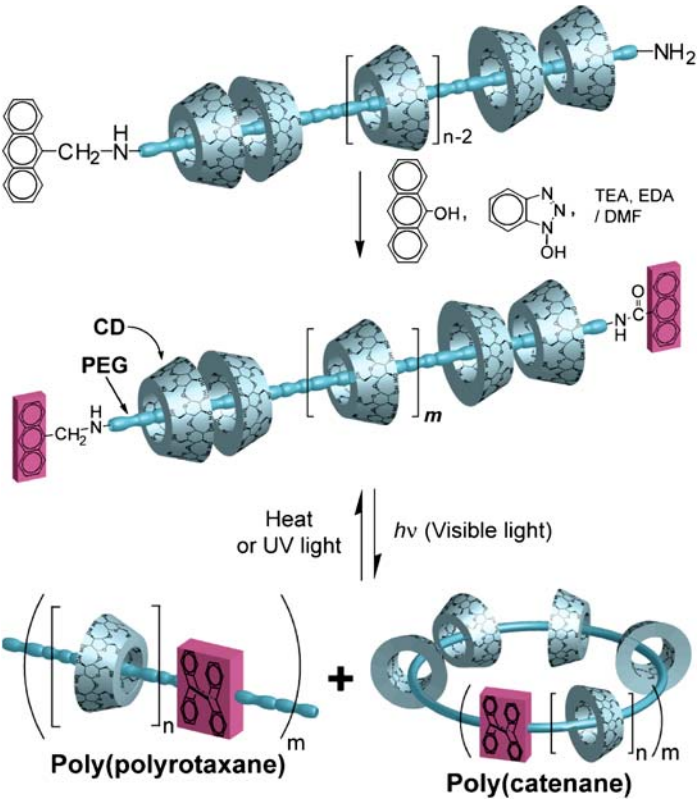

Scheme 10

4.6
One-Pot Synthesis of γ-Cyclodextrin Polyrotaxane

Some macrocyclic molecules currently inserted while preparing rotaxanes have a cavity of ca. 6 Å diameter, such as crown ether, cucurbituril (CB [6]), and α- and β-CDs, which make it relatively easy to prepare interlocked molecules. However, it is difficult to prepare rotaxanes or polyrotaxanes containing larger macrocyclic molecules having a cavity of more than 7.0 Å diameter by the threading method. γ-CD has a cavity of 7.5–8.3 Å diameter. Previously, the formation of tetraphenylcyclobutane blocking groups along the polymer main chain in the presence of both β- and γ-CDs was achieved upon irradiation with UV light in aqueous solutions, which are thought to be self-assembled spontaneously by γ-CD in the polyrotaxane and be composed mainly of β-CD polyrotaxane [134]. The 9-anthryl group is large enough to prevent α- and β-CDs from dethreading, but it is small enough for γ-CD to thread onto the polymer chain. However, the photocyclodimerization products of 9-anthracene groups are large enough to prevent γ-CD from dethread-

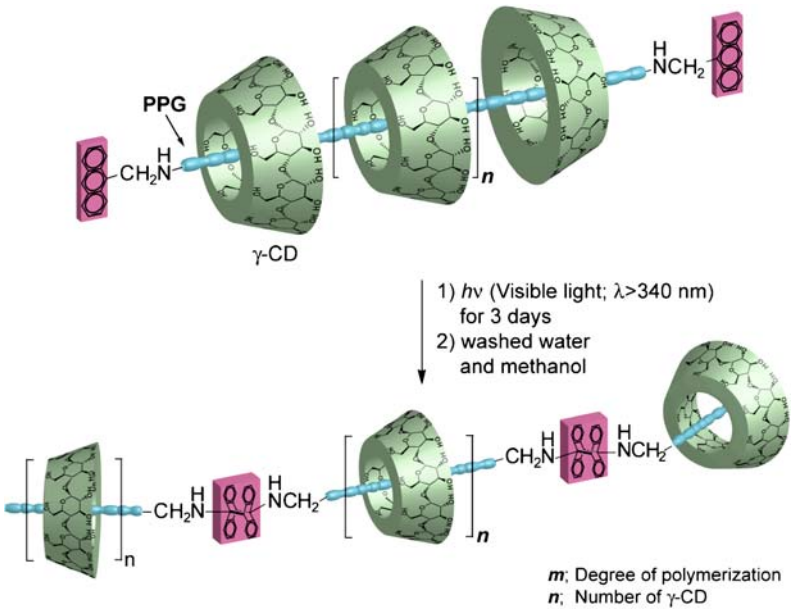

Scheme 11

ing [135–139]. Therefore, the authors chose PPG as an axle molecule and 9-anthryl groups as bulky stoppers for the PPG end. The authors investigated a new one-pot method to prepare polyrotaxanes containing γ-CDs by the photocyclodimerization reactions of 9-anthryl groups at the ends of the polymer chain in the presence of γ-CDs (Scheme 11) [140]. GPC data indicated that the molecular weight of γ-CD polyrotaxane was higher than that of the starting materials. The ^{1}H NMR spectrum of γ-CD polyrotaxane showed the absence of resonance bands due to the 9-anthryl group and a new signal appeared at 8 ppm, assignable to the cyclic dimer of 9-anthryl groups. The FT-IR spectrum showed absorption bands due to γ-CD moieties, indicating that γ-CD molecules are interlocked in γ-CD polyrotaxane.

4.7 Polyrotaxanes Prepared by Inclusion Polymerization (Polythiophene Polyrotaxanes)

Conducting polymers have attracted much attention as promising materials for sensors, because they have potential use as molecular wires as a foundation to put single-molecule electronics into practical use in the future. The authors expected to see interesting results from a π-conjugated polymer covered with organic compound insulation. The authors chose polythiophene as a π-conjugated polymer. Polythiophenes are an important representative class of π-conjugated polymers because of their thermal stability. Polythio-

phenes can be prepared by various chemical and electrochemical polymerization techniques. The authors investigated synthesis inclusion complexes of β-CD or of 2,6-dimethyl-β-CD (DM-β-CD) with bithiophene (2T) and their polymerization to obtain polyrotaxanes (Eq. 1) [141].

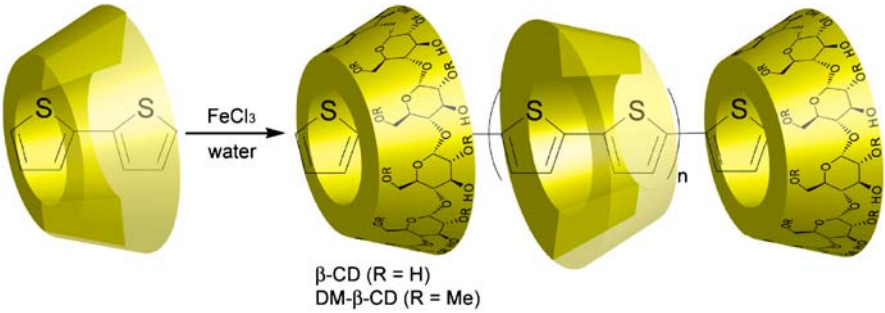

(1)

In order to obtain *pseudo*-rotaxane, the polymerizations of β-CD–2T and DM-β-CD–2T inclusion complexes were carried out in water using $FeCl_3$ as an oxidative initiator. ^{13}C CP/MAS NMR indicated that the DM-β-CD molecule in the inclusion complex with Poly(2T) had a symmetrical cyclic conformation, although DM-β-CD assumes an asymmetrical conformation in the crystal when not including a guest into the cavity. A polythiophene chain was included into the cavities of DM-β-CD. The signals in the MALDI-TOF MS spectrum of DM-β-CD–Poly(2T) were clearly assigned to proton adducts of poly(2T) and sodium or potassium cation adducts of DM-β-CD. The number-average molecular weight of poly(2T) was up to 5×10^3. Although there have been a few reports on the polymerization of thiophenes with CDs in water [142], the resulting poly(ethylenedioxy thiophene) did not contain any CD molecules, indicating that CD molecules came off from poly(ethylenedioxy thiophene) during the polymerization and a rotaxane-type structure was not formed.

5
Supramolecular Polymers Formed by CDs and Polymer Side Chains

In biological systems, macromolecules form supramolecular structures mainly through their side chains, leading to expression of various functions necessary for maintaining living activities [143]. Therefore, it is expected that supramolecular polymers in which their side chains interact through non-covalent bonds become more important not only for understanding details of biological systems but also for constructing highly functional artificial systems. More than twenty years ago, Iijima et al. [144–146] reported on

the interaction of CDs with water soluble polymers, including poly(sodium methacrylate), copolymers of sodium styrenesulfonate and styrene, and copolymers of sodium (meth)acrylate and styrene. In the case of copolymers containing styrene units, they suggested the interaction of CDs with phenyl side chains, but they did not characterize the structure of supramolecular polymers. In this section, the authors review recent examples of supramolecular polymers formed by CDs with polymer side chains.

5.1
Side Chain Polyrotaxanes

Ritter et al. [147–155] have been studying side chain polyrotaxanes. They synthesized side chain polyrotaxanes by amide coupling of polymer-carrying carboxylic acid moieties with various semirotaxanes of methylated β-CD(s) and an axle bearing an amine group at one end [147–154]. These works have been reviewed in an excellent review by Raymo and Stoddard [78]. Ritter et al. [155] reported recently a new type of side chain polyrotaxane. They polymerized inclusion complexes of di(meth)acrylates of butan-1,4-diol and hexan-1,6-diol with α-CD and with methylated β-CD using a redox initiator system in aqueous media, and characterized the polyrotaxane structure by IR and glass-transition temperature measurements.

5.2
Alkyl Side Chains

The authors studied the interaction of CDs with alkyl side chains attached to the poly(acrylamide) backbone with ^{1}H NMR spectroscopy and found that CDs bind alkyl side chains efficiently and selectively [156]. *n*-Butyl side chains interacted only with α-CD. On the other hand, *t*-butyl side chains interacted with β-CD and γ-CD, but did not interact with α-CD. The association constant for the complex formation of β-CD with a *t*-butyl side chain was larger than that for the complex formation of γ-CD, indicating that the *t*-butyl side chain fits well in the β-CD cavity. The association constant for the complex formation of α-CD with linear alkyl side chains increased with an increase in the carbon number of the alkyl side chain from butyl to dodecyl. Noteworthy is that CDs recognize alkyl chains on the polymer main chain more specifically than low molecular weight ones. This may be because CDs include polymer-carrying alkyl chains only from one direction.

5.3
Aryl Side Chains

The authors also investigated the interaction of CDs with aromatic side chains attached to the poly(acrylamide) backbone by several techniques including

steady-state fluorescence and circular dichroism (cd) spectroscopies [157]. (1-Naphthyl)methyl and (2-naphthyl)methyl side chains interacted most considerably with β-CD. Cd spectra indicated that β-CD included polymer-carrying 1Np groups shallowly, but it included deep polymer-carrying 2Np groups to form inclusion complexes, in which the longer axis of the 2Np group is rather parallel to the rotation axis of β-CD.

5.4 Utilization of Supramolecular Polymers Formed by CDs and Polymer Side Chains

Supramolecular polymers formed by CDs and polymer side chains have been utilized for controlling the association behavior of water soluble polymers. Akiyoshi et al. [158] reported that β-CD regulated the association and dissociation of hydrophobically modified pullulan in aqueous media. The self-aggregates of pullulan modified with cholesterol moieties were dissociated into molecularly dispersed polymers upon addition of β-CD, which interacts with cholesterol moieties to suppress hydrophobic associations. The self-aggregates were regenerated upon addition of 1-adamantanecarboxylic acid, which interacts with β-CD more strongly than cholesterol does. Yan et al. [159] utilized the complex formation of methyl β-CD with hydrophobically modified copolymers of methacrylic acid and ethyl acrylate to characterize the polymers molecularly dispersed in aqueous media, because it is usually difficult to characterize this type of polymer in aqueous media due to a stronger tendency for interpolymer hydrophobic association. Yan et al. determined the weight average molecular weight, hydrodynamic radius, and radius of gyration of these polymers in the presence of excess methyl β-CD. Hogen-Esch et al. [160–162] studied the interaction of β-CD with copolymers of *N*,*N*-dimethylacrylamide (DMA) and 2-(*N*-ethylperfluorooctane-sulfonamido)ethyl acrylate (FOSA) by viscometry. Upon addition of β-CD, the solution viscosity decreased because of suppression of hydrophobic associations of fluorinated side chains. Upon addition of sodium 1-adamantanecarboxylate to mixtures of β-CD and DMA/FOSA copolymers, the solution viscosity was recovered. Using these observations, controlled release of methyl orange was also investigated. Ravoo et al. [163] investigated the interaction of β-CD with poly(isobutene-*alt*-maleic acid)s modified with 4-*t*-butylphenyl or adamantyl groups by affinity capillary electrophoresis. From the effect of the β-CD concentration on the electrophoretic mobility of the polymers, the association constants for the complex formation of β-CD with hydrophobic side chains were determined. They deduced that the change in electrophoretic mobility upon complexation was caused by a transition of the polymer conformation from a compact conformation to an extended one with an increase in the β-CD concentration. Ritter et al. [164] reported copolymerization of *N*-isopropylacrylamide (NIPAM) with hydrophobic monomers included by methylated β-CD in aqueous me-

dia to form high molecular weight copolymers. Recently, they also examined the effect of methylated β-CD on the lower critical solution temperature of NIPAM copolymers bearing adamantane moieties [165]. Hu et al. [166, 167] synthesized a series of hydroxypropyl methylcellulose bearing azobenzene side chains and investigated their photoresponsive sol-to-gel transition behavior in the absence and presence of α-CD. Hu et al. observed that, after UV irradiation, the sol-to-gel transition occurred at a higher temperature in the absence of α-CD and at a lower temperature in the presence of α-CD.

When CD moieties linked together covalently interact with hydrophobic side chains to form inclusion complexes, these inclusion complexes may act as cross-links to form network structures, leading to an increase in solution viscosity, gelation, or phase separation. Wenz et al. [168, 169] studied the interaction of poly(isobutene-*alt*-maleic acid) bearing β-CD moieties with poly(isobutene-*alt*-maleic acid) bearing 4-*t*-butylanilide side chains and reported an increase in the solution viscosity. Gosselet et al. [170] reported on the interaction of a β-CD polymer, prepared by cross-linking with epichlorohydrin, with *N*,*N*-dimethylacrylamide/hydroxyethyl methacrylate copolymers bearing 2 mol % of adamantyl side chains. Mixing of these polymers led to a viscosity increase and phase separation. Guo et al. [171] studied the interaction of poly(acrylic acid)s bearing α- and β-CD moieties with octadecyl-modified poly(acrylic acid). They observed a maximum of solution viscosity at a 1 : 1 molar ratio of CD moiety and octadecyl side chain. The authors reported hydrogel formation from poly(acrylamide)-bearing azobenzene side chains and poly(allylamine) bearing-β-CD moieties [172]. When the azobenzene moieties took the *trans* form, a mixture of polymers forms hydrogel, but when the azobenzene moieties took the *cis* form, the mixture of polymers was a sol. Recently, the authors also investigated gel-to-sol and sol-to-gel transitions utilizing the complex formation of α-CD with dodecyl side chains attached to the poly(sodium acrylate) backbone [173]. When α-CD was added to a hydrogel of poly(sodium acrylate) modified with 5 mol % of dodecyl side chains, the viscosity decreased drastically. On the other hand, when an α-CD oligomer, prepared by cross-linking with epichlorohydrin, was added to a solution of poly(sodium acrylate) modified with 2 mol % of dodecyl side chains, the viscosity increased remarkably.

References

1. Lehn J-M (1995) Supramolecular Chemistry: Concepts and Perspectives. Wiley, Weinheim, Germany
2. Ciferri A (2000) Supramolecular Polymers. Marcel Dekker, New York
3. Fouquey C, Lehn J-M, Levelut A-M (1990) Adv Mater 2:254
4. Gulik-Krzywicki T, Fouquey C, Lehn J-M (1993) Proc Natl Acad Sci USA 90:163
5. Lehn J-M (1993) Makromol Chem, Macromol Symp 69:1

6. Sijbesma RP, Beijer FH, Brunsveld L, Folmer BJB, Hirschberg JHKK, Lange RFM, Lowe JKL, Meijer EW (1997) Science 278:1601
7. Hirschberg JHKK, Brunsveld L, Ramzi A, Vekemans JAJM, Sijbesma RP, Meijer EW (2000) Nature 407:167
8. Brunsveld L, Folmer BJB, Meijer EW, Sijbesma RP (2001) Chem Rev 101:4071
9. Castellano RK, Rebek J Jr (1998) J Am Chem Soc 120:3657
10. Castellano RK, Nuckolls C, Eichhorn SH, Wood MR, Lovinger AJ, Rebek J Jr (1999) Angew Chem Int Ed 38:2603
11. Castellano RK, Clark R, Craig SL, Nuckolls C, Rebek J Jr (2000) Proc Natl Acad Sci USA 97:12418
12. Knapp R, Schott A, Rehahn M (1996) Macromolecules 29:478
13. French D, Rundle RE (1942) J Am Chem Soc 64:1651
14. James WJ, French D, Rundle RE (1959) Acta Crystallogr 12:385
15. Hybl A, Rundle RE, Williams DE (1965) J Am Chem Soc 87:2779
16. Saenger W (1984) In: Atwood JL, Davies JED, MacNicol DD (eds) Inclusion Compounds, vol 2. Academic Press, London, Chapter 8
17. Le Bas G, Rysanek N (1987) In: Duchëne D (ed) Cyclodextrins and their industrial uses. Editions de Santë, Paris, Chapter 3
18. Harata K (1991) In: Atwood JL, Davies JED, MacNicol DD (eds) Inclusion Compounds, vol 5. Oxford University Press, New York, Chapter 9
19. Harata K (1996) In: Szejtli J, Osa T (eds) Cyclodextrins. Comprehensive Supramolecular Chemistry, vol 3. Pergamon, Oxford, U.K., Chapter 9
20. Harata K (1998) Chem Rev 98:1803
21. Hirotsu K, Higuchi T, Fujita K, Ueda T, Shinoda A, Imoto T, Tabushi I (1982) J Org Chem 47:1143
22. Kamitori S, Hirotsu K, Higuchi T, Fujita K, Yamamura H, Imoto T, Tabushi I (1987) J Chem Soc, Perkin Trans 2:7
23. Harata K, Rao CT, Pitha J, Fukunaga K, Uekama K (1991) Carbohydr Res 222:37
24. Di Blasion B, Pavone V, Nastri F, Isernia C, Saviano M, Pedone C, Cucinotta V, Impellizzeri G, Rizzarelli E, Vecchio G (1992) Proc Natl Acad Sci USA 89:7218
25. Hanesian S, Benalil A, Simard M, Bëlanger-Gariuepy F (1995) Tetrahedron 51:10149
26. Mentzafos D, Terzis A, Coleman AW, de Rango C (1996) Carbohydr Res 282:125
27. Harata K, Takenaka Y, Yoshida N (2001) J Chem Soc, Perkin Trans 2:1667
28. Liu Y, You C-C, Zhang M, Weng L-H, Wada T, Inoue Y (2000) Org Lett 2:2761
29. Liu Y, Fan Z, Zhang H-Y, Diao C-H (2003) Org Lett 5:251
30. Liu Y, Fan Z, Zhang H-Y, Yang Y-W, Ding F, Liu S-X, Wu X, Wada T, Inoue Y (2003) J Org Chem 68:8345
31. Eliadou K, Giastas P, Yannakopoulou K, Mavridis IM (2003) J Org Chem 68:8550
32. Miyauchi M, Hoshino T, Yamaguchi H, Kamitori S, Harada A (2005) J Am Chem Soc 127:2034
33. Hamasaki K, Ikeda H, Nakamura A, Ueno A, Toda F, Suzuki I, Osa T (1993) J Am Chem Soc 115:5035
34. Ueno A, Minato S, Suzuki I, Fukushima M, Ohkubo M, Osa T, Hamada F, Murai K (1990) Chem Lett 605
35. Wang Y, Ikeda T, Ikeda H, Ueno A, Toda F (1994) Bull Chem Soc Jpn 67:1598
36. Corradini R, Dossena A, Marchelli R, Panagia A, Sartor G, Saviano M, Lombardi A, Pavone V (1996) Chem Eur J 2:373
37. Corradini R, Dossena A, Galaverna G, Marchelli R, Panagia A, Sartor G (1997) J Org Chem 62:6283
38. Takahashi K, Imotani K, Kitsuta M (2001) Polym J 33:242

39. Inoue Y, Wada T, Sugahara N, Yamamoto K, Kimura K, Tong L-H, Gao X-M, Hou Z-J, Liu Y (2000) J Org Chem 65:8041
40. Yamada T, Fukuhara G, Kaneda T (2003) Chem Lett 32:534
41. Fukuhara G, Fujimoto T, Kaneda T (2003) Chem Lett 32:536
42. McAlpine SR, Garcia-Garibay MA (1996) J Am Chem Soc 118:2750
43. Zanotti-Gerosa A, Solari E, Giannini L, Floriani C, Chiesi-Villa A, Rizzoli C (1996) Chem Commun 119
44. Yamaguchi N, Nagvekar DS, Gibson HW (1998) Angew Chem Int Ed 37:2361
45. Bügler J, Sommerdijk NAJM, Visser AJWG, van Hoek A, Nolte RJM, Engbersen JFJ, Reinhoudt DN (1999) J Am Chem Soc 121:28
46. Tong L-H, Hou Z-J, Inoue Y, Tai A (1992) J Chem Soc, Perkin Trans 2 1253
47. McAlpine SR, Garcia-Garibay MA (1998) J Am Chem Soc 120:4269
48. Mirzoian A, Kaifer AE (1999) Chem Commun 1603
49. Harada A, Miyauchi M, Hoshino T (2003) J Polym Sci, Part A: Polym Chem 41:3519
50. Hoshino T, Miyauchi M, Kawaguchi Y, Yamaguchi H, Harada A (2000) J Am Chem Soc 122:9876
51. Fujimoto T, Uejima Y, Imaki H, Kawarabayashi N, Jung JH, Sakata Y, Kaneda T (2000) Chem Lett 29:564
52. Fujimoto T, Sakata Y, Kaneda T (2000) Chem Lett 29:764
53. Park JW, Song HE, Lee SY (2002) J Phys Chem B 106:5177
54. Gao X-M, Zhang Y-L, Tong L-H, Ye Y-H, Ma X-Y, Liu W-S, Inoue Y (2001) J Inclusion Phenom Macrocycl Chem 39:77
55. Fujimoto T, Sakata Y, Kaneda T (2000) Chem Commun 2143
56. Onagi H, Easton CJ, Lincoln SF (2001) Org Lett 3:1041
57. Kaneda T, Yamada T, Fujimoto T, Sakata Y (2001) Chem Lett 30:1264
58. Harada A, Kawaguchi Y, Hoshino T (2001) J Inclusion Phenom Macrocycl Chem 41:115
59. Harada A (2001) Acc Chem Res 34:456
60. Miyauchi M, Harada A (2005) Chem Lett 34:104
61. Miyauchi M, Takashima Y, Yamaguchi H, Harada A (2005) J Am Chem Soc 127:2984
62. Miyauchi M, Harada A (2004) J Am Chem Soc 126:11418
63. Sauvage JP, Dietrich-Buchecker C (eds) (1999) Molecular Catenanes, Rotaxanes and Knots: A Journey Through the World of Molecular Topology. Wiley, Weinheim
64. Amabilino DB, Stoddart JF (1995) Chem Rev 95:2725
65. Balzani V, Credi A, Raymo FM, Stoddart JF (2000) Angew Chem Int Ed 39:3348
66. Ashton PR, Baxter I, Cantrill SJ, Fyfe MCT, Glink PT, Stoddart JF, White AJP, Williams DJ (1998) Angew Chem Int Ed 37:1294
67. Ashton PR, Parsons IW, Raymo FM, Stoddart JF, White AJP, Williams DJ, Wolf R (1998) Angew Chem Int Ed 37:1913
68. Rowan SJ, Cantrill SJ, Stoddart JF, White AJP, Williams DJ (2000) Org Lett 2:759
69. Ogata N, Sanui K, Wada J (1976) J Polym Sci, Polym Lett Ed 14:459
70. Ogino H, Ohata K (1984) Inorg Chem 23:3312
71. Manka JS, Lawrence DS (1990) J Am Chem Soc 112:2440
72. Rao TVS, Lawrence DS (1990) J Am Chem Soc 112:3614
73. Isnin R, Kaifer AE (1991) J Am Chem Soc 113:8188
74. Wylie RS, Macartney DH (1992) J Am Chem Soc 114:3136
75. Wenz G, von der Bey E, Schmidt L (1992) Angew Chem Int Ed Engl 31:783
76. Harada A, Li J, Kamachi M (1997) Chem Commun 1413
77. Semlyen JA (1996) Large Ring Molecules. Wiley, Weinheim

78. Raymo FM, Stoddart JF (1999) Chem Rev 99:1643
79. Rowan SJ, Cantrill SJ, Cousins GRL, Sanders JKM, Stoddart JF (2002) Angew Chem Int Ed 41:898
80. Hubin TJ, Busch DH (2000) Coord Chem Rev 200–202:5
81. Harada A (1998) Acta Polym 49:3
82. Nepogodiev SA, Stoddart JF (1998) Chem Rev 98:1959
83. Pease AR, Jeppesen JO, Stoddart JF, Luo Y, Collier CP, Heath JR (2001) Acc Chem Res 34:433
84. Ballardini R, Balzani V, Credi A, Gandolfi MT, Venturi M (2001) Acc Chem Res 34:445
85. Schalley CA, Beizai K, Vogtle F (2001) Acc Chem Res 34:465
86. Collin J-P, Dietrich-Buchecker C, Gaviña P, Jimenez-Molero MC, Sauvage J-P (2001) Acc Chem Res 34:477
87. Blanco M-J, Consuelo Jimenez M, Chambron J-C, Heitz V, Linke M, Sauvage J-P (1999) Chem Soc Rev 28:293
88. Vogtle F, Safarowsky O, Heim C, Affeld A, Braun O, Mohry A (1999) Pure Appl Chem 71:247
89. Balzani V, Gómez-López M, Stoddart JF (1998) Acc Chem Res 31:405
90. Sauvage J-P (1998) Acc Chem Res 31:611
91. Chambron J-C, Dietrich-Buchecker CO, Sauvage J-P (1996) In: Hosseini MW, Sauvage J-P (eds) Templating, Self-Assembly, and Self-Organization. Comprehensive Supramolecular Chemistry, vol 9. Pergamon, Oxford, U.K., Chapter 2
92. Maciejewski M, Panasiewicz M, Jarminska D (1978) J Macromol Sci, Chem A12:701
93. Maciejewski M (1979) J Macromol Sci, Chem A13:77
94. Maciejewski M, Gwizdowski A, Peczak P, Pietrzak A (1979) J Macromol Sci, Chem A13:87
95. Maciejewski M (1979) Journal of Macromol Sci, Chem A13:1175
96. Maciejewski M, Durski Z (1981) Journal of Macromol Sci, Chem A16:441-450
97. Harada A, Kamachi M (1990) Macromolecules 23:2821–2823
98. Harada A, Kamachi M (1990) J Chem Soc, Chem Commun 1322
99. Harada A, Li J, Kamachi M (1993) Macromolecules 26:5698
100. Li J, Harada A, Kamachi M (1994) Bull Chem Soc Jpn 67:2808
101. Harada A, Li J, Kamachi M (1994) Macromolecules 27:4538
102. Li J, Harada A, Kamachi M (1994) Polym J 26:1019
103. Harada A, Okada M, Li J, Kamachi M (1995) Macromolecules 28:8406
104. Harada A, Okada M, Kamachi M (1998) Bull Chem Soc Jpn 71:535
105. Harada A, Li J, Suzuki S, Kamachi M (1993) Macromolecules 26:5267
106. Harada A, Suzuki S, Okada M, Kamachi M (1996) Macromolecules 29:5611
107. Harada A, Nishiyama T, Kawaguchi Y, Okada M, Kamachi M (1997) Macromolecules 30:7115
108. Harada A, Kawaguchi Y, Nishiyama T, Kamachi M (1997) Macromol Rapid Commun 18:535
109. Kawaguchi Y, Nishiyama T, Okada M, Kamachi M, Harada A (2000) Macromolecules 33:4472
110. Michishita T, Okada M, Harada A (2001) Macromol Rapid Commun 22:763
111. Michishita T, Takashima Y, Harada A (2004) Macromol Rapid Commun 2004:1159
112. Okumura H, Okada M, Kawaguchi Y, Harada A (2000) Macromolecules 33:4297
113. Okumura H, Kawaguchi Y, Harada A (2001) Macromolecules 34:6338
114. Okumura H, Kawaguchi Y, Harada A (2003) Macromolecules 36:6422
115. Harada A, Li J, Kamachi M, Kitagawa Y, Katsube Y (1998) Carbohydr Res 305:127

116. Kamitori S, Matsuzaka O, Kondo S, Muraoka S, Okuyama K, Noguchi K, Okada M, Harada A (2000) Macromolecules 33:1500
117. Udachin KA, Wilson LD, Ripmeester JA (2000) J Am Chem Soc 122:12375
118. Sakamoto K, Naruoka T, Kira M (2003) Chem Lett 32:380
119. Harada A, Li J, Kamachi M (1994) Nature 370:126
120. Harada A, Okada M, Kawaguchi Y (2005) Chem Lett 34:542
121. Peet J, Rusa CC, Hunt MA, Tonelli AE, Balik CM (2005) Macromolecules 38:537
122. Kihara N, Hinoue K, Takata T (2005) Macromolecules 38:223
123. Harada A, Li J, Kamachi M (1992) Nature 356:325
124. Harada A, Li J, Nakamitsu T, Kamachi M (1993) J Org Chem 58:7524
125. Harada A, Li J, Kamachi M (1994) J Am Chem Soc 116:3192
126. Harada A, Li J, Kamachi M (1993) Nature 364:516
127. Harada A (1995) Polym Prepr (Am Chem Soc, Div Polym Chem) 36:570
128. Harada A, Adachi H, Kawaguchi Y, Okada M, Kamachi M (1996) Polym J 28:159
129. Kawaguchi Y, Harada A (2000) Org Lett 2:1353
130. Kawaguchi Y, Harada A (2000) J Am Chem Soc 122:3797
131. Murakami H, Kawabuchi A, Kotoo K, Kunitake M, Nakashima N (1997) J Am Chem Soc 119:7605
132. Okada M, Harada A (2004) Org Lett 6:361
133. Okada M, Harada A (2003) Macromolecules 36:9701
134. Herrmann W, Schneider M, Wenz G (1997) Angew Chem Int Ed Engl 36:2511
135. De Schryver FC, Anand L, Smets G, Switten J (1971) J Polym Sci, Polym Lett Ed 9:777
136. Bouas-Laurent H, Castellan A, Desvergne JP (1980) Pure Appl Chem 52:2633
137. Desvergne JP, Bitit N, Castellan A, Webb M, Bouas-Laurent H (1988) J Chem Soc, Perkin Trans 2:1885
138. Desvergne JP, Bouas-Laurent H, Lahmani F, Sepiol J (1992) J Phys Chem 96:10616
139. Desvergne JP, Gotta M, Soulignac JC, Lauret J, Bouas-Laurent H (1995) Tetrahedron Lett 36:1259
140. Okada M, Takashima Y, Harada A (2004) Macromolecules 37:7075
141. Takashima Y, Oizumi Y, Sakamoto K, Miyauchi M, Kamitori S, Harada A (2004) Macromolecules 37:3962
142. Storsberg J, Ritter H, Pielartzik H, Groenendaal L (2000) Adv Mater 12:567
143. Voet D, Voet JG (1995) Biochemistry, 2nd ed. Wiley, New York
144. Iijima T, Uemura T, Tsuzuku S, Komiyama J (1978) J Polym Sci, Polym Phys Ed 16:793
145. Uemura T, Moro T, Komiyama J, Iijima T (1979) Macromolecules 12:737
146. Moro T, Kobayashi S, Kainuma K, Uemura T, Harada T, Komiyama J, Iijima T (1979) Carbohydr Res 75:345
147. Born M, Ritter H (1991) Makromol Chem, Rapid Commun 12:471
148. Born M, Koch T, Ritter H (1994) Acta Polym 45:68
149. Ritter H (1994) Angew Makromol Chem 223:165
150. Born M, Ritter H (1995) Angew Chem Int Ed Engl 34:309
151. Born M, Koch T, Ritter H (1995) Macromol Chem Phys 196:1761
152. Born M, Ritter H (1996) Macromol Rapid Commun 17:197
153. Noll O, Ritter H (1997) Macromol Rapid Commun 18:53
154. Noll O, Ritter H (1998) Macromol Chem Phys 199:791
155. Sarvothaman MK, Ritter H (2004) Macromol Rapid Commun 25:1948
156. Harada A, Adachi H, Kawaguchi Y, Kamachi M (1997) Macromolecules 30:5181
157. Harada A, Ito F, Tomatsu I, Shimoda K, Hashidzume A, Takashima Y, Yamaguchi H, Kamitori S (2005) J Photochem Photobiol A (in press)

158. Akiyoshi K, Sasaki Y, Kuroda K, Sunamoto J (1998) Chem Lett 27:93
159. Islam MF, Jenkins RD, Bassett DR, Lau W, Ou-Yang HD (2000) Macromolecules 33:2480
160. Tomczak S, Hogen-Esch TE (1999) Polym Prepr (Am Chem Soc, Div Polym Chem) 40:163
161. Tomczak S, Hogen-Esch TE (2000) Polym Prepr (Am Chem Soc, Div Polym Chem) 41:281
162. Tomczak S, Hogen-Esch TE (2001) Polym Prepr (Am Chem Soc, Div Polym Chem) 42:562
163. Ravoo BJ, Jacquier J-C (2002) Macromolecules 35:6412
164. Casper P, Glöckner P, Ritter H (2000) Macromolecules 33:4361
165. Ritter H, Sadowski O, Tepper E (2003) Angew Chem Int Ed 42:3171
166. Zheng P, Hu X, Zhao X, Li L, Tam KC, Gan LH (2004) Macromol Rapid Commun 25:678
167. Hu X, Zheng PJ, Zhao XY, Li L, Tam KC, Gan LH (2004) Polymer 45:6219
168. Weickenmeier M, Wenz G, Huff J (1997) Macromol Rapid Commun 18:1117
169. Wenz G, Weickenmeier M, Huff J (2000) In: Glass JE (ed) Associative Polymers in Aqueous Media. ACS Symposium Series 765, American Chemical Society, Washington, DC, Chapter 16
170. Gosselet NM, Borie C, Amiel C, Sebille B (1998) J Dispersion Sci Technol 19:805
171. Guo X, Abdala AA, May BL, Lincoln SF, Khan SA, Prud'homme RK (2005) Macromolecules 38:3037
172. Takashima Y, Nakayama T, Miyauchi M, Kawaguchi Y, Yamaguchi H, Harada A (2004) Chem Lett 33:890
173. Tomatsu I, Hashidzume A, Harada A (2005) Macromol Rapid Commun 26:825

Editor: K.-S. Lee

Adv Polym Sci (2006) 201: 45–155
DOI 10.1007/12_079
© Springer-Verlag Berlin Heidelberg 2006
Published online: 23 February 2006

Liquid Crystalline Dendrimers and Polypedes

Bertrand Donnio · Daniel Guillon (✉)

Groupe des Matériaux Organiques—GMO,
Institut de Physique et Chimie des Matériaux de Strasbourg—IPCMS,
UMR 7504—CNRS/Université Louis Pasteur, 23, rue du Loess, BP 43,
67034 Strasbourg Cedex 2, France
daniel.guillon@ipcms.u-strasbg.fr

1 Introduction 47

2 Supramolecular Liquid-Crystalline Dendrimers 48

3 Side-Chain Liquid-Crystalline Dendrimers 64
3.1 Silicon-Containing Dendrimers 64
3.1.1 Carbosilane Dendrimers 65
3.1.2 Siloxane Dendrimers 77
3.1.3 Carbosilazane Dendrimers 81
3.2 Polydamidoamine and Polypropyleneimine Dendrimers 83
3.2.1 Structure-Property Relationships 83
3.2.2 Tuning the Dimensions of the Nano-Dendritic Object 94
3.2.3 Theoretical Aspects 96
3.2.4 Chiral Properties 97
3.2.5 Amphiphilic PPI Dendrimers 98
3.2.6 Photoactive PPI Dendrimers 100
3.3 Dendrimers with Polyether Dendritic Cores 101
3.4 Dendrimers with Polyester Dendritic Cores 102

4 Main-Chain Liquid-Crystalline Dendrimers 104
4.1 Willow-Like Dendrimers 105
4.2 Octopus Dendrimers 107

5 Shape-Persistent Liquid-Crystalline Dendrimers 113

6 Liquid-Crystalline Metallodendrimers 117

7 Liquid-Crystalline Fullerodendrimers 126

8 Polypedes 133

9 Miscellaneous 139
9.1 Mesomorphic Dendrimers with Rigid Discotic Cores 139
9.2 Supramolecular Rod-Coil Block Codendrimers 141

10 Conclusions 145

References 146

Abstract The purpose of this review article is to give an account of the various types of dendritic systems that form liquid-crystalline mesophases and to describe the way they are organized within supramolecular organizations. It is shown that tuning of the mesophase structure can be achieved by an appropriate molecular design depending upon the chemical nature of the terminal mesogenic groups, dendritic core and dendrimer generation. The division of the subject in this review is made by the nature of the dendritic scaffold. After a general introduction on dendrimers, supramolecular liquid-crystalline dendrimers are first discussed. Then, a large part of the review is devoted to side-chain liquid-crystalline dendrimers with different chemical skeletons. The section concerning main-chain liquid-crystalline dendrimers is divided into two parts, the willow-like and the octopus dendrimers. Liquid crystals based on other types of dendritic matrices are finally discussed, including shape-persistent dendrimers, metallodendrimers, fullerodendrimers, polypedes and rod-coil block co-dendrimers.

Keywords Dendrimer · Dendritic · Liquid crystal · Mesogen · Mesophase · Polypede

Abbreviations

2D	two-dimensional
3D	three-dimensional
AFM	atomic force microscopy
Cr	crystalline phase
Col_h, Col_{ho}	hexagonal columnar phase (*p6mm* symmetry)
Col_r	rectangular columnar phase (*p2gg* or *c2mm* symmetry)
Col_{squ}	square columnar phase (*p4mm* or *p4mg* symmetry)
Col_{tet}	tetragonal columnar phase
Col_x	unidentified columnar phase
Cub	Cubic phases ($Pm\bar{3}n$ and $Im\bar{3}m$ lattice symmetries)
DMF	*N*,*N*′-dimethylformamide
DOBOB	3,4,5-tris[(4-dodecyloxy)benzyloxy]benzene unit
DP	degree of polymerization
DSC	differential scanning calorimetry
Fc	ferrocene
G	glassy or amorphous solid phase
I	isotropic liquid
LC	liquid crystalline
LCD	liquid crystalline dendrimer
MC-LCD	main-chain liquid crystalline dendrimer
M, M1, M2	unidentified mesophases
Tet, M_{tet}	3D body-centered tetragonal phase
MD	molecular dynamics
N	nematic phase
N*	chiral nematic or cholesteric phase
OPV	oligo(phenylenevinylene)
PAMAM	polyamidoamine
Pc	phthalocyanine
PE	pentaerythritol
PEO	polyethylene oxide
PPI	polypropyleneimine
Ps	spontaneous polarization
SC-LCD	side-chain liquid crystalline dendrimer

SmA	smectic A phase
SmB	smectic B phase
SmC	smectic C phase
SmC*	chiral smectic C phase
$SmCP_R$, $SmCP_F$	polar smectic phases
SmX	unidentified smectic phase
THF	tetrahydrofuran
UV	ultraviolet
XRD	X-ray diffraction

1 Introduction

Since their discovery in the late 1970s [1], dendrimers have led to the most impressive developments and rapidly expanding areas of current science [2–11]. This extraordinary enthusiasm is caused by the intrinsic and unique molecular features of the dendrimers [2–11] and the possibility of generating numerous and original chemical architectures, offering new synthetic concepts and challenges for chemists [12, 13] as well as raising several interesting theoretical questions [14, 15]. The word dendrimer comes from the Greek *dendros* meaning tree and *meros* meaning part. This is a class of aesthetic, compartmentalized, practically monodisperse supermolecules possessing a regular and controlled three-dimensional branched topology [2–11], with a geometrical rate of growth as the generation number increases. Consequently, these molecules can possibly carry a large number of functional groups per volume unit [16]. These features are the result of sophisticated genealogically directed syntheses consisting of controlled iterative methods involving successive and specific elementary steps (convergent or divergent directed sequential construction). Furthermore, such "supermolecules" are unique in that they lack entanglements, leading to a good solubility in almost all organic solvents and in principle to a lower intrinsic viscosity.

The combination of a precise functionality at the termini or in the cavities with large and defined macromolecular structures also offers many opportunities in materials science and medicine, as well as many fundamental aspects. Research in this area has been further boosted by the appreciation of their uses as potentially interesting candidates in widespread applications [17, 18]. They may be used, when suitably functionalized, in biology as drug or gene delivery devices (encapsulation of guests in the cavities of dendritic hosts) [19], because of their rough resemblance to some living components (bio-mimetism) [20–24], or in chemistry (multiredox, chiroptical, catalytic properties). Alternatively, as ideal functionalized oligomeric substances (incorporating active or reactive functions), they may be designed as materials with precise functionalities in which molecular level information is transferred from the initiator core to the periphery (or vice versa) with

the expectation of complementary and synergic phenomena (i.e. induction of new properties), and/or cooperative effects (i.e. amplification of the existing properties) [25–31]. Several excellent comprehensive review articles have emphasized many of these interesting assets of dendrimers [2–11, 14–16, 32–45].

Molecular engineering of liquid crystals is also an important issue for controlling the self-assembling ability [46, 47] and the self-organizing process of single moieties into controlled meso- and nanostructures [48–52]. It was therefore logical to functionalize such supermolecules in order to obtain well-defined giant-like liquid crystalline materials [53–58] with the possibility of discovering new types of mesophases and original morphologies [59–66]. The first liquid crystalline dendrimers (LCDs) to be reported were obtained by simply incorporating mesogenic groups within a hyperbranched dendritic scaffold either by random self-polymerization of an appropriate difunctionalized mesogenic monomer [67–73] or by the grafting of monofunctionalized mesogenic units at the terminal branches of a pre-formed tree-like polymer [71]: such hyperbranched polymers [74], a denomination presently preferred to dendrimers, are characterized by randomly branched structures with a high degree of branching and broad molecular weight distributions [75–77]. Despite their great interest, these systems will not be further discussed here as they are out of the scope of this review.

So far, most studies have focused on side-chain liquid crystalline dendrimers (SC-LCDs; Fig. 13). Induction of liquid crystalline properties may simply be achieved by grafting mesogenic promoters on the periphery of a dendrimer, though a few LCDs with non-mesogenic end-groups have also been reported [53–57]. Mesomorphism results essentially from both the enthalpic gain provided by anisotropic interactions, and the strong tendency for microphase separation due to the chemical incompatibility between the flexible dendritic core and the terminal groups as in AB-block copolymers [78]. The structure of the mesogen as well as the topology of attachment to the core (end-on and side-on; Fig. 13) determine the mesomorphism of the entire compound. The control of the ultimate molecular architecture (size and shape) can be modulated by the generation growth, the multiplicity of the branches and the connectivity of the focal core. Other sub-classes of LCDs that will also be considered in this review include supramolecular dendromesogens, shape-persistent, main-chain, polypedic, metal- and fullerene-containing LCDs.

2
Supramolecular Liquid-Crystalline Dendrimers

Such mesogenic systems represent a class by themselves often referred to as dendromesogens. The dendritic concept results from the self-organization of these dendromesogens into various liquid crystalline morphologies. Cylindrical supramolecular dendrimers are generally obtained by the self-assembly

of first generation monodendrons [79–85] (and of their corresponding side-group polymers [86–95]) that exhibit a tapered fan shape. The wide end of these molecules is usually made up of three flexible aliphatic chains such as in the DOBOB (3,4,5-tris[(4-dodecyloxy)benzyloxy]benzene unit; Fig. 1A) and 3,4,5-trialkoxybenzene derivatives (Fig. 1B), whereas the summit is made hydrophilic by using acid, ester or alcohol functions, or by grafting crown ethers or ethylene oxide chains. Malthête already successfully demonstrated the great aptitude of systems containing the DOBOB unit (Fig. 1A, $m = 12$) to self-organize into columnar mesophases. Indeed, unconventional mesogens such as the conical-like, pyramidal-like and the so-called diabolo-like mesogenic molecules [96–98] were produced by the connection of the DOBOB units to various multivalent molecular sub-units.

Self-assembly of such tapered dendritic molecules into infinite columns can be seen as an arrangement of "parts of a cake" to form a flattened circular slice followed by the stacking of these slices on top of another (Fig. 2), the central core of the columns being filled by the polar parts (crown ether, ethylene oxide segments) or the polymer backbone. This process is driven by micro-segregation of the different parts constituting the molecules, steric constraints as well as in some cases H-bonding interactions. The self-assembly ability of these systems into columnar organizations is strongly enhanced

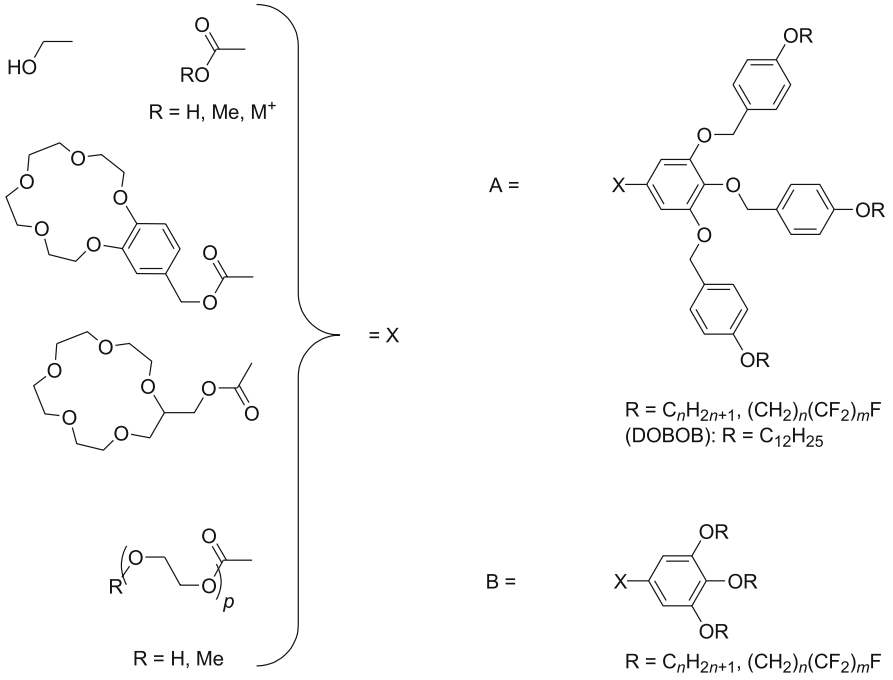

Fig. 1 Various types of flat tapered molecules self-assembling into cylindrical columns

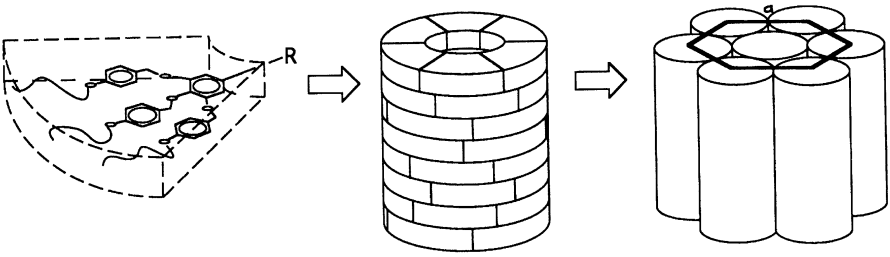

Fig. 2 Schematic representation of the self-assembling of flat tapered monodendrons into cylindrical columns and their self-organization into the Col_h phase

by fluorination of the dodecyl side chains (Fig. 1, R = $C_nH_{2n}C_mF_{2m+1}$ with $n + m = 12$ and $n, m = 4, 6, 8$) [99–101]. A rich mesomorphism was also promoted in alkali metal salts of 3,4,5-trialkoxybenzoic acids (G1-CO_2M, $n = 12$, 14, 16, 18) that were found to self-organize at low temperatures into Col_r ($M^+ = Na^+$, $m = 12$) or Col_h ($M = Li^+$, Na^+, K^+, Rb^+, Cs^+, $m = 12$, 14, 16, 18) phases and at high temperature into both $Pm\bar{3}n$ and $Im\bar{3}m$ cubic phases or only the cubic $Im\bar{3}m$ phase ($M = Li^+$, $m = 12$; $M = Li^+$, Na^+, K^+, $m = 14$; $M = Li^+$, Na^+, K^+, Rb^+, $m = 16$; $M = Li^+$, Na^+, K^+, Rb^+, Cs^+, $m = 18$), depending on chain-length and alkali metal [102].

Thus, essentially all the flat tapered molecules are found to lead to columnar structures, but when laterally attached to a flexible polymer backbone, the nature and symmetry of the phase was found to be determined by the degree of polymerization. And indeed, for some polystyrene, poly(methacrylate) [90] and poly(ethyleneimine) [92] polymers containing 3,4,5-tri(dodecyloxy)benzoyl minidendritic side-groups, those with a DP > 15–20 led to hexagonal columnar organizations, whereas those with lower DP self-organize into "inverse micellar-like" thermotropic cubic mesophases with $Pm\bar{3}n$ and $Im\bar{3}m$ space groups, respectively [90, 92]. About two macromolecules pair up to form inverse micellar-like objects with globular cores containing polymer backbones and aromatic groups, the alkyl chains radiating out to ensure a continuous matrix.

It was anticipated that a change in dendritic shape to a nearly spherical one should occur upon increasing the generation number [103]. And indeed, cone-shaped, hemisphere-like and even spherical monodendrons were obtained by increasing the generation number, producing spherical supramolecular dendrimers that in turn self-assemble into micellar cubic phases (Fig. 3). In addition, the rate of this dendritic deformation can be modulated by the degree of branching (branching multiplicity) and the "surface"-chain topology (position and number of terminal aliphatic chains).

This is first illustrated by the four generations of monodendrons based on the AB_3 building block unit shown in Fig. 4 [104, 105]. The substitution of the terminal benzyl ethers by three alkoxy groups (in their 3,4,5 positions)

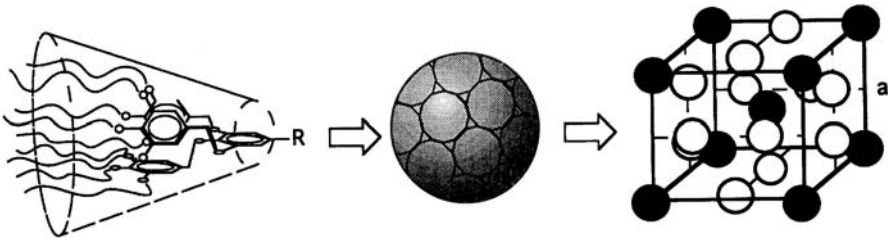

Fig. 3 Schematic representation of the self-assembling of conical-like monodendrons into spherical supramolecular dendrimers and their self-organization into cubic phases (here $Pm\bar{3}n$ symmetry)

allows only a restricted-cooperative rotation that requires the external benzyl ethers to be approximately orthogonal to the internal one, thus favoring the conical shape of the monodendron (Fig. 3). Starting from the second generation, all the dendrons (benzoates, corresponding benzyl alcohols and benzoic acids) exhibit in addition to the crystalline phase an isomorphous cubic liquid-crystalline phase with the $Pm\bar{3}n$ space group (Table 1).

Studies of electron density profiles and histograms computed from the X-ray diffraction data demonstrate that the cubic phase results from the self-assembly of these supramolecular dendrimers; the aromatic regions are centered around the corners, the center of the cubic lattice, and in the 1/4 and 3/4 positions along one of the bisectors of each face [106]. This model was finally confirmed by the analysis of the electron density profiles of the phase exhibited by a G2-CO_2H derivative with perfluorinated side-chains (Fig. 4, G2-CO_2H, R = $C_4H_8C_8F_{17}$) and doped with small amounts of the equivalent rubidium salt to modify the contrast [107]. This model is quite similar to that generally found in micellar lyotropic systems with the same symmetry [108–111]. The aggregation of the monodendrons into a supramolecular dendrimer is also favored by the H-bonding network generated by the apical acid or alcohol functions of the monodendrons, the former leading to the most stable cubic mesophase (Table 1). A convenient way to describe the cubic phase formed by these supramolecular dendrimers is to consider micelles with "polyhedral" shapes (vide infra). The fluorination of the terminal chains of the G2-CO_2Me monodendron (Fig. 4, R = $C_{12}H_{25}$ to R = $C_4H_8C_8F_{17}$) led to the transformation of the "spherical" supramolecular dendrimer into a pyramidal columnar supramolecular dendrimer. As a consequence, not only the phase symmetry was changed (cubic-$Pm\bar{3}n$ vs. Col_h-*p6mm*), but the stability considerably enhanced (Cr 22 Col_h 92 I) [112]. This unique result shows an interesting alternative for the control of the molecular conformation and its mechanism of self-assembly into pre-designed morphologies.

Continuing their investigations, Percec and coworkers also considered several generations of benzyl ether monodendrons containing only one aliphatic terminal chain on the outside benzyl groups (Fig. 5) [113]. Optical polarizing

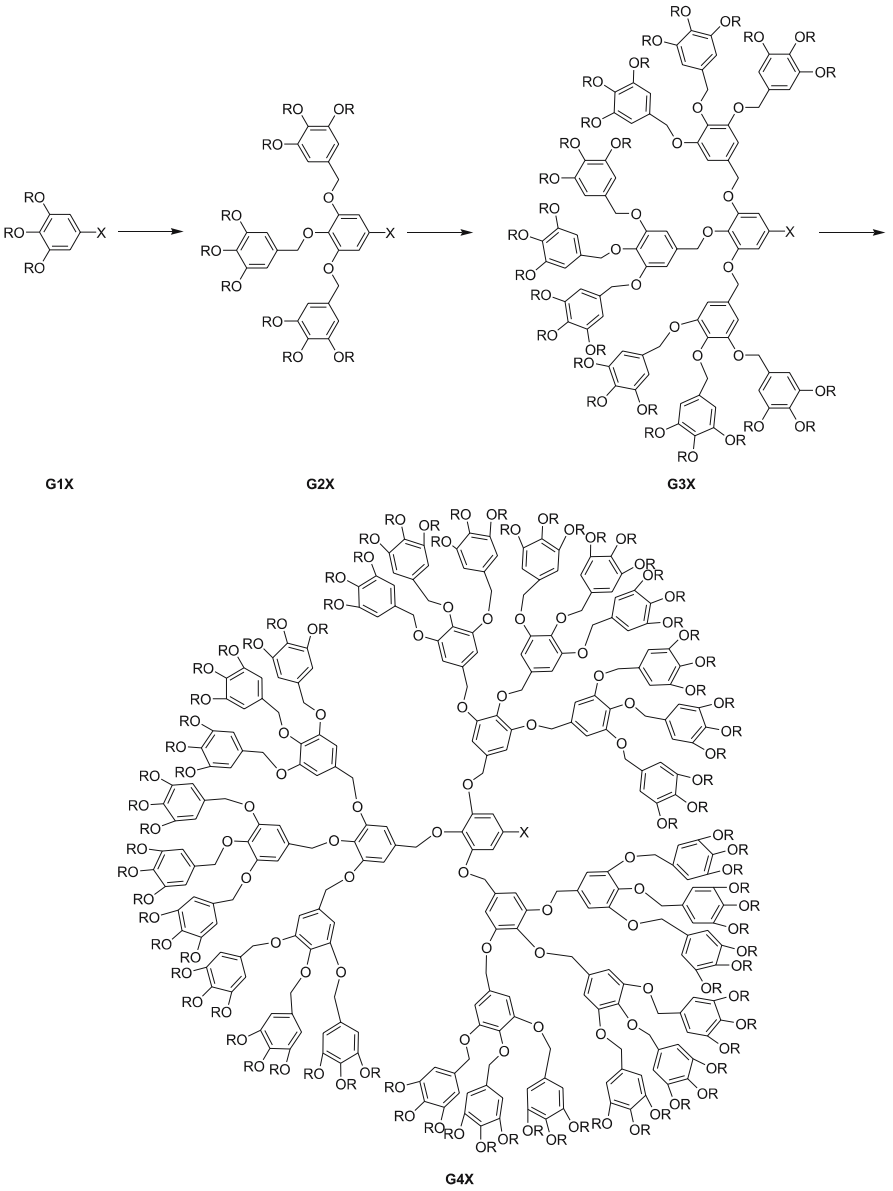

Fig. 4 Monodendrons based on the AB_3 building block unit (X = CO_2Me, CO_2H, CH_2OH; R = $OC_{12}H_{25}$)

microscopy studies and X-ray diffraction data show unambiguously the existence of a columnar mesophase (*p6mm* lattice) for the low generation dendrons and of a cubic mesophase ($Pm\bar{3}n$ lattice) for the third generation dendron (Table 2). Thus, the first two generations of monodendrons (G1-CO_2H

Table 1 Mesomorphic behavior of the monodendrons based on the AB_3 building block methyl 3,4,5-trishydroxybenzoate (X = CO_2Me, CO_2H, CH_2OH; R = $OC_{12}H_{25}$) [a,b]

G*n*X	X = CO_2CH_3	CH_2OH	CO_2H
G1	Cr 23 I	Cr 47 I	Cr 59 I
G2	Cr 58.5 (Cub 56) I	Cr 58 Cub 88 I	Cr 83 Cub 117 I
G3	Cr –11 Cub 94 I	Cr –12 Cub 106 I	Cr –12 Cub 139 I
G4	Cr –11 G 42 Cub 77 I		Cr –12 Cub 85 I

[a] Cubic phase with the $Pm\bar{3}n$ symmetry
[b] Phase in brackets: monotropic phase

and G2-CO_2Me) self-assemble into cylindrical supramolecular dendrimers. For an idealized model, it is convenient to view the columns as resulting from the stacking of cylindrical strata (taken at about ca. 4.5–4.7 Å thick), each containing a precise number of dendrons. In this idealized view, the former system is made up of four monodendrons, each having a shape equivalent to a quarter of a disk, whereas the latter is formed by two monodendrons with a half disk shape. The third generation monodendrons self-assemble into a spherical supramolecular dendrimer containing six monodendrons; those monodendrons undergo the most dramatic change in shape and become cone-like. So, a continuous change in the shape of the monodendron is induced by the generation number.

Therefore, for identical arborescence (here AB_3-type for both families of dendrons; Figs. 4 and 5), the number of terminal alkoxy chains can be greatly modified, simply by changing the nature of the terminal group. This straightforward modification affects significantly the mesophase behavior, as well as the self-assembling process. Indeed, the apparition of the cubic phase is delayed, and the increase in the number of alkyl tails (from 27 to 81) increases the size of the monodendrons from a sixth of a sphere (Fig. 5, G3-CO_2Me) to a hemisphere (Fig. 4, G4X).

In order to assess the criteria that govern the control of the shape and size of their supramolecular assemblies, Percec also investigated libraries of monodendrons that differ in their architecture on the periphery (number of peripheral aliphatic chains), in the internal repeat unit architecture (type of arborescence, i.e. branching multiplicity), in the generation number or core functionality and connectivity. For example, they studied the evolution of the mesomorphism in a series of dendrimers related to that shown in Fig. 5, but instead of grafting three 4-dodecyloxybenzyloxy groups at the periphery of the monomeric AB_3 building units, only two of them were attached to the AB_2 unit (the terminal chain number was changed from 3, 9, 27 in the former to 2, 6 to 18 for the latter from G1 to G3, respectively) [114]. The cubic phase appears from the second generation onwards ($Pm\bar{3}n$ lattice), whereas the first

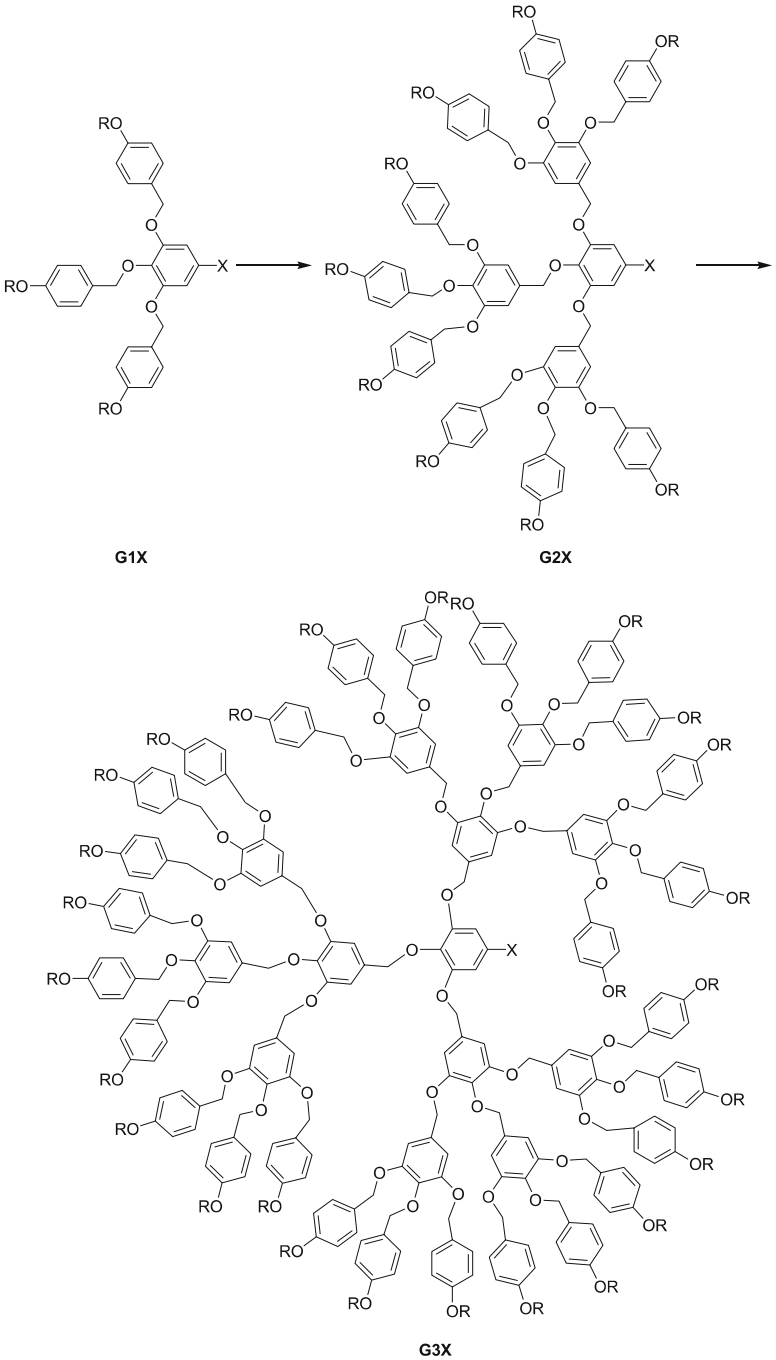

Fig. 5 Monodendrons based on the 3,4,5-AB_3 arborescence and with DOBOB as terminal group (X = CO_2Me, CO_2H; R = $OC_{12}H_{25}$)

Table 2 Mesomorphic behavior of the monodendrons based on the 3,4,5-AB_3 arborescence and with DOBOB as terminal group (X = CO_2Me, CO_2H; R = $OC_{12}H_{25}$) [a]

G*n*X	X = CO_2CH_3	CO_2H
G1	Cr 66 I	Cr 43 Col_h 145 I
G2	Cr –18 Col_{h1} 98 Col_{h2} 117 I	Cr 182 Cub 195 I
G3	Cr –17 G 47 Cub1 179 Cub2 197 I	

[a] Cubic phase with the $Pm\bar{3}n$ symmetry

generation forms a Col_h phase. Comparing these two series showed that the use of the AB_2 unit versus the AB_3 unit at the periphery led to an increase of the diameter of the supramolecular dendrimer, consequent to a decrease of the solid angle of the dendron. Upon increasing the generation number, all the dendrimers increase their solid angle until they become a single sphere. This trend was generally confirmed for this class of materials.

In another example, they considered the attachment of the first generation 3,4-bis(*n*-dodecan-1-yloxy)benzoyl ether monodendron to the periphery of Fréchet-type dendritic units (3,5-disubstituted benzyl ethers) leading to another class of mixed monodendrons (Fig. 6) [115]. Interestingly the second, third and fourth generation monodendrons (4, 8 and 16 terminal chains) self-assemble into supramolecular cylinders which in turn self-organize into a hexagonal columnar *p6mm* liquid-crystalline lattice. The fourth generation dendron is shown to be the first monodendron with a disk-like shape. The fifth generation dendron (32 chains) self-assemble into a cubic phase of $Pm\bar{3}n$ symmetry, where each monodendron is equivalent to a fifth of the supramolecular pseudo-spherical micelle.

Monodendrons based on the AB_3 arborescence (as those shown in Figs. 4 and 5) but with two terminal chains per peripheral phenyl group (as those shown in Fig. 6) were also synthesized up to the fifth generation (6, 18, 54, 162 dodecyloxy chains for G2 to G5, respectively) [116]. A cubic phase only with the same $Pm\bar{3}n$ 3D lattice was detected right from the second generation. All the above examples of cubic phases were found to result from the self-organization of dendrons which are conical or hemispherical in shape. However, the fifth generation monodendron is the first quasi-spherical functional monodendron that self-organizes into a cubic lattice ($Pm\bar{3}n$) to be reported (Fig. 12). The oblate spherical shape was confirmed by scanning force microscopy (the average diameter and average height of the molecule were found to be 6 and 5 nm, respectively, in a disordered monolayer of dendrons on a mica surface).

Two other isomeric libraries of self-assembling AB_2 monodendrons based on 3,4- and 3,5-disubstituted benzyl ether internal repeat units containing four first generation monodendrons, i.e., 3,4,5-tris(*n*-dodecan-1-

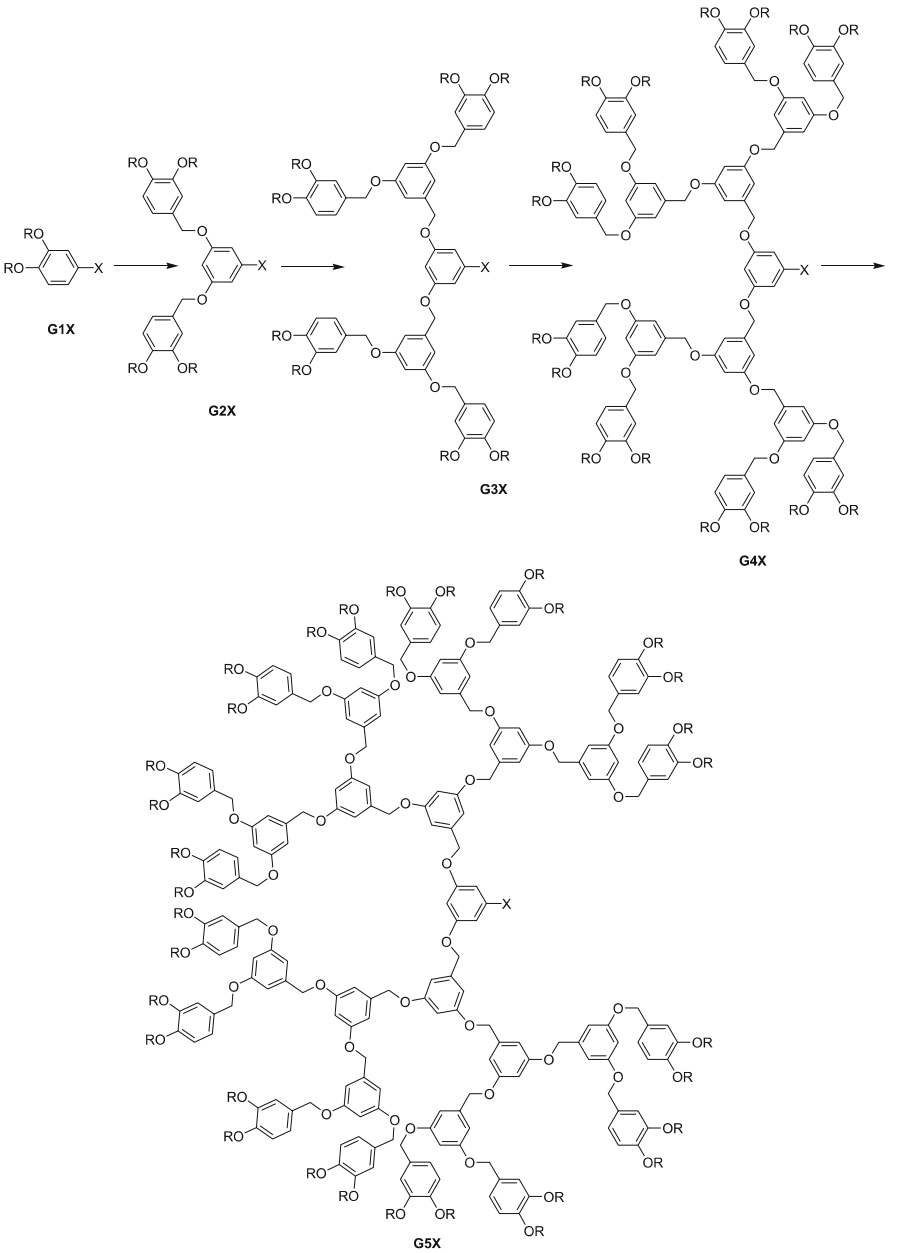

Fig. 6 Monodendrons based on the 3,5-AB_2 arborescence with 3,4-bis(*n*-dodecan-1-yloxy)benzoyl ether terminal groups (X = CO_2Me, CO_2H, CH_2OH; R = $OC_{12}H_{25}$)

yloxy)benzoyl ether, 3,4-bis(*n*-dodecan-1-yloxy)benzoyl ether, 3,4,5-tris(*n*-dodecan-1-yloxy)benzyloxy ether, 3,4-bis(*n*-dodecan-1-yloxy)benzyloxy ether, on their periphery were also considered (Fig. 7) [117]. It was shown that the supramolecular dendrimers derived from 3,4-dibenzyl ether monodendrons are spherical while the supramolecular dendrimers derived from 3,5-dibenzyl ether monodendrons are cylindrical. As a consequence, the monodendritic building blocks of the 3,4-disubstituted series have a cone-like shape while those of the 3,5-disubstituted series have a shape which corresponds to fragment of a disk or a disk-like shape (Fig. 12). In all the previous

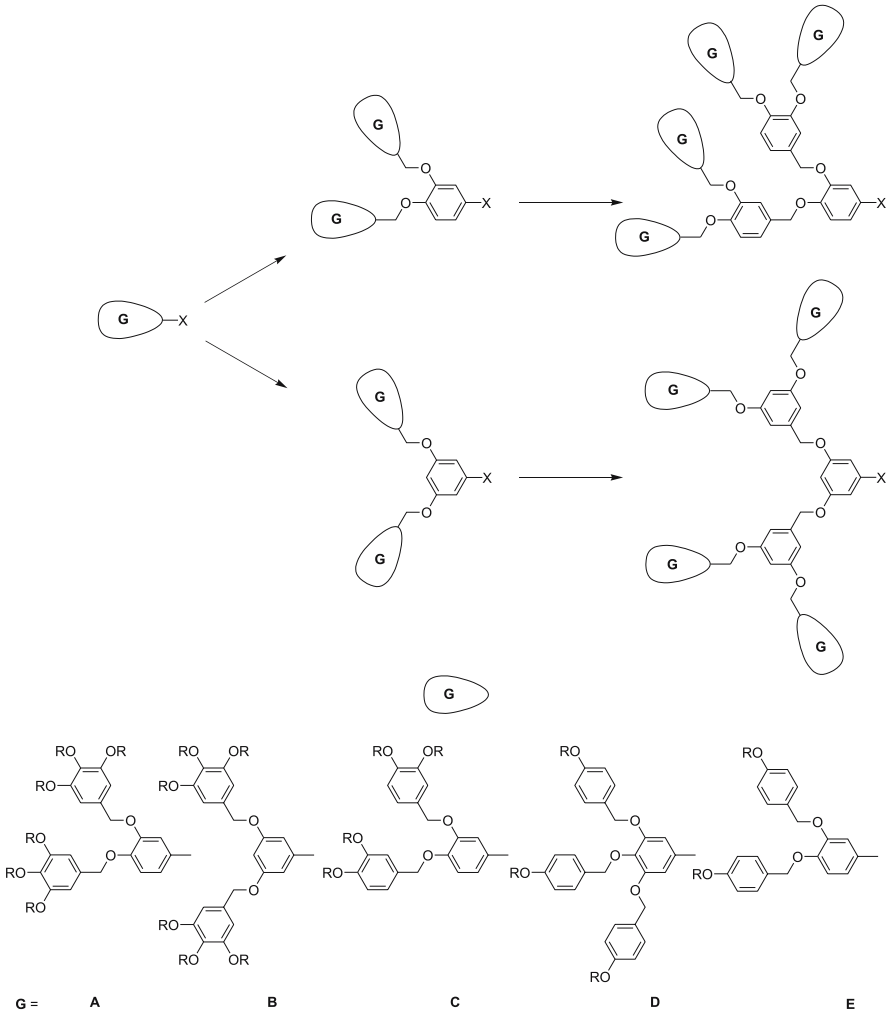

Fig. 7 Library of dendromesogens built up from a 3,4-AB_2, 3,5-AB_2, and mixed 3,4-3,5-type of arborescence (R = $OC_{12}H_{25}$, X = CO_2Me, CH_2OH, CO_2H)

libraries, the structure of the internal repeat unit determines the shape of the monodendron and of the supramolecular dendrimer. However, for the same internal repeat unit, the size of the monodendron and of the supramolecular dendrimer is determined by the structure of the unit on its periphery. On increasing the generation number, the shape of the monodendron changes from a fragment of a disk to a disk, to a cone, to half a sphere, and ultimately to a sphere. Please note that within all these libraries the library based on 3,5-disubstituted benzyl ethers provides the first example of supramolecular dendrimers able to change their shape in a reversible way as a function of temperature and also the first example of a spherical supramolecular dendrimer that self-organizes into a cubic phase of $Im\bar{3}m$ symmetry (Fig. 12).

Further studies by electron microscopy on some of the samples exhibiting the $Pm\bar{3}n$ cubic phase show the existence of grain boundaries and stacking faults [118]. These are all consistent with the presence of quasi-spherical assemblies or more precisely to polyhedral-like micelles, and moreover suggest that the supramolecular spheres are deformable, interacting with one another through a relatively soft pair potential [119]. The majority of such quasi-spherical assemblies are thus distorted into an oblate shape.

Wedge-shaped dendrons such as those described above form mainly columnar and cubic phases. However, a liquid-crystalline phase with a tetragonal three-dimensional unit cell (Tet phase) containing 30 globular supramolecular dendrimers has been reported recently. Each of these supramolecular dendrimers is the result of the self-assembly of 12 dendrons, as is shown in Fig. 8 [120, 121]. Interestingly, the complex tetragonal phase of symme-

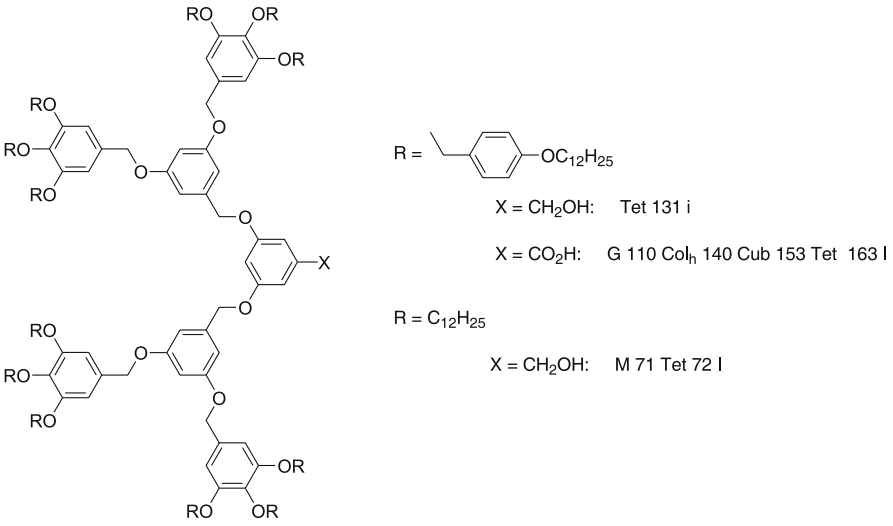

Fig. 8 Structure of the monodendrons with a 3,5-AB_2 arborescence showing the tetragonal phase

try $P4_2/mmm$ is shown to be the equivalent of tetrahedral closely packed Frank–Kasper structures [122] found in metals and metal alloys. The authors suggest that the analogy between dendrimers and metals lies in the role played by the "soft" *d* orbitals in the metals and the soft globular supramolecular dendrimers. In addition, with dendrons of the same family, quasiperiodic structures analogous to those found with some metal alloys, have been found. Whereas the characteristic length of the self-assembled quasicrystal is of a few Å in metal alloys, it is nearly 10 nm in the case of self-assembled dendrons.

Note that this geometrical model—that can be compared to the spherical micelle model used for cubic phases—which visualizes these 3D structures as an arrangement of space-filling polyhedra [123], as in the case of foams [124], appears more convenient for the description of the cubic structures than the 3D packing of spheres. In this view, the mean distances between the micellar nuclei can be represented by polyhedral hollow solids, the nature and type of which obviously are related to the symmetry of the cubic phase. Thus, for the $Im\bar{3}m$ phase, the symmetry is generated by the use of a single semi-regular Archimedean polyhedron, namely the truncated octahedron (a regular tetrakaidecahedron with 8 hexagonal and 6 square faces of identical edge) and located at the nodes of the cubic lattice ($N = 8 \times 1/8 + 1 \times 1 = 2$). Concerning the $Pm\bar{3}n$ space group, two polyhedra must be considered, namely the regular Platonic dodecahedron (12 pentagonal faces of same edge) located at the center and corners of the cubic cell ($8 \times 1/8 + 1 \times 1 = 2$) and a semi-regular 14-faced polyhedron (tetrakaidecahedron with two hexagonal faces and 12 pentagonal faces of same edge), occupying two of the four tetrahedral sites of each face of the cubic lattice ($6 \times 2 \times 1/2 = 6$).

In view of obtaining functional dendrons, crown ethers have been incorporated at the focal point of some of these dendromesogens (as in Fig. 1). The dendritic building blocks thus prepared self-assemble either spontaneously or after complexation with NaOTf in two-dimensional smectic B, smectic A, and *p6mm* hexagonal columnar and three-dimensional $Pm\bar{3}n$ cubic lattices with increasing generation [125]. A very delicate dependence is described between the shape of the dendritic crown ether and the stability of its supramolecular lattice obtained by complexation with NaOTf. Nevertheless, these supramolecular dendrimers represent interesting materials for selective ion transport.

In all the examples reported above concerning the self-assembly of dendrons based on AB_3, AB_2, and combinations of AB_3 and AB_2 building blocks, the shape and the diameter of the resulting supramolecular dendrimers were limited to less than 8 nm, mainly because of the solid angle of the dendron. In fact, because of the shape change of the self-assembling dendron as a function of generation, the increase in generation is generally not accompanied by an exaggerated increase of the supramolecular dimensions, despite the fact that the molecular weight increases exponentially. In order to produce supramo-

lecular dendrimers of larger dimensions, new libraries of compounds based on various combinations of AB, AB_2 and AB_3 building blocks have been designed and synthesized. This led to a very broad and original study (34 new compounds were reported) where the length of the branches, the number of terminal chains, the degree of branching and the multiplicity were systematically varied. Thus, two new families of dendritic mesogens such as the $(AB)_y$-AB_3 and $(AB)_y$-AB_2 series (Fig. 9; *y*: number of AB blocks; for the $(AB)_y$-AB_3 system, $y = 3n + 3 + m = 3 - 11$, and for the $(AB)_y$-AB_2 system $y = 2n + 3 + m = 2 - 7$) were first prepared [126].

Most of the first generation supramolecular dendrimers thus synthesized from the AB_3 building block (Fig. 9) self-organize into lamellar ($n = 1, 2$; $m = 0$), columnar hexagonal and rectangular ($n = 0, 1, 2$; $m = 0, 1$) and $Pm\bar{3}n$ cubic phases ($n = 0$; $m = 1, 2, 3$), whereas those derived from the AB_2 unit (Fig. 9) form lamellar ($n = 1, 2$; $m = 0, 3$) and columnar ($n = 0, 1, 2$; $m = 1, 2, 3$) phases only. The dimensions of the mesostructures are much larger (up to three times) than those of the phases of same symmetry exhibited by the highest generations of the supramolecular dendrimers obtained through the self-assembling of dendrons based on AB_3, AB_2, and combinations of AB_3 and AB_2 building blocks.

The corresponding families of the second generation of the AB_3 hybrid dendrons of the type $(AB)_y$-$(AB_3)^2$ (Fig. 10, $y = 0, 9, 18, 27$) and $(AB)_y$-$(AB_2)(AB_3)$ (Fig. 10, $y = 0, 6, 12$) were also prepared by varying the total number of benzyl AB groups *n* and *m*. A hexagonal columnar phase was obtained for the first series $(AB)_y$-$(AB_3)^2$ (Fig. 10, $n = 1, 2$), except for $n = 0$ which shows a $Pm\bar{3}n$ cubic phase and $n = 3$, which is crystalline. As for the mixed hybrid series $(AB)_y$-$(AB_2)(AB_3)$, a $Pm\bar{3}n$ cubic phase was obtained for all *n* (Fig. 10, $n = 0, 1, 2$), with an additional Col_h phase for $n = 2$. Unlike the previous series of the first generation, no smectic phases were detected.

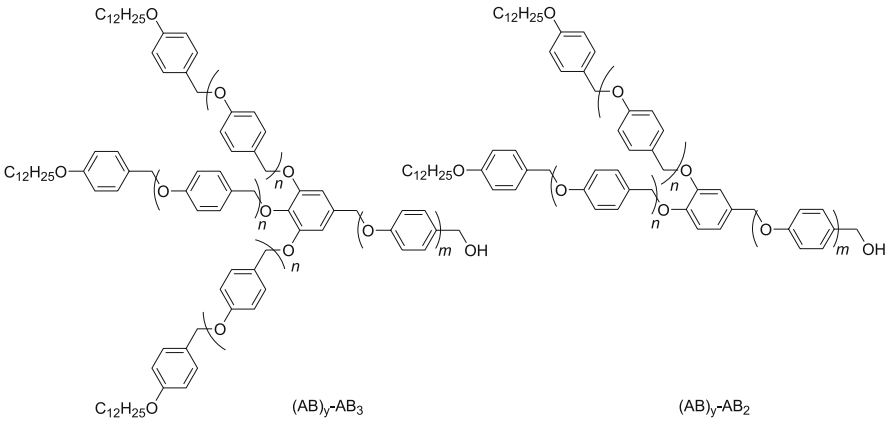

Fig. 9 Structure of the $(AB)_y$-AB_3 and $(AB)_y$-AB_2 dendrons of the first generation (*y*: number of AB blocks, see text)

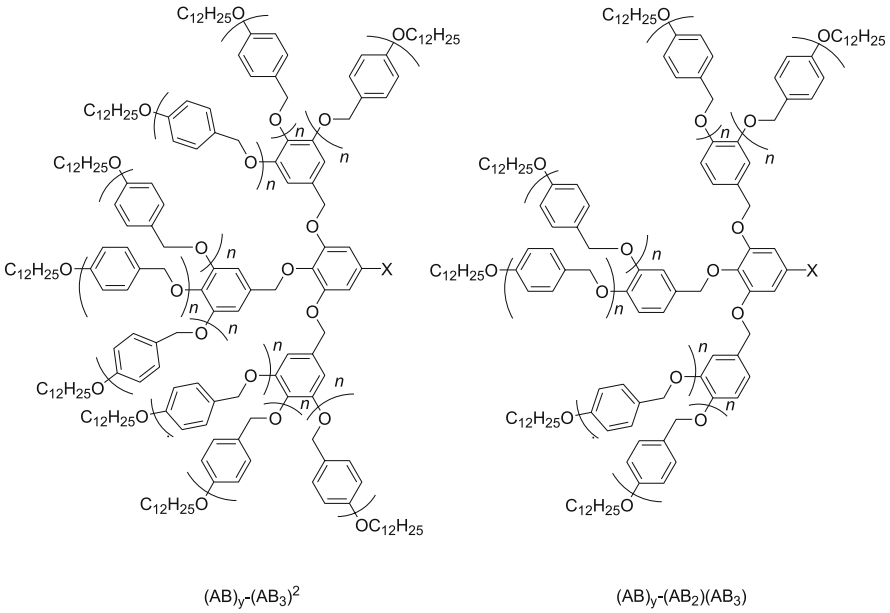

Fig. 10 Structure of the $(AB)_y$-$(AB_3)^2$ and $(AB)_y$-$(AB_2)(AB_3)$ hybrid dendrons of the second generation (y: number of AB blocks, see text)

Continuing in this direction, because of the large structural possibilities offered by this synthetic approach, other compounds with mixed hybrid structures could be prepared. A few isomeric dendrimers based on the (AB_2) unit with the 3,4 and 3,5 arborescence were also synthesized. The AB_2 hybrid dendrons $(AB)_y$-(3,4-AB_2)-$AB)_z$-(3,4-AB_2) (Fig. 11, $y + z = 4, 6, 12$, $z = 0, 2, 4$) yielded 3D cubic structures with an additional Col_h phase for the compound with $m = 1$ and $n = 0$. In contrast, the isomeric series $(AB)_y$-(3,4-AB_2)-$(AB)_z$-(3,5-AB_2) yielded mainly 2D columnar phases, namely a Col_h, then both Col_r and Col_h, and finally a single Col_r phase for the three compounds with $m = n = 0$, $m = 1$ and $n = 0$, and $m = 2$ and $n = 1$, respectively.

All the above examples show that supramolecular dendromesogens of various shape and dimensions (in the nanometer scale) can be obtained through a large variety of AB building blocks connected together according to various topologies, and through an efficient three-dimensional self-assembling process (Fig. 12). There is no doubt that such supramolecular nanostructures are of particular interest in complex soft matter in general, but represent also promising materials for optoelectronics, electronics and surface nanopatterning. Surface alignment and control of self-assembled columnar dendritic liquid crystals in thin films [127–129] as well as formation of Langmuir monolayers were also reported [130, 131].

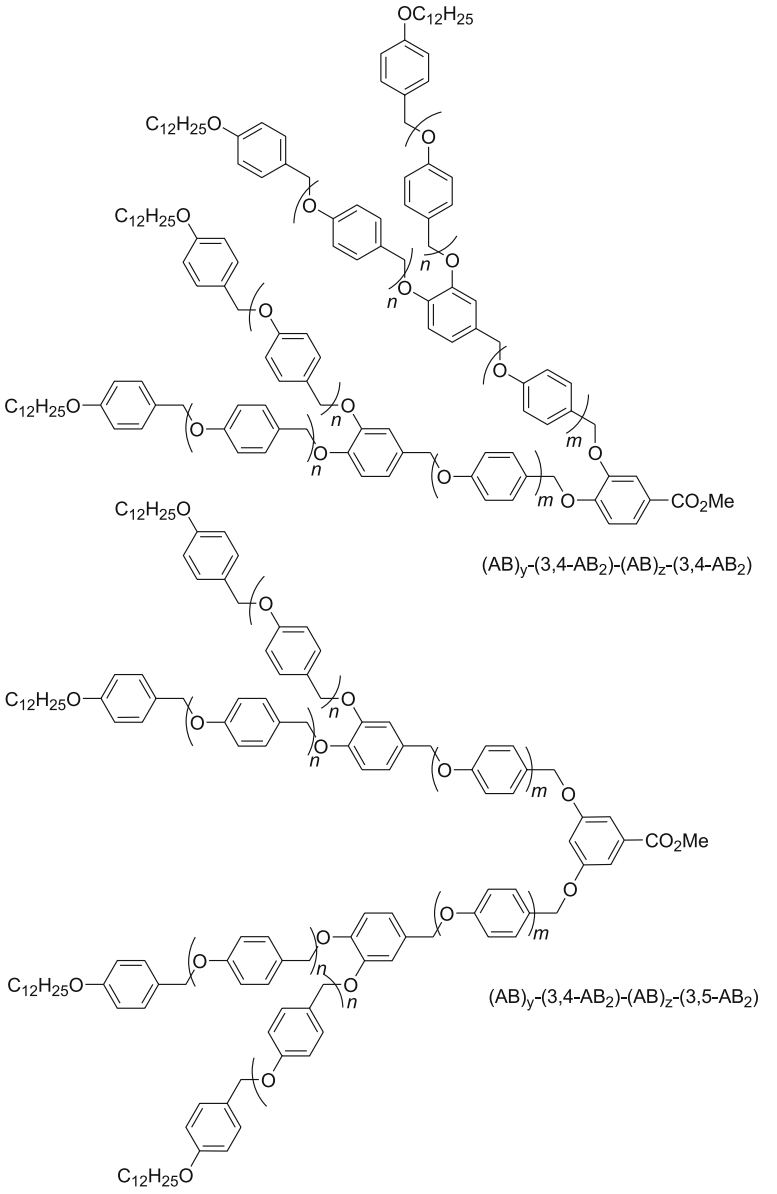

Fig. 11 Structure of the isomeric $(AB)_y$-(3,4-AB_2)-$(AB)_z$-(3,4-AB_2) and $(AB)_y$-(3,4-AB_2)-$(AB)_z$-(3,5-AB_2) hybrid dendrons of the second generation (*y* and *z*: number of AB blocks, see text)

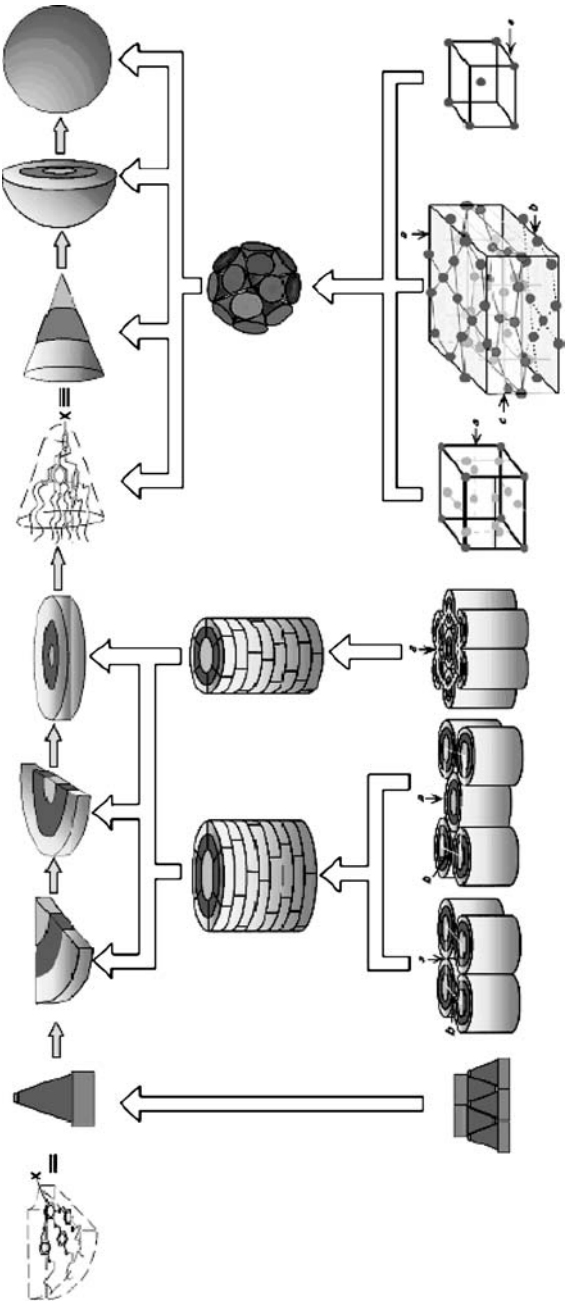

Fig. 12 Schematic representation of the self-assembly of dendromesogens into various type of mesophases (smectic, hexagonal and rectangular columnar, micellar cubic, and tetragonal phases) by the control of the molecular shape conformation (from flat tapered to cylindrical to conical and to spherical shape). From [126]

3
Side-Chain Liquid-Crystalline Dendrimers

The overall structure of such side-group LCDs (this terminology is used by analogy to side-chain liquid crystal polymers) consists of a flexible branched network with a branching multiplicity N_B, emanating from a single multivalent initiator core with a connectivity N_C, and mesogenic or pro-mesogenic units attached laterally (end-on) or terminally (side-on) at the termini of the branches (Fig. 13). The number of peripheral groups, Z, depends on these two structural parameters (N_C and N_B) as well as the generation number, G, according to the geometrical law: $Z = N_C N_B^G$. The control of the molecular conformation in such side-chain LC dendrimers will be considered thoroughly hereafter.

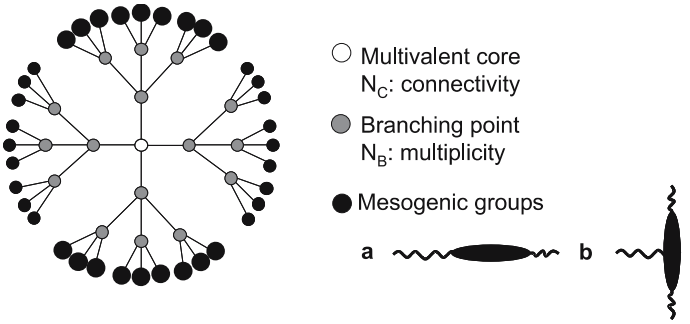

Fig. 13 Schematic 2D representation of an end-group dendrimer of second generation with a 4-fold core connectivity ($N_C = 4$), and a ternary branch multiplicity ($N_B = 3$). The mesogen can be attached terminally or laterally to yield **a** end-on or **b** side-on LCDs

3.1
Silicon-Containing Dendrimers

Silicon-containing dendrimers were the first heteroatom-based dendrimers synthesized, and three types of linkage were used at the branching points: carbosilane (Si – C), siloxane (Si – O) and carbosilazane (Si – N) bonds [41–45]. The carbosilane type represents the most important class of silicon-containing dendrimers mainly because of their excellent chemical and thermal stability, and the versatility of Si – C chemistry allowing access to macromolecules of high generation (up to the seventh) [43, 44]. Liquid crystalline dendrimers based on polycarbosilane and polysiloxane branched backbones have been reported by several groups.

3.1.1
Carbosilane Dendrimers

Frey and coworkers have prepared dendrimers-based on the carbosilane backbone with 4 (G0), 12 (G1), 36 (G2), and 108 (G3) cholesteryl end-groups via esterification of dendritic carbosilane polyols with cholesteryl chloroformate (Fig. 14) [132–134]. The fast increase in the number of terminal groups

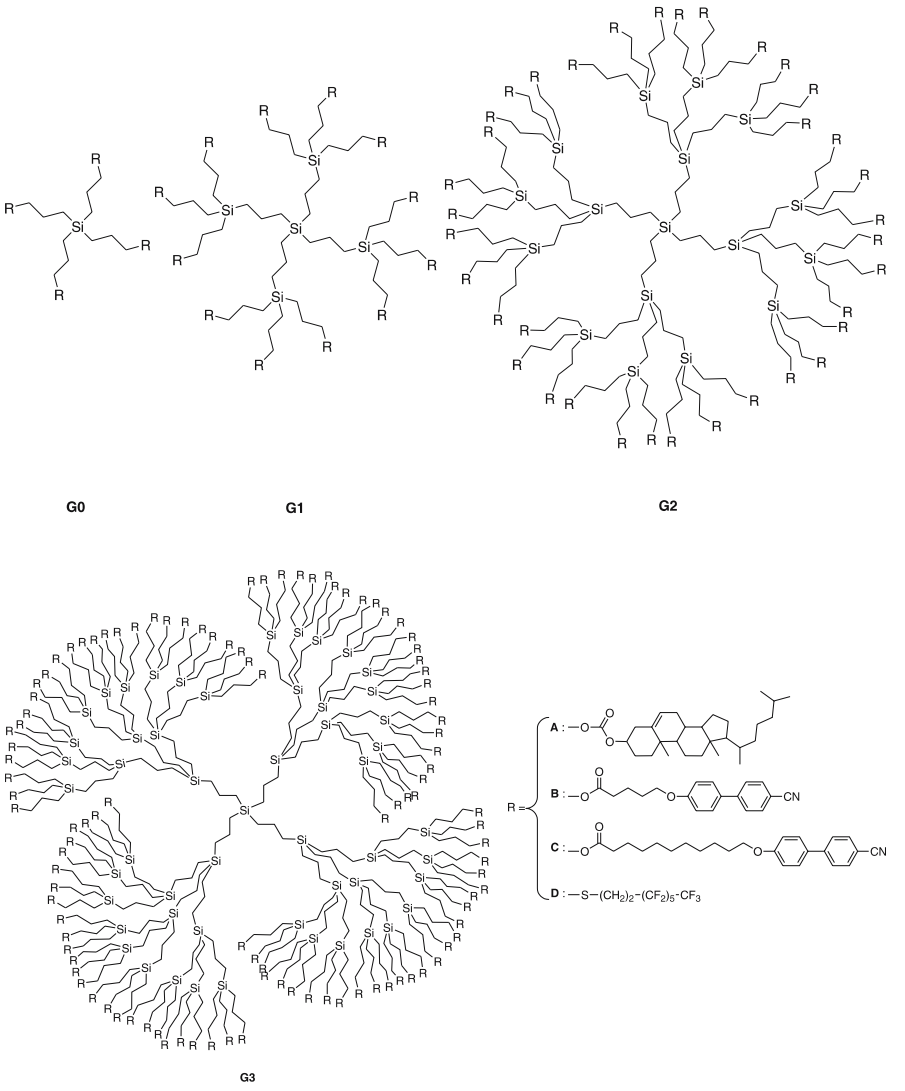

Fig. 14 Carbosilane dendrimers ($N_C = 4$, $N_B = 3$) from the zeroth to the second generation and the various groups attached at the periphery (R = A, B, C, D)

was because of the combination of a high core connectivity ($N_C = 4$) and the ternary degree of branching ($N_B = 3$), and despite the synthetic challenge, the polydispersity indices were in all cases close to unity. The mesomorphism of these dendrimers is nevertheless not totally clear. Indeed, the authors first reported that the G1 and G2 dendrimers (Fig. 14, R = A) were crystalline powders at ambient temperature and formed smectic mesophases between 80–90 °C and 130 °C, whereas that of the third generation was not mesomorphic. However, in a subsequent paper, and on the basis of X-ray diffraction experiments, they reported a lamellar structure for G1, but a 3D Col_h phase for G3, whereas it was not definite that G2 was mesomorphic [135]. These dendrimers were also found to be capable of self-assembly into ultrathin monolayers and multi-layer films.

In further studies, the same group investigated the effect of the nature of the mesogenic end groups and of the spacer length between the dendritic scaffold and the mesogen on the liquid crystalline properties. Thus, dendrimers of the first and second generation were prepared by esterification of the hydroxyl groups of the carbosilane arborols by derivatized cyanobiphenyl units (Fig. 14, R = B and C) [136, 137]. The four dendrimers possess a smectic mesomorphism identified by X-ray diffraction as SmA (R = B, G1: G 17 SmA 98 I and G2: G 17 SmA 130 I) and SmE and SmA phases (R = C, G1: G 14 SmE 67 SmA 106 I, G2: G 7 SmE 61 SmA 130 I). The clearing temperature was independent of the spacer length, but increased from G1 to G2.

Interestingly, besides the use of such classical calamitic mesogens, attachment of the non-mesomorphic perfluorinated alkyl chains to the same carbosilane polyols also yielded original mesomorphic systems. Thus, perfluorinated dendrimers of the zeroth to the third generation having 4, 12, 36, and 108 perfluoalkyl chains were prepared (Fig. 14, R = D) [138, 139]. Whereas G0 was obtained as a crystalline material devoid of mesomorphism (Cr 23 I), G1 and G2 exhibited a smectic phase (G1: G –30 SmA –15 I; G2: G –39 SmX) and G3 a Col_h phase (G –41 Col_h) [140, 141]; no transition to the isotropic liquid was detected for G2 and G3. In this series, mesomorphism clearly results from microphase segregation between the fluorophilic shell and the lipophilic interior of the dendrimer, since no mesogenic promoter is present [142]. The crossover behavior may be due to the increasingly dense packing of the perfluorinated chains at the periphery forcing the dendrimer core to deform and to adopt a more constrained conformation as the generation increased.

Terunuma and coworkers reported the properties of a different type of carbosilane dendrimer ($N_C = 3$, $N_B = 3$) bearing either cyanobiphenyl species or an optically active unit derived from 2-phenylpyrimidine at the periphery (Fig. 15). Only three branches emanated from the central silicon atom, the fourth valency being blocked by a phenyl group leading to 3 (G0), 9 (G1), and 27 (G2) terminal functional units.

All the dendrimers with cyanobiphenyl units (Fig. 15, R = A, $m = 5$) exhibited a single enantiotropic SmA phase, for which the stability was found

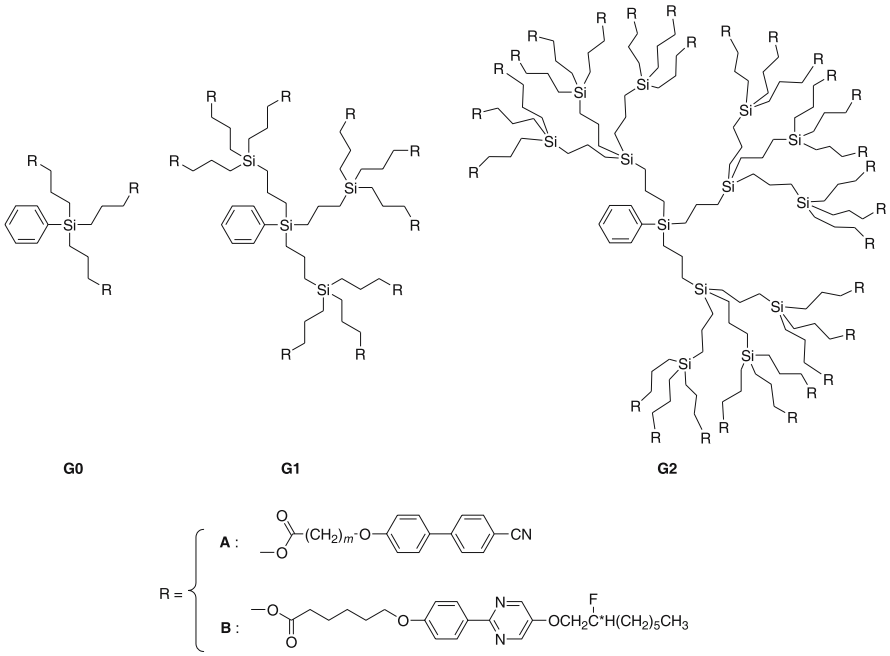

Fig. 15 Carbosilane dendrimers ($N_C = 3$, $N_B = 3$) functionalized by various R groups

to increase with generation number (Table 3) [143], whereas it was not affected to a great extent by the spacer length at a fixed generation (Fig. 15, R = A, $m = 4$–7) [144]. The dendrimers containing the chiral moieties (Fig. 15, R = B) exhibited a broad SmA phase only from room temperature up to around 80, 100, and 110 °C respectively [145]. However, the blends containing 10 wt % of the dendrimer with a non-chiral, liquid crystal material (also derived from 2-phenylpyrimidine), exhibited a broad ferroelectric SmC* phase from room temperature up to ca. 60 °C with additional SmA and N* phases before isotropization at 83–85 °C. No influence of the generation could be felt here, but the mixtures exhibited ferroelectric behavior, with an electro-optical switching time increasing with the generation number as in ferroelectric liquid crystalline polymers.

Table 3 Mesomorphic behavior of the compounds shown in Fig. 15

G*n*	Mesogen A ($m = 5$)	Mesogen B	Blend
G0	G 7 SmA 44 I	SmA 80 I	Cr 5.5 SmC* 62 SmA 71 N* 83 I
G1	G 14 SmA 72 I	SmA 105 I	Cr 7 SmC* 59 SmA 72 N* 85 I
G2	G 15 SmA 115 I	SmA 110 I	Cr 7 SmC* 56 SmA 72 N* 83 I

Let us also mention the only example of a bent-core molecule [146] fixed to the zeroth generation of a carbosilane core (Fig. 16) [147]. Truly speaking, this molecule, abusively referred to as a dendrimer, should be seen as a branched tetramer, since there is no branching, but the concept may be successfully applied for the supermolecules of higher generations (vide infra the case of PPI dendrimers bearing bent core mesogens). This compound exhibits a new type of polar smectic mesophase between the glassy state and the isotropic liquid (G 47 $SmCP_R$ 139 I), this organization resulting from a compromise between both the constraints imposed by the bent molecule and by the carbosilane moiety. By X-ray diffraction and optical microscopy, it was proposed that the molecules are tilted and adapt a polar order within the layers, but both the polar and tilt directions change randomly (no long-range orientational correlation between layers) in such a way that the polarization is cancelled, leading to an optically uniaxial phase. Switching into the ferroelectric organization ($SmCP_F$) can be achieved upon the application of a strong electric field due to the alignment of the polar directors of the layers parallel to the electric field. Once formed, the ferroelectric state remains stable, and spontaneous polarization as high as $P_S = 1400\ nC\ cm^{-2}$ could be measured.

Probably the most complete study on silicon-containing LCDs was that carried out by the group of Shibaev. The dendritic motif is based on a tetravalent core ($N_C = 4$), and a binary branching point ($N_B = 2$) leading to 4, 8, 16, 32, 64 and 128 terminal mesogens from G0 up to G5 (Fig. 17). The link with the mesogenic group is achieved by the hydrosilylation reaction between the peripheral double bonds of the dendrimer and the monosilylated mesogen. The effect of the nature of the mesogen and the generation of the dendrimer has been systematically analyzed.

These mesomorphic carbosilane dendrimers are characterized by a "surface" layer of mesogenic groups on the dendritic macromolecules of regular structures, responsible for the liquid-crystalline states of these compounds. The possibility of the creation of a liquid-crystalline shell around a central nucleus core formed by the soft dendritic matrix opens perspectives for the applications of such compounds. In a first paper [148], only the smallest generation (G1) of carbosilane dendrimer was synthesized and studied, the basic reaction used being hydrosilylation between the mesogen-containing fragments and the allyl groups of the dendritic matrix [149]. The liquid-

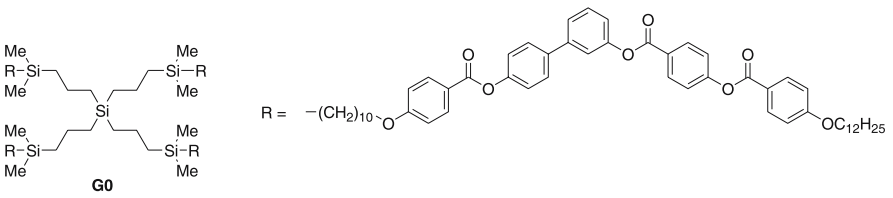

Fig. 16 Molecular structure of the zeroth generation dendrimer bearing a bent mesogen

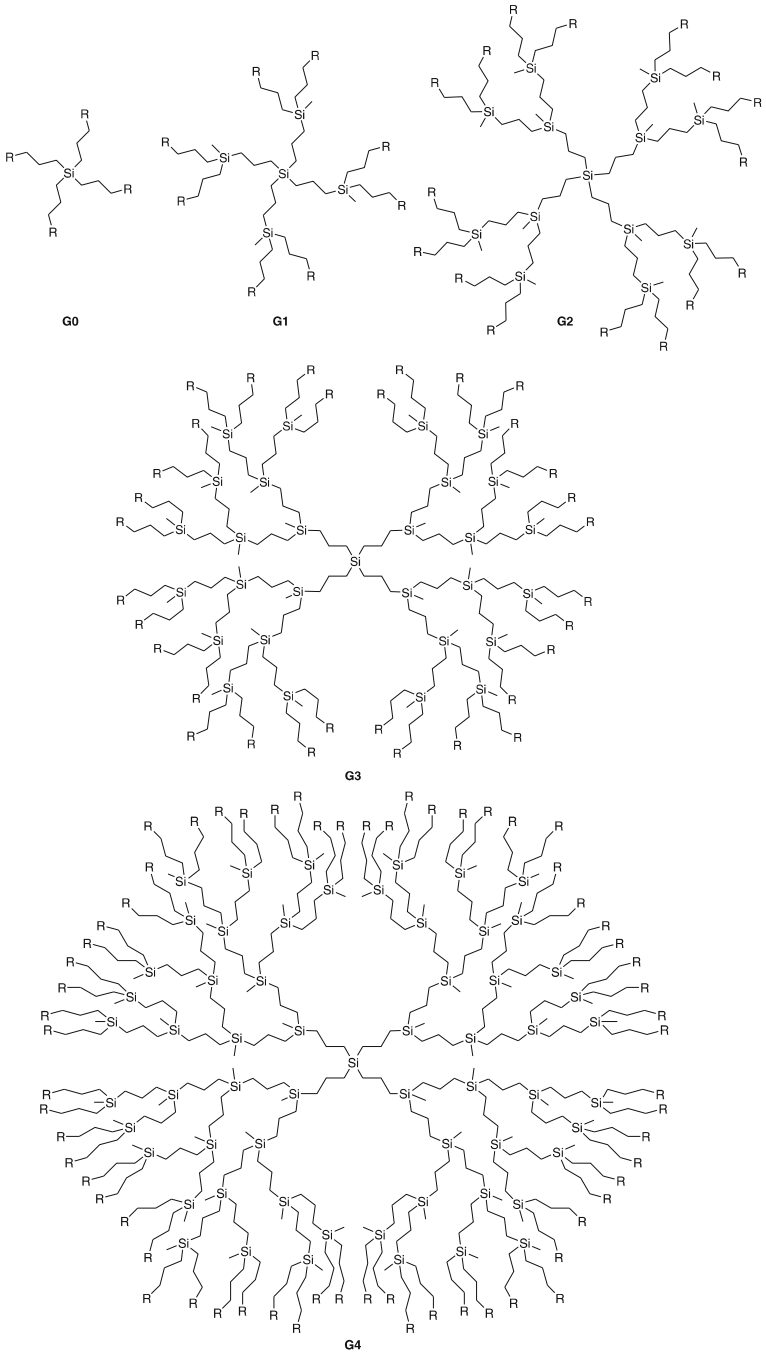

Fig. 17 Carbosilane dendrimer ($N_C = 4$, $N_B = 2$) from G0 to G4 bearing mesogenic R groups (G5 not reproduced here)

crystalline properties of the dendrimers were determined by optical polarizing microscopy in combination with differential scanning calorimetry (DSC) measurements and X-ray diffraction.

The phase behavior of the G1 compounds depends on the chemical nature of the terminal mesogenic groups. In the case of cholesteryl-containing dendrimers, a single smectic A phase was observed above a glassy phase, the glass transition temperature being below room temperature (Fig. 18, R = C: G –15 SmA 100 I). The layer spacing is in the range of 43–45 Å with an intermolecular distance of about 6 Å between the cholesteryl moieties. In the

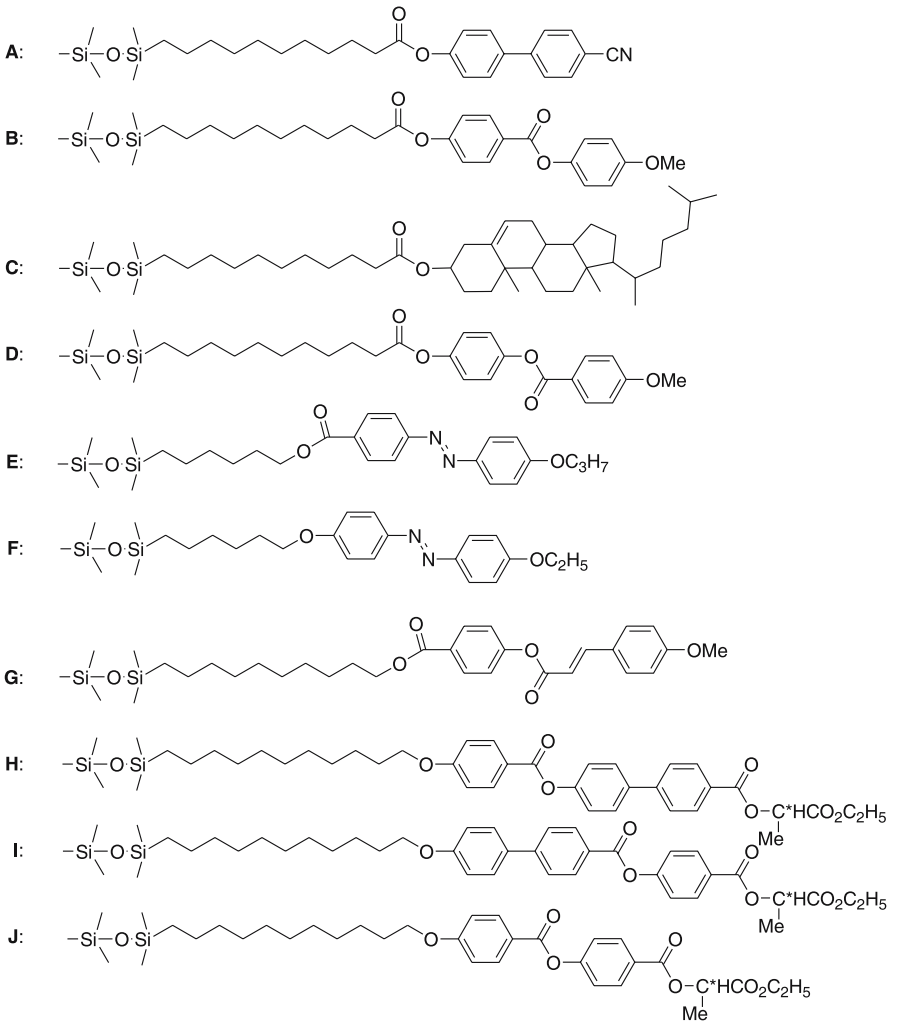

Fig. 18 Various R groups used for carbosilane-siloxy dendrimers shown in Fig. 17

other cases of cyanobiphenyl- (Fig. 18, R = A, Table 4) and methoxy phenyl benzoate-containing dendrimers (Fig. 18, R = B, Table 5), lamellar smectic A and C mesophases were identified with a layer spacing of about 42 Å; in these cases, two additional diffuse bands in the wide angle region of the X-ray diffraction patterns are related first to the intermolecular distance between the mesogenic groups (∼ 5 Å) and to the dendritic matrix itself (∼ 7 Å). Investigations of electro-optical properties of these dendrimers show that the dielectric polarization is proportional to the second power of the electric field in accordance with the Kerr law and that the Kerr constants are close to those of the low molar mass analogues of the corresponding mesogenic groups [150]. This suggests that the freedom in the orientation of the mesogenic groups is one of the most important factors influencing the capability of these compounds to form mesomorphic phases.

The synthesis of higher generations, up to the fifth one, was later described by the authors (Tables 4 and 5) [151, 152]. Following a divergent scheme, the strategy used for preparing the carbosilane dendrimers with terminal mesogenic groups (Fig. 18, R = A and B) involved three main steps: first the synthesis of carbosilane dendrimers with terminal allylic groups, then the modification of mesogens by the introduction of reactive terminal

Table 4 Mesomorphic behavior of the carbosilane dendrimers bearing cyanobiphenyl mesogens [a]

G*n*	R = A
G1	G –22.5 SmC 50 SmA 91.5 I
G2	G –21 SmC 55 SmA 89.5 I
G3	G –22.5 SmC 57 SmA 92 I
G4	G –21 SmA 109 I
G5	G –20 SmA T_X Col_r 121 Col_h 130 I

[a] T_X: transition temperature was not determined

Table 5 Mesomorphic behavior of the isomeric carbosilane dendrimers bearing methoxyphenyl benzoate (B) and anisic acid derivative (D) mesogens

G*n*	R = B	R = D
G1	G 30 SmC 77 I	G 30 SmC 52 SmA 58 I
G2	G 27 SmC 60 SmA 78 I	G 25 SmC 64 SmA 70 I
G3	G 15 SmC 67 SmA 81 I	G 10 SmC 65 SmA 79.5 I
G4	G 15.5 SmC 80 SmA 86 I	G 8 SmC 69 SmA 77.5 I
G5	G 12.8 Col_r 80.2 SmA T_X Col_h 96 I	G 0 M1 50 M2 95 I

groups such as Si – H and finally the attachment of these modified mesogenic groups onto the surface of the carbosilane dendrimers. Structural studies on both series of dendrimers, containing either terminal cyanobiphenyl or methoxyphenyl benzoate groups, show the existence of disordered smectic phases (smectic A and C) up to the fourth generation despite the assumed globular shape of the dendritic core [153], with layers of mesogenic groups alternating with layers formed by the carbosilane dendritic cores and aliphatic spacers. This model is supported by viscosity measurements in toluene and chloroform solutions of dendrimers which indicate that an increase in the generation number entails an increase in the crown size due to uncoiling of the terminal chains in the direction normal to the core surface [154, 155]. It is interesting to note that the layer spacing is almost constant with the low generation materials, and varies slightly for the high generation compounds, always in the range between 40 and 50 Å.

The phase diagram for the system G3 dendrimer (Fig. 18, R = A) and CCl_4, in the temperature range 0–90 °C, and concentration range 1–55 wt % was realized experimentally [156]. It showed two domains of phase co-existence: between 1 and 36.5 wt % of dendrimer, two phases coexist without varying their composition with temperature, and in the concentration range 36.5–55 wt %, the system separates into two phases, one being liquid-crystalline.

Molecular dynamics simulation studies of a third generation carbosilane dendrimer bearing cyanobiphenyl groups (Fig. 18, R = A) in solution have been carried out [157]. An hybrid model was used where the heavy atoms of the dendritic core are represented by Lennard-Jones sites and the mesogenic peripheral units by Gay–Berne potentials. It is shown that in the isotropic phase, the dendrimer adopts a spherical shape, with the alkyl chains (linking the mesogenic groups to the dendritic core) wrapping around the core and the terminal mesogenic units arranged randomly near the surface of the dendrimer. In the nematic and smectic solvents, the dendrimer core adopts a similar structure to the isotropic phase, but the terminal mesogenic units align to lie close to the solvent director. This occurs through a rearrangement of the alkyl chain conformations resulting in the dendrimer forming a rod shape. Such fluctuations in the conformations of the alkyl chains allow the dendrimer as a whole to become elongated along the nematic director and the peripheral mesogenic groups to align with an order parameter approaching that of the solvent. Such an elongation of dendrimers to form rod-shaped structures is consistent with the induction of lamellar phases in the bulk.

Unexpectedly, the fifth generation of the carbosilane LC dendrimers containing 128 terminal cyano groups not only form a lamellar but also supramolecular columnar mesostructures [158]. A smectic A phase exists at low temperature, for which the molecular organization is the same as that of the previous generations with a layer spacing of 53 Å despite the presence of the large number of peripheral mesogenic groups. At higher temperature,

this lamellar mesophase transforms firstly into a rectangular columnar phase, and on further heating into a hexagonal columnar phase. The explanation of this behavior given by the authors is based on a change of the molecular shape. With the increase of the temperature, the carbosilane LC dendrimers become less elongated and their shape more circular, favoring the formation of ellipsoidal columns. Each column consists of the stacking of ellipsoidal molecules, elongated in a direction perpendicular to the columnar axis. Further increase of the temperature leads to a more symmetrical shape of the LC dendrimers which become circular. The columns would then result from the stacking of these quasi-discoid molecules, and the arrangement of the latter into a hexagonal packing (Fig. 19). In both rectangular and hexagonal phases, the surface of the columns is covered by the mesogenic groups while their inner part consists of soft dendritic cores. A similar trend in the mesomorphic properties was observed with carbosilane dendrimers terminated with methoxyphenyl benzoate groups and with the mesogens based on anisic acid derivatives, isomeric system to B, (Fig. 18, R = B and D, Table 5) with little differences in the transition temperatures [159, 160].

The dielectric properties of fourth-generation mesogenic carbosilane dendrimers with alkyloxycyanobiphenyl terminal groups were studied. Permittivity and dielectric loss measurements were performed in the mesophase and isotropic phase in the range of electric field frequencies 1 kHz–100 MHz. A dispersion of permittivities was observed in this frequency range. It was shown that dispersion in the isotropic phase could be caused by two Debye-type relaxation processes. The activation energy of the low-frequency relaxation process decreased as the length of the alkyl chain of terminal dendrimer mesogen groups increased [161].

The analysis of these systems was completed by AFM studies [162, 163]. In particular AFM pictures of a monolayer of the fifth generation of the cyanobiphenyl-containing dendrimer shows patches with a thickness of ~ 3 nm on silicon substrate. These patches consist of individual particles. The

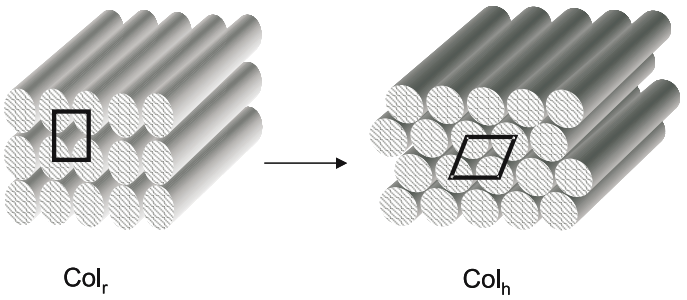

Fig. 19 Schematic diagrams of model structures formed by carbosilane LC dendrimers of the fifth generation (G5)

distance between the particles is close to the estimated size of one individual dendrimer which equals 5.5 nm according to X-ray diffraction data. Using a mica substrate, one can distinguish a rectangular two-dimensional packing. The structural ordering of some of these carbosilane LCDs within surface monolayers was studied, and found to strongly depend on the nature of the substrates (hydrophilic or hydrophobic) [164].

The influence of generation number on the phase behavior shows firstly that the glass transition temperature remains more or less constant and secondly that both the temperature and the enthalpy of the SmC-SmA transition increase whereas the enthalpy of the SmA-I transition temperature decreases with increasing the generation number. The increase of the transition temperatures is explained by a strengthening of the cooperative interactions of the increasing number of terminal mesogenic groups, and the decrease of the enthalpy by the more and more symmetrical shape of the LC dendrimers. According to the authors, these two opposite tendencies compete and result in the appearance of new supramolecular structures with a columnar morphology for the highest generation dendrimer [165].

In order to introduce electro-optical properties such as ferroelectric properties, Shibaev and coworkers first prepared carbosilane dendrimers of generation 1 to 3 with 8, 16 and 32 terminal ethyl-L-lactate-containing mesogenic groups (Fig. 18, R = H, I and J, Table 6) [166–169]. All the dendrimers exhibit a chiral smectic C mesophase above the glass transition in a broad temperature range, leading to ferroelectric properties (Table 6). For these dendrimers, the glass transition temperature does not depend on the generation number and is about –5 °C (Fig. 18, R = H and I) or –17 °C (Fig. 18, R = J). However, the decrease of the anisotropy of the mesogen leads to a strong diminution of the clearing temperature near to room temperature. The spontaneous polarization measurements were only possible at relatively high temperature, i.e. 80 °C, mainly because of the high viscosity of the materials at lower temperature. The highest values of Ps have been found to be around 140 nC cm^{-2}. The increase in generation number leads to a decrease in the value of Ps and to an increase in the switching time.

Table 6 Mesomorphic behavior of the carbosilane dendrimers bearing chiral mesogens (H, I and J)

G*n*	R = I	R = H	R = J
G1	G –5 SmC* 176 SmA 182 I	G –5 SmC* 175 I	G –17 SmC* 47 I
G2	G –5 SmC* 159 SmA 166 I	G –4 SmC* 167 I	G –17 SmC* 46 I
G3	G –5 SmC* 156 SmA 183 I	G –4 SmC* 158 I	G –17 SmC* 44 I
G4	G –4 Col_r 173 I	G – 4 Col_r 160 I	
G5	G –6 Col_r 178 I	G –6 Col_r 162 I	

The analogous dendrimers of higher generation (fourth and fifth, Table 6) exhibit only a rectangular columnar mesophase above the glass transition temperature, always about –5 °C [170]. According to the authors, each column consists of ellipsoidal disks of dendrimers as before, flattened towards the columnar axis in one direction and elongated perpendicular to that direction. The mesogenic groups are located entirely on the surface of the columns, while the inner part of the columns consists of the dendritic cores.

More recently, they also considered photosensitive dendrimers. The interest in such compounds is because of new opportunities provided by such systems in the production of various optical devices and the preparation of materials suitable for optical data storage. Moreover, the development of photoactive dendrimers capable of forming liquid-crystalline phases is particularly interesting, because a low viscosity of dendrimers is expected to induce a fast response of the so-called dendrimers to the action of an external field such as for example light irradiation (photosensitive materials). The first example concerns a liquid crystalline carbosilane dendrimer of first generation with azobenzene terminal groups (Fig. 18, R = E), exhibiting a smectic A mesophase (G –15 SmX 9 SmA 51 I) as for the dendrimers described above with various terminal mesogenic groups [171]. In this case, the azobenzene terminal moiety serves a dual function; on one hand, its rigid anisometric shape ensures the development of a mesomorphic state, and on the other hand, the presence of azo-chromophores ensures that the LC dendrimer is sensitive to light irradiation. It was shown that the $E - Z$ photopolymerization of the azobenzene groups proceeds both in solution and in film under UV irradiation. This process is reversible photochemically and thermally. In addition, it was shown that UV irradiation destroys the smectic ordering and gives rise to a transition to the isotropic liquid, because of the fact that the *Z*-isomer of an azobenzene moiety possesses a low anisometry. A very similar photochemical behavior is observed for the related non-mesomorphic azobenzene-containing dendrimers of higher generations (Fig. 18, R = F, G1, G3, and G5) [172].

The irradiation of the same dendrimer with a linearly polarized light (365 nm) results in an angular dependent E/Z photoisomerization, but the photo-orientation process was not observed practically. A quite different behavior is observed when the film of the dendrimer is irradiated with a linearly polarized green light (488 nm), where a well-pronounced linear dichroism is observed. However, the degree of photo-orientation of the azobenzene groups is rather low, the photo-induced parameter being much lower than the order parameter of the aligned smectic A phase [173]. In contrast, a strong effect is observed in different generations of carbosilane dendrimers where the terminal azobenzene moiety has a very slightly different chemical structure [172]. Under irradiation of the amorphous films by polarized light, a process of photo-orientation of azobenzene groups in the direction perpendicular to the direction of vector *E* of incident light is observed with three mean features.

First with UV radiation, the values of linear dichroism and of the order parameter do not depend on the generation number of the dendrimers. This indicates that a local surrounding of azobenzene groups in these films is similar independently of the molecular weight of the dendrimers. The second feature is the unusual behavior of the order parameter of the azobenzene groups under irradiation. After an increase at the beginning of the irradiation, the order parameter levels off and decreases down to zero, leading to a full degeneration of the orientational order of the system under prolonged light exposure. The third feature is the absence of photo-orientation processes under irradiation of the films by polarized light from an Ar-laser (488 nm).

Another carbosilane dendrimer of first generation containing terminal cinnamoyl groups (Fig. 18, R = G: G –28 SmA 58 I) which undergo *E*/*Z* photoisomerization was prepared according to a new synthetic approach, consisting of the synthesis of the dendrimer with terminal hydroxyl groups, followed by the coupling of 4-methoxycinnamoyl chloride [174]. In the liquid-crystalline phase under UV radiation, the dendrimer undergoes *E*/*Z* isomerization of the cinnamoyl groups, but also photo-cycloaddition leading to the formation of a three-dimensional network. These processes lead to a disordering effect and to an isothermal photo-induced smectic A to isotropic liquid phase transition.

As for the silane-containing dendrimers discussed above, some zeroth generation siloxysilanes were reported (Fig. 20). Again, these branched oligomers cannot be called dendrimers, but the interest of this study was the relationships between the core connectivity (N_C = 2, 3, and 4) and the mesomorphic

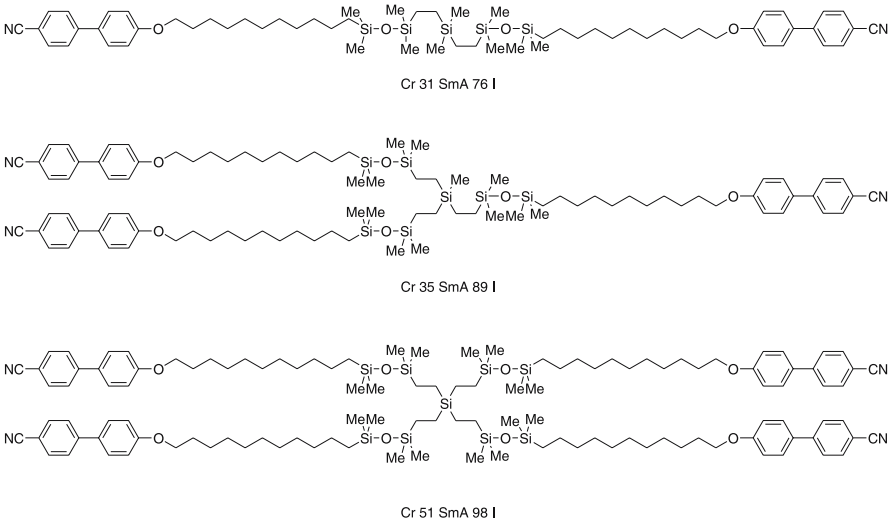

Fig. 20 Effect of the connectivity number of the core of some zeroth generation dendrimers

properties, able to bring useful information once extended to dendrimers. Thus, the linear dimer and the branched trimer and tetramer (Fig. 20) containing several cyanobiphenyl groups were prepared [175, 176]. As the number of mesogenic groups increases, the temperature range and the stability of the SmA phase increases quite steadily, but as expected the nature of the phase was not changed. Likely as the molecule becomes larger, the mesogenic arms have less freedom, and thus certain molecular conformations are more favored than others. As above, the smectic structures consist of a central silicon-containing layer, sandwiched between mesogenic groups, overlapping between layers. The related tetrakis(dimethylsilyl)silane functionalized by pro-mesogenic groups also gives rise to smectic phases [177].

3.1.2
Siloxane Dendrimers

There have been very few families of dendrimers built up around a pure siloxane core. One such dendrimer consisted of a dendritic methylsesquioxane matrix ($N_C = 3$, $N_B = 2$, Fig. 21) to which six terminal cholesteryl groups were attached via undecylene spacers [178]. This G1 compound exhibited a very broad temperature SmA phase (G –1.5 SmA 120 I). The molecules arrange in a single layer smectic phase with complete overlap of the cholesteryl mesogens separated by siloxane layers.

Cyanobiphenyl groups have been attached to tetrakis(dimethyloxy)siloxane to form a branched tetramer or tetrapede (Fig. 22, R = A, G0), which is similar to the siloxysilane derivative just discussed above (Fig. 20). Here again, whatever the spacer length, a smectic mesomorphism was detected, and a substantial increase of the mesophase stability and temperature range were observed as the aliphatic connector length increases; an additional unidentified phase was observed for $n = 9$, SmX (likely SmC) [179]. Lateral attachment of mesogenic groups onto such a tetravalent core led to the formation of a nematic phase above the SmC phase (Fig. 22, R = B, G0) [180].

In contrast to siloxanes, silsesquioxanes exist as ladder- or cage-type nanostructures, and are formed by complete hydrolytic condensation of their

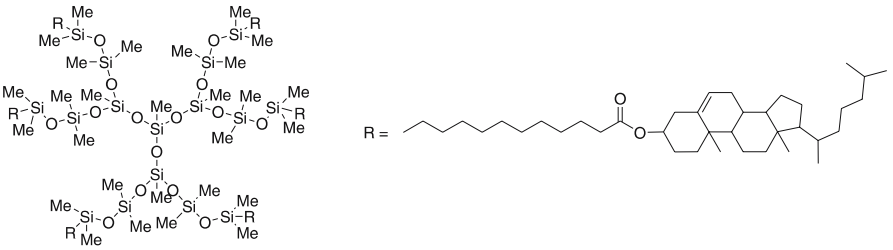

Fig. 21 Chemical structure of the dendritic methylsesquioxane matrix ($N_C = 3$, $N_B = 2$)

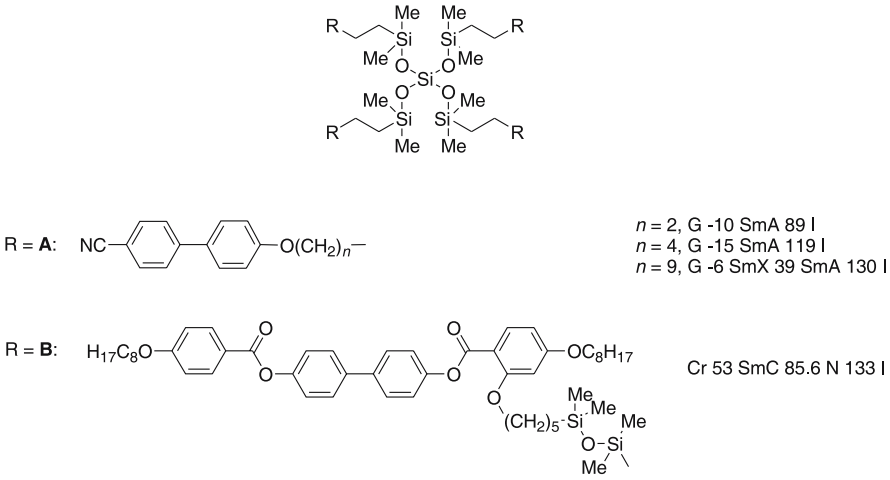

Fig. 22 Tetrakis(dimethyloxy)siloxane bearing four mesogenic groups with end-on and side-on attachment

trifunctional monomers Si_4O_6. Such 3D organosilicon cages are promising in the area of nanocomposites, as when suitably functionalized in the corners, they can be incorporated into organic systems to form hybrid inorganic–organic copolymers with novel properties [181]. The use of these silsesquioxane polyhedral frameworks as initiator cores for liquid crystal dendrimers has only been recently the focus of attention in accordance with the development of efficient syntheses as well as the improvement of the techniques of separation [182]. Such cage-like cores provide a useful central core because they possess several radial primary branches for derivatization, allowing the dense packing limit [183] to be reached at early generations. To start, several polyhedral liquid crystals have been prepared containing cubic cores such as the octa(hydrido)silsesquioxane and octa(dimethylsiloxy)octasilsesquioxane [184–187], and to a lesser extent the hexa(dimethylsiloxy)silsesquioxane [184] with a trigonal prismatic core and the deca(dimethylsiloxy)silsesquioxane [185] with a pentagonal prismatic core functionalized by eight, six, and ten mesogenic side groups (end-on), respectively (Fig. 23). These first generation polyhedral cage-like materials essentially display SmA and SmC phases often directly at the ambient and over broad temperature ranges; the exception are those cuboid materials giving rise to a nematic phase either after partial substitution of the cube [188–190], or by lateral attachment (side-on) of the mesogens [191].

As for the tetramers and dendrimers previously described, the mesogenic arms of the octasilsesquioxane-based materials can arrange parallel to one another; thus these supermolecules can pack together in layers to form a lamellar phase. Molecular simulations in the gas phase at absolute zero confirm this point of view and show that the minimized structure of the

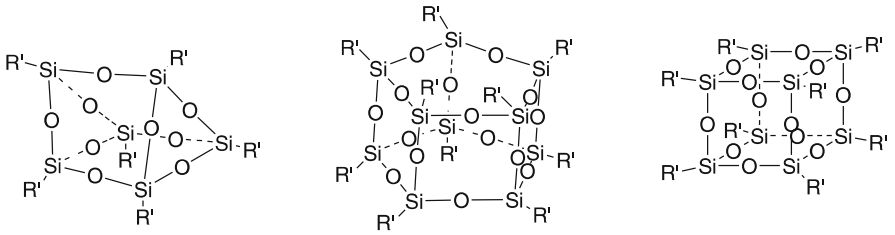

R' = R, R–SiMe$_2$O–, R is a mesogenic group

Fig. 23 Various polyhedral silsesquioxane backbone-based liquid crystals

cyanobiphenyl-substituted octasilsesquioxane is made by the cyanobiphenyl mesogenic arms packed together in a parallel arrangement thereby producing a supermolecular system that has a rod-like shape which is favorable to the formation of smectic A phases. Changing the chemical nature of the cyanobiphenyl groups by other mesogenic groups led to the induction of other smectic phases (eg., SmC) or to chiral phases (when chiral mesogens are attached).

Some dendrimers were eventually obtained by doubling the number of mesogenic groups fixed at each summit of the octa(dimethylsiloxy)octasilsesquioxane cage (Fig. 24). Branching was achieved by using either biforked carbosilane or malonate groups allowing for the preparation of materials containing 16 mesogenic units R (Fig. 24, R = B [192], D [175], F [57, 193] and G [175]). Substituted with cyanobiphenyl groups attached end-on, all first [186] and second generation [175, 192] systems yield to solely smectic phases, with in one case a decrease of the mesophase stability and temperature range on increasing the generation (Fig. 24, R = A → B), whereas the opposite was observed in the other case (Fig. 24, R = C → D). A more drastic change was, however, observed when the mesogens were laterally attached. Indeed, whereas the first generation system strongly promoted chiral nematic phases over broad temperature ranges, starting directly at the ambient [175, 194], the compound of the next generation appears to favor a columnar mesomorphism with both Col_r and Col_h phases being detected; the N* phase existed over a 6 °C temperature range only (Fig. 24, R = E → F). Moreover, in this study, the topology of mesogen attachment was found to strongly influence the mesomorphism (compare the isomeric compounds with R = F and G, Fig. 24). In order to understand the formation of such various mesophases, the authors proposed two extreme but feasible situations. One possibility results from the decoupling of the mesogens and the siloxane-cage thus acting independently, the cuboid core being surrounded by loosely packed mesogens. In the other possibility, the materials act as giant molecular systems, having either rod-like or disk-like shapes. To understand the forma-

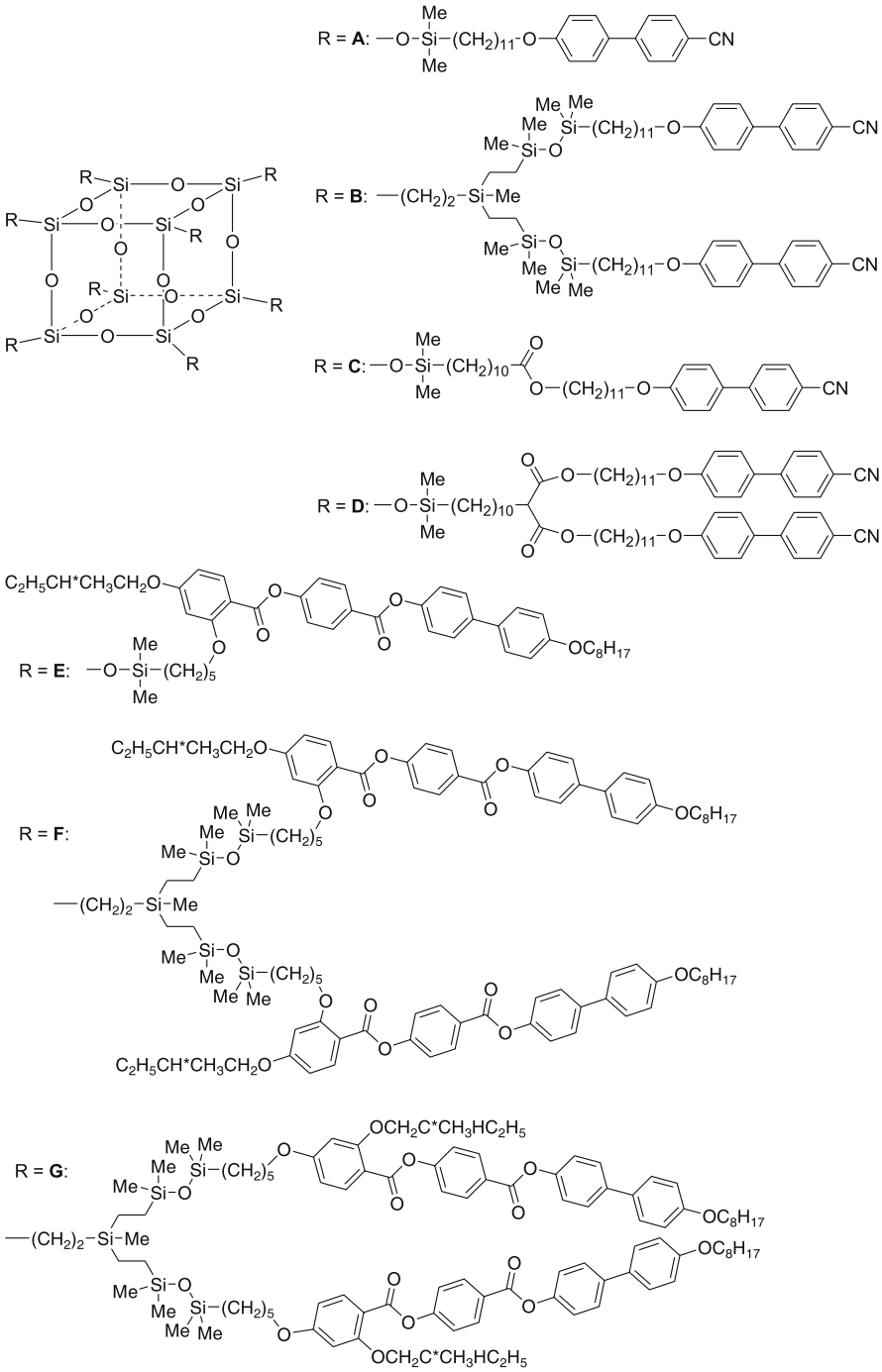

Fig. 24 Octa(dimethylsiloxy)octasilsesquioxane cage-like dendrimers

Table 7 Thermal behavior of the *R*-functionalized octa(dimethylsiloxy)octasilsesquioxane cage-like dendrimers

R	Transition temperatures
A	G –7 SmA 128.5 I
B	G –17.5 SmC 63 SmA 92 I
C	Cr 34.5 SmX 44 SmC 64 I
D	Cr 35 (SmC 30) SmA 96 I
E	G 24 N* 117 I
F	G 5.5 Col_r 30 Col_h 102 N* 108 I
G	Cr 133 SmC* 162 N* 165 I

tion of columnar mesophases, a "cotton-reel" model was proposed in which the dendrimer is assumed to have a cylindrical shape that has approximately the same height as its diameter. The long axes of the mesogenic units are roughly parallel to or slightly tilted with respect to the rotational axis that is normal to the cylinder. It seems that, contrary to the case of side-chain polysiloxane analogues where no columnar mesophase could be observed, the silsesquioxane core assists in the formation of the hexagonal and rectangular disordered structures, presumably through segregation of the siloxane cores from the mesogenic units in distinct columns.

3.1.3 Carbosilazane Dendrimers

Recently, a new dendritic system based on a carbosilazane core ($N_C = 3$, $N_B = 2$) with laterally attached mesogenic units (Fig. 25) [195–197] was synthesized. Depending on the mesogenic unit, these dendrimers exhibit a single, enantiotropic, room temperature nematic phase (Fig. 25, R = A), or in addition to the *N* phase, an additional SmC (G0, G1), or a Col phase (G2) between ca. 50 and 130 °C (Fig. 25, R = B) (Table 8). It is interesting to remark that although the molecular weight of these dendrimers doubles with each

Table 8 Mesomorphic behavior of the carbosilazane dendrimers

G*n*	Mesogen A	Mesogen B
G0	G –26 N 42 I	Cr 73 SmC 74.5 N 130.5 I
G1	G –23 N 40 I	Cr 58 SmC 74.5 N 130 I
G2	G –22 N 41 I	Cr 52 Col_x 73 N 126 I

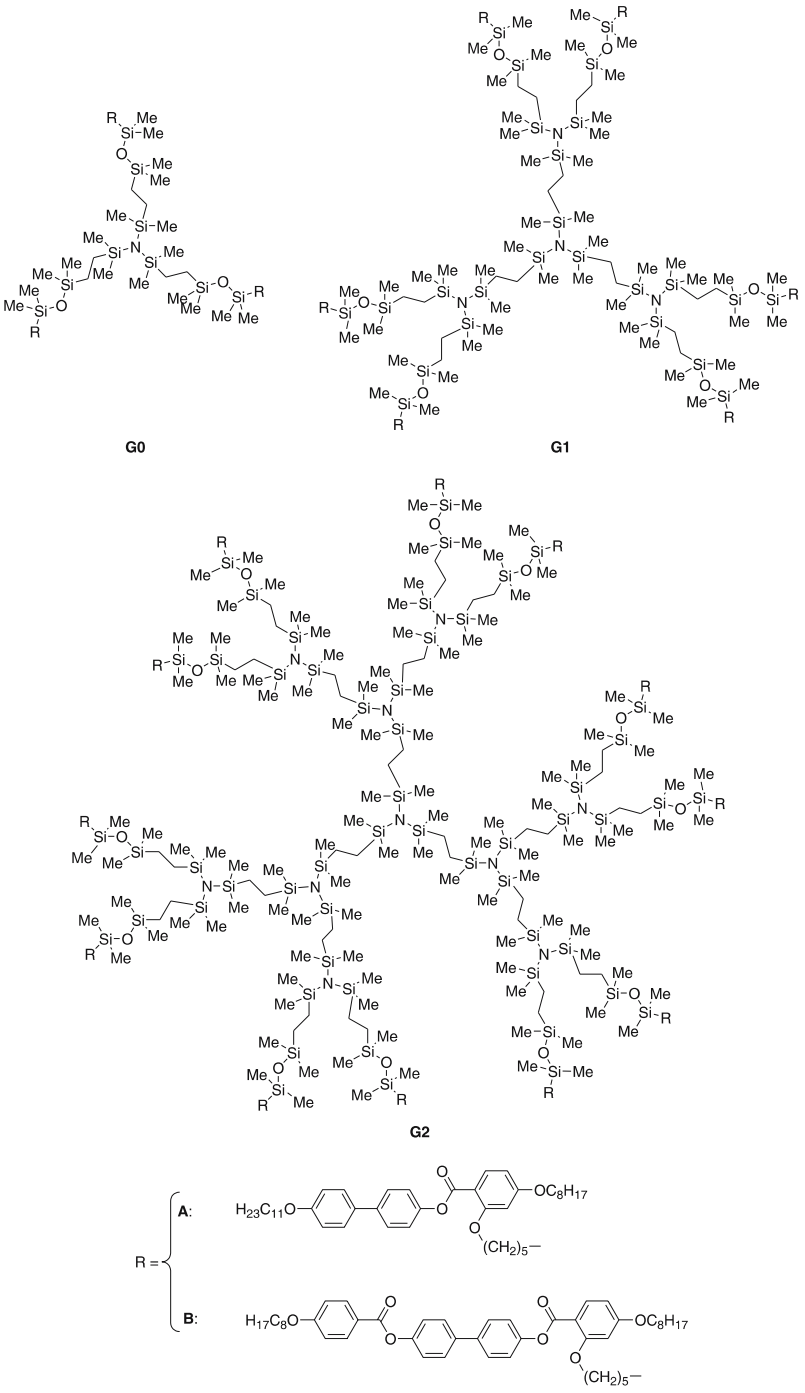

Fig. 25 Carbosilazane dendrimers

subsequent generation, the mesomorphic properties and transition temperatures are similar. This behavior has to be compared with the usual behavior of side-on liquid-crystalline polymers where a strong stabilization of the nematic phase is observed with increasing the degree of polymerization. This indicates that in the case of these nematic dendritic systems, the microphase separation of the silicon- and carbon-rich molecular moieties is not sufficiently pronounced on increasing generation to enhance the stability range of the mesophase. The orientational order and the dynamics of G0 in the nematic phase was analyzed by optical and dielectric studies, and confirmed the complete decoupling between the carbosilazane core and the mesogenic pendant groups [198].

3.2
Polydamidoamine and Polypropyleneimine Dendrimers

The dendritic motif of these systems is based on a tetravalent core ($N_C = 4$) and a binary branching point ($N_B = 2$) leading to 4, 8, 16, 32, 64 and 128 terminal mesogens from G0 up to G5 as was the case for some of the carbosilane dendrimers. These materials are built by the functionalization of the periphery of a pre-formed dendrimer poly(amidoamine) and poly(propyleneimine) (Fig. 26) with units (R) that promote the formation of supramolecular organizations giving rise to liquid crystal mesophases [53–57, 199]. For instance, the introduction of rod-like or disk-like units at the periphery of the original dendrimer leads to dendritic architectures that display liquid crystalline properties. The mesomorphic properties of these LC dendrimers (phase type, transition temperatures and thermodynamic stability) are determined by the enthalpy/entropy balance, the degree of chemical incompatibility of the constituent parts, their size and the structure of the (pro)mesogenic unit itself.

3.2.1
Structure-Property Relationships

In a pioneering work, Meijer et al. [200] described two series of PPI dendrimers functionalized with pentyloxy and decyloxy cyanobiphenyl mesogenic groups (Figs. 26 and 27, R = A and B). All the dendrimers with the pentyl spacer show liquid-crystalline phases above the glass transition temperature (between 10 and 30 °C) and below the isotropic liquid (ca. 130 °C). The dendrimers with the decyloxy spacer also exhibit liquid-crystalline behavior (between 100 °C and 114, 124 and 135 °C for G0, G2 and G4, respectively). X-ray diffraction experiments suggest that all the mesophases observed are smectic A in nature. One striking feature is the almost constant value of the layer spacing whatever the generation number for a given spacer. The authors explained the formation of smectic phases by a microphase separation between the mesogenic rigid units and the flexible dendritic skeleton.

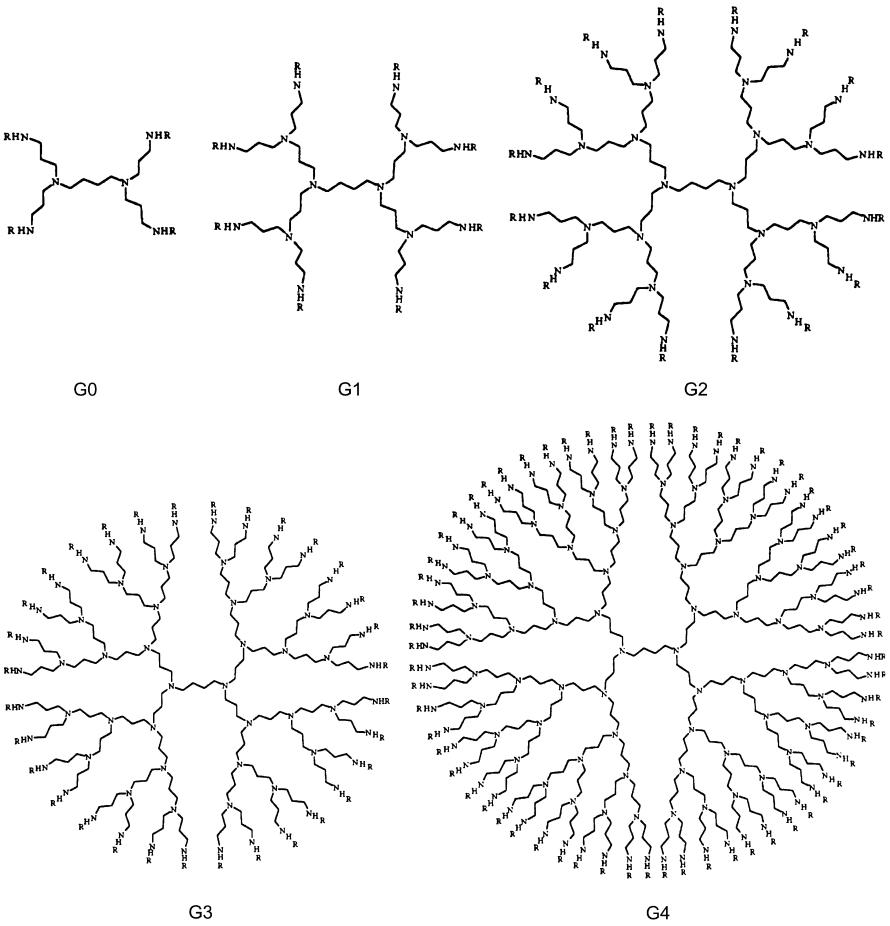

Fig. 26 Representation of the five generations of PPI dendrimers, functionalized by the R group. PAMAM dendrimers are closely structurally related: (i) the segment containing three methylene groups between two consecutive N junctions in the PPI dendrimer is replaced by the $-(CH_2)_2-CONH-(CH_2)_2-$ segment; (ii) the spacer between the two central N atoms is two methylene groups long (rather than four in the PPI)

The arrangement of the mesogenic end-groups is predominantly perpendicular with respect to the layer planes, with the dendritic cores located between these mesogenic sublayers. This orientation of the mesogenic groups is the same as for the low molecular weight cyanobiphenyl molecules which are well known to adopt antiparallel arrangements due to strong dipole–dipole interactions between the terminal cyano groups. The fact that the layer spacing does not vary as a function of the number of peripheral mesogenic units implies that the dendritic core should be in a pronounced distorted conformation, which seems to indicate an extension which occurs only in two

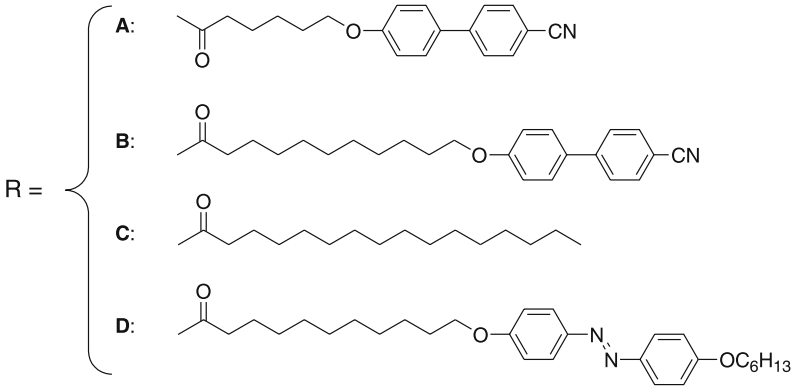

Fig. 27 Functional mesogenic groups used by Meijer

dimensions in a plane parallel to the smectic layers with increasing generation number.

The flexibility and thus the possibility of distortions of the PPI core was confirmed by the study of the self-assembly of amphiphilic dendrimers based on PPI dendrimers of five different generations with up to 64 end groups modified with long hydrophobic chains or azobenzene moieties (Fig. 27, R = C, D) [201, 202]. These molecules are able to arrange themselves in Langmuir monolayers in which the dendritic core is in contact with the water subphase and the alkyl chains are all pointing toward the air, forming a hydrophobic layer. Calculations showed that the shape of the dendritic core is distorted with an axial ratio of 1 : 2.5 for the first generations to approximately 1 : 8 for the three highest generations of dendrimers. Let us also remark that such dendrimers of the fourth generation (Fig. 27, R = B and C) were used as additives in a classical nematic matrix in order to develop electro-optical switches based on light scattering [203].

Note that this behavior is in marked contrast to that of the zeroth to the second generation of related PAMAM and PPI dendrimers ($N_C = 3$, $N_B = 2$) with 4′-cyanobiphenyl hydrogen glutarate that did not produce any mesomorphic behavior, except a lyotropic nematic phase in 80 wt % *N*,*N*′-dimethylformamide (DMF) solutions containing lithium bromide [204, 205].

Similarly, the functionalization of the G0, G1 and G2 PPI dendrimers with cholesteryl groups through carbamate linkage appeared to be the right strategy to induce mesomorphism in these systems [206]. They all exhibit a glass transition between 63 and 78 °C, and after a rich thermal history, all melt into birefringent fluids at ca. 149–162 °C, identified as a SmA phase. G0 then clears at 170 °C, whereas both G1 and G2 clear at 210 °C.

In another pioneering work, Lattermann et al. [207, 208] have also considered poly(propyleneimine) dendrimers (Fig. 26) of different generations but substituted with the non-mesogenic 3,4-bis(decyloxy)benzoate groups. Re-

markably, mesomorphic behavior was observed in the four first generation compounds (the G4 dendrimer was thought to be devoid of mesomorphism). Induction of mesophases was because of the chemical incompatibility between the dendritic core and the peripheral substituents. Contrary to the behavior of conventional non-mesomorphic and mesomorphic linear polymers the melting temperatures of these dendrimers decrease with increasing molar mass. The observed mesophases are all hexagonal columnar in nature, monotropic for G0, and enantiotropic for G1, G2 and G3 (G0: Cr 100 (Col_h 69) I; G1: Cr 100 Col_h 102 I; G2: Cr 76 Col_h 124 I; G3: Cr 60.5 Col_h 107.5 I). Recently, the G4 derivative was found to exhibit also a Col_h phase, and on cooling an additional monotropic cubic phase [209]. The lattice parameters of these hexagonal columnar phases did not correspond to the diameter of flat, two-dimensional, disk-like molecules, as determined from molecular modeling, even if a total interdigitation of the terminal aliphatic chains is assumed which is, on the other hand, not probable at all when taking into account the extremely dense packing of the alkyl chains in the outer shell. Thus, the formation of a columnar phase by a stacking of conventional flat disks can be excluded and the model of a spheroid (oblate or globular) structure of the dendrimer which can be accepted in solution is not valid in the liquid-crystalline phases. Consequently, the authors described the organization of the columnar phase of their dendrimers as resulting from the piling of three-dimensional cylindrical segments consisting of a polar core surrounded by an apolar shell. The corresponding thickness of the dendrimeric cylinder segments has been estimated to be around 10–12 Å, whereas their diameter has been determined by X-ray diffraction to be in the range of 40–50 Å. Such an anisotropic deformation of the polymeric structure is thought to be driven by the microphase separation in polar and apolar regions along the hexagonal columnar lattice. The G3 dendrimer bearing 4-decyloxybenzoate groups exhibits a transient SmA phase. Induction of lyotropic polymorphism was achieved in binary mixtures of some of these dendrimers bearing 4-decyloxybenzoate, 3,4-bis(decyloxy)benzoate and 3,4,5-tris(decyloxy)benzoate groups respectively with chloroform, cyclohexane, *n*-hexane, decane, decanol, THF, DMSO [209]. Some of these dendrimers were complexed with copper(II), and EPR spectroscopy was successfully applied for the determination of the structure and geometry of copper(II) coordination sites within the liquid crystalline dendrimers [210].

More recently, a systematic study of the properties of side-chain LC dendrimers has been undertaken on these PPI dendrimers and also on PAMAM systems by Serrano et al. [211]. In these dendrimers, the mesogenic group is connected to the dendritic scaffold by an imine linkage. In all cases, it was found that the enthalpic gain of the mesogenic units arranged as in a classical liquid crystalline mesophase dominates over the entropic tendency of the dendrimer core to adopt a globular isotropic conformation. The flexibility of the dendritic PAMAM and PPI cores allows the macromolecule to adopt

a microphase-separated molecular conformation which gives rise to various types of liquid crystalline supramolecular organizations. The chemical structure of the (pro)mesogenic units (shape, number of terminal alkoxy chains) determines the type of mesophase formed (nematic, lamellar, columnar).

LC dendrimers obtained by functionalization of the various generations of commercial amino-terminated PAMAM and PPI dendrimers with mesogenic units bearing one terminal alkoxy chain, namely 4-alkoxybenzoyloxysalicylaldehyde (Fig. 28, R = L_1), display as expected smectic mesophases and a nematic phase for G0 (Fig. 29) [212]. In this case and in agreement with the first suggestions of Meijer et al. [200], the molecular model proposed consists of cylinder-like shaped dendrimers in which the dendritic core occupies the central slab and the lateral mesogenic units are arranged parallel to each other, extending up and down from the molecular dendritic matrix (Fig. 30). This model explains the mesogenic behavior of these PAMAM and PPI derivatives since the dendrimeric supermolecules can be considered as large rods that would be ordered parallel to each other promoting the supramolecular order typical of smectic mesophases (Figs. 30 and 35).

In this type of supramolecular organization, the dendritic core deforms strongly with increasing generation number, since the layer spacing remains

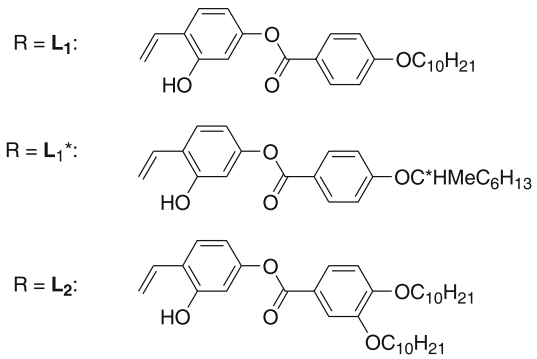

Fig. 28 Structure of the L_1, L_1* and L_2 mesogenic groups

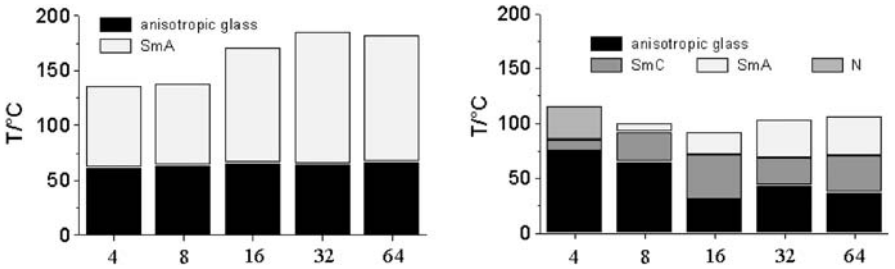

Fig. 29 Mesomorphism of PAMAM (*left*) and PPI (*right*) dendrimers functionalized by L_1

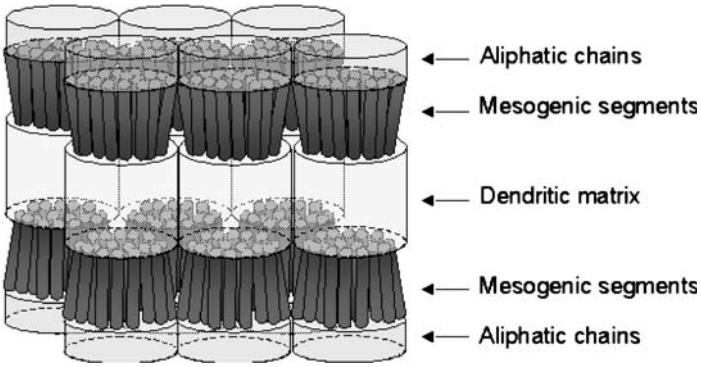

Fig. 30 Schematic representation of the molecular model for dendrimers with one-terminal-chain mesogenic units. Model for the Smectic A supramolecular organization (here G3-L_1 dendrimer)

around 4–5 nm whatever the molecular weight (Fig. 31). This deformation takes place in two dimensions in a plane parallel to the smectic layers. Systematic calculations performed from X-ray diffraction and volume data indicate that the diameter of the dendrimer cylinder increases from 1.3 nm up to 6 nm when going from the lowest generation up to the fourth one containing 64 peripheral mesogenic units. These results were further confirmed by MD calculations.

The same dendritic matrices functionalized with mesogenic units bearing two terminal alkoxy chains (3,4-dialkoxybenzoyloxysalicylaldehyde, Fig. 28, R = L_2) exhibit solely a hexagonal columnar mesophase (Fig. 32) [213, 214].

These dendrimers cannot be arranged in a molecular cylindrical model as that proposed for the smectic phases, since the cross-sectional area of the terminal chains is larger than the area occupied by the mesogenic units. In

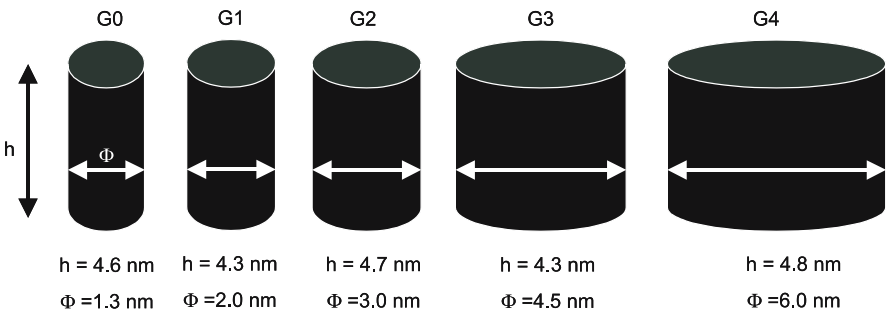

Fig. 31 Variation of the size of the elementary dendrimer cylinder as a function of generation number (G*n*). *Φ* is the diameter and *h* the height of the cylinder (i.e. lamellar periodicity)

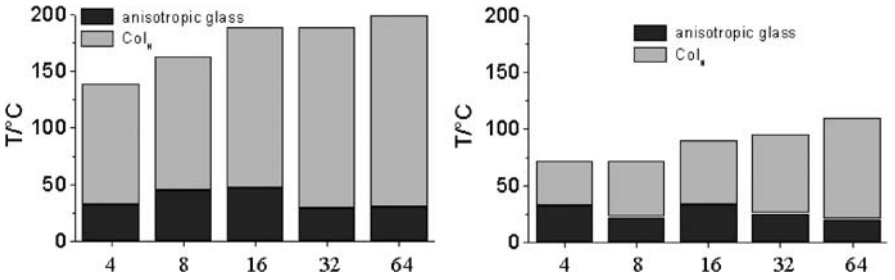

Fig. 32 Mesomorphism of PAMAM (*left*) and PPI (*right*) dendrimers functionalized by L_2

this case, the dendrimers tend to adopt a different and more stable conformation, so that the mesogenic units can be accommodated optimally. The most probable conformation consists of a disk-like radial arrangement that allows the filling of the space in three distinct regions corresponding to the central core, the rigid part of the mesogenic units and the terminal chains (Fig. 35). Therefore, the dendritic molecules fill up thick disks or disk equivalents: for the low generations, two or three molecules are needed to form a complete disk, and from the second generation onwards, just one molecule constitutes a disk, whose thickness depends on the generation number (Fig. 33). These molecular disks self-assemble into supramolecular cylindrical columns which are arranged according to a hexagonal symmetry.

This proposed model was further justified by MD simulation which reproduces the paving of the hexagonal lattice of the dendrimers in a flattened wedge conformation. The result of the calculation evidenced a good filling of the available volume. An enhancement of the micro-segregation over the entire simulation experiment time was also observed, contributing to the stabilization of the structure. Furthermore, the compensation of the molecular

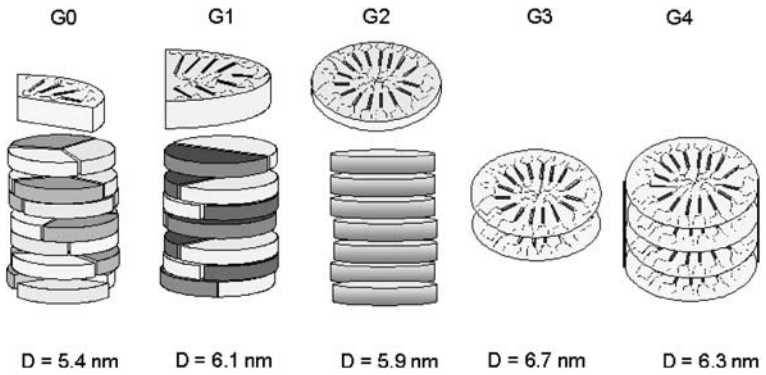

Fig. 33 Schematic representation of the molecular model for the dendrimers bearing the L_2 mesogenic unit. Model for the columnar supramolecular organization (*D*: intercolumnar distance)

areas at the dendritic/mesogen interfaces implies the tilt of the peripheral rigid segments with respect to the radial directions (Fig. 34).

It is interesting to note that the diameter of the columns does not vary significantly with the generation number. Indeed, it varies irregularly between 5.3 nm and 6.7 nm, despite the fact that the molecular weight of one single dendrimer varies between 2660 up to 48 500 Daltons when going from the lowest generation up to the fourth generation. In other words, this clearly indicates that the dendritic core deforms strongly in one main direction corresponding to that of the columnar axis, whereas the mesogenic units are arranged radially (Fig. 35) to ensure efficient lateral interactions within and between columnar slices. Similarly to the case of lamellar phases described above, systematic calculations performed from XRD and volume data indicate

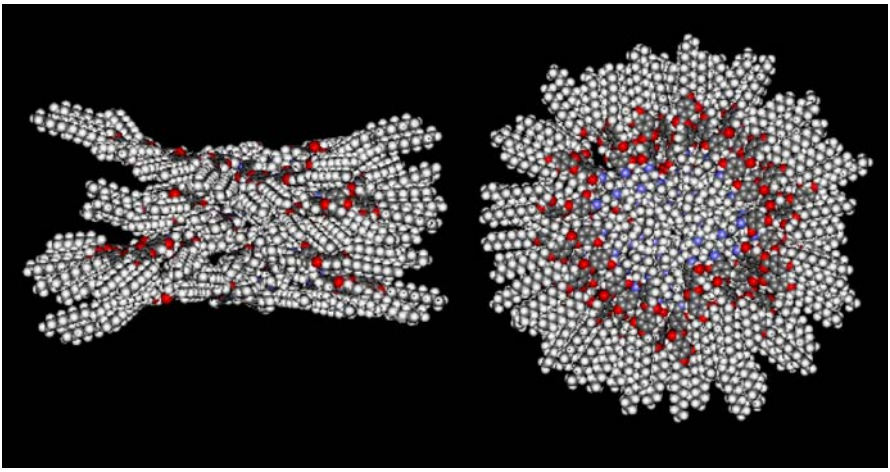

Fig. 34 Modelization of the self-organization of the G4-L_2 dendrimer into columns

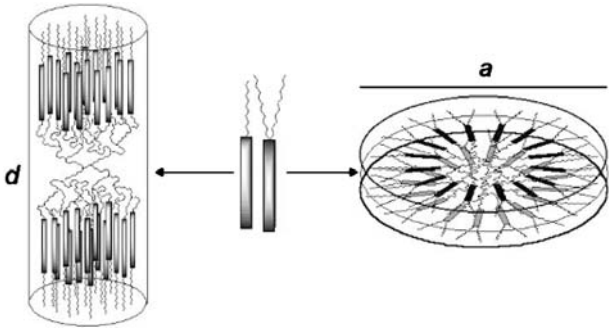

Fig. 35 Relationship between dendritic core deformation and mesogen type and the conformation of the side-chain liquid crystalline dendrimers

that the highest generation dendrimer (containing 64 peripheral mesogenic groups) can fill the equivalent of a disk 1.9 nm thick, whereas the second generation dendrimer containing 16 peripheral mesogenic groups alone fills a disk 0.5 nm thick. It has been found that, whatever the generation, there is on average 16 mesogenic units over 0.5 nm along the columnar axes.

To conclude this part, let us emphasize that both lamellar and columnar mesophases can be obtained with dendrimers, even with those of high molecular weight, the stability of the corresponding phases being ensured by lateral interactions between the (pro)mesogenic units and by a significant deformation of the conformation of the dendritic core. The difference in the symmetry of the mesophase is only related to a small difference in the molecular design of the peripheral mesogenic groups. Those with only one terminal end-chain produce lamellar mesophases by the lateral expansion of the dendritic matrix within the layer (prolate deformation), whereas those with two terminal end-chains lead to columnar mesophases by stretching of the matrix along the columnar axis (oblate deformation) (Fig. 35). Let us point out also that the dimensions (a few nanometers) of the elementary dendrimer cylinder can be tuned according to the generation number, but the fundamental dimensions of the mesophase structure (layer spacing for the lamellar phases and intercolumnar distance for the columnar phases) do not depend on the size of the dendrimer itself.

In the field of liquid crystals, it is well known that many of the materials displaying a columnar mesophase are constituted of disk-like (discotic) molecules, but very little attention has been paid to LC dendrimers containing discotic mesogenic units, for example based on hexa-substituted derivatives of triphenylene. The latter are also of special interest because of their photoconductive properties. A series of PPI-based dendrimers that incorporate discotic triphenylene mesogenic units (with decyloxy side-chains) at their periphery has been prepared and their properties investigated [215]. All the dendrimers except that of the zeroth generation (Cr 61 Col_r 79 I) show a hexagonal columnar mesophase over a wide temperature range (between ca. 40–50 °C and 110–115 °C). The XRD characterization of this mesophase reveals that its parameters are, here also, practically independent of the dendritic generation considered. In the model proposed by the authors, the flexible dendritic part adopts a cylindrical arrangement with the four generations having a similar diameter but their height increasing. Once more, the interactions between the mesogenic units determine the supramolecular structure and the dendritic central core adopts the elongated conformation necessary to allow this molecular arrangement.

Side-chain LC dendrimers exhibiting the nematic mesophase, which is the most disordered liquid crystalline phase, can also be achieved by the appropriate choice of the mesogenic unit(s) attached to the dendrimer central core. For example, side-chain PPI-derived dendrimers containing mesogenic units of type L_1 (Fig. 28) but with short terminal alkoxy chains (ethoxy, butoxy

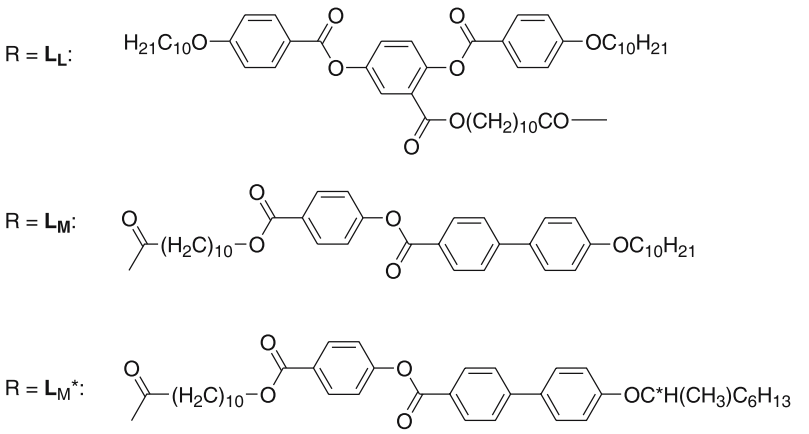

Fig. 36 Structure of the mesogenic groups for end-on and side-on dendrimers

and pentoxy) or mesogenic units attached laterally (Fig. 36, L_L, amide linkage), have been prepared in a similar approach to that employed in side-chain liquid crystal polymers [216, 217]. In this case, the side-by-side molecular arrangement typical of lamellar phases is disfavored, thus promoting a nematic order. For the end-on dendrimers, the clearing temperature range decreases with increasing generation number G0 to G3 (from ca. 120 to 70–80 °C), and then increases for G4 (to ca. 100 °C). No influence of the chain length was detected. Typically, the average temperature range of the nematic phase for the latter compounds phase remains almost generation independent (between ca. 25–30 °C and 70–80 °C), and decreases for the G4 dendrimer (G 14 N 53 I). Nematic or lamellar phases (SmC and SmA) have also been obtained with the third generation of PPI liquid-crystalline co-dendrimers containing various proportions of two types of pro-mesogenic units, i.e. one being laterally attached (Fig. 36, L_L) and one terminally attached (Fig. 36, L_M) [218] through an amide linkage. Decreasing the proportion of the side-on mesogens with respect to the end-on one contributes rapidly to the suppression of the nematic phase at the expense of the smectic phases (SmA and SmC). In these cases, ^{2}D NMR experiments carried out on one of these co-dendrimers have proved that the symmetry of the nematic phase is uniaxial, in contrast to the biaxial nematic phase observed for some side-on-polymers [219].

As described above, the presence of one or two terminal alkoxy chains in the chemical architecture of the mesogenic units induces a drastic modification in the thermotropic behavior of the dendrimer (from lamellar to columnar structures). The introduction of both types of mesogenic units (Fig. 28, L_1 and L_2) in different concentrations within the same dendritic structure, i.e. random co-dendrimers, should present a greater possibility of tuning the symmetry of the mesophase exhibited by the material. A series of such G3 co-dendrimers was synthesized, in which both types of mesogenic

units were introduced in various proportions [220]. The study of the phase diagram (Fig. 37) obtained for these PAMAM co-dendrimers revealed that, for intermediate compositions, two other mesophases (SmC and Col_r) appeared between the smectic A and the hexagonal columnar phases of the two homodendrimers, respectively. Co-dendrimers with a small content of the two-terminal-chain comonomer exhibit a smectic C phase below the smectic A phase. The appearance of the tilted smectic mesophase is a consequence of the increase in the total number of terminal chains for a constant size of the pre-dendritic matrix. The tilt of the molecule affords a larger area of the ideal cylinder base, which allows the accommodation of all the terminal chains (Fig. 38). Larger contents of the two-terminal-chain comonomer in the co-dendrimers favor the occurrence of a rectangular columnar mesophase. As the number of terminal chains increases, their accommodation within a cylindrical rod-like structure becomes unlikely. This elementary dendritic cylinder is deformed into some kind of parallelepiped structure, which in turn promotes the existence of a rectangular columnar mesophase (Fig. 38).

Thus, depending upon the relative concentration of each of the two monomers, orthogonal and/or tilted lamellar mesophases, or else rectangular and/or hexagonal mesophases can be obtained.

The molecular dynamics of the co-dendrimer G3-$(L_1)_{16}$ – $(L_2)_{16}$ in its two phases, i.e. a low temperature Col_r phase and a high temperature SmA phase, was studied by ^1H NMR relaxation [221]. In the high frequency range, the motions appear similar in both phases and are ascribed to reorientations of the dendritic segments, whereas in the low frequency ranges, notable differences in the dynamics between the columnar and layered phases were observed, and were discussed in terms of elastic deformations of the columns and layer undulations.

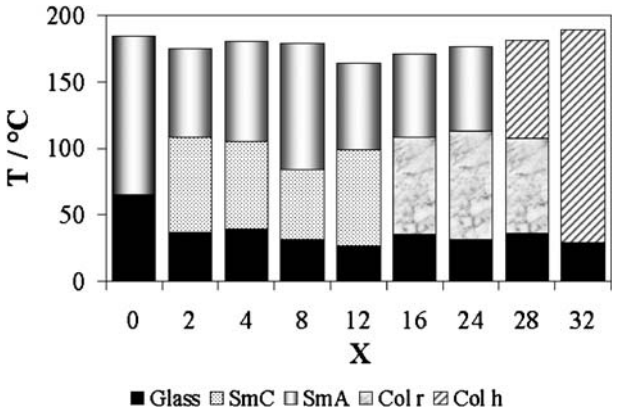

Fig. 37 Phase diagram of the co-dendrimer G3-$(L_1)_{1-x}$-$(L_2)_x$ (X: proportion of L_2 mesogens)

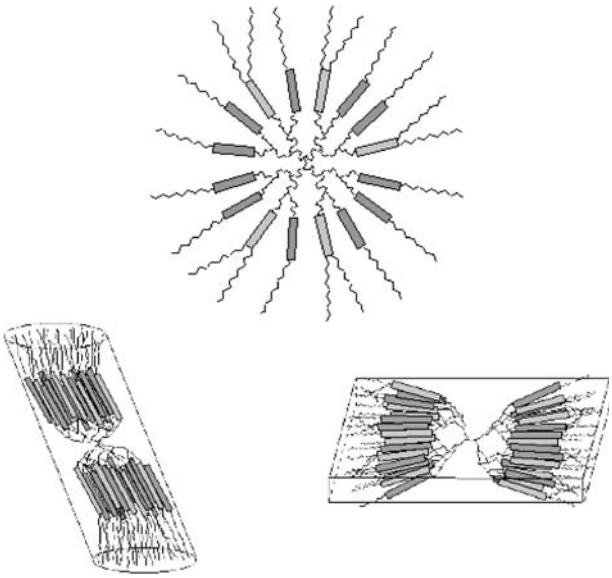

Fig. 38 Schematic representation of the molecular model for codendrimers with one- and two-terminal-chain mesogenic units (SmC and rectangular columnar phases)

As mentioned above, other PPI co-dendrimers have been obtained by mixing in their structures terminal- and laterally attached pro-mesogenic units using a dendritic matrix bearing 32 terminal amine groups [218]. It is shown that there is a gradual evolution from a nematic phase to an orthogonal lamellar phase through the appearance of a tilted smectic C phase (not present in the homodendrimers) when increasing the proportion of terminally attached mesogenic units. These studies confirm that the mesomorphic behavior of such block co-dendrimers could be modulated and controlled by a simple modification of the ratio of two pro-mesogenic units present around the dendritic core.

3.2.2
Tuning the Dimensions of the Nano-Dendritic Object

In order to further investigate the influence of the structure of the mesogenic units on the mesomorphic behavior of the dendrimers, bulky units have been introduced at the periphery of the third and fourth generations of amino-terminated PAMAM and PPI (Fig. 39, L_3, L_6, L_9), with the aim of achieving cubic mesophases, since the increased volume around the dendritic core could in principle force the dendrimer to adopt a globular conformation [199, 222].

However, all the dendrimers prepared showed only a hexagonal columnar mesophase, even those bearing the largest mesogenic units containing

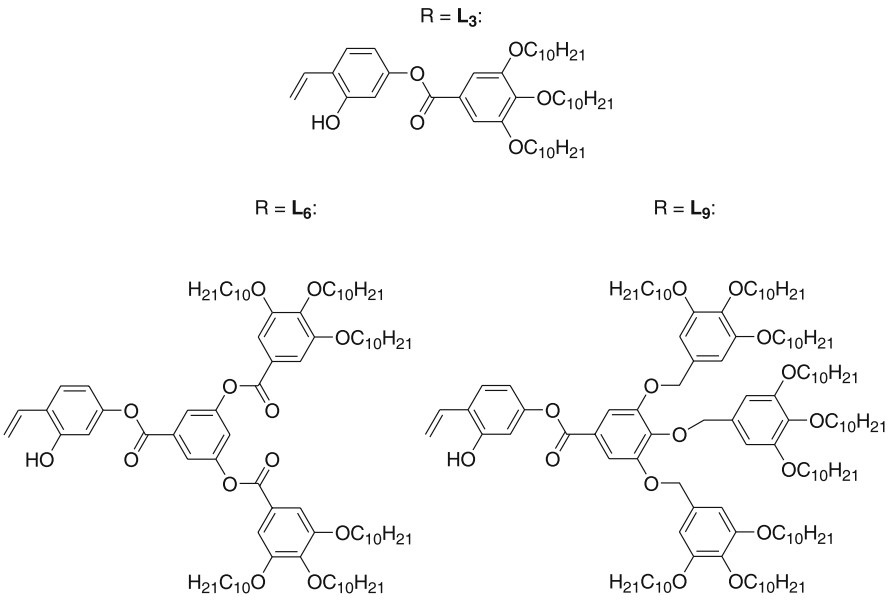

Fig. 39 Chemical structure of the bulky mesogenic units

nine terminal chains each. A model of organization of these dendritic supermolecules, deduced from X-ray diffraction results and theoretical calculations made thereof, was proposed. This molecular model implies a cylinder, whose inner part is occupied by the dendritic core and the bulky mesogenic units spreading around it, as shown in Fig. 40.

The dendritic core adopts an extended conformation which is possible due to the great flexibility (conformational freedom) of the PAMAM and PPI skeletons. In this way, the molecular model of thick disks proposed for the LC dendrimers with two-terminal chain mesogenic units is transformed into a model consisting of a long cylinder, which is the result of the axial elonga-

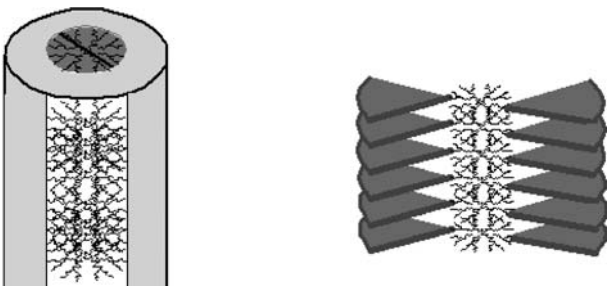

Fig. 40 Molecular model for the LC dendrimers with bulky mesogenic units

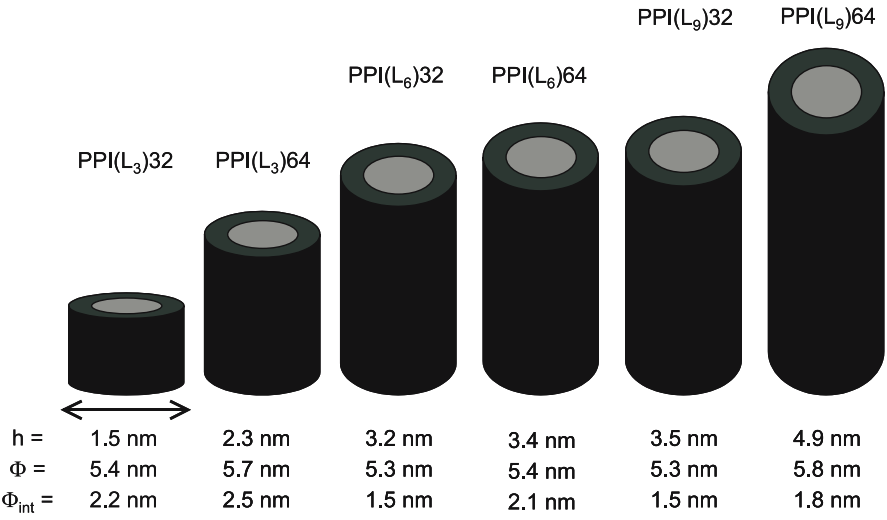

Fig. 41 Variation of the size of the elementary third and fourth generations dendrimer cylinder with bulky mesogenic groups. L_3, L_6 and L_9 are for the bulky groups containing 3, 6 and 9 terminal aliphatic chains, respectively. *h* is the height of the cylinder, Φ the diameter, and Φ_{int} is the internal diameter corresponding to the dendritic part only

tion of the oblate structure caused by the extended conformation adopted by the dendritic core in order to accommodate the bulky units around it. X-ray diffraction investigations show that the diameter of the cylinder is about the same whatever the generation and the bulky peripheral group (Fig. 41). But more detailed calculations indicate that the internal diameter of the cylinder corresponding to the dendritic core decreases when the bulkiness of the peripheral group increases, for example going from 2.5 down to 1.8 nm in the case of the fourth generation dendrimers, in agreement with an additional elongation of 2.6 nm of the dendritic core along the columnar axis. This example also emphasizes another way to tune the dimensions of the nano-dendritic objects by molecular engineering involving bulky peripheral groups. Note that other PPI dendrimers of the zeroth, second and fourth generation functionalized in the termini by anisotropic oligo(*p*-phenylene vinylene) units bearing three terminal dodecyloxy chains and lateral methylbutoxy side chains were reported to exhibit a lamellar mesomorphism between ca. 50–70 (melting) and 160–180 °C (clearing) [223].

3.2.3 Theoretical Aspects

A theoretical approach to identify the key topological and statistical ingredients for the description of the self-organization and of the mesomorphic behavior of such dendritic supermolecules has been developed [224–226].

The model is based on convex deformable hard body supermolecules that can interconvert between spherical and cylindrical states. In other words, the dendrimer is considered to be a deformable object that can exist in a certain number of conformational states governed by the intra-dendrimer interactions. Then, these objects are assumed to interact with one another as a whole in a way that is dictated by inter-dendrimer segmental interactions. It is shown that isotropic, nematic, smectic and columnar phases can be generated and that there is a strong thermodynamic selection of conformations according to their packing efficiency in each of the mesomorphic phases. In this model, the smectic and columnar phases are mainly stabilized by the anisometry of the global shape of the predominant supermolecular conformations. A second theoretical approach has been to consider directly the interactions among the dendritic segments in a pair-wise manner and to impose on the intra-dendritic pairs the configurational constraints dictated by their connectivity within the same dendrimer [227]. With this approach, the ensemble of dendrimers reduces to an ensemble of mesogenic dimers with spacers of different lengths corresponding to the different branch paths within the dendritic scaffold. This segmental approach is more suitable for the description of the mesomorphic properties that are sensitive to the ordering and to the motion of dendritic segments rather than of the dendrimer as a whole.

3.2.4 Chiral Properties

In order to get ferroelectric properties, a series of chiral PPI co-dendrimers bearing chiral and achiral terminal chains has been investigated [228]. Such an approach has been chosen to mimic the situation occurring in classical mixtures of low molecular weight liquid crystals using chiral dopants. It is shown that the presence of small quantities of the chiral mesogen unit (the chiral monomer is L_1* and the co-monomer is L_1; Fig. 28) favors the formation of the smectic C* ferroelectric phase and that this mesophase disappears only when the ratio of chiral terminal groups is larger than 75%. The stability of this smectic C* phase increases from the zeroth to the fourth generation of co-dendrimers. Unfortunately, ferroelectric behavior is revealed to be very poor. Switching was detected only in the small dendrimers (G0 and G1) and in co-dendrimers bearing a small number of chiral mesogenic units. Similarly, a third generation of PPI liquid-crystalline co-dendrimers containing various proportions of two types of pro-mesogenic units (Fig. 36; L_L, L_M^*) show a modulated SmC (or modulated SmA) and a N* (or N) phase for low contents of L_M^*, a SmC* for a ratio 40 : 60 of L_L/L_M^*, and a single SmA phase for a higher content of L_M^* [218].

Four PPI dendrimers of the zeroth and first generations containing bent-core molecules at the periphery were recently reported (Fig. 42, Table 9) [229]. These dendrimers exhibit a relatively high viscosity which is unfavorable for

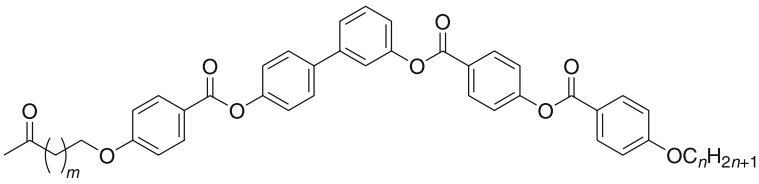

R = **B1** (n = 12, m = 3), **B2** (n = 16, m = 9)

Fig. 42 Structure of the bent mesogens

Table 9 Mesomorphic behavior of the dendrimers bearing bent-mesogens

Gn	Mesogen B1	Mesogen B2
G0	I 151 Col_r 104 Cr	I 144 SmX 113 Cr
G1	I 162 Col_r 120 Cr	I 149 SmX 122 Cr

detailed investigation of the physical properties. No switching and thus ferroelectric behavior could be observed for any of the dendrimers.

3.2.5 Amphiphilic PPI Dendrimers

The alkylation of PPI dendrimers of the third and fourth generation has been undertaken by reaction of all the amino end groups of the parent dendrimers with *n*-dodecyl isocyanate. While mesomorphism was not induced in these compounds, their corresponding protonated homologues were shown to exhibit thermotropic cubic phases of $Ia\bar{3}d$ symmetry [230]. This is attributed to the enhancement of the amphiphilic character and the subsequent "nanophase" segregation of the two incompatible parts. The proposed structure consists of 24 nearly spherical, multicationic dendrimeric entities located in the axes constituting the skeletal graph of the gyroid, while the aliphatic chains are located on each side of the minimal surface [231–234].

G0 to G4 generation amphiphilic PPI dendrimers with facial amphiphilic carboxylic acids were prepared (Fig. 43). Some of these ionic systems show a sequence with unconventional liquid crystalline phases, depending on the dendrimer generation, the structure of the facial amphiphilic acid and the external conditions (temperature and concentration) [235]. For example, different square columnar phases, as well as a channelled layered phase, i.e. a mesophase combining a layer structure with a hexagonal organization of columns have been observed (Table 10). The supramolecular dendrimers thus formed represent a new class of mesomorphic materials, whose properties can be tailored by the dendrimer generation and dendrimer-to-mesogen ratio. A single SmA phase is formed when there is no spacer (A0)

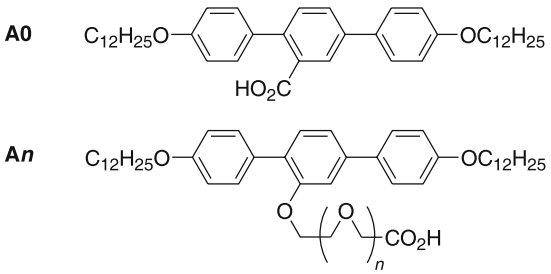

Fig. 43 Structure of the facial amphiphilic mesogenic side-groups A0 and A*n*

Table 10 Mesomorphism of the facial mesogen-containing dendrimers

G*n*	A0	A3	A4
G0	SmA 155 I	Col_h 87 I	Col_{squ} 109 I [a]
G1	SmA 159 I	Col^a_{squ} 116 I	Col_{squ}-*p4mm* 123 I
G2	SmA 165 I	Col^a_{squ} 125 I	Col_{squ}-*p4mm* 124 I
G3	SmA 167 I	Col^a_{squ} 124 I	
G4		Col^a_{squ} 117 I	Col_{squ}-*p4mm* 116 I

[a] Two co-existing columnar mesophases Col_{squ} with *p4mm* and *p4gm* symmetries

or when the amphiphilic spacer is short (A2) between the terphenylene and the dendrimer, whereas for the other materials with A3 and A4, solely Col_h and Col_{squ} phases were observed (Table 10). A dimorphism of two different columnar phases, with two different square 2D lattices (*p4mm* and *p4gm*), was observed for all the blends of the G*n*-A3 series, except for G0-A3, which leads to a Col_h phase only. As for the blends G*n*-A4, exclusively the *p4mm* square columnar phase was found for all generations except the G0 which showed the two square columnar phases (Table 10).

Ionic liquid crystals derived from the protonation of PPI dendrimers with a cholesteryl-based carboxylic acid led to materials exhibiting mesomorphic properties, which are dictated by the degree of protonation of primary amino groups [236]. G0 to G4 systems exhibit a glass transition at ca. 36–38 °C. At higher temperatures, they become birefringent fluids, followed by another transition at ca. 90–110 °C into a second mesophase. Both mesophases were identified as SmC* and SmA phases, respectively. They all decompose before clearing at 150 °C, the onset of the degradation. The mesophase stability was considerably reduced compared to the covalent systems [206].

Non-covalent thermotropic liquid crystal dendritic systems have been achieved recently by converting the amphiphilic surface of the dendrimers ($-NH_2$) into a hydrophobic shell (alkanoate chains). Tomalia et al. reported on the "non-aqueous lyotropic" behavior of supramolecular complexes re-

Table 11 Mesomorphism of the ionic dendrimers

G*n*	[PPI-H^+]·[$^-O_2CC_{17}H_{35}$]	[PPI-H^+]·[$^-O_2CC_{13}H_{27}$]	[PAMAM-H^+]·[$^-O_2CC_{17}H_{35}$]
G0	Cr 67 SmA 116 I	Cr 27 SmA 116 I	Cr 55 SmA 99 I
G1	Cr 55 SmA 134 I	Cr 28 SmA 125 I	Cr 71 SmA 130 I
G2	Cr 56 SmA 131 I	Cr 34 SmA 127 I	Cr 63 SmA 126 I
G3	Cr 48 SmA 127 I	Cr 11 SmA 73 I	Cr 53 SmA 130 I
G4	Cr 68 Col_{tet} 102 I	Cr 5 Col_h 78 I	Cr 62 SmA 133 I
G5			Cr 63 SmA 140 I

sulting from ionic interactions between the second generation of a PPI dendrimer ($N_C = 3$, $N_B = 2$, $Z = 12$) terminated with amino groups and octanoic acid [237]. The presence of a lamellar phase was detected by polarized light optical microscopy and X-ray diffraction for acid/dendrimer molecular ratios of 30 to 13. Similar ionic liquid crystal systems of PAMAM and PPI dendrimers (from G0 to G4) and long chain carboxylates were obtained recently [238–240]. All of the dendrimers, in approximately a 1 : 1 stoichiometry (primary amine groups : carboxylic acid groups) show lamellar phases (G0-G5) [238, 240], except for the highest generations of PPI dendrimers (G4) which exhibit columnar phases with hexagonal or tetragonal bidimensional symmetries, namely Col_h or Col_{tet} phases, depending on chain length (Table 11). It is also interesting to remark that such ionic dendrimers do not have aromatic mesogenic groups in their structure, which indicates that the ionic interactions play a key role in the formation of these thermotropic mesomorphic phases. For the PAMAM G3 dendrimer, the increase of stearic acid ratio with respect to primary amine groups leads to the transformation of the mesophases from SmA (for 0.11–1.5 ratio) to a columnar phase (for an acid/amine ratio of 2.33) [239].

PPI dendrimers (G1 to G4) functionalized on the periphery by pyridyl moieties (obtained by reacting 3-pyridyl isothiocyanate with the $-NH_2$ endgroups) form hydrogen-bonding supramolecular complexes when mixed with 3-cholesteryloxycarbonyl-propanoic acids [241]. The complexes are birefringent glasses at room temperature. Above the glass transition temperature (ca. 49–57 °C), they turned into viscous birefringent fluids, characterized as SmA phases. In all cases the isotropization could be reached, as the complexes decomposed at ca. 140 °C.

3.2.6 Photoactive PPI Dendrimers

In view of obtaining photo-responsive surfaces, photo-active Langmuir–Blodgett films based on the fourth generation PPI dendrimer, randomly sub-

stituted with palmitoyl- and azobenzene-containing alkyl chains, have been prepared (Fig. 27, R = C and D). The co-dendrimer thus obtained has a random functionalized shell with 32 functionalities on average [201, 202, 242]. This partial modification of the dendritic surface gives rise to materials which can be processed into stable Langmuir and Langmuir–Blodgett films where the dendrimer anchors the azobenzene units and hence prevents microphase separation of the azobenzene moieties, thereby facilitating reversible *cis-trans* isomerization.

In many of the PPI dendrimers described above, the mesogens are linked to the dendritic scaffold through an amide linkage. There is only one report concerning the same type of dendrimers coupled with rigid mesogens by ester linkages which show also smectic phases. These are obtained by using the zeroth and first generation PPI dendrimers and ω-(4′-cyanobiphenyloxy)alkyl acrylate [243, 244]. They all show ordered smectic phases (probably SmE) between ca. –10 °C and 90 °C. The advantage of such an approach is to cover the dendritic scaffold with a number of mesogen groups that is twice larger for identical generation than in the cases discussed above, i.e. 8, 16, 32, 64 and 128 groups for G0 to G4 (as in Fig. 26, but the NHR terminal functionality is replaced by a NR_2 functional end). A whole family of such dendrimers was synthesized, bearing peripheral 2,3-difluorobiphenyl mesogenic units [245]. Whereas the SmE-to-SmA phase transition is generation-independent (around 50 °C), a net enhancement of the mesophase stability is observed with generation (the clearing temperature increases linearly from 70 to 95 °C from G0 to G4).

3.3
Dendrimers with Polyether Dendritic Cores

Third-generation amphiphilic monodendrons extended by linear polyethylene oxide chains have shown to self-assemble into various supramolecular architectures. Thus, the AB-block copolymers with $n = 31$ (Fig. 44) melted at 63 °C from a crystalline lamellar into a $Pm\bar{3}n$ micellar cubic phase (clearing at 93 °C), whereas increasing the polyethylene oxide chain ($n = 96$) modifies substantially the phase sequence as a function of temperature: Cr 63 Col_h 114 Cub-$Ia\bar{3}d$ 190 lamellar 226 I; the cubic phase is likely continuous [246]. With an intermediate polyethylene oxide chain length ($n = 62$), the AB-block material melts from a crystalline lamellar phase into a Col_h phase (clearing at 175 °C) [247]. The dendrons themselves are not mesomorphic [248]. Here, mesomorphism clearly results from microphase segregation between the chemically incompatible parts, namely hydrophobic dendrons and hydrophilic linear polymer. Ionic conductivity of ion-doped samples was monitored in these different phases. It appears that it is strongly correlated to the mesophase behavior. Thus, charge transport has been measured in a nanostructured material in which the conducting medium is confined to either mi-

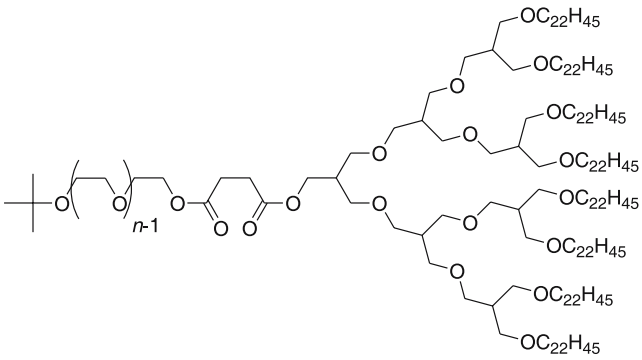

Fig. 44 Structure of the extended amphiphilic monodendrons with a polyether core

celles, infinite cylinders, lamellae or even bicontinuous networks throughout the entire macroscopic sample. This can be of importance in devices such as ion conductors, photovoltaic or electroluminescent cells.

Other dendritic frameworks were used, but did not always yield to mesomorphic systems. For instance, the polyalkylarylether dendrimers functionalized by azobenzene mesogens failed to show any liquid crystalline property despite the mesomorphic side-group promoter [249].

3.4
Dendrimers with Polyester Dendritic Cores

Hult and coworkers reported the first ferroelectric LCDs by attaching chiral mesogens onto a polyester dendritic core [250]. This dendritic core is quite original and is built by various generations of 2,2-bis(hydroxymethyl)propionic-based monodendrons that are coupled in the last stage of the reaction to 1,1,1-tris(hydroxyphenyl)ethane (Fig. 45, $N_C = 3$, $N_B = 2$) [251, 252]. The zeroth (G0), first (G1), second (G2) and third generation (G3) dendrimers end-capped with 3, 6, 12 and 24 mesogenic units (Fig. 45, R = A) were found to exhibit a SmC* phase (Table 12) [253, 254]. As the generation was increased, additional smectic mesophases could be observed for G2 and G3 among others, a SmA phase, and two unidentified tilted smectic phases M1 and M2; at the same time, the stability of the mesophases was enhanced. Moreover, once these compounds were placed into a surface-stabilized ferroelectric cell, all showed ferroelectric behavior upon the application of an external electric field, but electro-optical measurements did not reveal any cooperative effect since neither the spontaneous polarizations nor the tilt angles were found to be influenced by the generation number (at the same reduced temperature, $Ps \approx 35\ nC\,cm^{-2}$ and $\theta \approx 25°$). Similarly, the second harmonic generation and the dielectric relaxation processes [255] seemed insensitive to the increasing generation number.

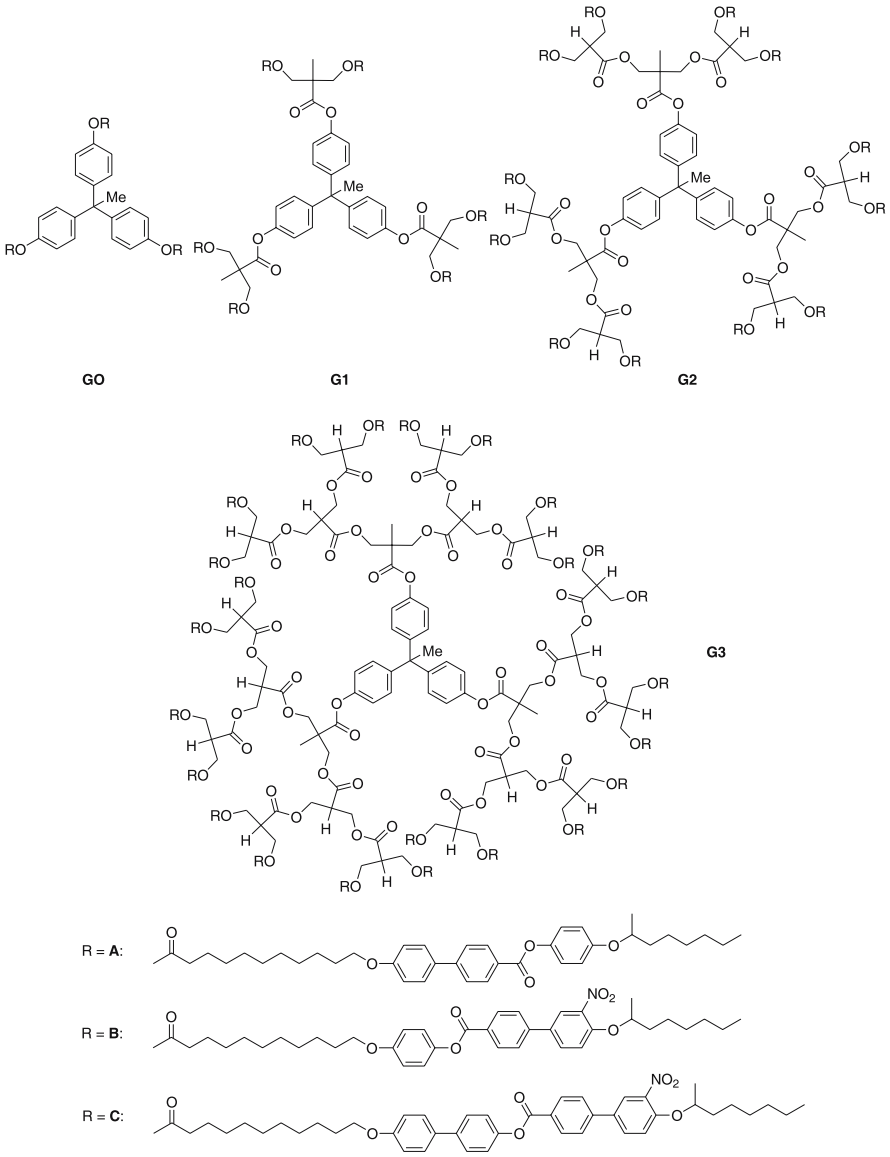

Fig. 45 Structure of the dendrimers with a polyester ramified core

The mesomorphic properties of the G2 dendrimer were substantially modified by the grafting of mesogenic units containing a nitro group (Fig. 45, R = B, C) [256]. In both cases, the two unidentified phases disappeared, and only the SmC* and SmA were observed (Table 12). For the dendrimer bearing the B moiety, the mesophases appeared at much lower temperatures than for the dendrimer functionalized by A groups, whereas for the compound bear-

Table 12 Mesomorphic behavior of the dendrimers with a polyester core

G*n*	R	Phase sequence
G0	A	Cr 77 SmC* 135 I
G1	A	Cr 82 SmC* 124 I
G2	A	Cr 84 SmC* 91 M1 121 M2 127 SmA 150 I
G2	B	G 34 SmC* 69 SmA 82 I
G2	C	G 70 SmC* 152 SmA 208 I
G3	A	Cr 84 SmC* 107 M1 130 M2 134 SmA 151 I

ing C groups, the liquid crystalline phases were substantially stabilized due to the elongation of the mesogenic core. Moreover, the crystalline phase of G2-A is suppressed to yield a glassy state instead in G2-B and G2-C.

4 Main-Chain Liquid-Crystalline Dendrimers

Regarding the dendrimers considered in this part, the branching points are no longer single atoms (C, N, Si) but consist of anisotropic molecular moieties instead. These units are linked together through long and flexible alkyl spacers and form therefore the dendritic matrix; the differentiation between side-chain and main-chain occurs at the first generation onwards (Fig. 46). The mesogenic groups are now present at every level of the dendritic hierarchy, and the dendrimers are forced to adopt constrained and regular structures. As such, the anisometric branches do not radiate isotropically as in side-chain dendrimers, but, on the contrary, favor preferentially an

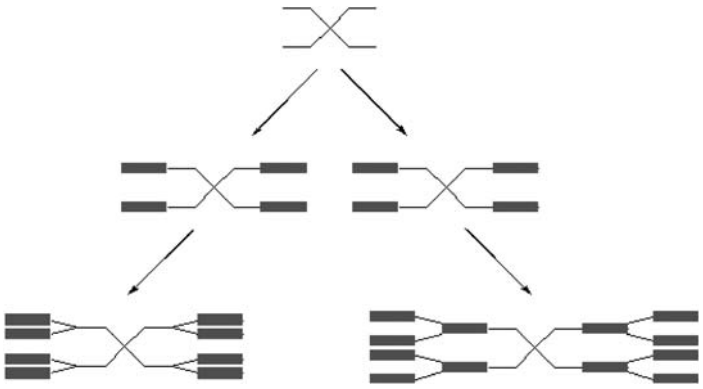

Fig. 46 Schematic of the structural difference between side-chain (*left*) and main-chain (*right*) dendrimers

anisotropic order by a gain in the enthalpy of the system in order to produce the most stable structure.

These main-chain dendrimers may represent an interesting alternative for the development of original molecular materials having a new architecture. Shibaev et al. foresaw the elaboration of such compounds, but have not yet reported on their synthesis and physical properties [151]. Up to now two families of such systems have been identified, namely the willow-like and the octopus dendrimers.

4.1 Willow-Like Dendrimers

The study of the so-called willow-like dendrons and dendrimers echoes a previous important study by Percec on non-regular hyperbranched polymers, another class of cascade macromolecules but distinct from the purely dendritic systems. Indeed, in the original study, Percec et al. synthesized cascade macromolecules by a random self-polymerization of tri-functionalized AB_2 mesogenic monomers derived from biphenylene, naphthalene and terphenylene moieties [67, 69]. These hyperbranched polymers exhibited a single nematic phase and did not crystallize on cooling; depending on the basic mesogenic unit, the nematic temperature range varied from 20 to ca. 80 °C. Because of such a statistical mode of construction [74–77], these hyperbranched macromolecules were characterized by a randomly branched structure with a high, and non-controllable degree of branching and broad molecular weight distributions. Despite these interesting results, they later synthesized regular dendrimers, based on the terphenylene monomer unit free of these imperfections [257–261]. Thus, the four generations of monodendrons (DH1-4) and the corresponding dendrimers (G1-4) resulting from the attachment of DH1-4 onto a tribenzoic acid were obtained by convergent methods with polydispersity indices close to unity (Fig. 47). All the monodendrons and dendrimers were mesomorphic and formed both enantiotropic nematic and smectic phases; only DH1 exhibits a single monotropic nematic phase (Table 13). Note that the corresponding hyperbranched system exhibited a single nematic phase (G 50 N 132 I). On average, the isotropization temperature increases with the generation as well as the stability of the nematic phase, but this effect is very much diluted for the third and fourth generation of both the monodendrons and dendrimers which exhibit an almost identical mesophase temperature range. The nature of the smectic phase is not clear, but on the basis of X-ray diffraction, a SmI or SmF phase (or the more ordered ones SmJ or SmG) seems most likely.

In these systems, the formation of both the nematic and smectic phases is attributed to a particular chain conformation implying that all the sub-units lie parallel to each other to give an overall rod-like shape, rather than a disk-like or spherical shape. This is possible since the racemic AB_2 monomer pos-

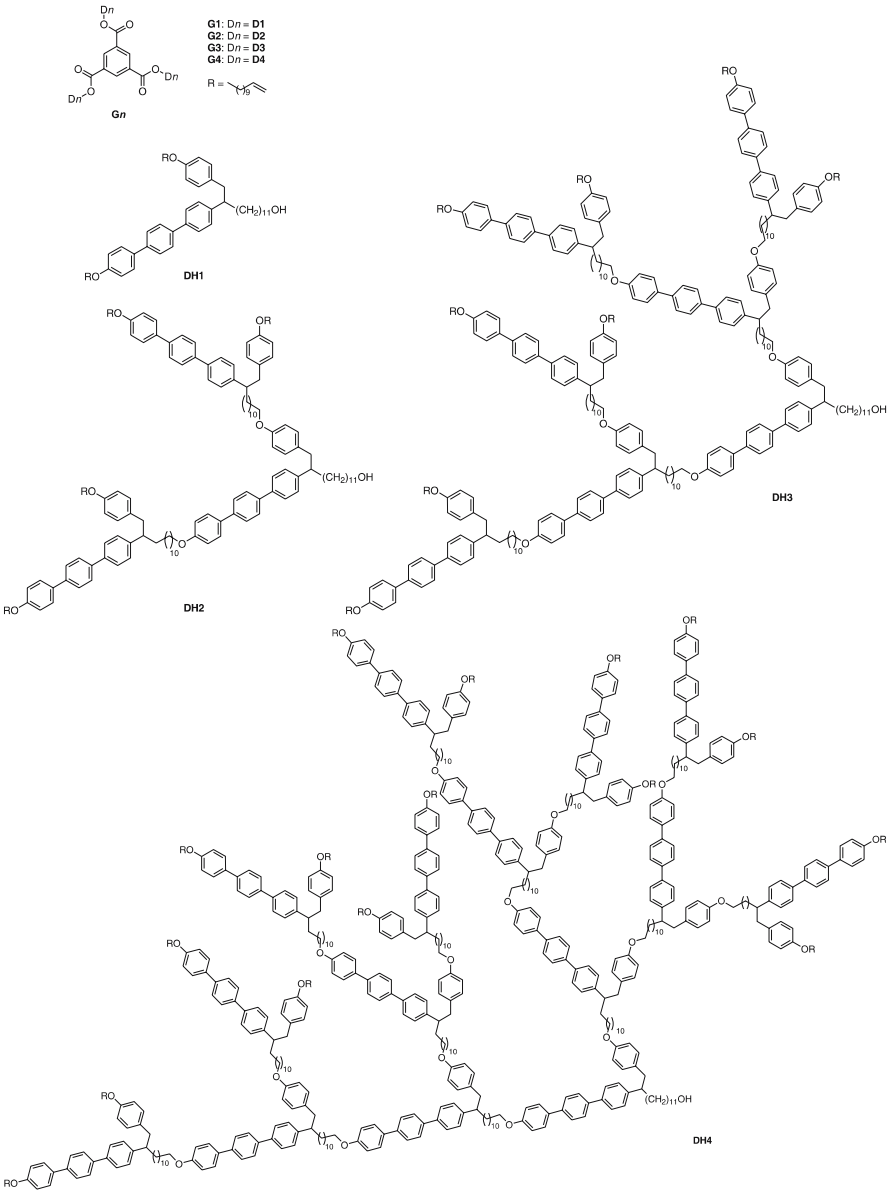

Fig. 47 Structure of the willow-like dendrons (DH*n*) and dendrimers (G*n*)

sesses a carbon linkage between the terphenylene and phenylene units, which exhibits conformational flexibility. Amongst the stable conformational isomers, the *anti* isomer has an extended conformation and leads to mesogens aligning in a parallel fashion, whereas the *gauche* isomer produces a kink in

Table 13 Mesomorphic behavior of the willow-like dendrimers (dendrons and dendrimers)

DH*n*	Dendrons	G*n*	Dendrimers
DH1	Cr 66 (N 54) I	G1	G 5 Cr 32 S 45 N 73 I
DH2	G 58 S 61 N 92 I	G2	G 20 S 42 N 96 I
DH3	G 52 Cr 63 SmX 69 N 105 I	G3	G 53 S 66 N 106 I
DH4	G 63 SmX 73 N 110 I	G4	G 49 S 70 N 108 I

the chain, resulting in a decrease of the temperatures. The subtle combination of both of these conformations of the monomeric sub-units allows for the induction of both smectic and nematic phases at rather accessible temperatures.

A series of polynorbornenes containing the second generation dendron D2 as a side group ($R = C_{11}H_{21}$), with different degrees of polymerization were also synthesized [262, 263]. They exhibit a nematic (over 2 °C), two SmA and a hexatic B phase on cooling from the isotropic liquid (which occurs at around 100 °C).

4.2 Octopus Dendrimers

For the octopus dendritic materials, a modular synthesis was elaborated for the preparation of the branches. Each constitutive part was prepared separately and later assembled selectively together. The anisotropic units selected were a tolane- or stilbene-based moiety, because of both their thermal stability and chemical versatility. Such poor mesogenic segments, despite their intrinsic anisotropy and rigidity, were also chosen in order to test whether mesomorphism could be induced solely by the dendrimerization process [264]. The dendritic branches, bearing mesogenic moieties and functionalized by a focal acid group, were coupled to a small tetra-podand core unit, bearing four amino groups, to yield the final dendrimer (Fig. 48).

Homolithic (Fig. 48, X = Y) [264, 265] and heterolithic (Fig. 48, $X \neq Y$) [264] dendrimers were synthesized and all of them were liquid crystalline. In such systems, mesomorphism was induced by the precise assembling of these non-mesogenic units within the dendritic frame. Moreover, the mesophase stability was found to greatly depend on the localization of the various units within the heterolithic systems (Fig. 51). Indeed, the principles of the modular construction can be applied here for the preparation of regular co-dendrimers made of at least two basic building blocks which can be arranged in a very controlled manner, alternated or segmented (Fig. 49). Only the former has been prepared to date. The possibility of creating such polyfunctional and discrete dendritic structures with the ability to self-organize

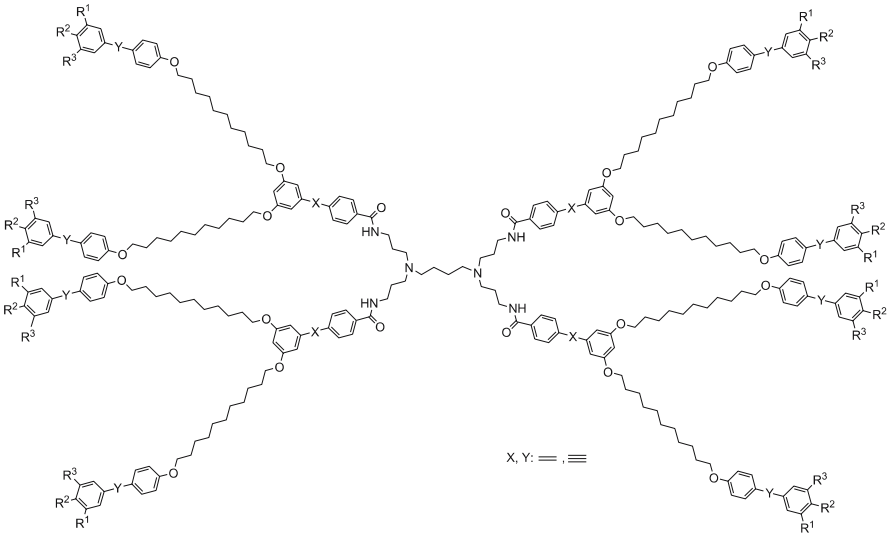

Fig. 48 Example of octopus LCD of the second generation (R^1, R^2 and R^3 stand for $OC_{12}H_{25}$ or H)

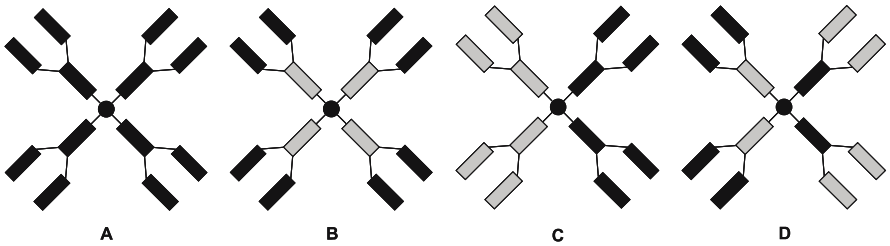

Fig. 49 Schematic representation of homolithic (**A**) and heterolithic alternated (**B**), segmented (**C**) and alternated-segmented (**D**) octopus-like dendrimers

into mesophases is an attractive strategy in the field of material science for the elaboration of multicomponent systems.

The dendrimers bearing only one aliphatic end-chain at the extremity of the outer tolane unit exhibit a smectic behavior (Fig. 48, $R^2 = OC_{12}H_{25}$, $R^1 = R^3 = H$). The X-ray diffraction patterns are characterized by the presence of 3–4 orders of reflection corresponding to a well-defined lamellar stacking. On the basis of these X-ray patterns, a high-temperature phase has been assigned as a disordered smectic A phase, whereas the other, low-temperature phase (due to an extra in-layer order) as a hexatic smectic B phase, the layer spacing being rather large, in the range 10–12 nm (homolithic derivative: SmB 101 SmA 121 I; heterolithic derivative: SmB 109 SmA 132 I). This confirms the prolate conformation of the dendrimers in both smectic phases with

the peripheral anisotropic units being almost perpendicular to the layer normal direction. In this case, the morphology of the smectic phases generated by such multiblock molecules is quite unique in that it possesses a two-level molecular organization, each being dependent on the other. It consists of an internal sub-layer made of tilted rigid segments with no correlation of the tilt, flanked by outer slabs inside which the mesogenic groups are arranged perpendicular to the layer (Fig. 50). Molecular modeling supports this view of strongly segregated multilayer structures, with interfaces between the various molecular parts. Obviously, these interfaces are not so well defined due to thermal fluctuations. Nevertheless, let us point out that because of this peculiar structural feature, such layered mesophases cannot exactly be described as purely SmA or SmB phases, and were referred to as "supersmectic" phases [264].

As for the other set of dendrimers bearing two (Fig. 48: $R^1 = R^2 = OC_{12}H_{25}$, $R^3 = H$, $X = / \neq Y$; $R^1 = R^3 = OC_{12}H_{25}$, $R^2 = H$, $X = Y =$ double bond: Col_h 42 I) or three aliphatic chains (Fig. 48: $R^1 = R^2 = R^3 = OC_{12}H_{25}$, $X = Y =$ double bond: Col_h 84 I) at the extremity of the outer tolane or stilbene part, they all exhibit a columnar mesophase with a hexagonal symmetry (Fig. 51) [264, 265]. The formation of columnar mesophases in non-discotic systems, and particularly with polycatenar mesogens [266, 267], is a consequence of the mismatch between the surface areas of the aromatic cores and the cross-section of the aliphatic chains, resulting in the curvature of all the interfaces, as has been discussed with SC-LCDs bearing polycatenar endgroups. In the present case, in order to compensate the discrepancy between the cross sections of both the anisometric segments and the chains, one can also imagine the former to be tilted and distributed in a "splay" fashion, with respect to the columnar axis, also resulting in the curvature of the in-

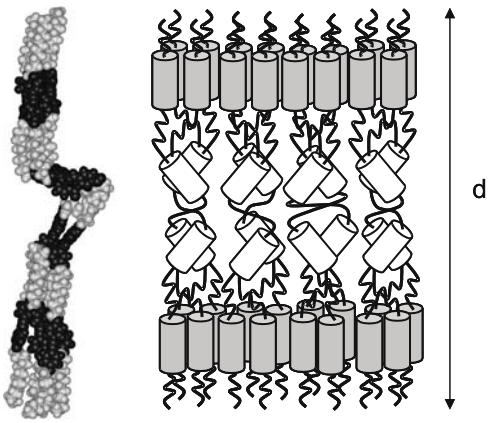

Fig. 50 Snapshot of the molecular conformation of the octopus dendrimers with 8 terminal chains and model for their molecular organization in smectic layers

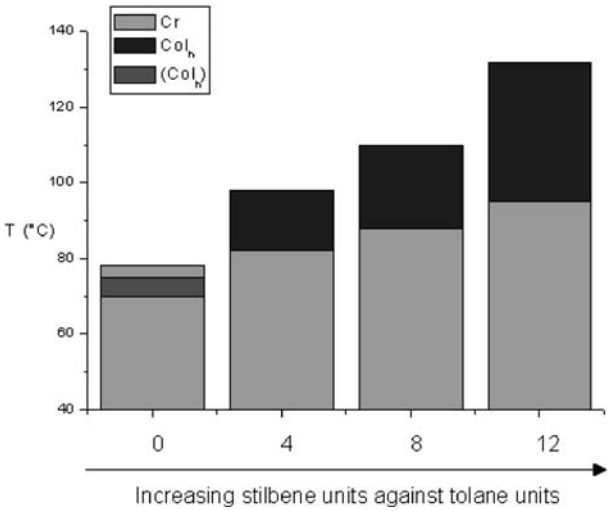

Fig. 51 Diagram showing the evolution of the mesophase stability from tolane-rich (*left side*) to stilbene rich (*right side*) octopus LCDs ($R^1 = R^2 = OC_{12}H_{25}$, $R^3 = H$)

terfaces [268, 269]. Indeed, the parameters of the hexagonal lattices obtained experimentally, $a = 9–10$ nm, correspond fairly well to the diameter of the dendrimers in a flattened conformation, ranging between 10 and 11 nm as estimated by MD simulation (Fig. 53). It is therefore highly probable that the octopus preferably adopts an oblate shape within the columns that is a flattened or wedge-like conformation with the anisotropic blocks lying more or less in the 2D hexagonal lattice plane, rather than a prolate conformation (cylindrical) as in the smectic systems.

As for the dendromesogens described by Percec et al. [79–85], where columnar structures are generated from the self-assembling of the most stable molecular conformations having either a wedge-like or half-disk shape, the mesophase formation of these dendrimers results from the self-assembling process into disks and columns of octopus molecules necessarily adopting pre-defined shapes. The overall molecular conformations of the dendrimers in the mesophase are driven by the steric congestion of the terminal aliphatic chains and depend on the segregation between the different constitutive blocks. In the present case, one ($R^1 = R^2 = R^3 = OC_{12}H_{25}$) or two ($R^1 = R^2 = OC_{12}H_{25}$, $R^3 = H$) molecular conformations likely predominate to satisfy the geometrical requirements. The supramolecular disks or columns thus result from the molecular association of two or three dendrimers (depending on the aliphatic chain substitution) in the appropriate conformation, as depicted in Fig. 52; and these columns are packed in a hexagonal lattice. Moreover, considering the diblock, alternated chemical nature of these octopus dendrimers, an *onion* morphology for the columns is most likely probable (Fig. 53) [264].

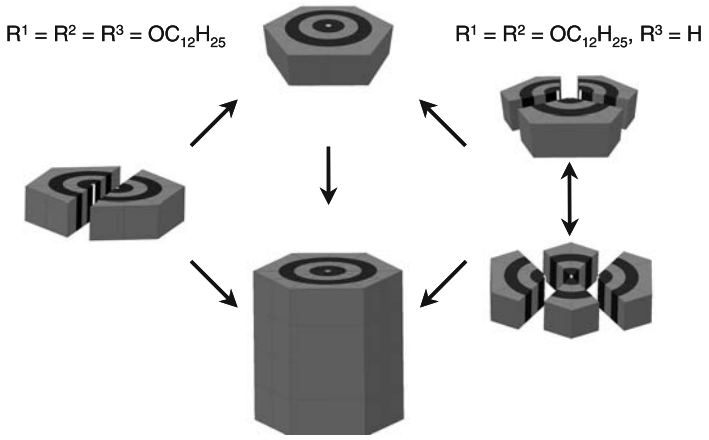

Fig. 52 Schematic representation of the self-assembling and self-organization processes of octopus-like dendrimers into the Col_h phase

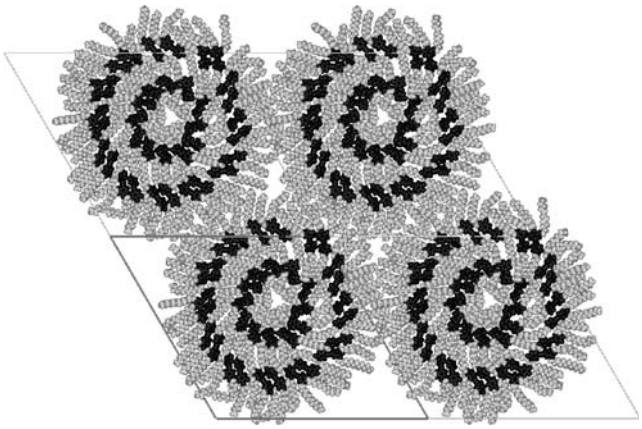

Fig. 53 Snapshot of the molecular conformation in the Col_h phase of a 16 chains octopus LCD

This model of an onion internal structure of the columns was supported by molecular dynamics on the homolithic stilbenoid system (Fig. 48, X = Y :=; $R^1 = R^2 = OC_{12}H_{25}$, $R^3 = H$). It showed good segregation at the molecular level by means of interlocked crowns of stilbenoid units belonging to the same generation, such crowns being stabilized by intermolecular interactions. Each crown was separated by neutral aliphatic coronas.

For these dendrimers, the morphology of the mesophase is thus determined by the number of alkyl chains grafted on the peripheral mesogenic group, i.e. the change in the number of terminal chains per end group modifies the relationships between the hard parts and the soft parts, and

consequently the molecules will adopt either a *parallel* (prolate) or *flat* (oblate) conformation. The formation of the smectic lamellar phases is the result of the parallel disposition of the mesogenic groups on both sides of the focal tetravalent core, the dendrimer adopting the shape of a giant elongated multipede (vide infra), and then organizing into layers. In contrast, the grafting of additional terminal chains at the periphery prevents such a parallel disposition of the pro-mesogenic groups, which are forced into a radial arrangement around the central moiety: the dendrimer can adopt the shape of a flat-tapered object and self-arrange into supra molecular columns.

To complete this analysis, the variation of the core connectivity number and the effect on the mesomorphism was studied [270]. Three new second generation main-chain dendrimers (with the same heterolithic branch: Fig. 48: $R^1 = R^2 = OC_{12}H_{25}$, $R^3 = H$, $X = / \neq Y$) were prepared from various amido-cores of zeroth generation and with different multiplicities: 1,4-diaminobutane ($N_C = 2$), tris(2-aminoethyl) amine ($N_C = 3$) and PAMAM-G_0 ($N_C = 4$); the latter was also prepared for the possibility to rigidify the core by additional hydrogen-bonds (amido groups) and the consequent effects on the mesophase stability. They all exhibit a broad Col_h phase. The transition temperatures and mesophase stability were found to be influenced by the nature and the connectivity number of the core (Fig. 54).

Since the overall number of peripheral chains per dendritic molecule is changed, while the lattice parameter of the Col_h phases remains roughly similar, the number of dendrimers self-assembling into columns is different in order to keep the total number of radiating chains constant as shown in Fig. 55.

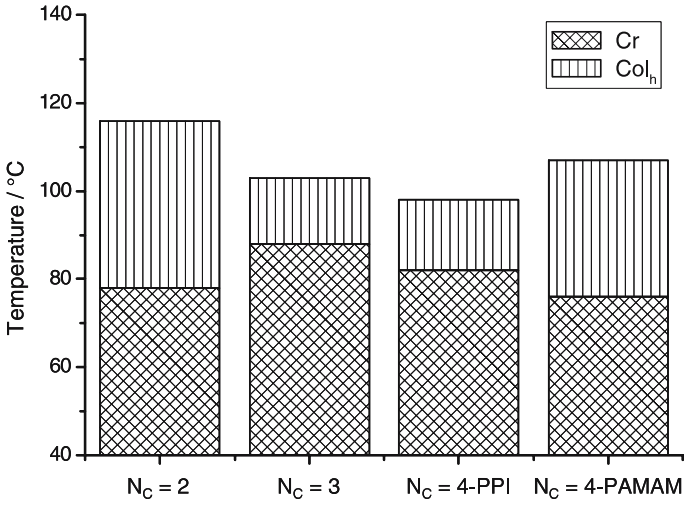

Fig. 54 Evolution of the mesophase stability from $N_C = 2$ to $N_C = 4$

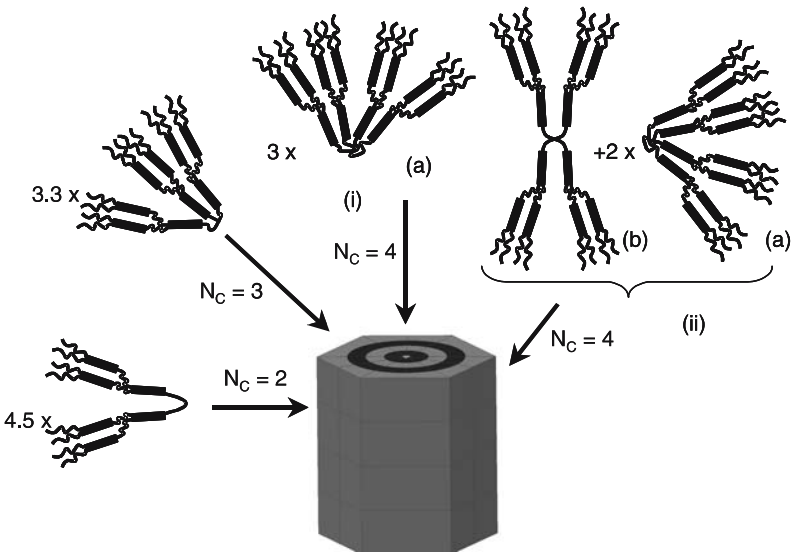

Fig. 55 Self-assembling and self-organization process into columns for the octopus dendrimers with various core connectivity numbers

5
Shape-Persistent Liquid-Crystalline Dendrimers

The so-called "shape-persistent LC dendrimers" represent an unusual and original family of dendrimers [271]. The particularity of these systems is the nature of the dendritic matrices, which are completely rigid and highly conjugated, and are different from the dendrimers described previously since they have the potential to be intrinsically mesogenic. Adequately functionalized by terminal aliphatic chains, they can behave as large, disk-shaped mesogenic molecules right from early generations potentially showing columnar mesomorphism. Because of their expanded and electron-rich core, such dendrimers should find many applications in materials science owing to their interesting photochemical and photophysical properties, and to their readily attainable nanoscale dimensions [271].

Pesak and Moore [272] described a convergent scheme for the synthesis of three generations of shape-persistent tolane-based dendrimers functionalized at the periphery by oligo(ethylene oxide) chains (Fig. 56). All the dendrimers, existing as stiff glasses at room temperature, were mesomorphic on heating, exhibiting wide temperature-range hexagonal columnar phases with clearing points increasing dramatically with the generation number (Table 14). Surprisingly, preliminary data for the dendrimer of the fourth generation indicated that this compound was amorphous.

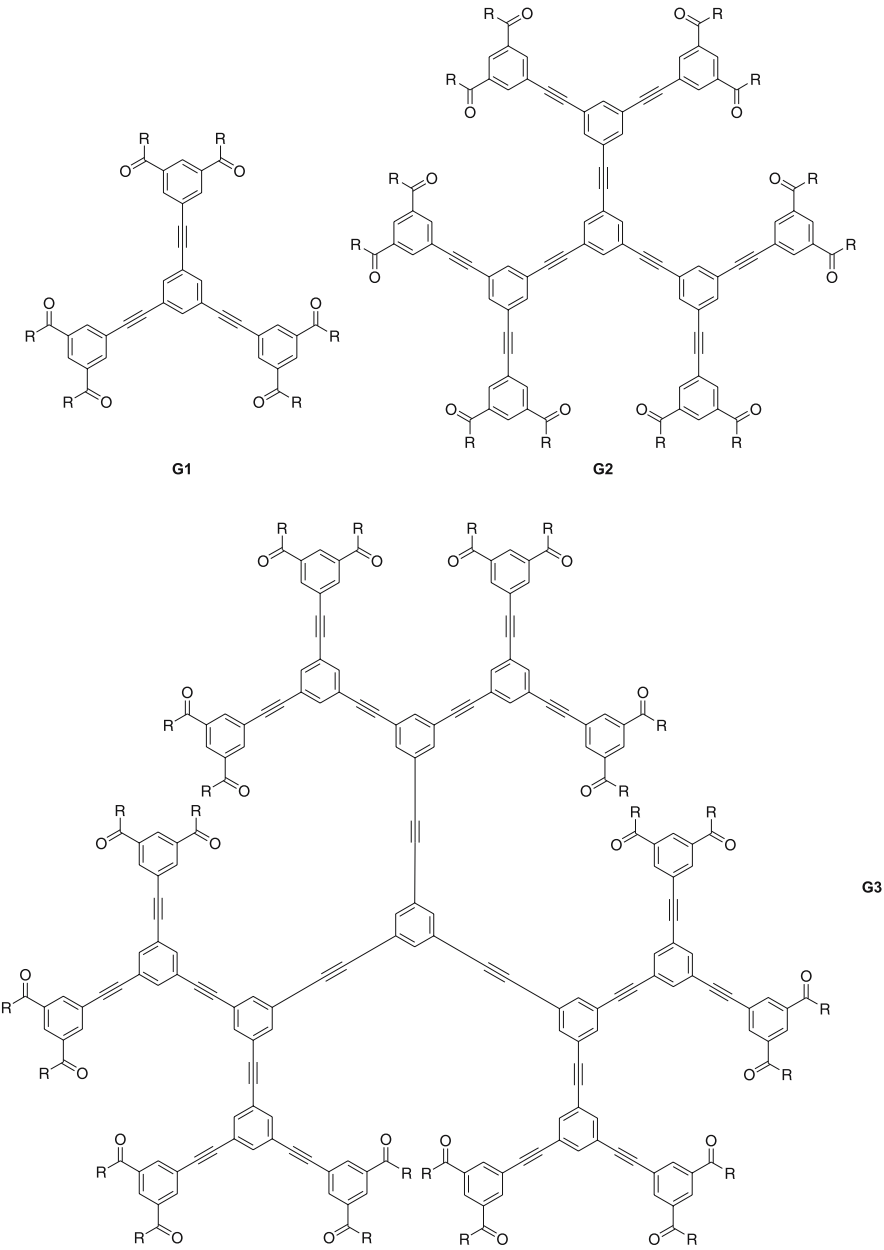

Fig. 56 Chemical structures of the tolanoid-like dendrimers (R = $O(CH_2CH_2O)_3Me$)

Stilbenoid-like dendrimers possessing an analogous molecular structure were reported by Meier to be mesomorphic too [273]. The five generations of stilbene-based dendrimers (Fig. 57) [274, 275] and the first two gener-

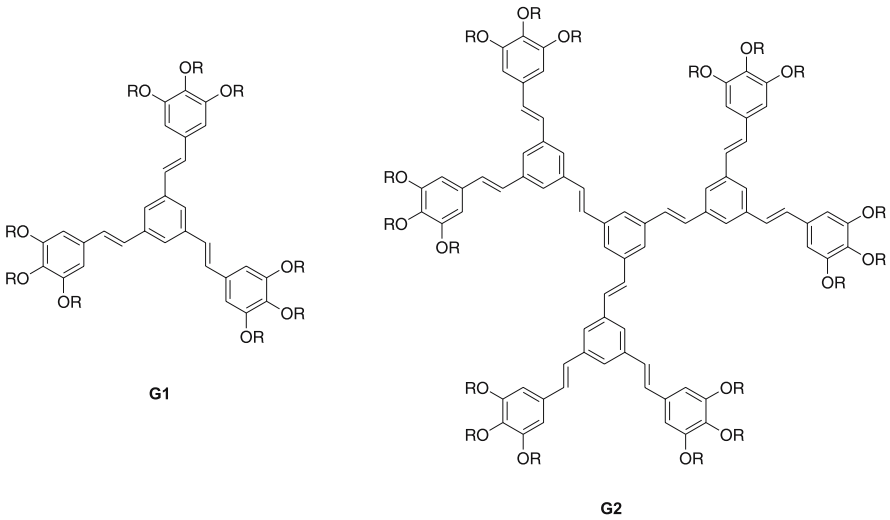

Fig. 57 Chemical structures of the stilbenoid-like dendrimers (R = OC_3H_7, OC_6H_{13}, $OC_{12}H_{25}$)

ations of distyrylbenzene-based dendrimers (Fig. 58) [276] were synthesized by a convergent scheme based on the Wittig–Horner reaction, which allowed an *E*-configuration with double bonds to be obtained. It was found that only generations G1 and G2 showed columnar mesophases as long as the alkoxy chains were long enough (R = OC_6H_{13}, $OC_{12}H_{25}$), whereas higher generations (not drawn here) failed to exhibit mesomorphism (Table 14). The unusual phase sequence Col_h-to-Col_o was attributed to the presence of several conformers whose distribution is temperature-dependent, leading to distortion of the columnar structures of the Col_h phase at high temperatures. Note that the elongation of the dendritic arms results in a huge stabilization of the mesophases. An interesting temperature-dependent ^{2}D NMR study carried out on the neat phases of the stilbenoid dendrimers (Fig. 57), selectively deuterated in specific positions, showed different molecular and segmental motions in the crystalline, liquid crystalline and isotropic phases [277]. It particularly revealed that G1 adopts an average planar shape, despite the significant deviation of the styryl arms from the molecular plane, whereas in contrast G2 does not show large angle motions. These motions are correlated with the photophysical properties of the materials (fluorescence, photochemistry and photo-oligomerization).

In these series of compounds, X-ray diffraction studies revealed that the inter-columnar distance significantly increases between G1 and G2, and then remains constant for G3, whereas the unit cell parameter *c* (representing the stacking periodicity between adjacent molecules in the column) nearly doubles on the passage from second to third generation. Molecular model-

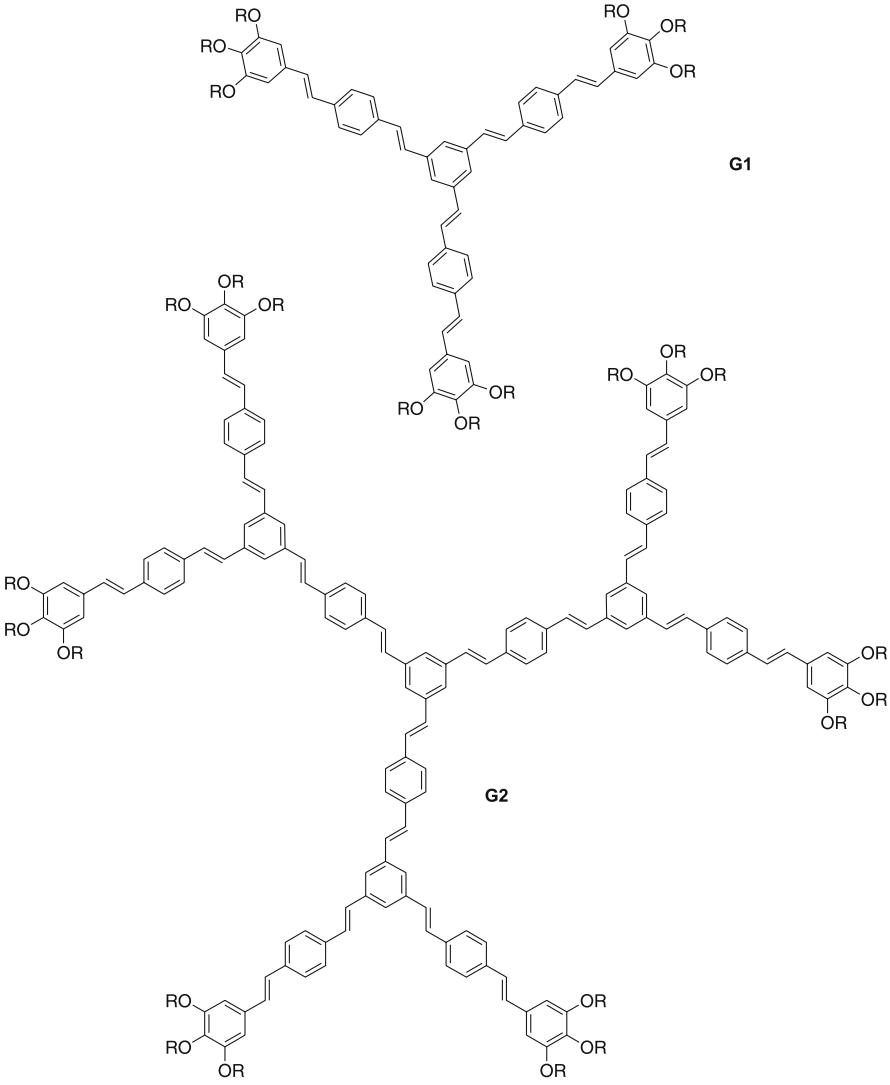

Fig. 58 Chemical structure of elongated distyrylbenzene-based dendrimers (R = OC_3H_7, OC_6H_{13}, $OC_{12}H_{25}$)

ing showed that in fact the dendrimers of the first and second generation have a planar conformation without any steric hindrance. In contrast, such a purely planar conformation is impossible for the largest dendrimers because of overcrowding of the terminal chains preventing as such a regular arrangement. For these compounds, the expansion of the molecule occurs in the molecular plane for the first generations to form megadisks and the growth expands out-of the molecular plane for higher generation numbers to

Table 14 Mesomorphism of the shape-persistent dendrimers

G*n*	Tolanoid dendrimers	Stilbenoid dendrimers ($R = OC_{12}H_{25}$)	Elongated Stilbenoid dendrimers ($R = OC_{12}H_{25}$)
G1	G –58 Col_{ho} 41 Col_h 62 I	Cr 38 Col_h 75 I	G 21 Col_h 108 I
G2	G –58 Col_{ho} 31 Col_h 181 I	Cr 11 Col_h 32 Col_o 99 I	G –27 Col_o 195 I
G3	G –52 Col_h 191 I		

form cylindrical objects. The stability of the columnar mesophases of these large unimolecular disks, which are formed by their face-to-face stacking is primarily enhanced in consequence to the increasing interactions between successive macrodisks. Then, the mesomorphic properties are lost once this out-of plane growth becomes too important because of steric repulsions and strong distortions of the molecular shape.

Structurally related dendrimers of the elongated stilbenoid systems based on a 1,3,5-triazine star-shape of the first generation having styryl or higher oligo(phenylenevinylene) arms were also prepared [278]. The four materials exhibit a liquid crystalline phase (still unidentified) with increasing phase stability on lengthening of the arms (clearing temperatures 109.5, 96.0, 233.3, and > 300 °C for mono-, di-, tri- and tetra(styrylbenzene) systems, respectively).

Other related dendrimers of the first [279] and second [280] generation based on the 1,3,5-triazine unit and tolane arms were also reported by Lee and Yamamoto. The dendrimers of the first generation bearing two chains exhibit a Col_h phase as expected. Surprisingly, the members of the second generation also showed a Col_h phase between 130 and 150 up to 170–230 °C, despite of the grafting of only one terminal chain per peripheral arm.

6
Liquid-Crystalline Metallodendrimers

Metallomesogens are metal complexes which exhibit liquid-crystalline properties, forming the same type of mesophases as found in purely organic materials. They may have a covalent (neutral) or an ionic character, and a large number of thermotropic [281, 282] and lyotropic [283] metal-containing liquid crystals have been reported. Metallomesogens are becoming a very important class of mesogenic materials, as new properties may be expected on the introduction of metals into a liquid-crystalline material. In addition, they offer wider possibilities for structural variations than simple organic materials as, for example, several types of coordination geometry can be envisaged

through the metal and by the use of polydentate ligands. This may in turn lead to new mesophases or new types of molecular organizations, which could eventually form the basis for new effects and devices.

While in general the vast majority of dendrimers prepared are purely organic systems, there has been some interest in the synthesis of dendrimers containing transition metals [34–40]. Indeed, their incorporation within a dendritic structure may find many applications in various areas of science as for example efficient catalysts because of the high concentration of active sites, electro-active molecules due to the multiredox centers, sensors due to their multivalent and selective binding ability, or as molecular antennas due to their particular photo-physical properties. These properties can be tuned and modulated depending on the location of the active moieties within the dendrimer: the metals can be incorporated at the core, throughout the structure or at the periphery of the dendrimer. Some interesting aspects concerning these "supra-supermolecular" systems have been discussed elsewhere [34–40, 48–52].

Only a few studies have looked at metal-containing liquid crystalline dendrimers. In these examples, the metal is either located at the core or in the branches of the dendrimer. The first report of a metallomesogen with a dendritic architecture can be backdated to 1993, though they were not described as such. Serrette et al. [284] prepared a first generation of "Fréchet–Percec" dendritic branch, which they then grafted around several coordinative salen-units varying in spacer length (Fig. 59: Y = – CH_2CH_2 –, – $CH_2CH_2CH_2$ –, – CH_2CMe_2 – CH_2 –). Induction of mesomorphism was observed upon complexation to the oxovanadyl metal ion (Table 15), probably due to the rigidification of the central chelating part, since the flexible ligands themselves were devoid of liquid crystalline properties. Infrared spectroscopy further revealed the formation of linear chain structures for complexes with Y = propyl and dimethylpropyl, whereas the complex with Y = – CH_2CH_2 – was

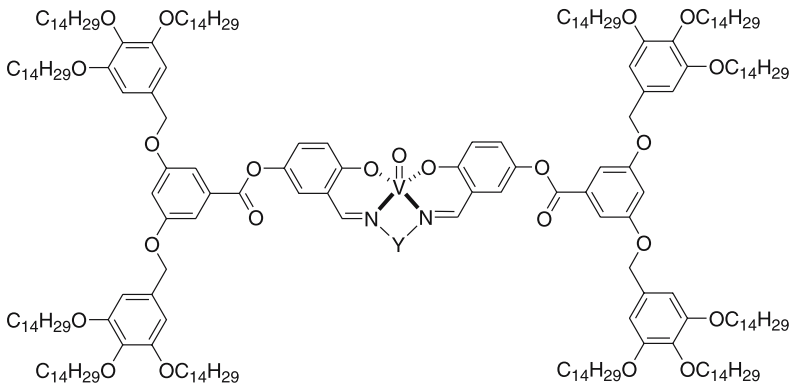

Fig. 59 Structure of the dendritic oxovanadyl complexes

Table 15 Thermal behavior of the dendritic oxovanadyl complexes as a function of the spacer Y

Y	Mesomorphism
$-CH_2CH_2-$	Col_{r1} 119.5 Col_{r2} 156 I
$-CH_2-CH_2-CH_2-$	Col_{h1} 36 Col_{h2} 97.5 Col_r 151 I
$-CH_2-CMe_2-CH_2-$	Col_h 55 Col_r 108 I

monomeric; it nevertheless displayed the largest mesomorphic range. The high-temperature mesophase was identified as a Col_r (*c2mm*) mesophase in all cases, and two of the complexes exhibited the Col_h-to-Col_r phase sequence (Table 15). The destabilization of the hexagonal structure at the expense of the rectangular phase was thought to be due to the bulkiness of the terminal groups and to their spatial requirements, and the driving force for the Col_h-to-Col_r transition may then be linked to the formation of linear chain structures. These could limit the lateral diffusion of the cores, and force the stacking of the core with limited conformational options.

Another series of related mesomorphic metallodendrimers, having the metal located at the core of the dendrimer, were also reported [285]. The dendritic ligands were obtained by condensation of the corresponding 1,3-dione with aminopropanol, and the dicopper complexes were then formed by the reaction with copper(II) acetate (Fig. 60). These ligands, also based on the first generation "Fréchet–Percec" dendron motif, were not themselves mesomorphic, but upon complexation, mesophases were observed whose sta-

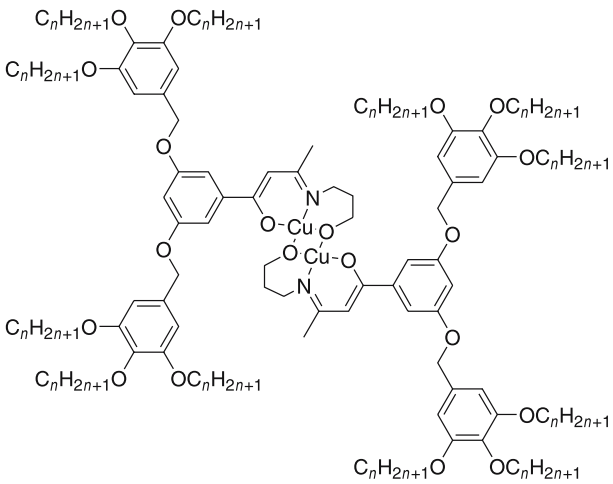

Fig. 60 Structure of the dicopper dendritic complexes

bility was found to be dependent on the number of chains and on their length. Induction of mesomorphism is also likely due to the rigidification of the chelating unit as above. The systems having one and two chains per terminal phenyl groups were not mesomorphic, but those with three chains showed a Col_h phase. The occurrence of the mesophase depended strongly on the chain-length. Thus, short- and long-chain derivatives (n = 5, 14 and 16) were not mesomorphic, whereas the intermediate chain length compounds (n = 6–9, 10, 12) displayed a Col_h phase with transition temperatures sensitive to the chain-length (between 80–100 °C for the melting temperature and 100–120 °C for the clearing temperature). The more circular core of the dicopper complexes with respect to that of the oxovanadyl ones just discussed above may explain the observation of only the Col_h phase for the latter.

Metallomesogens with branched, dendrimeric ligands L1 and L2 derived from tris(2-aminoethyl)amine were reported in 1996 by Stebani et al. (Fig. 61) [286]. This series of metallomesogens of the type $[MX_2(Li)]$ (i = 1 or 2) was obtained subsequently to the complexation of L1 and L2 with various metal salts, $CoCl_2$, NiX_2 (X = Cl, NO_3), CuX_2 (X = Cl, SCN and NO_3) and $ZnCl_2$. Depending on the metal, the complexes could be obtained with two possible coordination geometries, either with the trigonal bipyramidal mode giving rise to pentacoordinated ionic complexes ($[MXL]^+[X]^-$) (Fig. 61a) or

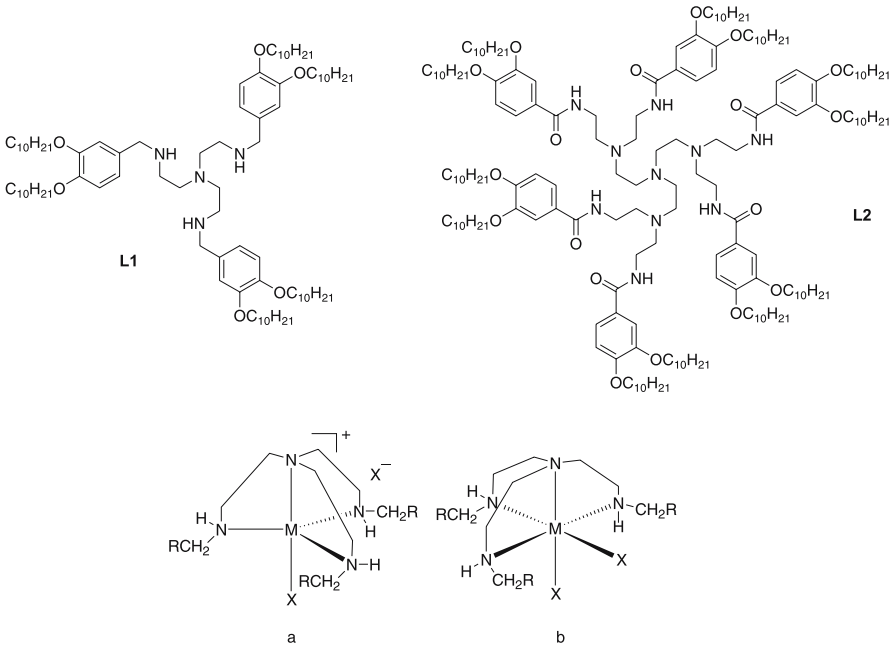

Fig. 61 Dendritic ligands L1 and L2, and the corresponding metal complexes in the trigonal bipyramidal (**a**) and octahedral (**b**) geometry

as the neutral octahedral complexes ([MX_2L]) (Fig. 61b). The distinction between these two modes of coordination was elucidated by infrared and UV/Vis spectroscopy: the copper(II) and cobalt(II) complexes adopted the trigonal bipyramidal structure and the nickel(II) complexes were octahedral, whereas it was not possible to determine the structure of the zinc(II) complexes. A Col_h phase was observed for quasi all the complexes with L1 between 40–60 °C and 65–85 °C, and up to 120 °C for the zinc(II) complex (Table 16), the exception being [$Ni(NO_3)_2$(L1)] which melted directly to the isotropic liquid at 46.5 °C.

Dendrimer L2 was itself mesomorphic, showing a monotropic Col_h phase, Cr (79.5 Col_h) 98.5 I, [287] which upon complexation to $CuCl_2$ became enantiotropic (Table 16). By UV/Vis spectrum, the complex was found to adopt a trigonal bipyramidal structure as [CuCl(L1)]Cl. Thus, a dendritic effect could be observed in this series in that the stability of the mesophase increased considerably with the dendrimer size; the complex [CuCl(L1)]Cl cleared at 75 °C whereas the clearing point of the complex [CuCl(L2)]Cl was 140 °C.

In these three series of dendrimers, the metal was located as the central node of the macromolecule, and induction of mesomorphism was systematically observed on complexation to the metal ion. When coordinated, the dendritic core is likely to lose its flexibility, its conformation being locked by the metal center, and thus the molecule adopts a molecular shape approximating that of a disk.

A quite different approach was used by Serrano et al. So far, whatever the generation number, the number of metallic centers was constant and equal to one, because the unique coordinative site was located at the center of the dendrimer and the metal was embedded within. Here, dendrimers based on the zeroth- and first-generation of PPI dendrimers and end-functionalized by four or eight coordinating 4-(alkoxybenzoyloxy)salicylaldimine were con-

Table 16 Mesomorphism of the metallodendromesogens

Dendrimers	Transition temperatures
[CoCl(L1)]Cl	G 56 Col_h 85.5 I
[$NiCl_2$(L1)]	G 40 Cr 47 Col_h 64.5 I
[$Ni(NO_3)_2$(L1)]	G 36 Cr 46.5 I
[CuCl(L1)]Cl	G 41 Col_h 75 I
[CuSCN(L1)](SCN)	G 41 Cr 48.5 Col_h 75 I
[$CuNO_3$(L1)](NO_3)	G 36 Cr 47.5 Col_h 79 I
[$ZnCl_2$(L1)]	G 60 Col_h 126 I
[CuCl(L2)]Cl	G 49 Col_h 140 I

sidered as potentially multicoordinative organic ligands [288]. Whereas all the organic dendromesogens were found to possess a smectic mesomorphism [213], the complexation of copper(II) affected strongly the mesomorphic properties of the corresponding complexes. Indeed, mesophase formation was either suppressed in some of the corresponding metallodendrimers (Fig. 62, G0: $n = 10$, mp: 179 °C; G1: $n = 10$, mp: 110 °C; $n = 14$, mp: 80 °C), or the mesophase temperature ranges strongly reduced for the mesomorphic complexes (Fig. 62, G0: $n = 14$, Cr 163 SmC 197 I; $n = 18$, Cr 167 SmC 187 I; G1: $n = 18$, Cr 35 SmC 108 I). Interestingly, the transition temperatures were raised upon complexation for the zeroth generation dendrimers, while for the first generation systems, the temperature interval was similar for the ligand and complex. By X-ray diffraction, the unique mesophase was identified as a SmC phase. The structure of the smectic phases of the dendritic ligands is explained by a parallel arrangement of the mesogenic units extending up and down from the molecular center. However, the complexation of copper(II) resulted in the breaking of this parallel arrangement, and in the opening of the branches, allowing as such interdigitation of the molecules located in neighboring layers. This model is in agreement with the diminishing of the layer

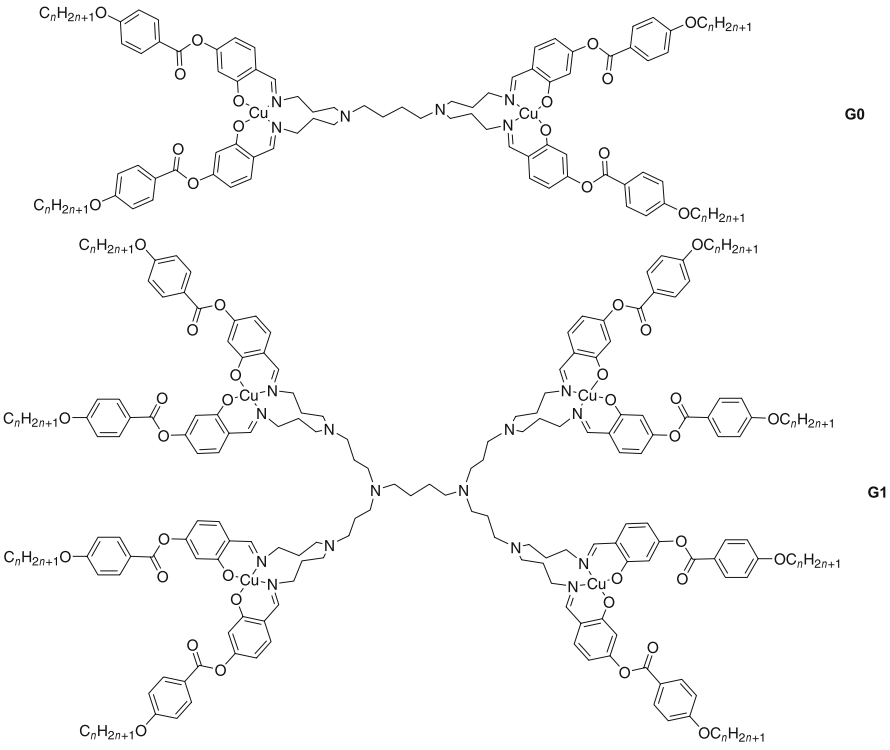

Fig. 62 Dimetallic and tetrametallic dendrimers

periodicity and with the increasing molecular area of the complexes compared to those of the ligands.

Deschenaux and co-workers have designed liquid-crystalline dendrimers based on aromatic polyester cores containing ferrocene [289] for the purpose of designing dendrimer-based molecular switching devices. All of the dendrimers were prepared by a convergent and iterative synthetic methodology leading to precisely monodisperse macromolecules. The dendrimers shown in Fig. 63 [290] and Fig. 64 [291–293] possess respectively 6 and 12 terminal groups (i.e. ferrocene units), each including a cholesteryl mesogenic promoter. Both dendrimers bearing a cholesteryl unit form an enantiotropic smectic A phase (G 47 SmA 150 I, and G 52 SmA 169 I). The other dendrimer (Fig. 64, R = B), for which the ferrocene unit is located at the periphery of the dendrimer, shows an unidentified smectic phase (SmA or SmC) between 119 and 256 °C. The higher temperatures observed for this compound are likely due to the elongated calamitic core unit used to promote the mesophase formation. The SmA mesophase was unambiguously determined by X-ray diffraction on powder and aligned samples. The structure of the mesophase can be explained by the formation of layers containing the dendrimer cores, with interdigitation of the mesogenic units from layer to layer.

A mixed [60]fullerene-ferrocene dendrimer (Fig. 65) was also found to be mesomorphic, showing a room temperature smectic A phase which cleared at 157 °C (no glass transition temperature was detected) [294, 295]. The mesophase was only slightly destabilized upon the addition of C_{60} when com-

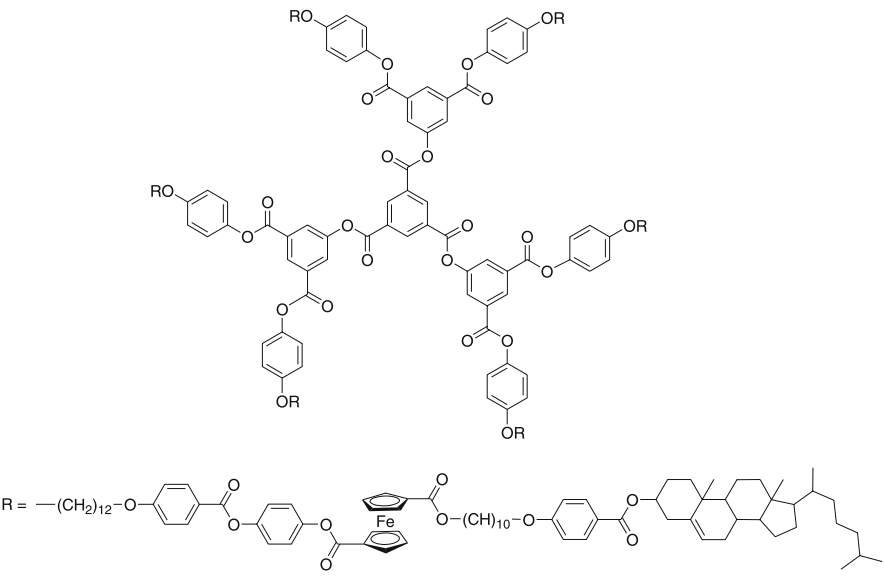

Fig. 63 Structure of the ferrocene-containing dendrimer with six mesogenic arms

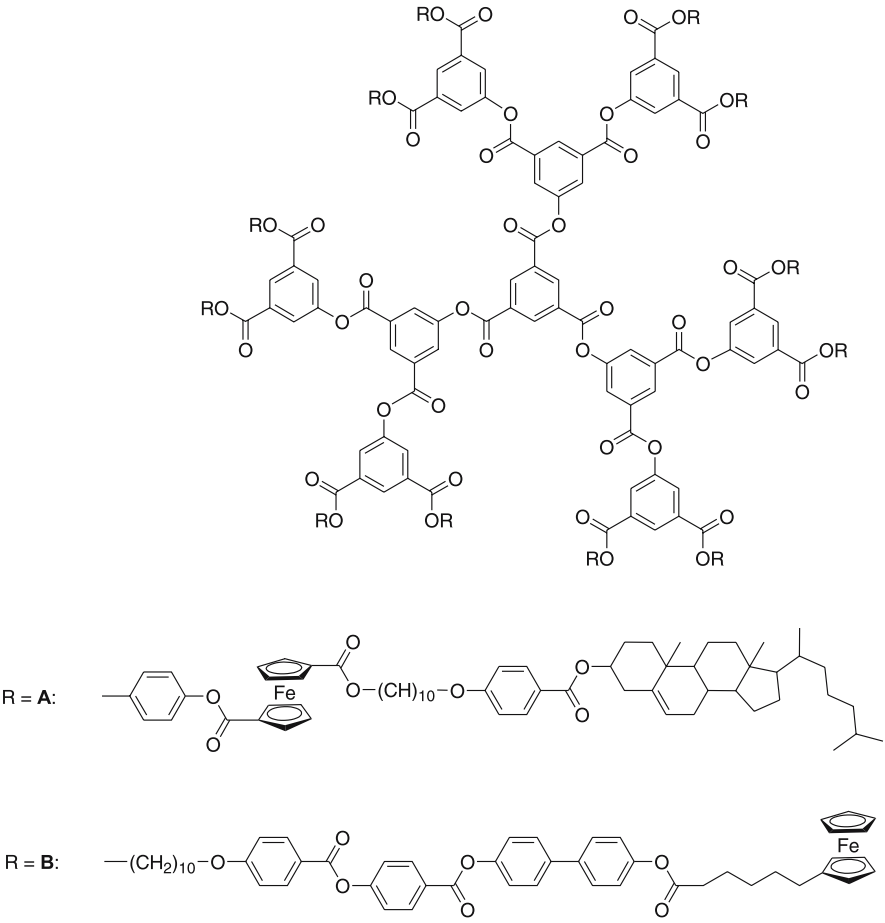

Fig. 64 Structure of the ferrocene-containing dendrimers with twelve mesogenic arms

pared to its malonate ferrocene-containing liquid crystalline dendrimer precursor (Fig. 65, SmA 169 I), probably because both species possess a similar size, and C_{60} is embedded within the dendritic matrix. The zeroth generation was also mesomorphic (SmA 118 I) [296]. This result showed that the association of fullerene (electron-acceptor unit) and ferrocene (electron-donor unit) within the same structure may be an attractive strategy to elaborate liquid-crystalline switches [297] based on the photo-induced electron transfer occurring from ferrocene to fullerene [298].

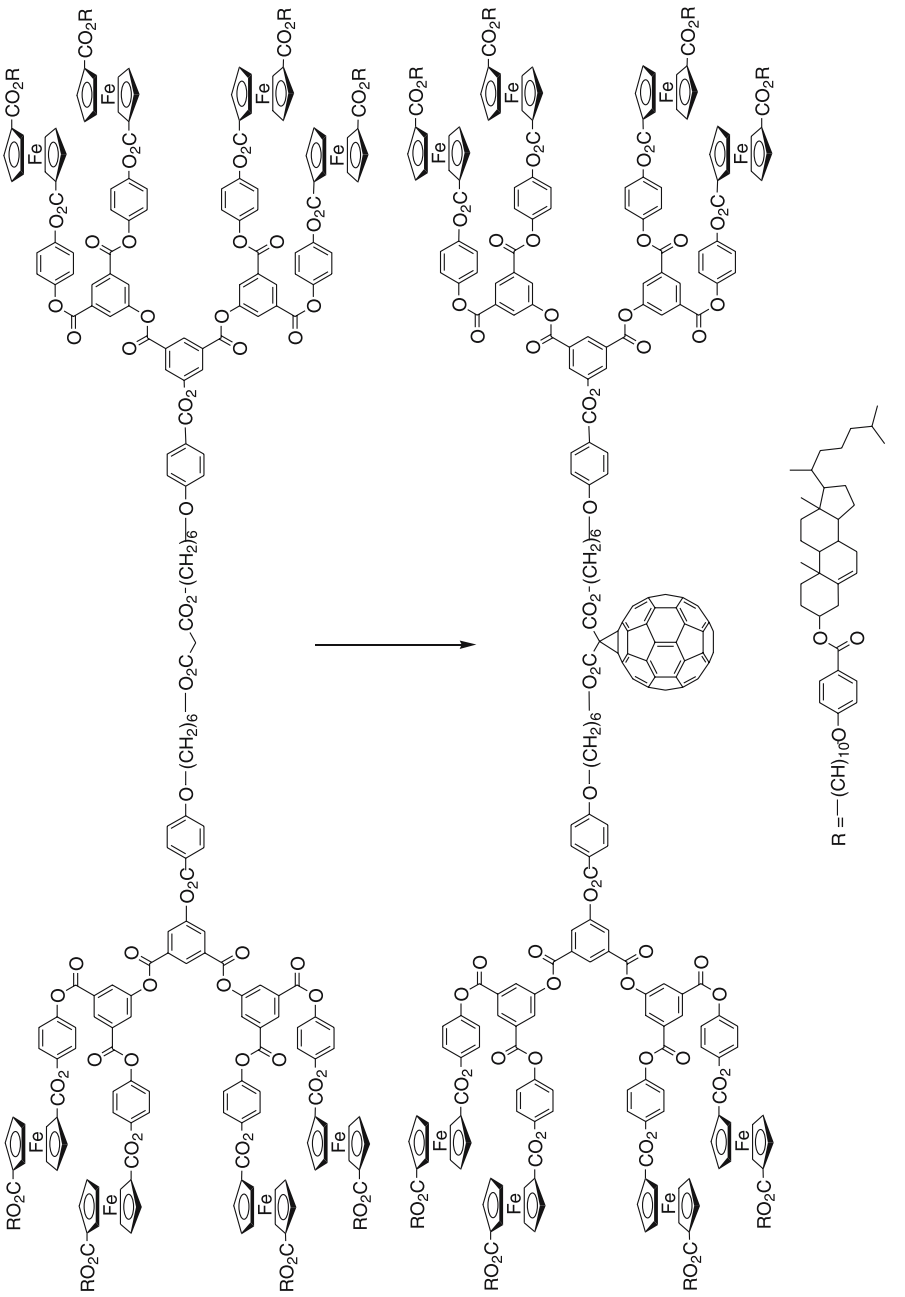

Fig. 65 Structure of the mixed [60]fullerene-ferrocene-containing dendrimer and of its precursory malonate

7
Liquid-Crystalline Fullerodendrimers

Following the work described above, Deschenaux and co-workers engaged in a more systematic study of the elaboration of fullerene-containing thermotropic dendrimers [299, 300] and on the understanding of how such a sphere-like structure could be inserted within liquid crystals in order to ultimately control the properties through dendrimer generation. The use of mesomorphic dendritic addends to functionalize C_{60} was thought to be a suitable solution to avoid aggregation of C_{60} units (decreasing the unfavorable interactions), and thus to favor the formation of mesophases.

An addition reaction of malonate-based dendritic addend onto C_{60} led to a new series of methanofullerodendrimers (Fig. 66) [301]. In such systems, C_{60} is buried within the large dendritic branches, and as a consequence the supramolecular organization of these fullerodendrimers is independent to the change of the generation number of the dendritic carapace (for G2, G3 and G4) and is similar to that of the corresponding malonate species. The mesophase stability was, however, slightly enhanced with generation for both systems (Fig. 67). The only drastic change concerned G1 where the nematic phase was suppressed and replaced by the SmA phase upon the insertion of C_{60}.

The G0 analogues (Fig. 66, G*n* = R) were also found to be mesomorphic, Cr 97 SmA 153 N 162 I and G 29 SmA 142 I, for the malonate and C_{60} adduct, respectively. The supramolecular organization of these dendrimers was deduced from a detailed X-ray diffraction analysis and molecular simulation. For G0, both arms of the molecules are folded towards the same direction, and then the structure consists of a head-to-tail arrangement of such conformers. As for G1, the molecule adopts a V-shape (constituted by pairs of mesogenic groups), and arranged in a head-to-tail fashion favored by the antiparallel packing of the polar end groups. For both structures, lamellae interact through a layer of fullerene. For the next system, G2, the branching part begins to have significant lateral extension with respect to the layer normal, and the two branches extend on both sides of the C_{60} nucleus. Then, for G3 and G4, the structure is solely governed by the polar cyano groups. The central part of the layer is constituted by the fullerene moiety embedded in the large dendritic segments, and the layer interface is formed by partially interdigitated mesogenic groups. In all cases mesophases are likely stabilized by dipolar interactions (antiparallel arrangement of the cyanobiphenyl units).

The corresponding G1 and G2 hemi-dendritic systems were also prepared for comparison (Fig. 68) [301]. Similar trends were observed in that the SmA phase was preferred to the nematic phase, suppressed upon the insertion of C_{60}. The same type of supramolecular organizations is suggested. Interestingly, the mesomorphic temperature range was strongly reduced in the hemi-dendrimers compared to that of the corresponding dendrimers. It was

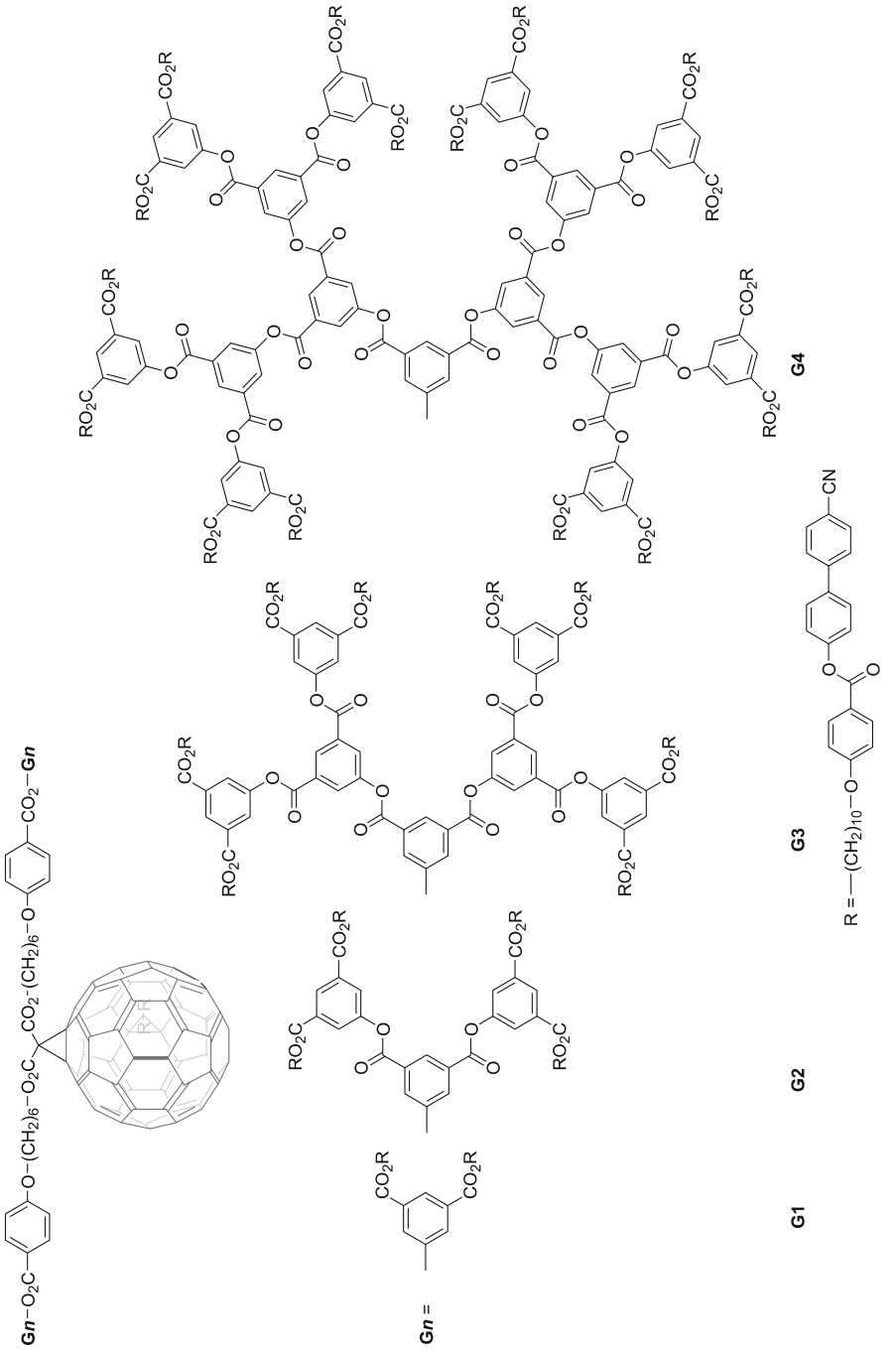

Fig. 66 Liquid crystalline malonate dendritic addends and corresponding methanofullerodendrimers

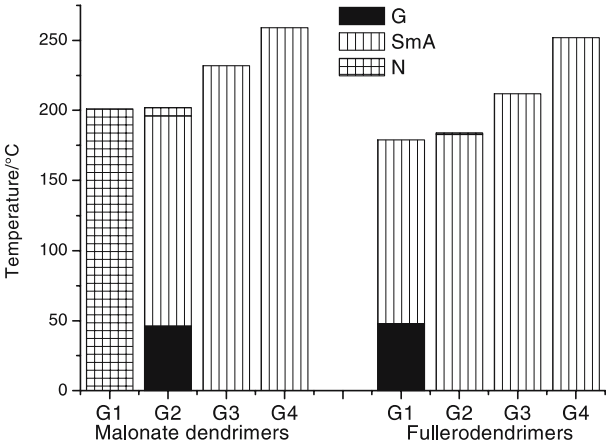

Fig. 67 Mesomorphic behavior of the malonate and corresponding methanofullerodendrimers

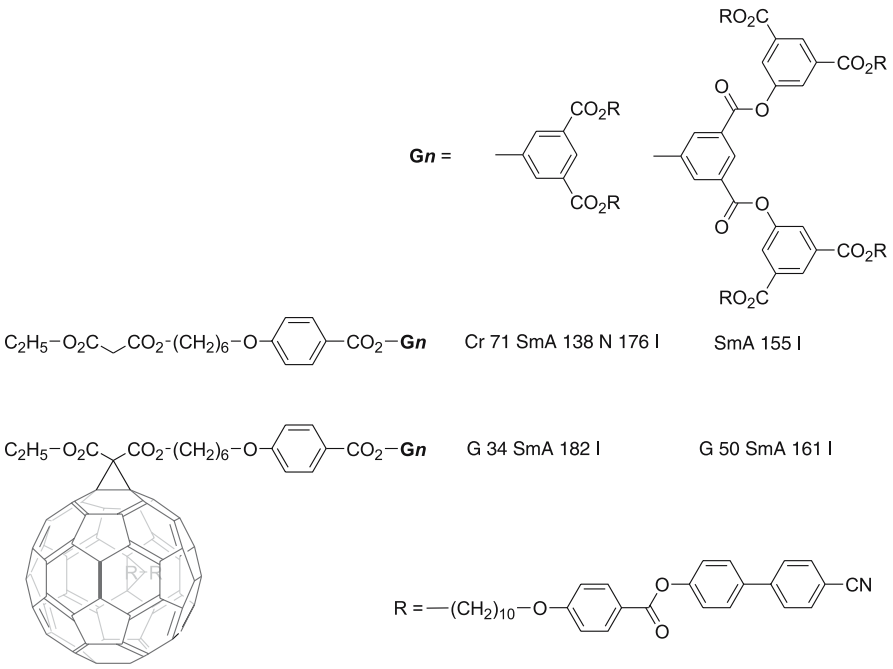

Fig. 68 Hemidendritic malonate and methanofullerene systems

also shown by the electro-optical Kerr effect and hydrodynamic methods that the hemidendrimers are more sensitive than dendrimers to the incorporation of fullerene in their structure (viscosity, shape changes) [302, 303].

Let us note that two homologues of the malonate addends and of the corresponding methanofullerene derivatives described above (Fig. 66) were also prepared with chiral pendant mesogenic groups, laterally attached (Fig. 69). Both the G1 [304] and G2 [57] fullerodendrimers were found to show a chiral nematic phase (Fig. 69, G1: G 26 N* 69 I; G2: G 24.3 N* 80.6 I), and are the first C_{60} derivatives that possess a chiral mesophase; the G1 C_{60}-free malonate was also mesomorphic (G 20 N* 113 I).

As for the silsesquioxane cages (Fig. 24, vide supra) [182], covalent adducts of [60]fullerene offer multiple possibilities for the design of highly functionalized derivatives. In particular, C_{60} can be used as an original initiator core or template for the construction of dendritic systems with high and variable connectivity number with various controllable geometries of attachment. Though, more appropriately referred to as polypedes [57], hexakis(methano)fullerene with 4 (Fig. 70B) [305] and 12 (Fig. 70A) [306] mesogenic groups derived from cyanobiphenyl proved to be mesomorphic. The hexa-adduct malonate difunctionalized in the two poles of the sphere exhibited a transient nematic phase (Cr 85 N 157 I), i.e. observed during the first heating only, while the hexa-adduct functionalized in the six apical positions of C_{60} showed an enantiotropic SmA phase (G 80 SmA 133 I). Unfortunately, no higher generations based on these poly-adducts of C_{60} have yet been reported.

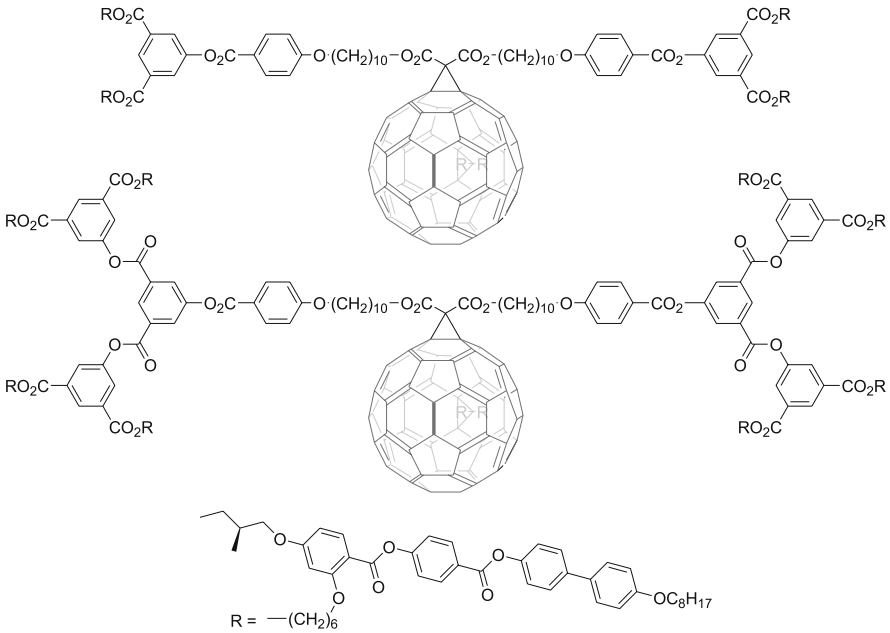

Fig. 69 First C_{60} derivative showing a chiral nematic phase

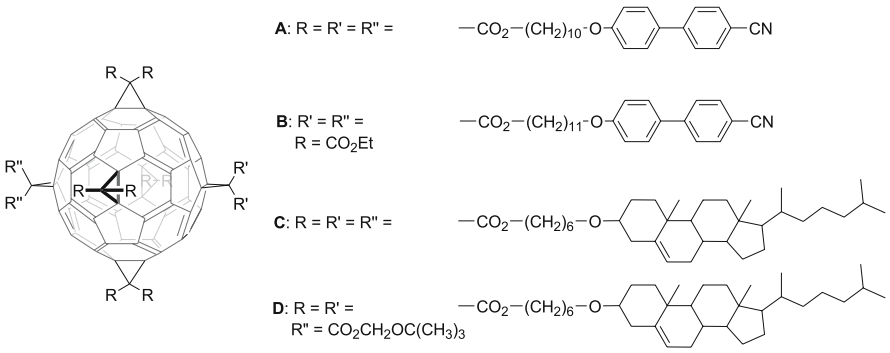

Fig. 70 Liquid crystalline hexakis(methano)fullerene materials

Following a judicious design and challenging chemistry, two novel hexaadducts bearing 12 (Fig. 70C) and 10 cholesteryl units (Fig. 70D), respectively, were reported by Felder-Flesch et al. [307] and found to be mesomorphic. They both exhibit a similar mesomorphic behavior, with a broad temperature SmA phase, quite different to that of the malonate mesogenic promoter for which a chiral nematic phase was observed (G 67 N* 88 I). On heating, a glass-to-SmA phase transformation is observed just above room temperature, followed by the transition to the isotropic liquid at 165 °C and 180 °C for the C and D systems, respectively. The supramolecular organization of these species within the smectic layer consists of an overall smectic bilayer structure in which one of the active moieties (C_{60}) is confined in a central sub-layer sandwiched by two outer-layers of cholesteryl groups; each single layer is separated by thin films of molten aliphatic chains. Moreover, and because of the quasi-spherical structure of C_{60}, the latter likely pave the sub-layer according to a 2D hexagonal arrangement (deduced from XRD and MD). The selected design, i.e polyaddition of cholesteryl moieties on the carbon sphere used as a spherical template to create new 3D architectures, then seems to be a method of choice to obtain stable anisotropic materials and prevent the C_{60} aggregation tendency. This approach should allow the preparation of a wide variety of fullerene hexaadducts, symmetrical or non-symmetrical and with a variable and controlled number of active pendant mesogenic units.

There has been one derivative of bis(methanofullerene) carrying two dendritic wedges (Fig. 71) that was claimed to show a mesophase between 40 and 70 °C, though the phase was not identified; the precursor itself displayed a nematic phase (Cr 48 N 63 I) [305].

Fulleropyrrolidines constitute an important family of C_{60} derivatives that have the advantage over the methanofullerene systems in that they lead to stable reduced species, allowing the development of fullerene-based redox molecular switches. In order to promote mesomorphism in such a mono-adduct structure, Deschenaux et al. decided to modify the C_{60} derivative by the use

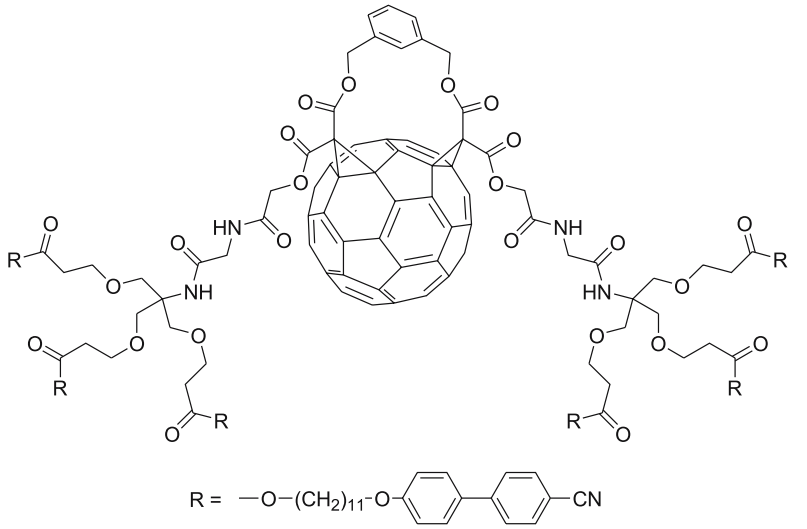

Fig. 71 Structure of the bis(methanofullerene) with dendritic wedges

of a dendritic addend bearing several cyanobiphenyl groups. Four generations of fulleropyrrolidines were prepared (Fig. 72) [308]. This appeared to be the right strategy since, with the exception of the first fulleropyrrolidine derivative that was found to be non-mesomorphic (Fig. 72, G1: Cr 178 I), all the other fullerene-based dendrimers gave rise to a SmA phase (Fig. 72, G2: G 44 SmA 168 I; G3: G 51 SmA 196 I; G4: G 36 SmA 231 I), the stability of which was found to increase with the generation number. The precursory aldehydes and alcohols showed essentially a broad SmA phase, except those of the first generation which showed a nematic phase above a crystalline phase. As for the molecular organization within the SmA phase, the G2 molecules are oriented in a head-to-tail fashion within the layers, and for each molecule the mesogenic groups point in the same direction interdigitating with mesogenic groups of adjacent layers. For the higher generation dendrimers, G3 and G4, the mesogenic units are positioned above and below the bulky dendritic cores, and interdigitation occurs between layers; C_{60} is now hidden in the dendritic core and has no influence in the supramolecular organization as was the case for the methanofullerodendrimers discussed above.

The first synthesized mesomorphic fulleropyrrolidine, G2, (Fig. 73A) [309] was chosen as a representative reference for a systematic variation of the R group in order to evaluate the effects on the mesomorphic properties. When R = H (Fig. 73B) [308], the compound exhibited a broad temperature range SmA phase (SmA 161 I). Modification of the R group by oligophenylenevinylene conjugates (OPV) led also to similar results (Fig. 73C: G 50 SmA 171 I, D: G 50 SmA 169 I) and indicated that the overall behavior is dominated by

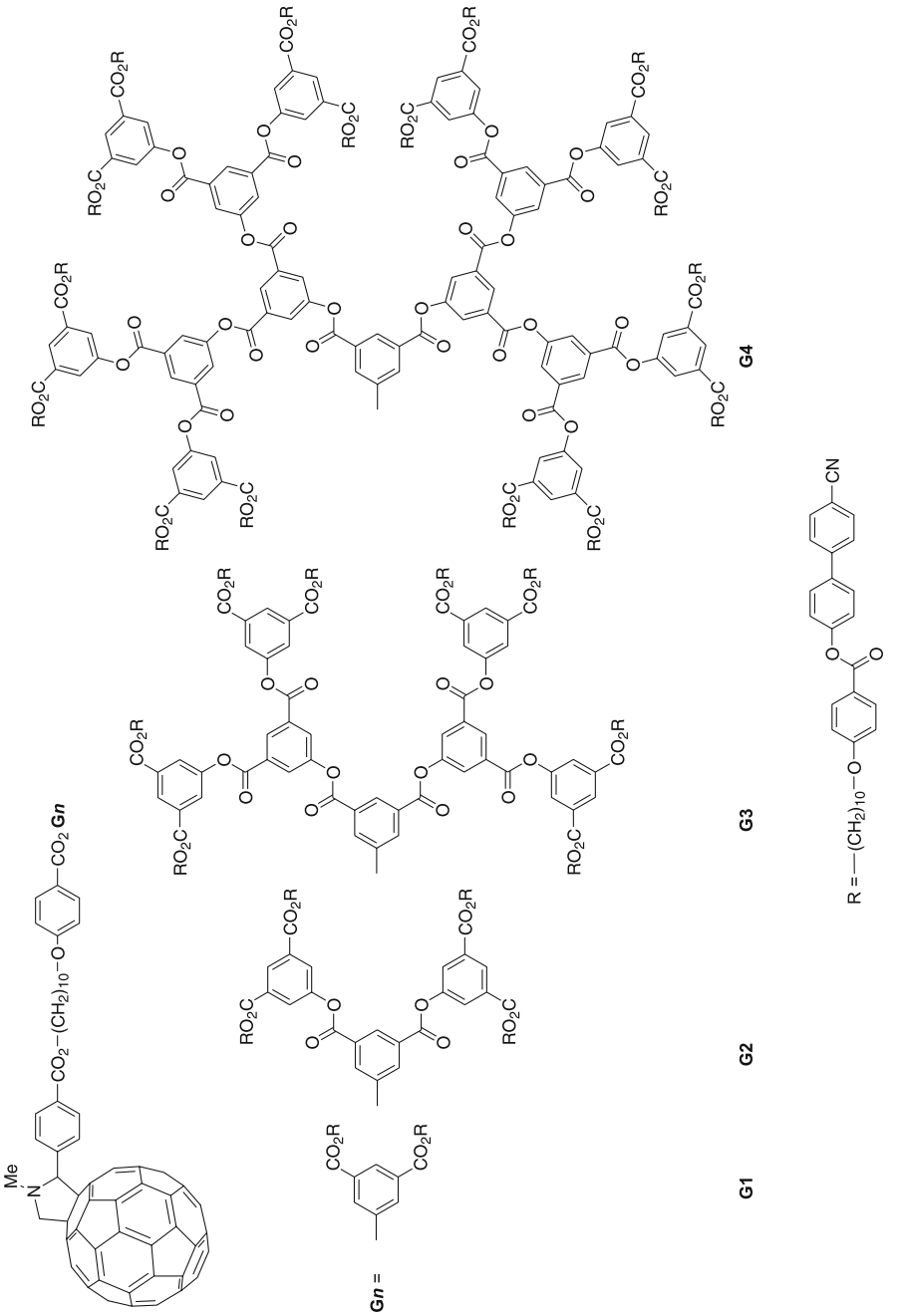

Fig. 72 Structure of the dendritic liquid-crystalline fulleropyrrolidines

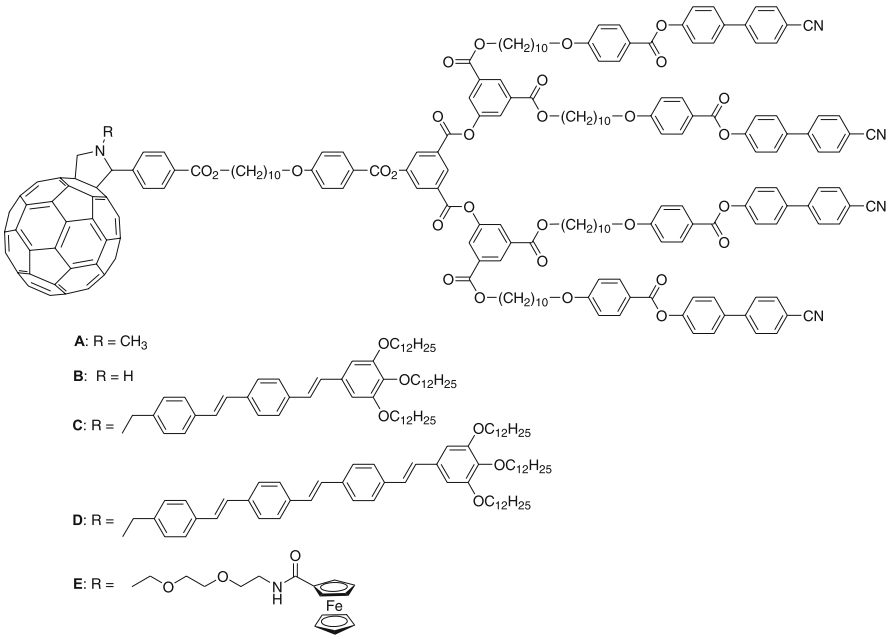

Fig. 73 Fulleropyrrolidine dendrimers of the second generation with various R groups

the dendritic framework [310]. Preliminary luminescence measurements in solution revealed a strong quenching of the oligo(phenylenevinylene) fluorescence by the C_{60} moiety, indicating that these donor-acceptor systems appeared suitable candidates for photovoltaic applications. Second-generation fulleropyrrolidine bearing a ferrocene unit (Fig. 73E) showed a SmA phase between 40 and 135 °C [311]. For this compound, photo-induced electron transfer was observed (through space mechanism) with a lifetime of the charge-separated state of 560 ns in THF. The association of Fc and C_{60} within a liquid-crystalline architecture could be an interesting method for the elaboration of supramolecular switches.

8 Polypedes

The molecular design of these materials is based on a central focal point to which mesogenic units are linked, so that restricted molecular topologies and limited molecular flexibility are induced [57]. They represent a class of materials intermediate between low molecular weight liquid-crystalline compounds and dendritic systems, and can be described as supermolecular entities or giant molecular systems made up of covalently attached

(end-on or side-on) identifiable molecular units (Fig. 74). These architectures once adequately functionalized may then self-organize into mesomorphic supramolecular assemblies with unusual morphologies. When all of the grafted units are the same, they can be considered as a first step of dendritic architectures (zeroth generation) or a polypedal supermolecule. Alternatively, if the mesogenic units are different to one another, they are referred to as multipedal supermolecules (Fig. 74) [57]. This approach also provides the access to several potentially interesting multicomponent structures and materials.

The most simple molecular topology of such systems reported so far is a tetrahedral supermolecule obtained by reacting tetrakis(dimethylsiloxy)-silane with alkenyloxy-cyanobiphenyls (Fig. 22), as discussed previously. Such tetramers exhibit smectic A liquid crystal phases [179]. For such end-on materials, microsegregation at the molecular level favors the formation of the smectic A phases in preference to the nematic phase exhibited by the mesogenic monomers themselves. The use of different polyhedral siloxane systems (Fig. 24) or the C_{60} polyhedron as the template for multi- and polypedal hexakis(methano)fullerenes (Fig. 70) substituted with a large number of terminally attached mesogenic groups confirm the same tendency to the formation of smectic A phases (vide supra).

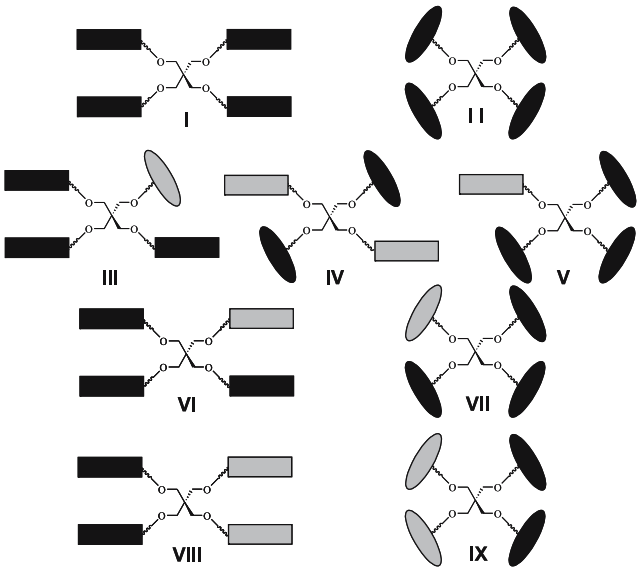

Fig. 74 Schematic representation of LC polypedes (all the mesogenic units are identical) and LC multipedes (either containing two different mesogenic units or two mixed end-on/side-on attachments)

The concept of multipedal liquid crystals was recently further developed by Saez and Goodby [312] who provided an elegant strategy to design tetrameric liquid crystalline polypedes and multipedes around a PE central core (Fig. 75) [57]. Liquid-crystalline materials were previously obtained with a PE central core to which were attached covalently mesogenic sub-units. Despite the large tetrahedral unit, PE was proved not to be particularly detrimental to the formation of mesophases, with a necessary condition, however, being that the peripheral units are strong liquid-crystalline promoters (e.g. calamitic, discotic, conical) and that the attachment is end-on [96–98, 313–322]. In this study, they used two types of mesogenic units, i.e. cyanobiphenyl and biphenyl benzoyloxybenzoate types (Fig. 75, R = A, B, C). The topology of attachment to the core (end-on for the cyanobiphenyl and side-on for the biphenyl benzoyloxybenzoate to yield the various structures I, II, III, and V, Fig. 74), and the chemical nature of the connection between PE and the mesogen (ether, ester and tetramethyldisiloxane moieties) have been used to tailor the mesomorphic properties. The pure cyanobiphenyl derivative (Fig. 75, type I, R = A) exhibits a smectic A phase, whereas all the other oligomers (Fig. 75, II, III, V) exhibit a chiral nematic phase. A chiral nematic phase was induced by the lateral attachment of the chiral phenylbenzoate unit to the core. The stability of the mesophases for the polypedes and multipedes is reported in Table 17.

Complementary dendritic hexamers based on a central scaffold made up of linked pentaerythritol and tri(hydroxymethyl)amino methane units have been found to also exhibit liquid-crystalline properties. This star-shaped scaffold was used to create supermolecules containing two different hemispheres, referred to thereafter as "Janus" supermolecular liquid crystals (Fig. 76) [323, 324]. One of the hemisphere contains three cyanobiphenyl end-groups, whereas the other lobe consists of three chiral phenyl benzoate mesogenic moieties laterally attached. The type of mesophase observed (N*

Table 17 Mesomorphic behavior of the tetrameric polypedes and multipedes

Compound type	Transition temperatures
Tetrapedes (Fig. 75)	
I (R = A)	G –34.3 SmA 21.1 I
III (R = A, R′ = C)	G –20 N* 18.6 I
V (R = B, R′ = A)	Cr 36.2 N* 58.8 I
II (R = B)	Cr 55.8 N* 79.7 I
Hexapedes (Fig. 76)	
R = A, R′ = B, $n = 9$	G –2.8 SmC* 33.8 N* 60.8 I
R = B, R′ = A, $n = 4$	G –7.9 N* 38.2 I

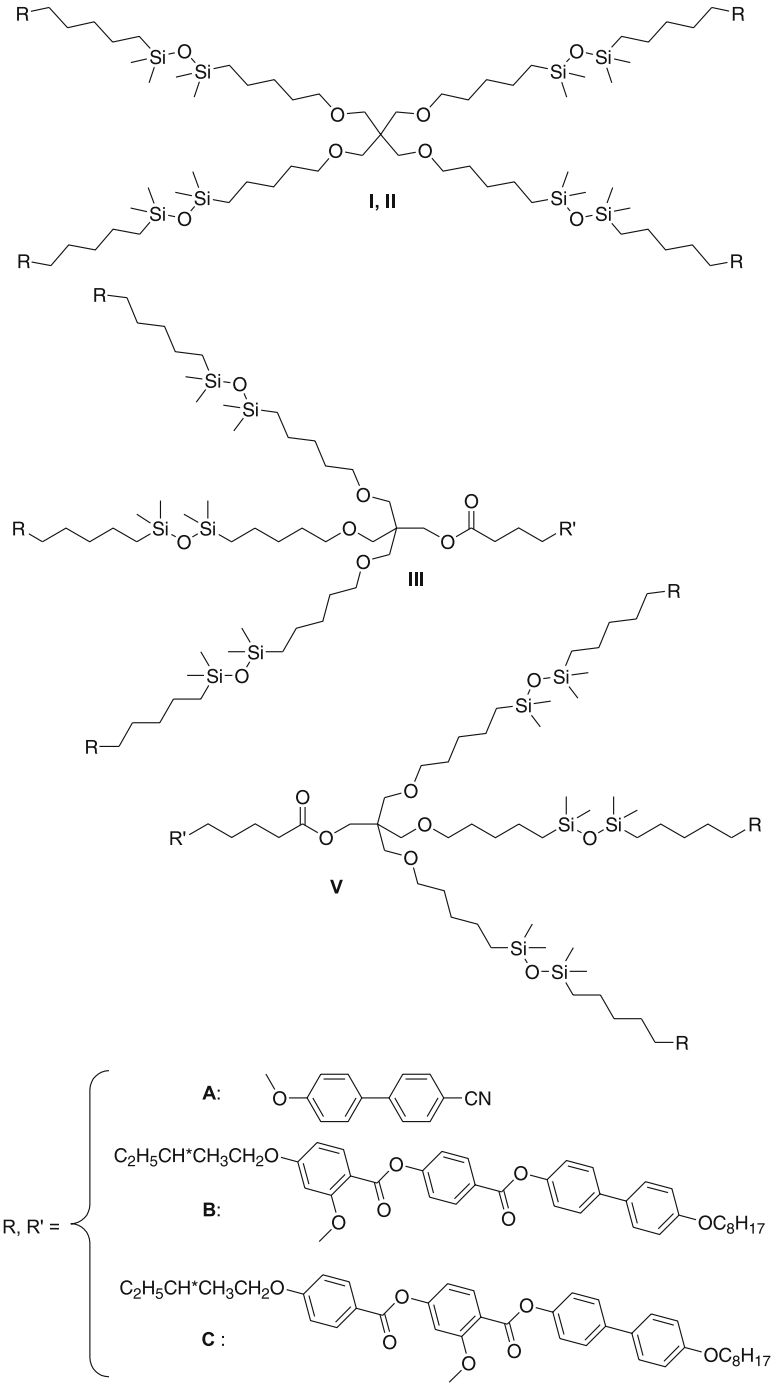

Fig. 75 Supermolecular liquid crystalline tetrapedes and multipedes

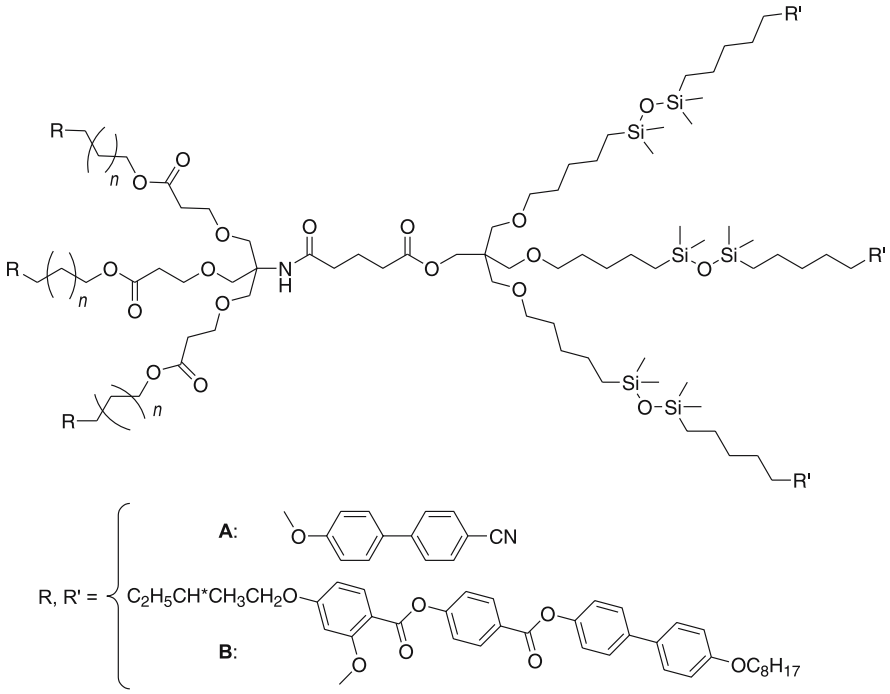

Fig. 76 Hexameric multipedes (Janus Liquid crystals)

or SmC*) depends on the overall topology of the molecule in respect to the inner core (in other words, which hemisphere carries which mesogen, Table 17).

In addition, these materials have very good thermal stabilities and nearly room temperature mesomorphic range and are serious candidates to compete with the famous commercial cyanobiphenyl compounds, and despite their high molecular weight, their physical properties are closer to those of low molecular mass materials than to polymers or dendrimers.

Table 18 Transition temperatures of the nematic supermesogens

G*n* (R)	I	II	III
G1 (A)	G 75 N 235 I	G 68 N 195 I	G 71 N 173 I (G 84 N 222 I) [a]
G2 (A)	G 106 N 183 I	G 108 N 197 I	G 102 N 187 I
G1 (B)	Cr 239 N > 360 I	Cr 200 N 310 I	Cr 150 N 305 I
G2 (B)	G 127 N 308 I	–	–

[a] Isomeric exo,exo-bicyclo[2.2.2]oct-7-ene-2,3,5,6-tetracarboxylic acid counterpart

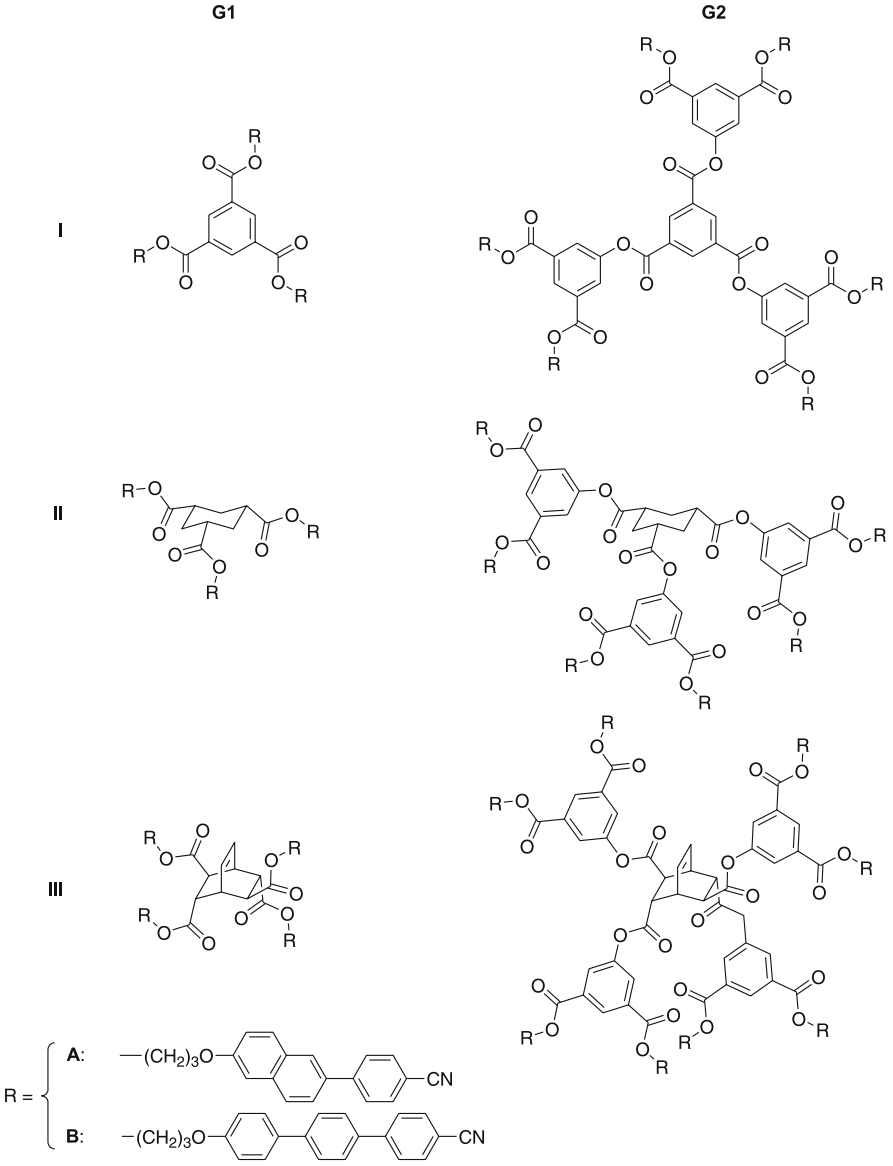

Fig. 77 Structure of the nematic glass-forming materials

Another nice piece of work was provided by Chen et al. [325, 326] on structurally related branched systems. In this work cyano-containing mesogenic pendants were grafted onto various polyvalent central cores.

These zeroth and first generation supermolecules were mesomorphic exhibiting almost exclusively a nematic phase (Table 18), which could be fur-

ther frozen into a glassy state. To assess the effects of the molecular structures on the thermal behavior, several structural parameters were systematically varied such as the shape and connectivity of the central cores namely 1,3,5-benzenetricarboxylic acids, *cis*,*cis*-1,3,5-cyclohexanetricarboxylic acids as well as bicyclo[2.2.2]oct-7-ene-(2,5)-*exo*-(3,6)-*endo*-tetracarboxylic acids, the mesogenic pendant and the spacer (Fig. 77).

Using the same strategy, photoresponsive glassy liquid crystals were also obtained using dithienylethene moieties [327].

9
Miscellaneous

9.1
Mesomorphic Dendrimers with Rigid Discotic Cores

Instead of having a flexible core, such as in the PAMAM and PPI LC dendrimers discussed in another section, the central node of the dendrimers can also be made of a rather rigid chemical unit. Fullerene-containing LC dendrimers are beautiful examples of such a morphology. Star-like discotic liquid crystals can also be considered as one of the first example of this category. The star-like heptamer of triphenylene has been shown to exhibit a hexagonal columnar mesophase between 69 and 122 °C (Fig. 78, R = R^1, R^2, R^3) [328]. Triphenylene has also been used as a central core from which oligomethyleneoxy-chains radiate symmetrically through amide bonds to be terminated by β-D-glucopyranosyl residues [329]. These unusual dendritic-like amphiphilic materials show two well-defined molecular regions, i.e. the central hydrophobic part and the peripheral hydrophilic part (Fig. 78, R = R^4, R^5, R^6, R^7). As a consequence, they exhibit amphotropic liquid crystalline properties, showing both thermotropic and lyotropic behavior. The nature of the molecular arrangements (hexagonal or rectangular) associated with the thermotropic columnar mesomorphism is shown to be strongly dependent on a delicate balance between the volume occupied by the central hydrophobic regions, corresponding to the triphenylene core and the side-chains, and the sizes of the hydrophilic sugar parts attached at the end of the chains. Note that Percec et al. reported hyperbranched liquid crystalline polyesters with discotic cyclotetraveratrylene mesogens as branching cores [330].

Peripheral substitution of phthalocyanine with one or four Fréchet-type dendrons (polyarylether without alkyl chains) surprisingly produces mesomorphic materials whose properties are dominated both by the columnar self-association of the Pc cores and by the glass-forming character of the dendritic wedges [331, 332]. The resulting glassy solids appear indefinitely stable towards crystallization and their structure is governed by the size, number and position of the dendritic wedges attached to the

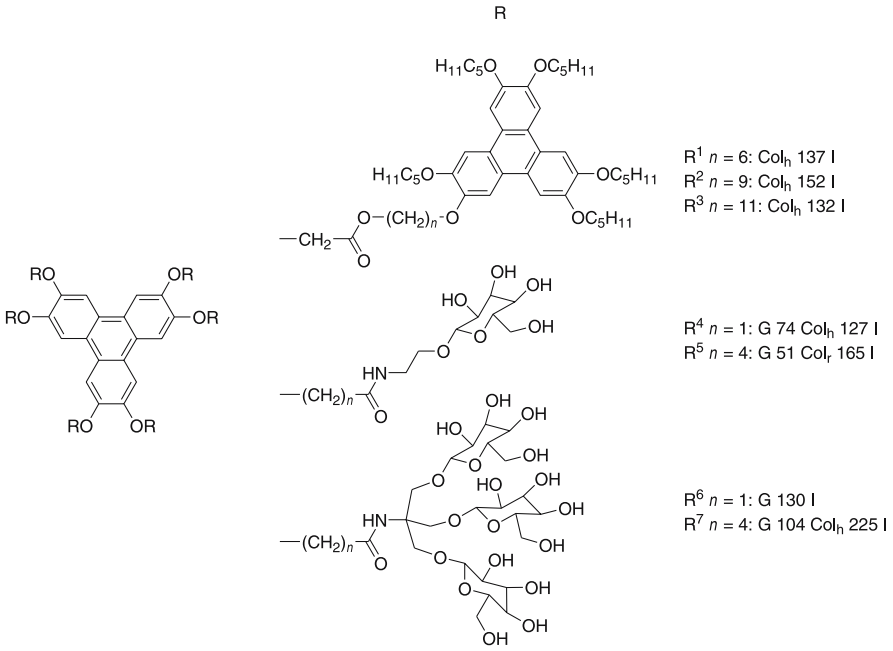

Fig. 78 Dendrimers with central triphenylene cores

Pc macrocycle. Some of them are mesomorphic and show a Col_h phase (Fig. 79: I-G1: G 115 Col_h 270 I; II-G1: G <– 20 Col_h > 320 I; II-G2: G 115 Col_h 250 I; II-G3: 94 Col_h 108 I) for which the structure of the columnar mesophase is frozen at room temperature (anisotropic glasses). The functionalization of these dendrons in the 3 and 5 position of the terminal rings by oligo(ethyleneoxy) chains $(OCH_2CH_2)_3OCH_3$, and their subsequent grafting onto the phthalocyanine of type I (Fig. 79) led to amphiphilic materials [333]. In concentrated ethanol solutions (~ 20–40% by mass), the compound with the functionalized G1 dendron behaves as a discotic amphiphile forming a columnar nematic lyotropic phase. In addition, it possesses a columnar mesophase stable from room temperature up to 260 °C. Systems of type III are not mesomorphic.

Another example of a rigid macrocycle used as the central core of a dendrimer is the porphyrin. First and second generation phenylene-based dendritic porphyrins with 8 and 16 long alkyl chains on their periphery have been studied (Fig. 80). Only the second generation exhibits mesomorphic behavior with the formation of a rectangular columnar mesophase upon heating (Cr 39 Col_r 110 I) [334]. A stable supramolecular 1 : 1 complex was formed between the second generation and C_{60}, which led to the enhancement of the mesophase stability of the formed (unidentified) columnar phase (Cr 99 Col 250 I).

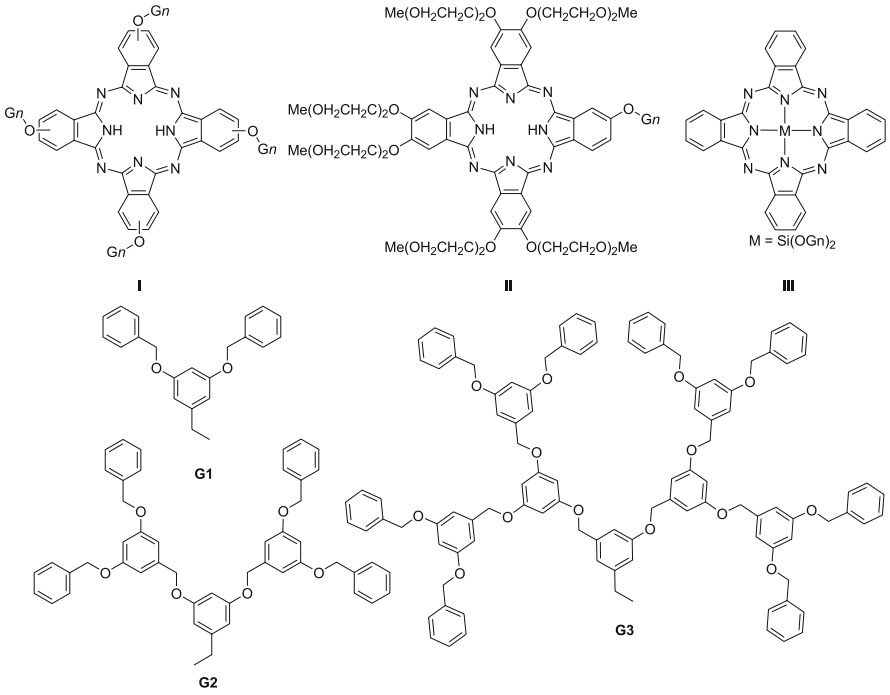

Fig. 79 Dendrimers with central phthalocyanine cores

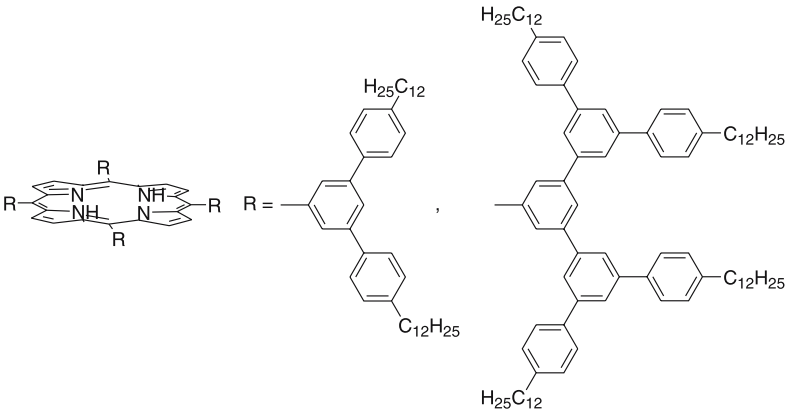

Fig. 80 Dendrimers with central porphyrin cores

9.2
Supramolecular Rod-Coil Block Codendrimers

In order to develop active materials for optics, supramolecular structures derived from rod-coil block copolymers appeared to be materials of par-

ticular interest [335]. Molecular dumbbells consisting of a conjugated rod and dendritic wedges have been synthesized and characterized, and their self-assembling behavior has been investigated (Fig. 81). For example, these dumbbell-shaped molecules are made of a conjugated rod segment consisting of three biphenyls connected through vinyl linkages, and of flexible amphiphilic dentritic wedges with different cross sections (Fig. 81) [336]. These molecular dumbbells self-assemble into discrete bundles of tuneable size that organize into three-dimensional superlattices. The molecules based on a dibranched dendritic wedge, organize into primitive monoclinic crystalline and body-centered tetragonal liquid crystalline (M_{tet}) structures, while the molecules based on tetra- and hexabranched dendritic wedges form only body-centered tetragonal liquid crystalline structures. The number of molecules per bundle decreases systematically when increasing the cross-section of the dendritic wedge (going down from 73 molecules for the dibranched wedge to 39 for the hexabranched wedge). Therefore, the size control of the bundles assembled from the rod building blocks is determined by the cross-section of the flexible segment attached to the rod ends. In addition, spectroscopic studies of these molecules demonstrate that the size of the optically active rod bundle has an influence on the photophysical properties of the conjugated rods (blue shift of the emission maximum when going from the dibranched to the hexabranched molecule).

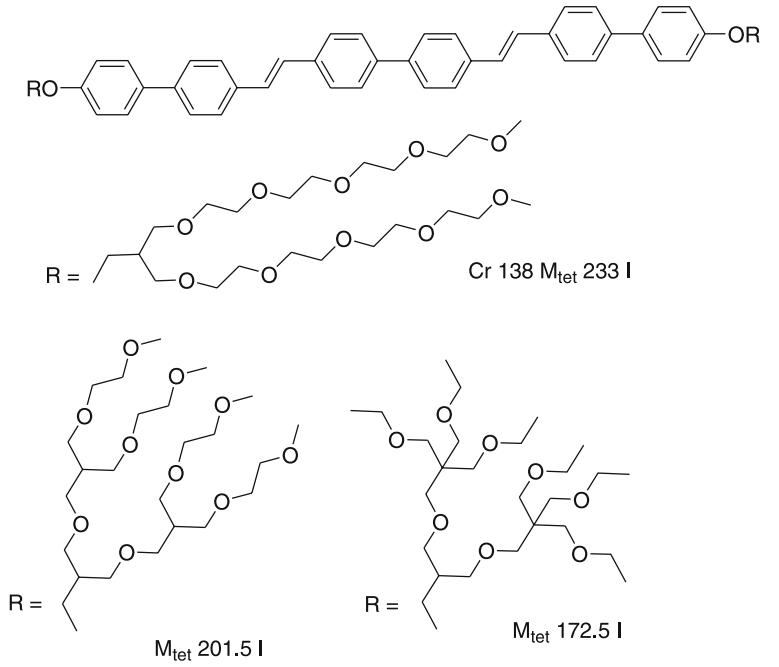

Fig. 81 Dumbbell-shaped molecules based on oligobiphenylene fragments

Another strategy to manipulate the aggregation structure assembled from a conjugated rod building block has been to connect hydrophilic, flexible dendritic branches to one side only, leading to a tree-shaped molecule. For example the latter consists of an octa-phenylene stem segment for the conjugation rod block and of oligo(ethylene oxide) dendrons for the flexible branches (Fig. 82) [337]. These molecular trees can also be considered as a new class of amphiphiles because they consist of a hydrophobic rod and a hydrophilic flexible head [338]. The molecular trees based on a small flexible head were found to self-assemble into a monolayer lamellar structure, whereas those with a larger head-group were found to self-assemble into bundles (containing seven molecules) that are organized according to a 3D primitive orthorhombic supercrystal. When both sides of the linear oligo-*p*-phenylene moiety are functionalized by amphiphilic dendritic wedges, formation of helical superstructures were observed in aqueous solutions [339].

New molecules based on a branched rod block and surrounding flexible ether-type coils represent a class of materials leading to similar self-organizations (Fig. 83, $n = 6$, 8). Such molecules have been shown, provided that the central rigid rod is long enough, to self-assemble into nanostructures (bundle type) that self-organize into a primitive monoclinic structure [340].

More recently, a novel combination of flexible and rigid conjugated parts has been tested, resulting in ABC wedge-coil triblock molecules made of a Y-shaped *p*-phenylene rigid wedge bearing aliphatic chains on one side and a flexible poly(ethylene oxide) (PEO) coil on the other side (Fig. 84A, $n = 12$, 17, 21, 34, 45, 77, 91, 114, 182) [341, 342]. These molecules self-assembled successively, as the length of the PEO chain is increased, into 3D micellar cubic phases with various symmetries (with $Im\bar{3}m$ for $n = 12$ and $Pm\bar{3}n$ for

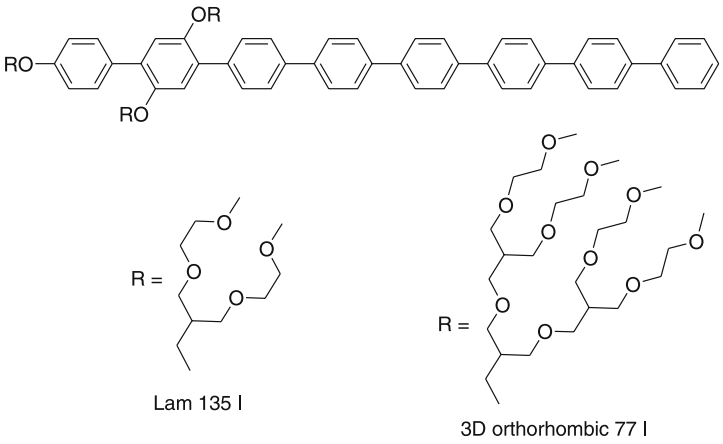

Fig. 82 Octa-*p*-phenylene molecular trees

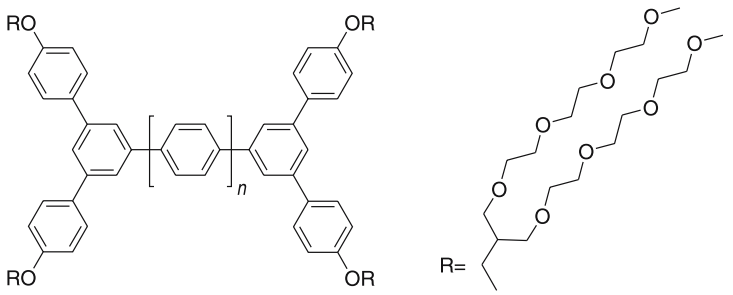

Fig. 83 Branched rod-block molecule with dendritic wedges

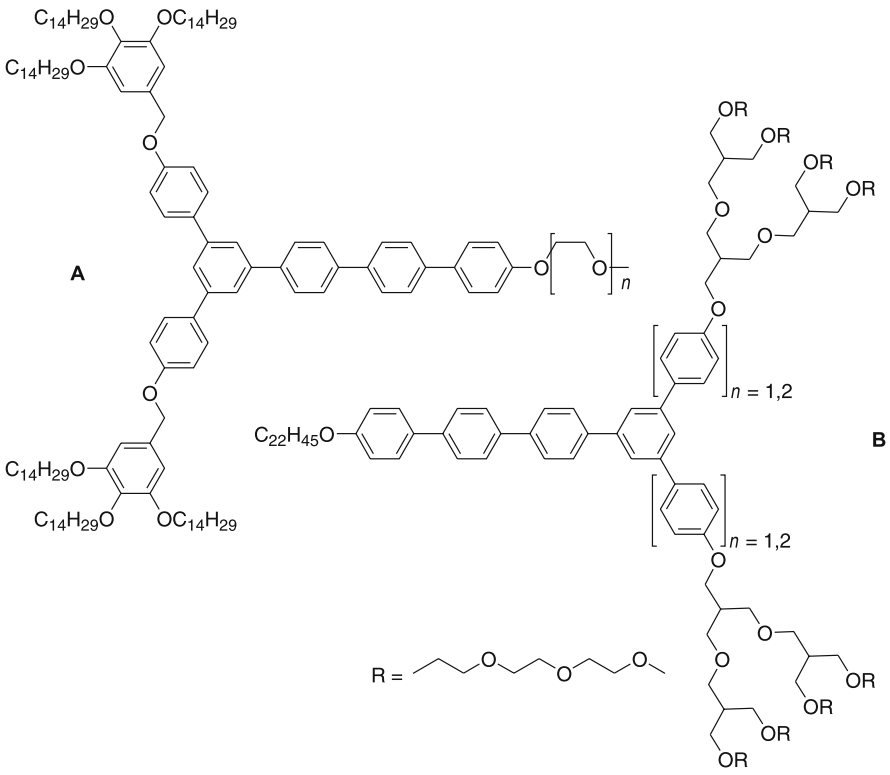

Fig. 84 Structure of the rigid wedge-flexible coil diblock molecules

$n = 17$), 2D hexagonal columnar ($n = 21$, 114, 182), 3D perforated lamellar ($n = 21$, 34), and smectic-like structures ($n = 45$, 77, 91). The melting temperatures remained almost the same (50–60 °C), whereas the clearing temperatures increased when increasing the PEO segment (from 80 to 145 °C). The primary force responsible for this structural change is believed to be

the combination of shape complementarity and microphase separation between the rigid and flexible segments. Among all the mesophases exhibited by such systems, let us point out the case of the unusual bilayered lamellar structure with in-plane ordered coil perforations (perforated lamellar mesophase).

This approach was pursued with the synthesis of "inverted" amphiphilic ABC triblock systems consisting of a hydrophilic dendritic block, a rigid aromatic part and a hydrophobic docosyl chain (Fig. 84B) [343]. X-ray scattering has demonstrated that the molecules with a rather rod-like aromatic unit self-organize into a 2D hexagonal columnar structure (B, $n = 1$: Col_h 36.4 I), while the molecules based on a more wedge-like aromatic unit self-organize into a 3D micellar cubic structure (B, $n = 2$: Cub-$Im\bar{3}m$ 46.1 I). The dimension (8.1 nm) of the hexagonal parameter implies that the rod-like rigid segments arrange axially with their preferred direction within a cross-sectional slice of the column, in which disordered docosyl chains pack in an interdigitated fashion. As for the cubic phase, it consists of a 3D body-centered arrangement of discrete polyhedral aggregates. Interestingly, dynamic light scattering and scanning electron microscopy studies of aqueous solution with the addition of $CHCl_3$ showed that these rigid-dendritic block molecules self-assemble into stable capsule-like micellar aggregates in the presence of a hydrophobic solvent.

10 Conclusions

The above examples show that liquid-crystalline phases can been produced with high molecular weight monodisperse dendrimers, dendrons and polypedes. Nematic, lamellar, columnar, cubic phases as well as less conventional mesophases are obtained depending upon the chemical nature of the terminal mesogenic groups, dendritic core and dendrimer generation. Such a tuning of the mesomorphic structure by an appropriate molecular design makes possible the development of new liquid-crystalline materials containing active molecular units with specific physical properties to be used in nanotechnology. The high sensitivity of such dendrimers to the surrounding environment (properties vs. molecular structure) could be, in principle, beneficial to some kinds of molecular sensors, i.e. to use such supermolecules as tools to test how properties in general may be altered or modulated through delicate external stimuli.

Acknowledgements B.D. and D.G. are grateful to Dr. Delphine Felder-Flesh (IPCMS) and Prof. Robert Deschenaux (Institute of Chemistry, Neuchâtel, Switzerland) for their kindness in reading the manuscript carefully, and offering us their critical and constructive remarks and comments. They are greatly acknowledged.

References

1. Tomalia DA, Fréchet JMJ (2002) Polym Sci A, Polym Chem 40:2719
2. Tomalia DA, Dupont Durst H (1993) Top Curr Chem 165:193
3. Ardoin N, Astruc D (1995) Bull Soc Chem Fr 132:875
4. Newkome GR, Moorefield CN, Vögtle F (eds) (1996) Dendritic Molecules: Concepts, Synthesis and Perspectives. Wiley, Weinheim
5. Ashton PR, Boyd SE, Brown CL, Nepogodiev SA, Meijer EW, Peerlings HWI, Stoddart JF (1997) Chem Eur J 3:974
6. Matthews OAN, Shipway N, Stoddart JF (1998) Prog Polym Sci 23:1
7. Newkome GR, Moorefield CN, Vögtle F (eds) (2001) Dendrimers and Dendrons: Concepts, Synthesis and Applications. Wiley, Weinheim
8. Voit BI (1995) Acta Polym 46:87
9. Fréchet JMJ, Tomalia DA (eds) (2001) Dendrimers and other Dendritic Polymers. Wiley Series in Polymer Sciences. Wiley, Weinheim
10. Special issues of C R Chim (2003) 6:709
11. Special issues of Prog Polym Sci (2005) 30:217
12. Grayson SM, Fréchet JM (2001) Chem Rev 101:3819
13. Hawker CJ (1999) Adv Polym Sci 147:113
14. Tomalia DA, Naylor AM, Goddard III WA (1990) Angew Chem Int Ed Engl 29:138
15. Tomalia DA (1994) Adv Mater 6:529
16. Feuerbacher N, Vögtle F (1998) Top Curr Chem 197:1
17. Issberner J, Moors R, Vögtle F (1994) Angew Chem Int Ed Engl 33:2413
18. Dykes GMJ (2001) Chem Technol Biotechnol 76:903
19. Boas U, Heegaard PMH (2004) Chem Soc Rev 33:43
20. Astruc D (1996) C R Acad Sci Paris Ser II 322:757
21. Uhrich K (1997) TRIP 5:388
22. Smith DK, Diederich F (1998) Chem Eur J 4:1353
23. Hecht S, Fréchet JMJ (2001) Angew Chem Int Ed 40:74
24. Cloninger MJ (2002) Curr Opinion Chem Bio 6:742
25. Chow HF, Mong TKK, Nongrum MF, Wan CW (1998) Tetrahedron 54:8543
26. Archut A, Vögtle F (1998) Chem Soc Rev 27:233
27. Fischer M, Vögtle F (1999) Angew Chem Int Ed 38:884
28. Inoue K (2000) Prog Polym Sci 25:453
29. Vögtle F, Gestermann S, Hesse R, Schwierz H, Windisch B (2000) Prog Polym Sci 25:987
30. Adronov A, Fréchet JMJ (2000) Chem Commun 1701
31. Beletskaya IP, Chuchurjukin AV (2000) Russ Chem Rev 69:639
32. Seebach D, Rheiner PB, Greiveldinger G, Butz T, Sellner H (1998) Top Curr Chem 197:125
33. Romagnoli B, Hayes W (2002) J Mater Chem 12:767
34. Constable EC (1997) Chem Commun 1073
35. Venturi M, Serroni S, Juris A, Campagna S, Balzani V (1998) Top Curr Chem 197:193
36. Gorman C (1998) Adv Mater 10:295
37. Newkome GR, He E, Moorefield CN (1999) Chem Rev 99:1689
38. Hearshaw MA, Moss JR (1999) Chem Commun 1
39. Stoddart FJ, Welton T (1999) Polyhedron 18:3575
40. Cuadrado I, Morán M, Casado CM, Alonso B, Losada J (1999) Coord Chem Rev 193–195:395
41. Majoral JP, Caminade AM (1998) Top Curr Chem 197:79

42. Majoral JP, Caminade AM (1999) Chem Rev 99:845
43. Frey H, Lach C, Lorenz K (1998) Adv Mater 10:279
44. Frey H, Schlenk C (2000) Top Curr Chem 210:69
45. Lang H, Lühmann B (2001) Adv Mater 13:1523
46. Collings PJ, Hird M (1997) Introduction to Liquid Crystals Chemistry and Physics. Taylor & Francis Ltd, London
47. Demus D, Goodby JW, Gray GW, Spiess HW, Vill V (eds) (1998) Handbook of Liquid Crystals. Wiley, Weinheim
48. Zeng F, Zimmerman SC (1997) Chem Rev 97:1681
49. Narayanan VV, Newkome GR (1998) Top Curr Chem 197:19
50. Constable EC, Housecroft CE (1998) Chimia 52:533
51. Emrick T, Fréchet JMJ (1999) Curr Opinion Coll Interface Sc 4:15
52. Smith DK, Diederich F (2000) Top Curr Chem 210:183
53. Goodby JW, Mehl GH, Saez IM, Tuffin RP, Mackenzie G, Auzély-Velty R, Benvegnu T, Plusquellec D (1998) Chem Commun 2057
54. Goodby JW (1999) Curr Opin Solid State Mater Sci 4:361
55. Ponomarenko SA, Boiko NI, Shibaev VP (2001) Polym Sci Ser A 43:1
56. Guillon D, Deschenaux R (2002) Curr Opinion Sol State Mater Sci 6:515
57. Saez IM, Goodby JW (2005) J Mater Chem 15:26
58. Hamley IW (2000) Introduction to Soft Matter: Polymers, Colloids, Amphiphiles and Liquid Crystals. Wiley, New York
59. Demus D (1989) Liq Cryst 5:75
60. Tschierske C (1996) Prog Polym Sci 21:775
61. Tschierske C (1998) J Mater Chem 8:1485
62. Tschierske C (2001) J Mater Chem 11:2647
63. Tschierske C (2002) Curr Opin Colloid Interface Sci 7:69
64. Tschierske C (2001) Annu Rep Prog Chem Sect C 97:191
65. Tschierske C (2002) Curr Opinion Coll Interface Sci 7:69
66. Cheng X, Prehm M, Das MK, Kain J, Baumeister U, Diele S, Dag L, Blume A, Tschierske C (2003) J Am Chem Soc 125:10977
67. Percec V, Kawasumi M (1992) Macromolecules 25:3843
68. Bauer S, Fischer H, Ringsdorf H (1993) Angew Chem Int Ed Engl 32:1589
69. Percec V, Chu P, Kawasumi M (1994) Macromolecules 27:4441
70. Hanh SW, Yun SYK, Jin JI, Han OH (1998) Macromolecules 31:6417
71. Sunder A, Quincy MF, Mülhaupt R, Frey H (1999) Angew Chem Int Ed 38:2928
72. Choi SH, Lee NH, Cha SW, Jin JI (2001) Macromolecules 34:2138
73. Park YS, Lee JW, Jin JI (2002) Bull Korean Chem Soc 23:1201
74. Flory PJ (1953) Principles of Polymer Chemistry. Cornell University Press, Ithaca, NY
75. Kim YH (1998) J Polym Sci A Polym Chem 36:1685
76. Frey H, Hölter D (1999) Acta Polym 50:67
77. Hult A, Johansson M, Malmström E (1999) Adv Polym Sci 143:1
78. Hamley IW (1998) The Physics of Block-Copolymers. Oxford University Press, Oxford
79. Percec V, Johansson G, Heck J, Ungar G, Batty SV (1993) J Chem Soc, Perkins Trans 1, 1411
80. Percec V, Heck JA, Tomazos D, Ungar G (1993) J Chem Soc, Perkin Trans 2, 2381
81. Percec V, Heck JA, Tomazos D, Falkenberg F, Blackwell H, Ungar G (1993) J Chem Soc, Perkin Trans 1, 2799
82. Percec V, Tomazos D, Heck JA, Blackwell H, Ungar G (1994) J Chem Soc, Perkin Trans 2, 31

83. Johansson G, Percec V, Ungar G, Abramic D (1994) J Chem Soc, Perkin Trans 1, 447
84. Ungar G, Batty SV, Percec V, Heck J, Johansson G (1994) Adv Mater Optics Electron 4:303
85. Chvalun SN, Blackwell J, Cho JD, Kwon YK, Percec V, Heck JA (1998) Polymer 39:4515
86. Kwon YK, Chvalun S, Schneider AI, Blackwell J, Percec V, Heck JA (1994) Macromolecules 27:6129
87. Percec V, Schlueter D, Ungar G, Cheng SZD, Zhang A (1998) Macromolecules 31:1745
88. Prokhorova SA, Sheiko SS, Möller M, Ahn CH, Percec V (1998) Macromol Rapid Commun 19:359
89. Percec V, Ahn CH, Cho WD, Jamieson AM, Kim J, Leman T, Schmidt M, Gerle M, Möller M, Prokhorova SA, Sheiko SS, Cheng ZD, Zhang A, Ungar G, Yeardley DJP (1998) J Am Chem Soc 120:8619
90. Percec V, Ahn CH, Ungar G, Yeardley DJP, Möller M, Shieko SS (1998) Nature 391:161
91. Chvalun SN, Blackwell J, Cho JD, Bykova IV, Percec V (1999) Adv Polym Sci 50:51
92. Yeardley DJP, Ungar G, Percec V, Holerca MN, Johansson G (2000) J Am Chem Soc 122:1684
93. Duan H, Hudson SD, Ungar G, Holerca MN, Percec V (2001) Chem Eur J 7:4134
94. Percec V, Holerca MN (2000) Biomacromolecules 1:6
95. Percec V, Bera TK (2002) Biomacromolecules 3:167
96. Malthête J, Collet A, Levelut AM (1989) Liq Cryst 5:123
97. Malthête J, Levelut AM (1991) Adv Mater 3:94
98. Malthête J (1996) New J Chem 20:925
99. Percec V, Johansson G, Ungar G, Zhou J (1996) J Am Chem Soc 118:9855
100. Johansson G, Percec V, Ungar G, Zhou JP (1996) Macromolecules 29:646
101. Jung HT, Kim SO, Hudson SD, Percec V (2002) Appl Phys Lett 80:395
102. Percec P, Holerca MN, Uchida S, Cho WD, Ungar G, Lee Y, Yeardley DJP (2002) Chem Eur J 8:1106
103. Naylor AM, Goddard WA, Kiefer GE, Tomalia DA (1989) J Am Chem Soc 111:2339
104. Balagurusamy VSK, Ungar G, Percec V, Johansson G (1997) J Am Chem Soc 119: 1539
105. Ungar G, Percec V, Holerca MN, Johansson GA, Heck JA (2000) Chem Eur J 6:1258
106. Hudson SD, Jung HT, Percec V, Cho WD, Johansson G, Ungar G, Balagurusamy VSK (1997) Science 278:449
107. Dukeson DR, Ungar G, Balagurusamy VSK, Percec V, Johansson GA, Glodde M (2003) J Am Chem Soc 125:15974
108. Vargas R, Mariani P, Gulik A, Luzzati V (1992) J Mol Biol 225:137
109. Luzzati V, Vargas R, Mariani P, Gulik A, Delacroix H (1993) J Mol Biol 229:540
110. Gulik A, Delacroix H, Kirschner G, Luzzati V (1995) J Phys France II 5:445
111. Luzzati V (1995) J Phys France II 5:1649
112. Percec V, Glodde M, Johansson G, Balagurusamy VSK, Heiney PA (2003) Angew Chem Int Ed 42:4338
113. Percec V, Cho WD, Mosier PE, Ungar G, Yeardley DLP (1998) J Am Chem Soc 120:11061
114. Percec V, Cho WD, Ungar G (2000) J Am Chem Soc 122:10273
115. Percec V, Cho WD, Ungar G, Yeardley DJP (2000) Angew Chem Int Ed 39:1597
116. Percec V, Cho WD, Möller M, Prokhorova SA, Ungar G, Yeardley DJP (2000) J Am Chem Soc 122:4249
117. Percec V, Cho WD, Ungar G, Yeardley DJP (2001) J Am Chem Soc 123:1302
118. Hudson SD, Jung HAT, Kewsuwan P, Percec V, Cho WD (1999) Liq Cryst 26:1493

119. Li Y, Lin ST, Goddard III WA (2004) J Am Chem Soc 126:1872
120. Ungar G, Liu Y, Zeng X, Percec V, Cho WD (2003) Science 299:1208
121. Zeng X, Ungar G, Liu Y, Percec V, Dulcey AE, Hobbs JK (2004) Nature 428:157
122. Ungar G, Zeng X (2005) Soft Matter 1:95
123. van der Vegt AK (2001) Order in space. VSSD, Edition on internet (http://www.vssd.nl/hlf)
124. Sadoc JF, Rivier N (eds) (1999) Foams and Emulsions. Kluwer, Dordrecht
125. Percec V, Cho WD, Ungar G, Yeardley DJP (2002) Chem Eur J 8:2011
126. Percec V, Mitchell CM, Cho WD, Uchida S, Glodde M, Ungar G, Zeng X, Liu Y, Balagurusamy VSK, Heiney PA (2004) J Am Chem Soc 126:6078
127. Jung HT, Kim SO, Ko YK, Yoon DK, Hudson SD, Percec V, Holerca MN, Cho WD, Moisier PE (2002) Macromolecules 35:3717
128. Yoon DK, Ko YK, Jung HT (2003) Liq Cryst 30:559
129. Yoon DK, Jung HT (2005) Mol Cryst Liq Cryst 412:417
130. Sidorenko A, Houphouet-Boigny C, Villavicencio O, Hashemzadeh M, McGrath DV, Tsukruk VV (2000) Macromolecules 16:10569
131. Pao WJ, Stetzer MR, Heiney PA, Cho WD, Percec V (2001) J Phys Chem B 105:2170
132. Frey H, Mülhaupt R, Lorenz K, Rapp U, Mayer-Posner FJ (1995) Polym Mater Sci Eng 73:127
133. Frey H, Lorenz K, Mülhaupt R, Rapp U, Mayer-Posner FJ (1996) Macromol Symp 102:19
134. Coen MC, Lorenz K, Kressler J, Frey H, Mülhaupt R (1996) Macromolecules 29:8069
135. Lorenz K, Hölter D, Frey H, Stühn B (1997) Polym Mater Sci Eng 77:168
136. Lorenz K, Hölter D, Stühn B, Mülhaupt R, Frey H (1996) Adv Mater 8:414
137. Trahasch B, Frey H, Lorenz K, Stühn B (1999) Colloid Polym Sci 277:1186
138. Lorenz K, Frey H, Stühn B, Mülhaupt R (1997) Macromolecules 30:6860
139. Stark B, Lach C, Frey H, Stuhn B (1999) Macromol Symp 146:33
140. Stark B, Stühn B, Frey H, Lach C, Lorenz K, Frick B (1998) Macromolecules 31:5415
141. Trahasch B, Stühn B, Frey H, Lorenz K (1999) Macromolecules 32:1962
142. Caminade AM, Turrin CO, Sutra P, Majoral JP (2003) Curr Opin Colloid Interface Sci 8:282
143. Terunuma D, Kato T, Nishio R, Matsuoka K, Kuzuhara H, Aoki Y, Nohira H (1998) Chem Lett 59
144. Terunuma D, Kato T, Nishio R, Aoki Y, Nohira H, Matsuoka K, Kuzuhara H (1999) Bull Chem Soc Jpn 72:2129
145. Terunuma D, Nishio R, Aoki Y, Nohira H, Matsuoka K, Kuzuhara H (1999) Chem Lett 565
146. Pelzl G, Diele S, Weissflog W (1999) Adv Mater 11:707
147. Dantlgraber G, Baumeister U, Diele S, Kresse H, Lühmann B, Lang H, Tschierske C (2002) J Am Chem Soc 124:14852
148. Ponomarenko SA, Rebrov EA, Bobrovski AY, Boiko NI, Muzafarov AM, Shibaev VP (1996) Liq Cryst 21:1
149. Platé NA, Shibaev VP (eds) (1987) Comb-Shaped Polymers and Liquid Crystals. Plenum, New York
150. Ryumtsev EI, Evlampieva NP, Lezov AV, Ponomarenko SA, Boiko NI, Shibaev VP (1998) Liq Cryst 25:475
151. Ponomarenko SA, Rebrov EA, Boiko NI, Muzafarov AM, Shibaev VP (1998) Polym Sci Ser A 40:763
152. Ponamorenko S, Boiko N, Rebrov E, Muzafarov A, Whitehouse I, Richardson R, Shibaev V (1999) Mol Cryst Liq Cryst 332:43

153. Richardson RM, Whitehouse IJ, Ponomarenko SA, Boiko NI, Shibaev VP (1999) Mol Cryst Liq Cryst 330:167
154. Lezov AV, Mel'nikov AB, Polushina GE, Ponomarenko SA, Boiko NI, Kossmehl E, Ryumtsev EI, Shibaev VP (1998) Doklady Akad Nauk 362:638
155. Lezov AV, Mel'nikov AB, Polushina GE, Antonov EA, Novitskaya ME, Boiko NI, Ponomarenko SA, Rebrov EA, Shibaev VP, Ryumtsev EI, Muzafarov AM (2001) Doklady Chem 381:313
156. Klenin VJ, Panina YuV, Yarotskii VI, Ponomarenko SA, Boiko NI, Shibaev VP (2001) Polym Sci Ser A 43:519
157. Wilson MR, Ilnystskyi JM, Stimson LM (2003) J Chem Phys 119:3509
158. Richardson RM, Ponomarenko SA, Boiko NI, Shibaev VP (1999) Liq Cryst 26:101
159. Ponomarenko SA, Agina EV, Boiko NI, Rebrov EA, Muzafarov AM, Richardson RM, Shibaev VP (2001) Mol Cryst Liq Cryst 364:93
160. Agina EV, Ponomarenko SA, Boiko NI, Rebrov EA, Muzafarov AM, Shibaev VP (2001) Polym Sci Ser A 43:1000
161. Kovshik AP, Ragimov DA, Kovshik SA, Boiko NI, Lezov AV, Ryumtsev EI (2003) Russ J Phys Chem 77:1041
162. Ponomarenko SA, Boiko NI, Shibaev VP, Magonov SN (2000) Langmuir 16:5487
163. Ponomarenko SA, Boiko NI, Zhu XM, Agina EV, Shibaev VP, Magonov SN (2001) Polym Sci Ser A 43:245
164. Genson KL, Holzmueller J, Leshchiner I, Agina E, Boiko N, Shibaev VP, Tsukruk VV (2005) Macromolecules 38:8028
165. Ponomarenko SA, Boiko NI, Shibaev VP, Richardson RM, Whitehouse IJ, Rebrov EA, Muzafarov AM (2000) Macromolecules 33:5549
166. Boiko N, Zhu X, Vinokur R, Rebrov E, Muzafarov A, Shibaev V (2000) Mol Cryst Liq Cryst 352:343
167. Boiko N, Zhu X, Vinokur R, Rebrov E, Muzafarov A, Shibaev V (2000) Ferroelectrics 243:59
168. Zhu XM, Vinokur RA, Ponomarenko SA, Rebrov EA, Muzafarov AM, Boiko NI, Shibaev VP (2000) Polym Sci Ser A 42:1263
169. Boiko NI, Lysachkov AI, Ponomarenko SA, Shibaev VP, Richardson RM (2005) Colloid Polym Sci 283:1155
170. Zhu XM, Boiko NI, Rebrov EA, Muzafarov AM, Kozlovsky MV, Richardson RM, Shibaev VP (2001) Liq Cryst 28:1259
171. Bobrovsky AY, Pakhomov AA, Zhu XM, Boiko NI, Shibaev VP (2001) Polym Sci Ser A 43:431
172. Bobrovski A, Ponomarenko S, Boiko N, Shibaev V, Rebrov E, Muzafarov A, Stumpe J (2002) Macromol Chem Phys 230:1539
173. Bobrovsky AY, Pakhomov AA, Zhu XM, Boiko NI, Shibaev VP, Stumpe J (2002) J Phys Chem B 106:540
174. Boiko N, Zhu X, Bobrovsky A, Shibaev V (2001) Chem Mater 13:1447
175. Mehl GH, Thornton AJ, Goodby JW (1999) Mol Cryst Liq Cryst 332:455
176. Mehl GH, Goodby JW (1999) Chem Commun 13
177. Kowalewska A, Lickiss PD, Lucas R, Stańczyk WA (2000) J Organomet Chem 597:111
178. Ponomarenko SA, Rebrov EA, Boiko NI, Vasilenko NG, Muzafarov AM, Freidzon YS, Shibaev V (1994) Polym Sci Ser A 36:896
179. Mehl GH, Goodby JW (1996) Chem Ber 129:521
180. Merkel K, Kocot A, Vij JK, Mehl GH, Meyer T (2004) J Chem Phys 121:5012
181. Kannan RY, Salacinski HJ, Butler PE, Seifalian AM (2005) Acc Chem Res 38:879
182. Mehl GH, Saez IM (1999) Appl Organomet Chem 13:261

183. De Gennes PG, Hervet H (1983) J Phys Lett 44:351
184. Mehl GH, Goodby JW (1997) Mol Cryst Liq Cryst 303:15
185. Kreuzer FH, Mauerer R, Spes P (1991) Makromol Chem-M Symp 30:215
186. Mehl GH, Goodby JW (1996) Angew Chem Int Ed Engl 35:2641
187. Saez IM, Styring P (1996) Adv Mater 8:1001
188. Sellinger A, Laine RM, Chu V, Viner C (1994) J Polym Sci Part A Polym Chem 32:3069
189. Laine RM, Zhang C, Sellinger A, Viculis L (1998) Appl Organometal Chem 12:715
190. Zhang C, Bunning TJ, Lainr RJ (2001) Chem Mater 13:3653
191. Elsäßer R, Mehl GH, Goodby JW, Photinos DJ (2000) Chem Commun 851
192. Saez IM, Goodby JW (1999) Liq Cryst 26:1101
193. Saez IM, Goodby JW, Richardson RM (2001) Chem Eur J 7:2758
194. Saez IM, Goodby JW (2001) J Mater Chem 11:2845
195. Elsäßer R, Mehl GH, Goodby JW, Veith M (2001) Angew Chem Int Ed 40:2688
196. Mehl GH, Elsäßer R, Goodby JW, Veith M (2001) Mol Cryst Liq Cryst 364:219
197. Elsäßer R, Goodby JW, Mehl GH, Rodriguez-Martin D, Richardson RM, Photinos DJ, Veith M (2003) Mol Cryst Liq Cryst 402:1
198. Tajber L, Kocot A, Vij JK, Merkel K, Zalewska-Rejdak J, Mehl GH, Elsässer R, Goodby JW, Veith M (2002) Macromolecules 35:8601
199. Barbera J, Donnio B, Gehringer L, Guillon D, Marcos M, Omenat A, Serrano JL (2005) J Mater Chem 15:4093
200. Baars MWPL, Söntjens SHM, Fischer HM, Peerlings HWI, Meijer EW (1998) Chem Eur J 4:2456
201. Stevelmans S, van Hest JCM, Jansen JFGA, van Boxtel DAFJ, de Brabander-van den Berg EMM, Meijer EW (1996) J Am Chem Soc 118:7398
202. Schenning APHJ, Elissen-Román C, Weener JW, Baars MWPL, van der Gaast SJ, Meijer EW (1998) J Am Chem Soc 120:8199
203. Baars MWPL, van Boxtel MCW, Bastiaansen CWM, Broer DJ, Söntjens SHM, Meijer EW (2000) Adv Mater 12:715
204. Suzuki K, Haba O, Nagahata R, Yonetake K, Ueda M (1998) High Perform Polym 10:231
205. Yonetake K, Suzuki K, Morishita T, Nagahata R, Ueda M (1998) High Perform Polym 10:373
206. Tsiourvas D, Felekis T, Sideratou, Paleos CM (2002) Macromolecules 35:6466
207. Seitz M, Plesnivy T, Schimossek K, Edelmann M, Ringsdorf H, Fischer H, Uyama H, Kobayashi S (1996) Macromolecules 29:6560
208. Cameron JH, Facher A, Lattermann G, Diele S (1997) Adv Mater 9:398
209. Usol'tseva N, Bykova V, Smirnova A, Grusdev M, Lattermann G, Facher A (2004) Mol Cryst Liq Cryst 409:29
210. Domracheva N, Mirea A, Schwoerer M, Torre-Lorente L, Lattermann G (2005) ChemPhysChem 6:110
211. Marcos M, Omenat A, Serrano JL (2003) C R Chimie 6:947
212. Barberá J, Marcos M, Serrano JL (1999) Chem Eur J 5:1834
213. Marcos M, Giménez R, Serrano JL, Donnio B, Heinrich B, Guillon D (2001) Chem Eur J 7:1006
214. Donnio B, Barberá J, Giménez R, Guillon D, Marcos M, Serrano JL (2002) Macromolecules 35:370
215. McKenna MD, Barberá J, Marcos M, Serrano JL (2005) J Am Chem Soc 127:619
216. Barberá J, Donnio B, Giménez R, Guillon D, Marcos M, Omenat A, Serrano JL (2001) J Mater Chem 11:2808

217. Pastor L, Barberá J, McKenna M, Marcos M, Martín-Rapún R, Serrano JL, Luckhurst GR, Mainal A (2004) Macromolecules 37:9386
218. Martín-Rapún R, Marcos M, Omenat A, Serrano JL, Luckhurst GR, Mainal A (2004) Chem Mater 16:4969
219. Severing K, Saalwächter K (2004) Phys Rev Lett 92:125501
220. Rueff JM, Barberá J, Donnio B, Guillon D, Marcos M, Serrano JL (2003) Macromolecules 36:8368
221. Van-Quynh A, Filip D, Cruz C, Sebastião PJ, Ribeiro AC, Rueff JM, Marcos M, Serrano JL (2005) Eur Phys J E 18:149
222. Rueff JM, Barberá J, Marcos M, Omenat A, Martín-Rapún R, Donnio B, Guillon D, Serrano JL (2006) Chem Mater 18:249
223. Precup-Blaga FS, Schenning APHJ, Meijer EW (2003) Macromolecules 36:565
224. Terzis AF, Vanakaras AG, Photinos DJ (1999) Mol Cryst Liq Cryst 330:517
225. Vanakaras AG, Photinos DJ (2001) J Mater Chem 11:2832
226. Terzis AF, Vanakaras AG, Photinos DJ (2000) Mol Cryst Liq Cryst 352:265
227. Vanakaras AG, Photinos DJ (2005) J Mater Chem 15:2002
228. Serrano JL, Marcos M, Martín R, González M, Barberá J (2003) Chem Mater 15:3866
229. Kardas D, Prehm M, Baumeister U, Pociecha D, Reddy RA, Mehl GH, Tschierske C (2005) J Mater Chem 15:1722
230. Tsiourvas D, Stathopoulou K, Sideratou Z, Paleos CM (2002) Macromolecules 35:1746
231. Diele S, Göring P (1998) In: Demus D, Goodby JW, Gray GW, Spiess HW, Vill V (eds) Handbook of Liquid Crystals. Wiley, Weinheim, vol 2B, chapter XIII, 887
232. Diele S (2002) Curr Opinion Coll Interface Sci 7:333
233. Kutsumizu S (2002) Curr Opinion Coll Interface Sci 7:537
234. Impéror-Clerc M (2005) Curr Opinion Coll Interface Sci 9:370
235. Cook AG, Baumeister U, Tschierske C (2005) J Mater Chem 15:1708
236. Felekis T, Tsiourvas D, Tziveleka L, Paleos CM (2005) Liq Cryst 32:39
237. Friberg SE, Podzimek M, Tomalia DA, Hedstrand DM (1988) Mol Cryst Liq Cryst 164:157
238. Ramzi A, Bauer BJ, Scherrenberg R, Froehling P, Joosten J, Amis EJ (1999) Macromolecules 32:4983
239. Ujie S, Yano Y, Mori A (2004) Mol Cryst Liq Cryst 411:483
240. Martín-Rapún R, Marcos M, Omenat A, Barberá J, Romero P, Serrano JL (2005) J Am Chem Soc 127:7397
241. Tsiourvas D, Felekis T, Sideratou Z, Paleos CM (2004) Liq Cryst 31:739
242. Weener JW, Meijer EW (2000) Adv Mater 12:741
243. Yonetake K, Masuko T, Morishita T, Suzuki K, Ueda M, Nagahata R (1999) Macromolecules 32:6578
244. Haba O, Okuyama K, Yonetake K (2001) Mol Cryst Liq Cryst 364:929
245. Haba O, Okuyama K, Osawa H, Yonetake K (2005) Liq Cryst 32:633
246. Cho BK, Jain A, Gruner SM, Wiesner U (2004) Science 305:1598
247. Cho BK, Jain A, Mahajan S, Ow H, Gruner SM, Wiesner U (2004) J Am Chem Soc 126:4070
248. Cho BK, Jain A, Nieberle J, Mahajan S, Wiesner U, Gruner SM, Türk S, Râder HJ (2004) Macromolecules 37:4227
249. Nithyanandhan J, Jayaraman N, Davis R, Das S (2004) Chem Eur J 10:689
250. Busson P, Ihre H, Hult A (1998) J Am Chem Soc 120:9070
251. Ihre H, Hult A, Fréchet JMJ, Gitsov I (1998) Macromolecules 31:4061
252. Malkoch M, Malmström E, Hult A (2002) Macromolecules 35:8307

253. Busson P, Örtegren J, Ihre H, Gedde UW, Hult A, Andersson G (2001) Macromolecules 34:1221
254. Örtegren J, Busson P, Ihre H, Gedde UW, Hult A, Eriksson A, Lindgren M, Andersson G (2001) Liq Cryst 28:861
255. Örtegren J, Tidlund J, Nykvist M, Busson P, Hult A, Sen S, Boyd RH, Gedde UW (2001) Polymer 42:10027
256. Busson P, Örtegren J, Ihre H, Gedde UW, Hult A, Andersson G, Eriksson A, Lindgren M (2002) Macromolecules 35:1663
257. Percec V (1997) From Molecular to Macromolecular Liquid Crystals. In: Collings PJ, Patel JS (eds) Handbook Of Liquid Crystal Research, chap 8. Oxford University Press, Oxford
258. Percec V, Chu P (1995) Polym Mater Sci Eng 73:125
259. Percec V, Chu P, Ungar G, Zhou J (1995) J Am Chem Soc 117:11441
260. Li JF, Crandall KA, Chu P, Percec V, Petschek RG, Rosenblatt C (1996) Macromolecules 29:7813
261. Jin AJ, Fisch MR, Mahajan MP, Crandall KA, Chu P, Huang CY, Percec V, Petschek RG, Rosenblatt C (1998) Eur Phys J 5:251
262. Liu Z, Zhu L, Shen Z, Zhou W, Cheng SZD, Percec V, Ungar G (2002) Macromolecules 35:9426
263. Liu Z, Zhu L, Zhou W, Cheng SZD, Percec V, Ungar G (2002) Chem Mater 14:2384
264. Gehringer L, Bourgogne C, Guillon D, Donnio B (2004) J Am Chem Soc 126:3856
265. Gehringer L, Guillon D, Donnio B (2003) Macromolecules 36:5593
266. Malthête J, Nguyen HT, Destrade C (1993) Liq Cryst 13:171
267. Nguyen HT, Destrade C, Malthête J (1997) Adv Mater 9:375
268. Fazio D, Mongin C, Donnio B, Galerne Y, Guillon D, Bruce DW (2001) J Mater Chem 11:2852
269. Smirnova AI, Fazio D, Iglesias EF, Hall CG, Guillon D, Donnio B, Bruce DW (2003) Mol Cryst Liq Cryst 396:227
270. Gehringer L, Bourgogne C, Guillon D, Donnio B (2005) J Mater Chem 15:1696
271. Moore JS (1997) Acc Chem Res 30:402
272. Pesak DJ, Moore JS (1997) Angew Chem Int Ed Engl 36:1636
273. Meier H, Lehmann M (1998) Angew Chem Int Ed Engl 37:643
274. Meier H, Lehmann M, Kolb U (2000) Chem Eur J 6:2462
275. Meier H, Lehmann M, Schnorpfeil C, Fetten M (2000) Mol Cryst Liq Cryst 352:85
276. Lehmann M, Schartel B, Hennecke M, Meier H (1999) Tetrahedron 55:13377
277. Lehmann M, Fischbach I, Spiess HW, Meier H (2004) J Am Chem Soc 126:772
278. Meier H, Holst HC, Oehlhof A (2003) Eur J Org Chem 4173
279. Lee CH, Yamamoto T (2001) Tetrahedron Lett 42:3993
280. Lee CH, Yamamoto T (2002) Bull Chem Soc Jpn 75:615
281. Binnemans K, Görller-Walrand C (2002) Chem Rev 102:2303
282. Donnio B, Guillon D, Deschenaux R, Bruce DW (2003) Metallomesogens. In: McCleverty JA, Meyer TJ (eds) Comprehensive Coordination Chemistry II. Elsevier, Oxford, vol 7, chap 7.9, 357
283. Donnio B (2002) Curr Opin Colloid Interface Sci 7:371
284. Serrette AG, Swager TM (1993) J Am Chem Soc 115:8879
285. Lai CK, Lu MY, Lin FJ (1997) Liq Cryst 23:313
286. Stebani U, Lattermann G, Wittenbger M, Wendorff JH (1996) Angew Chem Int Ed Engl 35:1858
287. Stebani U, Lattermann G (1995) Adv Mater 7:578

288. Barberá J, Marcos M, Omenat A, Serrano JL, Martínez JI, Alonso PJ (2000) Liq Cryst 27:255
289. Deschenaux R, Goodby JW (1995) In: Togni A, Hayashi T (eds) Ferrocenes: Homogeneous Catalysis, Organic Synthesis, Materials Sciences. Wiley, Weinheim, chap 9, 471
290. Deschenaux R, Serrano E, Levelut AM (1997) Chem Commun 1577
291. Chuard T, Béguin MT, Deschenaux R (2003) C R Chimie 6:959
292. Chuard T, Deschenaux R (2003) Chimia 57:597
293. Chuard T, Deschenaux R (2001) Chimia 55:139
294. Dardel B, Deschenaux R, Even M, Serrano E (1999) Macromolecules 32:5193
295. Chuard T, Dardel B, Deschenaux R, Even M (2000) Carbon 38:1573
296. Deschenaux R, Even M, Guillon D (1998) Chem Commun 537
297. Even M, Heinrich B, Guillon D, Guldi DM, Prato M, Deschenaux R (2001) Chem Eur J 7:2595
298. Guldi DM, Maggini M, Scorrano G, Prato M (1997) J Am Chem Soc 119:974
299. Chuard T, Deschenaux R (2002) J Mater Chem 12:1944
300. Guillon D, Nierengarten JF, Gallani JL, Eckert JF, Rio Y, Carreon MP, Dardel B, Deschenaux R (2003) Macromol Symp 192:63
301. Dardel B, Guillon D, Heinrich B, Deschenaux R (2001) J Mater Chem 11:2814
302. Yevlampieva NP, Dardel B, Lavrenko P, Deschenaux R (2003) Chem Phys Lett 382:32
303. Lavrenko P, Yevlampieva N, Dardel B, Deschenaux R (2004) Prog Colloid Polym Sci 127:61
304. Campidelli S, Eng C, Saez IM, Goodby JW, Deschenaux R (2003) Chem Commun 1520
305. Tirelli N, Cardullo F, Habicher T, Suter UW, Diederich F (2000) J Chem Soc, Perkin Trans 2, 193
306. Chuard T, Deschenaux R, Hirsch A, Schönberger H (1999) Chem Commun 2103
307. Felder-Flesch D, Rupnicki L, Bourgogne C, Donnio B, Guillon D (2006) J Mater Chem 16:304
308. Campidelli S, Lenoble J, Barberá J, Paolucci F, Marcaccio M, Paolucci D, Deschenaux R (2005) Macromolecules 38:7915
309. Campidelli S, Deschenaux R (2001) Helv Chim Acta 84:589
310. Campidelli S, Deschenaux R, Eckert JF, Guillon D, Nierengarten JF (2002) Chem Commun 656
311. Campidelli S, Vázquez E, Milic D, Prato M, Barberá J, Guldi DM, Marcaccio M, Paolucci D, Paolucci F, Deschenaux R (1994) J Mater Chem 14:1266
312. Saez IM, Goodby JW (2003) J Mater Chem 13:2727
313. Praefcke K, Psaras P, Eckert A (1993) Liq Cryst 13:551
314. Zab K, Joachimi D, Agert O, Neumann B, Tschierske C (1995) Liq Cryst 18:489
315. Andersch J, Diele S, Lose D, Tschierske C (1996) Liq Cryst 21:103
316. Van de Witte P, Lub J (1999) Liq Cryst 26:1039
317. Uedaira T, Koide N (2001) Mol Cryst Liq Cryst (2001) 365:23
318. Schulte JL, Laschat S, Vill V, Nishikawa E, Finkelmann H, Nimtz M (1998) Eur J Org Chem 2499
319. Pegenau A, Göring P, Tschierske C (1996) Chem Commun 2563
320. Pegenau A, Cheng XH, Tschierske C, Göring P, Diele S (1999) New J Chem 23:465
321. Pegenau A, Hegmann T, Tschierske C, Diele S (1999) Chem Eur J 5:1643
322. Cheng XH, Diele S, Tschierske C (2000) Angew Chem Int Ed 39:592
323. Saez IM, Goodby JW (2003) Chem Commun 1726
324. Saez IM, Goodby JW (2003) Chem Eur J 9:4869

325. Fan FY, Mastrangelo JC, Katsis D, Chen SH, Blanton TN (2000) Liq Cryst 27:1239
326. Fan FY, Culligan SW, Mastrangelo JC, Katsis D, Chen SH, Blanton TN (2001) Chem Mater 13:4584
327. Chen SH, Chen HMP, Geng Y, Jacobs SD, Marshall KL, Blanton TN (2003) Adv Mater 15:1061
328. Plesnivy T, Ringsdorf H, Schumacher P, Nütz U, Diele S (1995) Liq Cryst 18:185
329. Barberá J, Garcés AC, Jayaraman N, Omenat A, Serrano JL, Stoddart JF (2001) Adv Mater 13:175
330. Percec V, Cho CG, Pugh C, Tomazos D (1992) Macromolecules 25:1164
331. Brewis M, Clarkson GJ, Holder AM, McKeow NB (1998) Chem Commun 969
332. Brewis M, Clarkson GJ, Helliwell M, Holder AM, McKeown NB (2000) Chem Eur J 6:4630
333. Brewis M, Helliwell M, McKeown NB, Reynolds S, Shawcross A (2001) Tetrahedron Lett 42:813
334. Kimura M, Saito Y, Ohta K, Hanabusa K, Shirai H, Kobayashi N (2002) J Am Chem Soc 124:5274
335. Lee M, Cho BK, Zin WC (2001) Chem Rev 101:3869
336. Lee M, Jeong YS, Cho BK, Oh NK, Zin WC (2002) Chem Eur J 8:876
337. Yoo YS, Song JH, Oh NK, Zin WC, Park S, Chang T, Lee M (2004) J Am Chem Soc 126:6294
338. Holzmeuller J, Genson KL, Park Y, Yoo YS, Park MH, Lee M, Tsukruk V (2005) Langmuir 21:6392
339. Bae J, Choi JH, Yoo YS, Oh NK, Kim BS, Lee M (2005) J Am Chem Soc 127:9668
340. Yoo YS, Lee M (2005) J Mater Chem 15:419
341. Kim JK, Hong MK, Ahn JH, Lee M (2005) Angew Chem Int Ed 44:328
342. Bae J, Kim JK, Oh NK, Lee M (2005) Macromolecules 38:4226
343. Jang CJ, Ryu JH, Lee JD, Sohn D, Lee M (2004) Chem Mater 16:4226

Editor: K.-S. Lee

Adv Polym Sci (2006) 201: 157–224
DOI 10.1007/12_078
© Springer-Verlag Berlin Heidelberg 2006
Published online: 16 February 2006

Polymeric Betaines: Synthesis, Characterization, and Application

Sarkyt Kudaibergenov[1] (✉) · Werner Jaeger[2] · Andre Laschewsky[2]

[1]Institute of Polymer Materials and Technology, Satpaev Str. 18a, 050013 Almaty, Republic of Kazakhstan
ipmt-kau@usa.net

[2]Fraunhofer-Institute for Applied Polymer Research, Geiselbergstrasse 69, 14476 Potsdam-Golm, Germany
jaeger@iap.fhg.de, andre.laschewsky@iap.fhg.de

1 Introduction 160

2 Synthesis and Structure of Polymeric Carbo-, Sulfo-, and Phosphobetaines 161
2.1 Polycarbobetaines 162
2.2 Polysulfobetaines 168
2.3 Polyphosphobetaines 173
2.4 Narrowly Distributed Homopolymers and Block Copolymers 177
2.5 Polymeric Surfactants 179

3 Properties of Polybetaines in Solution, Condensed, and Gel States 181

4 Behavior of Hydrophobically Modified Polybetaines 196

5 Interpolymer, Polymer–Surfactant, and Coordination Complexes of Polybetaines 202

6 Application of Polybetaines 210

7 Concluding Remarks 215

References 217

Abstract This review summarizes mostly the literature data accumulated during the last decade on betaine-type polyampholytes. Synthetic pathways to polybetaines consisting of radical polymerization, the Michael addition reaction, and polymer-analogous transformation are discussed together with methods of controlled polymerization, such as group transfer polymerization, atomic transfer radical polymerization, and reversible addition fragmentation transfer. The role of intra- and interchain associates resulting in insolubility in pure water due to the formation of ionically cross-linked network structures, and solubility in saline water because of the disruption of the ionic networks, are outlined. Attention is also paid to the recent advancement of hydrophobically modified polymeric betaines with emphasis on phospholipid-containing vinyl polymers. Polymer complexes of polybetaines, in particular interpolyelectrolyte, polymer–surfactant, and polymer–metal complexes, are considered in the light of the competition between intra- and intermolecular ionic contacts and the cooperative character of interactions. Stimuli-sensitive behavior and morphological changes of polybetaine hydrogels triggered by

changes of the pH, ionic strength, water–organic solvent mixture, metal complexation, and DC electric field are discussed with respect to the ionization state of the macromolecules and the thermodynamic quality of solvents, as well as osmotic, chelating, and polarization effects. Some application aspects of polybetaines in medicine, biotechnology, hydrometallurgy, and the oil industry are also discussed.

Keywords Application · Complexes · Polymeric betaines · Solutions and gels · Zwitterions

Abbreviations

AMBNa	Sodium 3-acrylamido-3-methylbutanoate
AMPDAPS	3-[(2-Acrylamido-2-methylpropyl)dimethylammonio]-1-propanesulfonate
APDAPS	3-[*N*-(3-Acrylamido)propyl-*N*,*N*′-dimethylammonio]-propanesulfonate
APDMAE	2-(3-Acrylamidopropyldimethylammonio)-ethanoate
APE	Anionic polyelectrolyte
ATRP	Atom transfer radical polymerization
BMA	*n*-Butyl methacrylate
BSA	Bovine serum albumin
Chol	Cholesterol
CPE	Cationic polyelectrolyte
CRP	Controlled radical polymerization
CTA	Chain transfer agent
DADMAC	*N*,*N*-Diallyl-*N*,*N*-dimethylammonium chloride
DC	Direct current
DEAEM	2-(Diethylamino)ethyl methacrylate
DIPAEM	2-(Diisopropylamino)ethyl methacrylate
DLS	Dynamic light scattering
DMAAPS	*N*,*N*-Dimethyl(acrylamidopropyl)ammonium propanesulfonate
DMAEM	*N*,*N*-Dimethylaminoethyl methacrylate
DMAPS	*N*,*N*-Dimethyl-*N*-(2-methacryloyloxyethyl)ammonium propanesulfonate
DMF	Dimethylformamide
DMSO	Dimethyl sulfoxide
DNA	Deoxyribonucleic acid
EDMA	Ethylene dimethacrylate
EDTA	*N*,*N*-Ethylenediaminetetraacetic acid
ELISA	Enzyme-linked immunosorbent assay
GPC	Gel-permeation chromatography
GTP	Group transfer polymerization
HPLC	High-performance liquid chromatography
IEP	Isoelectric point
IPC	Interpolyelectrolyte complexes
LB	Langmuir–Blodgett
LCST	Lower critical solution temperature
MAA	Methacrylic acid
MEMA	2-(*N*-Morpholino)ethyl methacrylate
MPC	2-Methacryloyloxyethyl phosphorylcholine
NaPSS	Poly(styrenesulfonate sodium salt)
NIPAM	*N*-Isopropylacrylamide
PAA	Poly(acrylic acid)
PAAm	Polyacrylamide

PAESD	Poly(diallylaminoethanoate-*co*-sulfur dioxide)
PAMPS	Poly(2-acrylamido-2-methylpropanesulfonic acid)
PBA	Poly(butyl methacrylate)
PCB	Polycarbobetaine
PCEAC	Poly(carboxyethyl 3-aminocrotonate)
PCEAC-Ala	Poly(carboxyethyl 3-aminocrotonate) modified by β-alanine
PCEAC-Ea	Poly(carboxyethyl 3-aminocrotonate) modified by ethanolamine
PCEAC-Gly	Poly(carboxyethyl 3-aminocrotonate) modified by glycine
PCEAC-Lys	Poly(carboxyethyl 3-aminocrotonate) modified by lysine
PCECHAC	Poly(carboxyethyl 3-cyclohexylaminocrotonate)
PCEPAC	Poly(carboxyethyl 3-propylaminocrotonate)
PCMEDDAC	Poly3-[(2-carboxy-1-methylethyl)dodecylaminocrotonate]
PDADMAC	Poly(*N*,*N*-diallyl-*N*,*N*-dimethylammonium chloride)
PDI	Polydispersity index
PDMAPAA-Q	Quaternized poly*N*-[3-(dimethylamino)propyl]acrylamide chloride
PDMAPS	Poly[3-dimethyl(methacryloyloxyethyl)ammonium propanesulfonate]
PEG	Poly(ethylene glycol)
PEI	Polyethyleneimine
PEO	Poly(ethylene oxide)
PHMG	Poly(hexamethylene guanidine)
PMAA	Poly(methacrylic acid)
PMMA	Poly(methyl methacrylate)
PNIPAM-PC	Phosphorylcholine-based poly-*N*-isopropylacrylamide
polyAMPS	poly(2-acrylamido-2-methylpropanesulfonic acid)
polyCEACPhos	Poly(carboxyethyl 3-aminocrotonate) modified by phosphatidylethanolamine
polyTRIM	Poly(trimethylpropane trimethacrylate)
PPD	Pour point depressant
PPO	Poly(propylene oxide)
PSB	Polysulfobetaine
PVA	Poly(vinyl alcohol)
PVP	Poly(*N*-vinylpyrrolidone)
RAFT	Reversible addition fragmentation chain transfer
UCST	Upper critical solution temperature
VPPS	2-Vinylpyridiniopropanesulfonate
XPS	X-ray photoelectron spectroscopy
ZPE	Zwitterionic polyelectrolyte
a	Exponent of Mark–Kuhn–Houwink equation
A_2	Second virial coefficient
α	Ionization degree
α_e	Electrostatic expansion factor
$C_{protein}$	Protein concentration
C_s	Low molecular weight salt concentration
d_h	Hydrodynamic diameter
E	Voltage
E_A	Activation energy
$[\eta]$	Intrinsic viscosity
η_{sp}/C	Reduced viscosity
G_{el}	Electrostatic Gibbs energy
I_E	Fluorescence intensity of excimer

I_M	Fluorescence intensity of monomer
k_i	($i = 1, 2, 3, \ldots$) Microscopic ionization constant
K_i	($i = 1, 2, 3, \ldots$) Macroscopic ionization constant
K_t	Tautomeric constant
L	Distance
M_n	Number average molecular weight
M_w	Weight average molecular weight
μ	Ionic strength of the solution
pK_a	Ionization constant of acidic group
pK_b	Ionization constant of basic group
pH_c	Boundary between the primary and nonassociative phases
pH_{iep}	Isoelectric pH
pH_ϕ	Boundary between the primary and aggregate phases
R	Molar ratio of polyelectrolyte/polybetaine
R_g	Radius of gyration
R_h	Hydrodynamic radius
R_p	Propagation rate
t	Time
T_g	Glass transition temperature
Z_{pr}	Protein charge

1 Introduction

Polymeric betaines (also referred to as polyzwitterions) are macromolecules containing identical numbers of anionic and cationic species on the same monomer units. Thus, they present a special case of polyampholytes. In dependence on the nature of the ionic groups, polymeric betaines may be grouped into various subclasses, the most widespread ones being polycarbobetaines, polysulfobetaines, and polyphosphobetaines. The specific properties of polymeric betaines are dominated by the number and type of zwitterionic groups. In combination with hydrophobic and hydrophilic fragments, polymeric betaines can form well-defined nanosized assemblies, such as spheres, capsules, ultrathin films, or structured hydrogels. Also, self-organized systems such as monolayers, Langmuir–Blodgett (LB) multilayers, and vesicles are easily formed from hydrophobized polymeric betaines. Particularly, polyphosphobetaines—phospholipid-analogous polymers—have attracted much attention for the mimicking of biomembranes, good bio- and hemocompatibility, and nontrombogenicity. Moreover, the structural and behavioral similarity of polybetaines to biopolymers and biomembranes gives access to models for protein folding, or to biomimetic functions. Application areas of polybetaines include enhanced drag reduction, oil recovery, catalysts, drug delivery systems, and cosmetic and pharmaceutical formulations.

2
Synthesis and Structure of Polymeric Carbo-, Sulfo-, and Phosphobetaines

As the synthesis of polymeric betaines has already been the subject of several reviews [1–5], this chapter is focused on the developments and progress made during the last decade.

The polybetaines (or "polyzwitterions") are dipolar species, in which the cationic and anionic groups are separately bound to the same monomer unit and can be completely dissociated in a medium of sufficient dielectric permittivity. Typically, the use of the term "polybetaine" implies that the cation is a permanently cationic species, such as fully quaternized ammonium or phosphonium groups, and that the coexistence of the different charges applies to a broad range of physicochemical conditions, e.g., pH and ionic strength. The following overview also contains copolymers made of at least one zwitterionic monomer, as well as alternating copolymers of cationic and anionic monomers, giving rise to a zwitterionic constitutional repeat unit. However, polymers for which the zwitterionic structure is in equilibrium with a nonpolar form (such as polymeric merocyanines), or mesoionic polymers and polymeric ylides, are not discussed in this overview, except for some brief remarks. Also excluded are polyampholytes synthesized by statistical copolymerization of cationic and anionic monomers or corresponding ion pairs, as the oppositely charged groups are not regularly distributed within such copolymers.

As for any other functional polymer, polymeric betaines are accessible by two different synthetic routes: (1) the polymerization of zwitterionic monomers or (2) the zwitterionic functionalization of reactive precursor polymers. Both routes have inherent advantages and disadvantages. The polymerization of the zwitterionic monomers leads to polymers with 100% betaine functionality, but their molecular characterization is difficult for several reasons. For instance, the conformation of the polymers in aqueous solution is very sensitive, not only to the ionic strength but also to the type of added salt, and in the case of polycarbobetaines also to the pH. Furthermore, polymeric zwitterions often exhibit strong interactions with other matter, e.g., chromatographic columns. Hence, reliable GPC or HPLC measurements are very difficult to perform, if at all.

In contrast to the direct polymerization of zwitterionic monomers, the polymerization of precursor monomers is generally easy to conduct and leads to reactive polymers with adjustable molecular parameters whose characterization can usually be carried out without problems. However, neighboring group effects may involve complex reaction kinetics during the chemical functionalization to the betaine form, and the polymer-analogous reaction cannot be carried out to 100% yield in every case. Nevertheless providing a high yield, this strategy leads to well-defined polymeric betaines. Using different reagents, polymers with varied chemical structure but constant degree

of polymerization are available by this strategy. This is most useful for all investigations concerning structure–property–performance relationships.

The most widespread chemical classes of polybetaines are carbo-, sulfo-, and phosphobetaines, i.e., polymers with repeat units bearing simultaneously a quaternized ammonium group and a carboxylate, a sulfonate, or a phosphate group, respectively. These three classes will be focused on in the following discussion. Mostly, these polybetaines are prepared by free radical polymerization by virtue of the tolerance of this method to many functional groups and the presence of water, keeping in mind that most zwitterionic monomers are more or less hygroscopic. The preference for free radical polymerization was for a long time a major obstacle to preparing well-defined (model) polymers or complex polymer architectures, such as block copolymers. Therefore, the newly emerging methods of the so-called controlled radical polymerization (CRP) of both the zwitterionic and the reactive precursor monomers has given a fresh impetus to polybetaine synthesis in recent years [6, 7]. CRP of the precursor monomers in organic solvents or in bulk is now well known, but CRP in aqueous media has been established, too [4, 8, 9]. Atom transfer radical polymerization (ATRP) and particularly the reversible addition fragmentation transfer (RAFT) method are promising routes to overcome certain shortcomings in the polymerization of zwitterionic monomers. CRP in aqueous solution has not only been demonstrated to be a convenient method to polybetaines with defined end groups, but also to block copolymers containing betaine blocks. Moreover, the narrow molecular weight distributions of betaine polymers prepared by CRP improve and facilitate the precision of any physical or physicochemical measurement.

2.1 Polycarbobetaines

The chemical structure of most polycarbobetaines falls into one of three groups:

- Quaternary polypyrrolidinium compounds containing linear and branched alkylcarboxy groups
- Quaternary esters or amides of (meth)acrylic acid, in which the quaternary nitrogen is substituted by an alkoxy group of different chain length
- Polyzwitterions derived from polymeric heterocyclic or aromatic vinyl compounds

Polycarbobetaines may be synthesized via a number of reaction pathways by functionalization of suitable monomers or polymers, most commonly by reaction of a tertiary amine with a strained lactone, an α,β-unsaturated acid, a haloalkylcarboxylate, or a haloalkylcarboxylic ester followed by hydrolysis of the ester. Alternatively, the quaternization of halogen-containing

monomers and polymers with esters of amino acids were reported. Due to the possible protonation of the carboxylate moiety in aqueous (acidic) solution, the polymerization kinetics of carbobetaine monomers may be strongly pH dependent [10], but this aspect did not receive further attention. In some cases, the ionic strength of the solvent was increased by inorganic salts [11, 13], obviously to increase the solubility of the polymers.

The free radical cyclopolymerization of diallylammonium compounds leads to linear water-soluble polymers containing predominantly pyrrolidinium rings as the structural unit of the polymer chain [14, 15]. This well-established principle of polymer synthesis was used for the synthesis of the polycarbobetaines from their zwitterionic monomers (route (1), see above), which are summarized in Scheme 1.

Such polymers excel in their hydrolytic stability, as potentially labile carbon–heteroatom bonds are a priori absent. Polycarbobetaines of type **1a**, containing linear alkoxy groups with up to ten methylene groups separating N^+ and COO^-, were obtained by the polymerization of their pure monomers to provide polymers completely free of salt impurities [16, 17]. The monomers were synthesized by reacting diallylamine with an ester of ω-bromoalkanoic acids, followed by alkylation of the tertiary amine with CH_3I. The key step in the salt-free synthesis is the conversion of this cationic precursor to the zwitterionic monomer by treatment with an OH^--loaded anion-exchange resin. In a similar way, polymers **2a**, **2b**, and **3** were obtained by varying the length and the position of hydrophobic side chains [17]. However, the polymerization ability of diallylammonium monomers decreases generally with the size of the substituents on the nitrogen. Accordingly, high monomer and initiator concentrations were required to obtain polymers. The synthesis of **2a** and **3** needed peroxide initiators and a comparatively high temperature.

Several similar polycarbobetaines were prepared via polymer-analogous reaction, too (route (2), see above). Diallylammonium monomers bearing a carboxyalkyl group are reacted to form precursor polycations, which by subsequent hydrolysis of the ester group provide the desired polyzwitterions. In this way polymers **1b** were synthesized by complete hydrolysis of the cationic methyl ester precursors [18, 19]. Polymers **4** and **5** were obtained by a similar procedure [20, 21]. They are not classical polyzwitterions, because they may carry an excess charge in every monomer unit in dependence on the pH. Such so-called poly(ampholyte–electrolyte)s exhibit both polyelectrolyte and polyampholyte character simultaneously [3]. Photoinitiated cyclocopolymerization of 4-(*N*,*N*-diallyl-*N*-methylammonio)-butanoate with *N*,*N*-diallyl-*N*,*N*-dimethylammonium chloride (DADMAC) proceeded in NaCl-containing aqueous solution in a nearly ideal fashion, and resulted in copolymers **6** [22]. Copolymers with a large excess charge exhibit typical polyelectrolyte behavior, while those with a balanced charge show antipolyelectrolyte behavior like true polyzwitterions.

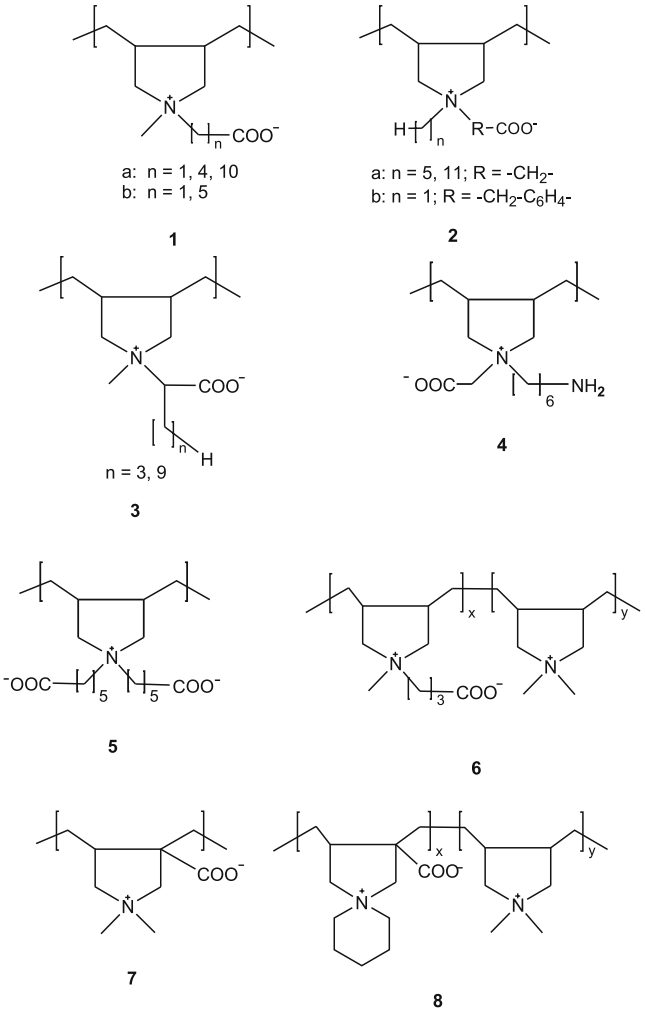

Scheme 1 Polycarbobetaines with quaternary pyrrolidinium units

An interesting extension of the cyclopolymerization strategy is the polymerization of allyl acrylate quaternary ammonium salts, where the resulting ester precursor of **7** is easily hydrolyzed by trifluoroacetic acid to the polybetaine [23]. Polyampholyte **8** was prepared by copolymerization with a high excess of DADMAC [24].

Poly(meth)acrylates and poly(meth)acrylamides offer at present the most versatile, straightforward access to polycarbobetaines (Scheme 2). Mostly, they are derived from quaternary esters or amides of (meth)acrylic acid and are prepared by free radical polymerization of the corresponding monomers. The pure monomers of **9a** [11], **9b** [12], and **9c** [13] are available by quaternization

of 2-acrylamido-2-methylpropanedimethylamine with bromoacetate, ethyl-4-bromobutyrate, or ethyl 6-bromohexanoate followed by saponification with an anion-exchange resin. Polymerization occured in 0.5 M NaBr using persulfate as initiator; the reaction was terminated at low conversion. Polymer **10a** was obtained by quaternization of poly(*N*,*N*-dimethylaminoethyl methacrylate) with 1,4-butyrolactone [25]. Polymers **10b–e** were synthesized for NMR studies and investigations of structure-dependent differences of the properties in solution [26]. Monomers were prepared by quaternization of the dimethylaminoalkyl (meth)acrylates or amides with propiolactone, and polymerized in 0.4 M aqueous solution using azo initiators. High yields were obtained after long reaction times, but such poly(3-ammoniopropanoates) are Mannich bases, and thus are subject to facile fragmentation. Light scattering studies of solutions of **10e** in deionized water indicate that the polymer exists as a mixture of individual chains and interchain associates [27]. Polymers **11** and **12** are prepared by the 2,2′-azobisisobutyronitrile-initiated polymerization of the zwitterionic monomers exhibiting surfactant properties in water. Monomers (and polymers) are tertiary acrylamides and, therefore, exhibit improved re-

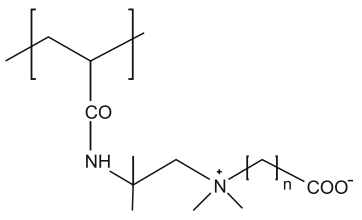

a: n =1; b: n = 3; c: n = 5

9

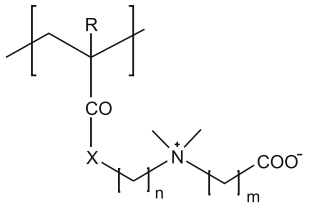

10

10	R	X	n	m
a	-CH_3	O	2	3
b	H	O	2	2
c	-CH_3	O	2	2
d	H	NH	3	2
e	-CH_3	NH	3	2

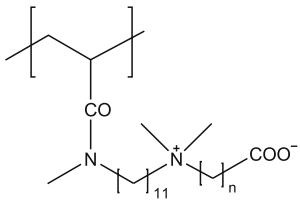

n = 1, 3

11

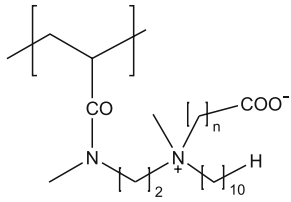

n = 1, 3

12

Scheme 2 Polycarbobetaines derived from quaternary esters or amides of (meth)acrylic acid

sistance to hydrolysis. This is a necessary presupposition for the success of the multistep monomer synthesis which includes the preparation of a mixed secondary–tertiary diamine, conversion to the tertiary acrylamide, alkylation by an ω-bromoester and, finally, conversion to the carbobetaine monomer by an OH^--loaded anion exchanger [28]. In this way, completely salt-free polybetaines are obtained. Notably, the "tail-end" type polymers **11** dissolve in highly polar solvents such as water. In contrast, the isomeric "head"-type polymers **12** dissolve in only some organic solvents, but are insoluble in water and, therefore, precipitate during the polymerization.

Polycarbobetaines derived from aromatic or heteroaromatic systems are listed in Scheme 3. The vinylimidazolium betaines **13** and **14** were prepared by alkylation of 1-vinylimidazole with the corresponding bromocarboxylic acid, and aqueous solution polymerization using an azo initiator [29]. Polymers **13b**, **15**, **16**, and **17b** were made by the addition of acrylic or propiolic acid to poly(4-vinylpyridine) and poly(*N*-vinylimidazole). Kinetic measurements revealed a mechanism consisting of two reactions: first, addition of two molecules of acid to the polymer; second, the formation of an equilibrium between the adduct and the betaine structure [30, 31].

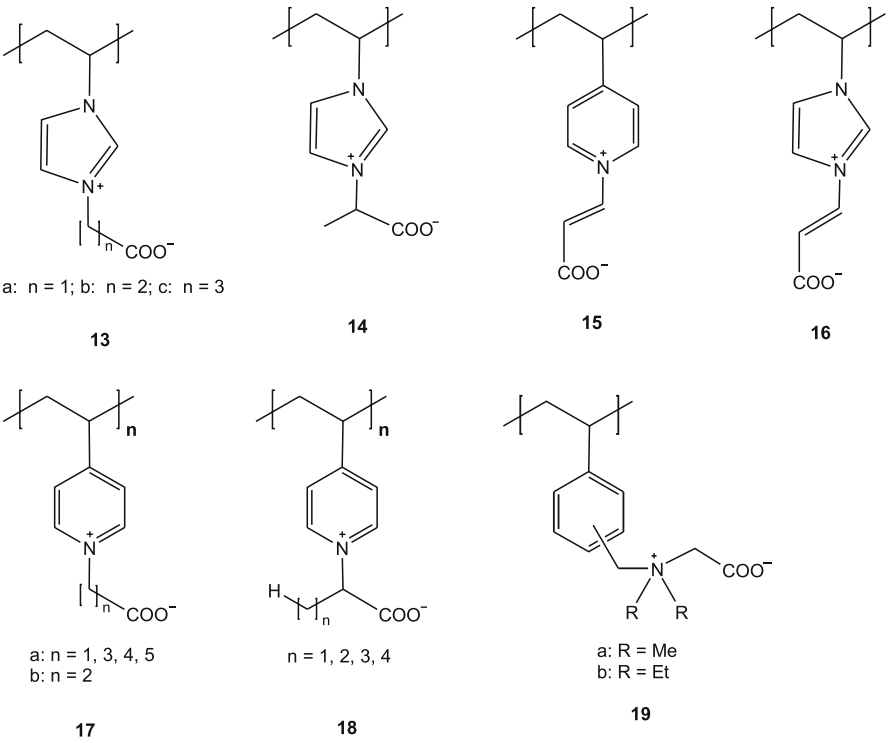

Scheme 3 Polycarbobetaines derived from aromatic or heteroaromatic systems

The *N*-oxyl-mediated CRP of 4-vinylpyridine [32] and vinylbenzyl chloride [33] results in useful precursors for the synthesis of polycarbobetaines with narrow molecular weight distribution. Alkylation with bromocarboxylic acid esters, or quaternization with amino acid esters, respectively, both followed by hydrolysis of the ester moiety, led to **17a**, **18**, and **19** with very high degrees of functionalization. This approach is extremely versatile and enables the facile variation of the alkyl spacer length between both charges, the length of an additional alkyl chain at the α carbon, and different substitution at as well as hybridization of the quaternary nitrogen [34, 35]. The influence of the chemical structure on the pH-dependent solution properties in aqueous systems and the interaction of the different charges of the polybetaines were demonstrated by capillary electrophoresis and charge titration [34–37]. Acid–base titrations of **17a** and **18** became possible provided the betaines were complexed by strong polyanions [38]. An interesting pathway to linear and cross-linked polycarbobetaines based on acrylic acid and the ethyl ester of 3-amino-2-butenoic acid comprises a Michael addition reaction of these reactants followed by a spontaneous polymerization [39, 40]. Also, cross-linked betaine gels were synthesized similarly in the presence of *N*,*N*-methylenebisacrylamide. The alternating copolymerization of maleamic acids and diallylammonium derivatives results in copolymers **20** with alternating cationic and anionic charges [41–43] (Scheme 4).

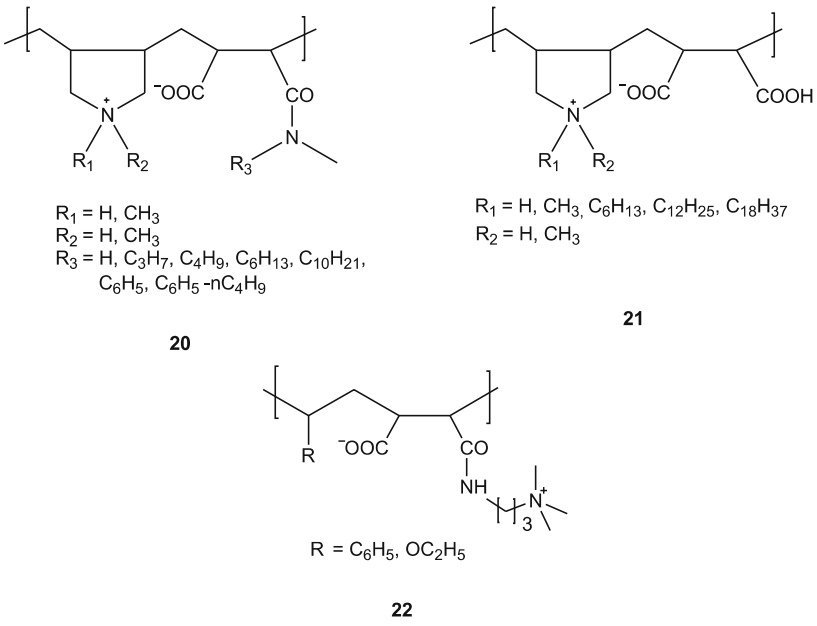

Scheme 4 Polycarbobetaines derived from alternating copolymers of maleic or maleamic acid

Increasing the chain length of R_3 results in an increase of the polymerization rate, probably caused by the formation of ordered structures in the monomer solution, as well as an increase of the surface-active properties of the polymers [42]. Polycarbobetaines **20** (R_1, $R_2 = CH_3$; $R_3 = H$, C_6H_5, C_6H_5-n-C_4H_9) form complexes with fatty acids which self-assemble into nanoparticles with sizes in the range of 3–5 nm [43]. Alternating copolymerization is also successful with maleic acid to give **21** [41, 44], the water solubility of which decreases with increasing length of R_1 [44]. Polymers **21** are used to prepare new organic–inorganic blends [45, 46], and multimetallic oxide catalysts therefrom after calcination.

Carbobetaine units are employed in many copolymers with uncharged monomers. Examples are the alternating copolymers of **1a** ($n = 1$) [47], **4** [20] or **5** [21] with SO_2, or alternating copolymers **22** with betaine structures derived from maleamic acid [48, 49].

Statistical copolymers were reported for *N*-vinylimidazole and **13b** [50], for acrylamide with **9a** [11], **9b** [12], and **9c** [13], and for terpolymers of acrylamide, sodium acrylate, and **9b** [51]. Several hydrolytically stable ammonioacetate and pyridiniocarboxylate monomers based on isobutylene with variable length of hydrophobic side chains did not homopolymerize, but these monomers with surfactant properties are suited for copolymerization with electron-poor monomers [52].

2.2 Polysulfobetaines

Similar to polycarbobetaines, the chemical structure of polysulfobetaines can be subsumed in several groups, where the different polymers bear an alkylsulfonate group. Most widespread are:

- Quaternary polypyrrolidinium compounds
- Quaternary esters or amides of (meth)acrylic acid
- Polyvinylpyridinium or polyvinylimidazolium compounds
- Ionenes

Also, various unconventional polymerizable sulfobetaines have been prepared occasionally in the context of hydrophobized polybetaines, and will be discussed in Sects. 2.5 and 4.

Sulfobetaines are typically prepared by alkylsulfonation of a monomeric or polymeric tertiary amine with strained sultones, usually 1,3-propanesultone or 1,4-butanesultone. An alternative route is the reaction of tertiary amines with a haloalkylsulfonate. Most of the early investigations on polymeric betaines relate to the sulfo derivatives **23a–e**, **24**, **25**, and **26** listed in Scheme 5 [1–4, 178].

In recent years, only a few new polysulfobetaines have been described. Polymers containing pyrrolidinium rings were synthesized by cyclopolymer-

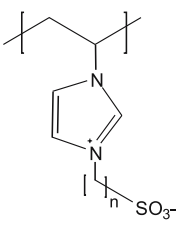

n = 2, 3, 4

24

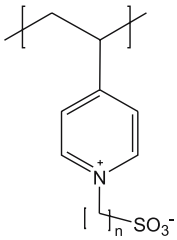

n = 3, 4

25

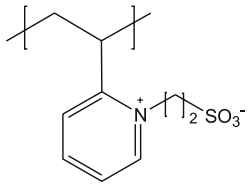

26

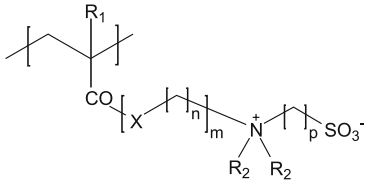

23

23	R_1	X	n	m	R_2	p
a	H	NH	3	1	$-CH_3$	3
b	$-CH_3$	O	2	1	$-CH_3$	3
c	H	O	2	1	$-CH_3$	3
d	$-CH_3$	O	2	2,3,4	$-CH_3$, $-C_2H_5$	4
e	$-CH_3$	NH	3	1	$-CH_3$	3

Scheme 5 Polysulfobetaines compiled in several reviews

ization of the corresponding diallylammonium sulfobetaines (Scheme 6). The monomers of **27** were prepared by the usual sultone procedure [17, 28, 53, 54]. The poly(electrolyte–zwitterion) **28** [55] and the polyampholyte copolymer **29** [56] are analogues to **5** and **6.** The photoinitiated copolymerization process leading to **29** is a random one; the reactivity ratios were determined by NMR spectroscopy. Cyclocopolymers containing less than 40 mol % of sulfobetaine show classical polyelectrolyte behavior.

As for polycarbobetaines, mechanistic studies of the polymerization of these sulfobetaine monomers are scarce. An example is the investigation of the influence of the ionic strength on the propagation rate of some ammoniosulfonates, which increases after adding NaCl [57]. Kinetic investigations of the polymerization of **23a** indicate that high monomer conversion can be achieved at lower temperatures. The conversion is enhanced in the presence of various salts in aqueous solution [58]. FTIR studies of the persulfate-initiated polymerization of **23b** in water showed significant changes of the overall rate equation and a decrease of the overall activation energy after adding inorganic salts [59].

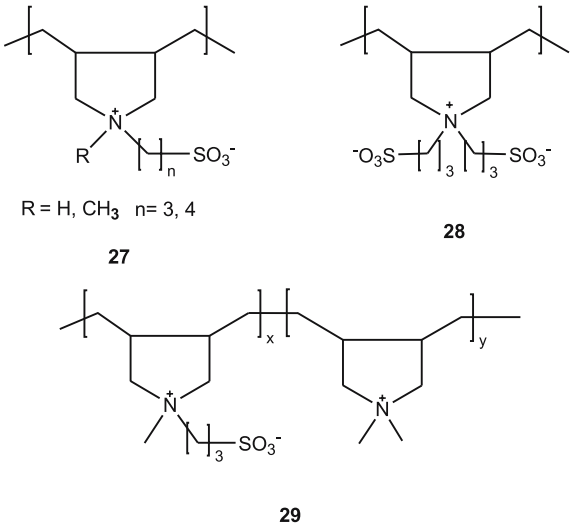

Scheme 6 Polysulfobetaines containing quaternary pyrrolidinium moieties

Several papers compare the properties of sulfobetaine (meth)acrylic polymers. NMR spectra and solution properties of **23a** and **23b** [59, 60] are correlated with data from the corresponding polycarbobetaines [26]. The photophysical and solution properties of pyrene-labeled **23c** were studied in terms of fluorescence emission. Addition of surfactants induces the formation of mixed micelles in aqueous solution [61]. Excluded volume effects of the unlabeled polymer were measured by light scattering [62], its adsorption on silica was studied by adsorbance measurement and ellipsometry [62, 63], and the electrostimulated shift of the precipitation temperature was followed at various electric field intensities [64]. Polysulfobetaines may accelerate interionic reactions, e.g., oxidation of ferrocyanide by persulfate [65]. The thermal and dielectric properties of polysulfobetaines **23d** were investigated. The flexible lateral chain of the polymers decreased T_g, for which a linear relationship with the number of C atoms was shown [66, 67].

A series of sulfobetaine monomers derived from *N*,*N*-dialkylaminophenylmethacrylamide were synthesized using conventional pathways and polymerized to give polymers **30** (Scheme 7). The NMR spectra and solution properties were compared with those of **31** and the corresponding cationic polyelectrolytes [68, 69].

Polysulfobetaines derived from alternating styrene–maleic anhydride copolymers **32** are easily prepared by ring opening of the anhydride moiety with 3-dimethylaminopropylamine, imidizing the resulting poly(amic acid) by heating, and alkylation with propane sultone [70–72]. For investigations of structure–property relationships additionally to **32b**, the polymers **33** and **34** were synthesized [71]. The ionene-like polymer **33** was prepared

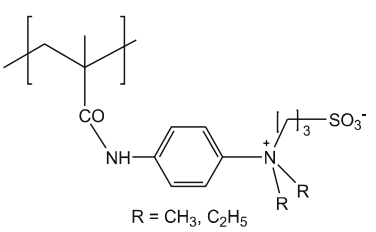

30

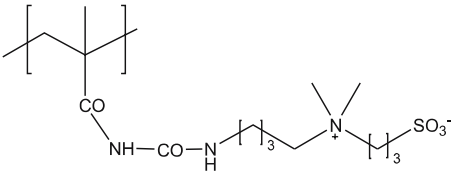

31

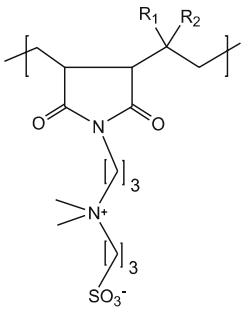

a: R_1 = H, R_2, C_6H_5
b: R_1, R_2 = H, H; H, CH_3; CH_3, CH_3; H, $C_{16}H_{33}$

32

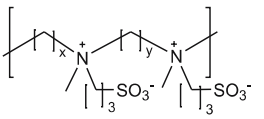

x, y = 3, 6; 6, 6 ; 6, 10

33

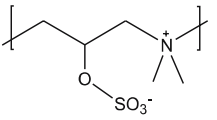

34

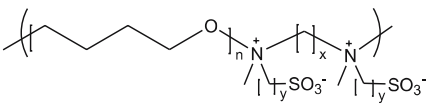

x = 3,6 y = 3,4

35

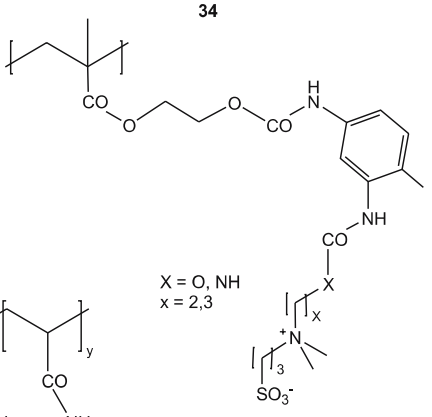

X = O, NH
x = 2,3

36

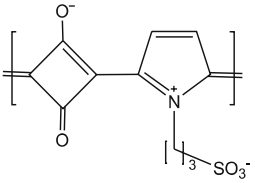

37

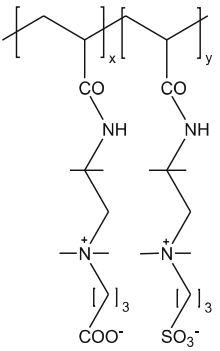

38

Scheme 7 Polysulfobetaines prepared for investigations of structure–property relationships

by dealkylation of a typical quaternary ionene polymer followed by reaction with propane sultone. The zwitterionic ionene **34** is made by reacting stoichiometric amounts of dimethylamine and epichlorhydrin, followed by sulfatation of the OH group. In the series **32b**, **33**, and **34**, the charged groups are increasingly moved from the side chain to the polymer backbone. This reduces markedly the solubility in aqueous solutions, as apparently the intermolecular Coulombic interactions are increased. Hydrophobic substituents and higher charge densities enhance these effects [71]. Several segmented poly(tetramethylene oxide) zwitterionomers **35** were investigated with respect to phase separation [73, 74]. Polysulfobetaines **36** were prepared via functionalization of the urethanes derived from 2,4-toluene diisocyanate, which bear a tertiary amino group [75].

Alternating sulfobetaine copolymers were reported for **27** with SO_2 [76], by analogy with the carbobetaine analogues described above. A very different approach was chosen for the alternating copolymer poly(ampholyte–electrolyte) **37**, by condensing sodium 3-(pyrrol-1-yl) propanesulfonate with squaric acid [77].

Many more papers deal with statistical copolymers containing sulfobetaine units, mostly prepared by free radical polymerization in solution. This includes copolymers of **23e** [78] or **23b** [79, 80] with butyl acrylate, of **23a** with styrene or *N*-vinylpyrrolidone [81], of **23e** with *N*-isopropylacrylamide (NIPAM) [82], and of **30** ($R = CH_3$) with methacrylamide [83]. Copolymers of *N*,*N*-dimethylmaleimidopropylammonium propanesulfonate and acrylamide [84] with a structure similar to **32** were labeled with naphthalene for investigations of the solution behavior on the microscopic level [85]. Statistical copolymers **38** containing both carbobetaine and sulfobetaine groups were obtained from the corresponding monomers in aqueous solution containing NaBr [86]. Their solubility behavior is complex and varies with composition, pH, and ionic strength.

Water-soluble graft copolymers of polysaccharides and polysulfobetaines were synthesized by grafting 3-dimethyl(methacryloyloxyethyl)ammonium propanesulfonate (DMAPS) onto hydroxyethyl cellulose using a ceric ammonium nitrate/EDTA initiating system [87]. Similar terpolymers containing additionally acrylamide were also described [88]. Sulfobetaine copolymers found a particular interest as hydrogels, e.g., for thermoreversible crosslinked hydrogels of NIPAM and 1-(3-sulfopropyl)-2-vinylpyridine [89] or DMAPS together with a cationic monomer [90], 1-vinyl-3-(3-sulfopropyl)imidazolium betaine [91], or *N*,*N*-dimethyl(acrylamidopropyl)ammonium propanesulfonate (DMAAPS) [92]. Other sulfobetaine hydrogels were made by copolymerization of 2-hydroxyethyl methacrylate and DMAPS [93], and superabsorbents were obtained by the copolymerization of sodium acrylate and DMAAPS together with a cross-linker [94, 95].

Polysulfobetaines were also used to modify surfaces. For instance, polysulfobetaines were grafted onto argon plasma-pretreated polytetrafluorethy-

lene films and the chemical composition of the surfaces was studied by X-ray photoelectron spectroscopy [96, 97]. Also, silica gel surfaces were modified by polysulfobetaines for different purposes, by grafting of 2-(dimethylamino)ethyl methacrylate with subsequent reaction with propanesultone [98]. Silicone rubber was also grafted after ozonization directly with betaine monomers [99]. In another example, polysulfobetaine grafts were prepared by first self-assembling a disulfide-functionalized azo initiator on a gold surface, and subsequently initiating the polymerization of the zwitterionic monomer to produce an ultrathin film of **23e** as a stimulus-sensitive hydrogel layer [100].

2.3 Polyphosphobetaines

Most of the known polyphosphobetaines are polymeric phospholipid analogues, as many research groups have been interested in mimicking lipid bilayer biomembranes with such polymers (see Sect. 4). The work up to the mid-1990s is described in the excellent review of the late D. O'Brien [101], who pioneered the field together with the groups of D. Chapman, S.L. Regen, H. Ringsdorf, and E. Tsuchida. Whereas the basic lecithin structure is maintained in most of these approaches, a plethora of polymerizing groups such as diynes [102, 103], (meth)acrylates [104–108], acrylamides [104–106], styrenes [109], dienes [110], and polyunsaturated fatty acids [111] have been incorporated at various positions of the phosphorylcholine moiety or of the fatty acid chains. Polymerization is mostly achieved by redox-initiated, or thermally or photochemically induced free radical polymerization of the zwitterionic monomers. Occasionally, the (different) polymerizable groups were cumulated in such reactive lipids, in order to achieve stepwise polymerization and cross-linking of self-organized structures [112–114]. An interesting extension of the use of such polymeric lipids is the preparation of organic nanotubes, as reviewed recently [115].

A major difficulty in the synthesis used to be the incorporation of the phosphatidylcholine moiety into the polymerizable lecithins. Nowadays, the main pathway to phosphobetaine vinyl monomers is the reaction of an OH group containing (meth)acrylate or (meth)acrylamide with 2-chloro-2-oxo-1,3,2-dioxaphospholane, with subsequent ring opening by trimethylamine leading to phosphorylcholine-containing compounds. This strategy is highly versatile [5]. Many of the known polymers which do not directly copy natural lecithins contain 2-methacryloyloxyethyl phosphorylcholine (MPC) as structural unit. Polymers based on MPC are well known for excellent bio- and blood compatibilities. They have delivered clinically proven benefits in various biomedical applications. A review compiles the literature up to 1997; attention is mainly focused on the development of phosphatidylcholine-analogous polymers, describing the synthesis of vinyl phospholipid poly-

mers, phospholipid-modified polypeptides, phospholipid organosiloxanes, and phospholipid urethanes [5] (Scheme 8). The published data of the last few years continue this development.

The kinetics of free radical polymerization of MPC leading to **39a** ($n = 2$) were studied in ethanol [116] and water [117]. In both cases a higher than normal dependence of the overall rate of polymerization on the monomer concentration was observed due to monomer aggregation. The presence of alkaline halides accelerated the polymerization in aqueous media [118]. Polymers **39a** with an increasing number of CH_2 groups between the ester and the phosphate group ($n = 4$, 6, 10) are available in good yields [118]. Several other polymeric methacrylates **39b** [119, 120] and fumarates **40** [121] bearing a phosphorylcholine moiety were synthesized and characterized. The phospholipid-analogous polymers **41a** and **41b**, prepared by radical polymerization in water, show the properties of polyelectrolytes in polar solvents [103]. Similar results were obtained with **42** [105]. Polymer **41b** containing a vitamin E moiety was easily prepared in high yield by polymerization in chlorobenzene/methanol [106]. A stacked bilayer structure was proposed from X-ray diffraction analysis.

A multistep reaction pathway leads to polymers **43** and **44** with phosphatidylcholine moieties in the main chain and long alkyl groups in the side chain [122]. These polymers exhibit thermotropic liquid-crystalline behavior. Polyamides **45** were obtained by interfacial polycondensation; they are insoluble in any normal solvent [123]. Poly-MPC capped with cholesteryl moieties at one or both polymer ends was prepared by the radical polymerization of MPC initiated with 4,4′-azobis[(3-cholesteryl)-4-cyanopentanoate] in the presence of a chain transfer agent [124]. The self-organization of these polymers was analyzed with fluorescence and NMR measurements.

Polyurethanes were modified with phosphobetaines to improve their hemocompatibility. Polyurethanes **46** containing cholesterol were synthesized by step growth polymerization. Surprisingly, they showed the viscosity behavior of common polyelectrolytes [125]. Excellent blood compatibilities were reached by introducing long-chain alkyl groups instead of cholesterol in polymer **46** [125], or by placing the phosphate group in the side chain [126]. The latter case results again in polymers with properties similar to those of the usual polyelectrolytes. Another variation led to segmented polyurethanes with polybutadiene and phosphobetaines in the main chain and long-chain alkyl groups in the side chain [127, 128]. A further successful attempt was the grafting of MPC and similar monomers onto polyurethane surfaces [129–131].

Microspheres containing a corona of polyphosphobetaines were obtained by emulsifier-free emulsion copolymerization of methyl methacrylate and 1-methyl-2-methacrylamidoethyl phosphorylcholine [132], MPC [133], or the fumarate monomers of **40** [133], as well as by precipitation polymerization of styrene with MPC macromonomers [134]. Poly-L-lactic acid nanoparti-

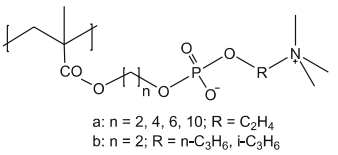

39

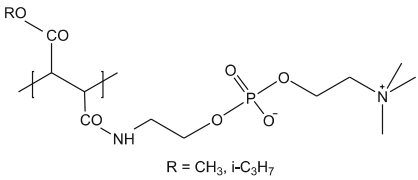

40

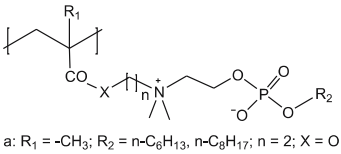

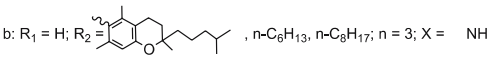

41

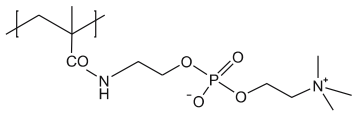

42

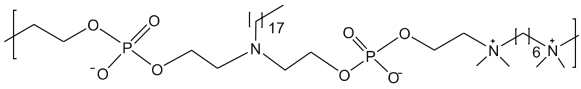

43

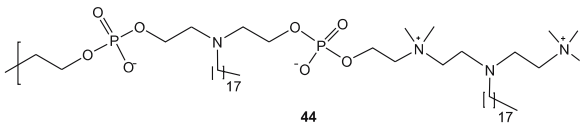

44

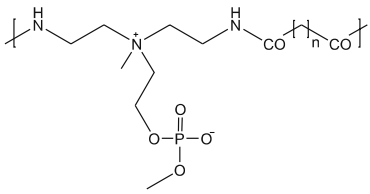

45

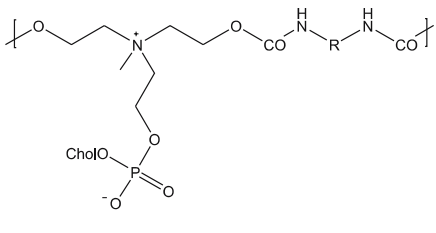

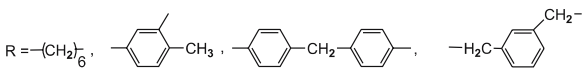

46

Scheme 8 Polymeric phospholipid analogues

cles covered with both bioinert phosphorylcholine groups and *p*-nitrophenyl ester groups are useful for immobilizing enzymes [135]. Surface modification of polypropylene membranes by tethering phosphatidylcholine analogous polymers created biocompatible interfaces [136, 137]. A similar result was obtained by reacting the OH groups of poly(acrylonitrile-*co*-hydroxyethyl methacrylate) membranes with 2-chloro-2-oxo-1,3,2-dioxaphospholane followed by ring opening with trimethylamine [138].

MPC is part of several statistical copolymers prepared by free radical polymerization. Copolymers with poly(ethylene glycol) monomethyl ether methacrylate show polyelectrolyte behavior [139]. The surface of copolymers with 2,2,2-trifluoroethyl methacrylate was analyzed by different methods. The amount of protein adsorbed could be strongly reduced [140]. Copolymers with 2-aminoethyl methacrylate were employed as DNA carrier [141]. The structure and hydrogen bonding of water in the vicinity of copolymers with *n*-butyl methacrylate was studied by vibrational spectroscopy [142], and copolymers with styrene were developed as effective blocking agents for the enzyme-linked immunosorbent assay (ELISA) method [143]. Several new monomers were only used for the synthesis of copolymers. Typical examples are **47**, useful for stable Langmuir–Blodgett films [144], and **48**, useful for coatings which are resistant to protein absorption [145] (Scheme 9).

Phosphobetaines are known as a component of hydrogels, too. MPC copolymers with methacrylic acid prepared by radical polymerization in water show spontaneous gelation [146]. To improve the hydrogel proper-

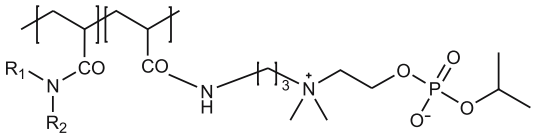

a: $R_1 = C_{18}H_{37}$, $R_2 = (CH_2)_8CH{=}CH(CH_2)_7CH_3$
b: $R_1 = R_2 = C_{18}H_{37}$
c: $R_1 = C_{22}H_{45}$, $R_2 = (CH_2)_8CH{=}CH(CH_2)_7CH_3$

47

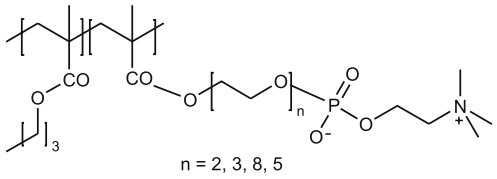

n = 2, 3, 8, 5

48

Scheme 9 Statistical phosphatidyl analogue copolymers

ties a new dimethacrylate cross-linker with a phosphorylcholine-like linkage was used in the copolymerization of MPC and 2-hydroxyethyl methacrylate [147]. Cross-linking of the acrylamide derivative of **39a** ($n = 2$) with *N*,*N*-methylenebisacrylamide leads to hydrogels whose degree of swelling decreases with increasing temperature [148]. Phosphorylcholine-based statistical terpolymers were obtained by adding phosphorylcholine groups to a preformed hydrophobically modified copolymer of NIPAM with several hydrophobic comonomers [149].

2.4 Narrowly Distributed Homopolymers and Block Copolymers

CRP is a powerful tool for the synthesis of both polymers with narrow molecular weight distribution and of block copolymers. In aqueous systems, besides ATRP, the RAFT method in particular has been used successfully. A number of uncharged, anionic, cationic, and zwitterionic monomers could be polymerized and several amphiphilic block copolymers were prepared from these monomers [150, 153]. The success of a RAFT polymerization depends mainly on the chain transfer agent (CTA) involved. A key question is the hydrolytic stability of the terminal thiocarbonyl functionality of the growing polymers. Here, remarkable progress could be achieved by the synthesis of several new dithiobenzoates [150–152].

The RAFT homopolymerization was mainly applied to vinylic sulfobetaines, for the synthesis of homopolymers as well as of block copolymers. The synthesis of the latter proceeds mainly in two steps: a macromolecular CTA of a monomer A is synthesized, which is subsequently employed in the polymerization of a monomer B. Polymers **49a**, **49b**, and **50** (Scheme 10) were prepared using 4-cyanopentanoic acid dithiobenzoate as CTA. M_w/M_n values between 1.04 and 1.08 at higher conversion were reported [154].

Recent attempts to prepare **26** by RAFT, however, failed [153]. Double hydrophilic block copolymers of NIPAM and **23e** [154], as well as of *N*,*N*-diethylacrylamide and **23b** [155], were prepared with the CTA benzyl dithiobenzoate, and exhibit LCST and UCST behavior in water. The new polymer **51** is also part of amphiphilic di- and triblock copolymers [152]. Diblock copolymers with poly(ethylene glycol) methyl ether acrylate, dimethylacrylamide, or 4-vinylstyrene sulfonate are macrosurfactants with a switchable hydrophobic block. Triblock copolymers containing additionally 4-vinylbenzoic acid differ in the nature of the hydrophilic part [152]. Near-monodisperse block copolymers of *N*,*N*-dimethacrylamide and **49a** were synthesized in different ways via macro-CTAs of both monomers as the first step. Such sulfobetaine block polymers form aggregates in pure water but are molecularly dissolved after addition of salt [152, 156, 157].

Another route to narrowly distributed sulfobetaine homopolymers and block copolymers is the functionalization of precursors prepared by group

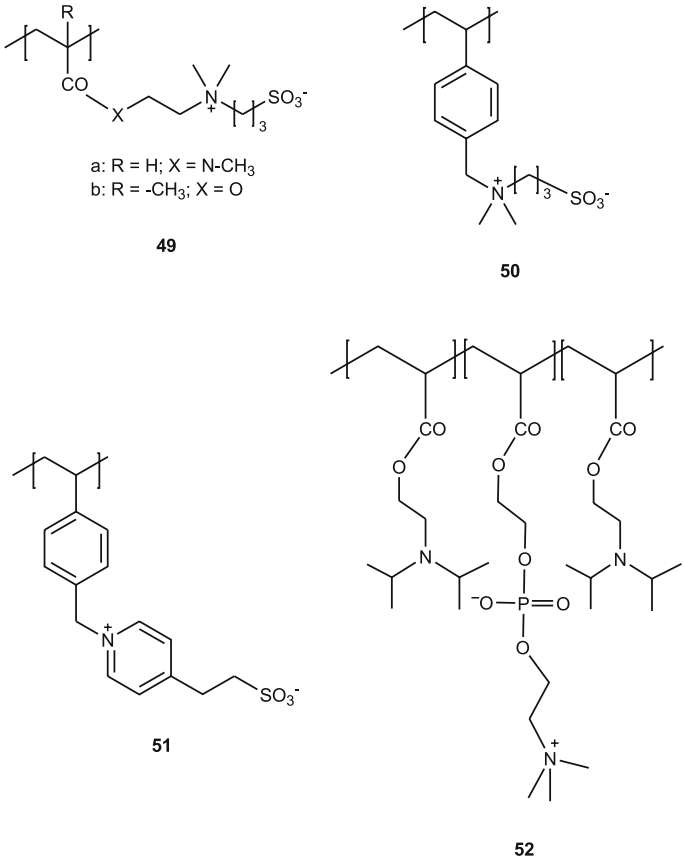

Scheme 10 Polysulfobetaines prepared by RAFT polymerization as homopolymers and part of block copolymers

transfer polymerization (GTP). Using 2-(dimethylamino)ethyl methacrylate (DMAEM), nearly monodisperse polymeric amines were made which were betainized in high yields via 1,3-propanesultone, resulting in **23b** [158, 159]. This principle was extended to block copolymers of *n*-butyl methacrylate (BMA) and DMAEM, resulting in hydrophilic–hydrophobic sulfopropylbetaine block copolymers BMA-*b*-**23b** [158, 160].

The synthesis of narrowly distributed polycarbobetaines **17a**, **18**, and **19** has already been mentioned. Block copolymers containing these structures and styrene were prepared likely by functionalization of reactive block copolymer precursors [161]. Well-defined block copolymers with phospholipid sequences were prepared using both RAFT and ATRP techniques.

Amphiphilic block copolymers composed of poly(butyl acrylate) and poly(2-acryloyloxyethyl phosphorylcholine) were synthesized via RAFT using a poly(butyl acrylate) macro-CTA with a ratio $M_w/M_n = 1.11–1.18$. The

conversion was followed by FT-NIR spectroscopy. The polymers have a strong tendency to aggregate in different solvent compositions [162]. RAFT polymerization of MCP leads to a dithioether end-capped macro-CTA used for the preparation of block copolymers with BMA with variable block length, whose associative properties [163] and interaction with enzymes [164] were investigated. MPC can also be polymerized in aqueous media via ATRP, showing first-order monomer kinetics to high conversion in protic solvents at ambient temperature. Polymers with relatively narrow polydispersities (M_w/M_n = 1.15–1.35) were thus obtained [165, 166]. Several MPC diblock copolymers were synthesized using the same principle. Macroinitiators were employed to prepare PEO-MPC and PPO-MPC diblocks, and the sequential monomer addition route was used for the block copolymerization of MPC with 12 different methacrylic comonomers. Generally high conversions were achieved with low polydispersities of 1.1–1.3 [167]. MPC-based ABA triblock copolymers with 2-(diisopropylamino)ethyl methacrylate (DIPAEM) **52** or 2-(diethylamino)ethyl methacrylate (DEAEM), prepared by ATRP using a bifunctional ATRP initiator, lead to polymers with adjusted block length. Polydispersities of the initial MPC homopolymers prior to the addition of the comonomer were less than 1.20, and final triblock polydispersities ranged from 1.5 to 1.8. The copolymers dissolve in acids but form freestanding gels at neutral pH [168]. Similarly obtained triblock copolymers with NIPAM building the outer block form gels over a narrow temperature range [169]. Folic acid functionalized MPC-*b*-DIPAEM or MPC-*b*-DEAEM block copolymers were synthesized by ATRP using a protected primary amine-based initiator. After deprotection, folic acid was chemically conjugated via the primary amine terminus of the MPC block with a degree of functionalization in the range 38–100%. The copolymers were designed for gene delivery and encapsulation of hydrophobic drugs [170]. Using a cholesterol-based macroinitiator, the ATRP of MPC results in block copolymers whose association behavior in aqueous solution was studied extensively [171].

2.5 Polymeric Surfactants

Zwitterionic polysoaps have been considered to combine ionic and nonionic polysoap behavior advantageously. The ionic groups with an overall neutral charge render the polymer very hydrophilic, avoid problems of a LCST, and hold the possibility of modifying the properties in solution by adding salt. A series of zwitterionic vinyl surfactants free of salt contamination was prepared by attaching a polymerizable moiety to a tertiary amine followed by sulfopropylation with propanesultone. The structural variation includes the nature and the position of the polymerizable moiety while keeping the length of the hydrophobic tail constant. Thus, polymers **53–56** with "head" or "tail"-end structure were obtained by free radical polymerization in wa-

ter or ethanol [172], and the effects of added salt on the solution properties [173] as well as on the molecular packing [174] were investigated. Furthermore, several alternating SO_2-containing polysoaps like **57** were synthesized by copolymerization of olefinic zwitterionic surfactants and SO_2, and a series of zwitterionic polysoaps containing oligo(ethylene oxide) spacers such as **58** was prepared [175]. Copolymers of sulfobetainic surfactant monomers of different geometry like that corresponding to **55** and polar nonionic comonomers such as acrylamide were synthesized and their

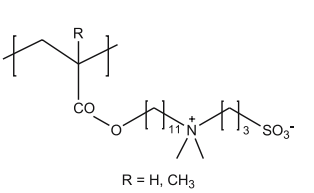

53

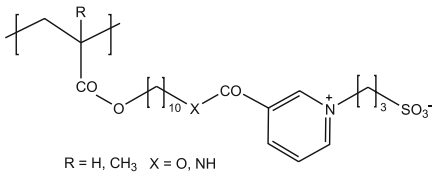

54

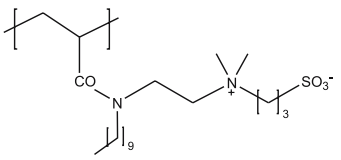

55

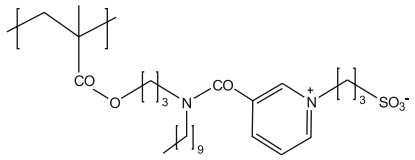

56

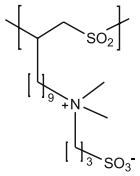

57

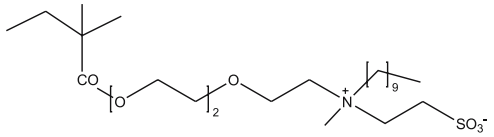

58

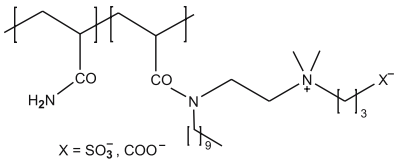

59

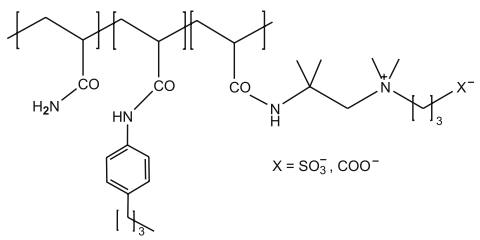

60

Scheme 11 Zwitterionic polysoaps

bulk and solution properties were extensively investigated [176]. A great number of polymeric surfactants all bearing the ammoniopropanesulfonate head group were prepared by radical homopolymerization of monomers containing diallyl, diene, or vinylcyclopropane moieties, thereby varying the density of surfactant side groups. The solubility of these polymers is dominated by the polymer geometry [176–178]. This work was continued by the synthesis of a series of polysulfobetaines with the principal structure of **53**, but variation of the spacer lengths and the substituents at the quaternary nitrogen. The influence of the structural variation on the bulk properties was the subject of detailed investigations [178]. A number of sulfobetaine monomers were characterized by one- and two-dimensional NMR spectroscopy [179]. Instead of synthesis by free radical chain growth polymerization, polymeric sulfobetaine surfactants were also synthesized from hydrophobized sulfopropylammonio monomers containing two olefinic groups by free radical step growth polymerization, namely via thiol/ene addition [180] (Scheme 11).

Copolymers **59** [181] and terpolymers **60** [182] were synthesized by micellar copolymerization and characterized with respect to their molecular and solution properties. The subject of further investigations was the interaction with low molecular weight surfactants [181, 183]. Another interesting use was made of hydrophobized sulfopropylammonio monomers as surface-active monomers (or "surfmers") [184]. Their use in emulsifier-free emulsion polymerizations [185] reduced the water uptake and improved the mechanical stability of the resulting filmed latexes.

3
Properties of Polybetaines in Solution, Condensed, and Gel States

The unique properties of polymeric betaines are strongly related to the interaction of the opposite charges in aqueous and aqueous salt solutions [1–4, 186]. One of the features of betaine-type polyampholytes is the tendency of the zwitterionic fragments to form a cyclic conformation of the cationic and anionic groups of neighboring monomer residues (intragroup), or a head-to-tail stacking (intrachain) within single macromolecules and interchain ion contacts between neighboring macromolecules. This results in the appearance of cross-linked networks (Scheme 12).

Therefore, polymeric betaines are usually sparingly soluble in pure water, and present gel-like characteristics, but they are soluble in salt-containing solutions. In contrast to ordinary polyelectrolytes, polymeric carboxy-, sulfo-, and phosphobetaines in dilute solutions have a very small disturbing effect on the structure of the hydrogen-bonding network of water molecules, because of the intra- and intertether proximity between the oppositely charged groups [187].

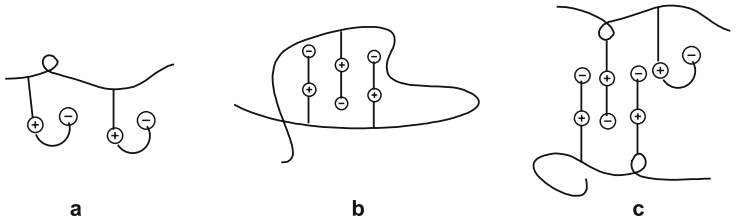

Scheme 12 Intragroup (**a**), intrachain (**b**), and interchain (**c**)salt bonds in polybetaines

According to molecular modeling calculations and NMR spectra [188], low molecular weight zwitterions are able to fold intramolecularly into a loop conformation in which the positive charge on one end of the molecule interacts with the negative charge on the other end, in dependence on the length and flexibility of the spacer. This folding motif can be useful for the design of supramolecular polymers by varying the linker length and its flexibility. The design of self-assembling molecules that are able to fold into predictable, specific conformations can help us to learn more about the self-organization, in particular protein folding processes.

Capillary electrophoresis proved to be a powerful tool for studying the intra- and interchain associations in various polycarboxybetaines as a function of the structure, the pH, and the molecular weight [35–37]. At low pH, the polymer particles migrate to the cathode side as the dissociation of the carboxylic groups is suppressed. The mobility differences of the charged species depend on their primary structure. For instance, the cationic group of **19b** is more effectively shielded by ethyl substituents than that of **19a**, which is surrounded by methyl groups. This lowers the association of the carboxylic groups with the quaternary ammonium groups. It is therefore easier to protonate the carboxylic functions in compound **19b**. The overall cationic charge of **19b** is higher, and the mobility is greater than that of **19a**. If intramolecular association prevails, the resulting electropherogram of the mixture of two samples of different molecular mass should be the overlap of the two single injections. When the electropherogram of the mixture results in a narrow peak with a mobility in between the peak maxima of the single injections, the dominating process should be intermolecular association. The intramolecular association is pH dependent. With increasing pH of the buffer solution the mobility of polycarboxybetaines drastically decreases due to the increased ionization of the carboxylic groups [36].

The effects of alkyl spacer length between both charged moieties with different substitution at, and with different hybridization of, the quaternized nitrogen were studied for a series of poly(carboxybetaines) derived from poly(4-vinylpyridine) and poly(vinylbenzyl chloride) by capillary electrophoresis, charge titration, and FTIR spectroscopy. A strong pH- and structure-dependent shift in electrophoretic mobilities is revealed for

the samples bearing different numbers of methylene groups between the charges [35–37]. The protonation of carboxylic units is increased with increasing charge distance and leads to enhanced mobility. The efficiency of the intramolecular electrostatic interaction is decreased by additional alkyl chains at the α carbon atoms. The "ion pair" formation ability of dimethyl- and diethylammonium acetate having sp^3 hybridization was compared with some sp^2-nitrogen-containing pyridiniocarboxylates. As expected, the intensity of interaction drops with an sp^3 hybrid orbital instead of an sp^2 ammonium ion. The findings of the FTIR measurements reveal that the association structures of the polycarboxybetaines are preformed in bulk. Strong interaction of sterically less shielded positive charges with a carboxylate moiety leads to increasing bond strength of the COO^- moiety and therefore to a higher wave number of the IR band (1643.1 cm^{-1}). The opposite happens with highly shielded cationic charges as in **19b** (1627.8 cm^{-1}) or with charges separated by four methylene spacers (1640.3 cm^{-1}). The increase in distance from one carbon up to four and ten carbons in polycarboxybetaines caused the carboxylate band to shift from 1632 to 1570 and 1561 cm^{-1} [16].

The pK_a values of ionizable groups in macromolecules can significantly differ from those of the isolated groups in solution because of interactions between neighboring ionizable groups, solvation effects, and conformational changes [189]. The approach developed in [190] for equimolar annealed polyampholytes can be applied to a comprehensive analysis of the potentiometric titration data of the polycarboxybetaines and -sulfobetaines derived from *N*,*N*-diallyl-*N*-carboethoxymethylammonium chloride and 3-(*N*,*N*-diallylammonio)-propanesulfonate [75, 191]. These zwitterionic polyelectrolytes can also exist in the form of anionic and cationic polyelectrolytes and in an uncharged form in dependence on pH (Scheme 13). The transformation from the uncharged form to the polyzwitterion or vice versa is determined by micro- and macroscopic ionization constants. The relationships between the microscopic (k_1, k_2, k_{12}, k_{21}) and macroscopic (K_1, K_2) ionization constants as well as the tautomeric (K_t) constant can be described as follows:

$$K_1 = k_1 + k_2$$
$$1/K_2 = 1/k_{12} + 1/k_{21}$$
$$K_1K_2 = k_1k_{12} = k_2k_{21}$$
$$K_t = k_1/k_2 = k_{21}/k_{12}\,.$$

As in the case of the simple amino acid glycine, the zwitterionic form of the polycarbobetaine should be more stable than its uncharged form because of $K_t \gg 1$. The polycationic form might be considered as a two-base acid having pK_a^1 and pK_a^2, which correspond to successive titration of COOH and NH^+ groups, while the polyanionic form can be considered as a two-base base with pK_b^1 and pK_b^2, which reflect the protonation of tertiary amine N groups and

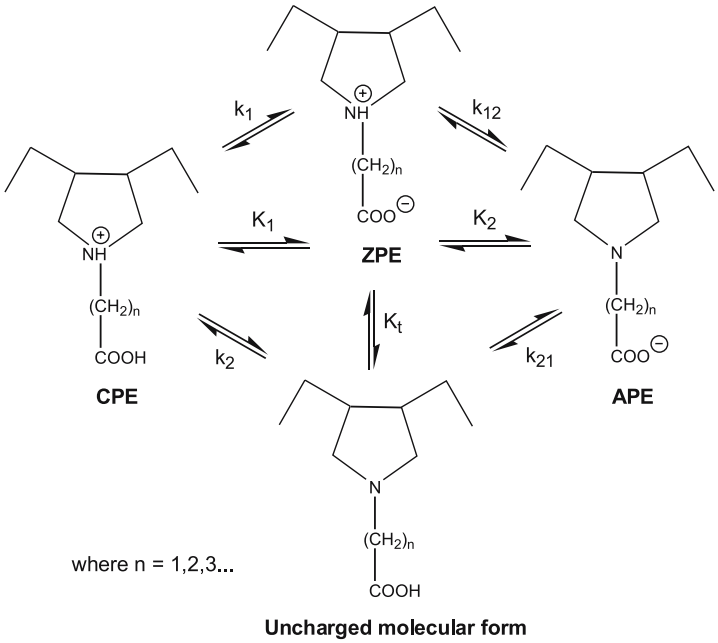

Scheme 13 Transformation of zwitterionic polybetaine (ZPE) to anionic (APE) and cationic (CPE) polyelectrolytes and uncharged molecular form [191]

carboxylate ions COO^-. In its turn, the polyzwitterionic form can serve as both an acid that loses protons and is converted to the polyanion (k_{12}), or as a base that binds protons and is transformed to the polycation (k_1).

Table 1 summarizes the values of k_1 and k_{12} determined in salt-free and saline water containing 0.1 M KCl, together with the solubilities of the poly-

Table 1 Ionization constants and solubility behavior of polycarboxybetaines and -sulfobetaines in salt-free water and 0.1 M KCl solutions

Polybetaine	Salt-free water		0.1 M KCl		Solubility	
	k_1	k_{12}	k_1	k_{12}	Salt-free water	0.1 M KCl
PCB ($n = 1$)	2.52	10.70	2.66	9.87	Soluble	Soluble
PCB ($n = 5$)	3.52	—	4.36	—	Soluble	Soluble
PCB-*co*-SO_2 ($n = 1$)	—	8.73	—	7.88	Insoluble	Insoluble
PCB-*co*-SO_2 ($n = 5$)	—	8.88	—	8.04	Insoluble	Soluble
PSB ($n = 1$)	—	10.82	—	9.88	Soluble	Soluble
PSB-*co*-SO_2 ($n = 1$)	—	8.51	—	7.54	Insoluble	Soluble
PSB-*co*-SO_2 ($n = 3$)	—	—	—	—	Insoluble	Insoluble

betaines. It is evident that the presence of the electron-withdrawing SO_2 unit considerably lowers k_{12}. As can be seen from Table 2, the polycarbobetaine with the shorter spacer ($n = 1$) is easier to protonate. The microscopic ionization constant k_1 of the polycarbobetaine with $n = 5$ in 0.1 M KCl is close to those of polycarboxylic acids. The strong acidic character of the polycarbobetaine with $n = 1$ may be attributed to a "nearest-neighbor effect" specific for polyampholytes [192]. Also, the changes in the dissociation constant of a weak acid (carboxyl) in the vicinity of strong basic (ammonium) groups based on Hill's theory should be taken into account [189].

The distribution of the cationic, anionic, and zwitterionic forms of the polyampholyte calculated from the k_1 and k_{12} and the viscosity data show that polybetaine molecules exist in the zwitterionic form and as a compact coil in the vicinity of the isoelectric point (IEP) (Fig. 1). Deviation from the IEP leads to prevalence of the anionic or cationic forms and expanding conformations.

The viscometric curves of the polyzwitterion form are not symmetrical, e.g., the increment in the reduced viscosity is significantly lower on the acidic side in contrast to the basic region. The reason is either the formation of hydrogen bonds between carboxylate ions and H^+ of the type $COO^- \cdots H^+ \cdots {}^-OOC$ that reduce the hydrodynamic volume of the polybetaines, or the specific binding of chloride ions to the protonated amine groups.

The intramolecular dipolar interaction in solution should decrease with increasing size of the substituents in the order: pyridinium $> N^+(CH_3)_2 > N^+(C_2H_5)_2$ [34]. The potentiometric titration curves of polybetaines resemble those of the titration of weak acids and weak bases. Measurements of the

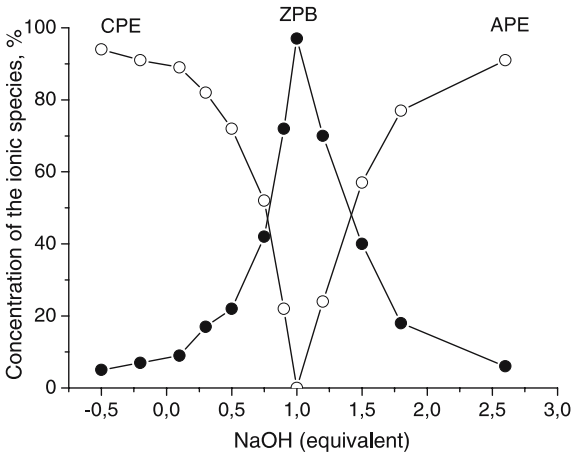

Fig. 1 Distribution curves for the anionic, cationic, and zwitterionic forms of polybetaines [191]

accessibility of the carboxylic group to protons show significant differences as a function of the chemical structure of polycarboxybetaines derived from poly(4-vinylpyridine) (**17**) and from poly(vinylbenzyl chloride) (**19**). Only 6% of the carboxylic groups of **17** were titrated in pure water. The addition of NaCl resulted in an increase of protonated carboxylates up to only 15%. The larger ethyl groups in **19b** are responsible for decreasing intramolecular interactions, so that a much higher proportion of acid groups can be titrated (up to 75% in 0.5 M NaCl). These results are in good agreement with viscosity measurements. Polycarboxybetaine **19b** shows a typical polyelectrolyte effect in water, while polycarboxybetaine **17** ($n = 1$) shows a nearly linear slope. The reason is that the free charges of the polycarboxybetaine **17** ($n = 1$) is close to zero in contrast to polycarboxybetaine **19b**, which has a noticeable number of free charges because of the hindered formation of an internal salt. The reduced viscosity of **19a** and **19b** passes through a minimum as a function of pH (Fig. 2) [193].

The difference in replacement of the IEP for **19a** ($pH_{IEP} = 3.6$) and **19b** ($pH_{IEP} = 2.9$) is probably connected with the different hydrophobicity of polycarboxybetaine chains, e.g., the cationic group of **19b** is more effectively screened by ethyl substituents, as they are bulkier than the methyl groups of **19a**. The effect of organic solvent on the solution behavior of **19b** was studied [193]. In saline water, the conformation of **19b** is compact due to the screening of the electrostatic repulsion by the neutral salt KCl. Addition of ethanol improves the thermodynamic quality of the solvent with respect to the hydrophobic parts of the macromolecules, and the reduced viscosity increases and has the maximal value at 60–80 vol % of ethanol in a water/ethanol mixture.

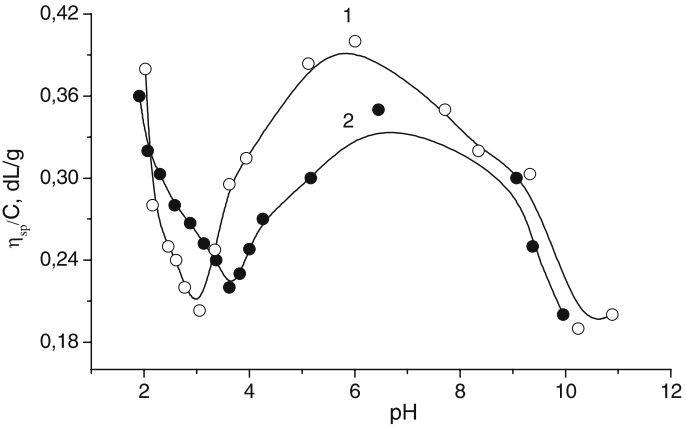

Fig. 2 Dependence of the reduced viscosity of **19b** (curve 1) and **19a** (curve 2) on pH in water. Concentration = 0.3 g/dL [193]

A reasonable explanation of this phenomenon may be the unfolding of the macromolecules due to preferential solvation of the betaine parts of **19b** by water, and of the benzyl ones by the organic solvent. The viscosity of **19b** decreases in pure ethanol because of the low solubility of ionic species and enhanced condensation of counterions to polyions.

The main distinction between polycarboxybetaines and -sulfobetaines is the difference in basicity, the carboxylate group in polycarboxybetaine being a stronger base than the sulfonate group of polysulfobetaine [13, 51]. In aqueous solution, the carboxylate group can be rendered nonionic by lowering the pH, whereas the sulfonate group remains anionic even at low pH due to the low pK_a. As a result, the reduced viscosity of polycarboxybetaine passes through a minimum undergoing a polyanion ↔ polyzwitterion ↔ polycation transition. In contrast, the polysulfobetaine does not exhibit an enhanced viscosity at low pH due to the weak basicity of the sulfonate group. A combination of static and dynamic laser light scattering was used to study the effects of temperature, pH, and ionic strength on inter- and intrachain interactions in poly(*N*,*N*-dimethylmethacrylamidopropylammonium propiolactone) [28]. An increase of the temperature to 50 °C shifts the equilibrium from associates toward individual chains. The addition of NaOH also suppresses interchain aggregates due to the ionization of carboxylic groups. The addition of a small amount of NaCl (at pH 12) at first enhances the dissociation of interchain associates, because both the hydrodynamic radius and molar mass decrease. The further addition of salt results in chain extension as the intrachain association is broken up. Thus intragroup, intrachain, and interchain ion contacts are disrupted at sufficiently high salt concentration. The solubility of polybetaines in aqueous solution depends on the nature of the anions and cations of added salts [194, 195]. For salts with a common anion (Cl^-) and monovalent cations, the solubility decreases as $K^+ > Na^+ > NH_4^+ > Li^+$, while for divalent cations the solubility decreases in the order $Ba^{2+} > Sr^{2+} > Ca^{2+} > Mg^{2+}$. In the presence of salts with a common cation (K^+) but different anions, the solubility decreases in the order $ClO_4^- > I^- > Br^- > Cl^- > F^-$. The Hofmeister lyotropic sequence can successfully be applied to describe the solubility behavior of most polybetaines.

The common feature of polyampholytes with betaine structure is that the viscosity of the solution and the second virial coefficient A_2 increase with increasing salt concentration [196] beyond a critical minimum value [173]. The Huggins constant K, which is generally considered to be related to polymer–solvent interaction, decreases as the salt content is increased. In other words, the solvent quality for polybetaines increases with increasing salt concentration. However, the properties of copolymeric polysulfobetaines [197, 198] based on styrene–*N*,*N*-dimethyl(maleimidopropyl)ammonium propanesulfonate, styrene–*N*,*N*-dimethyl(maleamidic acid)propylammonium propanesulfonate, or acrylamide–*N*,*N*-dimethyl(maleimidopropyl)ammonium propanesulfonate in aqueous salt solutions are different from the gen-

eral polysulfobetaines containing just a single sulfobetaine group [70, 199]. This may be attributed to the hydrophobic or hydrophilic character of macromolecules induced either by the presence of styrene segments or carboxylic (acrylamide) moieties in addition to sulfobetaine groups.

Poly(ampholyte–electrolyte)s containing both polybetaine and anionic (or cationic) polyelectrolyte can exhibit simultaneously both "antipolyelectrolyte" (the viscosity increases with growth of the ionic strength) and polyelectrolyte behavior (the viscosity decreases with increasing ionic strength) [22, 57]. The study in [56] provides an interesting opportunity to investigate which structural features—polyelectrolytic or polyzwitterionic—dictate the solution properties of novel poly(electrolyte–zwitterions) synthesized from sodium *N*-(3-sulfopropyl)-3-(*N*,*N*-diallylamino)propanesulfonate. As distinct from classical polybetaines, such poly(electrolyte–zwitterion)s have two negative and one positive charges in each monomer unit. This explains their very good solubility in water and many protic solvents except methanol, triethylene glycol, and acetic acid. In the absence of added salts, poly(electrolyte–zwitterion)s behave as typical polyelectrolytes. The polyelectrolyte effect disappears in salt-containing solutions, and the intrinsic viscosity values decrease with increase in various salt concentrations in favor of polyelectrolyte character. It is interesting to note that the hydrodynamic volume of poly(electrolyte–zwitterion)s increases continuously with increasing temperature in both 0.1 and 0.5 M NaCl. This property could be useful for viscosification of water at high temperatures. The polybetaines obtained by cyclopolymerization from *N*-(4-sulfobutyl)-*N*-methyl diallylammonium betaine show enhanced solubility in salt water, increased stability in the solid state, and enhanced thermal hydrolytic stability in comparison with betaines containing ester or amide linkages [56].

The aqueous solutions of aromatic and aliphatic polyzwitterions exhibit significantly different phase behavior: while **26** has an upper critical solution temperature (UCST) at 286 K, **23b** shows both an UCST at 306 K and an "apparent inverted" lower critical solution temperature (LCST) at 289 K [196, 200]. Compound **25** is insoluble over the whole temperature range between 273 and 373 K. Thus, **23b** is considered to be in a collapsed coil in water below the UCST due to intra- and/or interchain association.

The solution properties of a polybetaine containing the phosphatidylcholine group, poly[(2-methacryloyloxy)ethyl-2-(trimethylammonioethyl phosphate)], which has PO_4^- and $N^+(CH_3)_3$ groups separated by two methylene groups, were reported [201, 202]. A linear relationship between $[\eta]$ and $1/\mu$ was observed for the polyampholyte at low μ near pH_{IEP}. When $\mu > 0.0025$, $[\eta]$ increases as the attractive interactions between the oppositely charged units are diminished. By comparing the μ dependence of the electrostatic expansion factor of the polyampholyte with that of poly(sodium acrylate), it is suggested that there is a pronounced intramolecular attraction between the oppositely charged segments even when the pH deviates from

the IEP. For the sulfobetaine-type polyampholyte [66], the intrinsic viscosity $[\eta]$, second virial coefficient A_2, exponent a in the Mark–Kuhn–Sakurada equation, radius of gyration R_g, and hydrodynamic radius R_h increase with increasing salt concentration C_s. The exponents of the Mark–Kuhn–Sakurada equation are $a = 0.5$, 0.67, 0.70, and 0.70 for $C_s = 0.06$, 0.3, 1.0, and 4.0 M NaCl aqueous solution, respectively. Judging from the experimental results for $a = 0.5$, it was found that the NaCl solution of $C_s = 0.06$ M is a theta-solvent at 30 °C. The electrostatic expansion factors for the polyampholyte effect, α_e, were estimated over a wide range of molecular weights and C_s values. It was concluded that the chain expansion for a neutral polyampholyte is controlled by the nonionic excluded volume effect and the electrostatic excluded volume effect (polyampholyte effect) at moderate concentrations of added salt. The electrostatic expansion factor can reasonably be described by an α_e^3-type equation, although no such equation has so far been proposed for the polyampholyte.

The adsorption of **23** onto a silica surface from aqueous NaCl solutions with various concentrations was studied [203]. Comparison of the thickness of the adsorbed layer with the radius of gyration of **23** in NaCl solutions revealed the existence of collapsed (pancake)-, normal (fence)-, and elongated (pole)-like conformational regimes that were described theoretically by Joanny [204].

The three-dimensional plot [57] of R_h as a function of salt and polymer concentrations for cyclocopolymers consisting of sulfobetaine and cationic monomers shows that the value of R_h passes through a minimum at any polymer concentration as the ionic strength of the medium is increased. The initial decrease of R_h is attributed to the screening of electrostatic repulsions between positive charges by small ions. The minimum R_h corresponds to the collapsed state of the polymer chain. The reexpansion of the macromolecular chain with increasing ionic strength is due to the suppression of intramolecular dipole–dipole interactions between the sulfobetaine mer units.

Figure 3 shows the influence of pH on the viscosity and electrophoretic mobility of poly(carboxyethyl 3-aminocrotonate) (PCEAC) [205–211]. The minimal viscosity and the zero mobility are observed at extremely low pH (2.1–2.2) and correspond to the isoelectric point (IEP). The "asymmetric" character of chain stretching and the "anomalous" low magnitude of the IEP ($pH_{IEP} \approx 2.0$–2.1) may be explained by the different accessibility of the carboxylic and secondary amine groups to ionization. Carboxylic groups placed far from the polymer main chain can be ionized more easily than the secondary amine groups that are close to the main chain and in a hydrophobic environment. These results are in good agreement with the electrophoretic data, e.g., the number of negative charges on the macromolecules is significantly higher at pH > 2 than the number of positive charges at pH < 2. The values of R_g, A_2, and η_{sp}/C at pH = 2.1 (IEP) and 7.0, when the PCEAC chains are correspondingly in the collapsed and expanded state, correlate well with the data of Fig. 3 (Table 2).

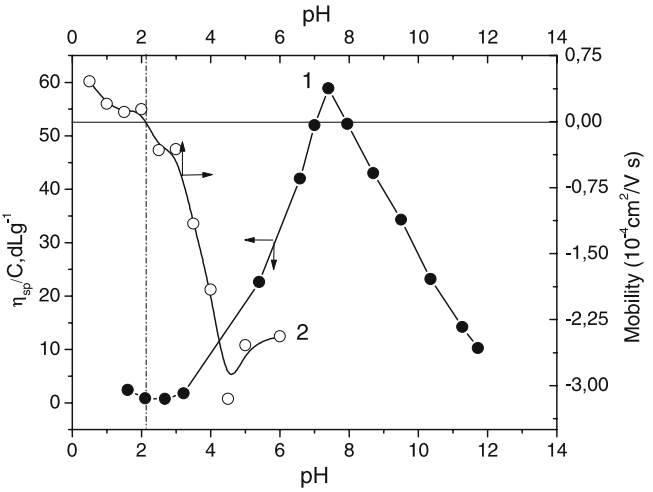

Fig. 3 Reduced viscosity (curve 1) and electrophoretic mobility (curve 2) of PCEAC vs pH of the solution [255]

Table 2 Hydrodynamic parameters of PCEAC in aqueous solution at different pH and μ = 0.1 [212]

Polybetaine	pH	$M_n 10^3$ [a]	PDI [a]	$M_w 10^3$	R_g, nm	η_{sp}/C, dL g^{-1}	$A_2 \times 10^{-4}$, cm^3 mol g^{-2}	Mean [b] d_h, nm	Peak [b] d_h, nm
PCEAC	2.1	—	—	44	—	0.5	– 38.8	40	18
	7.0	31	2.15	96	32	60.0	18.9	191	16

[a] Results are obtained using SEC
[b] DLS results are obtained at fixed polymer concentration and 90° scattering angle

The negative value of the second virial coefficient and the low value of the reduced viscosity at pH = 2.1 confirm a globular conformation of the polymer particles at the IEP [212]. The pH-dependent swelling behavior of the PCEAC gel is consistent with its linear analogue and a minimum at $pH_{IEP} \approx 2.1–2.2$.

The electrostatic self-assembly of thermally responsive copolymers of *N*-isopropylacrylamide with up to 10 mol % of the sulfobetaine monomer 3-[*N*-(3-methacrylamidopropyl)-*N*,*N*-dimethyl]ammonium propanesulfonate) and poly(ethylene oxide) modified with terminal cationic or anionic groups was studied in methanol and aqueous solutions by static light scattering, turbidimetry, viscometry, and rheological measurements [82]. The formation of graftlike complexes at stoichiometric dipole–ion ratio and their self-association was detected in the dilute and semidilute regime at temperatures below and above the LCST. The ability of the graftlike complexes

to associate below the LCST depended on the sulfobetaine content of the copolymers, the functionality of cationic or anionic groups, and the polymer concentration. The effect of the terminal group on the solution behavior of the graftlike complexes was less pronounced. With increasing temperature their semidilute aqueous solutions form gels, which are stable over a wide temperature range.

Polybetaines in the solid state are able to form ionic aggregates or clusters [2]. The microphase separation in various zwitterionomers was analyzed [67, 213, 214]. Copolymers based on five different sulfobetaine monomers and butyl methacrylate (or 2-ethoxyethyl acrylate) exhibited a biphasic morphology with the appearance of ion-rich and ion-poor phases in dependence on spacer length between positive and negative charges and on the bulkiness of the alkyl substituents at the quaternary ammonium functionality [213]. The cluster phase undergoes a glass transition at a higher temperature than the ion-poor matrix. A series of segmented poly(tetramethylene oxide) zwitterionomers of the ammonioalkanesulfonate ($N^+(CH_2)_pSO_3^-$, $p = 3, 4$) or the alkoxydicyanoethenolate ($N^+(CH_2)_pOCOC^-(CN)_2$, $p = 2, 3$) displays thermally stable biphasic structures as a result of the quantitative segregation of the dipolar segments within the highly mobile and weakly polar poly(tetramethylene oxide) matrix [74, 215]. Transition from a lamellar structure for the shorter poly(tetramethylene oxide) segments (high zwitterion density, lamellar spacings between 7 and 8 nm with a thickness of the zwitterionic layer of about 1 nm) to a hexagonal structure (low zwitterion density, radius of the zwitterionic cylinder of about 1.2 nm) for the longer ones is observed. Matrix polarity effects on the microphase separation in zwitterionic A_iB random copolymers (where A_i units are $-CH_2CH(CH_2R_i)O-$ corresponding to epichlorohydrin (PEC, $R_i = Cl$), glycidol (PGOH, $R_i = OH$), glycidyl acetate (PGAC, $R_i = OCOCH_3$), or glycidyl *p*-nitrobenzoate (PGNB, $R_i = OCOC_6H_4NO_2$); B unit is $-CH_2CH[CH_2O(CH_2)_2N^+(C_2H_5)_2(CH_2)_2OCOC^-(CN)_2]O-$, the ammonioethoxydicyanoethenolate type) were further analyzed [214, 216]. DSC and NMR results show that (1) PGOH zwitterionomers are monophasic (one T_g between 3 and 31 °C) as a result of hydrogen bonding; (2) PGNB zwitterionomers are likely monophasic (one T_g around 58 °C) as a result of strong dipolar and dispersion interactions; (3) PEC zwitterionomer is a biphasic material characterized by a quasi-quantitative segregation of the dipolar units in the "hard" phase (high $T_g \sim 22$ °C) and a segregation rate of PEC units in the "soft" phase (low $T_g \sim -18$ °C) of about 84%; and (4) PGAC zwitterionomers are monophasic (one T_g between – 12 and 15 °C), despite fairly close and weak van der Waals interactions and a fairly similar matrix mobility when compared to the previous PEC case. Thus, the development of a two-phase structure in random A_iB zwitterionomers is very sensitive to small variations of the matrix characteristics and of the A–B interactions. Microscopic structural features of three methacrylate polymers with different

numbers of diethylene glycol residues and sulfobetaine pendant groups (**23d**) were determined by WAXS, SAXS, SEM, TEM, scanning probe microscopy, and AFM [67]. The basic morphology of methacrylate-based polysulfobetaines was found to be a core–shell configuration of molecular aggregates embedded in an amorphous polymer matrix. The studied polysulfobetaines are crystalline systems that can be adequately described by a lamellar structure. As the number of pendant groups increases, the crystallinity decreases, and the lamellar aggregates become smaller.

Due to the high density in dipolar units and dipole moment, polybetaines have a strong binding capacity with respect to low molecular weight salts and may be used as solid electrolytes for high-energy batteries. Such behavior was demonstrated for a number of polybetaines blended with $LiClO_4$, $NaClO_4$, $NaNO_3$, NaBr, or NaI [16, 28, 174, 178, 217–219]. Equimolar mixtures of polycarbobetaines with NaI give homogeneous blends, as indicated by the missing signals of residual NaI in X-ray diffractograms demonstrating the full miscibility. Moreover, the small-angle peaks in the diffractogram of polycarbobetaine change or disappear, indicating modification or loss of the superstructure, and giving additional evidence for the miscibility of polymer and salt. Dielectric spectroscopy was used to analyze the molecular dynamics and the charge transport in mixtures of poly3-[*N*-(ω-methacryloyloxyalkyl)]-*N*,*N*-dimethylammonium propanesulfonate with NaI in the frequency range of 10^2–10^7 Hz and in the temperature range of 110–400 K for different salt concentrations (0, 100, and 200 mol %) [220]. One relaxation process is observed whose relaxation rate depends strongly on the length of the aliphatic spacer between the polymethacrylate main chain and the zwitterionic groups. This relaxation process with activation energy $E_A = 47$ kJ/mol is assigned to the fluctuation of the quaternary ammonium groups in the side chains. At higher temperatures, the dielectric properties and the conductivity are primarily dominated by the mobile inorganic ions: conductivity strongly depends on the salt concentration, showing a pronounced electrode polarization effect. The conductivity contribution can be quantitatively described by the hopping of charge carriers in the frame of a random free-energy model. The Barton–Nakajima–Namikawa relationship is fulfilled for the low-frequency regime and for the critical frequency.

Similar to polyelectrolyte gels, polybetaine gels are also sensitive to the variation of external stimuli such as pH, temperature, ionic strength, solvent nature, and DC electric field. The pH-dependent behavior of xerogels based on sodium acrylate and *N*,*N*-dimethyl(acrylamidopropyl)ammonium propanesulfonate is bell-shaped [94, 95]. The contraction of the hydrogels in the strong acidic region is explained by the suppression of the ionization of the sulfonate and carboxylic moieties by mineral acid. The sharp swelling of hydrogels in the region of pH 2–3 is accounted for by the ionization of mostly sulfonate groups (with $pK_a \approx 2.8$), which results in electrostatic repulsion by the negative charges. A roughly constant swelling of the hydrogels between

pH 4 and 10 is the result of the ionization of both the carboxylic and sulfonate groups. The considerable shrinking of gel specimens at pH > 10 is probably explained by the suppression of the polyelectrolyte effect by the excess of NaOH that plays the role of the low molecular weight electrolyte.

Discontinuous and continuous collapse of PCEPAC and poly(carboxyethyl 3-cyclohexylaminocrotonate) (PCECHAC) hydrogels was observed [221] in water/acetone and water/ethanol mixtures (Fig. 4). These results confirm the universal behavior of hydrogels with respect to the thermodynamic quality of solvents.

SEM pictures of PCECHAC taken in water/acetone mixtures are also in good agreement with the swelling–shrinking behavior of such hydrogels (Fig. 5). The average pore size of PCECHAC gel in pure water is 30–40 μm. Increasing the acetone content in the water/organic solvent mixture results in a decrease of the gel pore size down to 15–20 μm. In pure acetone the gel sample is in a collapsed state with pore sizes of 1–2 μm. The swelling of hydrogels in polar solvents changes in the sequence: water ≫ DMSO ≫ DMF > ethanol > acetone.

It is well known that polyelectrolyte gels swell, shrink, or bend when an external electric current is applied [222, 223]. The electric-stimuli property of polybetaine gels depends on the pH of the outer solution, the ionic strength, the applied voltage, and the direction of the electric field with respect to the gel specimen [208, 221]. The bending behavior of PCEPAC gels was studied under an externally imposed DC electric field. A gel rod placed parallel to the electrodes bends to the cathode side. If the electric stimulus is removed, the gel gradually returns to the original position. When the polarity of the electrodes is altered, the gel bends toward the opposite direction. The bending

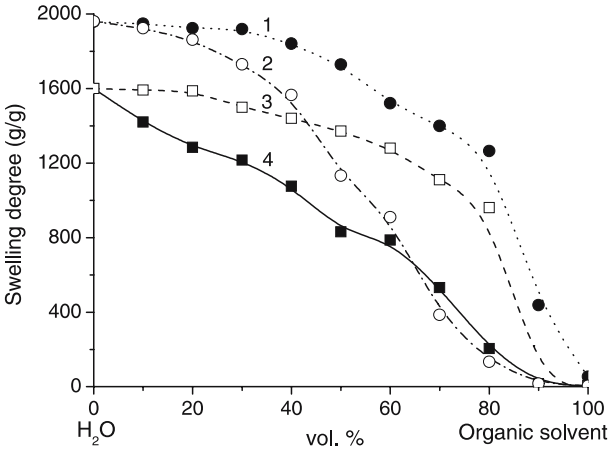

Fig. 4 Swelling–deswelling behavior of PCEPAC (1,2) and PCECHAC (3,4) gels in water/acetone (1,3) and water/ethanol (2,4) mixtures [221]

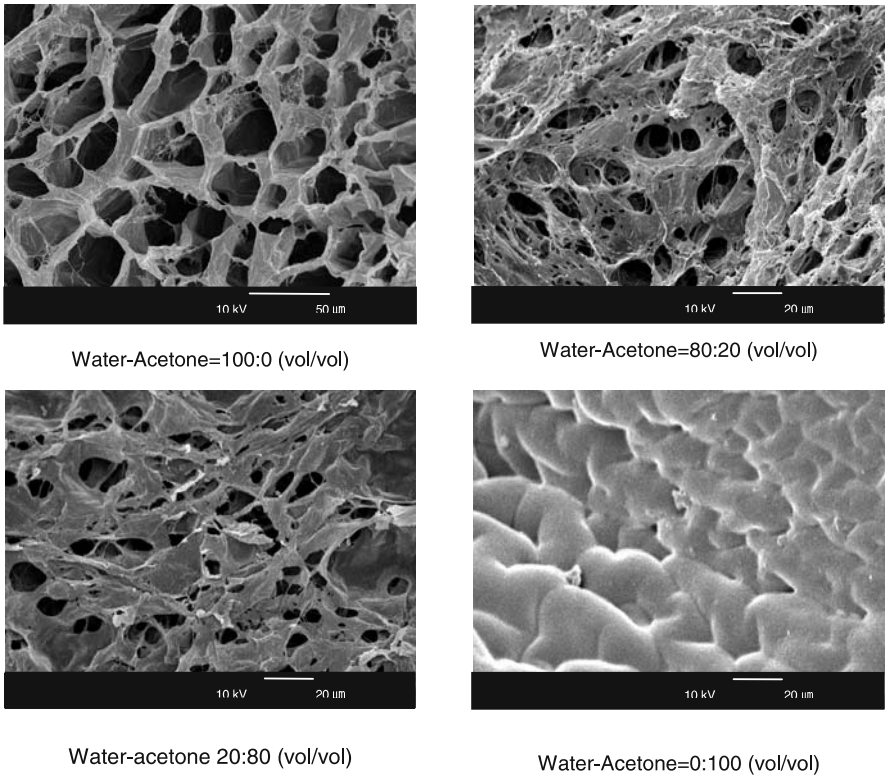

Fig. 5 SEM pictures of PCECHAC gel in water, acetone, and water/acetone mixtures [221]

angle increases with increasing voltage across the gel. The driving force of the bending toward the negative electrode is the swelling of the gel on the anode, and the shrinking on the cathode side induced by the osmotic pressure difference.

If the gel rod is placed perpendicular to the electrodes, the applied DC electric field causes a sharp appearance of pH gradient during 1–2 min [208]. After 5 min, the pH value becomes stable. The magnitude of the pH in the gel volume returns quickly to the initial state if the electricity is switched off. The values of $\Delta pH = pH_0 - pH_{t\to 0}$ (where pH_0 and $pH_{t\to 0}$ are the initial value of pH and pH value extrapolated to $t \to 0$, respectively) are a function of the DC electric field. Figure 6 presents the dependence of the pH on the distance $\pm L$ when the glass electrode is placed on the cathode or anode side of a gel specimen in comparison with its central section where $L = 0$.

Without an applied DC electric field, the pH gradient along the sample is uniform and equal to 5.46. An increase of the electric field shifts the pH gradient to the more acidic region. The dependence of the pH gradient on L is linear, but the slopes of the straight lines differ and depend on the value of

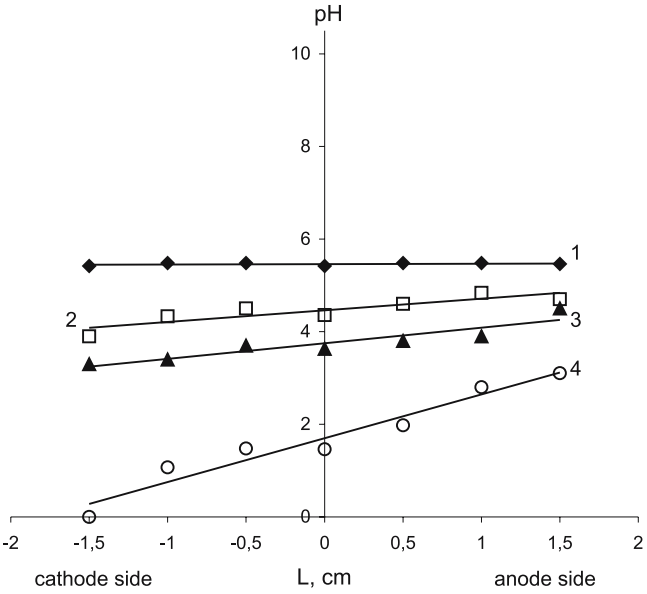

Fig. 6 Dependence of pH gradient on distance L without the imposed DC electric field (1) and at $E = 5$ (2), 10 (3), and 15 V (4) [208]

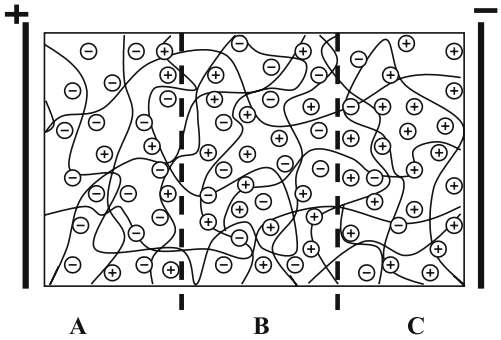

Scheme 14 Distribution of fixed and mobile charges in polybetaine gels under the imposed external DC electric field [208]

the applied DC electric field. In order to interpret these data, the distribution of fixed network charges and counterions along the gel specimen should be considered (Scheme 14).

The externally imposed potential across the gel causes the accumulation of negative fixed charges (COO^-) and mobile ions (OH^-) on the anodic side (zone A), while the accumulation of positive fixed charges (NH_2^+) and mobile ions (H^+) takes place on the cathodic side (zone C). Zone B probably contains an equal number of positive and negative charges.

As a result, zones A, B, and C have comparatively a basic, neutral, and acidic character, respectively. Increasing the DC electric current leads to the overall acidification of the gel sample (see Fig. 6, curve 4) due to the easy ionization of the acidic groups. Consequently, this narrows the zones B and C and expands zone A. Polybetaine hydrogel membranes of isopropyl-2-[2′-(trimethylammonium)ethyl phosphoryl] ethyl fumaramate and 2-hydroxyethyl methacrylate effectively enhance the water content in comparison with poly(2-hydroxyethyl methacrylate) [224]. The content of water in hydrogel membranes increases, but the amount of adsorbed BSA decreases with the increase of the betaine content in the feed. The values of the tensile strength and tensile elongation of the hydrogel reach 68.4 g mm^2 and 239%, respectively.

4
Behavior of Hydrophobically Modified Polybetaines

Hydrophobically modified polybetaines combine the behavior of zwitterions and amphiphilic polymers. Due to the superposition of repulsive hydrophobic and attractive ionic interactions, they favor the formation of self-organized and (micro)phase-separated systems in solution, at interfaces as well as in the bulk phase. Thus, glasses with liquid-crystalline order, lyotropic mesophases, vesicles, monolayers, and micelles are formed. Particular efforts have been dedicated to hydrophobically modified polyphosphobetaines, as they can be considered as polymeric lipids [5, 101, 225–228]. One can emphasize that much of the research on polymeric phospholipids was not particularly focused on the betaine behavior, but rather on the understanding of the lipid membrane, and on biomimicking. So, often much was learnt about biology and the life sciences, but little on polybetaines as such.

Although deviating chemically more from the natural prototype than polyphosphobetaines, hydrophobically modified polybetaines with other zwitterionic groups behave similarly. If the density and size of the hydrophobic fragments is reduced, the polymeric betaines become soluble in water (or in brine, see Sect. 3), but are still able to self-organize in aqueous solution and in bulk [17, 18, 28, 53, 172–174, 177, 178]. For instance, the low viscosities of so-called zwitterionic polysoaps are attributed to the intra- and intermolecular aggregation of the zwitterionic and hydrophobic side chains, keeping the hydrodynamic radius small. Simultaneously, X-ray studies of the same zwitterionic polysoaps reveal the formation of superstructures in the bulk. In the example in Scheme 15, both electrostatic attractions between ammonium and carboxylate groups and hydrophobic interactions between long hydrophobic side chains are the driving force of superstructure formation [17, 45, 174], supported by an appropriate spacer length in the polymer backbone.

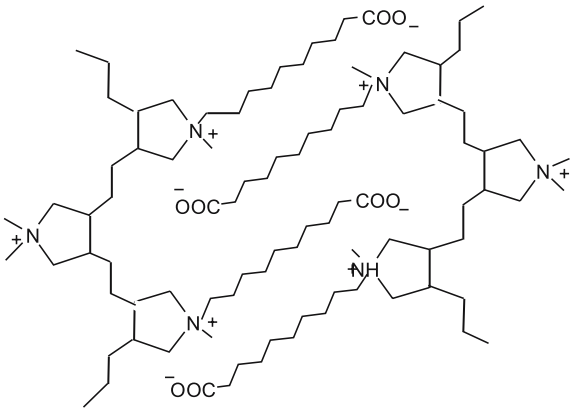

Scheme 15 Proposed spatial arrangement of the zwitterionic and hydrophobic parts in a hydrophobically modified polycarboxybetaine [17]

Fluorescent hydrophobes (naphthyl and pyrenyl groups) incorporated into the polysulfobetaines are a powerful tool for studying the formation of intra- and interpolymer aggregates in aqueous and aqueous salt solutions [85, 229–231]. Intermacromolecular hydrophobic association is observed as an increase in the excimer emission relative to that of the "monomer" emission, where I_E/I_M is the ratio of intensities of excimer and monomer fluorescence which reflects the extent of inter/intra macromolecular interactions. Intramolecular micellization is easily monitored by the quenching efficiency of the thallium ions. The decrease of I_E/I_M reflects the breaking of the intra- and interchain associations in aqueous salt solutions, leading to chain expansion.

The surface activity and solubilization capacity of amphoteric polysoaps were studied [172, 177, 178]. The surface activity of zwitterionic polysoaps is diminished by added salt due to their "antipolyelectrolyte" character. The sequence to solubilize hydrophobic dyes is often "mid-tail" > "head" > "tail-end" geometry. An extended study on the solubilization ability of hydrophobically modified polybetaines can be found in [232]. The surface activity of the cyclocopolymers containing the pH-responsive hydrophobic monomer *N*,*N*-diallyl-*N*-methylamine and the salt-sensitive sulfobetaine monomer 3-(*N*,*N*-diallyl-*N*-methylammonio) propanesulfonate was utilized to solubilize *p*-cresol within microdomains [233]. Other studies corroborate the general picture [182, 183].

Amphiphilic polybetaines that are end-capped by fluoroalkyl chains and which possess unique properties imparted by the fluorocarbon fragments were developed [234–236]. The polymers of common structure [R_F-**26**-R_F], [R_F-**23a**-R_F], and [R_F-(APDMAE)$_n$-R_F] (where APDMAE is 2-(3-acrylamidopropyldimethylammonio)-ethanoate and R_F is fluorinated hydrocarbons) were shown to exhibit a wide variety of dispersing, aggregate, and emulsion properties. The viscosity of [R_F-(APDMAE)$_n$-R_F] in water consid-

erably increases in comparison with that of [R_F-**23e**-R_F]. The gelation of [R_F-(APDMAE)$_n$-R_F] at a concentration of 10 g L^{-1} is connected with the aggregation of the end-capped fluoroalkyl segments and the strong ionic interactions between the betaine segments. Polymer [R_F-**23e**-R_F] could not form gels in water because of the electrostatic repulsion between the sulfonate units (Scheme 16), but was able to induce gelation in methanol. The reduction in the surface tension of water depends on the length of the fluoroalkyl segments in the polymers. The longer perfluoro-oxyalkylated polymers are more efficient for reducing the surface tension of water than the corresponding polymers with shorter fluoroalkyl chains, or polyAPDMAE without fluorinated end groups.

Whereas the above examples focused on end-capped polybetaines, the other molecular structural extreme is polymers end-capped with betaine groups, which are known, too. The dilute solution and bulk properties of such polymers with zwitterionic end groups were reviewed by Hadjichristidis et al. [237].

Block copolymers of **23b** and alkyl methacrylates [158] and diblock copolymers of **23b** with 2-(diethylamino)ethyl methacrylate (**23b**-DEAEM), 2-(diisopropylamino)ethyl methacrylate (**23b**-DIPAEM), or 2-(*N*-morpholino) ethyl methacrylate (**23b**-MEMA) exhibited reversible pH-, salt-, and temperature-induced micellization in aqueous solution under various conditions. The micelle diameters were 10–46 nm [238]. The micelles of these hydrophobically modified polybetaines consist of coronas from **23b** and cores from polyDEAEM, polyDIPAEM, or polyMEMA. In aqueous solution, the **23b**-MEMA diblock copolymers form micelles with cores of polyMEMA above an upper critical micelle temperature of about 50 °C, and reversibly betainized-DMAEM core micelles below a lower critical micelle temperature of approximately 20 °C [239].

Reversible pH-, salt-, and temperature-induced micellization has been reported for several other block copolymers containing a zwitterionic

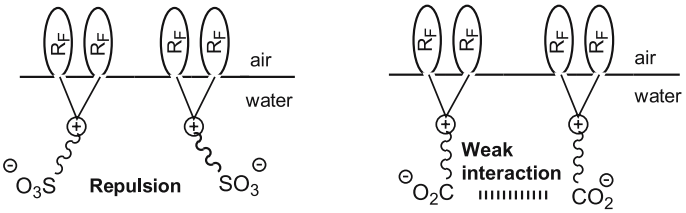

[R_F-(APDAPS)$_n$-R_F] [R_F-(APDMAE)$_n$-R_F]

R_F = $C_3F_7OCF(CF_3)CF_2OCF(CF_3)CF_2OCF(CF_3)$

Scheme 16 Surface arrangement of fluoroalkylated betaine-type polysoaps in aqueous solutions [236]

block [152, 154, 240–242]. In certain cases, multiple switching between complex self-organized structures becomes possible [152, 240–242].

Another parameter suitable for modifying the aggregation behavior of hydrophobically modifed polybetaines is the composition of the solvent used. This is exemplified in Fig. 7, which illustrates the changes of the intrinsic viscosity and of the swelling degree of linear and cross-linked poly3-[(2-carboxy-1-methylethyl)dodecylaminocrotonate] (PCMEDDAC) in water/DMSO mixtures [243]. The insoluble betaine parts of PCMEDDAC tend to aggregate in pure DMSO and form intra- or interchain associates surrounded by a hydrophobic corona. Addition of 10 vol % of water to DMSO considerably increases both the swelling degree and the intrinsic viscosity. A reasonable explanation of this phenomenon may be the unfolding of the macromolecules due to the preferential solvation of the betaine fragments of PCMEDDAC by water, and of the dodecyl chains by the organic solvent. However, a further enrichment of the solvent mixture by water causes the shrinking of the macromolecules, due to reversible micelle formation stabilized by hydrophobic interactions of the long alkyl chains. The insolubility of PCMEDDAC at more than 30 vol % of water is probably connected with a strong compactization of the polymer particles. A hypothetical structure of PCMEDDAC in DMSO, water/DMSO, and water environments is presented in Scheme 17.

The behavior of linear PCMEDDAC in water/DMF mixtures differs from the water/DMSO system. Increased temperatures increase the intrinsic viscosity of PCMEDDAC in DMSO, while they decrease it in DMF. This opposite behavior may be the result of the different solvent qualities with respect to the functional groups of PCMEDDAC.

A particular interest in hydrophobically modified phosphorylcholine polymers is due to the remarkable bio- and hemocompatibility of the surfaces

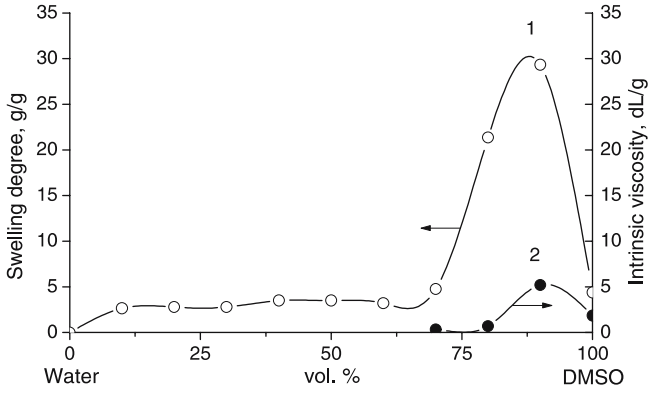

Fig. 7 Dependence of the swelling degree (1) and intrinsic viscosity (2) of PCMEDDAC on water/DMSO mixture [243]

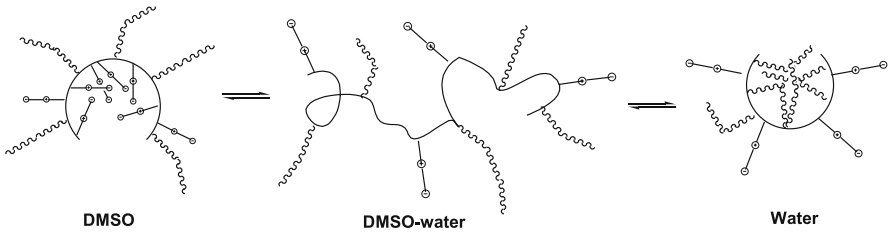

Scheme 17 Hypothetical scheme of the conformation of PCMEDDAC in DMSO, DMSO/water, and water solutions [243]

onto which they are coated. Conformational transitions of phosphorylcholine-based hydrophobically modified polybetaines were studied by ^{1}H NMR spectroscopy in D_2O, CD_3OD, and $CDCl_3$ [149]. The line broadening of the proton signals in D_2O indicates that the motion of the corresponding protons is restricted, providing evidence for the occurrence of hydrophobic microdomains stabilized by the association of the long alkyl chains. The assembly of the polymers in water is triggered by two cumulative effects: (1) hydrophobic interactions between the hydrocarbon chains and (2) ion pair formation between the phosphorylcholine groups. The hydrophobic interactions disappear when the polybetaine is dissolved in CD_3OD, while the solvation of the betaine moieties persists so that no aggregation is observed. In $CDCl_3$, however, inverse micelles are formed in which the core is made of agglomerated phosphorylcholine units and the corona is made of freely moving alkyl chains. In $CD_3OD/CDCl_3$ mixtures, a gradual conformational change from the swollen coil in CD_3OD to the collapsed structure in $CDCl_3$ is observed [244].

The behavior of polymerized phospholipids and analogues is exemplified in the following by the example of the new polyCEACPhos (poly(carboxyethyl 3-aminocrotonate) modified by phosphatidylethanolamine). The FTIR spectra of polyCEACPhos synthesized in bulk, chloroform, and ethanol are similar (Scheme 18) [245, 246].

The potentiometric titration curve of polyCEACPhos shows three bends due to the presence of three ionizing groups, namely OPOH, COOH, and

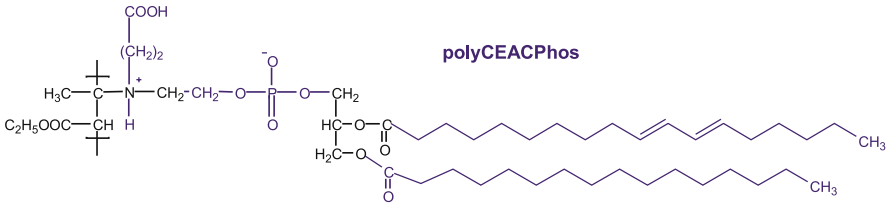

Scheme 18 Derived structure of phosphatidyl-containing poly(carboxyethyl 3-aminocrotonate) [245]

NH^+. The apparent ionization constants (pK_a) of OPOH, COOH, and NH^+ groups found from the Henderson–Hasselbalch equation are 2.57, 4.75, and 7.08, respectively. These values coincide well with the acidic strengths of phosphatidyl, carboxyl, and amine groups. The dependence of the pK_a on the ionization degree (α) plotted for the entire region of the potentiometric titration exhibits a nonmonotonic change of the pK_a (Fig. 8). The values of pK_a increase with α and show a local maximum at $\alpha \approx 0.4$. This is attributed to a change of polyCEACPhos from a compact conformation to an expanded polyelectrolyte-like state. The electrostatic Gibbs energy (G_{el}) that corresponds to the additional work required to remove the protons from the macromolecule was calculated according to the equation: $\Delta G_{el} = 2.303RTA$ (where R is the Boltzmann constant, T is absolute temperature, and A is area of conformational change). The value of $\Delta G_{el} = 45.72$ kJ mol^{-1} found for polyCEACPhos is much higher than that for poly(methacrylic acid) [247] and hydrophobically modified polyelectrolytes of 8.68 kJ mol^{-1} [248]. This is explained by a more stable compact conformation of polyCEACPhos, due to the stabilization of the globular structure by the hydrophobic interactions of the phospholipid fragments, which needs more electrostatic force to undergo the globule-to-coil transition.

The construction of biomembrane systems from polymers containing phosphatidylethanolamine and -choline analogues in the side chains by spreading at the air/water interface and by the Langmuir–Blodgett technique is of great interest [5, 101, 249, 250]. For instance, multilayers of dipalmitoyl-DL-α-phosphatidylethanol methacrylamide polymerized under γ radiation resemble a natural phospholipid structure and show a fine lamellar structure with a periodicity; the average monolayer was estimated to be 32 Å thick [251].

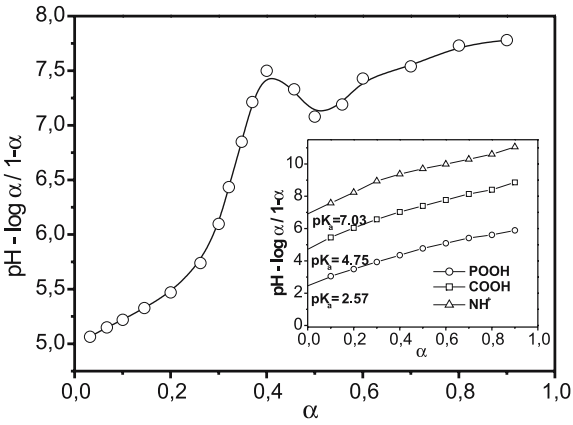

Fig. 8 Conformational transition and pK_a values of functional groups of polyCEACPhos in aqueous solution. [polyCEACPhos] = 1.4×10^{-3} mol L^{-1}, $T = 303$ K [245]

5
Interpolymer, Polymer–Surfactant, and Coordination Complexes of Polybetaines

The formation of interpolyelectrolyte complexes (IPC) of polybetaines with anionic or cationic polyelectrolytes differs in important aspects from the complex formation between two oppositely charged polyelectrolytes. In the latter case, the main driving force is the liberation of the low molar mass counterions, which is not possible for complexes with polybetaines. Also, the composition of the complexes with polybetaines may be nonstoichiometric, in contrast to the usual stoichiometric complexation found for two polyelectrolytes. Characteristic features of IPC formation of polybetaines are exemplified in the following for selected polysulfobetaines, polycarboxybetaines, and polyphosphobetaines.

Osada et al. [252] studied the complexation of **23b** with poly(2-acrylamido-2-methylpropanesulfonic acid) (polyAMPS), quaternized poly*N*-[3-(dimethylamino)propyl]acrylamide chloride (PDMAPAA-Q), and *x*, *y*-ionene bromides ($x = 3, 6$; $y = 3, 4$) in aqueous solution. Depending on the concentration and the mixing ratio of the constituent polymers, water-soluble IPCs were formed which exhibit an UCST, like the parent polybetaine. The UCST decreased markedly when a small amount of the polyanion polyAMPS was added to the solution of **23b**, and eventually disappeared at high concentrations of polyAMPS.

This pronounced change in the UCST indicates a strong interaction between the two polymers. The addition of the polycation PDMAPAA-Q until $R = 0.17$ (where R signifies the molar ratio of polyelectrolyte/polyDMAPS) decreases the UCST first from 65 to 15 °C. The mixtures with the cationic ionenes show a similar evolution of the UCST, but also exhibit a minimum at $R = 0.1$–0.17. Thus, when polycations are added to **23b**, the UCST decreases first, then passes through a minimum and increases again. This was attributed to the different geometrical structure of polyelectrolyte complexes (Scheme 19).

Since the ammonium cations are placed in the middle and the sulfonate anions at the end of the side chain of **23b**, the complex can be solubilized due to free anionic groups of **23b** (Scheme 19a). In contrast, PDMAPAA-Q and ionenes bind to **23b** via the sulfonate groups, which are located at the end of side chain (Scheme 19b and c). The ammonium cations of PDMAPS are thus strongly shielded as hydrophilic solubilizing groups because they are surrounded by two hydrophobic polymer main chains in the complex. Table 3 summarizes the yields and UCSTs of the IPCs resulting from the addition of anionic (PAA, PMAA, NaPSS), cationic (polyDADMAC, PDMAPAA-Q), and nonionic (polyacrylamide, PAAm) polymers to **23b**.

A "cascade"-type complexation with self-propagating association of **23b** was reported when small amounts of *x*, *y*-ionene bromides ($x = 3$ or 6; $y = 3$,

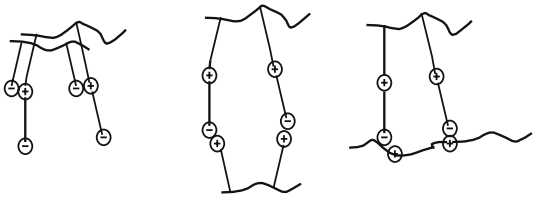

Scheme 19 Polyelectrolyte complexes of polybetaines with anionic (**a**) and cationic (**b**, **c**) polyelectrolytes [252]

Table 3 The yield and UCST of IPCs formed between polyDMAPS and anionic, cationic, and nonionic polymers at $\mu = 0.1$ M NaCl [252]

Polymer type	Polymer name	UCST (°C)	Yield [a] (mol %)
None	PDMAPS	65	—
Polycation	3,3-ionene bromide	26.1	93.1
	PDMAPAA-Q	— [b]	7.9
	PDADMAC	— [b]	11.9
Polyanion	PAMPS	11.6	— [c]
	PAA	11.5	— [c]
	PMAA	11.0	— [c]
	NaPSS	10.7	— [c]
Nonionic polymer	PAAm	11.4	— [c]

[a] Yield is defined as the weight ratio of precipitates to PDMAPS in feed
[b] No UCST was observed until 98 °C
[c] No precipitate was formed at 15 °C

4, 6, 10, or 12) were added [253]. Large amounts of IPCs are formed and precipitate. This behavior, specifically observed for polycations, is attributed to the particular geometry of the IPCs. The addition of some polycation to **23b** provides an overall cationic complex where the positive charges are located in the middle of two polymers (Scheme 20).

This may favor the subsequent complexation with more macromolecules of **23b** due to the suppressed thermal fluctuation and the solvation of the cations, and initiates a cascade reaction until most of the **23b** is consumed. In the case of added polyanions, however, the IPC is overall anionic, but with the negative charges on the surface of the complex. Therefore, the solvation is favored and an association of excess **23b** is unfavorable. The equilibrium at step 1 corresponds to chain initiation, and steps 2 and 3 to chain propagation. The observed phenomenon is useful for the selective separation of charged polymer systems.

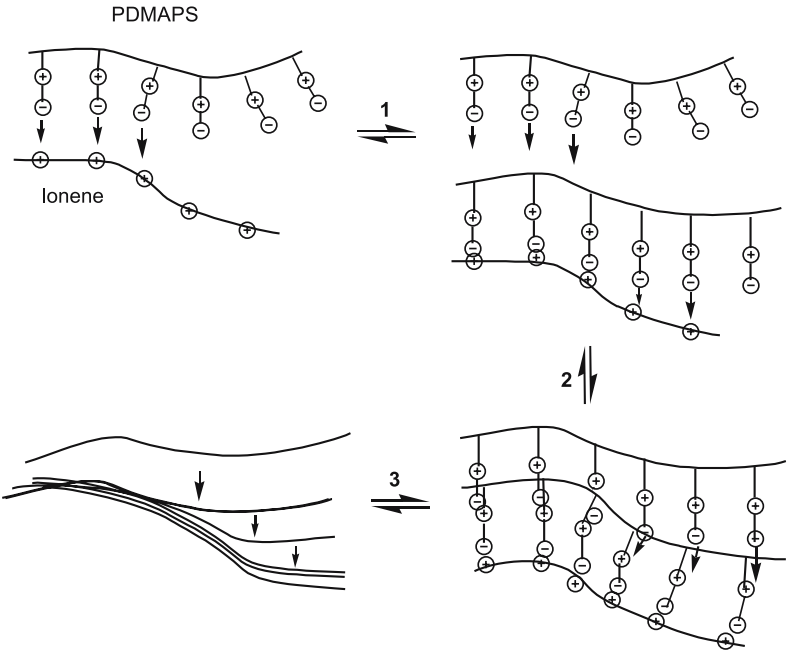

Scheme 20 A "cascade"-type complexation of polyDMAPS and ionene bromide [253]

For IPCs between polycarboxybetaines and negatively charged natural and synthetic polyelectrolytes such as DNA, PMAA, and NaPSS, competition between the intra- and intermacromolecular ion pairing was observed [38]. The weak interaction with DNA and PMAA with polycarboxybetaines was attributed to the formation of stable ion pairs between the carboxylate and quaternary ammonium groups within the repeat units of the polybetaine chains. In contrast, the sulfonate groups of NaPSS bind more strongly to the ammonium groups, thus destroying the internal ion pairs and liberating the carboxylate groups. The titration of 10^{-3} M polycarboxybetaine solution with 10^{-3} M NaPSS may result in soluble as well as insoluble IPCs [36]. The amount of positive charge involved in the IPC formation is pH dependent in the range of pH 1.4–4.0. It is extremely high (53–81%) at pH 1.5 and drastically low (0.7–13%) at pH 4.0. These findings can be interpreted by a competition of intra- and interpolymeric ion-pair associations. At low pH, when the dissociation of the carboxylic groups is suppressed, the polycarbobetaines are positively charged and efficently complexed by the sulfonate groups of NaPSS. But higher pH values provoke the cooperative formation of internal ion pairs between the ammonium and carboxylate groups.

Due to the simultaneous presence of ammonium and carboxylate groups, polycarboxybetaines are able to form interpolymer complexes stabilized by cooperative hydrogen or ionic bonds. Linear and cross-linked poly(carboxy-

ethyl 3-aminocrotonate)s (PCEAC) were involved in the complexation with anionic (PAA, NaPSS) and cationic (polyethyleneimine, poly(hexamethylene guanidine)) polyelectrolytes, as well as the nonionic polymers poly(*N*-vinylpyrrolidone), PEO, and poly(vinyl alcohol) [254]. The composition of the IPCs and some of their characteristics are summarized in Table 4.

IPC formation diminished the high viscosity and swelling degree of linear and cross-linked PCEAC by one to two orders of magnitude. The influence of external factors, such as temperature, pH, ionic strength, and thermodynamic quality of solvent, on the conformation (coil–globule) and volume (swelling–collapsing) transitions of the IPCs was studied [254].

The turbidimetric titration curves of BSA by PCEAC indicate three regions of complex formation [255]. The first region of constant turbidity is due to electrostatic repulsive forces between the oppositely charged protein and PCEAC that retard complex formation. The weak plateau on the curve can be considered as the region of primary or soluble complex formation. In the third region, the sharp increase in turbidity indicates phase separation. Here, pH_c represents the boundary between the nonassociative and primary phases, and pH_ϕ represents the boundary between the primary and aggregate phases. The phase boundaries of the PCEAC–BSA system as a function of pH and ionic strength are presented in Fig. 9. Complex formation takes place in the region between their isoelectric points. An increase of ionic strength leads to a shielding effect of charged groups of both the BSA and PCEAC, and increases both pH_c and pH_ϕ.

Table 4 Some characteristics of IPCs made of linear and cross-linked PCEAC and anionic, cationic, and nonionic polymers in water [254]

PCEAC	Polymer	Composition of IPC (mol/mol)	Intrinsic viscosity (dL/g)	Swelling degree (g/g)
Linear	—	—	14.2	—
	PVP	2 : 1	0.14	—
	PEG	2 : 1	0.13	—
	PVA	2 : 1	—	—
	PAA	1 : 1	—	—
	NaPSS	1 : 1	—	—
	PEI	1 : 1	0.08	—
	PHMG	2 : 1	0.11	—
Cross-linked	—	—	—	115
	PEI	1 : 1	—	8
	PHMG [a]	3 : 1	—	5

[a] PHMG is poly(hexamethylene guanidine)

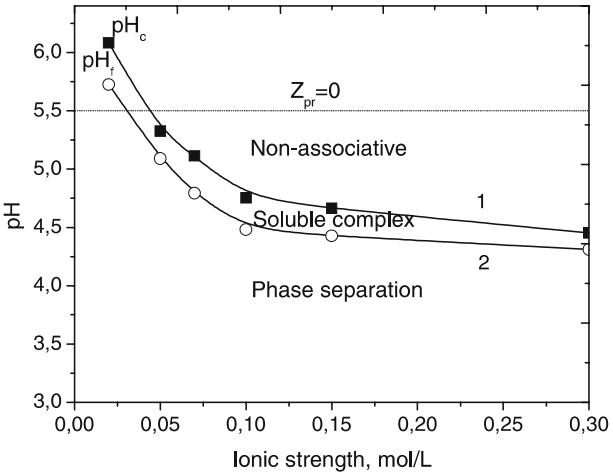

Fig. 9 Phase boundary for BSA/PCEAC. $C_{protein} = 1\ g\ L^{-1}$ [255]

The phase behavior of aqueous two-phase systems containing poly(diallylaminoethanoate-*co*-sulfur dioxide) (PAESD) and PEO is very sensitive to pH and salt concentration [256]. The reason is the dualistic character of PAESD, which can transform to a polyanion with expanded conformation at pH 7.89 and to a polybetaine with a collapsed structure at pH 7.37. At high pH, the mixture of PAESD and PEO is compatible because the hydrodynamic sizes of the two polymers are close. At low pH, however, PAESD and PEO are incompatible due to a large size asymmetry between the two polymers. The addition of salt was found to screen charges and to minimize the influence of pH on their compatibility. The coexistence curve of the PAESD–PEO aqueous two-phase system is described by a semiempirical two-parameter model. The model describes the experimental data accurately, especially when the size asymmetry of the two polymers increases. Further partitioning of two model proteins (BSA and cytochrome c) was studied in an aqueous two-phase system of PAESD and PEO as a function of polymer concentration, salt concentration, and pH [257]. Under all the pH values and salt concentrations investigated, cytochrome c prefers the PAESD-rich (bottom) phase due to its complexation with the protein. For BSA, the best uneven partitioning and separation were obtained at pH 7.89 and in 0.1 M KCl.

Cross-linking of **23b** by ethylene dimethacrylate (EDMA) leads to formation of porous monolithic sulfobetaine polymers [258]. Alternatively, grafting of the internal surfaces of porous poly(trimethylpropane trimethacrylate) (polyTRIM) by DMAPS provides grafted monoliths. Both synthesis routes yielded polymers capable of interacting reversibly with proteins in aqueous solutions. The SEM pictures show the copolymerized monolith poly(DMAPS-*co*-EDMA) comprised of spherical units with average diameter approximately

1.5–2 μm agglomerated into larger clusters transected by a large pore size. Such a structure allows liquids to be forced through the monolith sorbent without compression of the particles using flow rates suitable for chromatographic purposes. Indeed, poly(DMAPS-*co*-EDMA) monoliths adsorbed the basic proteins lysozyme, chymotrypsinogen A, and cytochrome c when loaded from pure water, whereas acidic and neutral proteins eluted in the void volume. It is reasonable to assume that the terminal sulfobetaine moieties interact electrostatically with the net cationic charges of basic proteins, because their elution is achieved by increasing the ionic strength according to the Hofmeister lyotropic series ($SCN^- > I^- > Br^- > Cl^-$). Perchlorate ions strengthened substantially the interactive forces between the proteins and the poly(DMAPS-*co*-EDMA) monoliths. The role of hydrophobic interactions in stabilizing polybetaine–protein complexes was tested using a strong promotor for hydrophobic interaction (2 M ammonium sulfate buffer, pH 7) as eluent. None of the model proteins was adsorbed on the monoliths. Thus, hydrophobic interactions were only minor for the interaction behavior of the sulfobetaine-based monoliths.

Interestingly, the interaction of polybetaines with many polyelectrolytes is strong enough and/or sufficiently kinetically favored to give nonstoichiometric complexes at interfaces, and thus to enable the formation of polyelectrolyte multilayers via the layer-by-layer technique [259, 260]. Such unusual variations of the layer-by-layer growth of ultrathin coatings are potentially useful for analyzing proteins, or for producing nonlinear optical coatings [261, 262]. The membranes of terpolymers having 2-methacryloyloxyethyl phosphorylcholine (MPC), methacryloyl or acryloyl poly(oxyethylene) macromonomers, and *n*-butyl methacrylate (BMA) were found to complex with BSA [263].

Low charge density, hydrophobically modified polybetaines were shown to interact and comicellize with nonionic, anionic, cationic, and amphoteric surfactants [181–183] and many ionic organic dyes [264, 265]. The association mechanism of hydrophobically modified polymers and surfactants in dependence on the concentration of interacting components can be modeled by two pathways (Scheme 21) [183].

The first pathway is the formation of mixed micelles or hemimicelles, composed of polymer-bound hydrophobes comicellized with surfactant molecules. Intermolecular physical cross-links often enhance the viscosity of the micellar solutions. The second pathway is intramolecular comicellization so that the hydrodynamic size of the associates contracts.

The addition of surfactants increases the viscosity much more for low charge density polybetaines than for high charge density polybetaines [183]. The addition of the anionic surfactant sodium dodecyl sulfate (SDS) produced the largest increase in solution viscosity for low charge density polybetaines, while the cationic *N*-dodecyl-*N*,*N*,*N*-trimethylammonium bromide, the zwitterionic *N*-dodecyl-*N*,*N*-dimethylammonio-1-propanesulfonate, and

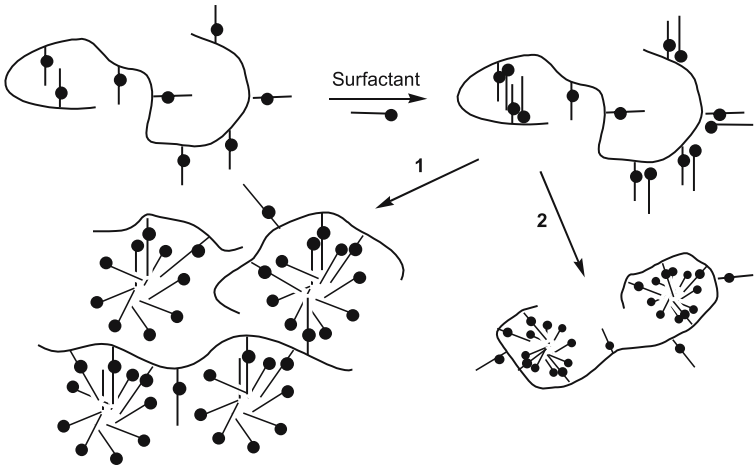

Scheme 21 Formation of hydrophobically modified polybetaine–surfactant complexes [182]

the nonionic Triton X-100 surfactants were less efficient. In most cases, high charge density polycarbobetaines exhibited diminished solution viscosity upon addition of surfactants.

The interaction between a phosphorylcholine-based polybetaine (equimolar copolymer PNIPA-PC of *N*-isopropylacrylamide and *N*-phosphorylcholine-*N*′-ethylenedioxybis(ethyl)acrylamide) and anionic, cationic, amphoteric, and neutral surfactants was studied by a fluorescence probe, isothermal titration calorimetry, and ^{1}H NMR spectroscopy [266]. The main results obtained in this study can be summarized as follows. The charge of the surfactant headgroup is the major determinant that controls the interactions. Only anionic surfactants associate with PNIPA-PC. For such associating systems, the surfactant concentrations at which binding first takes place are much lower than the respective critical micelle concentrations of the surfactants. The association between PNIPA-PC and the anionic surfactants occurs first via the electrostatic attraction between the surfactant headgroups and the polymer-bound ammonium groups. None of the mixed systems investigated underwent macroscopic phase separation, as the neutral comonomer (NIPAM) may act as solubilizing agent.

It is interesting to compare the behavior of polyelectrolyte–surfactant, polyampholyte–surfactant, and polybetaine–surfactant complexes. Addition of ionic surfactants to solutions of oppositely charged polyelectrolytes results in the precipitation of polyelectrolyte–surfactant complexes even at low polymer concentration. While partially charged polyampholytes are often insoluble in water, the association with either anionic or cationic surfactants results in solubilization due to the neutralization of one type of charge. The remaining nonneutralized charges confer polyelectrolyte character to the polyampholyte, ensuring its solubility. The addition of anionic or cationic surfactants

to polybetaines results in soluble polybetaine–surfactant complexes, converting the whole macromolecule either to a polycation or to a polyanion.

The interaction of low molar mass salts with polybetaines differs from the behavior of polyelectrolytes in that both low molar mass ions of the added salt may bind to the polymer [46, 47, 178, 267]. Typically, the intensity of interaction follows the well-known Hofmeister lyotropic series. This can be exploited for separation purposes. In particular, polycarboxybetaines containing acidic and basic groups are able to bind metal ions efficiently via their multidentate character. For example, poly(*N*-propylene glycine) (PPG), poly(1-isopropylcarboxylethyleneimine) (PIPCEI), and poly(ethylene alanine) (PEA) form five-membered chelate cycles [268]. The stability of polyampholyte–metal complexes with respect to bivalent ions decreases as $Zn^{2+} > Ni^{2+} > Cd^{2+} > Co^{2+} > Pb^{2+} > Fe^{2+} > Ca^{2+} > Mg^{2+}$ and coincides well with the stability constants of their complexes with EDTA. In another example, the binding ability of poly(carboxyethyl 3-aminocrotonate) modified by ethanolamine (PCEAC-Ea), glycine (PCEAC-Gly), β-alanine (PCEAC-Ala), and lysine (PCEAC-Lys) was studied with respect to various metal ions [269–275] (Table 5).

The polymer–metal complexes stabilized by the formation of intra- or intermacromolecular ionic and coordination bonds were precipitated. The adsorption capacity of linear polybetaines decreases with PCEAC-Gly > PCEAC-Ala > PCEAC-Lys, and depends on the metal cation to be bound with the following orders:

PCEAC-Gly:

$$Cd(II) > Cr(III) > Ga(III) > Cu(II) > Fe(III) \approx Ni(II) > Co(II) > Al(III)$$

PCEAC-Ala:

$$Cd(II) > Cr(III) > Ga(III) > Cu(II) > Co(II) > Fe(III) > Ni(II) > Al(III)$$

PCEAC-Lys:

$$Ga(III) > Cd(II) > Cu(II) > Cr(III) > Fe(III) > Co(II) > Ni(II) > Al(III)$$

Accordingly, the detailed polymer and betaine structures are important for the strength of the complexation. The high adsorption capacity of PCEAC-Gly and PCEAC-Ea in comparison with that of the parent PCEAC is probably due to the additional chelating groups such as OH and COOH that can form very stable mixed five- and six-membered cyclic structures with metal ions (Scheme 22).

The sorption of metal ions by betaine hydrogels is accompanied by gel contraction. At first, a thin colored layer is formed on the gel surface. Then the colored zone gradually moves into the gel interior. The driving force of this process is “ion-hopping transportation” of metal ions through intra- and intermolecular chelate formation, e.g., constant migration of metal ions deep into the gel volume by exchange of free ligand vacancies. In min-

Table 5 Metal ion binding capacity of linear PCEAC-Gly, PCEAC-Ala, and PCEAC-Lys [275]

Linear polybetaine	Amount of metal ion (mg) adsorbed by 1 g of linear polymer							
	Al(III)	Cd(II)	Co(II)	Cr(III)	Cu(II)	Fe(III)	Ga(III)	Ni(II)
PCEAC-Gly	153	984	345	791	600	373	726	366
PCEAC-Ala	164	1007	408	732	560	400	711	391
PCEAC-Lys	126	609	345	465	475	385	633	293

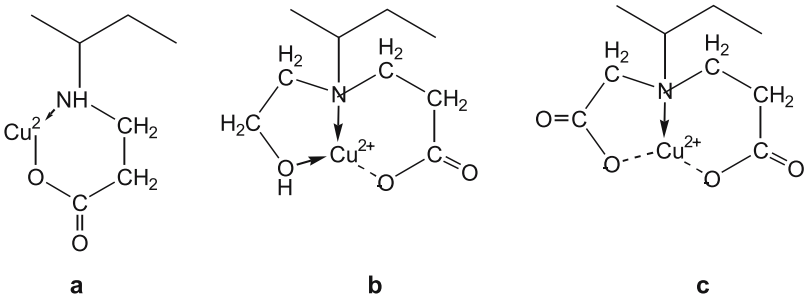

a b c

Scheme 22 Chelate complexes of Cu(II) with PCEAC (**a**), PCEAC-Ea (**b**), and PCEAC-Gly (**c**) [275]

eral acids, metal ions are replaced by protons and desorption of the metal ions takes place. Regeneration of the gel samples occurs in fresh water, e.g., the gel samples gradually return to the initial state. These experiments clearly demonstrate the ability of gel samples to adsorb and desorb metal ions several times. They imply the potential application of water-soluble and water-swelling polybetaines for purification of wastewater from metal ion contaminants.

6 Application of Polybetaines

Polybetaines are specialty polymers. Accordingly, they are typically discussed for high added value applications, or in cases where no satisfactory alternative materials exist. The application fields of polybetaines comprise, for instance, the oil industry, hydrometallurgy, biotechnology, medicine, and catalysis.

The drag reduction behavior was examined for poly3-[(2-acrylamido-2-methylpropyl)dimethylammonio]-1-propanesulfonate (AMPDAPS) [276]. In this study, the polybetaine excelled by having good long-term stability. The drag reduction properties of polyAMPDAPS and PEO in 0.5 M NaCl are compared in Fig. 10. PolyAMPDAPS retains approximately 60% of its initial level

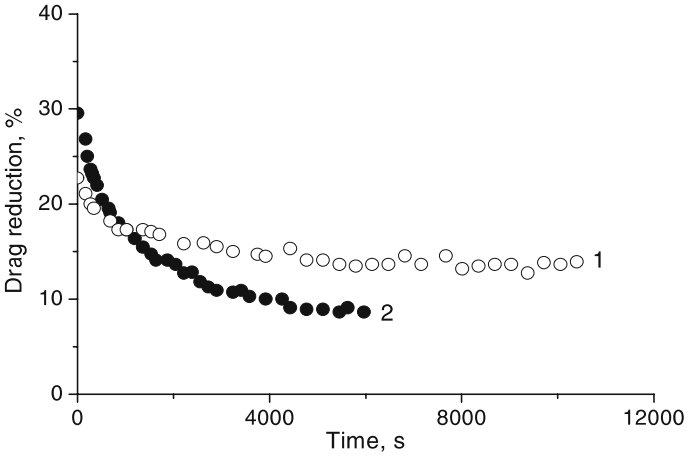

Fig. 10 Drag reduction profile for 3-ppm solutions of polymer of AMPDAPS (1) and PEO (2) in 0.5 M NaCl at $T_w = 1122$ dyne cm^{-2} in the rotating-disk rheometer [276]

of drag reduction after 100 min at 1000 rpm in the rotating disk. PEO retains only 28.5% of its initial drag reduction under similar conditions.

The most widely used synthetic and natural enhanced oil recovery polymers, such as partially hydrolyzed polyacrylamide, carboxymethyl(ethyl) cellulose, polysaccharides, or xanthan gums, are not suitable for high-temperature reservoirs (> 90 °C) with high-density brine fluid due to excessive hydrolysis and precipitation [277]. The main advantages of polymeric betaines over the mentioned standard polymers are: (1) thermostability (up to 120 °C); (2) brine compatibility; and (3) viscosification in brine solution [278]. Carbobetaines grafted onto hydroxyethyl cellulose were tested as a drilling-mud additive for clay hydration inhibition and mud rheological control [279]. An increase in the content of carbobetaine moieties resulted in an enhanced inhibitive ability, especially for saline mud.

Polybetaine gels were used for the separation of water and oil from water-in-oil emulsions [280]. These gels destructed water-in-oil emulsions by absorbing water, which was subsequently released under an externally imposed DC electric field that made the swollen gel shrink. The invention [281] concerns an improved process for stabilizing asphalt in a water emulsion using certain polybetaine surfactants as an asphalt emulsifier.

A hydrophobically modified polybetaine proved to be an efficient pour point depressant (PPD), to inhibit the deposition of wax, and to improve the viscosity of waxy crude oil from the Kumkol–Akshabulak oil field (western Kazakhstan) [282]. The inhibition of wax deposits in the presence of the hydrophobic polybetaine was interpreted in terms of its interference with the wax crystallization process, due to the formation of inverse micellar structures. While the zwitterionic parts on the polymer backbone stabilize the

Table 6 The pour point and kinematic viscosity of a Kumkol–Akshabulak oil mixture [282]

PCMEDDAC, 100 ppm	Kinematic viscosity (cSt)					Pour point (°C)
	20 °C	30 °C	40 °C	50 °C	60 °C	
Crude oil without depressant	9.87	5.43	4.07	3.22	2.76	15
Preheated oil without added depressant	9.40	5.68	4.21	3.33	2.76	6
Depressant prepared in DMF	7.44	5.81	4.42	3.46	2.91	0
Depressant prepared in *o*-xylene	7.21	5.56	4.33	3.10	2.80	3
Depressant prepared in *n*-hexane	7.37	5.60	4.36	3.13	2.89	– 3

small size of the aggregates, the hydrophobic side chains of the polymer provide nucleation sites and cocrystallize with the paraffins, thus modifying the paraffin crystal structure. The PPD effectiveness of poly3-[(2-carboxy-1-methylethyl)dodecylaminocrotonate] (PCMEDDAC) is shown in Table 6 for a Kumkol–Akshabulak oil mixture (89 : 11 wt %).

The best activity was observed for PCMEDDAC dissolved in *n*-hexane. Initial waxy crude oil behaves like a viscoplastic fluid. Doped by PCMEDDAC, waxy oil approaches a Newtonian liquid, and the shear stress decreases considerably due to the modification of the paraffin crystals by the hydrophobized macromolecules. In oily environments, PCMEDDAC forms micelles consisting of a hydrophilic core (made of the betaine groups) and a hydrophobic corona (made of the dodecyl groups). The PPD mechanism of PCMEDDAC with respect to waxy crude oil suggests the adsorption of definite fractions of paraffin molecules on the surface of micelles and further retardation of agglomeration.

The antipolyelectrolyte effect of polymeric betaines in saline media is used to thicken, retain saline water, or stabilize electrolyte-containing aqueous media. Polybetaines were applied to absorbing aqueous electrolyte solution [283], as viscosifying agents [284] for aqueous solutions within a wide salinity and temperature range, and as modifying agents for the surfaces of particles in aqueous suspensions.

The recovery of transition metal ions and organic impurities by both water-soluble and water-swelling polybetaines is especially important for hydrometallurgy processes and environmental protection [285]. The formation of five- or six-membered chelate "bridges", where transition metal ions bind to at least two monomeric units, is specific for polycarboxybetaines [286, 287]. Figure 11 shows the ability of PCEPAC hydrogels to absorb and desorb copper(II) ions [40, 269–275]. Adsorption of copper(II) ions starts from the gel surface, then the shell layer gradually moves into the gel interior. Desorption of copper(II) ions from the gel interior takes place in the medium of mineral acid due to destruction of ligand–metal complexes and replacement

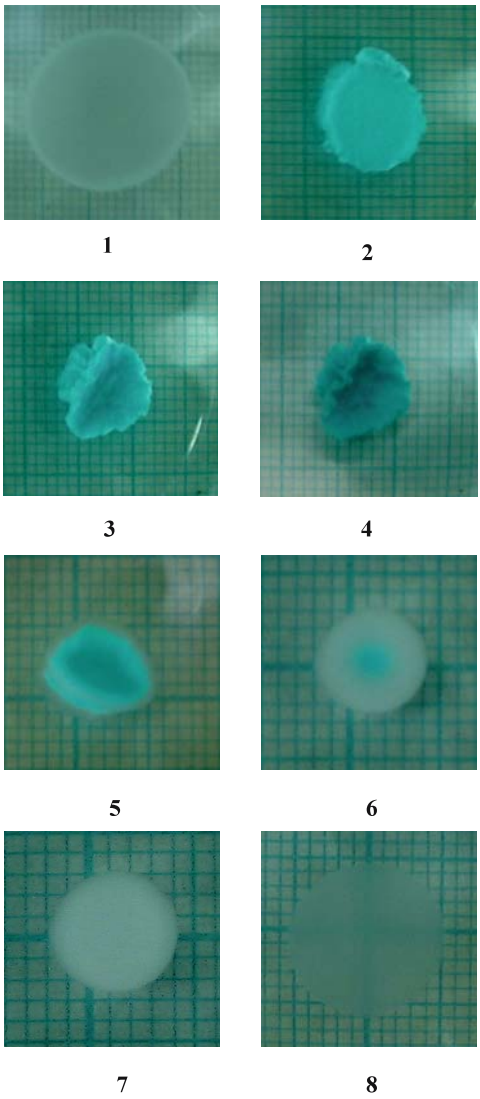

Fig. 11 Adsorption (1–4) and desorption (5–7) of copper(II) ions by a PCEPAC gel, and washing of the gel by water (8) as a function of time. Initial state (1), after 30 min (2), 1 h (3), 7 h (4), 3 min (5), 15 min (6), 1 h (7), 2 days (8) [273]

of metal ions by protons. According to UV/Vis measurements, up to 90% of copper(II) ions are released from the gel volume over 2 h. Regeneration of the gel sample can be realized in fresh water. As seen from Fig. 11, the gel sample gradually returns to its initial state after 2 days. Adsorption and desorption of copper(II) ions followed by gel regeneration were repeated ten times without the loss of gel capacity, durability, and reusability. Thus, the ad-

vantages of polycarbobetaine-type gels over others are: (1) high adsorption capacity (1 g of dry gel adsorbs up to 500 mg of copper(II) ions); (2) easy and fast desorption of metal ions by mineral acid (for instance, by 0.1 M HCl); (3) durability of the hydrogel materials (ten times repeatable use of the adsorbent); and (4) good mechanical stability (preservation of gel shape without cracks). Therefore, one can conclude that betaine-type hydrogels are attractive materials for the removal and recovery of metal ions from wastewater.

Among the various protein analysis and purification techniques, isoelectric focusing and chromatofocusing are the main tools for separating and purifying proteins for analytical and preparative purposes. However, the main disadvantage of these methods is that they use expensive polyampholyte buffers (a mixture of hundreds or thousands of low molecular weight amphoteric molecules) to generate linear or quasi-linear pH gradients and high applied voltage (up to 200 V/cm). Moreover, amphoteric buffers tend to associate with proteins and often yield irreproducible gradient shapes. A new approach [288–290] was developed for the electrophoretic resolution of proteins, which combines both the gel matrix and carrier ampholytes in one and the same sample, as in polycarbobetaine gels (Fig. 12).

In practice, the aqueous solution of proteins to be separated is injected by a syringe into the central section of the polyampholyte gel specimen. Then, the DC electric field is switched on, which induces the formation of a linear pH gradient along the gel sample. In its turn, the generated pH gradient promotes the migration of protein molecules until they are gradually localized at their isoelectric pH. Protein molecules will be separated and concentrated if the isoelectric pH of the proteins coincides with appropriate pH zones of the amphoteric gel.

Polybetaine-based materials [291] and polybetaines grafted (or adsorbed) onto an inorganic particle surface are applicable as a stationary phase for ion chromatography [292]. The separation capability of poly[3-diethyl(methylmethacryloylethyl)ammonium propanesulfonate] (polyDMAPS) grafted to silica gel and physically adsorbed onto silica gel was compared with respect

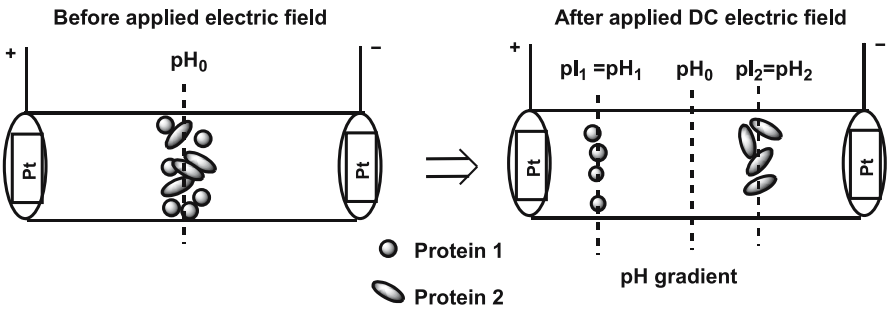

Fig. 12 Resolution of protein mixtures with the help of carbobetaine gels [288]

to various anions. The columns packed with polyDMAPS-grafted silica gel were able to separate Ce^{4+}, Li^{+}, Ca^{2+}, and Mg^{2+}. Moreover, the polyDMAPS-grafted silica gel has better durability than that of the physically immobilized polybetaine.

Polyetherurethanes end-capped with zwitterions of sulfobetaine via a hexamethylene diisocyanate spacer were found to show good blood compatibility [293]. Phospholipid-based polymers can serve as coatings for blood contact devices, drug carriers [294], and bioconjugates [295] due to their excellent biocompatibility, or as templates for the structure-directed synthesis of organic polymers [296]. The controlled permeation and release of drugs from polybetaine-coated implants provides a new approach to treating device-based infection, tumors, and stent restenosis [294].

The enzymatic activity profiles of the native papain and polybetaine-conjugated papain at 40 °C were compared [295]. The enzymatic activity of the native enzyme decreases continuously with the storage period, while papain maintains 50% of the initial enzymatic activity when conjugated with polybetaine. Enrichment of the polybetaine chain by hydrophobic monomers such as butyl methacrylate maintains the enzymatic activity of papain for 28 days. DMAEM-MPC diblock copolymers exhibit a stabilization effect with respect to DNA and can serve as a synthetic vector for gene delivery [297]. Highly condensed, sterically stabilized DMAEM-MPC/DNA complexes of 120–140-nm diameter or partly condensed with "spaghetti" structures are formed which prevent promiscuous interactions with tissues in the body. They potentially allow for the cell-specific delivery of the condensates following the attachment of a targeting ligand.

Fluoroalkylated end-capped 2-(3-acrylamidopropyldimethylammonio)-ethanoate (APDMAE) polymers (R_F-(APDMAE)$_n$-R_F) were found [235] to exhibit high antibacterial activity against *Staphylococcus aureus* or *Penicillium aeruginosa*. It is suggested that the cationic moieties in the betaine segments of the fluorinated APDMAE polymers are able to interact tightly with the negatively charged bacterial cell. In particular, the longer perfluorooxyalkylated APDMAE polymer was more active against both *S. aureus* and *P. aeruginosa* (below 10^3 colony-forming unit levels).

Several authors [298–300] reported on the preparation of platinum and palladium nanoparticles having a preferential diameter from about 1 to 2 nm stabilized by polymeric carbo-, phospho-, and sulfobetaines for fuel-cell catalysts and vinyl acetate production.

7 Concluding Remarks

The synthetic strategy, solution properties, complexation ability, and application aspects of polymeric carbo-, sulfo-, and phosphobetaines are outlined in

this review. The advantages and disadvantages of direct polymerization of the zwitterionic monomers and betainization of polymeric precursors are discussed. The newly developed controlled radical polymerization (CRP) of both the zwitterionic and the reactive precursor monomers in organic solvents, bulk, and aqueous media has become a powerful tool to obtain polybetaines with narrow polydispersities and defined end groups, as well as copolymers containing betaine blocks. The narrow molecular weight distribution of betaine polymers prepared by CRP supports the precision of any physical or physicochemical characteristics in solution and in the condensed and gel states. Atom transfer radical polymerization (ATRP), and particularly the reversible addition fragmentation transfer (RAFT) method, are promising routes to overcome certain shortcomings in the polymerization of zwitterionic monomers. A novel approach to designing zwitterionic polysoaps has been developed most recently.

The existence of intragroup, intrachain, and interchain interactions of the positive and negative charges in dependence on the length and flexibility of spacer between opposite charges determines the solubility, ionization ability, phase, volume, and conformational state of polymeric betaines in aqueous and saline media. The solubility of polybetaines in salt-containing solutions can satisfactorily be described by the charge/radius ratio, Hofmeister series, and Pearson theory. Transformation of zwitterionic species to anionic, cationic, and molecular forms can be determined by micro- and macroscopic ionization constants. The antipolyelectrolyte character comprising chain expansion upon addition of neutral salts is specific for polybetaines. Hydrophobically modified polybetaines exhibit reversible pH-, salt-, solvent-, and temperature-induced micellization and conformational transition from the coil (collapsed) to expanded (swollen) structure. The conformational and phase (or volume) transitions of linear and cross-linked polybetaines in response to pH, ionic strength, temperature, solvent nature, etc. expands our knowledge on the universality of synthetic and natural systems.

Interpolymer, polymer–surfactant, and coordination complexes of polybetaines are less developed. The "cascade"-type complexation observed for the polybetaine–polyelectrolyte system is similar to the "layer-by-layer" deposition found for oppositely charged polyelectrolytes. The behavior of the polybetaine–surfactant system differs from that of polyelectrolyte–surfactant and polyampholyte–surfactant complexes, leading to inter- or intramolecular comicellization or converting the whole macromolecule to either a polycation or polyanion.

The accumulated knowledge on synthesis–structure–property relationships can be exploited for technological purposes. Polymeric betaines are finding increased use in separation and enrichment technologies through combined adsorption, chelating, and ion-exchange processes. The antipolyelectrolyte effect can be applied to drag reduction, enhanced oil recovery, and desalination. Formation of a pH gradient within a monolithic betaine

gel, stimulated by an externally imposed DC electric field, may provide an alternative protein separation and purification principle.

Acknowledgements Financial support from INTAS-00/57, INTAS-00/113, and INTAS-Aral 1033 grants is greatly acknowledged.

References

1. Salamone JC, Rice WC (1998) Polyampholytes. In: Mark FH, Bikales NM, Overberger CG, Menges G (eds) Encyclopedia of polymer science and engineering, vol 11. Wiley, New York, p 514
2. Galin J-C (1996) Polyzwitterions. In: Salamone JC (ed) Polymeric materials encyclopedia, vol 9. CRC, Boca Raton, p 7189
3. Kudaibergenov SE (2002) Polyampholytes: synthesis, characterization, and application. Kluwer, New York
4. Lowe AB, McCormick CL (2002) Chem Rev 102:4177
5. Nakaya T, Li YL (1999) Prog Polym Sci 24:143
6. Matyjaszewski K (ed) (2000) Controlled/living radical polymerization. ACS Symp Ser 786. The American Chemical Society, Washington, DC
7. Matyjaszewski K, Davies TP (eds) (2002) Handbook of radical polymerization. Wiley, Hoboken
8. Qiu J, Charleux B, Matyjaszewski K (2001) Prog Polym Sci 26:2083
9. Cunningham MF (2002) Prog Polym Sci 27:1039
10. Topchiev DA, Mkrtchyan LA, Simonyan RA, Lachinov MB, Kabanov VA (1977) Polym Sci USSR 19:580
11. Kathman EE, White LA, McCormick CL (1997) Polymer 38:879
12. Kathman EE, White LA, McCormick CL (1997) Polymer 38:871
13. Kathman EE, McCormick CL (1997) J Polym Sci A 35:243
14. Butler GB (1992) Cyclopolymerization and cyclocopolymerization. Marcel Dekker, New York, p 51
15. Dautzenberg H, Jaeger W, Kötz J, Philipp B, Seidel C, Stscherbina D (1994) Polyelectrolytes—formation, characterization, application. Hanser, Munich, p 20
16. Favresse P, Laschewsky A (2001) Polymer 42:2755
17. Favresse P, Laschewsky A (1999) Macromol Chem Phys 200:887
18. Ali SA, Rasheed A, Wazeer MIM (1999) Polymer 40:2439
19. Ali SA, Aal-e-Ali (2001) Polymer 42:7961
20. Ali SA, Saeed MT (2001) Polymer 42:2785
21. Ali MM, Perzanowski HP, Ali SA (2000) Polymer 41:5591
22. Thomas DB, Vasilieva YA, Armentrout RS, McCormick CL (2003) Macromolecules 36:9710
23. Avci D, Mathias LJ (1999) J Polym Sci A 37:901
24. Avci D, Lemopulo K, Mathias LJ (2001) J Polym Sci A 39:640
25. Cardoso J, Gonzales L, Huanosta A, Manero O (1997) Polymer 38:4513
26. Liaw D, Huang C, Lee W, Borbely J, Kang E (1997) J Polym Sci A 35:3527
27. Niu A, Liaw D, Sang H, Wu C (2000) Macromolecules 33:3492
28. Bonte N, Laschewsky A (1996) Polymer 37:2011
29. Wielema TA, Engberts JBFN (1990) Eur Polym J 26:415
30. Barboiu V, Holerca MN, Streba E, Luca C (1996) J Polym Sci A 34:261
31. Barboiu V, Streba E, Luca C, Radu I, Grigoriu GE (1998) J Polym Sci A 36:1615

32. Bohrisch J, Wendler U, Jaeger W (1997) Macromol Rapid Commun 18:975
33. Wendler U, Bohrisch J, Jaeger W, Rother G, Dautzenberg H (1998) Macromol Rapid Commun 19:185
34. Jaeger W, Wendler U, Lieske A, Bohrisch J (1999) Langmuir 15:4026
35. Bohrisch J, Schimmel T, Engelhard H, Jaeger W (2002) Macromolecules 35:4143
36. Bohrisch J, Grosche O, Wendler U, Jaeger W, Engelhard H (2000) Macromol Chem Phys 201:447
37. Grosche O, Bohrisch J, Wendler U, Jaeger W, Engelhard H (2000) J Chromatogr A 894:105
38. Izumrudov VA, Zelikin AN, Jaeger W, Bohrisch J (2003) J Phys Chem B 107:7982
39. Didukh AG, Koizhaiganova RB, Khamitzhanova G, Bimendina LA, Kudaibergenov SE (2003) Polym Int 52:883
40. Koizhaiganova RB, Kudaibergenov SE, Geckeler KE (2002) Macromol Rapid Commun 23:1041
41. Hahn M, Jaeger W, Schmolke R, Behnisch J (1990) Acta Polym 41:107
42. Jaeger W, Hahn M, Lieske A, Zimmermann A (1996) Macromol Symp 111:95
43. Thünemann AF, Sander K, Jaeger W, Dimova R (2002) Langmuir 18:5099
44. Rullens F, Devillers M, Laschewsky A (2004) Macromol Chem Phys 205:1155
45. Rullens F, Devillers M, Laschewsky A (2004) J Mater Chem 14:3421
46. Rullens F, Delingue N, Laschewsky A, Devillers M (2005) J Mater Chem 15:1668
47. Ali SA, Rasheed A (1999) Polymer 40:6849
48. Lee W, Chen Y (2001) J Appl Polym Sci 80:1619
49. Lee W, Chen Y (2003) J Appl Polym Sci 89:2261
50. Luca C, Mihailescu S, Popa M (2002) Eur Polym J 38:1501
51. Kathman EE, McCormick CL (1997) J Polym Sci A 35:231
52. Favresse P, Laschewsky A, Emmermann C, Gros L, Linsner A (2001) Eur Polym J 37:877
53. Ali SK, Mazumder MAJ, Al-Muallem HA (2003) J Polym Sci A 41:172
54. Kaladas JJ, Kastrup R, Schulz DN (1998) Polymer Prepr 39:619
55. Mazumder MAJ, Umar Y, Ali Sk (2004) Polymer 45:125
56. Armentrout RS, McCormick CL (2000) Macromolecules 33:419
57. Liaw DJ, Liu JR, Chung KC (1993) J Macromol Sci A 30:51
58. Lee WF, Tsai CC (1995) J Appl Polym Sci 58:1423
59. Wang H, Hirano T, Seno M, Sato T (2003) Eur Polym J 39:2107
60. Lee WF, Tsai CC (1994) Polymer 35:2210
61. Liaw DJ, Huang CC (2002) Macromol Symp 179:209
62. Kato T, Takahashi A (1996) Ber Bunsen Phys Chem 100:784
63. Kato T, Kawaguchi M, Takahashi A (1999) Langmuir 15:4302
64. Georgiev G, Tzoneva A, Lyukov L, Iliev S, Kamenova I, Georgieva V, Kamenska E, Bund A (2004) Macromol Symp 210:393
65. Knoesel R, Galin JC (1997) Polymer 38:135
66. Cardoso J, Manrique R, Albores-Velasco M, Huanosta A (1997) J Polym Sci B 35:479
67. Cardoso J, Montiel R, Huanosta-Tera A (2005) J Polym Sci B 43:1152
68. Liaw DJ, Huang CC (2000) Macromol Chem Phys 201:1101
69. Liaw DJ, Huang CC, Sang HC, Kang ET (2001) Polymer 42:209
70. Lee WF, Lee CH (1997) Polymer 38:971
71. Buchweitz K (2000) Thesis, Technische Universität Berlin (Germany); Buchweitz K, Hahn M, Jaeger W, in preparation
72. Lee WF, Chen YM (2004) J Appl Polym Sci 91:726
73. Grassi B, Galin JC (1995) Macromolecules 28:7036

74. Grassi B, Meurer B, Scheer M, Galin JC (1997) Macromolecules 30:236
75. Lee WF, Chen CF, Yen SH (2001) J Appl Polym Sci 82:3447
76. Ali SA, Al-Muallem HA, Mazumder MAJ (2003) Polymer 44:1671
77. Chenthamarakshan CR, Ajayaghosh A (1998) Chem Mater 10:1657
78. Galin M, Galin JC (1997) Macromol Chem Phys 198:1021
79. Blom HP, Gauthier M, Li K, Nielsen KE (1998) J Appl Polym Sci 70:227
80. Gauthier M, Carrozzella T, Penlidis A (2002) J Polym Sci A 40:511
81. Berlinova IV, Dimitrov IV, Kalinova RG, Vladimirov NG (2000) Polymer 41:831
82. Nedelcheva AN, Novakov CP, Miloshev SM, Berlinova IV (2005) Polymer 46:2059
83. Liaw DJ, Huang CC, Sang HC, Wu PL (2000) Polymer 41:6123
84. Lee WF, Huang GY (1996) Polymer 37:4389
85. Liaw DJ, Huang CC, Kang ET (1997) Colloid Polym Sci 275:929
86. Kathman EE, White LA, McCormick CL (1997) Macromolecules 30:5297
87. Zhang LM, Chen LQ (2002) J Appl Polym Sci 83:2755
88. Hu ZH, Zhang LM (2002) J Macromol Sci Pure Appl Chem A 39:419
89. Xue W, Champ S, Huglin MB (2001) Eur Polym J 37:869
90. Lee WF, Chiu RJ (2002) J Appl Polym Sci 86:1592
91. Lee WF, Yeh PL (2000) J Appl Polym Sci 77:14
92. Lee WF, Yeh PL (1999) J Appl Polym Sci 74:2170
93. Lee WF, Chen CF (1998) J Appl Polym Sci 69:2021
94. Lee WF, Yeh PL (1997) J Appl Polym Sci 66:499
95. Lee WF, Tu YM (1999) J Appl Polym Sci 72:1221
96. Liu YX, Kang ET, Neoh KG, Tan KL, Huang CC, Liaw DJ (1999) J Appl Polym Sci 74:816
97. Kang ET, Shi JL, Neoh KG, Tan KL, Liaw DJ (1998) J Polym Sci A 36:3107
98. Arasawa H, Odawara C, Yokoyama R, Saitoh H, Yamauchi T, Tsubokawa N (2004) React Funct Polym 61:153
99. Yuan Y, Zang X, Ai F, Zhou J, Shen J, Liu S (2004) Polym Int 53:121
100. Heinz BS, Laschewsky A, Rekai ED, Wischerhoff E, Zacher T (2001) In: McCormick CL (ed) Stimuli-responsive water-soluble and amphiphilic polymers, ACS Symp Ser, vol 780. The American Chemical Society, Washington, DC
101. Armitage BA, Bennett DE, Lamparski HG, O'Brien DF (1996) Adv Polym Sci 126:54
102. Okada S, Peng S, Spevak W, Charych D (1998) Acc Chem Res 31:229
103. Norigaki K, Baumgart T, Jonas U, Offenhäuser A, Knoll W (2002) Langmuir 18:4082
104. Chen TM, Wang YF, Li YJ, Nakaya T, Sakurai I (1996) J Appl Polym Sci 60:455
105. Chen TM, Wang YF, Kuriu A, Li YJ, Kitamura M, Nakaya T (1996) Macromol Rep A 33:197
106. Chen TM, Wang YF, Sakaguchi T, Li YJ, Nakaya T (1997) Pure Appl Chem A 34:451
107. Orban JM, Faucher KM, Dluhy RA, Chaikof EL (2000) Macromolecules 33:4205
108. Kim K, Shin K, Kim H, Kim C, Byun Y (2004) Langmuir 20:5396
109. Im JY, Kim DB, Lee SH, Lee YS (2003) Langmuir 19:6392
110. Akama K, Yano Y, Tokuyama S, Hosoi F, Omichi H (2000) J Mater Chem 10:1047
111. Haider SS, Tanaka M, Alan MK, Nakajima SR, Baba N, Shimizu S (1998) Chem Lett 175
112. Liu S, O'Brien DF (2002) J Am Chem Soc 124:6037
113. Lei J, Sisson TM, Lamparski HG, O'Brien DF (1999) Macromolecules 32:73
114. Liu S, O'Brien DF (1999) Macromolecules 32:5519
115. Shimizu T, Masuda M, Minamikawa H (2005) Chem Rev 105:1401
116. Sato T, Miyoshi T, Seno M (2000) J Polym Sci A 38:509
117. Wang H, Miyamoto A, Hirano T, Seno M, Sato T (2004) Eur Polym J 40:2287

118. Wang YF, Chen TM, Li YJ, Korematsu A, Nakaya T (1996) Macromol Rep A 33:1
119. Oishi T, Uchiyama H, Onimura K, Tsutsumi H (1998) Polymer J 30:17
120. Oishi T, Yoshimura Y, Yamasaki H, Onimura K (2001) Polymer Bull 47:121
121. Oishi T, Fukuda T, Uchiyama H, Kondou F, Ohe H, Tsutsumi H (1997) Polymer 38:3109
122. Yamada M, Li Y, Nakaya T (1995) Pure Appl Chem A 32:1723
123. Wang YF, Chen TM, Li YJ, Kitamura M, Sakurai I, Nakaya T (1997) J Polym Sci A 35:3065
124. Li YJ, Shibata Y, Nakaya T (1995) Macromol Rapid Commun 16:253
125. Li YJ, Matthews KH, Kodama M, Nakaya T (1995) Macromol Chem Phys 196:3143
126. Yamada M, Li YJ, Nakaya T (1995) Pure Appl Chem A 32:1235
127. Li YJ, Nakamura N, Wang YF, Kodama M, Nakaya T (1997) Chem Mater 9:1570
128. Korematsu A, Li YJ, Murakami T, Sakurai I, Kodama M, Nakaya T (1999) J Mater Chem 9:647
129. Tomita T, Li YJ, Nakaya T (1999) Chem Mater 11:2155
130. Korematsu A, Tomita T, Kuriyama S, Hanada T, Sakamoto S, Nakaya T (1999) Acta Polym 50:363
131. Li YJ, Hanada T, Nakaya T (1999) Chem Mater 11:763
132. Sugiyama K, Ohga K (1999) Macromol Chem Phys 200:1439
133. Oishi T, Fukuda T, Uchiyama H, Kondou F, Ohe H, Tsutsumi H (1997) Polymer 38:3109
134. Uchida T, Furuzono T, Ishihara K, Nakabayashi N, Akashi M (2000) J Polym Sci A 38:3052
135. Komo T, Watanabe J, Ishihara K (2004) Biomacromolecules 5:342
136. Xu ZK, Dai QW, Wu J, Huang XJ, Yang Q (2004) Langmuir 20:1481
137. Deng HT, Xu ZK, Huang XJ, Wu J, Seta P (2004) Langmuir 20:10168
138. Huang XJ, Xu ZK, Wan LS, Wang ZG, Wang JL (2005) Langmuir 21:2941
139. Wang YF, Chen TM, Li YJ, Nakaya T (1996) Pure Appl Chem A 33:771
140. Inoue Y, Watanabe J, Ishihara K (2004) J Colloid Interface Sci 274:465
141. Sakaki S, Tsuchida M, Iwasaki Y, Ishihara K (2004) Bull Chem Soc Jpn 77:2283
142. Kitano H, Imai M, Mori T, Gemmei-Die M, Yokoyama Y, Ishihara K (2003) Langmuir 19:10260
143. Sakaki S, Iwasaki Y, Nakabayashi N, Ishihara K (2000) Polymer J 32:637
144. Wang Y, Chen T, Kitamura M, Nakaya T (1996) J Polym Sci A 34:449
145. Ishihara K, Fujike A, Iwasaki Y, Kurita K, Nakabayashi N (1996) J Polym Sci A 34:199
146. Nam KW, Watanabe J, Ishihara K (2002) Biomacromolecules 3:100
147. Kiritoshi Y, Ishihara K (2004) Polymer 45:7499
148. Wang YF, Chen TM, Kuriu A, Li YJ, Nakaya T (1997) J Appl Polym Sci 64:1403
149. Miyazawa K, Winnik FM (2002) Macromolecules 35:2449
150. McCormick CL, Lowe AB (2004) Acc Chem Res 37:312
151. Arotcarena M, Heise B, Ishaya S, Laschewsky A (2002) J Am Chem Soc 124:3787
152. Mertoglu M, Garnier S, Laschewsky A, Skrabania K, Storsberg J (2005) Polymer 46:7726
153. Mertoglu M, Laschewsky A, Skrabania K, Wieland C (2005) Macromolecules 38:3601
154. Donovan MS, Sumerlin BS, Lowe AB, McCormick CL (2002) Macromolecules 35:8663
155. Maeda Y, Mochiduki H, Ikeda I (2004) Macromol Rapid Commun 25:1330
156. Donovan MS, Lowe AB, Sanford TA, McCormick CL (2003) J Polym Sci A 41:1262
157. Yusa S, Shimada Y, Mitsukami Y, Yamamoto T, Morishima Y (2004) Macromolecules 37:7507
158. Lowe AB, Billingham NC, Armes SP (1996) Chem Commun 1555
159. Lowe AB, Billingham NC, Armes SP (1999) Macromolecules 32:2141

160. Vamvakahi M, Billingham NC, Armes SP (1998) Polymer 39:2331
161. Bohrisch J, Eisenbach CD, Jaeger W, Mori H, Müller AHE, Rehahn M, Schaller C, Traser S, Wittmeyer P (2004) Adv Polym Sci 165:1
162. Stenzel MH, Barner-Kowollik C, Davis TP, Dalton HM (2004) Macromol Biosci 4:445
163. Yusa S, Fukuda K, Yamamoto T, Ishihara K, Morishima Y (2005) Biomacromolecules 6:663
164. Miyamoto D, Watanabe J, Ishihara K (2005) J Appl Polym Sci 95:615
165. Lobb EJ, Ma I, Billingham NC, Armes SP (2001) J Am Chem Soc 123:7913
166. Ma I, Lobb EJ, Billingham NC, Armes SP, Lewis AL, Lloyd AW, Salvage JP (2002) Macromolecules 35:9306
167. Ma Y, Tang Y, Billingham NC, Armes SP, Lewis AL, Lloyd AW, Salvage JP (2003) Macromolecules 36:3475
168. Ma Y, Tang Y, Billingham NC, Armes SP, Lewis AL (2003) Biomacromolecules 4:864
169. Li C, Tang Y, Armes SP, Morris CJ, Rose SF, Lloyd AW, Lewis AL (2005) Biomacromolecules 6:994
170. Licciardi M, Tang Y, Billingham NC, Armes SP, Lewis AL (2005) Biomacromolecules 6:1085
171. Xu JP, Ji J, Chen WD, Shen JC (2005) Macromol Biosci 5:164
172. Laschewsky A, Zerbe I (1991) Polymer 32:2070
173. Köberle P, Laschewsky A, Lomax TD (1991) Macromol Rapid Commun 12:427
174. Tsukruk V, Mischenko N, Köberle P, Laschewsky A (1992) Makromol Chem 193:1829
175. Laschewsky A (1991) Colloid Polym Sci 269:785
176. Köberle P, Laschewsky A, van den Boogaard D (1992) Polymer 33:4029
177. Anton P, Laschewsky A (1993) Makromol Chem 194:601
178. Köberle P, Laschewsky A (1994) Macromolecules 27:2165
179. Laschewsky A, Touillaux R, Hendlinger P, Vierengel A (1995) Polymer 36:3045
180. Anton P, Laschewsky A (1995) Eur Polym J 31:387
181. Johnson KM, Poe GD, Lochhead RY, McCormick CL (2004) J Macromol Sci A 41:587
182. Johnson KM, Fevola MJ, McCormick CL (2004) J Appl Polym Sci 92:647
183. Johnson KM, Fevola MJ, Lochhead RY, McCormick CL (2004) J Appl Polym Sci 92:658
184. Abele S, Sjöberg M, Hamaide T, Zicmanis A, Guyot A (1997) Langmuir 13:176
185. Abele S, Zicmanis A, Graillot C, Guyot A (1999) Langmuir 15:1045
186. Kudaibergenov SE (1999) Adv Polym Sci 144:115
187. Kitano H, Imai M, Sudo K, Ide M (2002) J Phys Chem 106:11391
188. Schmuck C (2000) J Org Chem 65:2432
189. Mafe S, Garcia-Morales V, Ramirez P (2004) Chem Phys 296:29
190. Masuda S, Minagawa K, Tsuda M, Tanaka M (2001) Eur Polym J 37:705
191. Al-Muallem HA, Wazeer MIM, Ali SKA (2002) Polymer 43:4285
192. Merle Y (1987) J Phys Chem 91:3092
193. Ibraeva ZhE, Sigitov VB, Bimendina LA, Jaeger W, Bekturov EA, Kudaibergenov SE (2004) Dokl Akad Nauk Republic of Kazakhstan (in English) 1:65
194. Lee WF, Tsai CC (1994) J Appl Polym Sci 52:1447
195. Lee WF, Tsai CC (1995) Polymer 36:357
196. Schultz DN, Peiffer DG, Agarwal PK, Larabee J, Kaladas J, Soni L, Handwerker B, Garner RT (1986) Polymer 27:1734
197. Lee WF, Chen YM (2003) J Appl Polym Sci 89:1884
198. Lee WF, Chen YM (2004) J Appl Polym Sci 91:726
199. Lee WF, Hwong CY (1996) Polymer 37:4389
200. Huglin MB, Radwan MA (1991) Polymer Int 26:97

201. Nakaya T, Toyoda H, Imoto M (1986) Polym J 18:881
202. Muroga Y, Amano M, Katagiri A, Noda I, Nakaya T (1995) Polym J 27:65
203. Onabe T, Tanaka H (1999) Langmuir 15:4302
204. Joanny JF (1994) J Phys II France 4:1281
205. Huyghe G, Koizhaiganova R, Kudaibergenov S, Geckeler K (2002) In: Proceedings of the international monitoring conference on development of rehabilitation methodology of the environment of the Semipalatinsk region polluted by nuclear tests. Semipalatinsk, Kazakhstan, pp 87–90
206. Kudaibergenov SE (2002) International symposium on polyelectrolytes, Lund, Sweden, 15–19 June 2002, p 31
207. Noh JG, Sung YJ, Kudaibergenov SE, Geckeler KE (2002) Abstracts of the 2nd K-JIST/NAIST joint symposium on advanced materials, Nara, Japan, 6–9 November 2002, p 30
208. Kudaibergenov SE, Didukh AG, Moldakarimov SB (2002) In: Bohidar HB, Dubin P, Osada Y (eds) Polymer gels: fundamentals and applications. ACS, Washington, DC, p 149
209. Kudaibergenov SE, Sigitov VB, Didukh AG, Moldakarimov SB (2000) Polymer Prepr 41:724
210. Didukh AG, Sigitov VB, Kudaibergenov SE (2004) Poisk 4:4
211. Didukh AG, Sigitov VB, Kudaibergenov SE (2004) Vestn KazGU Ser Khim 3:168
212. Didukh AG, Koizhaiganova RB, Bimendina LA, Geckeler KE, Kudaibergenov SE (2005) Izv Akad Nauk RK Ser Khim 2:95
213. Gauthier M, Carrozzella T, Snell G (2002) J Polym Sci Polym Phys 40:2303
214. Biegle A, Mathis A, Meurer B, Galin JC (2000) Macromol Chem Phys 201:2401
215. Grassl B, Mathis A, Rawiso M, Galin JC (1997) Macromolecules 30:2075
216. Biegle A, Galin JC (2000) Macromol Chem Phys 201:1442
217. Bazuin GC, Zheng YL, Muller R, Galin JC (1989) Polymer 30:654
218. Ehrman M, Muller R, Galin JC, Bazuin GC (1993) Macromolecules 27:4910
219. Köberle P, Laschewsky A (1994) Macromol Symp 88:165
220. Rozanski SA, Kremer F, Köberle P, Laschewsky A (1995) Macromol Chem Phys 196:877
221. Didukh AG, Sigitov VB, Bimendina LA, Kudaibergenov SE, Noh JG, Sung YJ, Geckeler KE (2004) Izv Akad Nauk RK Ser Khim 1:96
222. Osada Y, Gong JP (1998) Adv Mater 10:827
223. Murdan S (2003) J Control Release 92:1
224. Oishi T, Yamasaki H, Onimura K, Fukushima T, Morihashi S (2004) J Appl Polym Sci 92:2552
225. Hupfer B, Ringsdorf H (1983) Chem Phys Lipids 33:355
226. Leaver J, Alonso A, Durrani AA, Chapman D (1983) Biochim Biophys Acta 732:210
227. Regen SL, Singh A, Oehme G, Singh M (1982) J Am Chem Soc 104:791
228. Ringsdorf H, Venzmer J, Winnik FM (1991) Macromolecules 24:1678
229. Liaw DJ, Huang CC, Sang HC, Kang ET (1998) Langmuir 14:3195
230. Liaw DJ, Huang CC, Sang HC, Kang ET (1999) Langmuir 15:5204
231. Liaw DJ, Huang CC, Kang ET (1999) Curr Trends Polym Sci 4:117
232. Anton P, Laschewsky A (1994) Colloid Polym Sci 272:1118
233. Cardoso J, Manero O (1991) J Polym Sci B 29:639
234. Sawada H, Katayama S, Ariyoshi Y, Kawase T, Hayakawa Y, Tomita T, Baba M (1998) J Mater Chem 8:1517
235. Sawada H, Umedo M, Kawaze T, Tomita T, Baba M (1999) Eur Polym J 35:1611
236. Sawada H, Umedo M, Kawase T, Baba M, Tomita T (2004) J Appl Polym Sci 92:1144

237. Hadjichristidis N, Pispas S, Pistikalis M (1999) Prog Polym Sci 24:875
238. Butun V (2004) Polymer 44:7321
239. Weaver JVM, Armes SP, Butun V (2002) J Chem Soc Chem Commun 19:2122
240. Virtanen J, Arotçaréna M, Heise B, Ishaya S, Laschewsky A, Tenhu H (2002) Langmuir 18:5360
241. Donovan MS, Lowe AB, Sanford TA, McCormick CL (2003) J Polym Sci A 41:1262
242. Maeda Y, Tsubota M, Ikeda I (2004) Macromol Rapid Commun 25:1330
243. Didukh AG, Koizhaiganova RB, Bimendina LA, Kudaibergenov SE (2004) J Appl Polym Sci 92:1042
244. Miyazawa K, Winnik FM (2002) Macromolecules 35:9536
245. Kudaibergenov SE, Ibraeva ZhE, Nepal D, Geckeler KE, Bimendina LA (2004) Vestn KazGU Ser Khim 4:483
246. Ibraeva ZhE, Nepal D, Geckeler KE, Bimendina LA, Kudaibergenov SE (2004) Dokl. Akad. Nauk Republic of Kazakhstan (in English) 3:25
247. Mandel M, Leyte JC (1972) Electroanal Chem 33:297
248. Wang C, Tam KC, Jenkins RD (2002) J Phys Chem B 106:1195
249. O'Brien DF, Ramaswami V (1989) In: Mark FH, Bikales NM, Overberger CG, Menges G (eds) Encyclopedia of polymer science and technology, vol 17. Wiley, New York, p 10
250. Ringsdorf H, Schlab B, Venzmer J (1988) Angew Chem Int Ed Engl 27:113
251. Nakaya T, Yamada M, Shibata K, Imoto M, Tsuchiya H, Okuno M, Nakaya S, Ohno S, Matsuyama T, Yamaoka H (1990) Langmuir 6:291
252. Chen L, Honma Y, Mizutani T, Liaw D-J, Gong JP, Osada Y (2000) Polymer 41:141
253. Okawa K, Gong JP, Osada Y (2002) Macromol Rapid Commun 23:423
254. Zhumadilova G, Yashkarova M, Bimendina L, Kudaibergenov S (2003) Polym Int 52:876
255. Didukh AG, Makysh GSh, Bimendina LA, Kudaibergenov SE (2003) In: Geckeler KE (ed) Advanced macromolecular and supramolecular materials and processes. Kluwer, New York, p 265
256. Waziri SM, Abu-Sharkh BF, Ali SA (2003) Fluid Phase Equilibr 205:275
257. Waziri SM, Abu-Sharkh BF, Ali SA (2004) Biotechnol Prog 20:526
258. Viklund K, Irgum K (2000) Macromolecules 33:2539
259. Rmaile HH, Bucur BC, Schlenoff JB (2003) Polymer Prepr 44(1):541
260. Salloum DS, Rmaile HH, Bucur C, Schlenoff JB (2004) Polymer Prepr 45(1):837
261. Laschewsky A, Mayer B, Wischerhoff E, Arys X, Bertrand P, Delcorte A, Jonas A (1996) Thin Solid Films 284:334
262. Koetse M, Laschewsky A, Mayer B, Rolland O, Wischerhoff E (1998) Macromolecules 31:9316
263. Oishi T, Tanaka H, Yamasaki H, Onimura K (2002) J Appl Polym Sci 86:1092
264. Bonte N, Laschewsky A, Mayer B, Vermylen V (1996) Macromol Symp 102:273
265. Bonte N, Laschewsky A, Vermylen V (1997) Macromol Symp 117:195
266. Miyazawa K, Winnik F (2003) Prog Colloid Polym Sci 122:149
267. Favresse P, Laschewsky A (1999) Macromol Chem Phys 200:887
268. Smets G, Samyn C (1979) In: Selegny E (ed) Optically active polymers. Reidel, Dordrecht
269. Mouton J, Khamitzhanova G, Kudaibergenov S, Geckeler KE (2002) Proceedings of the international monitoring conference on development of rehabilitation methodology of the environment of the Semipalatinsk region polluted by nuclear tests. Semipalatinsk, Kazakhstan, 21–24 September 2002, p 25
270. Khamitzhanova G, Syzdykbaeva Zh, Yashkarova M, Bimendina L (2002) Proceedings of the international monitoring conference on development of rehabilitation

methodology of the environment of the Semipalatinsk region polluted by nuclear tests. Semipalatinsk, Kazakhstan, 21–24 September 2002, p 30
271. Kudaibergenov SE, Bimendina LA, Sigitov VB, Yashkarova MG, Khamitzhanova G, Geckeler KE, Sung YJ, Noh JG, Choi SH (2003) Abstracts of the IUPAC 10th international symposium on macromolecule metal complexes, Moscow, 18–23 May 2003
272. Sigitov VB, Didukh AG, Tastanov KKh, Kudaibergenov SE (2003) Abstracts of the international conference devoted to the 40th anniversary of the macromolecular chemistry department of Kiev National Taras Shevchenko University, Kiev, Ukraine, 27–30 October 2003
273. Noh JG, Sung YJ, Geckeler KE, Kudaibergenov SE (2005) Polymer 46:2183
274. Koizhaiganova RB (2005) PhD thesis, Institute of Polymer Materials and Technology, Republic of Kazakhstan
275. Kudaibergenov SE, Choi SH, Geckeler KE, Annenkov VV (2005) Eur Polym J (in press)
276. Mumick PS, Welch PM, Salazar LC, McCormick CL (1994) Macromolecules 27:323
277. Sabhapondit A, Borthakur A, Haque I (2003) J Appl Polym Sci 87:1869
278. Sabhapondit A, Borthakur A, Haque I (2004) J Appl Polym Sci 91:2482
279. Zhang LM, Tan YB, Li ZM (2001) Carbohydr Polym 44:255
280. Didukh AG, Sigitov VB, Kudaibergenov SE (2004) Oil Gas 4:64
281. Water JM, James A (2003) US Patent 6,540,822
282. Kudaibergenov SE, Didukh AG, Koizhaiganova RB, Bimendina LA (2003) J Appl Polym Sci 92:1042
283. Ogura K, Sasaki K (1996) US Patent 5,512,644
284. Kudaibergenov SE, Kozhabekov DB, Geckeler KE (2002) Kazakhstan Patent 14007
285. Argiller JF, Audibert-Hayet A, Perchec PL, Carette PL (2002) US Patent 6,410,671
286. Smets G, Samyn C (1979) In: Selegny E (ed) Optically active polymers. Reidel, Dordrecht, p 179
287. Khvan AM, Chupov VV, Noa OV, Plate NA (1985) Vysokomol Soed Ser A 27:1243
288. Didukh AG (2005) PhD thesis, Institute of Polymer Materials and Technology, Republic of Kazakhstan
289. Kudaibergenov SE (2003) NATO advanced research workshop on modern technologies of secondary resources processing and creation of new composite materials on their basis, Tashkent, Uzbekistan
290. Lozinsky VI, Galaev IYu, Bloch KO, Damshkaln LG, Vasilevskaya VV, Burova TV, Didukh AG, Vardi P, Khokhlov AR, Grinberg VYa, Kudaibergenov SE, Mattiasson B (2003) 2nd Moscow international congress on biotechnology, Part 2, p. 182
291. Jiang W, Irgum K (1999) Anal Chem 71:333
292. Arasawa H, Odawara C, Yokoyama R, Saitoh H, Yamauchi T, Tsubokawa N (2004) React Funct Polym 61:153
293. Jiang Y, Qingfeng H, Baolei L, Jian S, Sicong L (2004) Colloids Surf B Biointerfaces 36:19
294. Xu JP, Ji J, Chen WD, Fan DZ, Sun YF, Shen JC (2004) Eur Polym J 40:291
295. Miyamoto D, Watanabe J, Ishihara K (2003) J Appl Polym Sci 95:615
296. Hentze HP, Kaler EW (2003) Curr Opin Colloid Interface Sci 8:164
297. Lam JKW, Ma Y, Armes SP, Lewis AL, Baldwin T, Stolnik S (2004) Polymer 45:2217
298. Xi X, Liu Y, Shi J, Cao S (2003) J Mol Catal 192:1
299. Bonsel H, Deckers G, Frank G, Millauer H, Soczka-Guth T (2002) US Patent 6,391,818
300. Hagemeyer A, Dingerdissen U, Millauer H, Manz A, Kuhlein K (2000) US Patent 6,074,979

Editor: S. Kobayashi

Adv Polym Sci (2006) 201: 225–296
DOI 10.1007/12_077
© Springer-Verlag Berlin Heidelberg 2006
Published online: 16 February 2006

Polyhedral Oligomeric Silsesquioxanes (POSS)-Containing Nanohybrid Polymers

K. Pielichowski[1] (✉) · J. Njuguna[2] · B. Janowski[1] · J. Pielichowski[1]

[1]Department of Chemistry and Technology of Polymers,
Cracow University of Technology, ul. Warszawska 24, 31-155 Kraków, Poland
k.pielich@usk.pk.edu.pl

[2]School of Industrial and Manufacturing Science, Cranfield University,
Cranfield, Bedfordshire, MK43 0AL, UK

1 Introduction 228

2 POSS Cages 230

3 Methods of POSS Cage Synthesis 231
3.1 Completely Condensed POSS 231
3.2 Incompletely Condensed POSS 232

4 Structure and Reactivity of POSS 235

5 Synthesis of POSS-Containing Polymers 246
5.1 Free Radical Polymerization 247
5.2 Polyaddition and Polycondensation 249
5.3 Ring-Opening Metathesis Polymerization (ROMP) 253

6 Synthesis of POSS-Dendrimer Cores 256
6.1 Convergent Method 257
6.2 Divergent Methods 260

7 Properties of POSS-Containing Nanohybrid Polymers 263
7.1 Mechanical Properties 264
7.2 Thermal Properties 265
7.3 Viscoelastic Properties—Rheological Behavior 270
7.4 Morphology of the POSS-Containing Nanohybrid Polymers 272
7.5 Interfacial Interactions, Compatibility and Dispersion Characteristics . . . 276
7.6 Catalytic Effects of POSS 281
7.7 Ion Mobility and Swelling Studies 282
7.8 Porosity 284

8 Applications 287

9 Concluding Remarks 289

References 290

Abstract Polyhedral oligosilsesquioxane (POSS)-based hybrid polymers have generated much interest recently, both from the academic and industrial points of view. POSS

are completely defined molecules of nanoscale dimensions that may be functionalized with reactive groups suitable for the synthesis of new organic–inorganic hybrids, thus providing the opportunity to design and build materials with extremely well-defined dimensions possessing nanophase behavior. POSS have been successfully incorporated into common polymers via copolymerization, grafting or blending. A variety of POSS-containing copolymers have been prepared and they have displayed great potential in the development of a wide range of hybrid nanomaterials with diverse properties. This work has critically evaluated the recent developments in syntheses of POSS polymer materials leading to POSS nanocomposites. The syntheses of POSS cages, monomers containing POSS cages, POSS-dendrimers' cores, POSS-containing polymers (nanobuilding blocks) and POSS nanocomposites are described in detail. This work also assesses the properties of POSS nanobuilding blocks that can be otherwise used for developing nanocomposites. Such properties include mechanical, thermal, flame-retardant and viscoelastic properties. Investigations into the structure, morphology and compatibility of POSS nanobuilding blocks have been reviewed. Other properties covered include the ion-mobility and swelling characteristics as well as porosity of POSS nanobuilding blocks. Lastly, existing and possible future applications are highlighted and final conclusions are drawn.

Keywords Applications · Nanohybrid polymers · POSS · Properties · Synthesis

Abbreviations

AIBN	2,2′-azobisisobutyronitrile
ATRP	atom-transfer radical polymerization
BDGE	1,4-butandiol diglycidyl ether
BSA	4,4′-[1,3-phenylenebis-(1-methylethylidene)]bisaniline
c-C_5H_9	cyclopentyl
c-C_6H_{11}	cyclohexyl
c-C_7H_{13}	cycloheptyl
m-CPBA	*meta*-chloroperbenzoic acid
DCPD	dicyclopentadiene
DDM	diaminodiphenylmethane
DGEBA	diglycidyl ether of Bisphenol A
DMA or DMTA	dynamic mechanical analysis
DP	degree of polymerization
DRIFTS	diffuse reflectance infrared Fourier transform (spectroscopy)
DSC	differential scanning calorimetry
EtO	ethoxyl
EXAFS	extended X-ray absorption fine-structure spectroscopy
E′	storage modulus
FTIR	Fourier-transform infrared spectroscopy
G′	shear storage modulus
G″	loss modulus
GPC	gel permeation chromatography
MALDI-TOF	matrix-assisted laser desorption ionization—time of flight (spectroscopy)
MDI	4,4′-methylenebis(phenylisocyanate)
Me	methyl group
MPDA	2-methyl-1,5-pentadiamine

MSD	mean square displacement
MW	molecular weight
1NB-POSS	norbornenylethyl-POSS
3NB-POSS	tris(norbornenylethyl)-POSS
NMR	nuclear magnetic resonance
OAPS	octaaminophenylsilsesquioxane
ODA	oxydianiline
ODPA	oxydiphthalic anhydride
OG	octaglycidyldimethylsiloxyoctasilsesquioxane
OHPS	octakis(3-hydroxypropyldimethylsiloxy)octasilsesquioxane
OMPS	octakis(3-methacryloxypropyldimethylsiloxy)octasilsesquioxane
PAA	poly(amic acid)
PALS	positron annihilation lifetime spectroscopy
PAPS	polyaminophenylsilsesquioxane
PAS	polyacetoxystyrene
PDMA	pyromellitic dianhydride
PDMAm	poly(*N*,*N*-dimethylacrylamide)
PEO	poly(ethylene oxide)
PMMA	poly(methyl methacrylate)
PN	polynorbornene
PPh_3	triphenylphosphine
PPO	poly(propylene oxide)
POSS	polyhedral oligomeric silsesquioxanes
POZO	poly(2-methyl-2-oxazoline)
PPSQ	polyphenylsilsesquioxane
PS	polystyrene
Pt(dvs)	platinum divinyltetramethyldisiloxane
PTMG	polytetramethylene glycol
PU	polyurethane
PVP	polyvinylpyrrolidone
ROMP	ring-opening metathesis polymerization
SAXS	small-angle X-ray scattering
SEM	scanning electron microscopy
SPM	scanning probe microscopy
SSA	specific surface area
STXM	scanning transmission X-ray microscopy
$\tan\delta$	mechanical loss factor
tert-Boc	*tert*-butoxycarbonyl
TEM	transmission electron microscopy
TG	thermogravimetry
T_g	glass temperature
TGDDM	tetraglycidyldiaminodiphenylmethane
THF	tetrahydrofuran
m-TMI	*meta*-isopropenyl-α,α'-dimethylbenzyl isocyanate
T	temperature
T_{ODT}	order-disorder transition temperature
Ts	tosyl (4-toluenesulfonyl) group
WAXD	wide angle X-ray diffraction
VMB	4-vinyl-4′-methyl-2,2′-bipyridine
ω	shear frequency

1 Introduction

The growth of new materials with specially designed chemical, mechanical or physical properties is becoming increasingly important in many fields of practical application. In this respect, recent years have seen increased demand for organic–inorganic hybrid polymer materials in a wide range of applications. These needs have been met with accelerated advances in polymer science and technology, taking benefit from nanophase technology geared towards enhancements to polymer materials. In order to accomplish the various practical requirements, a tailor-made material design is necessary, which includes direct control of both bulk and surface characteristics [1]. The nanostructure, degree of organization and properties that can be obtained for such materials certainly depend on the chemical nature of their components, but they also rely on the synergy between these components.

Interest in polyhedral oligomeric silsesquioxanes (POSS) materials is based on the facts that their rigid framework closely resembles that of silica and that they offer a unique opportunity for preparing truly molecularly dispersed nanocomposites [2, 3]. They combine a hybrid inorganic–organic composition, $R_n(SiO_{1.5})_n$, where R may be a range of organofunctional groups, while n is an even integer ≥ 4, with nanosized cage structures having dimensions comparable to those of most polymeric segments or coils [4]. POSS chemical reagents are nanostructured with sizes of 1–3 nm and can be thought of as the smallest particles of silica possible. However, unlike silica or silicones, each POSS molecule may contain nonreactive organic substituents that make the POSS nanostructure compatible with monomers or polymers. POSS molecules have been easily incorporated into common polymers via copolymerization, grafting or blending [5]. A variety of POSS-containing copolymers have been prepared using condensation, ring-opening metathesis and radical, both conventional, and atom-transfer, copolymerization techniques. Many varieties of substituents may be fixed onto the Si atoms at the corners of the cages to optimize polymer–POSS interactions and simultaneously to aid in the easy dissolution of the POSS moieties in common solvents for synthesis purposes. These groups may be incorporated into almost any conventional polymer and in a variety of different chain architectures. Thus, inorganic nature and multiple reactive functionalities of POSS make these compounds ideal for their use in the construction of organic–inorganic hybrid nanomaterials [6].

POSS have also been commonly employed in polymerization as building blocks for hybrid inorganic–organic nanocomposites. The nanobuilding block approach offers a powerful tool to control arrangement at the nanoscale because not only the building segments but also their macroscopic organization can be controlled completely [7]. Thus, a key point for the design of new hybrids is the tuning of the nature, extent and accessibility of the inner in-

terfaces [8]. In other words, systematic construction of nanocomposites using selectively designed building blocks offers an excellent chance to develop and tailor novel properties. However, to assemble the right segments in forming building blocks and to process them properly for target properties, a thorough understanding of nanostructure–processing–property relationships in nanocomposites is critical. Equally important, incorporation of nanosized components also offers the potential to greatly improve the reproducibility of composite properties because complete control of the smallest building segments offers the best potential for controlling macroscopic properties. Finally, detailed structure–processing–property studies of nanocomposites should eventually permit prediction of properties for specific applications.

Hybrids may be produced by blending POSS into a polymer matrix, by covalently bonding POSS into a polymer backbone, or by using POSS as a pendant group of a polymer. Using POSS as a pendant group of a linear polymer gives a linear organic–inorganic hybrid. The organic fragments in the building blocks range from rigid acrylenic [9, 10], acetylenic [9, 11] and olefinic bridging groups to flexible alkylenes ranging from 1 to 14 methylene groups in length. They also include a variety of functionalized groups such as amines, ethers, sulfides, phosphines, amides, ureas, carbamates and carbonates. In addition, bridging groups have included organometallics in which the metal is part of the bridge or pendant to the bridge [12]. In particular, organic–inorganic hybrid nanomaterials are generally achieved by forming a POSS macromonomer possessing a single polymerizable functional group, with the remaining vertices having inert organic groups. The macromonomer is then copolymerized with a suitable monomer, yielding the desired organic–inorganic hybrid material. Hybrids produced using this methodology include polypropylene-based blends and copolymers [13–15], polyurethanes [16], poly(alkyl methacrylates) [17, 18], poly(4-methyl styrene) [7, 19–21], ethene-propene [13] copolymers, epoxies [22–24], polynorbornene [25–27] and polysiloxanes [2, 28, 29] as cores in dendrimers [30] and in highly porous POSS-based network polymers [31]. Such polymers show many improved properties over those that use more traditional fillers, such as silica, including higher usage temperatures and increased fire retardance. These hybrid polymers also show improved properties, such as higher T_g, increased oxygen permeability and enhanced mechanical strength. This has led to proposed uses of these molecules as hard blocks or reinforcing particles in high-performance polymer materials.

These interesting POSS features, briefly mentioned above, have motivated this work to critically review recent developments in the syntheses of POSS polymer materials to form POSS nanocomposites. The work further examines the properties of POSS nanobuilding blocks that can otherwise be used for developing polymeric nanocomposites. In particular, the syntheses of POSS cages, monomers containing POSS cages, POSS-dendrimers' cores, POSS-containing polymers and POSS nanocomposites are covered in details. It should be emphasized that the assessment of the relationship between the

POSS nanobuilding blocks and the resultant POSS nanocomposites is beyond the scope of the current work. However, the enhanced properties of POSS nanobuilding blocks will be comprehensively reviewed. Such properties include mechanical, thermal, flame-retardant and viscoelastic properties. Investigations into POSS nanobuilding blocks' cube structure and reactivity, morphology, compatibility, dispersion, organization and catalytic effects, have been presented. Other properties covered include ion-mobility and swelling characteristics and porosity of the POSS nanobuilding blocks. Lastly, current and future applications are discussed.

2 POSS Cages

Silsesquioxanes exist in a variety of structures from random polymers to more ordered arrangements [32], but the POSS with their unique cage-like structures and nanoscale dimensions are of particular interest. Polyhedral silsesquioxanes $(RSiO_{1.5})_n$, where R = H, Cl, or a wide variety of organic groups, are unique structures generally formed by hydrolysis and condensation of trialkoxy- or trichlorosilanes. Several structural representations of silsesquioxanes with the empirical formula $RSiO_{1.5}$ are possible, e.g. trigonal prismatic (Si_6O_9) cages, cubane (Si_8O_{12}) cages, double five-ring ($Si_{10}O_{15}$) cages, double six-ring (Si_6O_9) cages (Fig. 1) and miscellaneous silsesquioxanes with an extra vertex have all been synthesized [33].

The two most common representations are of a ladder-type and a cubic structure, containing eight silicon atoms placed at the vertices of the cube. In essence, cubic silsesquioxanes can be thought of as the smallest silica particles possible that can be up to octafunctional; they may contain groups available for copolymerization or responsible for features like adhesion, light sensitization, catalytic activity and solubility. In other words, their well-defined almost cubic silica-like core surrounded by eight organic groups (R) makes them topologically ideal for the preparation of intimate nanocomposite materials, with the size of the inorganic region precisely defined by the size of the core. All or some of each type of functionality can in principle be introduced to a given platform. As "silica particles", studies of their copolymerization with organic monomers may represent the simplest models of silica-reinforced composites. When the silsesquioxane/organic copolymers do behave as silica-reinforced composites, then soluble, copolymerizable silsesquioxanes offer unique potential because single-phase composite processing becomes possible, as opposed to the two-phase monomer/silica filler mixtures typically used [34]. The Si_8O_{12} core can have a wide variety of functional groups attached to each vertex, leading to its use in a variety of different applications. For instance, Hasegawa [35] has developed effective routes to the related $((RMe_2SiO)SiO_{1.5})_8$ compounds. Their rigid framework

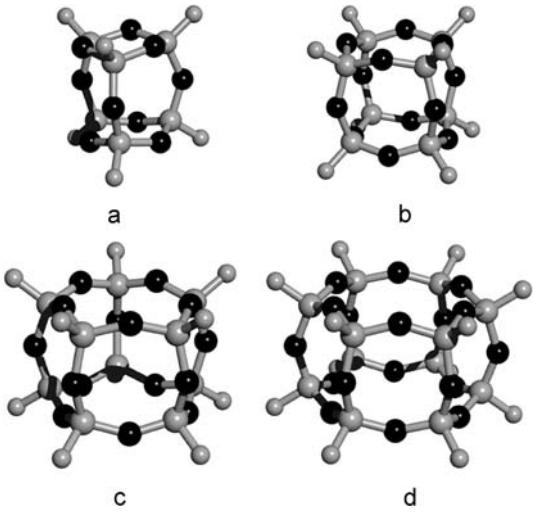

Fig. 1 Four typical structures of POSS cages: **a** trigonal prismatic (Si_6O_9) cage, **b** cubane (Si_8O_{12}) cage, **c** double five-ring ($Si_{10}O_{15}$) cage, and **d** double six-ring ($Si_{12}O_{18}$) cages

offers many appealing properties that have been exploited by, among others, Feher and coworkers to develop unique patterns of silica surfaces as models of zeolites [36], as novel sol–gel precursors [37], and by other groups for diverse applications [38].

3
Methods of POSS Cage Synthesis

POSS are an interesting class of three-dimensional Si/O clusters derived from the hydrolytic condensation of trifunctional organosilicon monomers. Since their discovery in the 1940s, many stoichiometrically well-defined POSS frameworks have been reported, but it was only recently that POSS frameworks with functionality suitable for most chemical applications have emerged. Several condensed (complete Si – O cage) and incompletely condensed (partial Si – O cage with multiple Si atoms capped with OH, also called silanols) POSS compounds of different cage sizes have been investigated [39]. The POSS-cage synthesis methods can be classified as hydrolitic condensation, and are hereby presented in the following subchapters.

3.1
Completely Condensed POSS

Without exaggerations, the ability of POSS to combine unique hybrid (inorganic–organic) chemical compositions with nanosized cage structures

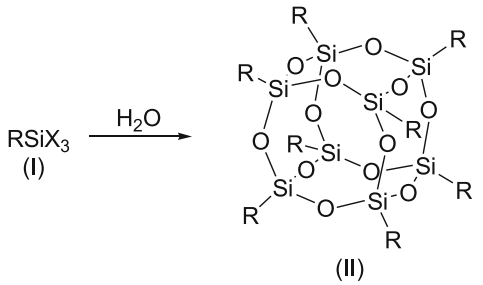

Scheme 1 Scheme of completely condensed polyhedral oligosilsesquioxanes synthesis by hydrolytic condensation of trichloro- or trialkoxysilanes

has long been important and interesting class of materials because of their unusual structures involving several rings connected together in a finite three-dimensional molecular skeleton. Of the two synthetic routes, the most common process used to obtain the polyhedral Si – O core of completely condensed POSS is by one-step hydrolytic condensation of trifunctional monomers $XSiY_3$, where X is a chemically stable organic substituent or H, and Y is a highly reactive substituent, such as Cl or alkoxy (Scheme 1). This is a difficult process that involves careful control of several factors, such as the concentration of initial monomer in the solution, nature of the solvent, type of catalyst employed, temperature, character of substituted X and functional group in the initial monomer, solubility of the polyhedral oligomers, quantity of water added and rate of its addition [33].

Generally, increase of temperature results in highly condensed polymers and therefore the temperature should be kept low, at room temperature or preferably subambient. Slow, careful addition of water helps to keep the concentration of silanol groups formed low, though this can also be done by the careful selection of a suitable solvent, such as an alcohol, which stabilizes the silanol group adequately. Some representative syntheses of completely condensed POSS $(XSiY_{1,5})_n$, by condensation of $XSiY_3$ precursors are given in Table 1.

3.2 Incompletely Condensed POSS

Increased interest in using incompletely condensed silsesquioxanes and oligosilsesquioxanes, containing more than one hydroxyl group, as molecular building blocks in many polymer systems, have been observed in recent times. This is mainly driven by significant property enhancements imparted by inclusion of a nanosized inorganic particulate into an organic matrix, yielding models for silica surfaces, building blocks for macromolecular networks and precursors to new families of silsesquioxane-containing

Table 1 Representative syntheses of completely condensed POSS $(XSiY_{1,5})_n$ by condensation of $XSiY_3$ precursors [246]

X	*n*	Y	Solvent	Catalyst	Yield %	Refs.
H	8	OCH_3	Cyclohexane	$HCl + CH_3COOH$	13	[40, 41]
H	10, 12, 14, 16	Cl	Benzene	$H_2SO_4 + SO_3$	15–35	[40]
CH_3	6	OC_2H_5	Benzene	HCl	—	[42]
CH_3	8	Cl	Methanol	HCl	37	[42–45]
CH_3	10,12	OC_2H_5	Benzene	KOH	—	[43, 45]
C_2H_5	6	OC_2H_5	Benzene	HCl	—	[46]
C_2H_5	8	Cl	Methanol	HCl	37	[43, 46]
C_2H_5	10	Cl	Butanol	HCl	16	[47]
c-C_6H_{11}	6	Cl	Acetone	HCl	7	[48]
c-C_6H_{11}	8	OCH_3	Nitrobenzene	OH	—	[43, 48]
$CH = CH_2$	8	OCH_3	Methanol	HCl	20	[49]
$CH = CH_2$	10	OCH_3	Butanol	HCl	—	[49]
C_6H_5	8	OCH_3	Benzene	$PhCH_2(CH_3)_3NOH$	88	[50–52]
C_6H_5	10	OC_2H_5	Tetrahydrofuran	Me_4NOH	—	[52]
C_6H_5	12, 22, 24	OC_2H_5	Tetrahydrofuran	Me_4NOH	—	[50, 52, 53]

polymers [54–62]. Of particular interest have been reactions of trisilanols with ligand-deficient trivalent-metal complexes, because of the inability of these trisilanols to support trigonal planar coordination environments that usually lead to more complex structures.

Feher and his team of researchers have also described a procedure for synthesis of three closely related groups of incompletely condensed POSS via slow hydrolytic condensation of cyclohexyltrichlorosilane $c\text{-}C_6H_{10}SiCl_3$ [63] in aqueous acetone (Scheme 2).

The published work claimed that hydrolytic condensation reactions of $c\text{-}C_5H_9SiCl_3$ led to 29% yield of $(c\text{-}C_5H_9)_7Si_7O_9(OH)_3$ (III), while that of $c\text{-}C_7H_{13}SiCl_3$ afforded $(c\text{-}C_7H_{13})_7Si_7O_9(OH)_3$ (V) and $(c\text{-}C_7H_{13})_6Si_6O_7(OH)_4$ (VI) in high yields (26% and 7%, respectively) within a few days. $(c\text{-}C_7H_{13})_6Si_6O_7(OH)_4$ (VI) tetrasilanols are formally derived from hydrolytic cleavage of two adjacent silicon atoms from the cube-octameric POSS. It was further claimed that $(c\text{-}C_7H_{13})_6Si_6O_7(OH)_4$ (VI) provided a tetrahydroxylic silsesquioxane ligand capable of accommodating two metal ions in a completely condensed silsesquioxane framework and therefore of significant importance in advancing chemical fields relevant to bimetallic silica-supported catalysts.

In recent years a remarkable trend has been observed towards actively exploring the reactions of silsesquioxanes with strong bases and acids, e.g. in Feher et al. [64–66] works on acid-mediated cleavage and rearrangement of $(c\text{-}C_6H_{11})_6Si_6O_9$ to $(c\text{-}C_6H_{11})_6Si_6O_8X_2$ and base-mediated cleavage of POSS (Scheme 3).

A good example of such a reaction is that in which cube-octameric polyhedral silsesquioxanes ($R_8Si_8O_{12}$) (VII) reacted with strong acids to produce $R_8Si_8O_{11}X_2$ frameworks, resulting from selective cleavage of one Si – O – Si linkage [67]. Subsequent hydrolysis afforded $R_8Si_8O_{11}(OH)_2$ (VIII) frameworks derived from the net hydrolysis of one Si – O – Si linkage in $R_8Si_8O_{12}$. The results of this work demonstrated that readily available $R_8Si_8O_{12}$ frameworks could be used as precursors to incompletely condensed Si/O frame-

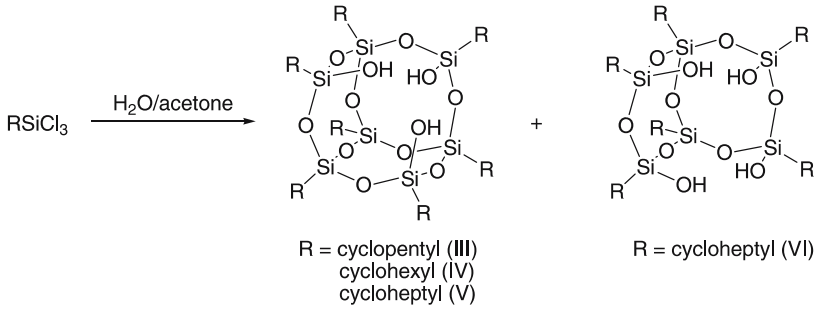

Scheme 2 Scheme of incompletely condensed POSS synthesis by slow hydrolytic condensation

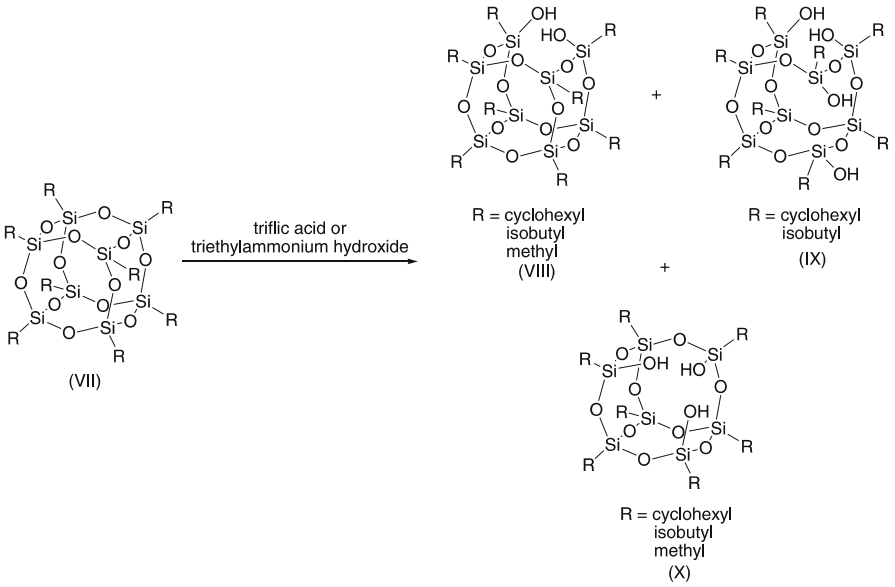

Scheme 3 Scheme of incompletely condensed POSS synthesis by acid- and base-mediated cleavage of completely condensed POSS

works and have important implications for the manufacture of hybrid inorganic–organic materials based on POSS.

Further developments have seen the inclusion of spherosilicates, which can be obtained at high yields from either silica or $(EtO)_4Si$ [68–70]. Such works reflect the expected revolution in the way that many classes of silsesquioxanes are prepared.

Experimental and theoretical parameters have been successfully developed to accurately model the gas-phase conformations of a variety of POSS compounds with different Si – O cage sizes and substituent groups. Incompletely condensed POSS molecules are commonly used to create specific condensed POSS systems by capping with the appropriate reactive functional group. Some of the POSS compounds were functionalized with cyclohexyl groups, but data has also been obtained for POSS functionalized with cyclopropyl, vinyl and phenyl groups [71].

4
Structure and Reactivity of POSS

Investigations on star polymers have determined that they constitute unique three-dimensional structures among the branched polymers since there is a large number of arm chains radiating from the central core and each

molecule has only one branching point [72, 73]. These works claimed that well-defined star polymers offer lower melt and solution viscosities compared to those of linear polymers. Evidently, living polymerization is one of the best methods to synthesize a variety of star polymers of well-defined architectures. Along this direction, Kobayashi et al. [74] and Kim et al. [75] have steadily studied a wide variety of functional materials based on ring-opening polymerization of 2-methyl-2-oxazoline, which is a good candidate for living polymerization because the obtained polyoxazoline had unique properties, such as hydrophilicity and good compatibility with common organic polymers. ^{1}H nuclear magnetic resonance (NMR) and gel permeation chromatography (GPC) results confirmed that star-shaped polyoxazolines with a POSS core, having at most four or five arms with different lengths out of eight possible arms, were obtained [76]. The different lengths of four or five arms were attributed to the steric hindrance and the different initiation rates for the eight initiation sites, which were derived from the unique structure of POSS, was due to inefficient commencement of the reaction. Also, the kinetic rate of polymerization initiated by methyl *p*-toluenesulfonate (MeOTs) was found to be much faster than that of polymerization initiated by cube-O-Ts, which is more evidence that confirms the steric hindrance imparted by POSS structure.

Zhang and Laine [77] reported on vinyl cubic polyhedral silsesquioxanes $(\text{vinylSiO}_{1.5})_8$ (XI) and $((\text{vinylMe}_2\text{SiO})\text{SiO}_{1.5})_8$ (XIV) that were epoxidized using ten equivalents of *m*-chloroperoxybenzoic acid (*m*-CPBA) per cube (Scheme 4).

The $((\text{vinylMe}_2\text{SiO})\text{SiO}_{1.5})_8$ (XIV) compound converts, quantitatively, to the octaepoxide, $((\text{epoxyMe}_2\text{SiO})\text{SiO}_{1.5})_8$ (XV). The $(\text{vinylSiO}_{1.5})_8$ (XI) cube was likewise fully epoxidized, as determined by NMR; however, efforts to isolate it led to intractable gels. Partial epoxidation was achieved using only three equivalents of *m*-CPBA.

The partially epoxidized compound was shown to have an average of two epoxy groups per cube. Both polyepoxides readily polymerized in the presence of Lewis acid catalysts or in reaction with amines. This suggested their potential as coupling agents in the synthesis of novel inorganic–organic hybrids.

Neumann and coworkers [6] reported the first synthesis and characterization of a novel POSS, possessing eight isocyanate groups (XVIII) (Scheme 5) *via* the hydrosilylation of *m*-isopropenyl-α,α'-dimethylbenzyl isocyanate (*m*-TMI) (XVII) by octakis(dimethylsiloxy)octasilsesquioxane ($Q_8M_8{}^H$) (XVI).

Initial attempts to obtain $Q_8M_8{}^{TMI}$ using dry toluene as the solvent afforded a product with incomplete substitution of the starting compound $Q_8M_8{}^H$, as evidenced by a peak in the ^{1}H NMR spectrum attributed to residual Si – H groups. Increased reaction time, temperature and catalyst concentration did not enable the reaction to be completed. In an effort to obtain complete substitution, dry tetrahydrofuran was used as a solvent for the reac-

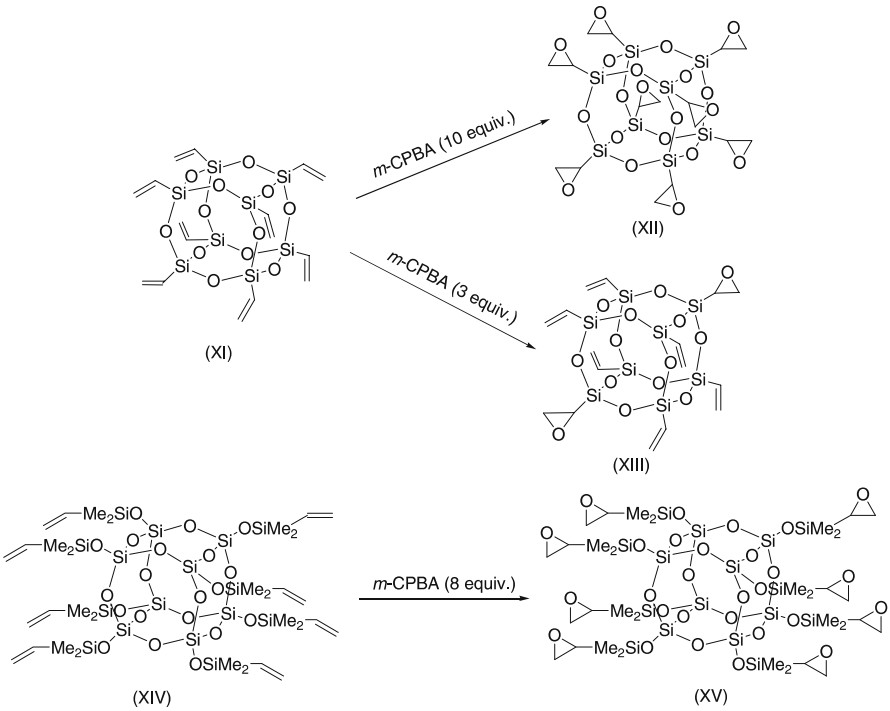

Scheme 4 Scheme of the epoxy-group-containing POSS synthesis by epoxydation of vinyl group [77]

tion. The presence of only two singlets in the ^{29}Si NMR spectrum confirmed that the cubic structure of POSS remained intact during the reaction. FT-IR and microchemical analysis provided further confirmation of the complete reaction of TMI with $Q_8M_8{}^{H}$ [1]. This POSS isocyanate is also suitable for synthesis of other compounds such as organic–inorganic dendrimers or star polymers.

Lichtenhan et al. [23, 24] prepared several monosubstituted POSS epoxides (XIX). The C_3-based chain epoxy (5–9 wt %) was used with 1,4-butanediol diglycidyl ether (BDGE) (XX), diglycidyl ether of Bisphenol A (DGEBA) (XXIII) and polyoxypropylene diamines (XXI) to prepare nano-reinforced epoxy network glasses (Scheme 6) [23].

The addition of a monofunctional POSS epoxy did not alter the shape of the viscoelastic spectrum despite their ability to shift it to higher temperatures. This means that the POSS epoxy nano-reinforcement did not contribute

[1] In silsesquioxane chemistry the symbols M and Q are used to represent framework silicon atoms which possess 3 and 0 organyl substituents, respectively. Subscripts are used to indicate the number of framework silicon atoms with the various designations.

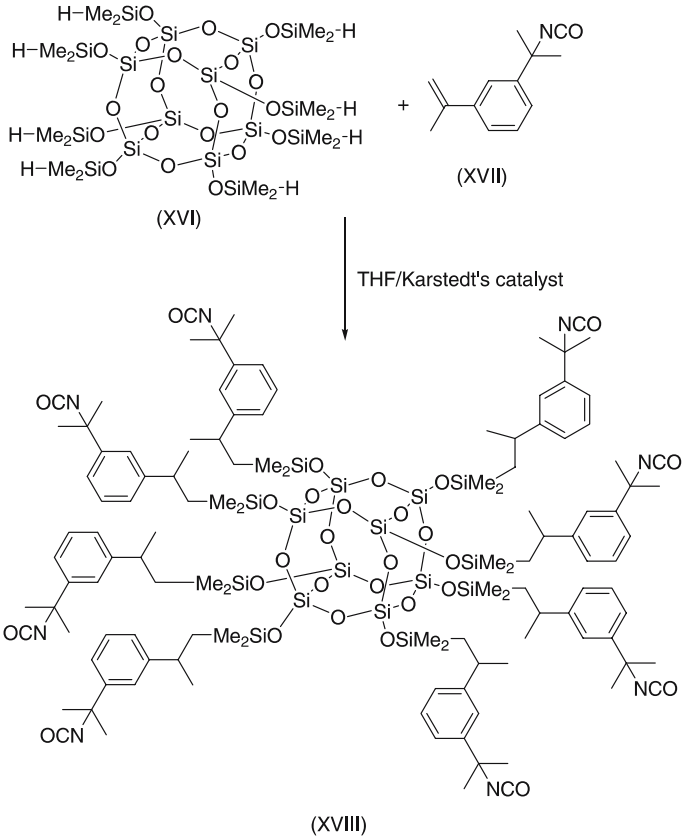

Scheme 5 Scheme for isocyanate-POSS by hydrosilylation of *m*-isopropenyl-α,α'-dimethylbenzyl isocyanate by octakis(dimethylsiloxy)octasilsesquioxane [6]

to the deformation process of the network while enhancing its thermal properties. The C_8-based chains exhibited excellent solubility in organic solvents, such as chloroform, THF, hexane and toluene [24]. The concentrations that can be reached in aliphatic or aromatic epoxides or curatives ranged from only 1 to 5 wt %. The researchers envisaged increasing the solubility of these POSS epoxides in aromatic-based epoxy resins by incorporating compatibilizing, nonreactive aromatic substituents or reactive aromatic epoxy functionalities into the cage and also developing difunctional POSS-epoxy monomers. Even more, the effects of cubes as inorganic crosslinkers was studied by comparing structure of DGEBA/OAPS (octaaminophenylsilsesquioxane) with DGEBA/DDM (diaminodiphenylmethane) structure [7]. The networks consisted of identical DGEBA/aniline segments and only the introduction of fully dispersed rigid silica particles as cube cores caused structural differences. In contrast, octaglycidyldimethylsiloxyoctasilsesquioxane, octaaminophenyl-

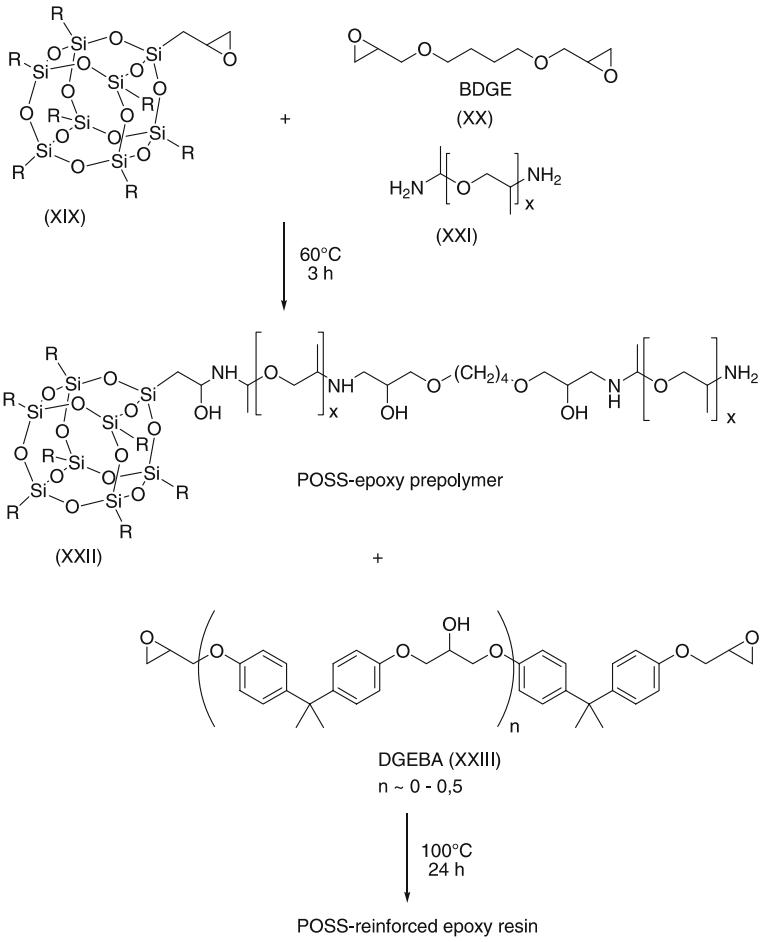

Scheme 6 Schematic representation of the curing cycle of the POSS-epoxy system [23]

silsesquioxane and polyaminophenylsilsesquioxane (OG, OAPS and PAPS, respectively) nanocomposites were used to study the effects of tether lengths on nanocomposite behavior because the OG/OAPS tether lengths were essentially half those of the DGEBA/OAPS or OG/DDM tethers.

Morrison et al. [78] NMR studies of the treated polymer revealed broadening of the resonance associated with the POSS silicon atoms at $\delta = -66$ ppm and a significant resonance at about -58 to -60 ppm, similar to those reported by Feher et al. [79] for the disilanol-functionalized POSS species.

The former indicated that the reaction with the triflic acid had indeed ring-opened a small proportion of the POSS species to produce silanol groups that can be further functionalized. Direct-polarization ^{29}Si NMR experiments indicated that the amount of POSS species reacting was relatively

small (10 vol %) and, although there was no evidence for the location of the reaction because of the relatively large size of the network's pores, it was expected that reaction would have taken place at both external and internal surface sites.

Apparently, one of the first steps in structure–property studies is the identification and characterization of pertinent structural features. The cubic topology of the molecule leads to some interesting opportunities to prepare micro- or mesoporous materials, as it is geometrically difficult to link cubes through only their corners and still fill all available space, although the degree of porosity must depend on the efficiency of polymerization and the flexibility of the organic polymerizable group. Harrison and Kannengisser [80], and, subsequently, Zhang et al. [81] have shown that porous polymers can be prepared by the hydrosilylation of octavinyl-POSS (XV-3) structures with octahydrido-POSS species (XIV-1). They reported polymeric materials (XVI) with high surface areas that showed adsorption isotherms consistent with volumes of the pores in the mesoporous regime (Scheme 7).

Furthermore, the proton NMR spectrum revealed more complicated resonance in the methylene region than would have been expected for the regular structure. This was accounted for by a small amount of addition at the β-position, rather than at the α-position (terminal CH_2) of the POSS vinyl groups. Such scenario has been reported for hydrosilylation under similar conditions revealing that the reaction is often regioselective at the α-position, especially when sterically hindered alkenes are used. However, in certain cases, such as the hydrosilylation of vinylsiloxanes to octahydridopentacyclosiloxanes (octahydrido-POSS) carried out by Bassindale and Gentle [82], there was up to 30% of β addition depending on the catalyst used. In Manson et al.'s [83] POSS system, the problem of β addition was at worst 5%, and could be reduced markedly by careful control of the temperature. High temperature (80 °C), such as that used in work [82], seemed to favor β addition, while lower temperature (room temperature) suppressed this unwanted side reaction. It was proposed that initial mixing of the reactions at ice-bath temperature might also suppress the undesired side reactions even further to the extent that the β addition could be reduced to levels that are generally difficult to quantify by NMR.

Other works on POSS proposed that the spacer cubes are more reactive than nonspacer cubes, based on the gelation times required to prepare the resultant polymers [81]. This characteristic was ascribed to steric effects, where the longer and more flexible $SiMe_2O$ spacers give the functional groups more freedom of movement, thus making them more accessible than functional groups on the nonspacer cubes. However, in hydrosilylation studies with 4-allyloxymethylbenzoate, the $(HSiO_{1.5})_8$ cube was found to be much more reactive than $HMe_2Si-O-SiMe_2H$. It was further noted that, because the Si – H environment in $HMe_2Si-O-SiMe_2H$ resembles that in the spacer cube, a closer look at this reactivity discrepancy was suggested.

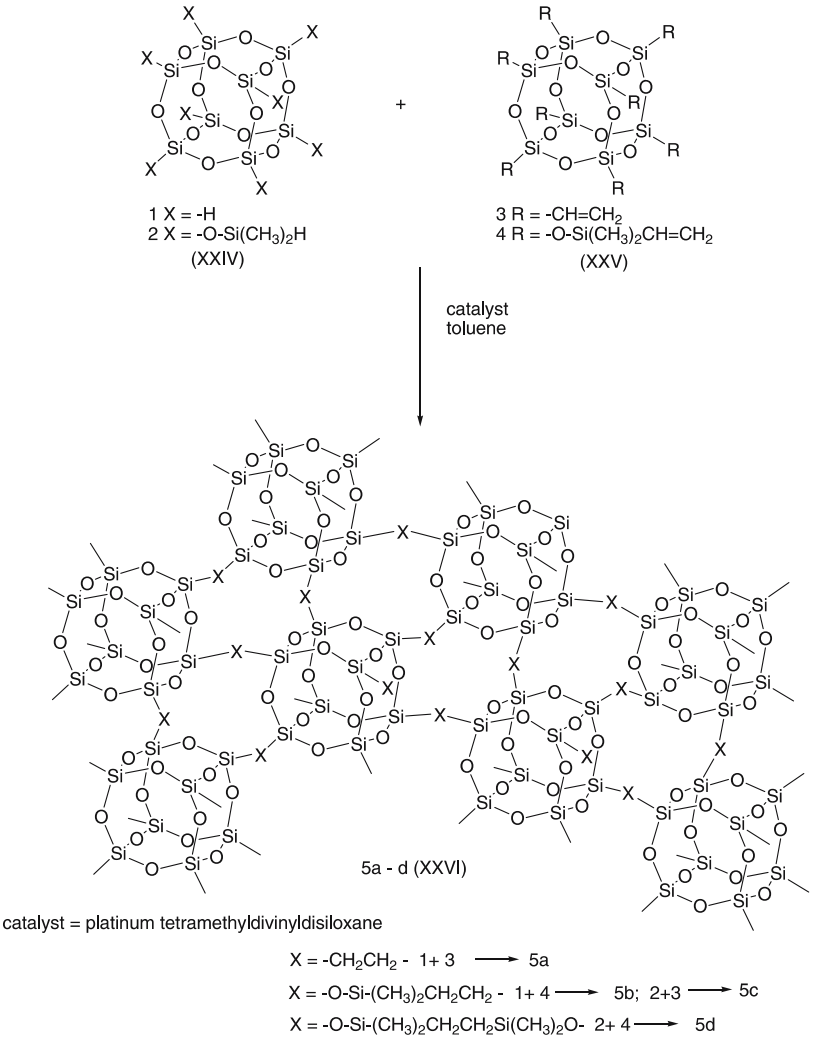

Scheme 7 Copolymerization of multifunctional vinyl POSS macromonomers 3 and 4 by hydrosilylation [81]

Sellinger and Laine [34] presented methacrylate/cube hybrids (XXIX) (Scheme 8) that can act as thermosets or photocurable monomers.

NMR showed substitutions at the opposite vertices of the cube. Although this substitution pattern is likely, no assignments regarding the exact positioning on the cube was made. Additionally, idealized structures indicated only tetrasubstituted hybrids. Differential scanning calorimetry (DSC) studies of freshly prepared tetramethacrylate cubes showed exotherm onsets at 50 °C with maxima at 120 °C, which probably result from inter- and/or in-

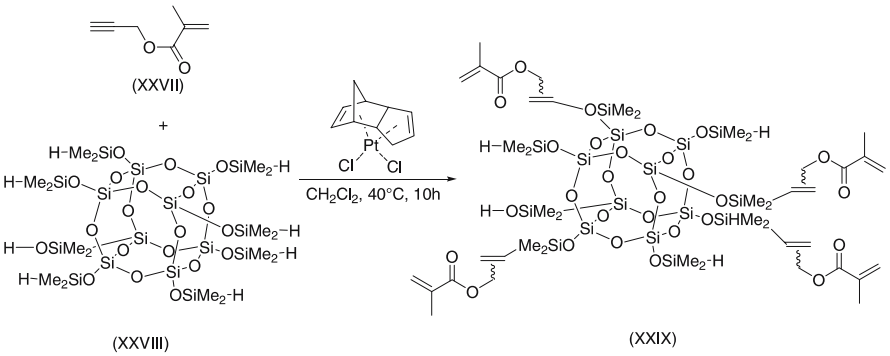

Scheme 8 Synthesis of the methacrylate functionalized POSS [34]

tramolecular alkene/Si – H hydrosilylation [34]. In contrast, the octasubstituted cubes, which had no Si – H bonds, showed exotherm onsets only at 100 °C with maxima at 170 °C due to methacrylate polymerization. Aged samples of the tetrasubstituted cubes or cubes prepared using a Pt/C catalyst showed slight onsets at 50–70 °C with maxima at 120 °C. When active catalyst was added to the aged samples, intense exothermic effects reappeared with onsets at 50 °C. Thus, the initial exotherms likely resulted from Pt-catalyzed hydrosilylation.

No observable thermal events occurred in subsequent heating/cooling cycles. Hydrocarbon-soluble methacrylate-functionalized cubes are highly reactive, viscous liquids that are readily polymerized either thermally or photochemically to produce clear, hard hybrid polymers containing up to 65% silica and thus paved the way for methods of producing novel copolymers.

Generally, POSS cages can be treated as spheres that pack hexagonally in a sequence in which spheres in one layer lie above the interstitial spaces in adjacent layers. Waddon and Coughlin [84] have shown that POSS monomers with alkyl corner units form a family of materials with structural similarities. POSS units with one norbornyl group in place of an alkyl clearly fit into the same pattern. Corner units occupied space in the structure and prevented close-packing of the spheres. When corner units were other than simply hydrogen atoms, the crystal structures had self-similar geometries, which were characterized by the same ratio of lattice parameters. In the case where the corner units were hydrogen atoms, spheres packed more closely and the stackings of adjacent layers were observed to be modified, as indicated by a different ratio of lattice parameters. Transmission electron microscopy (TEM) allowed correlation of the crystal structure with an external crystal habit. This showed the monomer to crystallize as well-defined, plate-like facetted crystals, showing a high degree of crystallographic regularity.

Fu et al. [85] studied the structural development of a unique polyurethane system having inorganic POSS molecules attached to the hard segments as

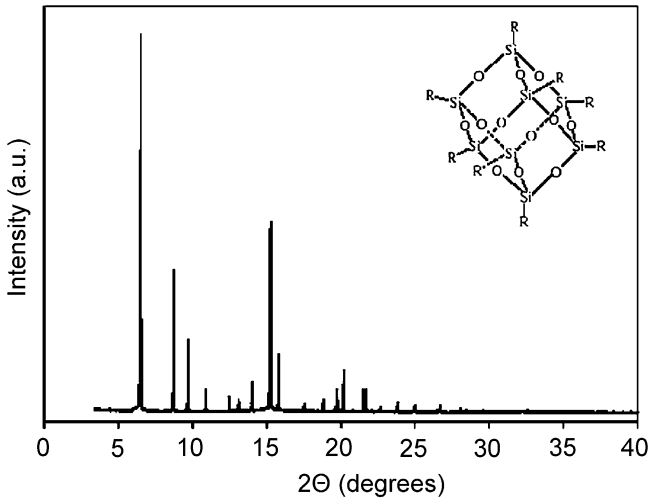

Fig. 2 The X-ray powder-diffraction profile of octacyclohexyl-POSS. The crystal can be indexed by rhombohedral unit cell with $a = 11.57$ Å, $\alpha = 95.58°$ [82]

nanoscale reinforcing agents. One was octacyclohexyl-POSS, which showed a rhombohedral unit cell with $a = 11.57$ Å, $\alpha = 95.58°$ (Fig. 2) while the other was hydrido-POSS, which showed a similar rhombohedral unit cell with $a = 11.53$ Å, $\alpha = 95.38°$.

A systematic X-ray pattern change was observed from POSS monomers to POSS-PU polymers, with an increase in the amorphous fraction and high disordering in the structure.

Simultaneous WAXD and SAXS techniques were applied to reveal the POSS crystal structural and POSS-PU morphological changes under deformation. The WAXD data indicated that POSS molecules formed nanoscale crystals in the hard segment domains. Under stretching, the full-width at half-maximum of the POSS crystal peak was found to decrease, which suggested the destruction of POSS crystals and also the hard segments.

Another hydrolytic condensation reaction resulted in the formation of ammonium-salt-substituted silsesquioxanes. Its free amine adduct was obtained by eluting solutions in ethanol or a 14 : 1 ethanol–water solution across a cation-exchange resin. The resulting free amine silsesquioxane was stable for 1–2 days at 25 °C, but decomposed to an ill-defined T-gel upon prolonged storage at room temperature or when the solvent was removed. Other neutralization led to the destruction of the Si/O framework. It was suggested that the free amine could be used to react with methyl acrylate, followed by an excess of ethylenediamine to produce a second-generation dendrimer that has free amine groups on the surface.

On the other hand, hydrosilylation is an efficient reaction for preparing hybrid crosslinked monomers in high yields from compounds bearing two

or more terminal olefinic moieties [86, 87]. This method has been used for synthesis of alkylene- and heteroatom-functionalized bridging groups. The addition of the Si – H groups in trichlorosilane or trialkoxysilanes is generally catalyzed with a noble-metal-containing catalysts, such as chloroplatinic acid or Karstedt's or Spier's catalyst. To cite a few good examples, methacrylate-functionalized cubes have been synthesized via Pt-catalyzed hydrosilylation of propargyl methacrylate [88, 89] with $(HSiO_{1.5})_8$ and $(HMe_2SiOSiO_{1.5})_8$. The propargyl route eliminates side reactions found with allyloxy chemistry [90].

It has been found that propargyl groups reacted in preference to methacrylate groups in Pt-catalyzed hydrosilylation, as modeled using triethylsilane [91]. Further, tetramethacrylate cubes have been reported as being photochemically curable by using visible light and free-radical initiators [34]. For example, the cubes, when mixed with camphorquinone (0.15 wt %), cure almost instantaneously in the presence of visible light (450 nm), forming clear, hard, crosslinked materials insoluble in common solvents. In addition, both compounds cured at 100 °C without initiator to produce clear, abrasion-resistant coatings.

Synthesis of the POSS macromonomer has also been successful via incompletely condensed trisilanol $(c\text{-}C_5H_9)_7Si_7O_9(OH)_3$ (XXX) prepared at 29% yield by the hydrolytic condensation reaction of cyclopentyltrichlorosilane in refluxing aqueous acetone [92]. The obtained trisilanol and triethylamine were dissolved in THF. The solution was cooled in an ice bath, and (3-acryloxypropyl)trichlorosilane (XXXI) in THF was added slowly to the mixture (Scheme 9).

The resulting solution was stirred at room temperature overnight. After the removal of insoluble salt by filtration, the filtrate was concentrated and poured into acetonitrile. The white precipitate was collected by filtration and dried in a vacuum to produce a solid material (XXXII).

To sum up, octakis(3-hydroxypropyldimethylsiloxy)octasilsesquioxane (OHPS) has also been synthesized by direct hydrosilylation of allyl alcohol with octakis(dimethylsiloxy)octasilsesquioxane, $(HSiMe_2O)_8Si_8O_{12}$

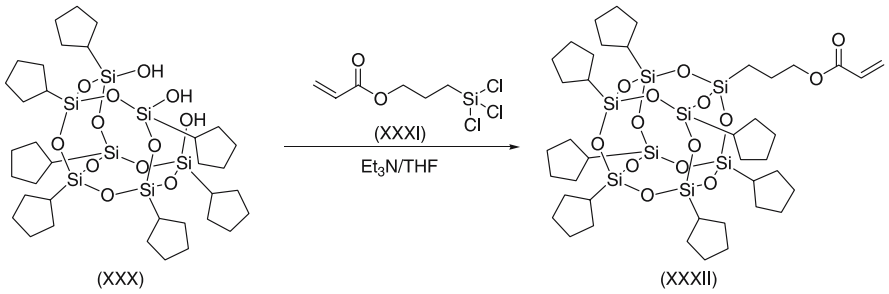

Scheme 9 Synthesis of the methacrylheptacyclopentyl-POSS [92]

($Q_8M_8{}^H$), using platinum divinyltetramethyldisiloxane (Pt(dvs)) as a catalyst [93]. It was proposed that direct hydrosilylation of $Q_8M_8{}^H$ with 2-allyloxyethanol also proceeds primarily *via* C- rather than O-silylation. In contrast, compounds such as 1,3,5,7-tetramethylcyclotetrasiloxane, 1,1,3,3-tetramethyldisiloxane (TMDS) or terminal Si – H functionalized poly(dimethylsiloxane) (PDMS-H, $M_w = 400$) gave significant amounts of O-silylation along with C-silylation. Initial catalyst concentration studies suggested that the catalytic cycle requires the intermediacy of Pt cluster complexes in contrast to recent studies on the mechanism of hydrosilylation that suggested monometallic complex catalysis. Even further, octakis(3-methacryloxypropyldimethylsiloxy)octasilsesquioxane (OMPS) was found to be easily prepared directly from OHPS. Previous unwanted polymerization that accompanies hydrosilylation of allyl or propargyl methacrylates was eliminated. Preliminary polymerization studies showed that OMPS readily polymerizes under UV light to give a crosslinked nanocomposite.

POSS reagents containing not more than one or two points of functionalization are desirable for the design of linear polymeric POSS systems. An efficient method for preparing such reagents involves the corner-capping of incompletely condensed POSS trisilanols $R_7T_7(OH)_3$. Corner capping of the POSS trisilanol can be carried out using a variety of trichlorosilane coupling agents to produce fully condensed T_8-POSS silicon–oxygen frameworks. Schwab et al. [94] synthesized POSS molecules $(SiO_{3/2})_n$ ($n = 8$, cage-like), with the cyclohexyl corner group, of $M_w > 1000$. This molecule was considerably larger than the regular size of polyurethane hard domains and was later used to produce a POSS-PU system in different work that resulted in a nanocomposite [95].

Lichtenhan and coworkers [96] have also used the functionalization method to prepare octameric T_8-POSS reagents in which only one corner is functionalized with a graftable or polymerizable group, leading to families of functionalized POSS R_7T_8-acrylic, α-olefin and -silane reagents suitable for the preparation of linear POSS polymers that have been prepared in this manner. Typically the macromonomers were prepared by dissolving POSS triols and triethylamine in THF. The solution was cooled in an ice bath, and a THF solution of (3-methacryloxypropyl)trichlorosilane was added dropwise over a 5-min period to the stirred solution. The mixture was allowed to warm to room temperature and reacted for 12 h. The reaction was then filtered to remove Et_3N – HCl, and the filter cake was washed with THF.

Removal of volatiles under reduced pressure and ambient temperature afforded a yellow solid that was subsequently dissolved in a minimum amount of benzene and precipitated into acetonitrile at five-fold excess. After filtration and drying under vacuum, the yield of POSS polymer white powder was 94%.

5
Synthesis of POSS-Containing Polymers

As a new paradigm, incorporation of POSS cages into polymers often results in interesting improvements in the materials' properties, including increases in use temperature, oxidation resistance and surface hardening, resulting in improved mechanical properties, as well as reductions in flammability and heat evolution [97]. Several works have focused on developing a repertoire of functionalized octahedral silsesquioxane (cube) macromonomers as a starting point for formulating nanocomposites with the objective of determining whether well-defined monomer/composite nanostructures and periodically placed organic/inorganic components might offer novel and predictable properties [7, 17, 19].

Apparently, when chain polymerization is performed, the inorganic part of the organically functionalized nanobuilding blocks plays the role of a side group or a crosslinking knot that does not participate in the chain construction. Depending on the chemical nature of the functionalities, the choice of synthesis mode definitively turns the expected structure and properties of the hybrid material toward those of polycondensates and related macrostructures or toward those of vinyl-type polymers [8]. Also, homopolymerization is a useful tool for obtaining materials in which properties reflect those of the precursor, whereas copolymerization broadens the field of possible structures with potential synergies between the organic backbone and inorganic side groups. For most technological uses and handling purposes, the nanoparticles have to be processed in bulk or as films, yet they must still exhibit their nanoscale-dependent properties, such as quantum dot, band-gap reduction, plasma resonance, nanomagnetism and superparamagnetism.

It is therefore possible that many nanocomposites using functionalized POSS derivatives with traditional polymers may be designed. For instance, a wide variety of octafunctional cubes has been prepared with polymerizable moieties that offer access to highly crosslinked thermosetting nanocomposites having controlled porosities with high surface areas [81], novel mechanical properties [81, 98–100], high thermal stabilities [101] and many other enhancements, such as ranging from dielectric properties to catalytic effects. In a complementary fashion, POSS materials offer access to robust thermoplastics with good-to-excellent properties including resistance to atomic oxygen [102–104]. Such enhancements have been shown to apply to a wide range of thermoplastic and a few thermoset systems based on methacrylates, styrene, norbornene, siloxanes and vinyl esters as well as epoxies [20, 21, 96, 105–109]. The synthesis of POSS monomers and their incorporation into the respective polymer systems has been demonstrated recently. A few examples of such synthetic processes are given in the following subsections.

In a few words, the synthetic approaches can be presented as condensation polymerization, ring-opening metathesis polymerization and free and

controlled/living radical polymerization [15, 26, 95, 96, 102, 110–113]. The nanobuilding block approach aims to create nanoparticle-based hybrid materials, however it includes the introduction of already synthesized nanoparticles into polymer or organic hosts, synthesizing the nanoparticles inside such matrixes, connecting particles with adequate organic spacers and polymerizing functionalized nanoparticles [8, 95, 105, 114].

5.1 Free Radical Polymerization

Monomethacrylate-functionalized POSS reagents are capable of being polymerized into novel linear silsesquioxane-based materials. Efforts to copolymerize these methacrylate-functionalized POSS with other acrylic comonomers have been successful [96, 112]. In a typical polymer synthesis, a 0.5 M toluene solution of macromonomer was prepared, to which 2,2′-azobis(isobutyronitrile) (AIBN) based on macromonomer was added from a stock solution. The clear solution was heated at 60 °C for 24 h and then precipitated into methanol. Further purification was performed by reprecipitation from toluene into methanol to yield white powder.

Conventional radical polymerization was engaged on investigations of organic–inorganic star-shaped polyoxazolines using octafunctional silsesquioxane as an initiator whereby the hybrid terpolymers with various POSS compositions were synthesized [92]. The 4-vinyl-4′-methyl-2,2′-bipyridine (VMB) in hybrid terpolymers was fixed at 10 mol % in the feed ratio. The *N*,*N*-dimethylacrylamide, VMB, POSS macromonomer and AIBN were dissolved in toluene (15% solution) under nitrogen. After bubbling with dry nitrogen gas for 5 min to release oxygen, the monomer solution was stirred at 60 °C for 2 days. After polymerization, the polymer was precipitated as a pale yellowish solid in an excess of hexane and dried under vacuum.

Recent advances in controlled/living radical polymerization as in the works of Matyjaszewski [115, 116] have offered a versatile tool to prepare model copolymers from a wide range of monomers such as styrenes or (meth)acrylates, enabling investigation of structure–property relationships [117]. In analogy to controlled/living cationic polymerizations, radical polymerizations can become controlled under conditions in which a low, stationary concentration of the active species is maintained and a fast, dynamic equilibrium is established between the active and dormant species. Such advances have been demonstrated by the ability to introduce methacrylate functional POSS monomers into polyacrylate materials for the synthesis of well-defined star diblock and ABA triblock copolymers using atom-transfer radical polymerization (ATRP) [118–121]. In these block copolymers, POSS moieties are attached to the copolymer backbone as pendant side-chain groups. In one of such work on POSS-containing ABA triblock copolymers, ATRP enabled the preparation of well-defined model copolymers possessing

a rubbery poly(*n*-butyl acrylate) (pBA) middle segment and glassy poly(3-(3,5,7,9,11,13,15-heptaisobutyl-pentacyclo(9.5.1.1^{3,9}.1^{5,1}5.1^{7,13})-octasiloxane-1-yl)propyl methacrylate (p(MAPOSS)) outer segments. By tuning the relative composition and degree of polymerization (DP) of the two segments, phase-separated microstructures were formed in thin films of the copolymer.

Elsewhere, poly(acetoxystyrene-*co*-isobutylstyryl-POSS)s (PAS-POSS) hybrid nanocomposites were prepared by a free-radical polymerization method [123]. The polymerization reactions were carried out under nitrogen using a vacuum-line system. A typical reaction example of experimental procedure for these polymers involved polymerization of acetoxystyrene and isobutylstyryl-POSS-monomers in dried toluene using the AIBN initiator (1 wt % based on monomer) at 80 °C under nitrogen atmosphere for 24 h. The product was then poured into excess cyclohexane under vigorous agitation to precipitate the copolymer, followed by purification in THF/cyclohexane and drying in a vacuum oven to afford a characteristic average of 40 wt % yield.

In another interesting development, Yei et al. [124] prepared POSS-polystyrene/clay nanocomposites using an emulsion polymerization technique. The emulsion polymerization for both the virgin polystyrene and the nanocomposite started with stirring a suspension of clay in deionized water for 4 h at room temperature. A solution of surfactant ammonium salt of cetylpyridinium chloride or POSS was added and the mixture was stirred for another 4 h. Potassium hydroxide and sodium dodecyl sulphate were added into the solution and the temperature was then raised to 50 °C. Styrene monomer and potassium persulfate were later on added slowly to the flask. Polymerization was performed at 50 °C for 8 h. After cooling, 2.5% aqueous aluminium sulphate was added to the polymerized emulsion, followed by dilute hydrochloric acid, with stirring. Finally, acetone was added to break down the emulsion completely. The polymer was washed several times with methanol and distilled water and then dried overnight in a vacuum oven at 80 °C. The obtained nanocomposite was reported to be exfoliated at up to a 3 wt % content of pristine clay relative to the amount of polystyrene.

In another work aimed at the preparation of POSS thermosets vinyl ester-POSS nanocomposite were synthesized [108]. First, multifunctional POSS nanoparticles, $((C_6H_5CHCHO)_4(Si_8O_{12})(CH=CHC_6H_5)_4)$, were dissolved in styrene to produce a transparent solution that was later mixed with a commercial vinyl ester resin to produce a clear, transparent solution containing 50 wt % styrene. Methyl ethyl ketone peroxide and cobalt naphthanate were added to the solution. The total formulation was then put into a mould without degassing and cured at room temperature for 24 h followed by postcuring in an oven at 90 °C and then by a further 5 h at 150 °C to afford vinyl ester-POSS multifunctional nanocomposite.

5.2 Polyaddition and Polycondensation

Choi and coworkers [7] synthesized epoxy-functionalized cube nanocomposites that were prepared from octaaminophenylsilsesquioxane (OAPS), PAPS, octa(dimethylsiloxypropylglycidyl ether) silsesquioxane (OG), DGEBA and diaminodiphenylmethane (DDM). In processing DGEBA/OAPS and DGEBA/PAPS nanocomposites, a variable *N* was first defined as the molar ratio of NH_2 (in OAPS) to epoxy groups (in DGEBA). A conventional stoichiometric ratio of 2 mol of epoxy to 1 mol of amine would occur at $N = 0.5$.

Later, OAPS/PAPS powder was weighed into a glass vial containing a magnetic stir bar. THF was then added to the vial and the OAPS/PAPS dissolved completely on stirring. DGEBA was then added to the solution and the mixture was stirred to give a homogeneous solution. The dark yellow, transparent solution was then transferred into an aluminium mould preheated to 50 °C. THF was slowly removed under vacuum at this temperature. Following removal of solvent after 30 min, the mixture was cured for 12 h at 50 °C, then 6 h at 100 °C, and finally 6 h at 150 °C under N_2, resulting in complete curing [125]. Similar works on OG/OAPS and OG/PAPS nanocomposites also involved the definition of *N* and a similar synthesis procedure as in the DGEBA/OAPS and DGEBA/PAPS nanocomposites as described above, except for the cure conditions because of the poor miscibility of OAPS/PAPS with OG.

Earlier results had demonstrated that the architecture of the organic tethers between vertices can be manipulated to optimize rigidity, processability and resulting thermomechanical properties [126, 127]. One of the works focused on imide nanocomposites prepared from OAPS (XXXIII) as a model nanobuilding block for rigid, high-temperature hybrid nanocomposite materials [126]. The OAPS units were linked from the NH_2 to the NH_2 vertex by reaction with various dianhydrides to form three-dimensional nanocomposites (Scheme 10).

Studies were then initiated using an extreme tether structure with zero flexibility prepared by solvent casting and then curing mixtures of OAPS with pyromellitic dianhydride (PMDA) (XXXIV) at 330 °C. The resulting materials (XXXV) were claimed to be extremely brittle such that it was difficult to take thermomechanical property measurements. Tether rigidity, length and crosslink densities were then modified using reactions of OAPS with oxydiphthalic anhydride (ODPA) and diluting with oxydianiline (ODA) to adjust nanocomposite stiffness. In Tamaki et al. [127], the synthesis of novel three-dimensionally structured polyimide by reaction of OAPS with PMDA was performed successfully. With model studies with phthalic anhydride provided useful cure conditions, stoichiometrically correct OAPS/PMDA nanocomposites were obtained following curing of *N*-methyl-2-pyrrolidone (NMP) and dimethylformamide (DMF) reaction solutions at lower temperatures and then

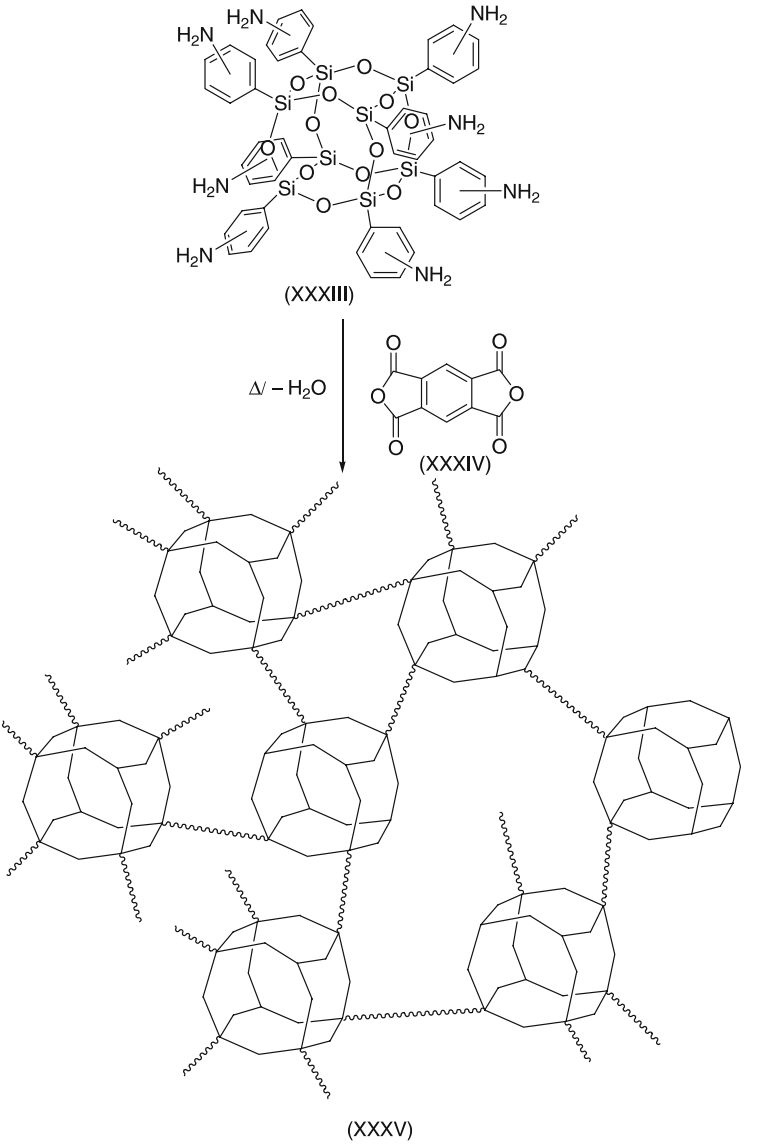

Scheme 10 Reaction of OAPS with pyromellitic dianhydride (PMDA) to form a nanocomposite with completely rigid imide tethers between cube vertices [126]

to > 350 °C under vacuum. The resulting materials offer thermal stabilities in air and N_2 of > 500 °C (5% mass-loss temperature) and char yields > 75% under nitrogen.

Another interesting work employed Schwab et al.'s [94] synthesis method to investigate the derivative of a POSS molecular structure $(SiO_{3/2}R)_8$ con-

taining R = cyclohexyl (octacyclohexyl-POSS) with one corner group substituted by a hydridomethylsiloxy group (hydrido-POSS) and a 3-(allylbisphenol-A) propyldimethylsiloxy group (BPA-POSS), thus obtaining POSS-polyurethane (POSS-PU) containing 34 wt % POSS molecules [95]. The BPA-POSS compound was a diol, which was used in the polyurethane synthesis as a chain extender. The POSS-PU used contained soft segments of poly(tetramethylene glycol) (PTMG), hard segments of 4,4′-methylenebis (phenyl isocyanate) (MDI) and BPA-POSS.

In another development, a rapid and versatile synthetic approach towards the study of $FeCl_3$-catalyzed hydrolytic polycondensation of suitable trichlorosilanes in a biphasic system, which yielded octasilsesquioxane $(BrCH_2CH_2CH_2)_8Si_8O_{12}$, was presented [1]. The work proposed that, depending on the functional group R attached to the T_8 cage, crosslinking of the monomeric building blocks could be carried out in different ways. Also, in the case of alkenyl-octasilsesquioxanes ($R = CH_2 = CH$- or $CH_2 = CH - CH_2$-), connection of the Si_8O_{12} units may be possible via polymerization or copolymerization with typical organic monomers such as vinyl acetate or acrylate.

In investigations of PU-POSS nanocomposite, pendant POSS were introduced through polycondensation reactions for segmented polyurethane-based elastomers [85]. The nanobrick $(HMe_2 - SiO)(c\text{-}C_6H_{11})_7Si_8O_{12}$ (XXXVI) was first grafted by hydrosilylation of 3,3′-diallylbisphenol A (XXVII) and then copolycondensed with poly(tetramethyleneglycol) and 4,4′-methylenebis (phenyl isocyanate) (MDI) (Scheme 11).

The inorganic nanobuilding blocks were found to be attached to the hard segments and greatly enhanced the tensile modulus and strength of the elastomer. Haddad et al. [111] and Fu et al. [128] have similarly provided works on condensation polymerization. The well-defined functionalized POSS have been prepared by the hydrosilylation reaction of terminal olefins with octahydridosilsesquioxane or direct hydrolytic condensation reactions of silane-bearing compounds [75, 100, 129]. However, clear explanation on the mechanism of direct hydrolytic condensation reaction has not been explored yet.

In a different work, octakis(3-methacryloxypropyldimethylsiloxy)octasilsesquioxane (OMPS) was easily prepared directly from octakis(3-hydroxypropyldimethylsiloxy)octasilsesquioxane (OHPS). Previous unwanted polymerization that accompanies hydrosilylation of allyl or propargyl methacrylates was first eliminated [93]. OHPS cube was first put into a Schlenk flask equipped with an addition funnel, a reflux condenser, and a magnetic stir bar. CH_2Cl_2 was then added to dissolve the OHPS followed by triethylamine addition and the mixture was cooled in an ice bath, followed by stirring for 15 min. Methacryloyl chloride was later added dropwise through the addition funnel. A light-pink precipitate of triethylammonium chloride formed on adding the methacryloyl chloride. After all the methacryloyl chloride was added, the reaction was further stirred at room temperature for 2 h. To isolate the methacrylate product, the reaction mixture was first filtered, and then the

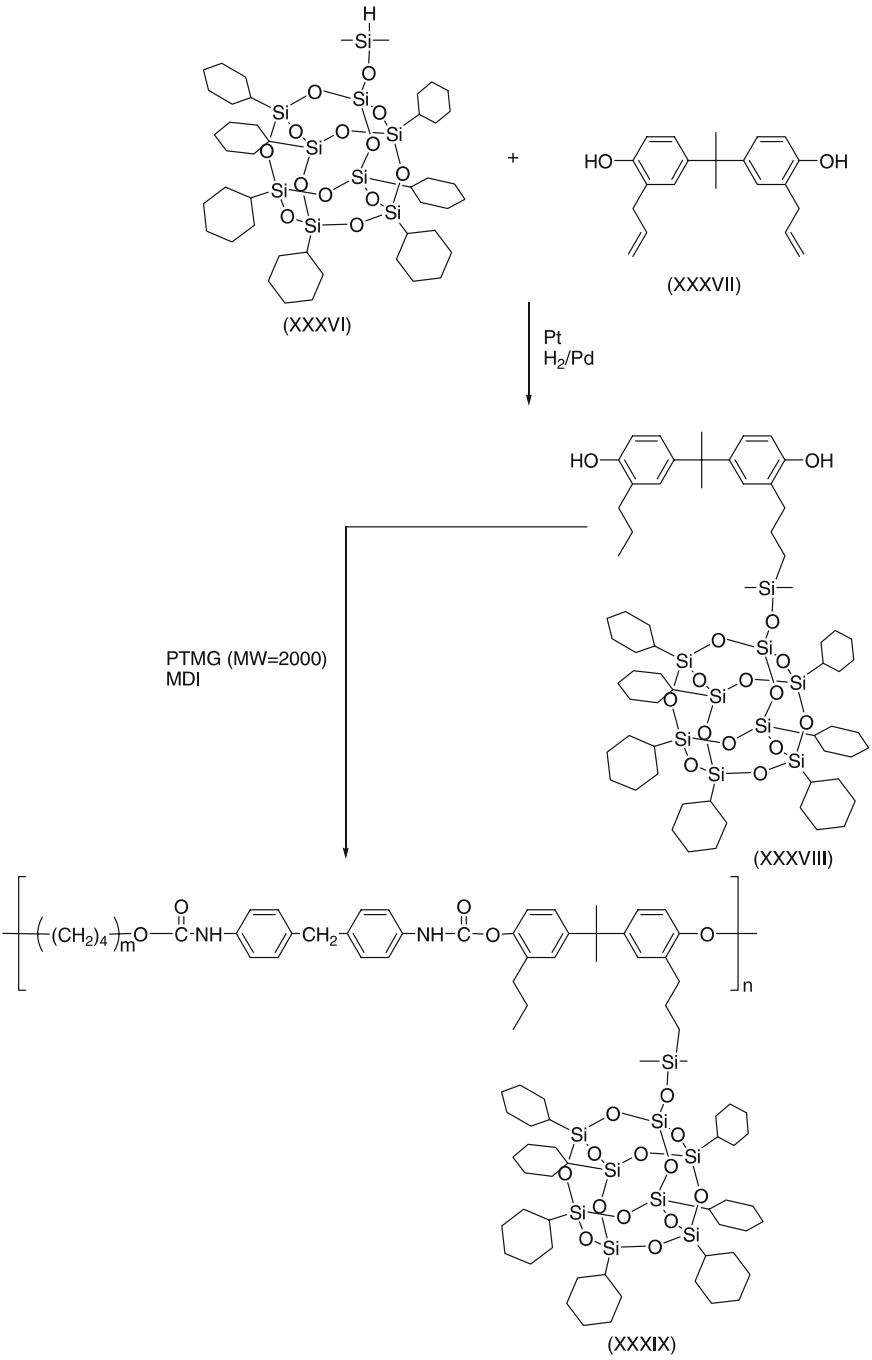

Scheme 11 Schematic diagram of the synthesis for POSS-polyurethane nanohybrid polymer [85]

filtrate was transferred to a separatory funnel and washed with water three times, 5% $NaHCO_3$ solution twice, 0.5 N NaOH twice, and lastly brine once. The solution was then dried over Na_2SO_4. Removal of the solvent gave OMPS as a clear, yellowish, slightly viscous oil that readily polymerized under UV light to give a crosslinked nanocomposite.

Tanaka et al. [101] synthesized octa(aminophenyl)silsesquioxane (OAPS), an aromatic amine-functionalized silsesquioxane free from aliphatic components. OAPS reacts rapidly with the 2-pyridinecarboxaldehyde under mild conditions, giving an imine that emits green light under UV illumination.

Leu et al. [130, 131] have demonstrated that covalently tethering nanoporous POSS to presynthesized polyimide chain ends or the side chains results in organic–inorganic nanocomposite materials with low dielectric constant and controllable mechanical properties. Recent work by this team of researchers reported on polyimide-tethered nanocomposites with well-defined architectures that were prepared by the copolymerization reaction of a new type of diamine monomer: POSS-diamine, 4,4′-oxydianiline (ODA), and pyromellitic dianhydride (PMDA) [132]. In the synthesis of poly(amic acid) (PAA), PMDA-ODA was first synthesized by first putting ODA into a three-necked flask containing NMP/THF under N_2 purge at 25 °C. Then, after the ODA had dissolved completely, PMDA, divided into three batches, was added to the flask batch-by-batch with a time interval of 0.5 h between batches. When PMDA had completely dissolved in the solution, the solution was stirred continuously for 1 h, and a viscous PAA solution was obtained. The mixture was then mixed for an additional 12 h using a mechanical stirrer. PMDA-ODA/POSS-diamine(copoly(amic acid)) was synthesized in a similar process except that various proportions of POSS-diamine were added. The PAA of PMDA-ODA and PMDA-ODA/POSS-diamine mixture were later cast onto glass slides and subsequently put in a vacuum oven at 40 °C for 48 h before the imidization step. Imidization of PMDA-ODA and POSS-PMDA-ODA was carried out by putting the samples in an air-circulation oven at 100, 150, 200, and 250 °C for 1 h and then at 300 °C for 0.5 h to ensure complete imidization. The polyimide-side-chain-tethered POSS nanocomposites presented self-assembly characteristics when the amount of POSS exceeded 10 mol %. Furthermore, POSS/polyimide nanocomposites had both lower and tunable dielectric constants, with a lowest value of 2.3, and controllable mechanical properties, compared to that of pure polyimide.

5.3
Ring-Opening Metathesis Polymerization (ROMP)

Jeon et al. have recently reported on ring-opening metathesis copolymerizations of cyclooctene and the POSS-norbornylene monomer performed with Grubbs's catalyst. Random copolymers were then formed and fully charac-

terized with POSS loadings as high as 55 wt %. Diimide reduction of these copolymers afforded polyethylene-POSS random copolymers [102].

The homopolymer of POSS-norbornyl was also synthesized and presumed to have a rigid backbone (Scheme 12).

Norbornyl–POSS hybrid copolymers having either cyclohexyl corner groups (c-C_6H_{11}-POSS) or cyclopentyl corner groups (c-C_5H_9-POSS) showed shape-memory effect. Samples containing 50 wt % of POSS macromonomer were mechanically drawn at temperatures above their glass-transition temperatures, followed by rapid quenching in liquid N_2. Interestingly, the types of corner groups in the POSS macromonomer affect the shape-memory behavior, with the c-C_6H_{11}-POSS copolymer showing lower percentage recovery

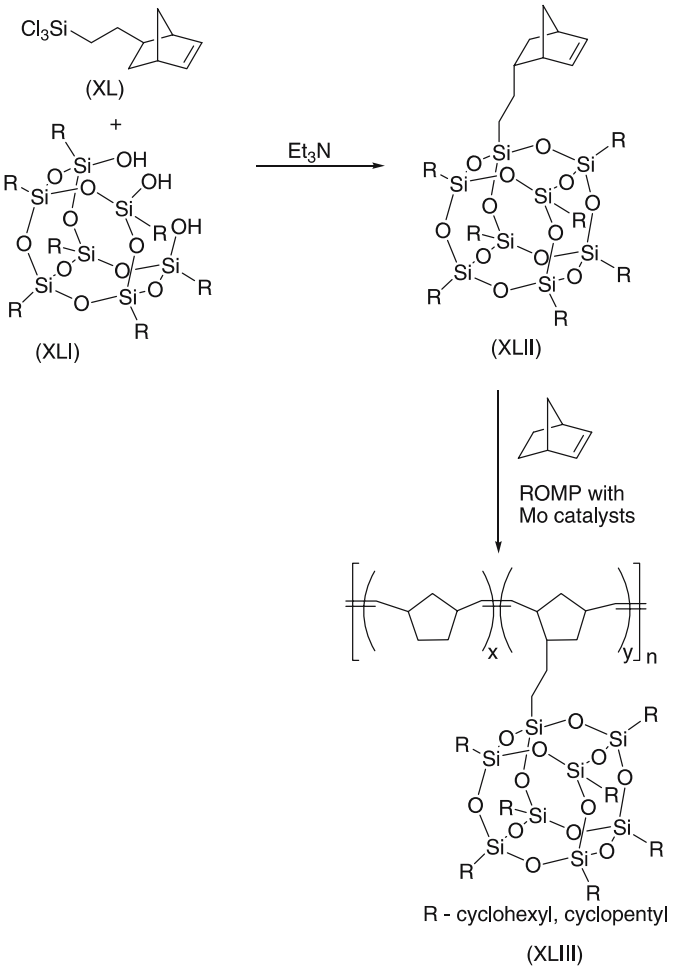

Scheme 12 Scheme of the polynorbornene-POSS copolymers synthesis [102]

than the *c*-C_5H_9-POSS copolymer due to enhanced aggregation of *c*-C_6H_{11}-POSS macromonomers. Additionally, incorporation of POSS comonomers within the polymer system was found to slightly reduce the percentage recovery, while improving thermal stability significantly [102].

In another work, Mather et al. [26] prepared random copolymers of norbornene/POSS-norbornene for microstructural and mechanical relaxation investigations. The POSS-norbornyl monomer was prepared by reaction of ethyl-trichlorosilane-substituted norbornene with cyclohexyl (*c*-C_6H_{11}-) or cyclopentyl (*c*-C_5H_9-) POSS triol in the presence of triethylamine. The random copolymers were synthesized under nitrogen using the ROMP catalyst, $Mo(C_{10}H_{12})(C_{12}H_{17}N)(OC_4H_9)_2$, in chloroform with various proportions of norbornene and the POSS-norbornyl derivatives (Scheme 12). The polymerizations were designed to yield polymers with degrees of polymerization of 500 by controlling the ratio of monomers to catalyst. The reactions were terminated by the addition of benzaldehyde. The polymers were later precipitated and purified by adding the chloroform solutions to a large excess of methanol and collecting the precipitate resulting in random copolymers in yields over 90%.

Kobayashi et al. [74] and Kim et al. [75] have also studied a wide variety of functional materials based on ring-opening polymerization of 2-methyl-2-oxazoline, which is a good candidate for living polymerization because the obtained polyoxazoline has advantageous properties, such as hydrophilicity and good compatibility with common organic polymers. Liquid-crystalline silsesquioxanes having various mesogenic moieties were synthesized by hydrosilylation reaction of octa(hydridosilsesquioxane) and terminal alkenes with mesogenic groups using hexachloroplatinic acid as a catalyst [75]. In a typical synthesis, octa(5-(4-methoxybiphenyloxy)pentyl)-octasilsesquioxane (cubic-OCH_3) was prepared. Hydridosilsesquioxane was dissolved in distilled 1,2-dichloroethane. The mixture was then stirred, and methoxybiphenyloxy-1-pentene and 1,2-dimethoxyethane solution of $H_2PtCl_6 \cdot 6H_2O$ were added. The reaction mixture was later refluxed for 24 h under nitrogen. The white precipitate appeared when the solution was cooled down to room temperature. The white crude product was recrystallized from 1,2-dichloroethane.

Most recently organic–inorganic hybrid thermoset copolymers have been prepared by ring-opening metathesis polymerization catalyzed with bis(tricyclohexylphosphine)benzylideneruthenium(II) dichloride [133]. Dicyclopentadiene (DCPD) and norbornenylethyl polyhedral oligomeric silsesquioxane (1NB-POSS) and tris(norbornenylethyl)-POSS (3NB-POSS) with isobutyl pendent groups have been copolymerized at 60 °C over a range of POSS loadings. For example, in a typical reaction, the reaction mixture for PDCPD-*co*-1NB-POSS with 20 wt % added POSS was composed of DCPD, 1NB-POSS, triphenylphosphine (PPh_3) in benzene and the catalyst-bis(tricyclohexylphosphine)benzylideneruthenium(II) dichloride in benzene. The addition of

PPh_3 was necessary to reduce the activity of the catalyst to allow sufficient time to fill the molds before gelation. Plaques were made by mixing the reactants in a beaker and pouring into a mould. The mould was placed into an oven at the cure temperature (60 °C) for 24 h and postcured at 100 °C for 4 h. Compression samples were made in a similar fashion in which the DCPD/POSS was poured into test tubes and cured as stated. It is important to note that the 1NB- and 3NB-POSS copolymers were synthesized from different lots of DCPD, and slight changes in the physical properties of the homopolymers were observed such that each POSS copolymer system could be compared to the PDCPD homopolymer cured from the same lot. In conclusion, the synthetic methodology allowed for synthesis of covalently bonded and well-dispersed inorganic moieties. At high 1NB-POSS loadings aggregates of approximately three to four POSS molecules were found, while 3NB-POSS remains uniformly dispersed over all loadings.

6
Synthesis of POSS-Dendrimer Cores

Dendrimers are molecules with a globular structure in which well-defined branches radiate from a central core, becoming more branched and crowded as they extend out to the periphery. Since the first successful synthesis of a symmetrical branched dendrimers [134], this class of polymers has received considerable interest, with possible applications ranging from drug-delivery agents, micelle mimics, nanoscale building blocks to high-performance polymers [134–137]. For example, the use of octafunctional POSS cores provides an easy route to highly functional dendrimers molecules. They may also be advantageous in tuning the properties of the dendrimer to suit the environment in which a particular application will occur.

Much of the interest in polyhedral silsesquioxane molecules in polymer chemistry is in their use as "hard blocks" to modify the thermal and mechanical stability of materials [114]. The use of POSS molecules in dendrimers should have a similar effect, leading to dendrimers with different properties from those based on, for example, tetravinylsilane cores. The properties of the dendrimers can also be altered by changing the length of the carbon chain between branching silicon atoms by using different alkenyl Grignard reagents in the alkenylation step. This will have a marked effect on the physical characteristics of the molecules, especially their size and the number of generations that can be synthesized before surface congestion becomes the size-limiting factor. Dendrimers are therefore almost certainly foreseen to play an important role in any catalytic utility of these molecules, affecting, e.g. the selectivity of a catalyst [135].

Dendrimers are generally prepared using two approaches: a divergent method, where successive dendrimer layers or generations are added to

a core, and a convergent method, where the arms of the dendrimer are synthesized first and subsequently attached together at a focal point to produce the final molecule. A major drawback with dendrimer synthesis, especially in the divergent method, is that it often requires many repetitive steps in order to build the dendrimer outwards leading to multiple steps that often result in low-yield preparations. However, initiative work by Jaffres and Morris [135] sorted out this problem by preparing POSS-dendrimers that can be used as supports for catalysts, combining a high number of active sites on the exterior of the molecule with the possibility of separating the catalyst from the reaction mixture using ultrafiltration techniques, so taking advantage of the relatively large size of the dendrimers to produce a molecule that combines the advantages of homogeneous and heterogeneous catalysts while minimizing the disadvantages of each. Since then, significant progress have been seen in the synthesis of POSS-dendrimers as shown in the follows.

6.1 Convergent Method

Several approaches to the production of dendrimers have been successfully developed. Of these methods, the convergent growth strategy couples together groups that will ultimately become the peripheral surface of the macromolecule to form wedge-shaped units termed dendrons [138, 139]. The dendrons are in turn coupled with multifunctional monomers to produce higher-generation dendrons that are finally reacted with a central core molecule to form the desired monodisperse dendrimer system of defined generation number and unique molecular weight. The convergent growth method allows for the production of monodisperse dendrimers by taking advantage of the relative ease of separation of the intermediate dendrons at each growth step and in the final coupling of the dendrons to the central core.

In addition, a wide variety of surface functionalities can be incorporated into the final structure by utilizing suitable molecular components at the outset of the convergent dendrimer synthesis or by deriving structures from the coupling of several different dendrons to the central core. Investigation involves the inclusion of recognition sites or chirality into the dendritic architecture with a long-term goal of ultimately developing soluble reaction supports for use in a clean chemical processes [140].

This approach has also been employed for synthesis of highly enantiomerically enriched cyclic silanes with silicon-centered chirality [141]. Zhang et al. [142] prepared second-generation dendrimers based on polyhedral silsesquioxane cores with up to 72 terminal groups at their surface (Scheme 13).

Repetitive hydrosilation/allylation of vinyl-functionalized polyhedral silsesquioxanes (XLIV) produced chlorosilyl- (XLV and XLVII) and allyl-derivatized (XLVI and XLVIII) dendrimers, respectively. Hydroboration/oxi-

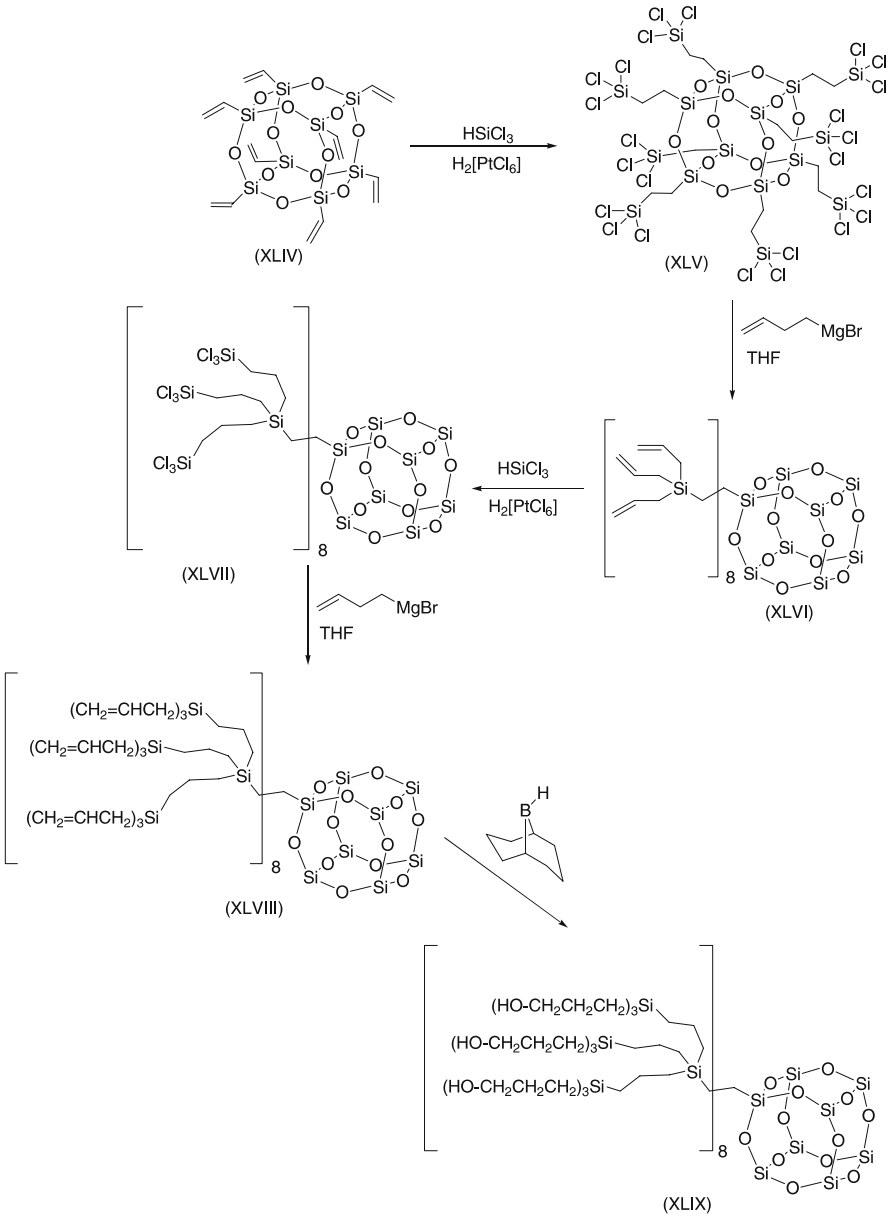

Scheme 13 Synthetic scheme for the production of 24-Cl dendrimer, 24-allyl dendrimer, 72-Cl dendrimer, 72-allyl, and POSS-72-OH dendrimer [142]

dation of the allyl-functionalized dendrimers produced alcohol (hydroxy)-terminated dendrimers (XLIX). The results showed the dendrimers to be relatively spherical, globular molecules, with a large proportion of the termi-

nal hydroxy groups located in a shell at the exterior of the dendrimer. Again, as the number of terminal groups on the dendrimers increased, the number of the dendrimer branches that back-fold towards the core of the dendrimer was also noted to increase. Experimental and modeling work illustrated two general features of the hydrosilation reactions in dendrimers. Firstly, steric influences are important in determining both the rate and regioselectivity the reactions, and, secondly, that the temperature is important in determining the regioselectivity. In general, it was found difficult to hydrosilate-unhindered allylsilanes in a regioselective manner. This was presumably because of the β-effect in silicon chemistry that tends to promote addition at the β-position in allylsilanes, instead of addition at the usually more favored α-position. It was further noted that in vinylsilanes the effect of the silicon would be expected to promote hydrosilation at the α-carbon of the vinyl group, thereby increasing the regioselectivity of the reaction.

Work report by Ropartz et al. [143] described a procedure whereby radical additions of HPR_2 (R = Et, Cy) onto alkenyl groups or nucleophilic substitution reactions on chlorosilanes by $LiCH_2PR_2$ (R = Me, Hex) were used to prepare first and second-generation alkylphosphine-containing dendrimers based on a polyhedral oligomeric silsesquioxane (POSS) core. The first generation dendrimers were built on 16 or 24 arms, which were chlorides, vinyl groups or allyl moieties. Hydrosilylation followed by vinylation or allylation of octavinyl-functionalized POSS gave these dendrimers. It follows that successive hydrosilylation/allylation followed by hydrosilylation/vinylation produced the framework for the second-generation dendrimers. The phosphorus-containing dendrimers were later on used as ligands for the hydrocarbonylation of alkenes (hex-1-ene, oct-1-ene, non-1-ene, prop-1-en-2-ol) in polar solvents (ethanol or THF) using the complexes $(Rh(acac)(CO)_2)$ or $(Rh_2\ (O_2CMe)_4)$ as a metal source. Linear-to-branched ratios up to 3 : 1 for the alcohol products were obtained for the diethylphosphine dendrimers. The reactions were found to proceed mainly via the formation of the corresponding aldehydes.

Kim et al. [92] synthesized hybrid star-shaped polyoxazolines having a POSS core by ring-opening polymerization of 2-methyl-2-oxazoline using various octafunctional POSS as an initiator with changing the feed ratio of POSS to 2-methyl-2-oxazoline. The core-first method, which uses an active multifunctional core to initiate growth of polymer chains, was applicable to make hybrid POSS-core star-shaped polyoxazolines. Various works by Coupar et al. [144] and Manson et al. [83] have prepared a number of POSS-based dendrimer molecules with functionalities ranging from terminal silane (Si – H), silanol (Si – OH), aromatic aldehyde, carboxylic acid and Schiff base groups and also prepared a number of phosphine functionalized dendrimers for use as catalytic ligands. Use of these molecules in combination with rhodium as the catalytic metal produced some very interesting results on the selectivity of hydroformylation reactions. Phosphines prepared from vinyl-

terminated dendrimers, i.e. with two carbons between the last silicon and the phosphorus atoms, show greatly improved selectivity, compared with similar small-molecule catalysts, towards the preferred long-chain aldehyde products [145]. On the other hand, those made from the Cl-functionalized dendrimers with only one carbon between the Si and P atoms, showed only a small improvement over their small molecule analogues [146]. It can then be justified to say that the length of the alkylene chain between the outermost silicon atom and the terminal functionality on the dendrimer is of crucial importance.

6.2 Divergent Methods

Divergent synthetic methods have been used to prepare a number of novel POSS-based dendrimers. Conversely, chloro-silyl or -vinyl dendrimers of the chosen generation number prepared using divergent methods can subsequently be used as synthetic platforms for other, more useful functional materials. Jaffres and Morris [147] have presented octavinyl-POSS species that have eight terminal vinyl groups on the exterior of an almost cubic core. Reaction at all eight of these terminal groups, with for example $HSiCl_3$, produces a first-generation dendrimer with a relatively large number of chloro groups at the exterior of the molecule. Vinylation of the dendrimer followed by further hydrosilation with $HSiCl_3$ produce dendrimers with 72 chloro groups. In this way dendrimers with a high number of terminal groups can be prepared in only three high-yielding synthetic steps. This reduces the number of steps required to produce such a high number of terminal groups compared to that needed for a core, citing terminal vinyl groups (e.g. tetravinylsilane) as a good example [148]. Importantly, this also reduces the need for wasteful isolation and purification steps during the synthesis. Another potential advantage of POSS-based dendrimers is the effect of the high multiplicity of the core on the structure of the molecule. The cubic shape and high multiplicity of the POSS core, in principle, can be amplified by the dendrimer branches to produce a fairly spheroidal, globular molecule with a large proportion of the terminal groups at, or near, the surface of the dendrimer, even at low generations [142]. Such molecules have been previously used as core species to produce what can be described as zeroth-generation dendrimers, for example, the octopus molecules [82, 149, 150] or the ferrocene derivatized octasilsesquioxane species [151]. Other works have reported the use of polyhedral silsesquioxanes as cores for dendrimers, based on functionalizing phosphine-derivatized dendrimers, and functionalizing the rather unstable γ-aminopropyl-derivatized silsesquioxane core [152, 153, 160].

The optimum conditions for divergent synthesis have been identified and molecular modeling studies have shown the resulting molecules to have low-energy conformations yielding relatively spherical structures with the major-

ity of the terminal groups on the exterior surface of the molecule [142]. Thus, energy-minimization and molecular-dynamics techniques have been used to model the architectures of the dendrimers.

Another work [154] reported the effects of monomer flexibility on overall dendrimer configuration. While it was found that dendrimers constructed of flexible monomers were more globular in shape, all dendrimers gave distributions of terminal groups throughout the molecules thought to be due to back-folding in the former case and branching-angle effects. Similar "back-folding" effects were reported by Cavallo and Fraternali [155], who reported the results of a molecular-dynamics study of the first five generations of polypropyleneimine with *N-tert*-Boc-*l*-phenylalanine terminal units. It was found that the shape of the dendrimer was generation-dependent, with higher generations becoming more spherical. Some back-folding of the terminal groups into the interior was also observed, similar to that reported by Zhang et al. [142].

Manson et al. [83] work reported the synthesis and full characterization of dioxolane (LII) and aldehyde (LIII) functionalized dendrimers (Scheme 14). The conditions of synthesis were shown to be important in determining whether the initial hydrosilylation reaction occurs at the α- or β-position.

NMR spectroscopy revealed that all the vinyl resonances on the cube had disappeared, indicating that, at least within the limits of detection by NMR, the reaction had gone to completion. Deeper investigations indicated that the products were of the correct mass for addition to all the corners of the POSS cube, although in the case of the dioxolane in the three-position an unidentified peak of lower mass was also present, leading to suspicion that unusual fragmentation of the molecular ion had occurred, as reported elsewhere [156]. Furthermore, a close look at the proton NMR spectrum revealed more complicated resonances in the methylene region than would have been expected for the structure as drawn.

Moreover, as mentioned earlier, cube-octameric polyhedral silsesquioxanes ($R_8Si_8O_{12}$) react with strong acids to produce $R_8Si_8O_{11}X_2$ frameworks resulting from selective cleavage of one Si – O – Si linkage [67]. Jaffres and Morris [135] reported a divergent synthetic route to dendrimers using POSS molecules as the core. The synthesis of the dendrimer molecules was accomplished, using a similar repetitive hydrosilation/vinylation procedures to those preferred previously by Zhou and Roovers [157], van der Made and van Leeuwen [158], and also by Seyferth et al. [159], to yield dendrimers with a high density of branch ends per generation. It was claimed that a cautious choice of hydrosilating agent ($HSiCl_3$, $H(CH_3)SiCl_2$ or $H(CH_3)_2SiCl$) produced dendrimers with varying numbers of chain ends, and alkenylating agents of different lengths produce molecules with different physical properties without resorting to repetitive synthesis of large numbers of generations.

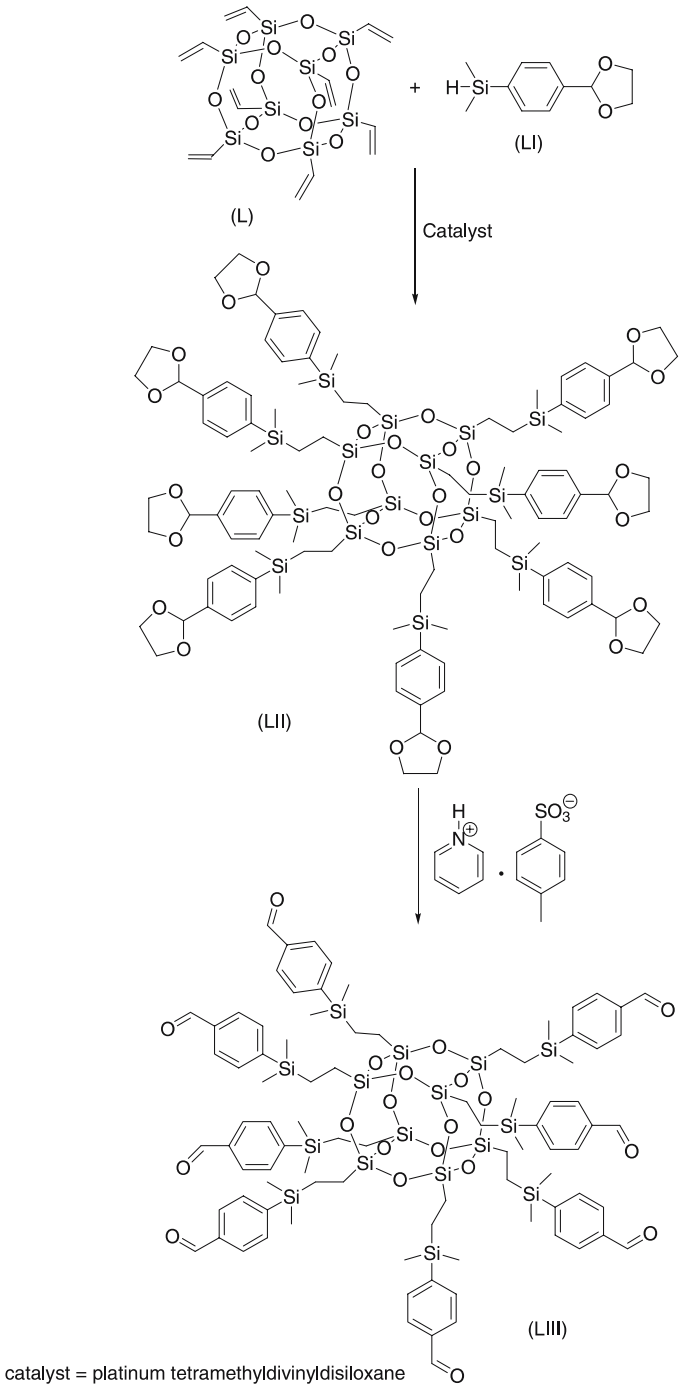

Scheme 14 Synthesis of dioxolane- and aldehyde-functionalized POSS-dendrimers [83]

7
Properties of POSS-Containing Nanohybrid Polymers

Interestingly, the mode of polymerization defines the type of participation of the nanobuilding blocks in the structure of the hybrid material. Conversely, the synthesis of linear organic/inorganic hybrid polymers containing POSS groups has recently received attention as a route to prepare novel nanocomposite materials. In the pursuit to understand the effect of POSS inclusions in polymeric hybrids, the synthesis of well-defined model copolymers of precise molecular weight, composition and architecture is required. Incompletely condensed silsesquioxanes have been extensively employed as models for silica surfaces [161–163], ligands [164–166], building blocks for network solids [167, 168] and precursors to new families of silsesquioxane-containing polymers [169, 170]. The last few decades have seen further developments and the use of oligosilsesquioxanes containing more than one hydroxyl group becoming important as building blocks for many metalosiloxanes. Of particular interest have been reactions of trisilanols with ligand-deficient trivalent-metal complexes because the inability of these trisilanols to support trigonal planar coordination environments is expected to produce more complex structures.

An exhaustive review of the synthesis and nature of nanoparticles is beyond the scope of this work, and readers are referred to more-specific sources. However, the properties of POSS-containing nanobuilding blocks are discussed in details in the following chapters. Just to mention briefly, the synthetic approaches can be presented as condensation polymerization [95, 111, 113], ring-opening metathesis polymerization (ROMP) [26, 102, 110], metallocene-mediated processes [15] and free-radical polymerization [96, 112] techniques. Additionally, recent advances in controlled/living radical polymerization [115, 116] have offered a versatile tool to prepare model copolymers from a wide range of monomers, e.g. styrene or (meth)acrylates, enabling investigation of structure–property relationships [117]. Such advances have been demonstrated by, e.g., the ability to introduce methacrylate functional POSS monomers into polyacrylate materials for the synthesis of well-defined star diblock and ABA triblock copolymers using atom-transfer radical polymerization (ATRP) [118–121]. In these block copolymers, POSS moieties are attached to the copolymer backbone as pendant side-chain groups.

Nanobuilding units are versatile and exhibit a large variety of interfaces between the organic and the inorganic components such as covalent bonding, complexation, electrostatic interactions, etc. [8]. These nanobuilding blocks with tunable functionalities can, through molecular recognition processes, permit the development of a new vectorial chemistry. However, depending on the set of chosen experimental conditions, these nanobuilding blocks keep or lose their integrity. Therefore, they can be used as true building blocks that

can be connected through organic spacers in surface-driven condensation reactions or treated as a reservoir of inorganic matter that can be delivered at the hybrid interface to build an extended inorganic network.

7.1 Mechanical Properties

Multifunctional POSS, containing four epoxide groups on the periphery, copolymerized with aliphatic diepoxides and an amine-curing agent increased and broadened the T_g, increased the tensile modulus, but lowered the flexural modulus over that of the neat epoxy resin [2] (Fig. 3).

Incorporation of monofunctional epoxy POSS into an amine-cured epoxy network increased and broadened the T_g without changing the crosslink density and enhanced the thermal properties. Additionally, it was found that the thermal and thermal–mechanical properties of resultant styrene-POSS vinylester resin nanocomposites were dependent on the percentage of POSS incorporated into the resin [171]. Over a range of POSS incorporations, the T_g of the copolymers changed very little, but the flexural modulus increased with increasing POSS content.

In one further work on epoxy-POSS, comparative studies were conducted on epoxy/ladderlike polyphenylsilsesquioxane (PPSQ) blends and the associated nanocomposites [2]. The work revealed that, although a decrease in the flexural strength and modulus of epoxy/POSS nanocomposites in comparison to the neat epoxy resin was observed, only flexural strength deteriorated in the epoxy/PPSQ blends compared to the neat epoxy resin. Flexural modulus of epoxy/PPSQ blends was reported to be much higher than that of the epoxy resin and also increased with an increase in POSS content. It was

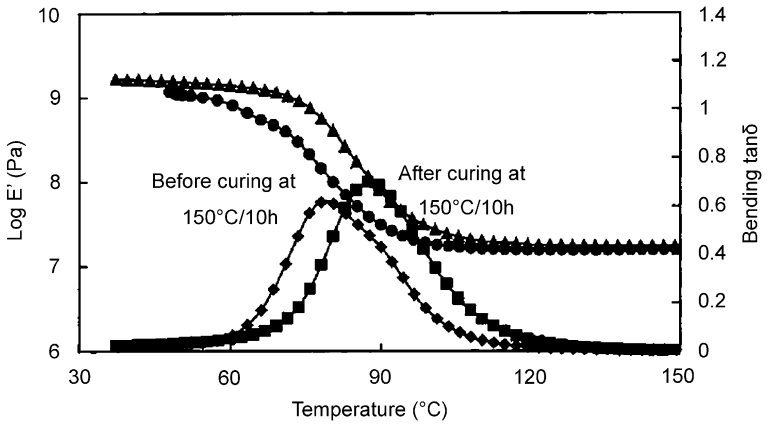

Fig. 3 Curves of bending modulus (E') and tan δ versus temperature at 1 Hz (from DMTA) of epoxy/POSS 75/25 (w/w) composite before and after curing at 150 °C/10 h [2]

further noted that the epoxy became harder and more brittle upon incorporation of POSS. In this respect, the flexural strength of the epoxy/PPSQ blends was lower than that of neat epoxy resin and it decreased sharply with an increase in PPSQ content. The sharp drop in flexural strength of the epoxy/PPSQ blend suggested that the adhesion between the resin and PPSQ phase was not strong in accordance with a low chemical-bond density connecting these phases.

For norbornene-POSS polymers, lack of mobility of the POSS units led to the conclusion that the reinforcement effect arises primarily due to the POSS units behaving as strong anchoring points [27]. In the case of a polynorbornene chain with the cyclopentyl rings (c-C_5H_9), the molecular-dynamic simulation approaches show diffused behavior above 200 °C and therefore the drop in the modulus was found to be higher than for the polynorbornene chain with cyclohexyl rings (c-C_6H_{11}) where the MSD remained very small at all temperatures. In addition, the results for the mechanical properties were also in agreement with the slower conformational dynamics observed in the case of (c-C_6H_{11}) versus (c-C_5H_9). It was also noted that the trends observed for the bulk and shear moduli follow similar lines to those seen in the tensile modulus case.

7.2 Thermal Properties

Lee and Lichtenhan [109] reported on thermal studies of monofunctional epoxy-substituted POSS monomer that was incorporated into a network composed of two difunctional epoxy monomers, the diglycidyl ether of bisphenol-A (DGEBA) and 1,4-butanediol diglycidyl ether (BDGE), at a DGEBA/BDGE 9 : 1 mole ratio.

The glass-transition region was observed by differential scanning calorimetry (DSC) to broaden with an increase in weight percent of the POSS, but there was no change on the onset temperature of the glass-transition range (Table 2) [23].

The topological constraints provided by the presence of POSS reinforcements slowed the motion of the network junctions.

Table 2 Differential scanning calorimetry results of POSS-containing epoxy glasses [23]

Sample	Onset of transition (°C)	Midpoint of transition (°C)	Endpoint of transition (°C)
Neat	66.9	71.2	75.3
5 wt % of POSS	67.2	74.8	80.3
10 wt % of POSS	67.2	78.9	83.4

Therefore, the time needed to reach structural equilibrium substantially increased relative to that for non-nanoreinforced networks. Elsewhere [172], thermal stability of the eightfold alkyl-substituted silsesquioxanes was reported to vary with n values. It was shown that when $n = 1$, the silsesquioxane sublimated at ambient temperature, while when $n = 2$, the silsesquioxane had a relatively high melting point (212 °C). For $n < 3$, derivatives showed a clear "odd–even" effect, with the compounds with odd numbers of carbon atoms exhibiting generally lower melting point. Thermogravimetry (TG) results under N_2 conditions showed that the onset of the weight loss was found to shift to higher temperatures with increasing alkyl chain length.

Although in air the onset of the decomposition was found at lower temperatures than in an N_2 atmosphere, the total weight loss was lower than under N_2, a phenomenon that was attributed to the formation of a crosslinked silicate network.

In another development, thermal analysis of POSS-containing ABA triblock methacrylate/butyl acrylate copolymers (Fig. 4) indicated the presence of two clear glass transitions in the microphase-separated system, with strong physical aging observed in samples annealed at temperatures near the T_g of the poly(methacryl-POSS) phase [122].

Wide-angle X-ray scattering indicated that rearrangement of POSS moieties observed in glassy domains further supported the occurrence of physical aging. It was found that the T_g of the poly(methacrylate-POSS) (p(MA-POSS)) phase from triblock copolymers sequestered in microphase-separated domains was nearly 25 °C higher than a poly(MA-POSS)-homopolymer of the comparable molecular weight, therefore suggesting a strong confinement-based enhancement of T_g in this system. In a different study, Zhu et al. [173] revealed an analogous sensitivity of polyethylene oxide (PEO) crystal stability on the matrix T_g of PEO/PS cylindrical diblocks and reported a similarly large T_g difference in aging behavior. However, in both studies, no definite explanations were given.

Similar reports to that of Ref. [122] based on DSC studies of cyclopentyl- and cyclohexyl-substituted POSS homopolymers reported the onset of decomposition occurring before observation of the T_g [96, 112]. This phenomenon was ascribed to retardation of segmental motion of polymer chains due to the presence of bulky side-chain groups at each repeat unit of the backbone [21]. In addition, another study [174] on diblock copolymers of polynorbornene (PN) and PN/POSS showed that increasing the length of the PN-POSS block had no effect on the PN-rich-phase T_g, with T_g of 55 °C, while the morphologies traversed the usual sequence of spheres–cylinders–lamellae. Other findings on POSS-methacrylate copolymers have shown that high-molecular-weight POSS-containing homopolymers ($M_w = 200\,000$) do not reveal a glass transition below thermal decomposition around $T = 400$ °C [96].

The aniline groups of octa(aminophenyl)silsesquioxane (OAPS) offer versatility both as reaction sites to which other nanobuilding blocks can be

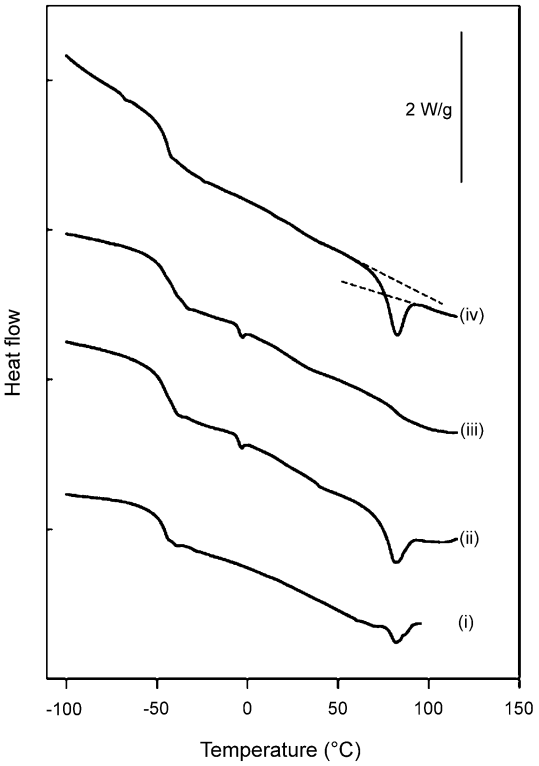

Fig. 4 Differential scanning calorimetry (DSC) characterization of triblock copolymer methacryl-POSS/*n*-butyl acrylate using a heating rate of 20 °C/min for the following thermal history: (i) the first scan (after cooling to $T = -100$ °C); (ii) heating scan following (i) and direct cooling to $T = 45$ °C for 40 hours of annealing and subsequent cooling at 20 °C/min to $T = -100$ °C; (iii) heating scan after (ii); (iv) heating scan following (iii) and direct cooling to $T = 45$ °C for 7 days of annealing and subsequent cooling 20 °C/min to $T = -100$ °C for reheating [122]

added and as starting points for generating other functional groups, thereby providing access to diverse and novel nanocomposites [28]. A key problem with almost all of the materials explored to date is that the aliphatic components limit the thermal stability of the resulting nanocomposites, strongly influence (lower) T_g, and decrease mechanical properties potentials. However, OAPS nanocomposites when reacted with diepoxides or dianhydrides were proposed to provide high-crosslink-density materials with good thermal stability, and good-to-excellent tensile and compressive strengths [19, 101]. Reacting OAPS with pyromellitic anhydride (PMA) at > 300 °C, yields material that exhibited a 5% mass loss at a temperature of 540 °C (air and N_2) and 75 wt % char yield at > 1000 °C/N_2. This robustness is exemplary and offers potential for many diverse applications.

The core-first method, which uses an active multifunctional core to initiate growth of polymer chains, was applicable to make hybrid POSS-core star-shaped polyoxazolines that showed an increase in T_g, compared to that of polyoxazoline initiated by methyl *p*-toluenesulfonate (MeOTs) with poly(2-methyl-2-oxazoline) (POZO) [76]. Other hybrid star-shaped polyoxazolines initiated by cube-OTs or cube-benzyl revealed the same phenomenon. This was attributed to the reduction of segmental mobility of POZO in star-shaped polyoxazolines, which was caused by the incorporation of hard, compact POSS moiety to the core of star polymer with the "core-first" technique. The conclusions were drawn that the thermal stabilities of star-shaped polymers increased as the POSS wt % was increased, and this was used as a measure of the effect of the inorganic POSS unit on polymer thermal properties.

In another report [81], thermal analyses of polyhedral octahydridosilsesquioxanes–$(HSiO_{1.5})_8$ and $((HSiMe_2O)SiO_{1.5})_8$ hydrosilylatively copolymerized with stoichiometric amounts of the octavinylsilsesquioxanes, $(vinylSiO_{1.5})_8$ and $((vinylSiMe_2O)SiO_{1.5})_8$ in toluene using platinum divinyltetramethyldisiloxane (Pt(dvs)) as catalyst indicated that the polymers are thermally stable to temperatures $> 300\,^{\circ}C$. Post-synthesis heat treatments at $> 100\,^{\circ}C$ promoted further reaction of residual functional groups, which changed polymer porosities. For polymers (i) $-CH_2-CH_2-$ and (ii) $-O-Si(CH_3)_2-CH_2-CH_2-$ bridges, a slight mass gain was observed just above $200\,^{\circ}C$ in air as residual Si – H groups oxidize. In polymer (iii) with $-O-Si(CH_3)_2-CH_2-CH_2-Si(CH_3)_2-O-$ unit, the oxidation was not as significant due to the lower concentration of Si – H groups. Further heating caused some mass loss above $350\,^{\circ}C$. On heating to $950\,^{\circ}C$, white silica residues resulted, with ceramic yields that correspond well to the theoretical calculations. All the polymers showed good-to-excellent thermal stability in N_2, apart from small mass gains that resulted from inevitable oxidation due to traces of O_2 in the N_2 purge gas used. It appeared that polymer (i), which had no siloxane spacer, was by $140\,^{\circ}C$ more stable than polymers (ii) and (iii), implying that the decomposition of (ii) and (iii) occurred at $300\,^{\circ}C$ probably due to fragmentation of the siloxane spacers. Continued heating in N_2 resulted in gray/black oxycarbides. DSC traces in N_2 of the first heating–cooling cycle for all the copolymers exhibited exotherms that disappeared in subsequent cycles. This observation likely corresponds to thermally promoted hydrosilylation of residual Si – H and vinyl groups. DRIFTS measurements made before and after DSC analysis confirmed this conclusion, as absorption intensities decreased significantly after cycling in the DSC. It was likely that this post-polymerization coupling of the residual groups influenced the crosslinking and, in turn, the copolymer porosity. The researchers suggested that the thermal history might be an important reason why similar materials have been reported to have quite different porosities. Also, the DSC exotherm-onset temperature decreased from 145 to $110\,^{\circ}C$, suggesting that the activation energy

for reaction of the residual functional groups decreased in all the polymers, a trend that agreed with the reactivity comparison in solution.

The effects of introducing POSS moieties onto polymeric chains as pendant groups have been explored too via atomistic molecular-dynamics simulations in the study of norbornene-POSS polymers [27]. The simulation predicted volume–temperature properties and X-ray scattering intensities that were in good agreement with experimental results for all three polymers studied. An increase in the glass-transition temperature was seen upon incorporation of the cyclopentyl (c-C_5H_9-POSS) and cyclohexyl rings (c-C_6H_{11}-POSS). The T_g for c-C_5H_9-POSS-containing polynorbornene was predicted to be higher than that for c-C_6H_{11}-POSS. Chain packing around the c-C_5H_9-POSS moieties was more efficient compared to that around c-C_6H_{11}-POSS moieties. This was traced to the intrinsic conformational attributes of the moieties arising out of the contrasting behavior of cyclopentyl versus cyclohexyl rings attached to the POSS polyhedral. Cyclopentyl groups are packed more efficiently around the POSS moieties and can approach the polyhedral cage composed of Si and O atoms more closely, compared to cyclohexyl groups, which tend to fan out, being subject to large steric hindrances.

To assess the thermal stability of the polymers and the effect of calcination on the porosity of the materials, samples of POSS copolymer were calcined under a steady flow of oxygen [78]. For each temperature studied, a sample was heated at 10 °C/min and allowed to remain at the set temperature for a period of 200 min. After being allowed to cool to room temperature, nitrogen absorption was used to determine the surface area. The reported results show a steady decrease in accessible surface area as the calcination temperature is increased. TG results showed that, at 400 °C, the mass lost by the sample is almost enough to account for all the organic component of the polymer and that the residue was essentially a mesoporous unordered silica.

In Neumann et al. [6], TG results of the octakis(m-isopropenyl-α,α'-dimethylbenzyl isocyanatodimethylsiloxy)octasilsesquioxane ($Q_8M_8^{TMI}$) under nitrogen displayed two degradation steps. The first loss of 15%, beginning at 250 °C, was attributed to cleavage of the peripheral arms attached to the POSS core, whereas the second weight loss began at 380 °C and was ascribed to breaking down of the core Si – O structure.

Xu et al. have investigated T_g of poly(acetoxystyrene-co-isobutylstyryl-POSS) (PAS-POSS) copolymers [175]. It was found that the presence of POSS at a relatively lower content actually reduces the dipole–dipole interactions of PAS molecules and plays an inert diluent role to decrease the self-association interactions of PAS molecules. The T_g of the PAS-POSS decreases with the increase of the POSS content (up to 1.47%) in the hybrid polymer (Fig. 5).

At a higher POSS content, the POSS–POSS and POSS–PAS interactions become dominant. As a result, the observed T_g of the PAS-POSS hybrid decreases and then increases with the increase of the POSS content.

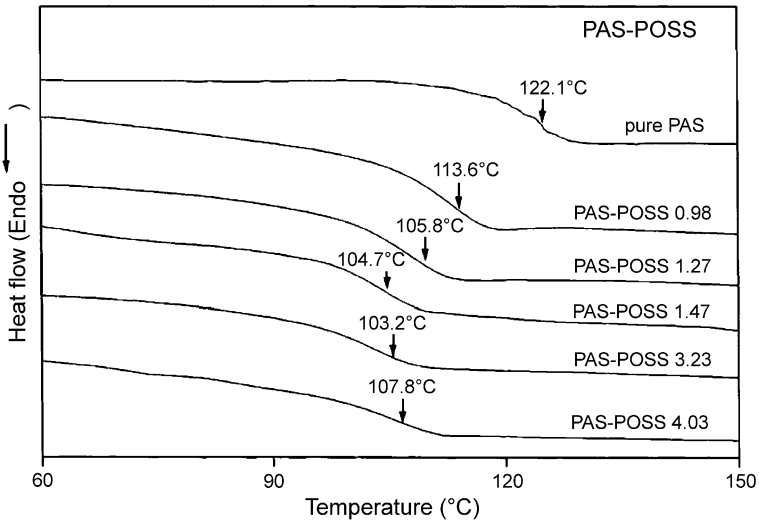

Fig. 5 Differential scanning calorimetry profiles of PAS and PAS-POSSs [175]

7.3 Viscoelastic Properties—Rheological Behavior

In the case of POSS-containing ABA methacrylate/butyl acrylate triblock copolymers, studies observed modest applicability of time–temperature superposition with lack of fluidity at even the highest temperatures and lowest frequencies probed, although this is not expected for microphase-separated morphologies [122]. This was clearly illustrated by comparison of the storage and loss modulus profiles with the expected fluid scaling of $G' \sim \omega^2$ and $G'' \sim \omega$. Indeed, a slope near 1/2 was observed for the low-frequency regions of both the storage and loss shear moduli. Such a response is consistent with other rheological observations for ordered block copolymers and also implicates elasticity derived from the microphase-separated morphology of a strongly segregated system as presented by Larson [176]. It was further observed that no indication of an order–disorder transition in the system at 170 °C, the highest temperature probed in the experiments, was found, but it was expected that T_{ODT} may be quite high due to the large incompatibility between the poly(methacrylate-POSS) (*p*MA-POSS), and poly(butyl acrylate), (*p*BA), phases.

No significant difference in the T_g of *p*BA-rich phase was observed for the ABA triblock copolymers, indicating a negligible influence of POSS on *p*BA softening in either the single- or two-phase systems [122]. The effect of a larger weight fraction of POSS in the $p(\text{MA-POSS})_{10}$-*b*-$p\text{BA}_{201}$-*b*-$p(\text{MA-POSS})_{10}$ copolymer was also seen in the DMA by doubling of the cryogenic modulus (below T_g of *p*BA) relative to $p(\text{MA-POSS})_6$-*b*-$p\text{BA}_{481}$-*b*-

p(MA-POSS)$_6$, which is consistent with another report for random copolymer systems containing POSS [26]. However, molecular weight for pure pBA was reported by Tong and Jerome [177] to be 28 000, which is substantially larger than the 8800 values for pMA [178, 179], but other work suggested that pBA behaves, after estimating the plateau modulus in shear of 0.1 MPa or 0.3 MPa in tension, as an ordinary entangled poly(n-butyl acrylate) [122].

According to a report presented by Fu et al. [180], the influence of POSS-triol on epoxy-amine reaction depends mostly on the magnitude of ΔT (T_g – T_c) used. Since T_g for epoxy cured with linear aliphatic diamine—2-methyl-1,5-pentadiamine (MPDA)—was higher than the T_g of the same epoxy cured with diamine-terminated polypropylene oxide (PPO), when cured at the same temperature, epoxy-cured MPDA showed a greater improvement in the value of T_g. Moreover, the addition of POSS-triol in tetraglycidyl diamino diphenyl methane (TGDDM) cured with MPDA also increased the rubbery plateau modulus (Fig. 6).

On the other hand, the glassy-state modulus was retained in all epoxy systems. The T_g improvement was caused by the promotion of the diffusion-controlled epoxy-amine reaction, hence, this promotion worked better in a network with a higher ΔT. Moreover, the addition of a small amount of POSS-triol ensured the consistency of the thermomechanical properties of epoxy networks with a high degree of steric constraints (high functionality of epoxy monomer), as evidenced by several parallel experiments. Because the addition of such a small amount of POSS-triol did not increase the viscosity of

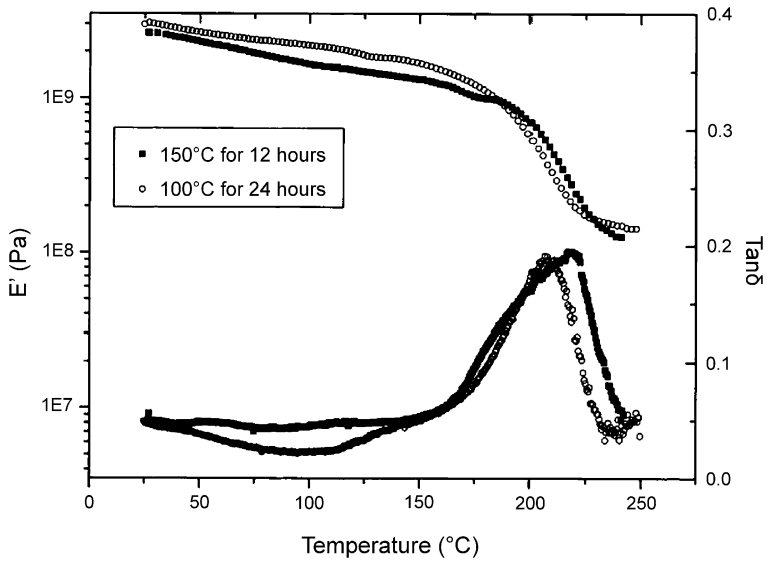

Fig. 6 Storage modulus (E') and tan δ versus temperature for TGDDM containing 1 wt % POSS-triol cured with MPDA at 150 °C for 12 h and at 100 °C for 24 h [180]

the epoxy resins, and did not accelerate the reaction in the pre-gelation stage, it was believed that the technology is of significant importance when used in the fabrication of fibre-reinforced epoxy composites using rapid processing methods such as the resin-transfer moulding process or vacuum-assisted resin-transfer moulding process.

7.4 Morphology of the POSS-Containing Nanohybrid Polymers

The effect of nanoconfinement on organization within microphase-separated domains of POSS-based copolymers is a phenomenon gaining increasing attention. While substantial work has been conducted on copolymers containing crystalline polymers with POSS segments, very limited attention has been given to the structure and morphology in block copolymers composed of amorphous segments with POSS groups [174].

Of particular interest is whether phase-separated domains of POSS are crystalline or glassy in nature. The POSS-rich-phase domains may serve as physical crosslinks, but there have been few investigations on the physical aging behavior in "pseudo"-network systems [181].

Prompted to question whether the glassy phase in ABA block copolymer would exhibit the same behavior and properties relative to the analogous POSS-containing homopolymers, Pyun et al. [122] investigated the POSS-containing ABA triblock microstructure by wide-angle X-ray scattering (WAXS).

In another development, WAXS results showed behavior intermediate between the high level of ordering in POSS monomer and the low ordering of POSS homopolymer, but very similar to previously reported observations on POSS-based multiblock polyurethanes (Fig. 7) [85].

By tuning the relative composition and degree of polymerization (DP) of the two segments, phase-separated microstructures were formed in thin films of the copolymer. Specifically, dynamic mechanical analysis (DMA) and transmission electron microscopy (TEM) observations revealed that, for a small molar ratio of *p*(MA-POSS)/*p*BA (DP = 6/481/6), no evidence of microphase separation was evident while a large ratio (1 : 2 : 1) revealed strong microphase separation (Fig. 8) [122].

Surprisingly, the microphase-separated material exhibited a tensile modulus larger than expected (ca. 2×10^8 Pa) for a continuous rubber phase for temperatures between a *p*BA-related T_g and a softening point for the *p*(MA-POSS)-rich phase.

Elsewhere [182], the morphology of polystyrene/poly(methyl methacrylate) blends with methyl methacrylate/POSS random copolymers (containing 5.5% m/m—PMMA-POSS5 [2]; 8.0% m/m – PMMA-POSS10 and 10.7% m/m—

[2] This number means content (mol %) of methacrylopropyl-POSS (PMA-POSS) in PMMA-POSS copolymers.

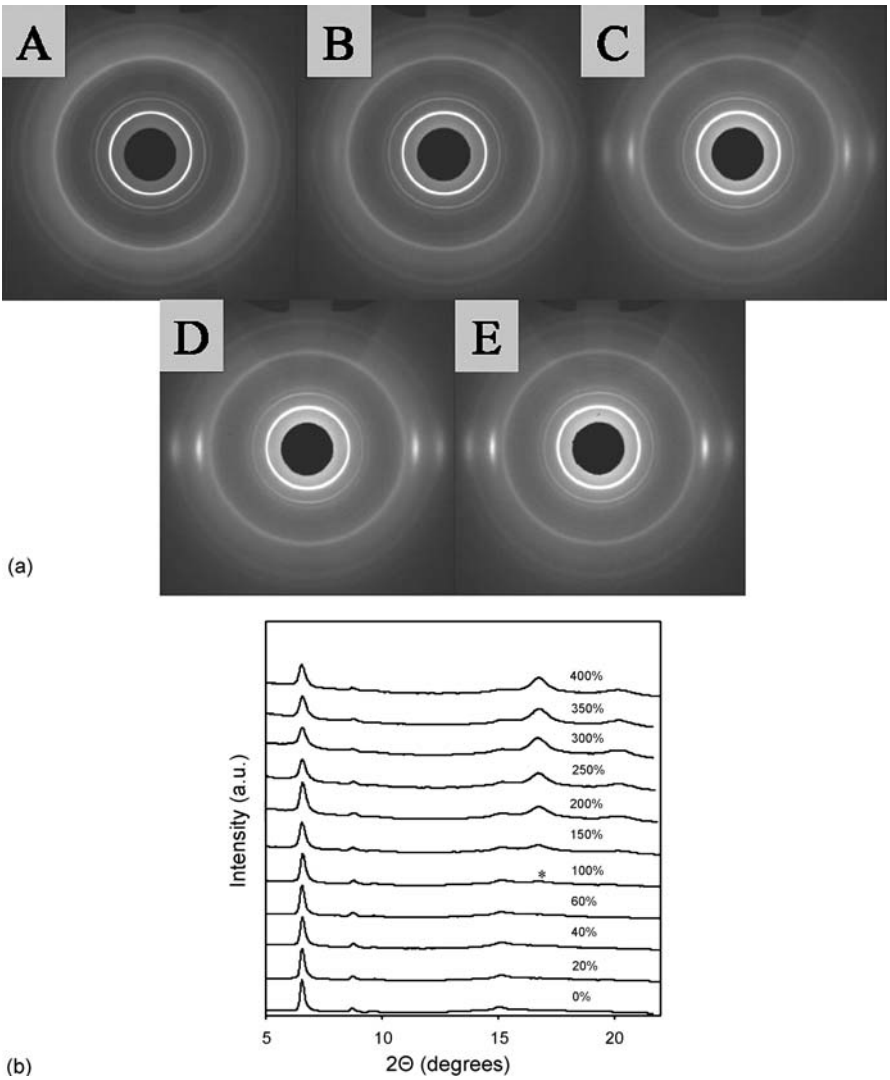

Fig. 7 **a** Two-dimensional WAXD patterns of POSS-containing nanohybrid polyurethanes at stretching ratio of: (A) 0; (B) 100; (C) 200; (D) 300, and (E) 400%. The exposure time of each pattern was 1 min. **b** WAXD profiles of POSS-containing nanohybrid polyurethanes along the equatorial direction at different strains. The asterisk symbol indicates the strain-induced crystallization of the soft segments [82]

PMMA-POSS15 cyclopentyl-POSS) as compatibilizer, using scanning transmission X-ray microscopy (STXM) and scanning probe microscopy (SPM) methods was examined.

STXM and SPM showed that bicontinuous microemulsion structure with well-defined wave vector has been formed, indicating that the interfacial ten-

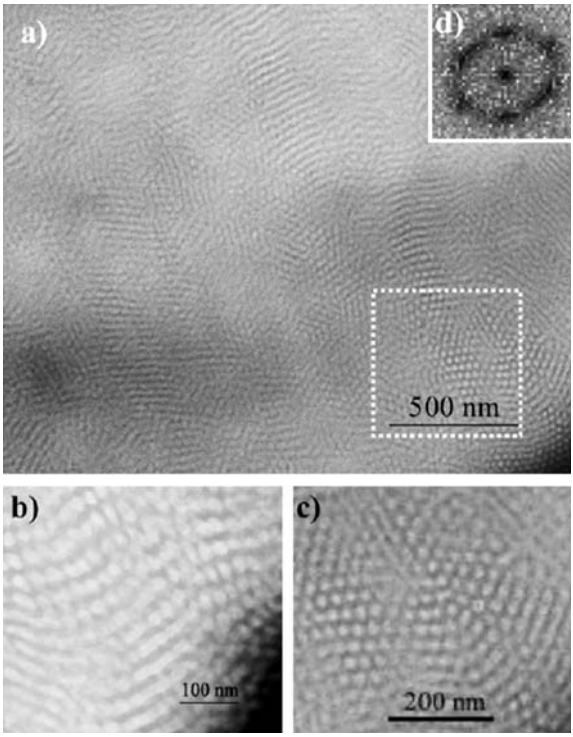

Fig. 8 Transmission electron microscopy (TEM) of thin sections of POSS triblocks prepared with cryomicrotomy at $T = -80\,^{\circ}C$ to yield samples of thickness ~ 50 nm. The microtomed sections were chemically treated with RuO_4, an agent selective for POSS. **a** Low-magnification micrograph showing overall morphology, **b–c** Higher-magnification micrographs revealing cylindrical morphology, **d** Fourier transform of selected area from micrograph (**a**) revealing symmetry consistent with local hexagonal packing of the cylinders [122]

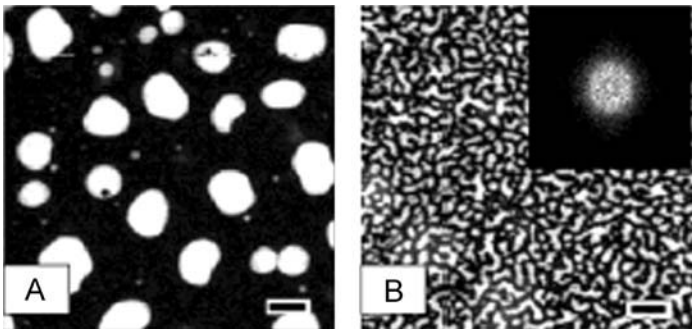

Fig. 9 STXM images of films after 24 h of annealing at 170 °C: **A** PS/PMMA with 2% (weight) cyclopentyl-POSS particle; **B** PS/PMMA with 10% cyclopentyl-POSS-PMMA copolymer (*black bars* in the image are 2 μm in length; both images are "PS" images which were taken at 285.2 eV) [182]

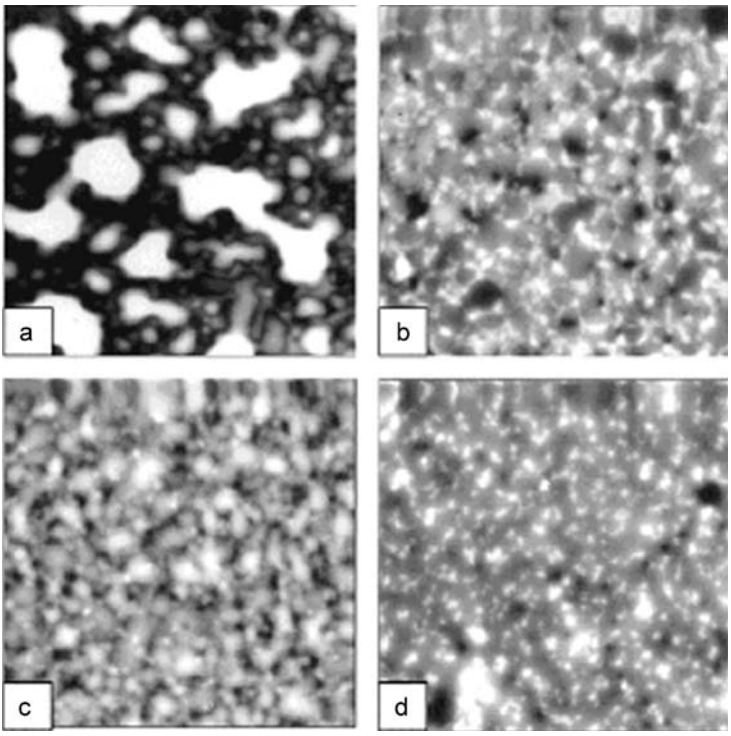

Fig. 10 SPM images of films after 96 h of annealing at 170 °C: **a** PS/PMMA–POSS0; **b** PS/PMMA–POSS5; **c** PS/PMMA–POSS10; **d** PS/PMMA–POSS15. (All images are 25 μm-by-25 μm scans) [182]

sion between the phases has been reduced. The topographical images show that size of the PS domains decreased when the POSS-PMMA copolymers were added (Figs. 9 and 10).

In Abad et al. [171] study of epoxy networks (from diglycidyl ether of bisphenol A (DGEBA) and glycidylisobutyl-POSS) containing POSS, the presence of smooth and rough macrodomains was described, as presented in Fig. 11.

Rough areas are POSS-rich regions (Fig. 11c) and smooth areas correspond to epoxy-rich regions (Fig. 11d). The primary phase separation occurred when adding DGEBA to the POSS-BSA precursor and was fixed by the polymerization reaction. The origin of this phase separation may be the incompatibility between the isobutyl groups of the POSS molecule with the aromatic epoxy-amine species. A secondary phase separation is observed in the smooth regions. Possibly, during the primary phase-separation process, the epoxy-rich phase was enriched in DGEBA, BSA, and a fraction of BSA-(POSS) (the species with only one cube attached to BSA). In the course of the formation of the epoxy-amine network, POSS was phase separated from the

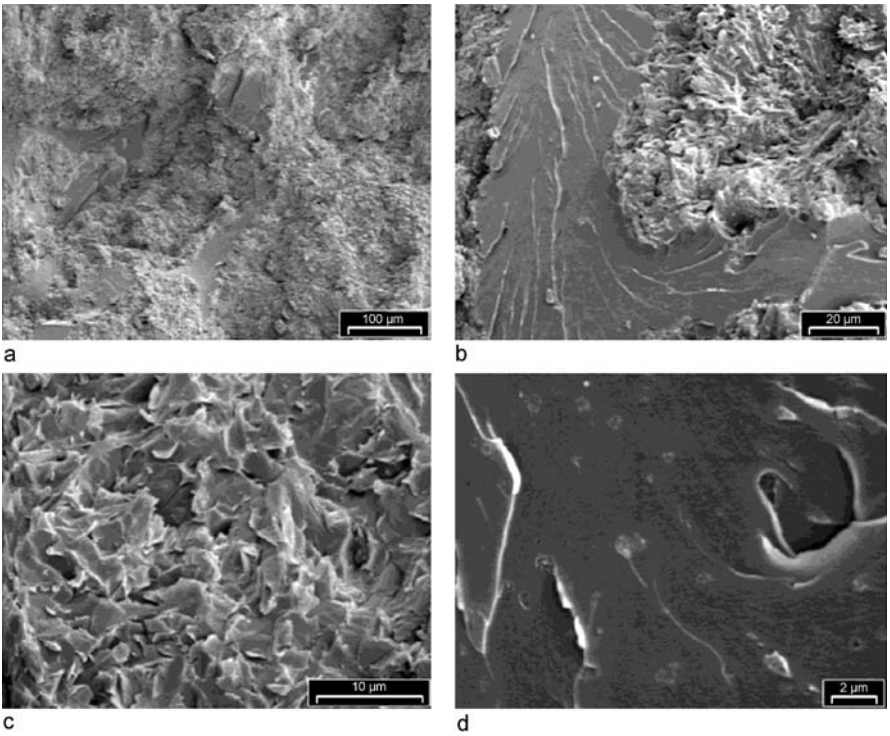

Fig. 11 SEM micrographs of the POSS-modified epoxy network: **a** general view showing the presence of rough and smooth regions; **b** magnification of coexisting rough and smooth regions; **c** rough domains; **d** smooth domains showing a dispersion of small particles [171]

epoxy-rich phase (smooth domains), leading to POSS-rich particles with sizes in the range 0.5–1 μm. This size of dispersed-phase particles is characteristic of a polymerization-induced phase-separation process.

7.5 Interfacial Interactions, Compatibility and Dispersion Characteristics

Kim et al. [183] prepared polymer hybrids by using three kinds of octasilsesquioxanes with hydroxyl groups and polymers such as poly(2-methyl-2-oxazoline) (POZO), poly(*N*-vinylpyrrolidone) (PVP) and poly(*N*,*N*-dimethylacrylamide) (PDMAAm). The obtained homogeneous and transparent hybrid films could be dissolved in different solvents and cast again without any separation. It was found that the high homogeneity of polymer hybrids was the result of hydrogen-bonding interaction between octasilsesquioxanes and organic polymers, as confirmed by the carbonyl stretching shifts in IR measurements (Fig. 12).

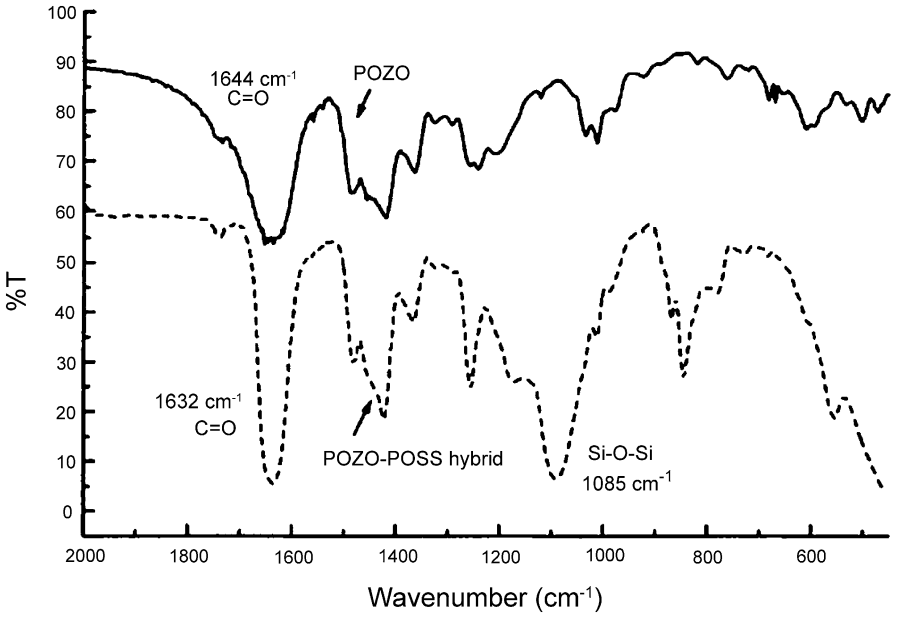

Fig. 12 FT-IR spectra of POZO and POZO-POSS polymer hybrid [245]

Also, the influence of flexibility of the eight arms bound to silica-like core on the homogeneity of polymer hybrids was examined to reveal that the solubility of POSS and transparency of polymer hybrids from POSS were closely dependent on this flexibility. It was found as well that remaining inorganic parts of polymer hybrids in TGA matched well with the calculated contents of inorganic parts. In a more recent work, the same researchers investigated on ternary polymer hybrids POZO, PVP and aminopropylsilsesquioxane (cube-aminopropyl) utilizing the sol–gel reaction of tetramethoxysilane (TMOS) [184]. In this hybrid system, hydrogen-bonding interactions played a critical role in the formation of the transparent polymer hybrids. Polymer hybrids using POZO showed high transparency and homogeneity in a wide range of the feed ratios of POZO to cube-aminopropyl. On the other hand, in the case of polymer hybrids using PVP, a higher cube-aminopropyl ratio brought about the phase separation, indicating the aggregation of the cube-aminopropyl itself. The homogeneity of ternary polymer hybrids was found to be closely dependent on the difference between the strength of the hydrogen-bonding interaction of polymer and residual silanol groups of silica gel and the strength of that of polymer and cube-aminopropyl. It was also observed that the initial decomposition temperature of the polymer hybrids increased with increasing cube-aminopropyl ratio.

In another work it has been claimed that epoxy/PPSQ blends have several similarities to the epoxy/multifunctional POSS nanocomposites; the main-

chain structure of PPSQ is quite similar to that of the POSS [2]. The PPSQ used in this work had some Si – OH groups present which might have displayed some reactivity with the aliphatic epoxides of the epoxy resin. However, this PPSQ had no other functional groups that could react with components of the epoxy system during curing. Finally, PPSQ molecules (M_w = 4636) were substantially larger than the multifunctional POSS, which had M_w of 1305. Thus, the volume of their microphases was expected to be larger than those of POSS, even when the PPSQ was completely compatible and molecularly dispersed in the epoxy. The epoxy/PPSQ (95/5) blend was found to be transparent, but the (9 : 1) blend was slightly translucent. In contrast, the epoxy/PPSQ (85/15) blend was opaque, leading to speculation that some phase separation had occurred in this blend. It was reported that some PPSQ precipitated within liquid resin mixtures after all the THF solvent had evaporated during the preparation of blends with higher amounts of PPSQ (less or equal to 20%).

Hydrosilylation of allyl alcohol with octakis(dimethylsiloxy)octasilsesquioxane, $(HSiMe_2O)Si_8O_{12}$ ($Q_8M_8^H$) was discovered to provide C-silylation at C = C, which provides one-step access to octakis(3-hydroxypropyldimethylsiloxy)octasilsesquioxane (OHPS), and hence an efficient route to octakis(3-methacryloxypropyldimethylsiloxy)octasilsesquioxane (OMPS) [93]. The success of the reaction with 2-allyloxyethanol suggested that a broad spectrum of OH-functionalized cubes can be synthesized using this facile methodology, and thus provided access to a wide variety of macromonomers incorporating ester functionality on the periphery of octasilsesquioxane cores, such as the octamethacrylatesilsesquioxane. Although OHPS is very stable as a dry powder, in the reported work it turned into viscous oil in methanol solution after a few days. GPC analysis indicated a significant amount of high-molecular-weight species, a phenomenon also explained by the backbiting process. The results were contrary to the anticipation that, as a dry powder, the OH groups on OHPS are likely to be immobilized by H-bonding between OH groups, and thus are unable to backbite. On dissolution in methanol, H-bonding with methanol competes with that between the propanol groups and provides the propanol groups with the mobility essential for backbiting to occur. In another words, OHPS provided a basis for the development of polyester nanocomposite precursors, e.g. polyester nanocomposites [185]. These compounds also offer potential utility for developing new ligands for inorganic and organometallic chemistry [164, 186], and as cores for hyperbranched or dendritic materials [67, 187].

Organic–inorganic OAPS particles that have a cubic silica core and eight amino-phenyl groups have been extensively studied. OAPS can be easily dissolved in NMP, which facilitates proper mixing between POSS and polyamic acid (PAA). For instance, Huang et al. [188] terminated PAA by anhydride groups in that only a small excess amount (5% mole) of the dianhydride was added. When the OAPS/NMP solution was mixed with the PAA/NMP

solution, the amine groups of OAPS reacted readily with the terminal anhydride groups of PAA, which resulted in the formation of amide bonds. During the imidization process, the amide bonds were converted into imide groups. As a result, the linkage between the polyimide and the POSS was the phenyl group and the imide group. The amine groups of OAPS may also react with the side carboxylic groups of the PAA to form amide bonds, thus offering an alternative method. However, the chance of forming the amide bonds between POSS and side carboxyl groups is small due to the low reactivity of the latter. Furthermore, this kind of the ortho amide bonds is not stable in the process of imidization. In this case, two adjacent amide bonds are transformed into one amine group and one imide group. However, linkage between the polyimide and the POSS is still the phenyl group and the imide group. In a parallel study by Choi et al. [19] of OAPS and PAPS, in ^{29}Si NMR spectra Si peaks at 68.0 and 76.0 ppm representing $T_2(Ph)(OR)$[3] and $T_3(Ph)$, respectively, were reported. $T_2(Ph)(OR)$ was proposed to contain only hydroxyl groups (R = H) because potential alcoxy groups in the polyphenylsilsesquioxane starting materials are most likely removed during nitration by nitric acid. The PAPS 5% mass-loss temperature (140 °C) was blamed for condensation reactions between these hydroxyls. Otherwise, the PAPS-ceramic yield was expected to be lower than that of OAPS because of the presence of uncondensed Si – OH units. However, according to the study, the ceramic yield (41.4%) was reportedly higher than expected, suggesting that some Si units had lost phenyl groups, forming Si – OH groups in the process. Supportive work has also been presented by Prado et al. [31] and Zhu et al. [189].

Elsewhere, no evidence for intermolecular aggregation was seen from the packing analysis in case of norbornene-POSS polymers [190]. However, the researchers warned that this did not imply that aggregation could not occur since the temporal and spatial scales employed in the atomistic-level simulations in the work did not permit such a determination. Rather, it was demonstrated that, in the case where no aggregation was present, the beneficial effects of incorporating the POSS moieties were realized nevertheless. The source of the reinforcement was therefore traced to the low mobility of the POSS moieties, which behave as strong anchoring points in the polymeric matrix, rather than any specific intermolecular interactions between the POSS moieties. In addition, transparent ternary polymer hybrids consisting of random copolymer and POSS were prepared via two simultaneous physical interactions (hydrogen bonding and aromatic ($\pi - \pi$) interactions) coexisting in one system [190].

In another work, the POSS-24Cl dendrimer was found to react with vinylmagnesium bromide to give a 24-vinyl dendrimer [142]. However, POSS-24Cl also reacted with allylmagnesium bromide to give a 24-allyl dendrimer,

[3] The symbol T represents framework silicon atom which poses one organyl substituent. Subscripts are used to indicate the number of framework silicon atoms with the various designations.

POSS-24-allyl, in a similar manner to that shown in other carbosilane dendrimer preparations. This allylation reaction occurred almost quantitatively and once recovered from solution, the purity was sufficient to be used in subsequent reactions without any further purification, as it was confirmed by NMR studies. The POSS-24-allyl dendrimer was hydrosilylated by trichlorosilane to give the POSS-72Cl dendrimer. In this case, the hydrosilylation was more effectively catalyzed by Karstedt's catalyst (a platinum divinylsiloxane complex), allowing the reaction to be completed at or below room temperature. Purification and characterization of this dendrimer was claimed to be hard due to the difficulty of removing all the solvent (THF) from the product, presumably because of the long dendrimer arms—a common problem in many high-generation dendrimer syntheses due to effectively trapped solvent molecules. ^{13}C NMR clearly showed that, in the hydrosilation of POSS-24-allyl by trichlorosilane, silicon was only connected to the α-carbon atoms of the allyl groups. This is consistent with previous work by the same team of researchers on hydrosilation reactions, which showed that reaction at low temperature lead to addition exclusively at the α-carbon [147].

In yet another work, NMR studies were performed to address two main points concerning the hydrosilylation route, i.e. whether hydrosilylation can produce either linear $Si-CH_2-CH_2-Si$ (β-hydrosilylation) or branched $Si-CH(CH_3)-Si$ bridges (α-hydrosilylation) [81]. On this point, the bridge geometry certainly affects the development of the network microstructure and therefore the resultant porosity, pore volume and pore-size distribution. Thus, identification of the types and quantification of the bridges that are formed during hydrosilylation is essential. Analysis of both ^{13}C and ^{29}Si NMR results would give a quantitative estimation of the number of crosslink sites and hence the crosslink density. In conclusion, the work observed that the inversion-recovery cross-polarization (IRCP) technique allowed the proposal of definitive assignments for all ^{13}C lines in polymers studied and showed that β-hydrosilylation is the main crosslinking reaction. Moreover, segmental motion of the bridging carbons was detected along the transition of the hybrid polymers. Furthermore, solid-state ^{13}C and ^{29}Si MAS-NMR (MAS—magic angle spinning) analyses of POSS indicated that β-hydrosilylation was the primary process that occurs during copolymerization for all polymers studied [81].

Laine et al. [77] synthesized epoxy-containing silsesquioxanes and, although these compounds were soluble in common solvents, they contained crystalline phase and therefore were not practical for processing in dense, single-phase nanocomposites. To improve processability and impart the potential for toughening, the same group devised the synthesis of liquid silsesquioxane with the epoxide tethered to the cube *via* a flexible spacer [125]. The photochemically cured polymers gave hard, scratch- and solvent-resistant materials containing up to 65% of masked silica. As an additional feature, analysis by matrix-assisted laser desorption ionization

time-of-flight (MALDI-TOF) mass spectroscopy at various stages of oxidation illustrated how species are formed containing *n* carboxylic groups, where *n* ranges from 0 for the freshly prepared octaaldehydes to 8 for fully oxidized species [83]. As a matter of fact, the synthesis of octacarboxylic-acid-functionalized POSS species is attractive because of their potential uses in supramolecular chemistry and as building blocks in macromolecular engineering experiments. However, some attempts to prepare a pure sample of the octacarboxylic acid have been reported fruitless—a fact mainly blamed on unchanged aldehyde groups that contaminate it to some extent, as characterized by ^{1}H NMR and confirmed by CHN analysis. On the other hand, attempts to use mild oxidizing agents in solution proved difficult because of solubility problems.

7.6 Catalytic Effects of POSS

The influence of phenyl-trisilanol polyhedral silsesquioxane (POSS-triol) on the thermo-mechanical properties and curing of epoxy-amine networks was investigated using DMA and FTIR to demonstrate that the addition of soluble POSS-triol can be used to improve the crosslinking of epoxy-amine networks [81]. Two of the most common epoxy monomers, diglycidyl ether of bisphenol A (DGEBA) and tetraglycidyldiaminodiphenylmethane (TGDDM) were used. These epoxies were cured with linear aliphatic diamine—2-methyl-1,5-pentadiamine or diamine-terminated polypropylene oxide. Using an identical curing schedule, when minor amounts of POSS-triol were added to the epoxy-amine networks, resulted in a significant improvement in the value of T_g. Due to the small quantity of POSS-triol used, this enhancement in T_g was attributed to the catalytic activity of phenyl-trisilanol POSS that could have promoted a more completely cured epoxy network. This argument is consistent with observed increases in the rubbery-plateau modulus due to increases in the crosslink density. However, unlike other catalysts such as phenol, acceleration of reaction in the pre-gelation stage by this acidic POSS-silanol was not observed. Because of its nanoscopic size, it promoted additional epoxy-amine crosslinking in the post-vitrification stage, which was dominated by a diffusion-controlled mechanism.

A significant amount of work has been reported in the literature concerning the nature of reactions between epoxides and amines. The curing kinetics of epoxy can be accelerated by many factors, such as the hydroxyl groups generated during cure, the addition of alcohols and Lewis acids. Among them, the catalytic effect of alcohols has been widely acknowledged. The catalytic efficiency of alcohols and phenols can be approximately proportional to their acidity, which explains the high catalytic activity of phenol. This is because acids or electrophilic species accelerate the addition of most nucleophiles considerably by the reversible formation of the more reactive conjugated acid

of the epoxide, as in the case of Lewis acids [191, 192]. The influence of silanol groups on the epoxy curing kinetics has been studied by some researchers at high concentration of silica fillers, which have silanol groups on the filler surface, and reported that it could accelerate the reaction of certain epoxy resins [193–195], or at least in the circumstances where aluminum complex was present [196]. Elsewhere it have been claimed that it is possible to incorporate titanium into the polymer and so this scenario is a distinct possibility [78]. Unfortunately, while the cyclopentyltitanium chloride ($CpTiCl_3$) species used as the titanium source is excellent for characterization of the resulting polymers (equidistant carbon atoms are convenient marker in EXAFS spectroscopy), for this type of material to be useful for catalysis, the Cp units should be removed by calcination in oxygen. Unluckily, the polymer network itself is not thermally stable enough to allow this activation procedure, and so catalytically active polymeric materials must be prepared that do not need this extra calcination step. Nevertheless, it was claimed that catalytic functional materials are achievable in this system.

Interestingly, the fascinating reactions of POSS molecules with triflic acid in solution also occur in the polymeric species, with evidence that a number of the POSS units in the polymers are ring-opened by having one or more of the Si – O – Si linkages broken. Similar reactions also occur with dilute sodium hydroxide. These reactions open up the exciting possibility of derivatizing the polymers with metals. One obvious use of such metal-derivatized polymers is as catalysts, possibly used in a similar way to other porous solids like zeolites and mesoporous silica. In fact, there are potential advantages of using inorganic–organic hybrid polymers, including the fact that the presence of organic regions in the structure must surely affect the hydrophobicity of a catalyst, which can be truly important in a number of reactions [78].

7.7 Ion Mobility and Swelling Studies

Ion mobility is based on the measurement of the amount of time it takes for an ion to drift through a buffer gas under the influence of a weak electric field. This drift time inherently contains information about the conformation of the ion. Differently shaped ions have various collision cross sections and hence different mobilities (and drift times) when drifting through the gas. Thus, various computational methods are then used to generate model structures of the ions and calculate their cross sections for comparison to experiment. For instance, X-ray crystallography and NMR spectroscopy are usually used to obtain structural data on POSS molecules. However, POSS-polymer systems can be difficult to examine with these methods since synthetic polymers exist as a mixture of chain lengths; data can thus only be obtained for the entire polymer distribution as a collective using these methods. In this respect, detailed information about how POSS interacts with one particular

polymer chain is almost impossible to obtain. However, by combining mass spectrometry with the ion-mobility experiments, conformational data can be measured for one POSS-oligomer system at a time and detailed information about how the POSS molecules interact with the polymer chains can be obtained [197, 198].

Several condensed (complete Si – O cage) and incompletely condensed (partial Si – O cage with multiple Si atoms capped with OH, also called silanols) POSS compounds of different cage sizes (Si_6O_9, Si_8O_{12}, $Si_{10}O_{15}$, $Si_{12}O_{18}$) have been investigated [39]. Experimental and theoretical parameters have been successfully developed to accurately model the gas-phase conformations of a variety of POSS compounds with different Si – O cage sizes and substituent groups. Incidentally, incompletely condensed POSS molecules are commonly used to create specific condensed POSS systems by capping with the appropriate reactive functional group. In this work, some of the POSS compounds were functionalized with cyclohexyl groups, but data were also obtained for POSS functionalized with cyclopropyl, vinyl and phenyl groups [71]. In addition, X-ray collision cross sections of these structures were compared to those obtained from the ion-mobility measurements, and the theoretical modeling to check the validity of the calculations and also to determine if any structural changes occurred when POSS was introduced to the gas phase, was performed. Good agreement between theoretical and experimental cross sections was observed for all of the POSS systems, with differences falling within 1–2%. The theoretical work indicated that the sodium ion, used to cationize the POSS compounds, essentially acted as a "spectator ion" and simply attached to oxygen in the Si – O cage or interacted with the vinyl and phenyl groups. In neither case did the Na^+ ion significantly alter the structure of the POSS cage. It was envisioned that the parameterizations developed in the study could be confidently used to accurately model POSS-polymer systems in which detailed conformational information is not well known.

Elsewhere, the mobility of the POSS moieties in the polymer has been addressed via the mean squared displacements during the study of norbornene–POSS polymers [27]. In both cases the MSD was very small, with that for cyclohexyl-POSS (*c*-C_6H_{11}-POSS) being smaller compared to cyclopentyl-POSS (*c*-C_5H_9-POSS). Conformational dynamics were also retarded by the presence of the POSS moieties as ascertained via the computation of the torsional autocorrelation function. It was demonstrated that the main-chain dynamics were sensitive not only to the presence, but also to the nature of the POSS moieties; the dynamics were slower in the case of the polymer with *c*-C_6H_{11}-POSS pendant groups compared to *c*-C_5H_9-POSS pendant groups. These results were found to be in good agreement with the mechanical properties predicted from simulations in the same report where the tensile, bulk and shear moduli for *c*-C_5H_9-POSS/norbornene and *c*-C_6H_{11}-POSS/norbornene copolymers showed an increase and less change with increasing temperature compared to the polynorbornene homopolymer.

Kim and Chujo [199] prepared organic–inorganic hybrid gels having functionalized silsesquioxanes via a common radical polymerization method, i.e. by metal-complex formation between bipyridine groups of the terpolymers and various metal ions. Highly concentrated solutions of terpolymers with iron(II) sulfate or ruthenium(III) chloride gave hybrid gels in good yields. On the other hand, no hybrid gel was formed with nickel(II) chloride even at much higher concentrations of nickel ions due to rapid ligand-exchange reactions causing the polymer network to disappear as a result of a change in the nature of the coordination bonds from an intermolecular network to an intramolecular network. The stability of the hybrid gels was related to the nature of the solvent and the properties of the metal, i.e. on the coordination strength between the bipyridine group and the metal ion. Also, the degree of swelling of the hybrid gels in water showed a sudden drop with only a small amount of POSS in the hybrid gel because of the increased hydrophobicity caused by the seven cyclopentyl groups of POSS. The critical "turning" percentage of POSS moiety, above which the degree of swelling in nonpolar solvents changes, was reportedly greater than 10 mol % in the hybrid gel due to the increase of physical crosslinking points caused by the occurrence of hydrophobic interactions between the cyclopentyl groups in POSS, which resulted in a volume-phase transition. The work concluded that the degree of swelling and the thermal stability of the gels in various solvents were dependent on the content of POSS moiety in the hybrid gel where ruthenium gel was considerably more stable than the iron and nickel gels. The hybrid gels containing POSS had properties characteristic of hydrogels as well as those of lipogels depending on the content of POSS in the hybrid gel. By analysis of the degree of swelling, it was concluded that the amount of POSS moiety in the hybrid gel has a significant effect on the degree of swelling in this system.

7.8 Porosity

Much of the research to date has been successfully focused on engineering of the size of pores through the choice of the bridging groups. Parallel to this, parameters allowing control of the pore-size distributions are well understood. More recently, however, the focus has shifted to building functionality into the bridging groups to make materials with controlled porosity that are capable of selective adsorption or catalysis [200].

POSS, particularly the cubic $(RSiO_{1.5})_8$ octamers, offer 4,4′ cage structures akin to those found in Linde A and related zeolites [201]. Zeolites are the epitome of high surface area, controlled-porosity materials and are typically made by hydrothermal processes. In principle, the polymerization of selected organofunctional cubic silsesquioxanes could offer access to organic–inorganic hybrids with controlled surface area, porosity and functionality via nonaqueous methods. It follows that the main aspects of POSS-nanobuilding

blocks' porosity characteristics include control over the porosity, pore size and pore templating. To date, there is sufficient understanding through empirical data available to predict with fair confidence if a given bridging group under a defined set of sol–gel polymerization [202, 203] conditions will be porous [12]. To start with, porosity is a key property of materials used for the preparation of catalysts, chromatographic supports, membranes and adsorbent materials. High surface areas and control over the pore size are important goals for synthetic design of materials.

The ability to tailor nonporous-bridged polysilsesquioxanes may be useful for fabricating chemical barriers, dense membranes or optical coatings. It is also important to note that, because of the sensitivity of the sol–gel process to factors such as pH, catalyst, temperature, solvent and aging time, these factors must be carefully controlled to permit the structure–property effects of the bridging group to be determined reproducibly. On this point of interest, less-compliant networks prepared with basic catalysts give condensed networks and/or rigid bridging groups that retain their porosity after drying. For instance, arylene- [9, 11] and ethenylene-bridged [176] polysilsesquioxanes give rise to materials with surface areas as high as $1800\,m^2/g$. The high surface area contains large contributions from ultra micropores with mean pore diameters < 20 Å. Loy et al. [194] showed that alkylene-bridged polysilsesquioxanes prepared with base catalysts and bridging groups up to 10 carbons in length are in the form of mesoporous xerogels of $20\,Å <$ mean pore diameter $< 500\,Å$. The mean pore diameter was shown to be roughly proportional to the length of the bridging groups. Introduction of unsaturated functionalities such as olefinic or aromatic groups into the organic bridges might have decreased the flexibility and further prevented collapse of pores during drying.

Admittedly, in recent times, intense efforts have been directed toward the development of new micro- and mesoporous materials because of their utility (or potential utility) as catalysts and catalyst supports, dielectric materials for electronic applications media for optical and sensor applications and selective permeability membranes. The most extensively explored synthetic approach is *via* sol–gel polymerization of tri- or tetraalkoxysilanes and other metal alkoxides [81]. Controlled hydrolysis and condensation of silanes under acidic or basic conditions result in crosslinked gels that can be air-dried to give xerogels or supercritically dried to produce aerogels. For example, POSS aerogels based on organo-bridged bis(trialkoxy)silanes that provide access to micro- and mesoporous materials with surface areas up to $1000\,m^2/g$, pore volumes up to $0.6\,mL/g$ and very well defined micro- and/or mesoporosity have been prepared [194, 195]. The obtained results suggested that the inorganic – O – Si – O – moieties are built up through hydrolysis and condensation of bistrialkoxysilane monomers with the organic portion retained intact. Other researchers have also shown that organofunctional cubic silsesquioxanes can be polymerized to form porous hybrid polymers [205]. Elsewhere it

has been suggested that the length of the bridges between the cubes is a critical factor in determining porosity. Only materials with six-atom bridges were suggested to be porous, while shorter (four-atom) or longer (seven-atom) bridges led to nonporous materials. Other works reported specific surface areas (SSAs) for polymers prepared by hydrosilylation to be in the range of 150–570 m^2/g [205]. Still on porosity, another work prepared polymers whose preliminary porosity measurements revealed that they exhibited high SSAs, even with bridge lengths of two to four atoms [80].

Zhang et al. [81] suspected that these discrepancies arose as a consequence of differences in synthesis conditions, such as concentrations of the monomers and catalysts, type of solvent, etc., and the conditions used to dry the materials, a fact observed elsewhere too [12]. The investigators went even further and presented a standard syntheses of porous POSS-polymers and offered detailed analysis of the degree of condensation that occurs during polymerization, and also a study of the types of pores generated during the crosslinking process, aiming to establish the structure–property relationships that would in turn permit the synthesis of hybrids with controlled surface area, porosity and functionality. Nitrogen sorption provided a view of the pore sizes in the 10–500 Å range, while PALS allowed identification of pores in the cubes ($\sim$ 3 Å) and in between of the cubes (10–11 Å); SAXS provided overlapping confirmation of the two methods.

In yet another interesting study of POSS-nanobuilding blocks' porosity, POSS-based network polymers were prepared using hydrosilation copolymerization reactions of a silyl-functionalized POSS molecule with a vinyl-functionalized moiety [206]. However, the N_2 adsorption isotherm obtained was not of the classical type, normally associated with mesoporous materials, as it contained a non-closing hysteresis where the two branches remain nearly horizontal and parallel over a wide range of pressures. The low-pressure hysteresis extended to the lowest attainable pressures, indicating that some of the adsorption was irreversible under particular experimental conditions. This phenomenon was associated with the swelling of a non-rigid porous structure or with the irreversible uptake of molecules in pores or through pore entrances of about the same width as the adsorbate molecules. This unusual behavior was therefore probably due to the presence of micropores as well as mesopores in the polymer, and due to the flexible nature of the organic linking groups.

The use of the organic group as a template for porosity is just another method for creating porosity. While this a common strategy in the preparation of zeolites, this has only recently been applied in hybrid sol–gel materials [12]. Templating relies on an organic group to occupy space until calcination, chemical oxidation, chemical rearrangements or hydrolysis eliminate the template. This leaves a pore whose size and shape roughly corresponds to that of the organic molecule. One work performed templating serendipitously with acetylene-bridged polysilsesquioxanes that lost acetylene during thermolysis [9]. An alternative approach used low-

temperature, inductively coupled plasma to burn away organic bridging groups in crosslinked polysilsesquioxane xerogels and resulted in porous silica gels [86, 87]. However, when the xerogels were porous before oxidation, the mean pore diameter shifted to larger sizes. When nonporous alkylene-bridged polysilsesquioxane xerogels were treated, mesoporous silica gels were obtained. The size of the pores increased as the length of the bridging group increased. Elsewhere, the bridged polysilsesquioxanes were subsequently used to template porosity in silica membranes [207].

8 Applications

Incorporation of POSS, for example as a pendant group of a linear polymer, generally increases oxygen permeability and glass-transition and degradation temperatures, while reducing flammability. There is enough evident that POSS and POSS-hybrid nanomaterials have many applications in a wide variety of fields, ranging from surface modifiers and coatings to catalysts and membrane materials. Such inorganic–organic hybrid polymers possess several attractive properties such as increased thermal stability, higher glass-transition temperature, better flame and heat resistance and enhancements in the modulus and melt strengths [24]. Importantly, these property enhancements occur at low POSS contents (< 10 mol %). Moreover, POSS chemistry is very flexible and therefore offers even accelerated possibilities. For example, the OAPS synthesized by Tanaka et al. [101] reacts rapidly with the 2-pyridinecarboxaldehyde under mild conditions, giving an imine that emits green light under UV illumination. This type of imine offers potential for forming metal chelate complexes for sensor, electrochemical, photonic and catalytic applications. The OAPS itself contains an inorganic core as a foundation and rigid arylamine moieties serving as highly functional anchors; therefore, OAPS was suggested to provide access to numerous materials with a high density of functional groups in a very small volume. Some of these materials can be thus used as structural "bricks" to construct a large number of thermally robust nanocomposite materials nanometer-by-nanometer.

It is evident that the incorporation of POSS cages into polymeric materials often results in substantial improvements in polymer properties and offer the possibility to control the mechanical, chemical and physical properties of the system during polymerization as well. Intense efforts have recently been directed toward the development of new porous materials because of their utility and potential utility as catalysts and catalyst supports [208, 209], dielectric materials for electronic applications [210], media for optical [211] and sensor [212] applications, and selectively permeability membranes [213] and precursors [10] for POSS nanocomposites. Significant property enhancements imparted by the inclusion of a nanosized inorganic

particles into an organic matrix include models for silica surfaces, well-defined ligands, building blocks for network solids and precursors to new families of silsesquioxane-containing polymers [54–62]. While the primary application of hybrid polysilsesquioxanes has been for surface modification as coupling agents such as those with sulfides in the bridging group that are used with silica-filled rubber, POSS nanomaterials offer reinforcements and improved end products [143]. For example, the methacrylate-functionalized cubes synthesized via Pt-catalyzed hydrosilylation of propargyl methacrylate with $(HSiO_{1.5})_8$ and $(HMe_2SiOSiO_{1.5})_8$ results into compounds cured at 100 °C without an initiator to produce clear, abrasion-resistant coatings [88, 89]. Also, bridged polysilsesquioxanes have been applied as a part of coating formulations [12]. Materials with alkylene [214], ether [215] and urea [216] functionalized hybrid groups can result in the formation of tough and relatively hard films, applied for protection of easily scratched surfaces. POSS hybrid coatings can also be used as protective layers for metals or for microelectronic applications such as low-*k* dielectrics and photoresists [217, 218].

A more recent application took advantage of the more hydrophobic, yet readily gelled, alkylene-POSS as encapsulating sol–gel networks for enzymes and cells [219]. Most recently, functional POSS have been prepared for use as high-capacity adsorbents [220] since the same functionalities that make suitable ligands for catalysts can also be used to bind metals in adsorbent materials. Functional groups that have been employed in the preparation of crosslinked hybrid materials include epoxy [17, 19, 77, 221], amine [101, 222], methacryloyl [93], vinyl [81], alkyl halide [223], and hydrido [81]. Even further, high surface area and chemical functionality make POSS materials excellent candidates for catalyst supports [208]. Incorporation of dyes the like of anthracene, terphenylene, coumarin, fullerene, oligothiophenes, lanthanide complexes, triarylamines, nitroaromatics, phthalocyanines, porphyrins, and phenylenevinylidene functionalities into the sol–gel POSS matrix is another useful strategy for preparing waveguides, lasers, sensors, light-emitting diodes and nonlinear optical (NLO) materials [9, 12, 224–234]. The use of a dye molecule as a bridging group provides an exceptionally high loading of chromophores and ensures against leaching and/or phase separation of the dye molecule. The fine degree of control over bulk chemical and physical properties in addition to capability to manipulate the properties by incorporating chromophores in the organic component has made these POSS-based materials attractive candidates for applications ranging from optical-device fabrication [235, 236] to catalyst supports [237] and ceramics. For example, dithienylethene-bridged polysilsesquioxanes that are photochromic materials, which refractive index can be reversibly photoswitched, offer significant potential for optical components for wave guiding [238]. Optical properties can also be manipulated by incorporating chromophores in the bridging organic component [12]. POSS dendrimers possible applications range from drug-delivery agents, micelle mimics, nanoscale building

blocks, high-performance polymers and nanoscale reactors [134–137]. The rigid spheroidal architecture of these molecules leads to properties such as low intrinsic viscosity, high solubility and miscibility, and high reactivity due to the presence of many chain ends. An alternative application that has achieved some attention is that of catalysis where dendrimers have some striking advantages over both homogeneous and heterogeneous catalysts including the possibility of preparing highly active yet recyclable catalysts [114, 135, 239–241]. POSS-dendrimer systems are currently under investigation as biomimetic catalysts, building blocks for fabrication of designed biomaterials, molecular carriers for chemical catalysts and potential vehicles for delivery of drugs and immunogens [242], and as selective molecular gates [243], as well as light-emitting diodes, signal amplifiers, frequency converters and other photonic devices [244].

9 Concluding Remarks

The incorporation of POSS cages into polymeric materials often results in major improvements in polymer properties, including increases in use temperature, oxidation resistance and surface hardening, resulting in improved mechanical properties, as well as reductions in flammability and heat evolution. As a result, POSS-based hybrid polymers have recently generated much interest. Appropriate choice of the outer groups confers a wide range of tailored properties to the molecule, e.g., the surface properties and the miscibility behavior that can be changed by the choice of hydrophobic or hydrophilic attachments. Nevertheless, the nature of the interface between the organic and inorganic components, together with the connectivity and functionality of the nanobuilding blocks are of primary importance in determining the final structure of the hybrid materials.

In principle, there are several ways to adapt the POSS-nanobuilding blocks approach to create nanoparticle-based hybrid materials, yet, creating the hybrid structures requires fine-tuning at the hybrid interface level. Further, the nanoparticles have to be functionalized to be compatible with the organic components of the hybrid. In this case, colloidal interactions must be taken into account, in addition to the chemical nature of the system. The resulting hybrid networks can be either amorphous or nanostructured, or can even exhibit long-range ordering. Enhancements have been shown to apply to a wide range of POSS-polymer thermoplastics and a few thermoset systems, such as those based on siloxanes, vinyl esters, methacrylates, styrene, norbornene, ethylene, epoxies and urethanes. The applications of the resultant materials is therefore immense and of many diversities.

So far these well-defined functionalized POSS have been prepared by the hydrosilylation reaction of terminal olefins with octahydridosilsesquiox-

ane or direct hydrolytic condensation reaction of silane-bearing compounds. However, the clear explanation on the mechanism of direct hydrolytic condensation reaction has not been explored yet. The relationships between the structures of POSS molecules and of polymer matrix, and the resulting rheological and mechanical property changes in POSS nanocomposites needs further understanding. In addition, some of the reported ad hoc synthetic procedures need to be standardized to foresee significant developments in acquiring greatly improved properties as forecasted. This need can be reflected by the great variation in the resultant material properties, in which some remarkable improvements have been reported, while at the same time significant property deterioration have been observed, e.g. enhanced thermal properties at the expense of mechanical properties or vice versa; therefore better understanding and optimization procedures are a must for further advances in chemistry and technology of these materials. Furthermore, some of these synthetic procedures are yet to be established for large-scale production. Also, much of the reported works on POSS-monomers, nanobuilding blocks and nanocomposites cover POSS-cubic cages, while there is hardly any work on other POSS-cages. It is important to mention that, despite these shortcomings, advances in POSS-based hybrid polymers are currently fast-growing and looks very promising. POSS commercial products and industrial applications are readily available; with the ongoing demands for better quality applications, one would only expect continuous growth in all areas of POSS chemistry and in particular the nanocomposites area.

To sum up, this work has reviewed the recent developments in syntheses of POSS polymer materials, otherwise used for developing nanocomposites. Examination of the relationships between the POSS-nanobuilding blocks and the resultant POSS nanocomposites, though vital, is beyond the scope of the current work. The syntheses of POSS cages, monomers containing POSS cages, POSS-dendrimers' cores, POSS-containing polymers (nanobuilding blocks) and POSS nanocomposites is described in fine details. The enhanced properties of POSS-nanobuilding blocks have been critically reviewed and conclusions drawn. Such properties include mechanical, thermal and flame-retardant, and viscoelastic properties. Investigations in to POSS-nanobuilding blocks' structure/reactivity, morphology and compatibility have also been reviewed. Other properties covered include ion-mobility, swelling characteristics and porosity of the POSS-nanobuilding blocks.

References

1. Lucke S, Stoppek-Langner K (1999) Appl Surf Sci 144–145:713
2. Li GZ, Wang L, Toghiani H, Daulton TL, Koyama K, Pittman Jr CU (2001) Macromolecules 34:8686
3. Ramirez C, Vilarino JML, Abad MJ, Barral L, Bouza R, Cano J, Diez FJ, Garcia-Garabal S, Lopez J (2004) J Appl Polym Sci 92:1576

4. Lichtenhan JD, Schwab JJ, Reinerth WA Sr (2001) Chem Innov 31:3
5. Haddad TS, Stapleton R, Jeon HG, Mather PT, Lichtenhan JD, Phillips S (1999) Polym Prepr 40:496
6. Neumann D, Fisher M, Tran L, Matisons JG (2002) J Am Chem Soc 124:13998
7. Choi J, Kim SG, Laine RM (2004) Macromolecules 37:99
8. Sanchez C, Soler-Illia GJAA, Ribot F, Lalot T, Mayer CR, Cabuil V (2001) Chem Mater 13:3061
9. Shea KJ, Loy DA, Webster OW (1992) J Am Chem Soc 114:6700
10. Corriu RJP (2000) Angew Chem Int Ed 39:1376
11. Corriu RJP, Moreau JJE, Thepot P, Man MWC (1992) Chem Mater 4:1217
12. Choi KM, Shea KJ (1998) In: Wise G, Wnik G, Trantolo M, Graham B (eds.) Photonic Polymer Synthesis. Marcel Dekker, New York, p 437
13. Kim GM, Qin H, Fang X, Mather PT (2003) J Polym Sci Polym Phys 41:3299
14. Fu BX, Yang L, Somani RH, Zong SX, Hsiao BS, Phillips S, Blanski R, Ruth P (2001) J Polym Sci, Polym Phys 39:2727
15. Zheng L, Farris RJ, Coughlin EB (2001) Macromolecules 34:8034
16. Fu BX, Hsiao BS, White H, Rafailovich M, Mather PT, Jeon HG, Phillips S, Lichtenhan J, Schwab JJ (2000) Polym Int 49:437
17. Choi J, Harcup J, Yee AF, Zhu Q, Laine RM (2001) J Am Chem Soc 123:11420
18. Gao F, Culbertson BM, Tong Y, Schricker SR (2001) Polym Prepr 41:580
19. Laine RM, Choi J, Lee I (2001) Adv Mater 13:800
20. Haddad TS, Lichtenhan JD (1996) Macromolecules 29:7302
21. Romo-Uribe A, Mather PT, Haddad TS, Lichtenhan JD (1998) J Polym Sci Polym Phys 36:1857
22. Sellinger A, Laine RM (1996) Macromolecules 29:2327
23. Lee A, Lichtenhan JD (1998) Macromolecules 31:4970
24. Shockey EG, Bolf AG, Jones PF, Schwab JJ, Chaffee KP, Haddad TS, Lichtenhan JD (1999) Appl Organomet Chem 13:311
25. Andrews R, Weisenberger MC (2004) Curr Opin Solid State M 8:31
26. Mather PT Jeon HG, Romo-Uribe A, Haddad TS, Lichtenhan JD (1999) Macromolecules 32:1194
27. Bharadwaj BK, Berry RJ, Farmer BL (2000) Polymer 41:7209
28. Laine RM, Tamaki R, Choi J (2002) World Patent WO 02100867
29. Lichtenhan JD, Vu NQ, Carter JA (1993) Macromolecules 26:2141
30. Shan L, Verghese KNE, Robertson CG, Reifsnider KL (1999) J Polym Sci Polym Phys 37:2815
31. De A Prado LAS, Radovanovic E, Pastore HO, Yoshida IVP, Torriani IL (2000) J Polym Sci Polym Chem 38:1580
32. Baney RH, Itoh M, Sakakibara A, Suzuki T (1995) Chem Rev 95:1409
33. Harrison PG (1997) J Organomet Chem 542:141
34. Huang J, Lim PC, Shen L, Pallathadka PK, Zeng K, He C (2005) Acta Mater 53:2395
35. Hasegawa I (1989) Chem Commun 208
36. Bartsch M, Bornhauser P, Calzaferri G (1994) J Phys Chem 98:2817
37. Agaskar PA (1991) Inorg Chem 30:2708
38. Schockey E, Lichtenhan JD (1994) Polym Prepr 35:525
39. Gidden J, Kemper PR, Shammel E, Fee DP, Anderson S, Bowers MT (2003) Int J Mass Spectrom 222:63
40. Frye CL, Collins WT (1970) J Am Chem Soc 92:5586
41. Muller R, Khole R, Sliwinski S (1959) J Prakt Chem 9:71
42. Sprung MM, Guenther FO (1955) J Am Chem Soc 77:3990

43. Barry AJ (1955) J Am Chem Soc 77:4248
44. Sprung MM, Guenther FO (1955) J Am Chem Soc 77:6045
45. Vogt LH, Brown JF (1963) Inorg Chem 2:189
46. Sprung MM, Guenther FO (1955) J Am Chem Soc 77:3996
47. Voronkov MG, Lavrent'yev VI, Kovrigin VM (1981) J Organomet Chem 220:285
48. Brown JF, Vogt LH (1965) J Am Chem Soc 87:4313
49. Voronkov MG (1979) Zh Obshch Khim 49:1522
50. Brown Jr JF (1965) J Am Chem Soc 87:4317
51. Sprung MM, Guenther FO (1958) J Polym Sci 28:17
52. Brown JF, Vogt LH, Prescott PI (1964) J Am Chem Soc 86:1120
53. Brown JF (1963) J Polym Sci 1C:83
54. Tishchenko G, Bleha M (2005) J Membrane Sci 248:45
55. Bent M, Gun'ko Y (2005) J Organomet Chem 690:463
56. Pielichowski K, Janowski B (2004) World Polymer Congress MACRO 2004—Conference Proceedings, p 169
57. Njuguna J, Pielichowski K: Composites A, submitted
58. Lee Y-J, Huang J-M, Kuo S-W, Lu J-S, Chang F-C (2005) Polymer 46:173
59. Chen Y, Kang E-T (2004) Mater Lett 58:3716
60. Chen W-Y, Wang Y-Z, Kuo S-W, Huang C-F, Tung P-H, Chang F-C (2004) Polymer 45:6897
61. Lee Y-J, Kuo S-W, Su Y-C, Chen J-K, Tu C-W, Chang F-C (2004) Polymer 45:6321
62. Ni Y, Zheng S, Nie K (2004) Polymer 45:5557
63. Feher FJ, Budzichowski TA, Blanski RL, Weller KJ, Ziller JW (1991) Organometallics 10:2526
64. Feher FJ, Soulivong D, Lewis GT (1997) J Am Chem Soc 119:11323
65. Feher FJ, Nguyen F, Soulivong D, Ziller JW (1999) Chem Commun 1705
66. Feher FJ, Soulivong D, Nguyen F (1998) Chem Commun 1279
67. Feher FJ, Wyndham KD (1998) Chem Commun 323
68. Feher FJ, Terroba R, Ziller JW (1999) Chem Commun 2309
69. Feher FJ, Terroba R, Ziller JW (1999) Chem Commun 2153
70. Feher FJ, Terroba R, Jin R-Z (1999) Chem Commun 2513
71. Gidden J, Jackson AT, Scrivens JH, Bowers MT (2002) J Am Soc Mass Spectr 13:499
72. Angot S, Taton D, Gnanou Y (2000) Macromolecules 33:5418
73. Kobayashi S, Kaku M, Saegusa T (1988) Macromolecules 21:334
74. Kim KM, Keum DK, Chujo Y (2002) Polym Prepr Jpn 51:304
75. Kim KM, Chujo Y (2001) Polym Bull 46:15
76. Kamigaito M, Ando T, Sawamoto M (2001) Chem Rev 101:3689
77. Zhang C, Laine RM (1996) J Organomet Chem 521:199
78. Morrison JJ, Love CJ, Manson BW, Shannon IJ, Morris RE (2002) J Mater Chem 12:3208
79. Feher FJ, Soulivong D, Eklund AG (1998) Chem Commun 399
80. Harrison PG, Kannengiesser R (1996) Chem Commun 415
81. Zhang C, Babonneau F, Bonhomme C, Laine RM, Soles CL, Hristov HA, Yee AF (1998) J Am Chem Soc 120:8380
82. Bassindale AR, Gentle TE (1993) J Mater Chem 3:1319
83. Manson BW, Morrison JJ, Coupar PI, Jaffres PA, Morris RE (2001) Dalton Trans 1123
84. Waddon AJ, Coughlin EB (2003) Chem Mater 15:4555
85. Fu BX, Hsiao BS, Pagola S, Stephens P, White H, Rafailovich M, Sokolov J, Mather PT, Jeon HG, Phillips S, Lichtenhan J, Schwab J (2001) Polymer 42:599

86. Loy DA, Jamison GM, Baugher BM, Russick EM, Assink RA, Prabaker S, Shea KJ (1995) J Non-Crystal Solids 186:44
87. Loy DA, Baugher BM, Prabaker S, Assink RA, Shea KJ (1995) Mater Res Soc Symp Proc (Adv Porous Mater) 371:229
88. Sellinger A, Laine RM (1994) Polym Prepr 35:665
89. Harvey DF, Lund KP, Neil DA (1992) J Am Chem Soc 114:8424
90. Laine RM, Sellinger A, Chu V, Viney C (1994) J Polym Sci Polym Chem 32:3069
91. Lewis LN, Sy KG, Bryant Jr GL, Donahue PE (1991) Organometallics 10:3750
92. Kim KM, Ouchi Y, Chujo Y (2003) J Mater Chem 49:341
93. Zhang C, Laine RM (2000) J Am Chem Soc 122:6979
94. Schwab JJ, Lichtenhan JD, Carr MJ, Chaffee KP, Mather PT, Romo-Uribe A (1997) Polym Prepr 77:549
95. Devaux E, Rochery M, Bourbigot S (2002) Fire Mater 26:149
96. Lichtenhan JD, Otonari YA, Carr MJ (1995) Macromolecules 28:8435
97. Schwab JJ, Lichtenhan JD (1998) Appl Organomet Chem 12:707
98. Zhang C, Baranwal R, Laine RM (1995) Polym Prepr 36:342
99. Liu H, Zheng S (2005) Macromol Rapid Commun 26:196
100. Laine RM, Zhang C, Sellinger A, Viculis L (1998) Appl Organomet Chem 12:715
101. Tamaki R, Tanaka Y, Asuncion MZ, Choi J, Laine RM (2001) J Am Chem Soc 123:12416
102. Jeon HG, Mather PT, Haddad TS (2000) Polym Int 49:453
103. Hoflund GB, Gonzalez RI, Philips SH (2001) J Adhes Sci Technol 15:1199
104. Feher FJ, Soulivong D, Eklud AG, Wyndham KD (1997) Chem Commun 1185
105. Mather PT, Jeon HG, Romo-Uribe A, Haddad TS, Lichtenhan JD (1998) Macromolecules 32:1194
106. Barral L, Diez FJ, Garcia-Garabal S, Lopez J, Montero B, Montes R, Ramirez C, Rico M (2005) Eur Polym J 41:1662
107. Dodiuk H, Kenig S, Blinsky I, Dotan A, Buchman A (2005) Int J Adhes Adhes 25:211
108. Li GZ, Wang L, Toghiani H, Daulton TL, Pittman Jr CU (2002) Polymer 43:4167
109. Liu H, Zhang W, Zheng S (2005) Polymer 46:157
110. Zheng L, Farris RJ, Coughlin EB (2001) J Polym Sci Polym Chem 39:2920
111. Haddad TS, Lee A, Phillips SH (2001) Polym Prepr 42:88
112. Haddad TS, Choe E, Lichtenhan JD (1996) Mater Res Soc Symp Proc 435:25
113. Fu BX, Zhang W, Hsiao BS, Johansson G, Sauer BB, Phillips S, Blanski R, Rafailovich M, Sokolov J (2000) Polym Prepr 41:587
114. Lichtenhan J (1995) Comments Inorg Chem 17:115
115. Matyjaszewski K (ed) (1998) Controlled Radical Polymerization. Proceedings of a Symposium at the 213th ACS National Meeting 685:483
116. Matyjaszewski K (ed) (2000) Controlled/Living Radical Polymerization. Progress in ATRP, NMP, and RAFT. Proceedings of a Symposium on Controlled Radical Polymerization 768:484
117. Matyjaszewski K (2001) Macromol Symp 174:51
118. Wang JS, Matyjaszewski K (1995) Am Chem Soc 117:5614
119. Pyun J, Matyjaszewski K (2000) Macromolecules 33:217
120. Matyjaszewski K, Xia J (2001) Chem Rev 101:2921
121. Patten TE, Matyjaszewski K (1999) Acc Chem Res 32:895
122. Pyun J, Matyjaszewski K, Wu J, Kim GM, Chun SB, Mather PT (2003) Polymer 44:2739
123. Xu H, Kuo S-W, Huang C-F, Chang F-C (2002) J Polym Res 9:239
124. Yei D-R, Kuo S-W, Su Y-C, Chang F-C (2004) Polymer 45:2633

125. Sellinger A, Laine RM (1996) Chem Mater 8:1592
126. Choi J, Tamaki R, Kim SG, Laine RM (2003) Chem Mater 15:3365
127. Tamaki R, Choi J, Laine RM (2003) Chem Mater 15:793
128. Mather PT, Romo-Uribe A, Otonari Y, Carr MJ, Lichtenhan JD (1997) Soc Plast Eng Symp Proc 1817
129. Unno M, Suto A, Takada K, Matsumoto H (2000) Bull Chem Soc Jpn 73:215
130. Leu C-M, Reddy GM, Wie KH, Shu CF (2003) Chem Mater 15:2261
131. Leu C-M, Chang Y-T, Wei KH (2003) Chem Mater 15:3721
132. Leu C-M, Chang, Y-T, Wei K-H (2003) Macromolecules 36:9122
133. Constable GS, Lesser AJ, Coughlin EB (2004) Macromolecules 37:1276
134. Tomalia D, Dewald R (1985) US Patent 4,507,466
135. Jaffres PA, Morris RE (1998) Dalton Trans 2767
136. Ardoin N, Astruc D (1995) Bull Soc Chim Fr 132:875
137. Dagani R (1996) Chem Eng News 74:30
138. Romagnoli B, Hayes W (2002) J Mater Chem 12:767
139. Zeng F, Zimmerman SC (1996) J Am Chem Soc 118:5326
140. Hayes W, Osborn HMI, Osborne SD, Rastall RA, Romagnoli B (2003) Tetrahedron 59:7983
141. Oestreich M, Schmid UK, Auer G, Keller MA (2003) Synthesis-Stuttgart 17:2725
142. Zhang X, Haxton KJ, Ropartz L, Cole-Hamilton DJ, Morris RE (2001) Dalton Trans 3261
143. Ropartz L, Foster DF, Morris RE, Slawin AMZ, Cole-Hamilton DJ (2002) Dalton Trans 1997
144. Coupar PI, Jaffres P-A, Morris RE (1999) Dalton Trans 2183
145. Ropartz L, Foster D, Morris RE, Cole-Hamilton DJ (2001) Chem Commun 361
146. Ropartz L, Schwarz G, Foster D, Morris RE, Cole-Hamilton DJ (2000) Inorg Chem Commun 714
147. Jaffres P-A, Morris RE (1998) Dalton Trans 2770
148. Matthews OA, Shipway AN, Stoddart JF (1998) Prog Polym Sci 23:1
149. McCusker C, Carroll JB, Rotello VM (2005) Chem Commun 996
150. Bassindale AR, Gentle TE (1996) J Organomet Chem 521:391
151. Moran M, Casado CM, Cuadrado I, Losada J (1993) Organometallics 12:4237
152. Hong B, Thoms TPS, Murfee HJ, Lebrun MJ (1997) Inorg Chem 36:6146
153. Ropartz L, Morris RE, Foster DF, Cole-Hamilton DJ (2002) J Mol Catal A: Chem 182–183:99
154. Cavallo L, Fraternali F (1998) Chem Eur J 4:927
155. Gorman CB, Smith JC (2001) Acc Chem Res 34:60
156. Murfee HJ, Thoms TPS, Greaves J, Hong B (2000) Inorg Chem 39:5209
157. Zhou LL, Roovers J (1993) Macromolecules 26:963
158. van der Made AW, van Leeuwen PWNM (1992) Chem Commun 1400
159. Seyferth D, Son DY, Rheingold AL, Ostrander RL (1994) Organometallics 13:2683
160. Saez IM, Goodby JW, Richardson RM (2001) Chem Eur J 7:2758
161. Feher FJ, Phillips SH, Ziller JW (1997) Chem Commun 829
162. Feher FJ, Budzichowski TA, Rahimian K, Ziller JW (1992) J Am Chem Soc 114:3859
163. Feher FJ, Newman DA, Walzer JF (1989) J Am Chem Soc 111:1741
164. Feher FJ, Budzichowski TA (1995) Polyhedron 14:3239
165. Murugavel R, Chandrasekhar V, Roesky HW (1996) Acc Chem Res 29:183
166. Herrmann WA, Anwander R, Dufaud V, Scherer W (1994) Angew Chem Int Ed Engl 33:1285

167. Abbenhuis HCL, van Herwijnen HWG, van Santen RA (1996) Chem Commun 1941
168. Abbenhuis HCL, Krijnen S, van Santen RA (1997) Chem Commun 331
169. Li GZ, Cho H, Wang L, Toghiani H, Pittman Jr CU (2005) J Polym Sci Polym Chem 43:355
170. Lichtenhan JD, Noel CJ, Bolf AG, Ruth PN (1996) Mater Res Soc Symp Proc 435:3
171. Abad MJ, Barral L, Fasce DP, Williams RJJ (2003) Macromolecules 36:3128
172. Bolln C, Tsuchida A, Frey H, Mulhaupt R (1997) Chem Mater 9:1475
173. Zhu L, Mimnaugh BR, Ge Q, Quirk RP, Cheng SZD, Thomas EL, Lotz B, Hsiao BS, Yeh F, Liu L (2001) Polymer 42:9121
174. Haddad TS, Mather PT, Jeon HG, Chun SB, Phillips SH (2001) Mater Res Soc Symp Proc 628:cc2.6.1
175. Xu H, Kuo SW, Lee JS, Chang FC (2002) Macromolecules 35:8788
176. Larson RG (1999) The Structure and Rheology of Complex Fluids. Oxford University Press, New York
177. Tong JD, Jerome R (2000) Macromolecules 33:1479
178. Fujino K, Senshu K, Kawai H (1961) J Colloid Sci 16:262
179. Wu S (1989) J Polym Sci Polym Phys Ed 27:723
180. Fu BX, Namani M, Lee A (2003) Polymer 44:7739
181. Tant MR, Wilkes GL (1981) Polym Eng Sci 21:325
182. Zhang W, Fu BX, Seo Y, Schrag E, Hsiao B, Mather PT, Yang NL, Xu D, Ade H, Rafailovich M, Sokolov J (2002) Macromolecules 35:8029
183. Kim KM, Inakura T, Chujo Y (2001) Polym Bull 46:351
184. Kim KM, Adachi K, Chujo Y (2002) Polymer 43:1171
185. Majoros I, Marsalko TM, Kennedy JP (1997) Polymer Bull 38:15
186. Feher FJ, Tajima RL (1994) J Am Chem Soc 116:2145
187. Hong B, Thomas TPS, Murte HJ, Lebrun MM (1997) Inorg Chem 36:6146
188. Jun-Chao H, Chao-Bin H, Yang X, Yi MK, Jie D, Ping SY (2003) Polymer 44:4491
189. Zhu B, Katsoulis DE, Keryk JR, McGarry FJ (2000) Polymer 41:7559
190. Kim KM, Chujo Y (2003) J Polym Sci Polym Chem 41:1306
191. Aylott JW, Richardson DJ, Russell DA (1997) Analyst 122:77
192. Dire S, Pagani E, Babonneau F, Ceccato R, Carturan G (1997) J Mater Chem 7:67
193. Brinker CJ, Scherer GW (1990) Sol–Gel Science: The Physics and Chemistry of Sol–Gel Processing. Academic Press, San Diego
194. Loy DA, Russick EM, Yamanaka SA, Baugher BM (1997) Chem Mater 9:2264
195. Loy DA, Shea KJ (1995) Chem Rev 95:1431
196. Mackenzie JD (1997) In: Pope EJA, Sakka S, Klein LC (eds.) Sol–Gel Science and Technology. American Ceramic Society, Westerville, OH, p 25
197. Bowers MT, Kemper PR, von Helden G, van Koppen PAM (1993) Science 260:1446
198. Clemmer DE, Jarrold MF (1997) J Mass Spectrom 32:577
199. Kim KM, Chujo Y (2003) J Mater Chem 13:1384
200. Shea KJ, Loy DA (2001) Chem Mater 13:3306
201. Breck DW (1984) Zeolite Molecular Sieves. Wiley, New York
202. Matejka L, Plestil J, Dusek K (1998) J Non-Cryst Solids 226:114
203. Matejka L, Dusek K, Plestil J, Kriz J, Lednicky F (1998) Polymer 40:171
204. Hoebbel D, Pitsch I, Heidemann D (1992) Eurogel'91 467
205. Hoebbel D, Endres K, Reinert T, Pitsch I (1994) J Non-Cryst Solids 176:179
206. Rouquerol F, Rouquerol J, Sing K (1999) Adsorption by Powders and Porous Solids: Principles, Methodology and Applications. Academic Press, San Diego
207. Brinker CJ, Sehgal R, Hietala SL, Deshpande R, Smith DM, Loy DA, Ashley CS (1994) J Membr Sci 94:85

208. Schubert U (1994) New J Chem 18:1049
209. Lopez T, Bosch P, Navarrete J, Asomoza M, Gomez R (1994) J Sol-Gel Sci Technol 1:193
210. Jeng S-P, Taylor K, Seha T, Chang M-C, Fattaruso J, Havemann RH (1995) VLSI Technology Symposium Digest 61
211. Hsuie G-H, Lee R-H, Jeng R-J (1997) Chem Mater 9:883
212. Aylott JW, Richardson DJ, Russell DA (1997) Analyst 122:77
213. Dire S, Pagani E, Babonneau F, Ceccato R, Carturan G (1997) J Mater Chem 7:67
214. Loy DA, Carpenter JP, Alam TM, Shaltout R, Dorhout PK, Greaves J, Small JH, Shea KJ (1999) J Am Chem Soc 121:5413
215. Li C, Glass T, Wilkes GL (1999) J Inorg Organomet Polym 9:79
216. Vlasova NN, Pestunovich AE, Pozhidaev YN, Kirillov AI, Voronkov MG (1989) Izv Sib Otd Akad Nauk SSSR Ser Khim Nauk 2:106
217. Jin C, List S, Yamanaka S, Lee WW, Taylor K, Hsu W-Y, Olsen L, Luttmer JD, Havemann R, Smith D, Ramos T, Maskara A (1997) Mater Res Soc Symp Proc 443:99
218. Koike N, Tsukagoshi H (1985) Japanese Patent 60169847
219. Reetz M, Zonta A, Simpelkamp J (1995) Angew Chem Int Ed Engl 34:301
220. Kirillov AI, Panezhda EV, Pozhidaev YN, Belousova LY, Vlasova NN, Voronkov MG (2000) Zh Prikl Khim 73:520
221. Laine RM, Choi J, Costa ROR (2000) Polym Prepr 41:524
222. Tamaki R, Choi J, Laine RM (2001) Polym Mater Sci Eng 84:564
223. Costa ROR, Vasconcelos WL, Tamaki R, Laine RM (2001) Macromolecules 34:5398
224. Corriu RJP, Moreau JJE, Thepot P, Man WCM, Chorro C, Lere-Porte JL, Sauvajol JL (1994) Chem Mater 6:640
225. Suratwala T, Gardlund Z, Davidson K, Uhlmann DR, Watson J, Peyghambarian N (1998) Chem Mater 10:190
226. Xia H, Zhu C, Gan F, Chen Y, Yu B, Cai R, Huang Z (1997) Fullerene Sci Technol 5:1621
227. Ki CD, Kim JK, Hwang SS, Hong SI (2000) Polym Prepr 41:600
228. Gaudiello JG, Ghosh PK, Bard AJ (1985) J Am Chem Soc 107:3027
229. Taylor-Smith RE, Choi KM (2000) Polym Mater Sci Eng 83:237
230. Li W, Wang Q, Cui J, Chou H, Shaheen SE, Jabbour GE, Anderson J, Lee P, Kippelen B, Peyghambarian N, Armstrong NR, Marks TJ (1999) Adv Mater 11:730
231. Han S, Li Z, Ji S, Dai D, Zhang R, Zhu C, Wang C (2000) J Sol-Gel Sci Technol 18:137
232. Ribeiro AO, Biazzotto JC, Serra OA (2000) J Non-Cryst Solids 273:198
233. Ciuffi KJ, Sacco HC, Biazzotto JC, Vidoto EA, Nascimento OR, Leite, CA, Serra OA, Iamamoto Y (2000) J Non-Cryst Solids 273:100
234. Corriu RJP, Hesemann P, Lanneau GF (1996) Chem Commun 1845
235. Corriu R (1998) Polyhedron 17:925
236. Cerveau G, Corriu RJP, Framery E (2000) J Mater Chem 10:1617
237. Lindner E, Schneller T, Auer F, Mayer HA (1999) Angew Chem Int Ed 38:2155
238. Biteau J, Chaput F, Lahlil K, Boilot J-P (1998) Chem Mater 10:1945
239. Tomalia D, Dvornic P (1994) Nature 372:617
240. Knapen J, van der Made AW, de Wilde JC, van der Leeuwen PWNM, Wijkens P, Grove DM, van Koten G (1994) Nature 372:659
241. Haggin J (1995) Chem Eng News 73:26
242. Newkome GR, He E, Moorefield CN (1999) Chem Rev 99:1689
243. Kovvali AS, Chen H, Sirkar KK (2000) J Am Chem Soc 122:7594
244. Andronov A, Frechet JMJ (2000) Chem Commun 1701
245. Kim KM, Ouchi Y, Chujo Y (2003) Polym Bull 49:341
246. Li G, Wang L, Li H, Pittman Jr CU (2001) J Inorg Organomet Polym 11:123

Editor: K. Dusek

Author Index Volume 201

Author Index Volumes 1–100 see Volume 100
Author Index Volumes 101–200 see Volume 200

Donnio, B. and *Guillon, D.*: Liquid Crystalline Dendrimers and Polypedes. Vol. 201, pp. 45–156.

Guillon, D. see Donnio, B.: Vol. 201, pp. 45–156.

Harada, A., Hashidzume, A. and *Takashima, Y.*: Cyclodextrin-Based Supramolecular Polymers. Vol. 201, pp. 1–44.
Hashidzume, A. see Harada, A.: Vol. 201, pp. 1–44.

Jaeger, W. see Kudaibergenov, S.: Vol. 201, pp. 157–224.
Janowski, B. see Pielichowski, K.: Vol. 201, pp. 225–296.

Kudaibergenov, S., Jaeger, W. and *Laschewsky, A.*: Polymeric Betaines: Synthesis, Characterization, and Application. Vol. 201, pp. 157–224.

Laschewsky, A. see Kudaibergenov, S.: Vol. 201, pp. 157–224.

Njuguna, J. see Pielichowski, K.: Vol. 201, pp. 225–296.

Pielichowski, J. see Pielichowski, K.: Vol. 201, pp. 225–296.
Pielichowski, K., Njuguna, J., Janowski, B. and *Pielichowski, J.*: Polyhedral Oligomeric Silsesquioxanes (POSS)-Containing Nanohybrid Polymers. Vol. 201, pp. 225–296.

Takashima, Y. see Harada, A.: Vol. 201, pp. 1–44.

Subject Index

2-(3-Acrylamidopropyldimethylammonio)-ethanoate (APDMAE) 215
Antipolyelectrolyte 212

Betaines 157
Bipyridinium (viologen) 28
2,2-Bis(hydroxymethyl)propionic-based monodendrons 102
Bis(methanofullerene) 131
Bithiophene 35
Butanediol diglycidyl ether (BDGE) 237
1,4-Butyrolactone 165

Carbobetaine gels, resolution of protein mixtures 214
Carbosilane 64, 65
– polyols 65
Carbosilane-siloxy dendrimers 70
Carbosilazane 64, 81
Cholesteryl chloroformate 65
6-Cinnamoyl-β-cyclodextrin 15
Coordination complexes 202
Crown ether 33
Cucurbituril 33
Cyclodextrin, aromatic tethers 10
– polyrotaxanes 31
Cyclohexyltrichlorosilane 234

Dendrimers, carbosilane 65
–, carbosilazane 81
–, central triphenylene cores 140
–, distyrylbenzene-based 116
–, fullerene-ferrocene 123
–, LC 45
–, main-chain liquid-crystalline 104
–, mesomorphic, rigid discotic cores 139
–, metallodendrimers, liquid-crystalline 117
–, PPI, amphiphilic 98
–, shape-persistent liquid-crystalline 113
–, side-chain liquid-crystalline 64
–, silicon-containing 64
–, stilbenoid-like 115
–, tolanoid-like 114
–, willow-like 105
Dendromesogens 48
N,*N*-Diallyl-*N*,*N*-dimethylammonium chloride (DADMAC) 163
4-(*N*,*N*-Diallyl-*N*-methylammonio)-butanoate 163
Dicopper dendritic complexes 119
Diglycidyl ether of bisphenol A (DGEBA) 237
Distyrylbenzene-based dendrimers 116
DOBOB 49
Drug delivery devices 47
Dumbbell 142

Epoxy network, POSS-modified 276
Ethylene dimethacrylate 206
2-(*N*-Ethylperfluorooctane-sulfonamido) ethyl acrylate (FOSA) 37

Ferrocene-containing dendrimer 123
Frank–Kasper structures 59
Fullerene-ferrocene dendrimer 123
Fullerodendrimers, liquid-crystalline 126
Fulleropyrrolidines 130

Gene delivery devices 47
Glass-forming materials, nematic 138

Hexa(ethylene glycol) 21
Hexakis(methano)fullerene 130
Host-guest interactions 1, 3
Hydrocinnamoyl-β-cyclodextrin 13

Inclusion complex 1

Interpolyelectrolyte 157
Inversion-recovery cross-polarization 280

Kumkol–Akshabulak oil mixture 212

Malonate-based dendritic addend 126
Mesogens 45
Mesophase 45
Metallodendrimers, liquid-crystalline 117
Metallodendromesogens, mesomorphism 121
Metallomesogens 117
2-Methacryloyloxyethyl phosphorylcholine (MPC) 207
Methanofullerene dendrimers 127
Methylsesquioxane 77
Molecular shuttle 28
Molecular tubes 1, 28
Molecular wires 34
Monodendrons, 2,2-bis(hydroxy-methyl)propionic-based 102
Multipedes 135

Nanohybrid polymers, POSS-containing 263
Norbornene–POSS polymers 283

Octaaminophenylsilsesquioxane 249
Octa(dimethylsiloxy)octasilsesquioxane 78
Octa(hydrido)silsesquioxane 78
Octakis(dimethylsiloxy)octasilsesquioxane 236
Octa-*p*-phenylene molecular trees 143
Octopus dendrimers 107
Oligo(ethylene oxide) 113
Oligophenylenevinylene conjugates (OPV) 131
Oligosilsesquioxanes 232
Onion morphology 110
Oxovanadyl complexes 119

PAMAM, mesomorphism 87
Papain 215
PEG 26
Pentaerythritol 135
Photocyclodimerization 33
Phthalocyanine 139
PNIPA-PC 208
Poly(acrylamide) 36
Poly3-[(2-acrylamido-2-methylpropyl)dimethylammonio]-1-propanesulfonate 210
Poly(3-ammoniopropanoates) 165
Poly(carboxyethyl 3-aminocrotonate) 209
Poly3-[(2-carboxy-1-methyl-ethyl)dodecylaminocrotonate] 212
Poly(catenane)s 32
Poly(diallylaminoethanoate-*co*-sulfur dioxide) (PAESD) 206
Poly[3-diethyl(methylmethacryloylethyl) ammonium propanesulfonate] 214
Poly(*N*,*N* –dimethylacrylamide) (PDMAAm) 276
Poly(*N*,*N*-dimethylaminoethyl methacrylate) 165
Poly(dimethylsilane)s (PSi) 25
Poly(dimethylsiloxane)s (PDMS) 25
Poly(DMAPS-*co*-EDMA) 207
Poly(ethylene alanine) (PEA) 209
Poly(ethylene oxide) (PEO) coil 143
Poly(isobutene-*alt*-maleic acid) 38
Poly(1-isopropylcarboxylethyleneimine) (PIPCEI) 209
Poly(meth)acrylamides 164
Poly(meth)acrylates 164
Poly(2-methyl-2-oxazoline) (POZO) 276
Poly(oxytrimethylene) 26
Poly(polyrotaxane) 32
Poly(*N*-propylene glycine) (PPG) 209
Poly(propyleneimine) dendrimers 85
Poly(tetrahydrofuran) 26
Poly(trimethylpropane trimethacrylate) 206
Poly(*N*-vinylpyrrolidone) (PVP) 276
Polyaminophenylsilsesquioxane 239
Polybetaines, gel states 181
–, interpolymers 202
Polybutadienes (PB) 25
Polycarbobetaines 162
–, quaternary pyrrolidinium units 164
Polycarbosilane 64
Polydamidoamine dendrimers 83
Polyether dendritic cores 101
Polyhedral oligosilsesquioxane (POSS) 225
Polyisoprenes (PIP) 25
Polymer–surfactant 202

Polyoxypropylene diamines 237
Polypedes 45, 133
Polyphosphobetaines 160, 173
Polypropyleneimine dendrimers 83
Polyrotaxanes 1, 20
Polysiloxane 64
Polysulfobetaines 168
Polythiophene polyrotaxanes 34
Polyzwitterions 160
Porphyrins 140
POSS cages 230
POSS-dendrimer cores 256
POSS-triol 281
Pour point depressant (PPD) 211
PPI dendrimers, amphiphilic 98
– –, mesomorphism 87
– –, photoactive 100
Pullulan 37
Pyromellitic dianhydride 249

Rod-coil block codendrimers, supramolecular 141
Rotaxanes 1, 21

SC-LCDs 48
Silicon-containing dendrimers 64
Siloxane 64
– dendrimers 77
Silsesquioxanes 77, 225, 230
–, cages 129
Star-like discotic liquid crystals 139
Stilbenoid-like dendrimers 115
Supermesogens, nematic 137
Supramolecular liquid-crystalline dendrimers 48
Supramolecular polymer 1
Surfactants 179

Tetra(ethylene glycol) dibromide 22
Tetraglycidyldiaminodiphenylmethane (TGDDM) 271, 281
Tetrakis(dimethyloxy)siloxane 77
Tetraphenylcyclobutane blocking groups 33
Tolanoid-like dendrimers 114
3,4,5-Tris[(4-dodecyloxy)benzyl-oxy]benzene 49

Ureido pyrimidinone 3

4-Vinyl-4'-methyl-2,2'-bipyridine 247